HIGH-RESOLUTION CLIMATE PROJECTIONS FOR VIETNAM

TECHNICAL REPORT

IMHEN | CSIRO | Australian Aid

JUNE 2014

J.J. Katzfey, J.L. McGregor, and R. Suppiah
CSIRO Climate Adaptation Flagship

CITATION

Katzfey, JJ, McGregor, JL and Suppiah, R (2014). High-Resolution Climate Projections for Vietnam: Technical Report. CSIRO, Australia. 266 pp.

PHOTOGRAPHY COURTESY OF MATTHEW INMAN • CSIRO

ACKNOWLEDGEMENTS

We acknowledge the World Climate Research Programme's Working Group on Coupled Modelling, which is responsible for CMIP, and we thank the climate modelling groups for producing and making available their model output. For CMIP the U.S. Department of Energy's Program for Climate Model Diagnosis and Intercomparison provides coordinating support and led development of software infrastructure in partnership with the Global Organization for Earth System Science Portals.
This paper is a contribution to the Commonwealth Scientific Industrial Research Organiation (CSIRO) Climate Adaptation Flagship.

We acknowledge their efforts and also wish to thank the editors and reviewers who gave many useful suggestions to improve the text: R. Krishnan, V. Veldore, M. Thatcher, J. Johnson and H. Cat.

Many scientists contributed to the research and writing of this report. Use the following citations for individual chapter:

- **Chapter 1:** Katzfey JJ (2014) About the project. In: Katzfey JJ, McGregor JL and Suppiah R (eds) High-resolution climate projections for Vietnam: Technical report. CSIRO, Australia
- **Chapter 2:** Katzfey JJ, McGregor JL, Suppiah R and Hoffmann P (2014) Methods for developing projections. In: Katzfey JJ, McGregor JL and Suppiah R (eds) High-resolution climate projections for Vietnam: Technical report. CSIRO, Australia
- **Chapter 3:** Suppiah R and Thang N (2014) Observed climate variability of Vietnam. In: Katzfey JJ, McGregor JL and Suppiah R (eds) High-resolution climate projections for Vietnam: Technical report. CSIRO, Australia
- **Chapter 4:** Katzfey JJ, Smajgl A and Erwin T (2014) Understanding and use of climate projections. In: Katzfey JJ, McGregor JL and Suppiah R (eds) High-resolution climate projections for Vietnam: Technical report. CSIRO, Australia
- **Chapter 5:** Khiem M, Katzfey JJ and Hoffmann P (2014) Model performance for current climate. In: Katzfey JJ, McGregor JL and Suppiah R (eds) High-resolution climate projections for Vietnam: Technical report. CSIRO, Australia
- **Chapter 6:** Katzfey JJ and Khiem M (2014) Vietnam's future climate. In: Katzfey JJ, McGregor JL and Suppiah R (eds) High-resolution climate projections for Vietnam: Technical report. CSIRO, Australia
- **Chapter 7:** Nguyen KC, Hoffmann P, Abbs D, Chattopadhyay M, Nguyen H, Quang T, Tory K (2014) Climate features and extremes. In: Katzfey JJ, McGregor JL and Suppiah R (eds) High-resolution climate projections for Vietnam: Technical report. CSIRO, Australia
- **Chapter 8:** Church J, Monselesan D, White N, Zhang X and Platten S (2014) Changes in sea level. In: Katzfey JJ, McGregor JL and Suppiah R (eds) High-resolution climate projections for Vietnam: Technical report. CSIRO, Australia
- **Chapters 9-15:** Katzfey JJ, Thang N and Khiem M (2014) Regional reports. In: Katzfey JJ, McGregor JL and Suppiah R (eds) High-resolution climate projections for Vietnam: Technical report. CSIRO, Australia.

ACRONYMS

ABM	Agent-Based Model
ADB	Asian Development Bank
AOGCM	Atmosphere-Ocean Global Climate Model
APHRODITE	Asian Precipitation Highly Resolved Observational Data Integration Towards Evaluation of Water Resources
AVHRR	Advanced Very High Resolution Radiometer
BBN	Bayesian Belief Network
CABLE	Community Atmosphere Biosphere Land Exchange
CAM	Community Atmosphere Model
CCAM	Conformal Cubic Atmospheric Model
CDD	Consecutive Dry Days
CDD	CSIRO Direct Detection (for tropical cyclones)
CFC	Chlorofluorocarbon
CGE	Computable General Equilibrium
CMAP	Climate Prediction Center Merged Analysis of Precipitation
CMIP3	Coupled Model Intercomparison Project Phase 3
CMIP5	Coupled Model Intercomparison Project Phase 5
CORDEX	Coordinated Regional Climate Downscaling Experiment
CPAC	Central Pacific
CRU	Climatic Research Unit, University of East Anglia
CSIRO	Commonwealth Scientific and Industrial Research Organisation
CTU	Can Tho University
CVP	Curvature Vorticity Parameter
CWD	Consecutive Wet Days
DDC	Data Distribution Centre
DFAT	Department of Foreign Affairs and Trade
DTR	Diurnal Temperature Range
ECI	Extreme Climate Indices
ECMWF	European Centre for Medium Range Weather Forecasts
ENSO	El Niño Southern Oscillation
EPAC	Eastern Pacific
ERA-40	ECMWF Re-Analysis 40 km data archive
ERA-Interim	ECMWF Re-Analysis Interim (Latest version of the ECMWF global reanalysis)
ES	East Sea
ESM	Earth System Model
ETCCDI	Expert Team on Climate Change Detection and Indices
GCM	Global Climate Model
GDP	Gross Domestic Product
GEV	Generalised Extreme Value (distribution)
GFDL	Geophysical Fluid Dynamics Laboratory
GHG	Greenhouse Gas
GIA	Glacial Isostatic Adjustment
GIS	Geographic Information System
GMSL	Global Mean Sea Level
GPCP	Global Precipitation Climatology Project
GPI	Genesis Potential Index
GPI-M	Murakami modification of the GPI
HCMC	Ho Chi Minh City
HUS	Hanoi University of Science
HWDI	Heat Wave Duration Index
IBTrACS	International Best Track Archive for Climate Stewardship (National Climatic Data Center, NOAA)
ICE-5G	An ice model that analyses GIA processes
IFRC	International Federation of the Red Cross
IMHEN	Institute of Meteorology, Hydrology and Environment
IOD	Indian Ocean Dipole
IPCC	Intergovernmental Panel on Climate Change
ITCP	International Centre for Theoretical Physics
ITCZ	Inter-Tropical Conversion Zone
JTWC	Joint Typhoon Warming Center
LAM	Limited Area Model
MONRE	Ministry of Natural Resources and Environment
MSLP	Mean Sea Level Pressure
NASA	National Aeronautics and Space Administration
NCAR	National Center for Atmospheric Research
NCEP	National Center for Environmental Protection
NOAA	National Oceanic and Atmospheric Administration
OBS	Observations
OWZP	Okubo-Weiss-Zeta Parameter
PACCSAP	Pacific-Australia Climate Change Science and Adaptation Planning program
PCCSP	Pacific Climate Change Science Program
PDF	Probability Density Function
PDO	Pacific Decadal Oscillation
PIG	Pine Island Glacier
PSMSL	Permanent Service for Mean Sea Level
RCP	Representative Concentration Pathways
RCM	Regional Climate Model
RMSE	Root Mean Square Error
RSL	Relative Sea Level
RSMC	Regional Specialized Meteorological Center
RX1	Yearly maximum 1-day precipitation
RX5	Yearly maximum 5-day precipitation
SIC	Sea Ice Concentration
SIHYMETE	Sub-Institute of Hydro-Meteorology and Environment of South Vietnam

SIMCLIM	A flexible software package that links data and models in order to simulate the impacts of climatic variations and change.
SMB	Surface Mass Balance
SOI	Southern Oscillation Index
SPI	Standard Precipitation Index
SRES	Special Report on Emissions Scenarios
SST	Sea Surface Temperature
SSTA	Sea Surface Temperature Anomaly
T2m	Temperature at 2 meters (same as Tave)
TC	Tropical Cyclone
TCRM	Tropical Cyclone Risk Model (Geoscience Australia)
TOPEX	Topography Experiment (Satellite using radar altimeter from 1992-2006)
TRMM	Tropical Rainfall Measuring Mission
UHSLC	University of Hawaii Sea Level Center
UTC	Coordinated Universal Time
VND	Vietnamese Dong (currency)
WMO	World Meteorological Organisation
YGP	Yearly Genesis Parameter

ABBREVIATIONS

1.1 SEASONS

FIMS	First Inter-Monsoon Season (AM: April-May)
SWMS	South West Monsoon Season (JJAS: June, July, August, September)
SIMS	Second Inter-Monsoon Season (ON: October-November)
NEMS	North East Monsoon Season (DJFM: December, January, February, March)

1.2 REGIONS

NW	North West
NE	North East
ND	North Delta
NC	North Central
SC	South Central
CH	Central Highlands
S	South

1.3 EMISSION SCENARIOS

A1FI- SRES	A1FI is the fossil-fuel intensive scenario
B1-SRES	B1 scenario assumes introduction of clean and resource-efficient technologies
B2-SRES	Medium scenario, with less rapid change
A2-SRES	More divided, independent regional development
RCP	Representative Concentration Pathway

MODELS[1]

ACCESS1.0	Version of the Australian Community Climate and Earth-System Simulator that uses the MetOffice's MOSES land surface model and cloud scheme
ACCESS1.3	Version of ACCESS that uses the new PC2 cloud scheme and the CABLE land surface scheme
CanESM2	Canadian Earth System Model
CCSM4	Community Climate System Model version 4, from NCAR
CNRM-CM5	The CMIP5 version of the Earth System Model developed jointly by CNRM-GAME (Météo-France and CNRS) and CERFACS since 1995
CSIRO-Mk3.6.0	CSIRO climate model version 3.6
FGOALS-g2	Flexible Global Ocean-Atmosphere-Land System model (China) – grid point
FGOALS-s2	Flexible Global Ocean-Atmosphere-Land System model (China) - spectral
GFDL-CM3	Geophysical Fluid Dynamics Laboratory Climate Model version that includes cloud-aerosol interactions
GFDL-ESM2M	Geophysical Fluid Dynamics Laboratory C\ Earth System Model
GISS-ES-H	NASA Goddard Institute for Space Studies with H version ocean.
HadCM3	Hadley Centre Climate Model version 3
HadCM3Q	Version Q of the HadCM3 model
HadGEM2-CC	Hadley Centre Global Environment Model version 2 for Climate Change
HadGEM2-ES	Hadley Centre Global Environment Model version 2 - Earth System
INMCM4	Institute for Numerical Mathematics (Russia) Climate Model
IPSL-CM5A-LR	Institut Pierre Simon Laplace climate model – low resolution
IPSL-CM5A-MR	Institut Pierre Simon Laplace climate model – medium resolution
MIROC4h	Japanese Model for Interdisciplinary Research on Climate version 4
MIROC5	Japanese Model for Interdisciplinary Research on Climate version 5
MIROC-ESM	Japanese Model for Interdisciplinary Research – Earth System Model
MIROC-ESM-CHEM	MIROC-ESM with Chemistry
MPI-ESM-LR	Low resolution version of Max Planck Institute Earth System Model
MRI-CGCM3	Meteorological Research Institute (Japan) Coupled Ocean-Atmosphere General Circulation Model
NorESM1-M	The Norwegian Earth System Model
PRECIS	Providing REgional Climates for Impacts Studies (MetOffice)
RegCM4.2	Regional Climate Model system version 4

1 See **http://cmip-pcmdi.llnl.gov/cmip5/availability.html** for more details.

GLOSSARY

Aerosol	A gaseous suspension of fine solid or liquid particles
Agent-based modelling	A class of computational models for simulating the actions and interactions of autonomous agents
Albedo	The proportion of the incident light or radiation reflected by a surface
Anomaly	Difference from mean
Anthropogenic	Originating from human activity
Arakawa-Schubert closure assumption	A minimization method used to determine the mass fluxes of a family of moist convective elements within a grid cell
Bias	Differences of the modelled means from those of the observations
Bi-cubic horizontal interpolation	A two-dimensional interpolation method using data from 16 grid points for each interpolated value
Biosphere	The regions of the surface and atmosphere of the earth or other planet occupied by living organisms
Cartesian representation	A three-dimensional coordinate system whose coordinate axes are orthogonal straight lines
Climatological gradient	Mean gradients for a particular month or season
Climatology	Average over a long time period, usually several decades
Climate projection	A climate projection is a statement about the likelihood that something will happen several decades to centuries in the future
Cold surge	A wind event accompanied by an abrupt drop in temperature
Computationally expensive	Requiring a large amount of computer resources
Convection	Heat transfer in the atmosphere by the circulation of currents from one region to another
Convergence	A net flow of air into a given region
Cyclonic disturbance	Rotational disturbance having a length scale greater than about 1000 km
Diurnally-varying	Varying in a 24-hour period
Dynamical downscaling / downscaled simulation	Explicitly simulating atmospheric dynamical and thermodynamical processes using a model to obtain fine-scale climate with information provided by a prior coarse simulation
Eddy	A circular movement of air
El Niño	A warm ocean current that flows along the equator from the date line and south off the coast of Ecuador at Christmas time
El Niño / Southern Oscillation (ENSO)	Pattern of sea surface temperature oscillations in the tropical Pacific
Emergence	The appearance of new properties
Ensemble	A set of a number of different climate simulations with some common feature, such as emission scenario
Evapotranspiration	Transfer of water from the land to the atmosphere by evaporation
Forecast	A prediction of future weather conditions
Glacial Isostatic Adjustment	Post ice-age continental rebound
Global-scale performance	A ranking derived from the general agreement of the GCMs over the whole globe with observations of temperature, rainfall and MSLP
Gradient	Slope or rate of change
Gravitational fingerprint	Change in the gravitational field due to changes in the ocean and ice distribution
Grell scheme	A simplified version of the Arakawa-Schubert cumulus convection scheme
Insolation	The amount of solar radiation reaching a given area
Lateral boundary reflection	Refection of atmospheric waves at the lateral boundaries of a limited-area model
Limited-area model	A weather or climate model on a limited domain and requiring forcing from another model, especially at its lateral boundaries
Mercator conformal projection	A map projection of the Earth derived by projecting an ellipsoid
Monin–Obukhov similarity theory	A common method for treating turbulent transfer near the Earth's surface
Monsoon surge	The temporary extension of deep monsoon flow into a region not normally dominated by persistent monsoon flow

Multivariate analysis	Analysis using multiple variables
NINO3.4	Index of sea surface temperature changes in the central Pacific
Onset date	Start date of monsoon
Orographic lifting	When an air mass is forced from a low elevation to a higher elevation as it moves over rising terrain
Orography	Height of terrain
Pacific Decadal Oscillation	A pattern of Pacific climate variability that shifts phases on at least an inter-decadal time scale
Parameterisations	Treatment of a sub-grid scale process in terms of resolvable model variables
Pentad	Average over 5 days
Polar front	The region separating air masses of polar origin from those of tropical or subtropical origin
Projections	Climate projections are plausible descriptions of the future climate, based on assumptions of global development and the resulting levels of greenhouse gas concentrations. They are not a prediction of a specific event, like a weather forecast, but instead provide a range of possible changes over a longer time period.
Radiation balance	The equation containing both incoming and outgoing thermal radiation
Radiative forcing	The difference between radiant energy received by the earth and energy radiated back to space
Radiosonde	A lightweight package of weather instruments fitted with a radio transmitter and carried aloft by a balloon
Schmidt transformation	A global coordinate transformation devised by Schmidt
Semi-Lagrangian horizontal advection	A numerical technique that averages the equations of motion along a trajectory between a grid point and its departure point
Simulations	Recreations of current or future climate generated by computer models
Skill-score	A scaled representation of forecast error
Spurious vertical velocity	Vertical velocity produced by artefacts of the model numerics
Standard deviation	A quantity calculated to indicate the extent of deviation for a group as a whole
Southern Hemisphere Sub-Tropical High	A high pressure system that prevails over the oceans at latitudes of about 30°S
Synoptic scale disturbance	Disturbance having a length scale greater than about 1000 km
Stratosphere	The zone of the atmosphere above the troposphere that is characterised at first by isothermal conditions and then a gradual temperature increase. The earth's ozone is concentrated here.
Thermocline	An abrupt vertical gradient of temperature in the ocean
Time Series	Sequential data over a particular period
Topography	The arrangement of the natural and artificial physical features of an area
Total-variation-diminishing vertical advection	A particular numerical method for vertical transport of air with good stability properties
Trade wind	A wind blowing steadily toward the equator from the northeast in the northern hemisphere or the southeast in the southern hemisphere
Tropical depression	An early stage of tropical cyclone with wind less than 35 knots
Tropopause	The boundary between the troposphere and the stratosphere
Troposphere	The lowermost layer of the atmosphere marked by considerable turbulence and, in general, a decrease in temperature with increasing height
Tropospheric aerosol	A gaseous suspension of fine solid or liquid particles in the lower part of the atmosphere
Variable-resolution	Having grid cells of varying size
Vortices	Spiralling motions of air within a limited area

CONTENTS

Acknowledgements i
Acronyms ii
Abbreviations iii
Models iii
Glossary iv
Foreword xxv

PART 1 1

Executive summary – Part 1 2

1 About the project 4
1.1 Project aims 4
1.2 What are climate projections? 4
1.3 How to use the climate projections from this study 5

2 Methods for developing projections 6
2.1 Observational datasets 6
2.1.1 Station data variables 6
2.1.2 Global datasets and variables 6
2.1.3 ERA-40 and ERA-Interim datasets 6
2.1.4 NCEP reanalysis 7
2.1.5 The CRU Dataset 7
2.1.6 GPCP 7
2.1.7 APHRODITE 7
2.2 Emission scenarios for CMIP5 8
2.3 Climate Models 8
2.3.1 GCM selection for downscaling 9
2.4 Bias correction of SSTs 12
2.5 Dynamical downscaling models 13
2.5.1 Introduction 13
2.5.2 Conformal Cubic Atmospheric Model (CCAM) 14
2.5.3 RegCM4.2 14
2.5.4 PRECIS 14
2.6 Dynamical downscaling methods 14
2.6.1 CCAM 15
2.6.2 RegCM4.2 15
2.6.3 PRECIS 15

3 Observed climate variability of Vietnam 18
3.1 Overview 18
3.2 Atmospheric circulation and rainfall 19
3.2.1 South West Monsoon Season 19
3.2.2 Second Inter-Monsoon Season 20
3.2.3 North East Monsoon Season 22
3.2.4 First Inter-Monsoon Season 23
3.3 Trends in temperature and rainfall of Vietnam 25
3.4 Climate drivers 25
3.4.1 El Niño-Southern Oscillation (ENSO) 25
3.4.2 Tropical cyclones 27
3.4.3 Impact of aerosols on rainfall 28
3.5 Summary and knowledge gaps 28

4 Understanding and use of climate projections 30
4.1 Climate variables of interest 30
4.2 Temporal (time) scales 31
4.3 Spatial scales 31
4.4 Treatment of uncertainty 31
4.4.1 Representing climate uncertainties 32
4.4.2 Examples of uncertainty management in impact and risk assessments 32
4.5 Understanding climate projections 33
4.6 Climate Futures Tool 34
4.6.1 Delivering climate projections to end-users and stakeholders 34
4.6.2 The Climate Futures Framework 35
4.6.3 Use of the Climate Futures Tool in impact assessment 35
4.7 Using an integrated assessment model to assess policy options 38
4.7.1 Modelling methods 38
4.7.2 Determining required assessment model inputs and outputs 39
4.7.3 Agent-based modelling workshops in Vietnam 40
4.8 Summary 41

5 Model performance for current climate 42
5.1 Introduction 42
5.2 Observational datasets and validation methods 42
5.3 An assessment of the new generation of global climate models over South East Asia 42
5.3.1 Introduction 42
5.3.2 Data and methods 42
5.3.3 Results 42
5.4 Downscaled simulations within ERA-Interim 46
5.4.1 Validation of temperature for Vietnam 46
5.4.2 Validation of rainfall for Vietnam 48
5.4.3 Validation of the annual cycles of temperature and rainfall for the seven sub-regions 51
5.4.4 Spatial patterns of circulation 54
5.5 Performance of RCMs downscaled from GCMs 55
5.5.1 Validation of temperature for Vietnam 55
5.5.2 Validation of rainfall for Vietnam 57
5.6 Summary 59

6 Vietnam's future climate 60
6.1 Climate change projections for Vietnam from CMIP5 simulations 60
6.2 Climate change projected by RCMs for Vietnam by mid-century (2045-2065) 60
6.3 Climate change projected by RCMs for Vietnam at the end of the century (2080-2100) 66
6.4 Knowledge gaps 73
6.5 Summary 73

7 Climate features and extremes 74
7.1 Tropical cyclones in Vietnam 74
7.1.1 Tropical cyclone detection in GCM simulations 75
7.1.2 Tropical cyclone detection in CCAM simulations 79
7.1.3 Summary 83
7.2 Extreme rainfall 84
7.2.1 Methods and data 84
7.2.2 Assessment of downscaled simulations of the current climate (1980-2000) 85
7.2.3 Projected changes of extreme indices by mid-century (2045-2065) for RCP 8.5 88
7.2.4 Projected changes of extreme indices by end of the century (2079-2100) for RCP 8.5 90
7.2.5 Summary 92
7.3 Heatwaves and hot days 93
7.3.1 Introduction 93
7.3.2 Observed HWDI 93
7.3.3 Assessment of model simulations of the current climate 94
7.3.4 Future changes in heatwaves and hot days 94
7.3.5 Summary 96
7.4 Droughts 97
7.4.1 Introduction 97
7.4.2 SPI and drought computation 97
7.4.3 Future changes in droughts 100
7.4.4 Summary 104
7.5 Monsoons 104
7.5.1 Data and method 104
7.5.2 Current climate 105
7.5.3 Future RCM changes in the summer monsoon under RCP 8.5 by mid-century 110
7.5.4 Future changes in the summer monsoon under RCP 8.5 by the end of the century 112
7.5.5 Summary 113

8 Changes in sea level 114
8.1 Sea-level rise: observations and methods 114
8.1.1 Historical sea-level rise 115
8.1.2 Reasons for historical sea-level change 118
8.1.3 The ability of models to simulate sea-level rise 119
8.2 Projections of 21st century sea-level change 120
8.2.1 Contributions to globally-averaged 21st century sea-level rise 120
8.2.2 Regional projections for Vietnam 122
8.3 Discussion 124

PART 2 **127**

Executive Summary – Part 2 **128**

9 North West regional report **129**
9.1 Description 129
9.2 Observed climate 129
9.2.1 Temperature 130
9.2.2 Rainfall 130
9.2.3 Extremes 131
9.3 Climate projections 133
9.3.1 GCM results 133
9.3.2 Regional model results 136
9.4 Summary 142

10 North East regional report **143**
10.1 Description 143
10.2 Observed climate 143
10.2.1 Temperature 144
10.2.2 Rainfall 144
10.2.3 Extremes 145
10.3 Climate projections 147
10.3.1 GCM results 147
10.3.2 Regional model results 150
10.4 Summary 156

11 North Delta regional report **157**
11.1 Description 157
11.2 Observed climate 157
11.2.1 Temperature 158
11.2.2 Rainfall 158
11.2.3 Extremes 159
11.3 Climate projections 161
11.3.1 GCM results 161
11.3.2 Regional model results 165
11.4 Summary 170

12 North Central regional report **171**
12.1 Description 171
12.2 Observed climate 171
12.2.1 Temperature 172
12.2.2 Rainfall 172
12.2.3 Extremes 173
12.3 Climate projections 175
12.3.1 GCM results 175
12.3.2 Regional model results 178
12.4 Summary 184

13 South Central regional report **185**
13.1 Description 185
13.2 Observed climate 185
13.2.1 Temperature 186
13.2.2 Rainfall 186
13.2.3 Extremes 187
13.3 Climate projections 189
13.3.1 GCM results 189
13.3.2 Regional model results 192
13.4 Summary 198

14 The Central Highlands regional report **199**
14.1 Description 199
14.2 Observed climate 199
14.2.1 Temperature 200
14.2.2 Rainfall 200
14.2.3 Extremes 201
14.3 Climate projections 203
14.3.1 GCM results 203
14.3.2 Regional model results 206
14.4 Summary 212

15 South regional report **213**
15.1 Description 213
15.2 Observed climate 213
15.2.1 Temperature 214
15.2.2 Rainfall 214
15.2.3 Extremes 215
15.3 Climate projections 217
15.3.1 GCM results 217
15.3.2 Regional model results 220
15.4 Summary 226

References **227**

Appendix 1:
Development of an integrated assessment tool **235**

FIGURES

Figure 2-1: Comparison of equivalent CO_2 concentrations (ppmv) from SRES (A1B, A1FI, A2, B1) and RCP (3, 4.5, 6.0, 8.5) approaches (Meinshausen *et al*., 2011). 8

Figure 2-2: An illustration of the various processes included in GCMs and their interactions. Source: CMAR Graphics. 9

Figure 2-3: SST changes in the tropical Pacific (°C) from the nine best-performing models (MIROC4h is not available so results are given for MIROC5) for the months July-August by 2071-2100 compared with 1971-2000, based on the RCP 8.5 emission scenario. 11

Figure 2-4: Mean (top panel) and standard deviation (bottom panel) of July SSTs for the period 1982-2011 from (a, d; left) uncorrected ACCESS1.0 results, (b, e; middle) corrected ACCESS1.0 results and (c, f; right) observed data from the Optimum Interpolation SST dataset version 2 (Reynolds *et al*., 2007). 13

Figure 2-5: CCAM grids used for the 50 km global (C192 grid; top) and 10 km (C96 grid; bottom) downscaled simulations over Vietnam (plotting every 2nd grid point). 16

Figure 3-1: Major climate drivers that influence the climate of Vietnam. ITCZ: Inter-tropical Convergence Zone, ES: East Sea, ENSO: El Niño-Southern Oscillation phenomenon. 18

Figure 3-2: Average MSLP (left panel) and winds at the 850 hPa level (right panel) during the South West Monsoon Season (SWMS) for the current climate (1975-2004). Source: ERA-Interim. 19

Figure 3-3: Inter-annual variability (days) of the onset (date) of the South West Monsoon over the South region of Vietnam from 1979 to 2011. Grey, red and green bars depict neutral, El Niño and La Niña years, respectively. 20

Figure 3-4: Mean seasonal rainfall (mm day^{-1}) (left panel) and its inter-annual variability (right panel) during the South West Monsoon season (SWMS) for the period 1979-2007. Inter-annual variability is shown by the standard deviation (mm day^{-1}). Source: APHRODITE. 20

Figure 3-5: Average MSLP (left panel) and winds at the 850 hPa level (right panel) during the Second Inter-Monsoon season (SIMS) for the period 1975-2004. Source: ERA-Interim. 21

Figure 3-6: Mean seasonal rainfall (mm day^{-1}, left panel) and its inter-annual variability (right panel) during the Second Inter-Monsoon Season (SIMS) for 1979-2007. The inter-annual variability is shown by the standard deviation (mm day^{-1}). Source: APHRODITE. 21

Figure 3-7: Average MSLP (left panel) and winds at the 850 hPa level (right panel) during the North East Monsoon season (NEMS) for the period 1975-2004. Source: ERA-Interim. 22

Figure 3-8: Mean seasonal rainfall (mm day^{-1}, left panel) and its inter-annual variability (right panel) during the North East Monsoon Season (NEMS). The inter-annual variability is shown by the standard deviation (mm day^{-1}) for the period 1979-2007. Source: APHRODITE. 23

Figure 3-9: Average MSLP (left panel) and winds at the 850 hPa level (right panel) during the First Inter-Monsoon Season (FIMS) for the period 1975-2004 Source: ERA-Interim. 24

Figure 3-10: Mean seasonal rainfall (mm day^{-1}, left panel) and its inter-annual variability (right panel) during the First Inter-Monsoon Season (FIMS) from 1979-2007. Inter-annual variability is shown by the standard deviation (mm day^{-1}). Source: APHRODITE. 24

Figure 3-11: Mean temperature and rainfall trends from 1961 to 2011. Trends in temperature are shown as °C per decade and rainfall as percentage per decade. Source: Vietnam station observations. Filled circles show that the trend is significant at the 95% level. 25

Figure 3-12: Schematic representations of sea surface temperature anomalies, thermocline, east-west circulations and rainfall along the equator over the Indo-Pacific region for (a) El Niño, (b) La Niña and (c) neutral conditions of the El Niño-Southern Oscillation phenomenon. Source: Australian Bureau of Meteorology. 26

Figure 3-13: Relationship between the seasonal NINO3.4 index and normalised seasonal station rainfall amounts for the S region for 1979-2011. Green dots represent individual years. Normalised rainfall is defined as the yearly seasonal rainfall anomalies from the long-term mean divided by the standard deviation of the time series. 27

Figure 3-14: Monthly frequency of tropical cyclones affecting Vietnam. Source: Ngu (2000). 28

Figure 3-15: Difference in annual rainfall (mm day^{-1}) between CMIP5 GCM ensemble simulations with anthropogenic aerosol-only forcing and those with all anthropogenic forcings for the period 1975-2004. 28

Figure 3-16: Difference in seasonal rainfall (mm day^{-1}) between CMIP5 GCM ensemble simulations with anthropogenic aerosol-only forcing and those with all anthropogenic forcings for the period 1975-2004. (a) First Inter-Monsoon Season (FIMS), (b) South West Monsoon Season (SWMS), (c) Second Inter-Monsoon Season (SIMS) and (d) North East Monsoon Season (NEMS). 29

Figure 4-1: Projected changes in annual mean temperature in Canberra in 2070 based on simulations with the OzClim scenario generator (**www.csiro.au/ozclim**; Page and Jones, 2001). Results are presented for temperature changes using one model (CSIRO Mark 3.0) with one emission scenario (A1) and three climate sensitivities (red); one model (CSIRO Mark 3.0) with the six IPCC illustrative scenarios (green); and eight models with the six IPCC scenarios (blue). Coloured arrows on the axis identify the minimum and maximum results for each ensemble of results. 32

Figure 4-2: Example of appropriate and inappropriate use of climate model projections in impact assessment. For both of the above figures, rainfall (R) and temperature (T) projections from three different global climate models (GCMs) are applied in a hypothetical impact model. In (a), each pair of global climate model scenarios is applied independently to the impact assessment model, resulting in a range of different climate impacts. In (b), projections of rainfall and temperature from different models are paired to yield extreme scenarios of climate change, which are then applied to the impact model. Source: CSIRO and BoM (2007). 33

Figure 4-3: Scatter plot representing GCM annual mean temperature vs annual rainfall output classified into climate futures. 35

Figure 4-4: Home page of Vietnam Climate Futures Tool: **climatetool.vnclimate.vn**. 36

Figure 4-5: Example Climate Futures matrix showing a hypothetical 'best' case (green outlined box), 'worst' case (red outlined box) and 'most likely' case (black outlined box) for ND region with RCP 8.5 for end of century. Note likelihood colour coding is based only on the GCMs. 37

Figure 4-6: Conceptualisation of link between climate projection data and assessment of adaptation options. 38

Figure 4-7: List of required features for an integrated assessment model. Inputs are in top box, outputs in bottom box. Colour coding explains the suitability of existing modelling capacity implemented in agent-based methodology: green identifies aspects that can easily implemented in an agent-based model, yellow are dimensions that can be implemented in agent-based modelling depending on the resolution, and red marks aspects that cannot be easily implemented in an agent-based model for Vietnam. 40

Figure 5-1: Relationship between pattern correlation and RMSE values for annual MSLP and temperature for the larger domain (60-160°E, 15°S-50°N) for the period 1975-2004. Note the best models tend to sit towards the top left corner and the worst models tend to sit towards the bottom right corner of the figure. Names of the model simulations are shown in the column on the right. 43

Figure 5-2: Annual average model temperature biases (°C) based on the difference between model simulations and observed values for the period 1975-2004. 43

Figure 5-3: Relationship between pattern correlation and RMSE values for annual rainfall for ERA-Interim and CRU data for the larger domain (60-160°E, 15°S-50°N) for the period 1975-2004. Note the best models tend to sit towards the top left corner and the worst models tend to sit towards the bottom right corner of the figure. Names of the model simulations are also shown in the column at the right. 44

Figure 5-4: Annual rainfall bias (mm day^{-1}) between model simulations and observations for the period 1975-2004. Observations are from CMAP data. 45

Figure 5-5: Seasonal rainfall bias (mm day^{-1}) between model simulations and observations for four seasons for the period 1975-2004. (a) First Inter-Monsoon Season, (b) South West Monsoon Season, (c) Second Inter-Monsoon Season and (d) North East Monsoon Season. 45

Figure 5-6: Seasonal mean surface air temperature (°C) for NEMS (winter; top) and SWMS (summer; bottom) for CRU (observations, left column) and biases of the three model simulations (PRECIS for the period 1990-2007 and CCAM and RegCM4.2 for 1980-2000). 47

Figure 5-7: Simulations of average precipitation (mm day^{-1}) over Vietnam for two seasons (NEMS, top and SWMS, bottom) for APHRODITE (observations) compared with the three model outputs (CCAM and RegCM4.2 for the 1980-2000 period and PRECIS for 1990-2007). 49

Figure 5-8: Simulations of the percentage difference of rainfall for two seasons (NEMS, top and SWMS, bottom) over Vietnam for APHRODITE (observations) compared with the three model outputs (CCAM and RegCM4.2 for the 1980-2000 period and PRECIS for 1990-2007). 50

Figure 5-9: Annual cycle of temperature (°C) by month, averaged over the seven sub-regions and over the whole of Vietnam for three simulations (RegCM4.2, PRECIS, CCAM), together with station observations (STN) and the CRU gridded dataset, for the period 1980-2000 (PRECIS for 1990-2007). 52

Figure 5-10: Annual cycles of precipitation (mm day^{-1}) averaged over the seven sub-regions and over whole of Vietnam for three simulations (RegCM4.2, PRECIS, CCAM), together with station observations (STN) and APHRODITE gridded dataset (APH) for the period 1980-2000 (PRECIS for 1990-2007). 53

Figure 5-11: 850 hPa wind speed (m s^{-1}, shown by shading) and direction during NEMS (winter, top) and SWMS (summer, bottom), averaged over the 1980-2000 period for ERA-40 and the RegCM4.2 and CCAM model simulations. The PRECIS period is 1990-2007. 54

Figure 5-12: Observed CRU surface air temperature (Tave) (left) and biases for CCAM and RegCM4.2 (°C) for two seasons (NEMS, top and SWMS, bottom) over Vietnam for the 1980-2000 period. 56

Figure 5-13: The annual cycle of the temperature (°C) by month averaged over the whole of Vietnam for two RCM simulations (CCAM and RegCM4.2) compared with CRU gridded observations and local observations (STN) for the period 1980-2000. 57

Figure 5-14: NEMS (winter) and SWMS (summer) precipitation average (mm day^{-1}) during a 1980-2000 baseline period over Vietnam for APHRODITE (observations), and the percentage difference of CCAM and RegCM4.2 relative to the APHRODITE dataset. 58

Figure 5-15: The annual cycle of precipitation (mm day^{-1}) by month averaged over the whole of Vietnam for two RCM simulations (CCAM and RegCM4.2) compared with the APHRODITE dataset and local observations (STN) for the period 1980-2000. 59

Figure 6-1: Increase in temperature (°C) and changes in rainfall (%) projected by the GCM ensembles by the end of this century over South East Asia. Values are multi-model means. 60

Figure 6-2: Multi-model mean rainfall changes (mm day^{-1}) projected by the eight-member RCM ensemble for the four seasons at mid-century for RCP 8.5. 61

Figure 6-3: Agreement on sign-of-increase of rainfall changes (%) from RCM projections by the eight-member ensemble for the four seasons at mid-century for RCP 8.5. 62

Figure 6-4: Standard deviation of the rainfall changes (mm day^{-1}) from RCM projections by the eight-member ensemble for the four seasons at mid-century for RCP 8.5. 62

Figure 6-5: Multi-model mean maximum temperature changes (°C) projected by the eight-member RCM ensemble for the four seasons at mid-century for RCP 8.5. 63

Figure 6-6: Standard deviation of maximum temperature changes (°C) from RCM projections by the eight-member ensemble for the four seasons at mid-century for RCP 8.5. 63

Figure 6-7: Multi-model mean of minimum temperature changes (°C) projected by the eight-member RCM ensemble for the four seasons at mid-century for RCP 8.5. 64

Figure 6-8: Standard deviation of minimum temperature changes (°C) from RCM projections by the eight-member ensemble for the four seasons at mid-century for RCP 8.5. 64

Figure 6-9: Multi-model mean of average temperature changes (°C) projected by the eight-member RCM ensemble for the four seasons at mid-century for RCP 8.5. 65

Figure 6-10: Standard deviation of multi-model average temperature changes (°C) from RCM projections by the eight-member ensemble for the four seasons at mid-century for RCP 8.5. 65

Figure 6-11: Projected changes in annual temperature (Tave, left) and rainfall (right) by 2080-2100 under RCP 8.5. Temperature changes are in °C and rainfall changes are in mm day^{-1}. Values are multi-model means of the eight-member RCM ensemble. 66

Figure 6-12: Multi-model mean rainfall changes (mm day^{-1}) projected by the eight-member RCM ensemble for the four seasons at the end of the century for RCP 8.5. 67

Figure 6-13: Agreement of sign-of-increase of rainfall changes (%) from RCM projections by the eight-member ensemble for the four seasons at the end of the century for RCP 8.5. 67

Figure 6-14: Standard deviation of rainfall changes (mm day^{-1}) from RCM projections by the eight-member ensemble for the four seasons at the end of the century for RCP 8.5. 68

Figure 6-15: Multi-model mean maximum temperature changes (°C) projected by the eight-member RCM ensemble for the four seasons at the end of the century for RCP 8.5. 69

Figure 6-16: Standard deviation of maximum temperature changes (°C) for RCM projections by the eight-member ensemble for the four seasons at the end of the century for RCP 8.5. 69

Figure 6-17: Multi-model mean minimum temperature changes (°C) projected by the eight-member RCM ensemble for the four seasons at the end of the century for RCP 8.5. 70

Figure 6-18: Standard deviation of minimum temperature changes (°C) for RCM projections by the eight-member ensemble for the four seasons at the end of the century for RCP 8.5. 70

Figure 6-19: Multi-model mean average temperature changes (°C) projected by the eight-member RCM ensemble for the four seasons at the end of the century for RCP 8.5. 71

Figure 6-20: Standard deviation of average temperature changes (°C) for RCM projections by the eight-member ensemble for the four seasons at the end of the century for RCP 8.5. 72

Figure 7-1: The number of tropical storms and typhoons (per month) that affected Vietnam during the period 1945 to 1998. Source: ReliefWeb. 75

Figure 7-2: Spatial distribution of annual tropical cyclone genesis in (a) IBTrACS data, (b) detected in ERA-interim using the CDD method and (c) detected in ERA-Interim using the OWZP method. Occurrence is expressed as the number of cyclones per year within a 5° x 5° grid cell. 77

Figure 7-3: Percent change in tropical cyclone formation over the East Sea for the end of the century based upon different detection methods for various GCMs. 79

Figure 7-4: Inter-annual variability of the number of tropical storms over the northwest Pacific from 1945 to 2011 from IBTrACS (blue), JTWC (black) and WMO (green) datasets. Solid black line shows decrease in TC frequency for IBTrACS from 1980. 80

Figure 7-5: Inter-annual variability of observed (JTWC, black; IBTrACS, blue; WMO, green) and CCAM-simulated (red) tropical cyclone numbers over the East Sea from 1979 to 2001. CCAM simulations were at 50 km resolution forced by ERA-Interim. 81

Figure 7-6: Monthly frequencies of tropical cyclones by month from observations (dashed) and from the 50 km ERA-Interim forced CCAM simulation (solid) over the East Sea for El Niño events (red lines) and La Niña events (blue lines) for the period 1979-2001. 82

Figure 7-7: Relationship between observed tropical cyclone numbers (JTWC, y-axis) and CCAM-simulated TCs (x-axis) for El Niño, La Niña and neutral conditions over the East Sea for the period 1979-2001. Perfect fit lines and their equations are shown by black, red and blue dashed lines for the total number of TCs and those for El Niño and La Niña years, respectively. The 50 km CCAM simulation was forced by ERA-Interim data. 82

Figure 7-8: Projected changes in the number of tropical cyclone days over the western Pacific by the end of the century for RCP 8.5. Changes are calculated as the difference between projections from a four-member 50 km CCAM simulation ensemble for the period 2079-2100 compared with a baseline period, 1980-2000. 83

Figure 7-9: The seven climatic sub-regions of Vietnam (outlined in colour) and meteorological stations (squares) used in this project. NW, NE, ND, NC denote regions in northern Vietnam and SC, CH and S denote regions in southern Vietnam. 84

Figure 7-10: Observed spatial patterns of mean one day (RX1, a) and five day (RX5, b) extreme rainfall indices (mm day^{-1}), consecutive wet days (CWDs, c) and consecutive dry days (CDDs, d) derived from the APHRODITE daily rainfall data for the period from 1979 to 2007. 85

Figure 7-11: Spatial patterns of mean one day (RX1, a) and five day (RX5, b) extreme rainfall indices (mm day^{-1}), consecutive wet days (CWDs, c) and consecutive dry days (CDDs, d) derived from the CCAM multi-model simulations for the period 1980-2000 at 10 km resolution. 86

Figure 7-12: Spatial patterns of mean percentage bias of one day (RX1, a) and five day (RX5, b) extreme rainfall indices, consecutive wet days (CWDs, c) and consecutive dry days (CDDs, d) for the period 1980 to 2000. Biases are the multi-model mean of the CCAM simulations for the period 1980-2000 at 10 km resolution relative to the APHRODITE daily rainfall data. 86

Figure 7-13: Projected extreme indices by mid-century (2045-2065) from the 10 km CCAM multi-model mean for RCP 8.5. RX1 (a) and RX5 (b) are shown as mm day^{-1}, while CWD (c) and CDD (d) are shown as number of days. 89

Figure 7-14: Multi-model mean projected changes of extreme indices by mid-century (2045-2065) from 10 km CCAM simulations for RCP 8.5. RX1 (a) and RX5 (b) are shown as changes in mm day^{-1}, while CWD (c) and CDD (d) are shown as number of days. All changes are relative to the baseline period (1980-2000). 89

Figure 7-15: Percentage of agreement on the direction of change (increase positive)/(decrease negative) of RX1 (a), RX5 (b), CWD (c) and CDD (d) among the 10 km CCAM simulations for the period 2045-2065 compared with the baseline period 1980-2000. The results were interpolated to 30 km resolution. 90

Figure 7-16: Multi-model mean projected changes of extreme indices by end of the century (2079-2100) from 10 km CCAM simulations for RCP 8.5. RX1 (a) and RX5 (b) are shown as changes in mm day^{-1}, while CWD (c) and CDD (d) are shown as number of days. All changes are relative to the baseline period (1980-2000). 91

Figure 7-17: Percentage of agreement on the direction of change (increase positive)/(decrease negative) of RX1 (a), RX5 (b), CWD (c) and CDD (d) among the 10 km CCAM simulations for the period 2080-2100 compared with the baseline period 1980-2000. The results were interpolated to 30 km resolution. 91

Figure 7-18: Observed (a) HWDI, and (b) maximum number of consecutive hot days (Tmax > 35°C) based on station data for the period 1980-2000. 93

Figure 7-19: Tmax biases (a) and mean absolute error (b) for CCAM 10 km simulation forced by ERA-Interim reanalyses compared with observations for the period 1980-2000 (°C). 94

Figure 7-20: Changes in the number of heatwaves (a-b, in events) and their average duration (c-d, in days) for 2045-2065 (a,c) and 2080-2100 (b,d) based on the HWDI from the ensemble of CCAM projections at 10 km and RegCM4.2 projections at 20 km for RCP 8.5. Changes are relative to the baseline period 1980-2000. 95

Figure 7-21: Multi-model ensemble standard deviation of the number of heatwaves (events) derived from the HWDI index for 2045-2065 (a) and for 2080-2100 (b) and their average duration (days) for 2045-2065 (c) and for 2080-2100 (d) for RCP 8.5. Based on CCAM simulations at 10 km resolution and RegCM4.2 at 20 km resolution. Changes are relative to the baseline period 1980-2000. 95

Figure 7-22: Changes in the number of hot days for 2045-2065 (a) and 2080-2100 (b) for RCP 8.5. Values are multi-model mean changes from the CCAM and RegCM4.2 ensembles. Also shown are multi-model ensemble standard deviations (days year^{-1}) for 2045-2065 (c) and for 2080-2100 (d). Changes are relative to the baseline period 1980-2000. 96

Figure 7-23: Number (a, b) and average duration (c, d, in months) of extreme and severe agricultural droughts (a, c) and hydrological droughts (b, d) based on APHRODITE rainfall from 1979 to 2007. 98

Figure 7-24: Observed trends (year^{-1}) for 3-month SPI (left) and 12-month SPI (right) based on APHRODITE for the period 1979-2007. Note that a positive (negative) trend in SPI is associated with wet (drought) conditions. Note that results have been interpolated to the 25 km APHRODITE grid. 98

Figure 7-25: Observed trends for 3-month SPI (left) and 12-month SPI (right), based on CCAM ERA-Interim results at 10 km resolution for 1979-2007. Note that results have been interpolated to the 25 km APHRODITE grid. 99

Figure 7-26: Number of 3-month (a) and 12-month (b) drought events, and average 3-month (c) and 12-month (d) drought duration based on the CCAM 10 km simulation forced by the ERA-Interim reanalysis from 1979 to 2007. Note that results have been interpolated to the 25 km APHRODITE grid. 99

Figure 7-27: Projected changes in the number of extreme agricultural droughts for 2045-2065 (a) and severe agricultural droughts for 2080-2100 (b), both in events per period, and their average duration in months for 2045-2065 (c) and for 2080-2100 (d) based on the 3-month SPI values calculated using CCAM ensemble simulations at 10 km resolution for RCP 8.5. 100

Figure 7-28: Ensemble standard deviations of the number of extreme agricultural droughts for 2045-2065 (a) and severe agricultural droughts for 2080-2100 (b) and their average duration in months for 2045-2065 (c) and for 2080-2100 (d) based on the 3-month SPI values calculated using CCAM ensemble simulations at 10 km resolution for RCP 8.5. 101

Figure 7-29: Agreement on the increase in the number of extreme agricultural droughts for 2045-2065 (a) and severe agricultural droughts for 2080-2100 (b) and their average duration for 2045-2065 (c) and for 2080-2100 (d) in percent based on the 3-month SPI values calculated using CCAM ensemble simulations at 10 km resolution for RCP 8.5. 101

Figure 7-30: Projected changes in the number of extreme and severe hydrological droughts for 2045-2065 (a) and for 2080-2100 (b) in events per period and their average duration in months for 2045-2065 (c) and for 2080-2100 (d) based on the 12-month SPI values calculated using CCAM ensemble simulations at 10 km resolution for RCP 8.5. 102

Figure 7-31: Ensemble standard deviations of the number of extreme and severe droughts for 2045-2065 (a) and for 2080-2100 (b) and their average duration in months for 2045-2065 (c) and for 2080-2100 (d) based on the 12-month SPI values calculated using CCAM-ensemble simulations at 10 km resolution for RCP 8.5. 103

Figure 7-32: Agreement on the increase in the number of extreme and severe droughts for 2045-2065 (a) and for 2080-2100 (b) and their average duration for 2045-2065 (c) and for 2080-2100 (d) in percent based on the 12-month SPI values calculated using CCAM-ensemble simulations at 10 km resolution for RCP 8.5. 103

Figure 7-33: NCEP R-2 climatological winds at the 850 hPa level and APHRODITE rainfall (shaded, mm day^{-1}) over Vietnam and surrounding areas for April to December for the period 1979 to 2007. 105

Figure 7-34: Observed area-averaged zonal wind at 850 hPa (U850, green) and 200 hPa (U200, red) levels and averaged rainfall (blue) from station data for three regions in South Vietnam (SC, CH and S) and four regions in North Vietnam (NW, NE, ND and NC) for the period 1979-2011. The arrow shows the beginning of the month of May. 106

Figure 7-35: As in Figure 7-34 but for the CCAM 10 km simulation. 107

Figure 7-36: Onset dates of the summer monsoon for three regions in South Vietnam (S, CH and SC) for the period 1980 to 2000. The mean onset is shown by the dotted line, red and green boxes show spread from the first quartile (Q1) and third quartile (Q3) to the median, respectively, and blue boxes denote Q1. Whiskers show spread from the minimum to Q1 and from the maximum to Q3. The horizontal axis shows station observations (left), six CCAM simulations (middle) and the CCAM ensemble mean (right). The zero value on the vertical axis represents 1 May, with positive numbers indicating later dates and negative numbers earlier dates. 108

Figure 7-37: As in Figure 7-36 but for North Vietnam. 109

Figure 8-1: Schematic diagram of the major changes that influenced sea level during the 20th century and will continue to drive sea-level change during the 21st century and beyond. 114

Figure 8-2: Estimates of global mean sea-level rise from 1880 to present from Church and White (2011). 115

Figure 8-3: The regional trends in sea level over the period 1993 to 2012 based on satellite altimeter data for (a) the globe and (b) the region around Vietnam. The locations of tide gauge data used in Figure 8-4 (following) are indicated in (b). 115

Figure 8-4: Monthly sea-level data for the coast of Vietnam from 1960 to 2010. The data that appear to be of useful quality are bounded by the short vertical red lines with the suspect data outside these windows shown in light grey. 117

Figure 8-5: The sum of the modelled contributions to sea-level change from ocean thermal expansion, increased glacier melting and changes in land-water storage. The light grey lines represent individual models, with the black line showing the adjusted model mean after an allowance for the impact of the lack of volcanic simulations in the model spin-up, natural variability on glacier contributions and a potential long-term ice-sheet contribution are included. The 20th century estimates of global mean sea level are indicated by the blue (Church and White, 2011) and green (Ray and Douglas, 2011) lines with the shading indicating the uncertainty estimates (two standard deviations). The satellite altimeter data since 1993 is shown in red. The results are given (a) for the period 1900 to 2010 and (b) for 1990 to 2010. The dotted black line is after inclusion of the Shepherd *et al*. (2012) ice-sheet observational estimates but excluding the peripheral glacier contribution (to avoid double counting). The red line is the average rate from the altimeter record. Note different vertical scales in the plots. (Adapted from Church *et al*., 2013). 119

Figure 8-6: Contributions (in mm) to 21st century sea-level rise calculated using the results of individual AOGCMs. (a) Global-averaged ocean thermal expansion. (b) Glacier contributions using the Marzeion *et al*. (2012) model. (c) Contributions from the surface mass balance of the Greenland Ice Sheet. For RCP 8.5 and RCP 2.6 the multi-model mean values with 5-95% uncertainty ranges (shaded areas) are shown. For RCP 6.0 and RCP 4.5, only the multi-model mean values are shown. 121

Figure 8-7: Projection of regional sea-level change (in mm) due to ocean density and circulation change for 2081-2100 compared with 1986-2005, derived from CMIP5 models under four different RCPs. The global mean sea level has been removed from each panel; thus positive values indicate higher (and negative values indicate lower) local sea-level change than the global average. The stippling (black shading) indicates regions where climate models tend to agree, with the magnitude of multi-model mean exceeding the inter-model standard deviation. 122

Figure 8-8: Projection of regional sea-level rise for 2081-2100 compared with 1986-2005 for four emission scenarios: RCP 2.6 (top left), RCP 4.5 (top right), RCP 6.0 (bottom left) and RCP 8.5 (bottom right). These regional sea-level projections combine the global-average sea-level projections (thermal expansion, glacier, ice sheets and land storage). Regional 5-95% uncertainties come from uncertainty in the global-mean projections and uncertainty in the regional distribution associated with ocean dynamics, gravitational fingerprints and GIA. These vary little over the displayed domain, with values around 130 mm for RCP 2.6 and 150 mm for RCP 8.5. 123

Figure 8-9: Observed and projected relative sea-level change from 1950 to the end of the century near four locations around the coast of Vietnam: (a) Phuquoc, (b) Nhabe, (c) Sontra, and (d) Hondau. The observed tide-gauge relative sea-level records (since the late 1970s) are indicated in light blue, with the satellite record (since 1993) in light green. Multi-model mean projections (black lines) for the RCP 8.5 and RCP 2.6 emission scenarios with 5-95% uncertainty range are shown by the red and blue shaded regions from 1995 to 2100. The dashed lines are an estimate of inter-annual variability in sea level (5–95% uncertainty range about the projections) and indicate that individual monthly averages of sea level can be above or below longer-term averages. 125

Figure 9-1: The North West region with provinces. Insert shows location of region in Vietnam. 129

Figure 9-2: Trend in annual mean surface air temperature (°C per decade) in the North West (NW) region for the period 1961 to 2011. A blue circle indicates a decreasing trend and a red circle shows an increasing trend. A filled circle means that the trend is statistically significant at the 90% confidence level. 130

Figure 9-3: Time series of regionally-averaged annual surface air temperature (°C, red) for the NW region with a trend line (dashed). Annual values are shown by black dots. 130

Figure 9-4: Trend in annual rainfall (% per decade) in the NW region for the period 1961 to 2011. A blue circle indicates an increasing trend and a red circle shows a decreasing trend. A filled circle means that the trend is significant at the 90% confidence level. 130

Figure 9-5: Time series of regionally-averaged annual rainfall (mm day^{-1}, blue) for the NW region with a trend line (black dashed line). Annual values are shown by black dots. 130

Figure 9-6: Trends in Tmax (upper left), Tmin (upper right), TX90p (lower left), and TN10p (lower right) in the NW region for the period 1961 to 2011 (°C per decade for Tmax and Tmin; days per decade for TX90p and TN10p). A blue circle indicates a decreasing and a red circle shows an increasing trend. A filled circle means that the trend is significant at the 90% confidence level. 131

Figure 9-7: Trends in RX1 and RX5 (% per decade), R95p (mm $year^{-1}$), CWD and CDD (days per decade) in the NW region for the period 1961 to 2011. A blue circle indicates an increasing and a red circle shows a decreasing trend for all but CDD, where red indicates an increasing and blue a decreasing number of days. A filled circle means that the trend is significant at the 90% confidence level. 132

Figure 9-8: Regionally averaged seasonal surface air temperature changes (°C) for NW. For each season, the time series graph of projections by global climate models (GCM) is shown on the left for the higher (RCP 8.5) greenhouse gas scenario. Black line is from historical GCM runs, red line is the multi-model median projection from GCMs using RCP 8.5. Shadings are between 10% and 90% of 20-year mean values. GCM values have been corrected for 1995-2005 mean bias. Bars on the right for each season show the end-of-century summary of projections by global climate models (GCM, left) and regional climate models (RCM, right) for both lower (RCP 4.5) and higher (RCP 8.5) scenarios. 133

Figure 9-9: Regionally averaged seasonal maximum air temperature changes (°C) for NW. For each season, the time series graph of projections by global climate models (GCM) is shown on the left for the higher (RCP 8.5) greenhouse gas scenario. Black line is from historical GCM runs, red line is the multi-model median projection from GCMs using RCP 8.5. Shadings are between 10% and 90% of 20-year mean values. GCM values have been corrected for 1995-2005 mean bias. Bars on the right for each season show the end-of-century summary of projections by global climate models (GCM, left) and regional climate models (RCM, right) for both lower (RCP 4.5) and higher (RCP 8.5) scenarios. 134

Figure 9-10: Regionally averaged seasonal minimum air temperature changes (°C) for NW. For each season, the time series graph of projections by global climate models (GCM) is shown on the left for the higher (RCP 8.5) greenhouse gas scenario. Black line is from historical GCM runs, red line is the multi-model median projection from GCMs using RCP 8.5. Shadings are between 10% and 90% of 20-year mean values. GCM values have been corrected for 1995-2005 mean bias. Bars on the right for each season show the end-of-century summary of projections by global climate models (GCM, left) and regional climate models (RCM, right) for both lower (RCP 4.5) and higher (RCP 8.5) scenarios. 135

Figure 9-11: Regionally averaged seasonal precipitation changes (mm $month^{-1}$ on left axis and % on right axis) for NW. For each season, the time series graph of projections by global climate models (GCM) is shown on the left for the higher (RCP 8.5) greenhouse gas scenario. Black line is from historical GCM runs, red line is the multi-model median projection from GCMs using RCP 8.5. Shadings are between 10% and 90% of 20-year mean values. GCM values have been corrected for 1995-2005 mean bias. Bars on the right for each season show the end-of-century summary of projections by global climate models (GCM, left) and regional climate models (RCM, right) for both lower (RCP 4.5) and higher (RCP 8.5) scenarios. 136

Figure 10-1: The North East region with provinces. Insert shows location of region in Vietnam. 143

Figure 10-2: Trend in annual surface air temperature (°C per decade) in the North East (NE) region for the period 1961 to 2011. A blue circle indicates a decreasing trend and a red circle shows an increasing trend. A filled circle means that the trend is statistically significant at the 90% confidence level. 144

Figure 10-3: Time series of regionally-averaged annual surface air temperature (°C, red) for the NE region with a trend line (dashed). Annual values are shown by black dots. 144

Figure 10-4: Trends in annual rainfall (% per decade) in the NE region for the period 1961 to 2011. A blue circle indicates an increasing trend and a red circle shows a decreasing trend. A filled circle means that the trend is significant at the 90% confidence level. 144

Figure 10-5: Time series of regionally-averaged annual rainfall (mm day^{-1}, blue) for the NE region with a trend line (black dashed line). Annual values are shown by black dots. 144

Figure 10-6: Trends in Tmax (upper left), Tmin (upper right), TX90p (lower left), and TN10p (lower right) in the NE region for the period 1961 to 2011. A blue circle indicates a decreasing and a red circle shows an increasing trend. A filled circle means that the trend is significant at the 90% confidence level. 145

Figure 10-7: Trends in RX1, RX5, R95p, CWD, and CDD in the NE region for the period 1961 to 2011. A blue circle indicates an increasing and a red circle shows a decreasing trend for all but CDD, where red indicates an increasing and blue a decreasing number of days. A filled circle means that the trend is significant at the 90% confidence level. 146

Figure 10-8: Regionally averaged seasonal surface air temperature changes (°C) for NE. For each season, the time series graph of projections by global climate models (GCM) is shown on the left for the higher (RCP 8.5) greenhouse gas scenario. Black line is from historical GCM runs, red line is the multi-model median projection from GCMs using RCP 8.5. Shadings are between 10% and 90% of 20-year mean values. GCM values have been corrected for 1995-2005 mean bias. Bars on the right for each season show the end-of-century summary of projections by global climate models (GCM, left) and regional climate models (RCM, right) for both lower (RCP 4.5) and higher (RCP 8.5) scenarios. 147

Figure 10-9: Regionally averaged seasonal maximum air temperature changes (°C) for NE. For each season, the time series graph of projections by global climate models (GCM) is shown on the left for the higher (RCP 8.5) greenhouse gas scenario. Black line is from historical GCM runs, red line is the multi-model median projection from GCMs using RCP 8.5. Shadings are between 10% and 90% of 20-year mean values. GCM values have been corrected for 1995-2005 mean bias. Bars on the right for each season show the end-of-century summary of projections by global climate models (GCM, left) and regional climate models (RCM, right) for both lower (RCP 4.5) and higher (RCP 8.5) scenarios. 148

Figure 10-10: Regionally averaged seasonal minimum air temperature changes (°C) for NE. For each season, the time series graph of projections by global climate models (GCM) is shown on the left for the higher (RCP 8.5) greenhouse gas scenario. Black line is from historical GCM runs, red line is the multi-model median projection from GCMs using RCP 8.5. Shadings are between 10% and 90% of 20-year mean values. GCM values have been corrected for 1995-2005 mean bias. Bars on the right for each season show the end-of-century summary of projections by global climate models (GCM, left) and regional climate models (RCM, right) for both lower (RCP 4.5) and higher (RCP 8.5) scenarios. 149

Figure 10-11: Regionally averaged seasonal precipitation changes (mm month^{-1} on left axis and % on right axis) for NE. For each season, the time series graph of projections by global climate models (GCM) is shown on the left for the higher (RCP 8.5) greenhouse gas scenario. Black line is from historical GCM runs, red line is the multi-model median projection from GCMs using RCP 8.5. Shadings are between 10% and 90% of 20-year mean values. GCM values have been corrected for 1995-2005 mean bias. Bars on the right for each season show the end-of-century summary of projections by global climate models (GCM, left) and regional climate models (RCM, right) for both lower (RCP 4.5) and higher (RCP 8.5) scenarios. 150

Figure 11-1: The North Delta region with provinces. Insert shows location of the region in Vietnam 157

Figure 11-2: Trend in annual mean surface air temperature in the North Delta (ND) region (°C per decade) for the period 1961 to 2011. A blue circle indicates a decreasing and a red circle shows an increasing trend. A filled circle means that the trend is significant at the 90% confidence level. 158

Figure 11-3: Time series of regionally-averaged annual surface air temperature (°C, red) for the ND region with a trend line (dashed black line). Annual values are shown by black dots. 158

Figure 11-4: Trends in annual rainfall in the ND region (% per decade) for the period 1961 to 2011. A blue circle indicates an increasing and a red circle shows a decreasing trend. A filled circle means that the trend is significant at the 90% confidence level. 158

Figure 11-5: Time series of regionally-averaged annual rainfall (mm day^{-1}, blue) for the ND with a trend line (dashed black line). Annual values are shown by black dots. 158

Figure 11-6: Trends in Tmax (upper left), Tmin (upper right), TX90p (lower left), and TN10p (lower right) in the ND region for the period 1961 to 2011. A blue circle indicates a decreasing trend and a red circle shows an increasing trend. A filled circle means that the trend is significant at the 90% confidence level. 159

Figure 11-7: Trends in RX1, RX5, R95p, CWD, and CDD in the ND region for the period 1961 to 2011. A blue circle indicates an increasing trend and a red circle shows a decreasing trend for all but CDD, where red indicates an increasing and blue a decreasing number of days. A filled circle means that the trend is significant at the 90% confidence level. 160

Figure 11-8: Regionally averaged seasonal surface air temperature changes (°C) for ND. For each season, the time series graph of projections by global climate models (GCM) is shown on the left for the higher (RCP 8.5) greenhouse gas scenario. Black line is from historical GCM runs, red line is the multi-model median projection from GCMs using RCP 8.5. Shadings are between 10% and 90% of 20-year mean values. GCM values have been corrected for 1995-2005 mean bias. Bars on the right for each season show the end-of-century summary of projections by global climate models (GCM, left) and regional climate models (RCM, right) for both lower (RCP 4.5) and higher (RCP 8.5) scenarios. 161

Figure 11-9: Regionally averaged seasonal maximum air temperature changes (°C) for ND. For each season, the time series graph of projections by global climate models (GCM) is shown on the left for the higher (RCP 8.5) greenhouse gas scenario. Black line is from historical GCM runs, red line is the multi-model median projection from GCMs using RCP 8.5. Shadings are between 10% and 90% of 20-year mean values. GCM values have been corrected for 1995-2005 mean bias. Bars on the right for each season show the end-of-century summary of projections by global climate models (GCM, left) and regional climate models (RCM, right) for both lower (RCP 4.5) and higher (RCP 8.5) scenarios. 162

Figure 11-10: Regionally averaged seasonal minimum air temperature changes (°C) for ND. For each season, the time series graph of projections by global climate models (GCM) is shown on the left for the higher (RCP 8.5) greenhouse gas scenario. Black line is from historical GCM runs, red line is the multi-model median projection from GCMs using RCP 8.5. Shadings are between 10% and 90% of 20-year mean values. GCM values have been corrected for 1995-2005 mean bias. Bars on the right for each season show the end-of-century summary of projections by global climate models (GCM, left) and regional climate models (RCM, right) for both lower (RCP 4.5) and higher (RCP 8.5) scenarios. 163

Figure 11-11: Regionally averaged seasonal precipitation changes (mm month^{-1} on left axis and % on right axis) for ND. For each season, the time series graph of projections by global climate models (GCM) is shown on the left for the higher (RCP 8.5) greenhouse gas scenario. Black line is from historical GCM runs, red line is the multi-model median projection from GCMs using RCP 8.5. Shadings are between 10% and 90% of 20-year mean values. GCM values have been corrected for 1995-2005 mean bias. Bars on the right for each season show the end-of-century summary of projections by global climate models (GCM, left) and regional climate models (RCM, right) for both lower (RCP 4.5) and higher (RCP 8.5) scenarios. 164

Figure 12-1: The North Central region with provinces. Insert shows location of region in Vietnam. 171

Figure 12-2: Trend in annual surface air temperature (°C per decade) in the North Central (NC) region for the period 1961 to 2011. A blue circle indicates a decreasing trend and a red circle shows an increasing trend. A filled circle means that the trend is statistically significant at the 90% confidence level. 172

Figure 12-3: Time series of regionally-averaged annual surface air temperature (°C, red) for the NC region with a trend line (dashed). Annual values are shown by black dots. 172

Figure 12-4: Trends in annual rainfall (% per decade) in the NC region for the period 1961 to 2011. A blue circle indicates an increasing trend and a red circle shows a decreasing trend. A filled circle means that the trend is significant at the 90% confidence level. 172

Figure 12-5: Time series of regionally-averaged annual rainfall (mm day^{-1}, blue) for the NC region with a trend line (black dashed line). Annual values are shown by black dots. 172

Figure 12-6: Trends in Tmax (upper left), Tmin (upper right), TX90p (lower left), and TN10p (lower right) in the NC region for the period 1961 to 2011. A blue circle indicates a decreasing trend and a red circle shows an increasing trend. A filled circle means that the trend is significant at the 90% confidence level. 173

Figure 12-7: Trends in RX1, RX5, R95p, CWD, and CDD in the NC region for the period 1961 to 2011. A blue circle indicates an increasing and a red circle shows a decreasing trend for all but CDD, where red indicates increasing and blue decreasing number of days. A filled circle means that the trend is significant at the 90% confidence level. 174

Figure 12-8: Regionally averaged seasonal surface air temperature changes (°C) for NC. For each season, the time series graph of projections by global climate models (GCM) is shown on the left for the higher (RCP 8.5) greenhouse gas scenario. Black line is from historical GCM runs, red line is the multi-model median projection from GCMs using RCP 8.5. Shadings are between 10% and 90% of 20-year mean values. GCM values have been corrected for 1995-2005 mean bias. Bars on the right for each season show the end-of-century summary of projections by global climate models (GCM, left) and regional climate models (RCM, right) for both lower (RCP 4.5) and higher (RCP 8.5) scenarios. 175

Figure 12-9: Regionally averaged seasonal maximum air temperature changes (°C) for NC. For each season, the time series graph of projections by global climate models (GCM) is shown on the left for the higher (RCP 8.5) greenhouse gas scenario. Black line is from historical GCM runs, red line is the multi-model median projection from GCMs using RCP 8.5. Shadings are between 10% and 90% of 20-year mean values. GCM values have been corrected for 1995-2005 mean bias. Bars on the right for each season show the end-of-century summary of projections by global climate models (GCM, left) and regional climate models (RCM, right) for both lower (RCP 4.5) and higher (RCP 8.5) scenarios. 176

Figure 12-10: Regionally averaged seasonal minimum air temperature changes (°C) for NC. For each season, the time series graph of projections by global climate models (GCM) is shown on the left for the higher (RCP 8.5) greenhouse gas scenario. Black line is from historical GCM runs, red line is the multi-model median projection from GCMs using RCP 8.5. Shadings are between 10% and 90% of 20-year mean values. GCM values have been corrected for 1995-2005 mean bias. Bars on the right for each season show the end-of-century summary of projections by global climate models (GCM, left) and regional climate models (RCM, right) for both lower (RCP 4.5) and higher (RCP 8.5) scenarios. 177

Figure 12-11: Regionally averaged seasonal precipitation changes (mm month^{-1} on left axis and % on right axis) for NC. For each season, the time series graph of projections by global climate models (GCM) is shown on the left for the higher (RCP 8.5) greenhouse gas scenario. Black line is from historical GCM runs, red line is the multi-model median projection from GCMs using RCP 8.5. Shadings are between 10% and 90% of 20-year mean values. GCM values have been corrected for 1995-2005 mean bias. Bars on the right for each season show the end-of-century summary of projections by global climate models (GCM, left) and regional climate models (RCM, right) for both lower (RCP 4.5) and higher (RCP 8.5) scenarios. 178

Figure 13-1: The South Central region with provinces. Insert shows location of the region in Vietnam. 185

Figure 13-2: Trend in annual mean surface air temperature (°C per decade) in the South Central region (SC) for the period 1961 to 2011. A blue circle indicates a decreasing trend and a red circle shows an increasing trend, while a filled circle indicates that the trend is statistically significant at the 90% level. 186

Figure 13-3: Time series of regionally-averaged annual surface air temperature (°C, red) for region SC with a trend line (dashed black line). Annual values are shown by black dots. 186

Figure 13-4: Trends in annual rainfall (% per decade) in the SC region for the period 1961 to 2011. A blue circle indicates an increasing trend and red circle shows a decreasing trend, while a filled circle shows that the trend is statistically significant at the 90% level. 186

Figure 13-5: Time series of regionally-averaged annual rainfall (mm day^{-1}, blue) for region SC with trend line (dashed black line). Annual values are shown by black dots. 186

Figure 13-6: Trends in Tmax (upper left), Tmin (upper right), TX90p (lower left), and TN10p (lower right) in the SC region for the period 1961-2011. A blue circle indicates a decreasing trend and red an increasing trend, while a filled circle means that the trend is significant at the 90% level. 187

Figure 13-7: Trends in RX1, RX5, R95p, CWD, and CDD in the SC region for the period 1961-2011. A blue circle indicates an increasing and red a decreasing trend for all but CDD, where red indicates an increasing and blue a decreasing number of days. A filled circle means that the trend is significant at the 90% level. 188

Figure 13-8: Regionally averaged seasonal surface air temperature changes (°C) for SC. For each season, the time series graph of projections by global climate models (GCM) is shown on the left for the higher (RCP 8.5) greenhouse gas scenario. Black line is from historical GCM runs, red line is the multi-model median projection from GCMs using RCP 8.5. Shadings are between 10% and 90% of 20-year mean values. GCM values have been corrected for 1995-2005 mean bias. Bars on the right for each season show the end-of-century summary of projections by global climate models (GCM, left) and regional climate models (RCM, right) for both lower (RCP 4.5) and higher (RCP 8.5) scenarios. 189

Figure 13-9: Regionally averaged seasonal maximum air temperature changes (°C) for SC. For each season, the time series graph of projections by global climate models (GCM) is shown on the left for the higher (RCP 8.5) greenhouse gas scenario. Black line is from historical GCM runs, red line is the multi-model median projection from GCMs using RCP 8.5. Shadings are between 10% and 90% of 20-year mean values. GCM values have been corrected for 1995-2005 mean bias. Bars on the right for each season show the end-of-century summary of projections by global climate models (GCM, left) and regional climate models (RCM, right) for both lower (RCP 4.5) and higher (RCP 8.5) scenarios. 190

Figure 13-10: Regionally averaged seasonal minimum air temperature changes (°C) for SC. For each season, the time series graph of projections by global climate models (GCM) is shown on the left for the higher (RCP 8.5) greenhouse gas scenario. Black line is from historical GCM runs, red line is the multi-model median projection from GCMs using RCP 8.5. Shadings are between 10% and 90% of 20-year mean values. GCM values have been corrected for 1995-2005 mean bias. Bars on the right for each season show the end-of-century summary of projections by global climate models (GCM, left) and regional climate models (RCM, right) for both lower (RCP 4.5) and higher (RCP 8.5) scenarios. 191

Figure 13-11: Regionally averaged seasonal precipitation changes (mm $month^{-1}$ on left axis and % on right axis) for SC. For each season, the time series graph of projections by global climate models (GCM) is shown on the left for the higher (RCP 8.5) greenhouse gas scenario. Black line is from historical GCM runs, red line is the multi-model median projection from GCMs using RCP 8.5. Shadings are between 10% and 90% of 20-year mean values. GCM values have been corrected for 1995-2005 mean bias. Bars on the right for each season show the end-of-century summary of projections by global climate models (GCM, left) and regional climate models (RCM, right) for both lower (RCP 4.5) and higher (RCP 8.5) scenarios. 192

Figure 14-1: The Central Highlands region with provinces. Insert shows location of region in Vietnam. 199

Figure 14-2: Trends in annual mean surface air temperature (°C per decade) in the Central Highland (CH) region for the period 1961-2011. A blue circle indicates a decreasing trend and a red circle shows an increasing trend, while a filled circle indicates that the trend is statistically significant at the 90% level. 200

Figure 14-3: Time series of regionally-averaged annual surface air temperature (°C, red) for the CH region, with trend line (dashed black line). Annual values are shown by black dots. 200

Figure 14-4: Trends in annual rainfall in the CH region (% per decade) for the period 1961-2011. A blue circle indicates an increasing trend and a red circle shows a decreasing trend. A filled circle shows that the trend is statistically significant at the 90% level. 200

Figure 14-5: Time series of regionally-averaged annual rainfall (mm day^{-1}, blue) for the CH region, with a trend line (dashed black line). Annual values are shown as black dots. 200

Figure 14-6: Trends in Tmax (top left), Tmin (top right), TX90p (bottom left), and TN10p (bottom right) in the CH region for the period 1961-2011. A blue circle indicates a decreasing trend and a red circle shows an increasing trend. A filled circle means that the trend is statistically significant at the 90% level. 201

Figure 14-7: Trends in RX1, RX5, R95p, CWD, and CDD in the CH region for the period 1961-2011. A blue circle indicates an increasing trend and red a decreasing trend for all but CDD, where red indicates an increasing and blue a decreasing number of days. A filled circle means that the trend is significant at the 90% level. 202

Figure 14-8: Regionally averaged seasonal surface air temperature changes (°C) for CH. For each season, the time series graph of projections by global climate models (GCM) is shown on the left for the higher (RCP 8.5) greenhouse gas scenario. Black line is from historical GCM runs, red line is the multi-model median projection from GCMs using RCP 8.5. Shadings are between 10% and 90% of 20-year mean values. GCM values have been corrected for 1995-2005 mean bias. Bars on the right for each season show the end-of-century summary of projections by global climate models (GCM, left) and regional climate models (RCM, right) for both lower (RCP 4.5) and higher (RCP 8.5) scenarios. 203

Figure 14-9: Regionally averaged seasonal maximum air temperature changes (°C) for CH. For each season, the time series graph of projections by global climate models (GCM) is shown on the left for the higher (RCP 8.5) greenhouse gas scenario. Black line is from historical GCM runs, red line is the multi-model median projection from GCMs using RCP 8.5. Shadings are between 10% and 90% of 20-year mean values. GCM values have been corrected for 1995-2005 mean bias. Bars on the right for each season show the end-of-century summary of projections by global climate models (GCM, left) and regional climate models (RCM, right) for both lower (RCP 4.5) and higher (RCP 8.5) scenarios. 204

Figure 14-10: Regionally averaged seasonal minimum air temperature changes (°C) for CH. For each season, the time series graph of projections by global climate models (GCM) is shown on the left for the higher (RCP 8.5) greenhouse gas scenario. Black line is from historical GCM runs, red line is the multi-model median projection from GCMs using RCP 8.5. Shadings are between 10% and 90% of 20-year mean values. GCM values have been corrected for 1995-2005 mean bias. Bars on the right for each season show the end-of-century summary of projections by global climate models (GCM, left) and regional climate models (RCM, right) for both lower (RCP 4.5) and higher (RCP 8.5) scenarios. 205

Figure 14-11: Regionally averaged seasonal precipitation changes (mm month^{-1} on left axis and % on right axis) for CH. For each season, the time series graph of projections by global climate models (GCM) is shown on the left for the higher (RCP 8.5) greenhouse gas scenario. Black line is from historical GCM runs, red line is the multi-model median projection from GCMs using RCP 8.5. Shadings are between 10% and 90% of 20-year mean values. GCM values have been corrected for 1995-2005 mean bias. Bars on the right for each season show the end-of-century summary of projections by global climate models (GCM, left) and regional climate models (RCM, right) for both lower (RCP 4.5) and higher (RCP 8.5) scenarios. 206

Figure 15-1: The South region with provinces. Insert shows location of the region in Vietnam. 213

Figure 15-2: Trend in annual mean surface air temperature in the South (S) region (°C per decade) for the period 1961-2011. A blue circle indicates a decreasing trend and a red circle shows an increasing trend, while a filled circle indicates that the trend is statistically significant at the 90% level. 214

Figure 15-3: Time series of regionally-averaged annual surface air temperature (°C, red) for the S region, with a trend line (dashed). Annual values are shown by black dots. 214

Figure 15-4: Trend in annual rainfall (% per decade) in the S region for the period 1961-2011. A blue circle indicates an increasing trend and a red circle shows a decreasing trend. A filled circle indicates that the trend is statistically significant at the 90% level. 214

Figure 15-5: Time series of regionally-averaged annual rainfall (mm day^{-1}, blue) for the S region, with a trend line (dashed black line). Annual values are shown by black dots. 214

Figure 15-6: Trends in Tmax (upper left), Tmin (upper right), TX90p (lower left), and TN10p (lower right) in the S region for the period 1961-2011. A blue circle indicates a decreasing trend and a red circle shows an increasing trend, while a filled circle shows that the trend is statistically significant at the 90% level. 215

Figure 15-7: Trends in RX1, RX5, R95p, CWD, and CDD in the S region for the period 1961-2011. A blue circle indicates an increasing trend and a red circle shows a decreasing trend for all but CDD, where red indicates increasing and blue decreasing number of days. Filled circles show that the trend is statistically significant at the 90% level. 216

Figure 15-8: Regionally averaged seasonal surface air temperature changes (°C) for S. For each season, the time series graph of projections by global climate models (GCM) is shown on the left for higher (RCP 8.5) greenhouse gas scenario. Black line is from historical GCM runs, red line is the multi-model median projection from GCMs using RCP 8.5. Shadings are between 10% and 90% of 20-year mean values. GCM values have been corrected for 1995-2005 mean bias. Bars on the right for each season show the end-of-century summary of projections by global climate models (GCM, left) and regional climate models (RCM, right) for both lower (RCP 4.5) and higher (RCP 8.5) scenarios. 217

Figure 15-9: Regionally averaged seasonal maximum air temperature changes (°C) for S. For each season, the time series graph of projections by global climate models (GCM) is shown on the left for the higher (RCP 8.5) greenhouse gas scenario. Black line is from historical GCM runs, red line is the multi-model median projection from GCMs using RCP 8.5. Shadings are between 10% and 90% of 20-year mean values. GCM values have been corrected for 1995-2005 mean bias. Bars on the right for each season show the end-of-century summary of projections by global climate models (GCM, left) and regional climate models (RCM, right) for both lower (RCP 4.5) and higher (RCP 8.5) scenarios. 218

Figure 15-10: Regionally averaged seasonal minimum air temperature changes (°C) for S. For each season, the time series graph of projections by global climate models (GCM) is shown on the left for the higher (RCP 8.5) greenhouse gas scenario. Black line is from historical GCM runs, red line is the multi-model median projection from GCMs using RCP 8.5. Shadings are between 10% and 90% of 20-year mean values. GCM values have been corrected for 1995-2005 mean bias. Bars on the right for each season show the end-of-century summary of projections by global climate models (GCM, left) and regional climate models (RCM, right) for both lower (RCP 4.5) and higher (RCP 8.5) scenarios. 219

Figure 15-11: Regionally averaged seasonal precipitation changes (mm month^{-1} on left axis and % on right axis) for S. For each season, the time series graph of projections by global climate models (GCM) is shown on the left for the higher (RCP 8.5) greenhouse gas scenario. Black line is from historical GCM runs, red line is the multi-model median projection from GCMs using RCP 8.5. Shadings are between 10% and 90% of 20-year mean values. GCM values have been corrected for 1995-2005 mean bias. Bars on the right for each season show the end-of-century summary of projections by global climate models (GCM, left) and regional climate models (RCM, right) for both lower (RCP 4.5) and higher (RCP 8.5) scenarios. 220

TABLES

Table 1-1: Names and abbreviations for the seven climatic regions of Vietnam used in this report, correlated with regional designations used in previous reports. 4

Table 2-1: Details of observed station data from Vietnam for the period 1961-2011. 6

Table 2-2: Climate variables and details of a number of global and regional gridded datasets. 7

Table 2-3: List of CMIP5 GCMs based on their average performance in different evaluation studies. Models selected for downscaling in this project are indicated by blue shading. 10

Table 2-4: Strengths and limitations of the six GCMs selected for downscaling. 12

Table 2-5: List of RCMs used in this project, with their resolution, number of levels, and some details of the simulations. 17

Table 3-1: Correlation coefficients between SST anomalies (SSTA), which are represented by the NINO3.4 index, and regional station rainfall anomalies of Vietnam from 1979-2011. Statistically significant values at the 95% confidence level are bold. 27

Table 4-1: Common climate variables used in impact and risk assessment. Adapted from CSIRO and BoM (2007). 30

Table 4-2: Model selection for key climate futures for a hypothetical impact assessment given in Figure 4-5. 37

Table 5-1: Observational datasets used for validation of RCM simulations for Vietnam. 42

Table 5-2: Summary of the RCM set-ups. 46

Table 5-3: Tave validation of RCMs relative to station observational data. Bold numbering indicates the best-performing model. 48

Table 5-4: Tmax validation of RCMs relative to station observational data. Bold numbering indicates the best-performing model. 48

Table 5-5: Tmin validation of RCMs relative to station observational data. Bold numbering indicates the best-performing model. 48

Table 5-6: Rainfall validation of RCMs relative to station data across Vietnam. Bold numbering indicates the best-performing model for each statistic. 51

Table 5-7: Summary of the GCM forced RCM set-ups for current climate validation. 55

Table 5-8: Tmax validation of multi-model mean of RCMs for current climate (1980-2000) relative to station data. Bold numbering indicates the best-performing model for each statistic. 56

Table 5-9: Tmin validation of multi-model mean of RCMs for current climate (1980-2000) relative to station data. Bold numbering indicates the best-performing model for each statistic. 57

Table 5-10: Rainfall validation of RCMs relative to observational data for the period 1980-2000. Bold numbering indicates the best-performing model for each statistic. 58

Table 6-1: Temperature changes (°C) for Vietnam annually and by season by the end of the century (2080-2100) under RCP 4.5, including a measure of agreement and spread. Values are RCM ensemble means. 72

Table 6-2: Temperature changes (°C) for Vietnam annually and by season by the end of the century (2080-2100) under RCP 8.5, including a measure of agreement and spread. Values are RCM ensemble means. 72

Table 6-3: Rainfall changes (mm day^{-1}) for Vietnam annually and by season by the end of the century (2080-2100) under RCP 4.5, including a measure of agreement and spread. Values are RCM ensemble means. 73

Table 6-4: Rainfall changes (mm day^{-1}) for Vietnam annually and by season by the end of the century (2080-2100) under RCP 8.5, including a measure of agreement and spread. Values are RCM ensemble means. 73

Table 7-1: Percent change in tropical cyclone formation by the end of the century based upon GCMs using different methods. 78

Table 7-2: Regional values and standard deviation of RX1 and RX5 (with percent bias) and CWD and CDD (day bias) for the observations and the CCAM 10 km ensemble means. The indices are derived from daily station-averaged rainfall (OBS) and area-averaged daily rainfall from CCAM ensemble simulations for the seven sub-regions. 87

Table 7-3: Extreme indices and standard deviation and the percent change. The two periods used are 1980-2000 (current climate) and 2045-2065 (mid-century) for RCP 8.5. 88

Table 7-4: Drought classification based on the standardized precipitation index (SPI). Note only extreme and severe droughts (bold) are considered here. 97

Table 7-5: Summer monsoon onset dates (as Julian dates) and observed standard deviations for the current climate (1980-2000). Ensemble-mean bias (mean minus observations in days) is shaded. 108

Table 7-6: Rainfall intensity, or accumulated rainfall amount (mm) and rainfall duration (days) for the seven sub-regions of Vietnam during the summer monsoon season for the current (1980-2000) climate, and the ensemble-mean percentage bias relative to observations (shaded). 110

Table 7-7: Accumulated rainfall amount (mm) during the summer monsoon season from high-resolution CCAM simulations for the current and future climate at mid-century and the percentage change under RCP 8.5 (shaded). 111

Table 7-8: Duration (in days) of the summer monsoon rainy season from high-resolution CCAM simulations for the current and future climate at mid-century and change under RCP 8.5 (shaded). 111

Table 7-9: Accumulated rainfall amount (mm) during the summer monsoon season from high-resolution CCAM simulations for the current and future climate at end of the century and the percentage change under RCP 8.5 (shaded). 112

Table 7-10: Duration (in days) of the summer monsoon rainy season from high-resolution CCAM simulations for the current and future climate at the end of the century and change under RCP 8.5 (shaded). 112

Table 8-1: Sea-level trends. The table gives the locations, start and end dates, record length trend, trend from 1993 to the end of the tide-gauge record, and the altimeter trend for the closest available altimeter grid point from 1993 to the end of the tide-gauge record, each with the standard deviation of the trend in brackets. Note that for Coto and Phuquoc, we have truncated the data to end in 2002 and 1998 because of concerns about the data after this time; these truncations are also applied to the corresponding altimeter data. 118

Table 9-1: Observed climate variables and ranges for the NW region. Nguyen and Nguyen (2004). 129

Table 9-2: Summary of the multi-model mean and range of projected changes in annual and seasonal average, maximum and minimum temperature (°C) for the NW region relative to the baseline period (1980-2000) for RCP 8.5. Green colouring is for increases less than 2°C, yellow from 2-4°C and orange greater than 4°C. 137

Table 9-3: Projected changes in annual and seasonal mean temperature (°C) for the NW region relative to the baseline period (1980-2000) under different SRES emission scenarios (B1, B2, A2, A1B) from a previous study (MONRE, 2012) and the latest PRECIS projections (ensemble means). Green colouring is for increases less than 2°C, yellow from 2-4°C and orange greater than 4°C. Source: IMHEN. 137

Table 9-4: Projected changes in annual and seasonal average temperature by model (°C) for the NW region relative to the baseline period (1980-2000) for RCP 8.5 from eight RCM experiments. Green colouring is for increases less than 2°C, yellow from 2-4°C and orange greater than 4°C. 138

Table 9-5: Projected changes in annual and seasonal maximum temperature by model (°C) for the NW region relative to the baseline period (1980-2000) for RCP 8.5 from eight RCM experiments. Green colouring is for increases less than 2°C, yellow from 2-4°C and orange greater than 4°C. 139

Table 9-6: Projected changes in annual and seasonal minimum temperature by model (°C) for the NW region relative to the baseline period (1980-2000) for RCP 8.5 from eight RCM experiments. Green colouring is for increases less than 2°C, yellow from 2-4°C and orange greater than 4°C. 140

Table 9-7: Projected changes in annual and seasonal mean rainfall and its ranges (%) for the NW region relative to the baseline period (1980-2000) for RCP 8.5. Changes are the multi-model means from eight simulations. Orange colouring is for decreases less than -10%, green for changes between -10% to +10% and blue for increases greater than +10%. 141

Table 9-8: Projected changes in annual and seasonal rainfall (%) for the NW region relative to the baseline period (1980-2000) for SRES emission scenarios (B1, B2, A2, A1B) from a previous study (MONRE, 2012) and the latest PRECIS projections (ensemble means). Orange colouring is for decreases less than -10%, green for changes between -10% to +10% and blue for increases greater than +10%. Source: IMHEN. 141

Table 9-9: Projected changes in annual and seasonal mean rainfall by model (%) for the NW region relative to the baseline period (1980-2000) for RCP 8.5 from the eight RCMs. Orange colouring is for decreases less than -10%, green for changes between -10% to +10% and blue for increases greater than +10%. 142

Table 10-1: Observed climate variables and ranges for the NE region. Nguyen and Nguyen (2004). 143

Table 10-2: Summary of the multi-model mean and range of projected changes in annual and seasonal average, maximum and minimum temperature (°C) for the NE region relative to the baseline period (1980-2000) for RCP 8.5. Green colouring is for increases less than 2°C, yellow from 2-4°C and orange greater than 4°C. 151

Table 10-3: Projected changes in annual and seasonal mean temperature (°C) for the NE region relative to the baseline period (1980-2000) under different SRES emission scenarios (B1, B2, A2, A1B) from a previous study (MONRE, 2012) and the latest PRECIS projections (ensemble means). Green colouring is for increases less than 2°C, yellow from 2-4°C and orange greater than 4°C. Source: IMHEN. 151

Table 10-4: Projected changes in annual and seasonal average temperature by model (°C) for the NE region relative to the baseline period (1980-2000) for RCP 8.5 from eight RCM experiments. Green colouring is for increases less than 2°C, yellow from 2-4°C and orange greater than 4°C. 152

Table 10-5: Projected changes in annual and seasonal maximum temperature by the models (°C) for the NE region relative to the baseline period (1980-2000) for RCP 8.5 from eight RCM experiments. Green colouring is for increases less than 2°C, yellow from 2-4°C and orange greater than 4°C. 153

Table 10-6: Projected changes in annual and seasonal minimum temperature by model (°C) for the NE region relative to the baseline period (1980-2000) for RCP 8.5 from eight RCM experiments. Green colouring is for increases less than 2°C, yellow from 2-4°C and orange greater than 4°C. 154

Table 10-7: Projected changes in annual and seasonal mean rainfall and its ranges (%) for the NE region relative to the baseline period (1980-2000) for RCP 8.5. Changes are the multi-model means from eight simulations. Orange colouring is for decreases less than -10%, green for changes between -10% to +10% and blue for increases greater than +10%. 155

Table 10-8: Projected changes in annual and seasonal rainfall (%) for the NE region relative to the baseline period (1980-2000) for SRES emission scenarios (B1, B2, A2, A1B) from a previous study (MONRE, 2012) and the latest PRECIS projections (ensemble means). Orange colouring is for decreases less than -10%, green for changes between -10% to +10% and blue for increases greater than +10%. Source: IMHEN. 155

Table 10-9: Projected changes in annual and seasonal mean rainfall by model (%) for the NE region relative to the baseline period (1980-2000) for RCP 8.5 from the eight RCMs. Orange colouring is for decreases less than -10%, green for changes between -10% to +10% and blue for increases greater than +10%. 156

Table 11-1: Observed climate variables and ranges for the ND region. Nguyen and Nguyen (2004). 157

Table 11-2: Summary of the multi-model mean and range of projected change in annual and seasonal average, maximum and minimum temperature (°C) for the ND region relative to baseline period (1980-2000) for RCP 8.5. Green colouring is for increases less than 2°C, yellow from 2-4°C and orange greater than 4°C. 165

Table 11-3: Projected changes in annual and seasonal mean temperature (°C) for the ND region relative to baseline period (1980-2000) under different SRES emission scenarios (B1, B2, A2, A1B) from a previous study (MONRE, 2012) and the latest PRECIS projections (ensemble means). Green colouring is for increases less than 2°C, yellow from 2-4°C and orange greater than 4°C. Source: IMHEN. 165

Table 11-4: Projected changes in annual and seasonal average temperature by model (°C) for the ND region relative to the baseline period (1980-2000) for RCP 8.5 from eight RCM experiments. Green colouring is for increases less than 2°C, yellow from 2-4°C and orange greater than 4°C. 166

Table 11-5: Projected changes in annual and seasonal maximum temperature by model (°C) for the ND region relative to the baseline period (1980-2000) for RCP 8.5 from eight RCM experiments. Green colouring is for increases less than 2°C, yellow from 2-4°C and orange greater than 4°C. 167

Table 11-6: Projected changes in annual and seasonal minimum temperature by model (°C) for the ND region relative to the baseline period (1980-2000) for RCP 8.5 from eight RCM experiments. Green colouring is for increases less than 2°C, yellow from 2-4°C and orange greater than 4°C. 168

Table 11-7: Projected changes in annual and seasonal mean rainfall and its ranges (%) for the ND region relative to the baseline period (1980-2000) for RCP 8.5. Changes are the multi-model means from eight simulations. Orange colouring is for decreases less than -10%, green for changes between -10% to +10% and blue for increases greater than +10%. 169

Table 11-8: Projected changes in annual and seasonal rainfall (%) for the ND region relative to the baseline period (1980-2000) for SRES emission scenarios (B1, B2, A2, A1B) from a previous study (MONRE, 2012) and the latest PRECIS projections (ensemble means). Orange colouring is for decreases less than -10%, green for changes between -10% to +10% and blue for increases greater than +10%. Source: IMHEN. 169

Table 11-9: Projected changes in annual and seasonal mean rainfall by model (%) for the ND region relative to the baseline period (1980-2000) for RCP 8.5 from the eight RCMs. Orange colouring is for decreases less than -10%, green for changes between -10% to +10% and blue for increases greater than +10%. 170

Table 12-1: Observed climate variables and ranges for the NC region. Nguyen and Nguyen (2004). 171

Table 12-2: Summary of the multi-model mean and range of projected change in annual and seasonal average, maximum and minimum temperature (°C) for the NC region relative to the baseline period (1980-2000) for RCP 8.5. Green colouring is for increases less than 2°C, yellow from 2-4°C and orange greater than 4°C. 179

Table 12-3: Projected changes in annual and seasonal mean temperature (°C) for the NC region relative to the baseline period (1980-2000) under different SRES emission scenarios (B1, B2, A2, A1B) from a previous study (MONRE, 2012) and the latest PRECIS projections (ensemble means). Green colouring is for increases less than 2°C, yellow from 2-4°C and orange greater than 4°C. Source: IMHEN. 179

Table 12-4: Projected changes in annual and seasonal average temperature by model (°C) for the NC region relative to the baseline period (1980-2000) for RCP 8.5 from eight RCM experiments. Green colouring is for increases less than 2°C, yellow from 2-4°C and orange greater than 4°C. 180

Table 12-5: Projected changes in annual and seasonal maximum temperature by model (°C) for the NC region relative to the baseline period (1980-2000) for RCP 8.5 from eight RCM experiments. Green colouring is for increases less than 2°C, yellow from 2-4°C and orange greater than 4°C. 181

Table 12-6: Projected changes in annual and seasonal minimum temperature by model (°C) for the NC region relative to the baseline period (1980-2000) for RCP 8.5 from eight RCM experiments. Green colouring is for increases less than 2°C, yellow from 2-4°C and orange greater than 4°C. 182

Table 12-7: Projected changes in annual and seasonal mean rainfall and ranges (%) for the NC region relative to the baseline period (1980-2000) for RCP 8.5. Changes are the multi-model means from eight simulations. Orange colouring is for decreases less than -10%, green for changes between -10% to +10% and blue for increases greater than +10%. 183

Table 12-8: Projected changes in annual and seasonal rainfall (%) for the NC region relative to the baseline period (1980-2000) for SRES emission scenarios (B1, B2, A2, A1B) from a previous study (MONRE, 2012) and the latest PRECIS projections (ensemble means). Orange colouring is for decreases less than -10%, green for changes between -10% to +10% and blue for increases greater than +10%. Source: IMHEN. 183

Table 12-9: Projected changes in annual and seasonal mean rainfall by model (%) for the NC region relative to the baseline period (1980-2000) for RCP 8.5 from the eight RCMs. Orange colouring is for decreases less than -10%, green for changes between -10% to +10% and blue for increases greater than +10%. 184

Table 13-1: Observed climate variables and ranges for the SC region. Nguyen and Nguyen (2004). 185

Table 13-2: Summary of multi-model mean and range of projected change in annual and seasonal average, maximum and minimum temperatures (°C) for the SC region relative to the baseline period (1980-2000) for RCP 8.5. Green colouring is for increases less than 2°C, yellow from 2-4°C and orange greater than 4°C. 193

Table 13-3: Projected changes in annual and seasonal mean temperature (°C) for the SC region relative to the baseline period (1980-2000) for various SRES emission scenarios (B1, B2, A2, A1B) from a previous study (MONRE, 2012) and the latest PRECIS projections (ensemble mean). Green colouring is for increases less than 2°C, yellow from 2-4°C and orange greater than 4°C. Source: IMHEN. 193

Table 13-4: Projected changes in annual and seasonal average temperature by model (°C) for the SC region relative to the baseline period (1980-2000) for RCP 8.5 from the eight RCM experiments. Green colouring is for increases less than 2°C, yellow from 2-4°C and orange greater than 4°C. 194

Table 13-5: Projected changes in annual and seasonal maximum temperature by model (°C) for the SC region relative to the base line period (1980-2000) for RCP 8.5 from the eight RCM experiments. Green colouring is for increases less than 2°C, yellow from 2-4°C and orange greater than 4°C. 195

Table 13-6: Projected changes in annual and seasonal minimum temperature by model (°C) for the SC region relative to the baseline period (1980-2000) for RCP 8.5 from the eight RCM experiments. Green colouring is for increases less than 2°C, yellow from 2-4°C and orange greater than 4°C. 196

Table 13-7: Projected changes in the annual and seasonal mean rainfall and its range (%) for the SC region relative to the baseline period (1980-2000) for RCP 8.5. Changes are the multi-model means from eight simulations. Orange colouring is for decreases less than -10%, green for changes between -10% to +10% and blue for increases greater than +10%. 197

Table 13-8: Projected changes in annual and seasonal rainfall (%) for the SC region relative to the baseline period (1980-2000) for various SRES emission scenarios (B1, B2, A2, A1B) from a previous study (MONRE, 2012) and the latest PRECIS projections (ensemble mean). Orange colouring is for decreases less than -10%, green for changes between -10% to +10% and blue for increases greater than +10%. Source: IMHEN. 197

Table 13-9: Projected changes in annual and seasonal mean rainfall by model (%) for the SC region relative to the baseline period (1980-2000) for RCP 8.5 from the eight RCM experiments. Orange colouring is for decreases less than -10%, green for changes between -10% to +10% and blue for increases greater than +10%. 198

Table 14-1: Observed climate variables and their ranges for the CH region. Nguyen and Nguyen (2004). 199

Table 14-2: Summary of multi-model mean and range of projected change in annual and seasonal average, maximum and minimum temperatures (°C) for the CH region relative to the baseline period (1980-2000) for RCP 8.5. Green colouring is for increases less than 2°C, yellow from 2-4°C and orange greater than 4°C. 207

Table 14-3: Projected changes in annual and seasonal mean temperature (°C) for the CH region relative to the baseline period (1980-2000) for various SRES emission scenarios (B1, B2, A2, A1B) from a previous study (MONRE, 2012) and the latest PRECIS projections (ensemble means). Green colouring is for increases less than 2°C, yellow from 2-4°C and orange greater than 4°C. Source: IMHEN. 207

Table 14-4: Projected change in annual and seasonal average temperature by model (°C) for the CH region relative to the baseline period (1980-2000) for RCP 8.5 from the eight RCM experiments. Green colouring is for increases less than 2°C, yellow from 2-4°C and orange greater than 4°C. 208

Table 14-5: Projected change in annual and seasonal maximum temperature by model (°C) for the CH region relative to the baseline period (1980-2000) for RCP 8.5 from the eight RCM experiments. Green colouring is for increases less than 2°C, yellow from 2-4°C and orange greater than 4°C. 209

Table 14-6: Projected change in annual and seasonal minimum temperature by model (°C) for the CH region relative to the baseline period (1980-2000) for RCP 8.5 from the eight RCM experiments. Green colouring is for increases less than 2°C, yellow from 2-4°C and orange greater than 4°C. 210

Table 14-7: Projected changes in annual and seasonal mean rainfall and its range (%) for the CH region relative to the baseline period (1980-2000) for RCP 8.5. Changes are the multi-model means from eight simulations. Orange colouring is for decreases less than -10%, green for changes between -10% to +10% and blue for increases greater than +10%. 211

Table 14-8: Projected changes in annual and seasonal rainfall (%) for the CH region relative to the baseline period (1980-2000) for SRES emission scenarios (B1, B2, A2, A1B) from a previous study (MONRE, 2012) and the latest PRECIS projections (ensemble means). Orange colouring is for decreases less than -10%, green for changes between -10% to +10% and blue for increases greater than +10%. Source: IMHEN. 211

Table 14-9: Projected changes in annual and seasonal mean rainfall by model (%) for the CH region relative to the baseline period (1980-2000) for RCP 8.5 for the eight RCMs. Orange colouring is for decreases less than -10%, green for changes between -10% to +10% and blue for increases greater than +10%. 212

Table 15-1: Observed climate variables and ranges for the South region. Nguyen and Nguyen (2004). 213

Table 15-2: Summary of multi-model mean and range of projected change in annual and seasonal average, maximum and minimum temperatures (°C) for the S region relative to the baseline period (1980-2000) for RCP 8.5. Changes are from eight RCM simulations. Green colouring is for increases less than 2°C, yellow from 2-4°C and orange greater than 4°C. 221

Table 15-3: Projected changes in annual and seasonal mean temperature (°C) for the S region relative to the baseline period (1980-2000) for different SRES emission scenarios (B1, B2, A2, A1B) from a previous study (MONRE, 2012) and the latest PRECIS projections (ensemble means). Green colouring is for increases less than 2°C, yellow from 2-4°C and orange greater than 4°C. Source: IMHEN. 221

Table 15-4: Projected change in annual and seasonal average temperature by model (°C) for the S region relative to the baseline period (1980-2000) for RCP 8.5 for eight RCMs. Green colouring is for increases less than 2°C, yellow from 2-4°C and orange greater than 4°C. 222

Table 15-5: Projected change in annual and seasonal maximum temperature by model (°C) for the S region relative to the baseline period (1980-2000) for RCP 8.5 for eight RCMs. Green colouring is for increases less than 2°C, yellow from 2-4°C and orange greater than 4°C. 223

Table 15-6: Projected change in annual and seasonal minimum temperature by model (°C) for the S region relative to the baseline period (1980-2000) for RCP 8.5 for eight RCMs. Green colouring is for increases less than 2°C, yellow from 2-4°C and orange greater than 4°C. 224

Table 15-7: Projected changes in annual and seasonal mean rainfall and its range (%) for the S region relative to the baseline period (1980-2000) for RCP 8.5. Changes are the multi-model means from eight simulations. Orange colouring is for decreases less than -10%, green for changes between -10% to +10% and blue for increases greater than +10%. 225

Table 15-8: Projected changes in annual and seasonal rainfall (%) for the S region relative to the baseline period (1980-2000) for SRES emission scenarios (B1, B2, A2, A1B) from a previous study (MONRE, 2012) and the latest PRECIS projections (ensemble means). Orange colouring is for decreases less than -10%, green for changes between -10% to +10% and blue for increases greater than +10%. Source: IMHEN. 225

Table 15-9: Projected changes in annual and seasonal mean rainfall by model (%) for the S region relative to the baseline period (1980-2000) for RCP 8.5 for the eight RCMs. Orange colouring is for decreases less than -10%, green for changes between -10% to +10% and blue for increases greater than +10%. 226

FOREWORD

Climate change has been recognized as one of the greatest challenges of the 21st Century. The Intergovernmental Panel on Climate Change (IPCC) has indicated the projected increase of global mean surface temperatures for 2081–2100 relative to 1986–2005 is likely be in the ranges derived from the concentration-driven CMIP5 model simulations, that is, 0.3°C to 1.7°C (RCP 2.6), 1.1°C to 2.6°C (RCP 4.5), 1.4°C to 3.1°C (RCP 6.0), 2.6°C to 4.8°C (RCP 8.5).This is likely to be associated with changes to weather patterns and sea-level rise, which will impact on ecosystems, water resources, agriculture, forests, fisheries, industries, urban and rural settlements, energy usage, tourism and health.

Since 1960, average temperatures have risen by approximately 0.5 to 0.7°C and sea levels have increased by 20 cm within Vietnam (MONRE, 2009). The government of Vietnam is deeply concerned about the consequences of climate change and is committing considerable efforts to better understand these impacts. As part of this, they have introduced the *National Target Program to Respond to Climate Change*, which requires the development and update of climate change scenarios to provide a basis for impact assessment by ministries, sectors, cities and provinces. In 2009, climate change and sea-level rise scenarios were developed for the whole of Vietnam. A further update of these scenarios is expected by 2015 (MONRE, 2009).

A key priority identified by stakeholders was the need to better understand the likely effects of climate change at the local level, since most of the impacts occur at this scale. More localised climate change projections will help identify the people and sectors at risk, and in doing so, will support Vietnam in the challenging task of prioritising its climate change responses. To address this gap, Australia's Agency for International Development (under the Department of Foreign Affairs and Trade, DFAT) has supported the *High-resolution Climate Projections for Vietnam* project discussed in this report to help refine Vietnam's climate change projections. The project will provide crucial inputs into the next update of the *Climate Change and Sea Level Rise Scenarios for Vietnam* by providing more detailed climate change projections at 10 km resolution across Vietnam. The project was funded by the Australian Department of Foreign Affairs and Trade (DFAT) under its Research for Development Alliance with the Commonwealth Scientific and Industrial Research Organisation (CSIRO). Delivery partners were the Institute of Meteorology, Hydrology and Environment (IMHEN) and the Hanoi University of Science – Vietnam National University (HUS) in Vietnam and CSIRO in Australia.

This publication is the final volume in a series of *High-resolution Climate Projections for Vietnam* reports. It contains full details of our approach, results and analysis, targeted towards a more technical audience. Part 1 describes the methods used to produce the climate simulations for Vietnam, while Part 2 contains detailed analyses of the projections for seven sub-regions of Vietnam.

Other available reports associated with the project are:

- **Summary for Policy Makers**, developed for the purpose of communicating the climate projection information to a more general audience
- **Regional Brochures**, which present climate projections for each of the seven regions in Vietnam.
-

PART 1

- METHODOLOGY AND MODEL SET-UP
- CURRENT CLIMATE VALIDATION
- FUTURE CLIMATE PROJECTIONS FOR VIETNAM
- UNDERSTANDING AND USE OF CLIMATE PROJECTIONS

EXECUTIVE SUMMARY – PART 1

Climate change has been recognized as one of the greatest challenges facing our planet, not only for the environment, but also for economic development, with changes occurring in the physical, ecological and socio-economic systems. Atmospheric greenhouse gas concentrations increased rapidly in the past century and are almost certain to continue increasing in the future (IPCC, 2013). Global climate model experiments indicate a global warming of 0.3 to 4.8°C for 1981-2100 relative to 1986-2005 (IPCC, 2013). This is likely to be associated with changes to weather patterns, sea-level rise and impacts on ecosystems, water resources, agriculture, forests, fisheries, industries, urban and rural settlements, energy usage, tourism and health.

Located in South East Asia, with a tropical monsoon climate and a coastline of more than 3200 km, Vietnam is one of the most disaster-prone countries in the world. Most of the disasters that occur in the country are related to weather and climate, and consequently climate change and climate variability are likely to pose increasing threats to Vietnam and its inhabitants in the near and long-term future (MONRE, 2009). The purpose of the *High-resolution Climate Projections for Vietnam* project was to further climate science research and capacity building in Australia and Vietnam and to produce high-resolution climate projections to support the government of Vietnam in its efforts to update its national *Climate Change and Sea-Level Rise Scenarios* by 2015. This update is required to incorporate new climate science information released by the Intergovernmental Panel on Climate Change and provide more detailed projections at a regional level, enabling more effective adaptation planning.

This section of the technical report details the methodology used to generate the new climate projections, gives a summary of the current climate and trends across Vietnam, provides validation of the simulations of the current climate and future projections for Vietnam, and provides guidance to users on utilization of the climate change projections. Regional climate models (RCMs) were used to produce high-resolution simulations using the latest available coarse-resolution global climate model (GCM) simulations from the Coupled Model Intercomparison Project Phase 5 (CMIP5). Six GCMs were selected on the basis of their ability to realistically capture current climate and climate features such as El Niño-Southern Oscillation (ENSO): CNRM-CM5, CCSM4, NorESM1-M, ACCESS1.0, MPI-ESM-LR and GFDL-CM3.

The RCMs used in this study were CSIRO's Conformal-Cubic Atmospheric Model (CCAM), RegCM4.2 (developed by ICTP in Trieste, Italy), and the UK Met Office's Providing Regional Climates for Impacts Studies (PRECIS) model. The two-step method used to generate the high-resolution regional climate simulations is known as dynamical downscaling. First, data from the GCMs (approximately 200 km resolution) are used as input into an RCM run globally at finer resolution (50 or 100 km, depending on the regional model used in the next step). Then data from this simulation are used as input into the same RCM, or a different one, to produce the high-resolution simulation (10 or 20 km).

CCAM is a variable-resolution model, which means it can be run globally on an even grid or on a stretched grid with high resolution over the area of interest. In the projections generated here, only sea surface temperature and sea ice information from CMIP5 GCMs were used as inputs. These inputs were corrected to more realistically match the current climate. RegCM4.2 and PRECIS are limited area models (LAMs) that are run only over the area of interest, with input of more atmospheric variable information such as temperature, pressure, and wind speed at the lateral boundaries of the limited domain. CCAM simulations were completed for a continuous period from 1970-2100, while due to computer resource constraints those of RegCM4.2 were for time slices: current climate (1980-2000), mid-century (2045-2065), and the end of the century (2080-2100). Two sets of projections were completed, using two of the most recent IPCC Representative Concentration Pathways (effectively equivalent to emission scenarios): RCP 4.5 (lower) and RCP 8.5 (higher).

Updated sea-level rise projections for the oceans surrounding Vietnam were developed using information from the latest global models, with added understanding of other contributing factors such as glacial melting and changes in land-based water resources. All four Representative Concentration Pathways (RCP 2.6, 4.5, 6.0 and 8.5) were considered.

As the first step in understanding the climate of Vietnam, current climate trends and variability of temperature and rainfall as well as the impacts of climate drivers such as ENSO and tropical cyclones were analysed in detail, both annually and for monsoon-based seasons.

The ability of GCMs and RCMs to simulate the current climate (1980-2000) was validated by comparing their output with observations from 70 stations in Vietnam and global observational or reanalysis datasets such as ERA-40, ERA-Interim or gridded observational datasets such as APHRODITE and CRU. Statistical measures used included pattern correlation and Root Mean Square Error (RMSE). RCMs were forced both by the ERA-Interim reanalysis dataset and by data from the six CMIP5 GCMs (which may have biases) to compare performance.

Eight downscaled projections of future climate for Vietnam and the sub-regions were then produced to show Vietnam-wide changes in temperature and rainfall. Only the results for the high emission scenario for both mid-century (20-year period centred on 2055) and the end of the century (20-year period centred on 2090), relative to the period 1980-2000 are presented in this report. The multi-model mean changes are presented, along with the percent agreement of the sign-of-change among the downscaled results and the spread among the model projections (using the standard deviation of the model changes as a measure). The latter two provide some measure of confidence in the projections.

The data generated in this study are further analysed to determine changes in monsoon onset date and tropical cyclone frequency. Extreme indices such as 1-day and 5-day rainfall and the heat wave duration index (HWDI) were computed to indicate possible changes in drought duration and frequency.

Climate change projections are inherently uncertain. The future climate will be determined by a combination of factors, including levels of greenhouse gas and aerosol emissions, unexpected events (e.g. volcanic eruptions), a range of human activities, and sensitivity of the climate system to greenhouse gases and aerosols, as well as natural variability. Exactly how these factors will unfold is unknown. Climate models have different internal dynamics and parameterisations, and thus respond somewhat differently to the same inputs, producing a range of possible futures. This concern is partly addressed in the current study by selecting CMIP5 GCMs that reproduce current climate reasonably well, then using techniques for bias correction of sea surface temperatures (SSTs) that improve their representation in the current climate, but preserve the projected climate change signal and the internal variability. In addition, multi-model means of variables such as temperature and rainfall are assessed to capture the central estimates of possible futures.

The Climate Futures Tool (**http://climatetool.vnclimate.vn/**) allows the end user to see the spread of possible projections for the seven sub-regions of Vietnam. In addition, the tool guides the end user in choosing possible projections that may be used to assess the impact of climate change for different applications.

KEY FINDINGS

Temperature is projected to increase across all seven sub-regions, with annual changes ranging from 1.6°C to 3.2°C for RCP 4.5, and 2.4°C to 5.1°C for RCP 8.5 by 2090, with more hot days and heatwaves.

Rainfall is projected to change in some seasons and regions. There are significant variations in projections, with annual changes ranging from -12% to +20% for RCP 4.5, and -17% to +34% for RCP 8.5 by 2090. In general, summer rainfall is projected to decrease throughout Vietnam. Projections indicate likely rainfall increases for central Vietnam in all other seasons.

Changes in the frequency and intensity droughts and extreme rainfall amounts are projected to vary across Vietnam, which could have large impacts on agriculture and water resources when coupled with the effects of temperature increases.

Fewer but possibly more intense tropical cyclones (typhoons) are projected. The complexity of tropical cyclone formation makes them hard to predict, so this is an area requiring further investigation.

Sea level continues to rise, with a projected range of increase of between 100 and 400 mm by 2050 and increase to 300-600 mm for RCP 2.6 to 900 mm for RCP 8.5 by to the end of the century. Further increases are projected beyond 2100.

RECOMMENDATIONS

This research has revealed some new insights into the potential future climate in Vietnam, given our current understanding. In assessing the impact of these projections, careful analysis is required. For example, while the results suggest little change in annual rainfall, the projected decrease in rainfall during the summer monsoon season may have significant hydrological implications, which could impact areas such as water resource planning and agriculture. This may potentially be made worse by the projected increase in the frequency of droughts and the more intense extreme rainfall. Users should collaborate with climate experts and other advisors to identify the best means for applying these new findings in their planning processes and in future project design.

The Climate Futures Tool (**http://climatetool.vnclimate.vn/**), developed as part of this project, can be used to select relevant climate projection information for a preliminary assessment. The tool allows users to identify a smaller number of plausible 'futures' that are most relevant to their application, including at least the 'most representative' (where most models agree), the 'best' (most desirable) and the 'worst' (least desirable) cases.

The results presented from this research are only the first step in developing a greater understanding of future climate in Vietnam. Further research is needed to fully understand the drivers behind projected changes, especially for rainfall, and implications for other climate features such as typhoons and droughts.

Part 1 (Chapters 1-8) of this technical report gives more information on the methodology used to produce the simulations for this study, as well as details of the current and future climate simulations over all of Vietnam. For analysis of the simulations for the seven sub-regions of Vietnam, see Part 2 (Chapters 9-15). More information about the project is also available on the project website: **www.vnclimate.vn**.

1 ABOUT THE PROJECT

The *High-resolution Climate Projections for Vietnam* (HCPV) project was funded by the Australian Department of Foreign Affairs and Trade (DFAT) under its Research for Development Alliance with the Commonwealth Scientific and Industrial Research Organisation (CSIRO). The purpose of the project was to further climate science research and capacity building in Australia and Vietnam, through delivery partners The Institute of Meteorology, Hydrology and Environment (IMHEN) and the University of Science – Vietnam National University (HUS) in Vietnam and CSIRO in Australia.

1.1 PROJECT AIMS

There have been many previous studies of impacts of climate change over South East Asia and possible changes to weather patterns over Vietnam. In an earlier study by the Asian Development Bank (1994), simulations from nine global climate models were used to project temperature and rainfall for northern and southern Vietnam. Subsequently, climate change projections have been used to assess the impacts of climate change for the tropics (Hulme and Viner, 1998). A number of studies have focused on climate change and its likely impact on various sectors of Vietnam (Waibel, 2008; Asian Disaster Preparedness Center, 2003; Eckert and Waibel, 2009). Most projections are derived from multiple model results, using simple averages or weighted values based on statistical measures of model reliability, such as the correlation between observed and simulated climate patterns. The underlying assumption is that projections are likely to be more reliable from models that simulate the present climate well.

The aims of this project were to:

- Improve understanding of potential future climate changes in Vietnam.
- Integrate past and current research for a more complete assessment of the potential effects of climate change.
- Provide information necessary for appropriate planning and investment to adapt to climate change.
- Develop innovative communication tools to ensure that the data generated are widely accessible.

A key priority identified by stakeholders was the need to better understand the likely effects of climate change at the local level, since most of the impacts occur at this scale. More localised climate change projections will help identify the people and sectors at risk.

The project had six main components:

- **Component 1**: Review of previous observation data and climate drivers in Vietnam
- **Component 2**: Dynamical downscaling to produce regional climate simulations
- **Component 3**: Analysis of climate projections
- **Component 4**: Regional sea-level projections
- **Component 5**: Assessment of response options
- **Component 6**: Communication and management

The project will provide crucial inputs into the next update of the *Climate Change and Sea Level Rise Scenarios for Vietnam* in 2015 by providing more detailed climate change projections at 10 km resolution across Vietnam.

1.2 WHAT ARE CLIMATE PROJECTIONS?

Climate projections are plausible descriptions of the future climate, based on assumptions of global development and the resulting levels of greenhouse gas concentrations. They are not a prediction of a specific event, like a weather forecast, but instead provide a range of possible changes over a longer time period. Projections are created using computer simulations of the climate systems with these greenhouse gas concentrations as inputs. The response of the climate models to these concentrations leads to different climate change signals and a range of possible climate futures for any given location.

Global climate models are the best available tools for simulating future climates based on various greenhouse gas and aerosol emission scenarios because they are able to couple the atmosphere and oceans and incorporate their complex linked interactions over the entire Earth system. However, they are computationally expensive and have a relatively coarse resolution, so that projections may typically be for a 200 km grid box. At this low resolution, it is not possible to take into account regional effects such as topography or land use. For this reason, regional climate models, which are high-resolution atmospheric models formulated with the same dynamical equations of motion as the GCMs, are used to dynamically downscale the GCM results and provide more detailed climate change projections at 10 km resolution across Vietnam.

In this project, climate projections are given for seven climatic regions[2] (see Table 1-1 below) as well as for the whole of Vietnam. These regions will be used throughout the report to describe climate changes at the regional level.

Table 1-1: Names and abbreviations for the seven climatic regions of Vietnam used in this report, correlated with regional designations used in previous reports.

CLIMATIC REGIONS USED IN THIS REPORT	PREVIOUS REGIONAL DESIGNATIONS
North West (NW)	R1 or B1
North East (NE)	R2 or B2
North Delta (ND)	R3 or B3
North Central (NC)	R4 or B4
South Central (SC)	R5 or N1
Central Highlands (CH)	R6 or N2
South (S)	R7 or N3

2 The regions and their abbreviations follow the conventions in *Climate Change and Sea Level Rise Scenarios for Vietnam* (MONRE, 2009).

WHAT'S NEW

This project builds on existing work and uses the latest available information from the Coupled Model Intercomparison Project Phase 5 (CMIP5) simulations, which will be used in the next Intergovernmental Panel on Climate Change (IPCC) *Fifth Assessment Report* (AR5; 2013). It presents a range of possible climate futures over Vietnam with the following new information and approaches (see Chapter 2 for more details):

- **Greenhouse gases and aerosols:** the latest projections for future greenhouse gas and aerosol concentrations were used.[3] For this project, only the lower and higher concentrations were considered, while four concentration trends were considered for sea-level rise projections.[4]
- **Global simulations:** results from the new generation of global climate models[5] were used.
- **Regional projections**: different regional modelling approaches were used to develop more detailed projections for Vietnam, and results were summarised for the seven climate sub-regions of Vietnam.
- **Seasonal analysis**: in addition to reviewing of annual changes, seasonal changes were also assessed using monsoon-based seasons.
- **Climate features:** the impact of climate change on a range of extremes was assessed.
- **Regional sea-level assessment:** simulations of regional sea-level changes were developed using information from the latest global models with added understanding of other contributing factors, such as glacial melting and changes in land-based water resources.
- **Data access**: the web-based Climate Futures Tool was developed to simplify assessment of the climate projections.

1.3 HOW TO USE THE CLIMATE PROJECTIONS FROM THIS STUDY

The purpose of this technical report is to document in detail the methodology used in the *High-resolution Climate Projections for Vietnam* (HCPV) project. The report is organised in two sections: Part 1 (Chapters 1-8) covers the methodology used to produce the dynamically downscaled simulations and presents annual and seasonal climate projections by both GCMs and RCMs for all of Vietnam, while Part 2 (Chapters 9-15) gives detailed projections of future climate for each of the seven sub-regions of Vietnam. In both parts, the data generated are presented in tables and figures to make them more accessible.

Chapter 2 describes methods for developing the projections, including the selection of GCMs, RCMs, datasets for validation and emission scenarios, as well as downscaling model set-up and bias correction techniques. Chapter 3 analyses the current climate of Vietnam and observed trends, including climate drivers and variability, for four monsoonal-based seasons and annual periods.

In Chapter 4 there is extensive discussion of how to understand and use climate projections, and how the choice of spatial and temporal time scales, resolution, and methods of dealing with uncertainty affects results. Assessment methods such as the Climate Futures Tool and Agent-Based Modelling are also described.

Model performance and validation of both GCM and RCM simulations of current climate are given in Chapter 5, followed by analysis of climate change projections for Vietnam by GCMs and RCMs for mid-century and the end of the century in Chapter 6.

Chapter 7 examines projected changes to climate extremes such as tropical cyclones, extreme rainfall, heatwaves and droughts, as well as monsoon onset date, while Chapter 8 discusses projected sea-level changes for coastal areas of Vietnam.

As noted above, this study has incorporated current understanding of the processes that drive climate change, as well as the most up-to-date CMIP5 GCM data and RCP emission scenarios. To address the inherent uncertainty in future projections, a range of GCMs, RCMs and emission scenarios has been used for the simulations, as well as techniques such as ensemble predictions and calculation of multi-model means to ensure that a broad range of plausible changes to the climate of Vietnam have been evaluated. However, before the results of this study are used for adaptation assessments or planning purposes, their suitability for the application must be carefully considered.

Climate models are continually developing, which will lead to improved climate projections. In addition, understanding of and confidence in climate projections will increase as research continues. Users should ensure that any climate projections they are working with are updated every two to three years or in line with updates provided by the Intergovernmental Panel on Climate Change.

3 The plausible future trends (scenarios) in greenhouse gas concentrations used in this study are called Representative Concentration Pathways (RCPs). These new scenarios (2.6, 4.5, 6.0 and 8.5) represent increasing concentrations of greenhouse gases. They replace the older emission scenarios from the IPCC *Fourth Assessment Report* (AR4) – *Special Report on Emission Scenarios* (SRES).

4 Because of computer resource constraints only two RCPs (8.5 and 4.5) were used to develop the new climate projections. RCP 4.5 represents lower concentrations and impacts, while RCP 8.5 represents higher concentrations and impacts. For sea-level rise projections, where there are fewer computer resource constraints, all four RCPs (2.6, 4.5, 6.0 and 8.5) were used.

5 This refers to global model results currently available from the *Climate Model Intercomparison Project Phase 5* (CMIP5).

2 METHODS FOR DEVELOPING PROJECTIONS

This chapter describes the methods used in this study to provide high-resolution climate scenario information for Vietnam. The study employs high-resolution climate models known commonly as Regional Climate Models (RCMs). The RCMs are able to produce simulations that downscale (refine) information from prior simulations by selected Global Climate Models (GCMs) from the Coupled Model Intercomparison Project Phase 5 (CMIP5), which provided data for the *Fifth Assessment Report* of the IPCC. The CMIP5 simulations were driven by several Representative Concentration Pathways (RCPs) for envisaged greenhouse gas emissions. The RCM simulations in this study are validated for current climate conditions by comparing the simulations against a range of current climate observational datasets. Section 2.1 gives details of the available validating observational datasets used. Section 2.2 describes the RCP emission scenarios used in this study and relates them to the SRES emission scenarios used for previous IPCC assessments. Section 2.3 provides a brief overview of global climate modelling and describes the procedures used in this study to choose six GCMs to be dynamically downscaled to finer resolution. Section 2.4 describes the methodology used to correct the Sea Surface Temperature (SST) biases of the GCMs before they are used to drive the RCMs. In Section 2.5, a discussion of the methodologies used to dynamically downscale the GCM climate change information to fine resolution over Vietnam is provided, as well as descriptions of the RCMs used for downscaling, followed in Section 2.6 by a discussion of the configuration of the models used for the downscaled simulations.

2.1 OBSERVATIONAL DATASETS

This study produces high-resolution climate-change information by using several RCMs to dynamically downscale simulations by six selected GCMs. The selection of the six GCMs was guided by comparing their output against available observational datasets. The datasets were also required for validating the subsequent dynamically downscaled fine-resolution simulations for present-day conditions. This section lists and describes the derivation and contents of the available data, from station datasets to gridded global and regional datasets.

2.1.1 Station data variables

Observed daily data of temperature, rainfall, wind speed, potential evapotranspiration and humidity are available from about 70 stations in Vietnam for the present climate, from 1961 to 2011 (see Table 2-1). Only 61 stations had sufficient good quality data to be useful in this study.

Table 2-1: Details of observed station data from Vietnam for the period 1961-2011.

CLIMATE VARIABLES	NUMBER OF STATIONS
Daily 2 m Temperature	70
Daily Maximum Temperature	70
Daily Minimum Temperature	70
Daily Rainfall Amount	70
Daily Potential Evaporation	69
Daily Minimum Relative Humidity	68
Relative Humidity at 13h	69
Daily Maximum Wind Speed	68

2.1.2 Global datasets and variables

A number of global gridded datasets are available for studying present climate and climate variability, and also for comparing with global climate simulations performed for the IPCC. Some of the datasets include enough climate variables over an appropriate geographic area to make them useful for studies that focus on the regional scale in the Asia-Pacific area. The global atmospheric component datasets include the ERA-40 and ERA-Interim datasets from the European Centre for Medium-range Weather Forecasts (ECMWF) and a reanalysis[6] dataset from the National Center for Environmental Prediction (NCEP), USA. Sets of global precipitation data include the Climate Research Unit (CRU) datasets and the Global Precipitation Climatology Project (GPCP) dataset. The APHRODITE dataset covers most parts of Asia and Europe. Table 2-2 provides details of data available from each global and regional dataset.

2.1.3 ERA-40 and ERA-Interim datasets

Both ERA-40 and ERA-Interim reanalyses were produced by the ECMWF in collaboration with many other institutions. The reanalyses incorporate meteorological observations from September 1957 to August 2002 for ERA-40 and from January 1979 to present for ERA-Interim. The observing system changed considerably over this reanalysis period, with data assimilation provided by a succession of satellite-borne instruments from the 1970s onwards, supplemented by increasing numbers of observations from aircraft, ocean buoys and other surface platforms, but with a declining number of radiosonde ascents since the late 1980s. The observations used were obtained from many sources. These reanalysis datasets contain many atmospheric variables on a sub-daily time scale. Details of the procedure for creating this dataset and variables available are given by Uppala *et al*. (2005).

6 A reanalysis dataset is produced by taking observed data from many sources (land stations, ocean vessels, satellites) and using a computer program to assimilate the data, producing a dataset that is consistent over space and time on a regular grid.

2.1.4 NCEP reanalysis

The NCEP/NCAR (National Center for Atmospheric Research) reanalysis is an alternative data assimilation system to ERA-40, using past data from 1948 to the present. Output of the NCEP reanalysis products continues to be released. All variables are resolved every 6 hours (00, 06, 12 and 18 UTC), and monthly and annual data are also available. The data are on a 2.5° × 2.5° horizontal grid (144 × 73 regular grid points) for each of 17 pressure levels. The surface and tropopause data are also on the same horizontal grid. Seasonal and annual climatologies can be calculated using monthly data. A detailed description of the reanalysis dataset was given by Kalnay *et al*. (1996).

2.1.5 The CRU Dataset

The CRU Global Climate Dataset, available through the IPCC Data Distribution Centre, consists of a multivariate analysis on a 0.5° × 0.5° horizontal resolution grid for global land areas, excluding Antarctica. There is a monthly time series for the period 1901-2012. Data are available for eleven surface variables:

- precipitation and wet-day frequency
- mean, maximum and minimum temperature
- vapour pressure and relative humidity
- sunshine percentage and cloud cover
- frost day frequency
- potential evapotranspiration

Climatologies also include sunshine percentage and wind speed. Details of this dataset are provided by New *et al*. (1999) and Mitchell and Jones (2005).

2.1.6 GPCP

The GPCP dataset has spatial and temporal patterns of precipitation globally from 1979 to the present over the land and oceans. This dataset has been created by the NASA Goddard Space Flight Center from sounding observations and observations from over 6,000 rain gauge stations, in addition to geostationary and low-orbit infrared and passive microwave data from satellites. Merged precipitation data are on a 2.5° × 2.5° global grid. Uncertainties associated with the estimates are also provided as part of the GPCP products. The GPCP data can be used to investigate changes in precipitation characteristics on seasonal to inter-annual time scales and also for validating simulated precipitation from coupled ocean-atmospheric models for the present-day climate. Further details of this dataset can be found in Adler *et al.* (2003).

2.1.7 APHRODITE

APHRODITE is the Asian Precipitation Highly Resolved Observational Data Integration Towards Evaluation of Water Resources project. The APHRODITE project began in 2006 to develop state-of-the-art daily precipitation datasets on high-resolution grids covering the whole of Asia with 0.25° latitude × 0.25° longitude grid resolution. This daily precipitation dataset has been created from station data from Asia and Europe, by sub-regions. The sub-regions are Northern Eurasia, Monsoon Asia, the Middle East and Japan. Compared with other global precipitation datasets, this dataset has higher resolution, so it captures the effects of orography over complex mountainous regions such as the Himalayas and parts of South East Asia, and also over parts of Europe. The dataset is available for the period 1951 to 2007. Details of selected stations, algorithms for spatial interpolation, quality control and the products available are given by Yatagai *et al.* (2012).

Table 2-2: Climate variables and details of a number of global and regional gridded datasets.

CLIMATE VARIABLES	DESCRIPTION	SOURCES
Rainfall	Average annual, monthly, daily rainfall (1951-2007)	APHRODITE
Temperature	Average, annual, monthly and daily temperature (1961 to present)	
Rainfall	Monthly, 1979 to present	Global Precipitation Climatology Project (GPCP)
Precipitation and wet-day frequency; mean, maximum and minimum temperature; vapour pressure and relative humidity; sunshine percentage and cloud cover; frost frequency; wind speed	Monthly climatology (1961-1990)	Climate Research Unit, East Anglia (CRU)
Atmospheric variables at surface and upper levels and rainfall	Daily time scale (1957 to 2002)	ERA-40 ERA-Interim
Atmospheric variables at surface and upper levels and rainfall	6 hourly (00, 06, 12 and 18 UTC), monthly and annual data (1948 to present)	NCEP reanalysis

2.2 EMISSION SCENARIOS FOR CMIP5

GCMs provide the best available tools for simulating broad-scale future climates based on various greenhouse gas and aerosol emission scenarios. The global and regional simulations for the period through 2005 presented in this project were driven by observed changes in greenhouse gases and aerosols. Some simulations included direct and indirect effects of aerosols, some included ozone depletion, and some included volcanic aerosols and solar forcing. The latest 21st century (from 2006 onwards) climate change simulations for the *Fifth Assessment Report* of the IPCC are driven by Representative Concentration Pathways (RCPs). The RCPs describe a wide range of potential futures for the main drivers of climate change: greenhouse gases, air-pollutant emissions and land use changes. For the current project, the lower RCP 4.5 and higher RCP 8.5 emission scenarios are defined in terms of radiative forcings of 4.5 and 8.5 Wm^{-2} by the end of the 21st century. RCP 8.5 represents the upper range of concentrations, while RCP 4.5 is near the lower range of concentrations. GCM climate change simulations produced for prior IPCC assessments used the alternative SRES emission scenarios for evolving concentrations of CO_2 and other greenhouse gases. The evolution over time of the equivalent CO_2 concentrations for a range of SRES and RCP concentrations is shown in Figure 2-1. It can be seen that RCP 8.5 approximately follows the A1FI- SRES emission scenario and RCP 4.5 follows the B1-SRES emission scenario.

2.3 CLIMATE MODELS

GCMs include complex interactions of atmospheric flow, clouds, radiative transfer, and biospheric behaviour, as well as ocean and sea ice behaviour. The various processes included in GCMs and their interactions are illustrated in Figure 2-2. This complexity makes GCMs effective tools for simulating broad-scale features of future climate, but it also makes them computationally expensive due to the large number of processes being modelled and the large number of simulations required for use in intercomparisons such as CMIP5, where various research organisations around the world run their models under similar conditions to compare model performance. As a consequence, GCM resolution is usually restricted to 100 km or coarser. GCMs all have biases and various inadequacies due to such factors as model configuration, resolution, differing internal dynamics and parameterisations. For this project, suitable outputs from up to 24 GCMs were available, but due to computational cost, it was only possible to run a modest number of downscaled simulations, with a sample of possible emission scenarios. For this reason, it is desirable to select the most credible GCMs for downscaling. The selection criteria we used to choose the GCMs for this study are discussed in Section 2.3.1.

Figure 2-1: Comparison of equivalent CO_2 concentrations (ppmv) from SRES (A1B, A1FI, A2, B1) and RCP (3[7], 4.5, 6.0, 8.5) approaches (Meinshausen *et al*., 2011).

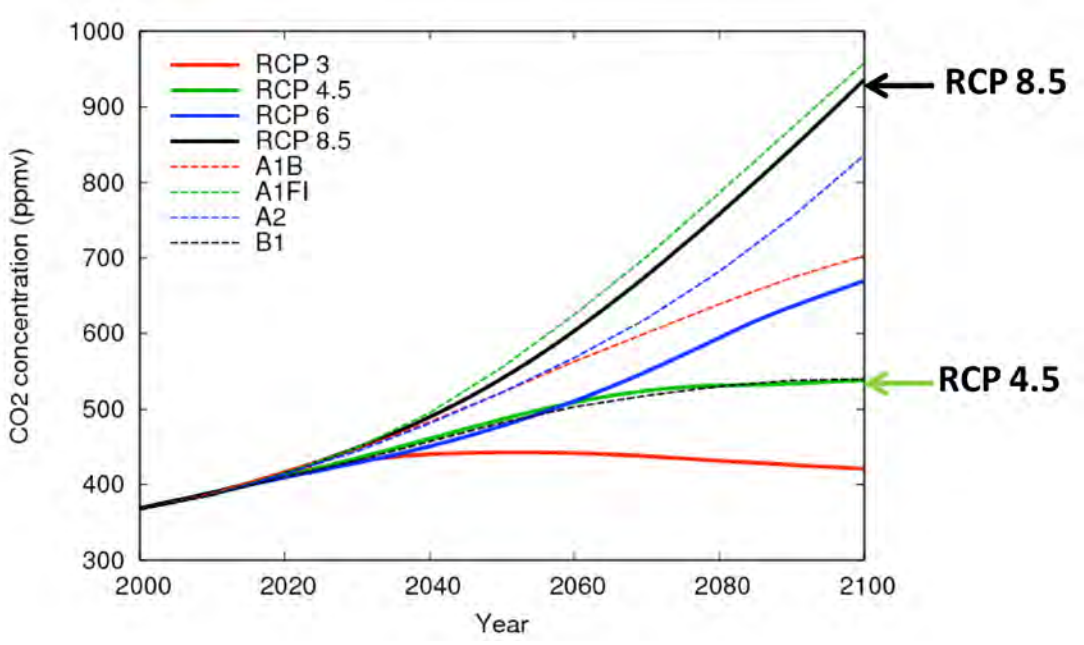

7 Note that for the lowest emission scenario, called RCP 2.6 in this report, the radiative forcing peaks at 3 Watts m^{-2} then declines to 2.6 Watts m^{-2} by the end of the 21st century.

Figure 2-2: An illustration of the various processes included in GCMs and their interactions. Source: CMAR Graphics.

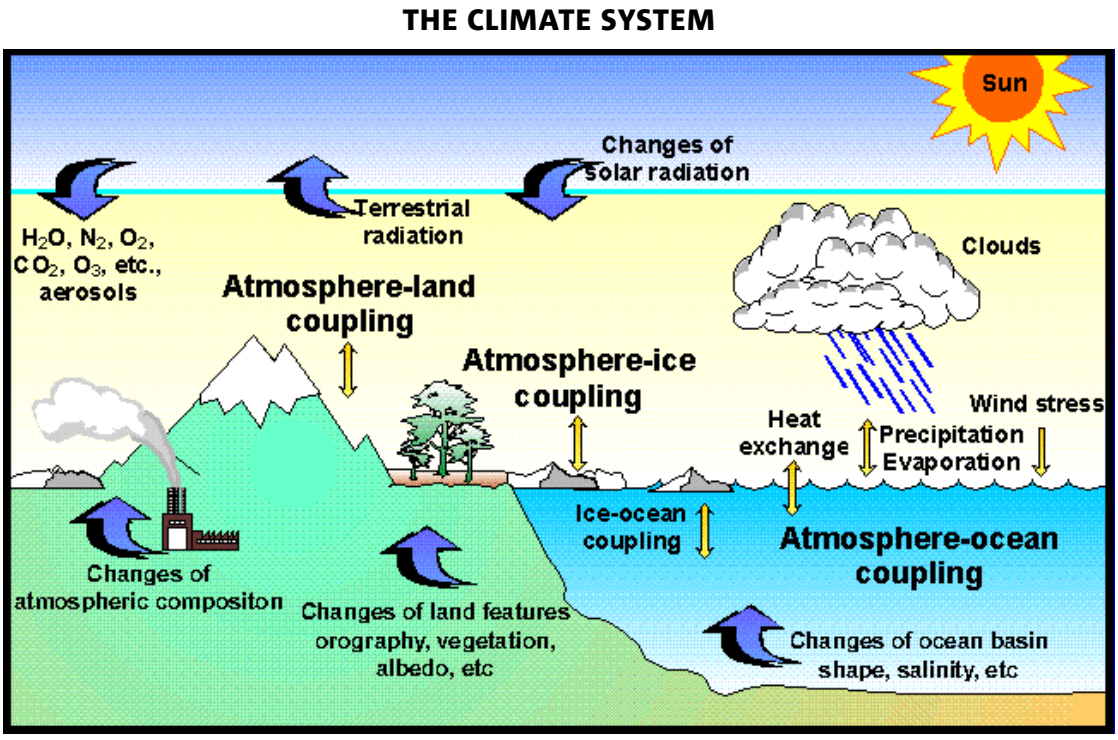

Climate modelling over the Asian region involves particular complexities, including regional processes (such as tropical convection, monsoons and tropical cyclones), complex land use and significant orography (including the Himalayas and the Tibetan plateau). Extra effects from snow and snow melt must also be considered. Monsoon behaviour in the region is difficult to simulate well in GCMs. This is partly related to a lack of horizontal detail in GCMs, meaning that the various topographic interactions with the atmospheric flow and also the air-sea interaction process are not adequately captured. The complex topography also affects the ability to properly represent relevant physical processes within the models. In addition, GCMs still have problems in fully capturing the inter-annual variability of the ocean temperatures related to El-Niño Southern Oscillation (ENSO).

There is thus a requirement for quite fine resolution over the Asian region to resolve the complex topographic and coastal features and processes. One approach, called dynamical downscaling, is to use high-resolution atmospheric models, or RCMs, formulated with the same dynamical equations of motion as the GCMs. The dynamical downscaling technique has been available for over 20 years, and a number of review papers are available, including those of McGregor (1997), Wang *et al*. (2004b), Evans *et al*. (2012) and Katzfey (2013). The GCMs typically have a horizontal resolution of 100 to 200 km, whereas the RCMs in this project have resolution of 10 to 50 km. As described in Section 2.5, the various RCMs used in this study provide comprehensive simulations of atmospheric, radiative and land processes, but do not include separate ocean model simulations.

2.3.1 GCM selection for downscaling

The performance of 24 GCMs is compared in this section and the GCMs are ranked according to their present-day performance over the South East Asia region. As a result of the comparison, the following six GCMs were selected to be downscaled to fine resolution for this project:

1. CNRM-CM5
2. CCSM4
3. NorESM1-M
4. ACCESS1.0
5. MPI-ESM-LR
6. GFDL-CM3

Downscaling the results of all available CMIP5 GCMs is computationally too expensive at present. However, to reflect the uncertainty of the climate projections, ensemble simulations of GCMs are needed. For this project, data from a subset of six different GCMs provide a compromise between computational costs and the provision of a range of different climate change signals that arise from model-to-model variations. The decision on which of the available models to downscale was based on three criteria:

- First, the models should capture the observed spatial patterns of the current climate with small values of Root Mean Square Error (RMSE) and high pattern correlations. The observed climatology of atmospheric variables such as Mean Sea Level Pressure (MSLP), temperature and rainfall should be reproduced by the models, as well as the observed trends.

- The second criterion relates to the downscaling method applied in this project. Since only the bias- and variance-corrected SSTs and sea ice concentrations (SIC) are used from the GCM outputs to initialise the climate simulations by some RCMs, oceanic features should be simulated well by the selected GCMs. The representation of larger scale phenomena such as ENSO, which have a large impact on the climate variability of Vietnam and surrounding countries (see Section 3.4.1), is crucial for the results of the regional climate simulations.
- The third criterion used is the selection of models to represent the full range of possible future changes in SSTs, to address the uncertainty inherent in climate modelling and capture the most probable/realistic range of changes in climate variables such as temperature and rainfall.

Initially, a ranking of the models based on the first two criteria was prepared using studies that focused on CMIP5 simulations. At the time of this study, there were over 30 evaluation studies available, but most of them do not provide a ranking, or consider only a small subset of the CMIP5 models. For the first criterion, results of the analyses conducted in this project and results of three additional studies were incorporated. Based on the results of the validation of model simulations of current climate (see Chapter 5), the GCMs were ranked according to the RMSE values for annual temperature and rainfall (Table 2-3) as well as the pattern correlation of the annual rainfall. The ranking by Bhend (personal communication), which is based on the analyses of Bhend and Whetton (2013), was constructed using the agreement between observed and simulated temperature trends. Watterson *et al*. (2013a, b) ranked the models using a skill score, which combined the agreement of the models with observations of temperature, rainfall and MSLP. Watterson *et al*. (2013a) ranked the models on global-scale performance, while Watterson *et al*. (2013b) provided a ranking focusing just on results for Asia.

For the second criterion, a review of the three different studies that focused on SSTs was conducted. Grose *et al*. (2013) analysed the GCM SSTs in the Pacific Ocean with a special focus on the two El Niño regions (the Central and Eastern Pacific regions). They also investigated the observed and simulated frequency of extremes of the ENSO phenomenon, El Niño and La Niña events. Kim and Yu (2012) correlated the spatial patterns of the two types of El Niño with the observed patterns, while Kug *et al*. (2012) focused on the temporal correlation between both types. Results of these studies indicate how well the spatial and temporal patterns of the ENSO phenomenon are represented in the models.

The rankings of the individual studies were averaged to yield a final ranking of the models. If there was more than one ranking from a single study (e.g. for rainfall and temperature) these rankings were averaged in order to produce just one ranking per study. Not all studies considered had the same number of GCMs used in the rankings. Therefore, the rankings were normalized by the number of models analysed in the individual studies. Consequently, the possible range of the averaged score could vary between 0.15 (best model of the set of 24 models) and 1.0 (worst model). The final scores for the different models are listed in Table 2-3.

Table 2-3: List of CMIP5 GCMs based on their average performance in different evaluation studies. Models selected for downscaling in this project are indicated by blue shading.

RANK	GCM	AVERAGE SCORE
1	CNRM-CM5	0.31
2	CCSM4	0.34
3	ACCESS1.3	0.35
4	NorESM1-M	0.35
5	ACCESS1.0	0.39
6	MPI-ESM-LR	0.41
7	GFDL-CM3	0.42
8	HadGEM2-CC	0.44
9	MIROC4h	0.46
10	MIROC5	0.47
11	GFDL-ESM2M	0.48
12	MRI-CGCM3	0.51
13	HadCM3	0.53
14	IPSL-CM5A-MR	0.53
15	HadGEM2-ES	0.54
16	FGOALS-g2	0.57
17	CSIRO-Mk3.6.0	0.57
18	INMCM4	0.61
19	CanESM2	0.61
20	MIROC-ESM-CHEM	0.69
21	GISS-ES-H	0.70
22	IPSL-CM5A-LR	0.71
23	FGOALS-s2	0.80
24	MIROC-ESM	0.84

The third and final criterion used is based upon the magnitude and pattern of the SST change. The range of changes in both spatial pattern and magnitude of SSTs for nine of the best-performing models is shown in Figure 2-3. NorESM1-M shows the smallest increase in magnitude and GFDL-CM3 the largest increase. The magnitude changes in CNRM-CM5 and CCSM4 are small as well, while ACCESS1.3 and ACCESS1.0 show larger increases. MPI-ESM-LR simulated a moderate increase. Based on these results, the top six models were selected for the project (shaded in Table 2-3). Note that ACCESS1.0 was selected to replace ACCESS1.3. ACCESS1.3 had a slightly better score because it performed well in the study by Kug *et al*. (2012), but that study did not include ACCESS1.0 because it was not available at the time of the evaluation. Table 2-4 presents a short summary of the strengths and limitations of the selected models.

Figure 2-3: SST changes in the tropical Pacific (°C) from the nine best-performing models (MIROC4h is not available so results are given for MIROC5) for the months July-August by 2071-2100 compared with 1971-2000, based on the RCP 8.5 emission scenario.

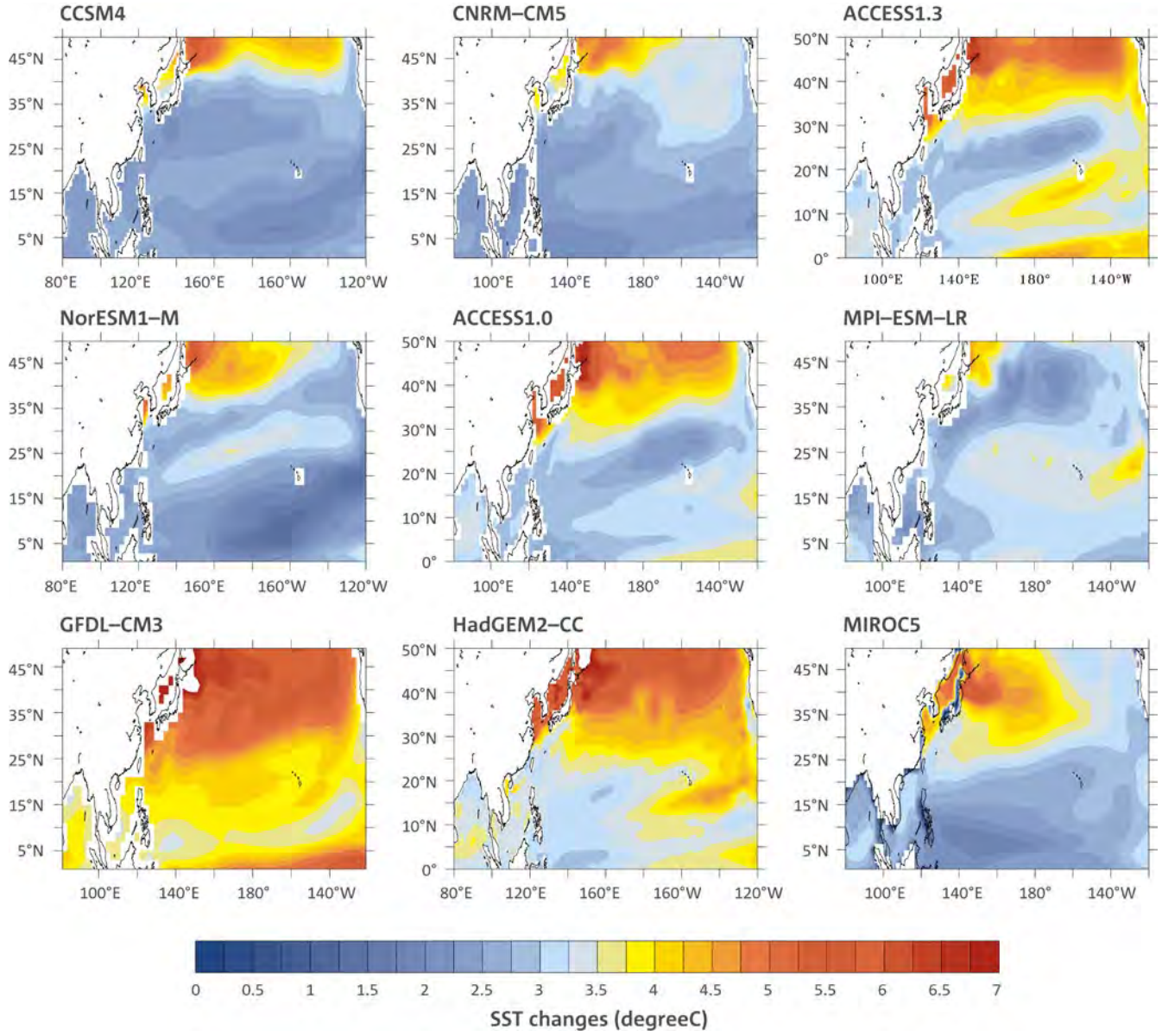

Table 2-4: Strengths and limitations of the six GCMs selected for downscaling.

GCM	STRENGTHS	LIMITATIONS
CCSM4	• Good agreement with mean rainfall and temperature observations over South East Asia • ENSO pattern well reproduced	• Observed temperature trends poorly reproduced • Less realistic SST pattern in the tropical Pacific
CNRM-CM5	• ENSO pattern well reproduced • Good agreement with rainfall observations over South East Asia • Good agreement with observations globally and over Asia	• Observed trends poorly reproduced over South East Asia • Too few ENSO events
NorESM1-M	• ENSO pattern and tropical Pacific SSTs well reproduced	• Poor agreement with rainfall observations over South East Asia
ACCESS1.0	• SSTs in the Pacific well reproduced • Observed temperature trends well reproduced • Good agreement with observations globally	• Poor agreement with rainfall observations over South East Asia
MPI-ESM-LR	• ENSO pattern and SSTs in the Pacific well reproduced • Good agreement with temperature observations over South East Asia	• ENSO variability not well reproduced
GFDL-CM3	• Good agreement with rainfall observations over South East Asia	• Poor agreement with temperature observations over South East Asia

2.4 BIAS CORRECTION OF SSTs

As previously discussed in this chapter, GCMs simulate the global climate reasonably well, but still have biases and do not simulate inter-annual variability in the atmospheric and oceanic system (e.g. ENSO) realistically. To improve the dynamical downscaling results, Sea Surface Temperature (SST) biases in GCMs can be corrected before the GCM results are used by RCMs (at least in the global CCAM; LAMs which use atmospheric data from GCMs cannot use this technique). The deficiencies or biases of GCMs, due to differing model configurations and physics, if not corrected before downscaling can cause unrealistic behaviour of the RCM simulations and thereby affect the reliability of the climate projections. In previous downscaling simulations with CCAM, a simple correction of the climatological monthly means was applied to GCM SSTs (Katzfey *et al.*, 2009 and Nguyen *et al.*, 2012). However, this method preserved the inter-annual (year-to-year) variation of GCM SSTs. Therefore, GCM errors in variability of SSTs, such as those related to ENSO, were also imposed upon the downscaled simulations. Several studies have shown that this variability, especially in the tropical Pacific, is still unsatisfactorily modelled even by the latest CMIP5 GCMs. Therefore a newly-developed method that corrects both the mean and variability of monthly model SSTs was applied in this project. Consequently, while the climate change signals of the GCMs are preserved in the downscaled simulations, the location of the ENSO variability is more realistic. It should be noted that the frequency of the ENSO variability is coming from the GCMs and was not adjusted.

The GCM SSTs are corrected to match the Optimum Interpolation SST dataset version 2 (Reynolds *et al.*, 2007), which contains daily SST and SIC data on a 0.25° longitude by 0.25° latitude grid for the period 1982 (September) to 2011. The dataset is based on measurements conducted by NOAA's polar orbiting AVHRR meteorological satellites[8] in combination with buoy data and ship measurements. Since the GCM data are monthly averages, both SST and SIC daily data are averaged monthly for the computation of the bias correction. Additionally, prior to correction the model SSTs and SIC are interpolated to match the observation grid.

In the bias correction method, the following steps are conducted for each month of the year separately (see Katzfey *et al.,* 2009 for more details of the previous bias correction procedure):

1. The SST data is de-trended for 30-year backward running trends.
2. The standard deviation (SD), which is a measure of the year-to-year variability of the de-trended 30-year period, is calculated.
3. The yearly anomalies are corrected using the ratio of the observed SD to the model SD.
4. Monthly biases are then calculated and subtracted, giving the bias- and variance-corrected SSTs.

8 See **http://noaasis.noaa.gov/NOAASIS/ml/avhrr.html** for more information on AVHRR satellites.

Problems due to differences between SIC distribution in the GCMs and in the observations are avoided in the bias correction by reducing the correction near the ice edges as a function of SIC. In addition, the correction is linearly reduced from the equator to 50°N and 50°S. This means that the full variance correction is applied at the equator, but no variance correction is applied north of 50°N or south of 50°S. This step is necessary to avoid problems arising from the possible shift of strong ocean currents such as the Gulf Stream in a future climate. When omitting this step, the change signal can be quite different between corrected and uncorrected SSTs for those regions.

As an example, Figure 2-4 shows the uncorrected and corrected July SSTs from the ACCESS1.0 GCM as well as the observed SSTs in the tropical Pacific for the period 1982-2011. As intended, the GCM SSTs are very close to the observed SSTs after the correction. Also the standard deviation is very similar to the observations, especially close to the equator.

2.5 DYNAMICAL DOWNSCALING MODELS

2.5.1 Introduction

As mentioned at the beginning of this chapter, dynamical downscaling with RCMs is used in this study to produce fine-scale climate change information with appropriate data provided by six GCMS selected from the CMIP5 simulations. The RCMs, like GCMs, solve the atmospheric equations of motion and the associated parameterisations for moist and dry processes, turbulence, radiation and surface interactions with land and sea. Several different RCMs are employed in this study by the various participating institutes.

RCMs have become important tools for the prediction of climate variability and change in the regions of southern and eastern Asia. For instance, Afiesimama *et al*. (2006) used RegCM3 (RegCM model, version 3) to simulate the Indian summer monsoon and showed that the average rainfall over the region is well represented by the model, which demonstrates considerable skill in reproducing the extreme rainfall regimes. Francisco *et al*. (2006) applied the RegCM model to simulations of monsoonal rainfall over the Philippines and found that the model could reproduce observed monsoonal rainfall patterns well.

At CSIRO, the Conformal-Cubic Atmospheric Model (CCAM; McGregor 2005b; McGregor and Dix 2008) is used for dynamical downscaling. This adopts the fairly recent development of using a variable-resolution GCM as an RCM, where the region of interest can have fine resolution (10 km or less) and be represented by many grid points, while areas on the opposite side of the globe may have extremely coarse resolution and be represented by only two or three grid points. Because the model is global, it is easier to incorporate large-scale dynamical processes that affect the small region studied.

For their dynamical downscaling RCM simulations, IMHEN and HUS have employed several limited-area models (LAMs), driven at their lateral boundaries by coarser resolution host simulations but run at higher resolution only over the smaller area of interest, due to computational limitations. Details of the various limited-area RCMs are provided later in this section.

Figure 2-4: Mean (top panel) and standard deviation (bottom panel) of July SSTs for the period 1982-2011 from (a, d; left) uncorrected ACCESS1.0 results, (b, e; middle) corrected ACCESS1.0 results and (c, f; right) observed data from the Optimum Interpolation SST dataset version 2 (Reynolds *et al*., 2007).

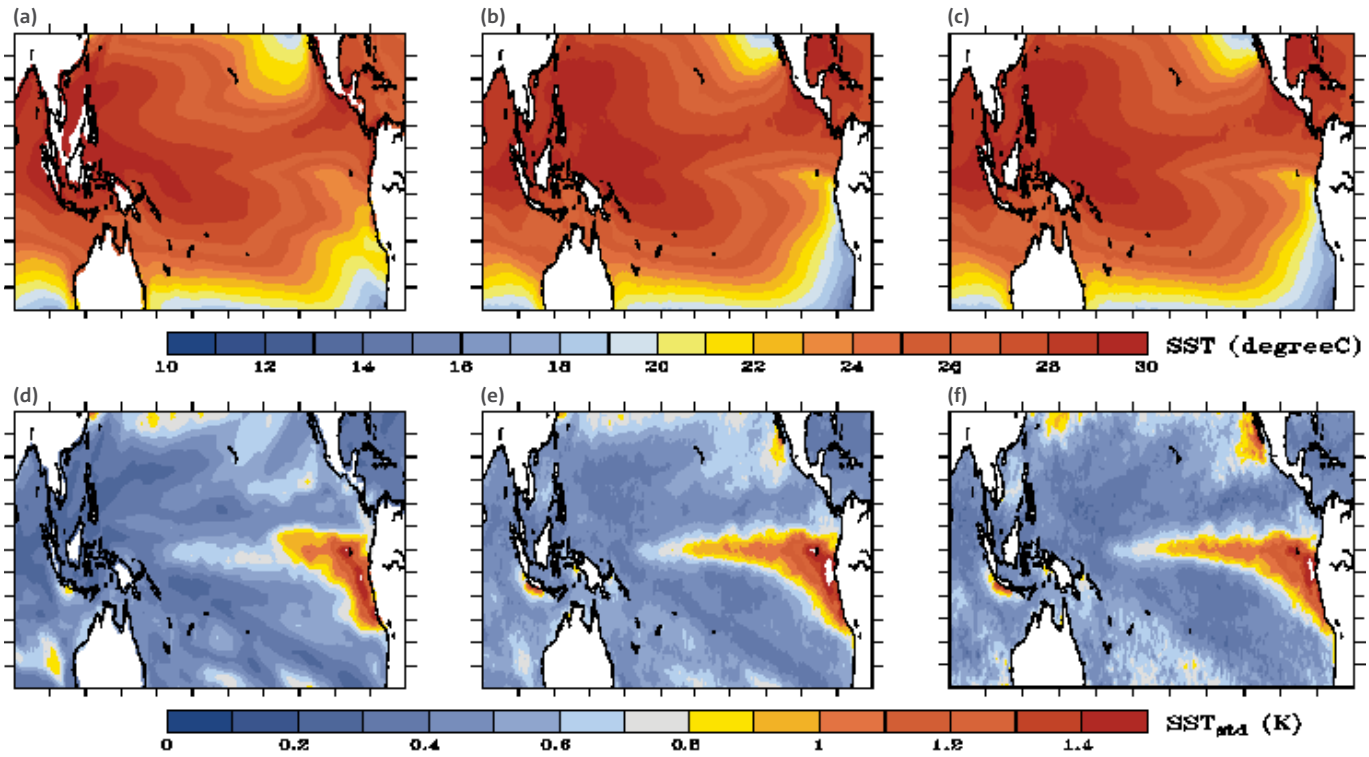

Unlike variable-resolution GCMs which have no lateral boundaries, limited-area RCMS can experience reflections of atmospheric waves near their lateral boundaries, which can produce spurious vertical velocities and associated rainfall near those boundaries. Thus the simulated rainfall is usually ignored near the lateral boundaries of limited-area RCMs. Until recently it was considered to be quite expensive to run RCMs for long simulations, so only a small number of runs were typically performed. However, with computational advances, it has become possible to run RCMs to obtain climate simulations downscaled from a variety of host models and scenarios.

Each model used in this study is described briefly below, giving key features of its formulation and parameterisations. For more complete descriptions of the models, refer to the references.

2.5.2 Conformal Cubic Atmospheric Model (CCAM)

CCAM is a variable-resolution global atmospheric model that has been developed at CSIRO (McGregor 2005b; McGregor and Dix 2001, 2008). CCAM includes a fairly comprehensive set of physical parameterisations to represent sub-grid scale atmospheric processes that are not directly simulated by the model. The updated GFDL parameterizations for long-wave and short-wave radiation (Schwarzkopf and Ramaswamy 1999; Freidenreich and Ramaswamy, 1999) are employed, with interactive cloud distributions determined by the liquid- and ice-water scheme of Rotstayn (1997). The simulations also include the scheme of Rotstayn and Lohmann (2002) for the direct and indirect effects of sulphate aerosols. The model employs a stability-dependent boundary-layer scheme based on Monin–Obukhov similarity theory (McGregor *et al*., 1993). The CABLE biosphere-atmosphere exchange model is included, as described by Kowalczyk *et al*. (2006), having six layers for soil temperatures, six layers for soil moisture (solving the Richards equation), and three layers for snow. The cumulus convection scheme uses mass-flux closure as described by McGregor (2003), and includes downdrafts and detrainment. CCAM also includes a simple parameterisation to enhance SSTs under conditions of low wind speed and large downward solar radiation, affecting the calculation of surface fluxes.

The dynamical formulation of CCAM includes a number of distinctive features. The model is non-hydrostatic, with two-time-level semi-implicit time differencing. It employs semi-Lagrangian horizontal advection with bi-cubic horizontal interpolation (McGregor, 1993; McGregor, 1996), in conjunction with total-variation-diminishing vertical advection. The grid is un-staggered, but the winds are transformed reversibly to/from C-staggered locations before/after the gravity wave calculations, providing improved dispersion characteristics (McGregor, 2005a). Three-dimensional Cartesian representation is used during the calculation of departure points, and also for the advection or diffusion of vector quantities. CCAM may be employed in quasi-uniform mode or in stretched mode by utilising the Schmidt (1977) transformation. Further details of the model dynamical formulation are provided by McGregor (2005b).

2.5.3 RegCM4.2

The Regional Climate Model version 4.2 (RegCM4.2) developed at the Abdus Salam International Centre for Theoretical Physics (ICTP) in Trieste, Italy, is used in the project. RegCM4.2 is a primitive equations, hydrostatic, compressible, limited-area model with sigma-pressure (σ) vertical coordinates. The model runs with 18 vertical σ-levels. The experiments conducted in this project use the Grell scheme with a simplified form of the Arakawa-Schubert closure assumption for convective parameterization (Grell, 1993; Arakawa & Schubert, 1974). Exchanges of energy, moisture, and momentum between the land surface and the atmosphere are computed using the Biosphere-Atmosphere Transfer Scheme (BATS; Dickinson *et al*., 1993). The domain covers 100°E to 120°E and 6°N to 25.5°N with horizontal resolution of 20 km for both east-west and north-south directions. The Mercator Conformal projection is used. SST and lateral boundary conditions are updated every 6 hours.

2.5.4 PRECIS

While not part of this project, some previous results from the PRECIS model are presented in this report. PRECIS is a regional climate modelling system developed by the UK Met Office Hadley Centre. It is based on the atmospheric component of the HadCM3 climate model (Gordon *et al*., 2000) and is extensively described by Jones *et al*. (2004). PRECIS consists of a coupled atmospheric and land-surface model describing processes related to dynamical flow, atmospheric sulphur cycle, clouds, precipitation, radiation, land surface and deep soil. The atmospheric component of the PRECIS model is a hydrostatic version of the full primitive equations model. A full description of the model and its parameterisation scheme is documented in Jones *et al*. (2004). There are 19 vertical levels based on hybrid vertical coordinates, the lowest at approximately 50 m and the highest at 0.5 hPa (Simmons and Burridge, 1981). For this project, PRECIS is used as a limited-area model. It has been configured for a domain extending from about 5°S to 35°N and 92.5°E to 122°E with a horizontal resolution of 0.22° in both latitude and longitude, which corresponds approximately to 25 km.

2.6 DYNAMICAL DOWNSCALING METHODS

The following section describes the methods used to produce the dynamically-downscaled simulations for this study. The process had two steps:

1. Global simulations with initial input from six CMIP5 GCMs (see Section 2.3.1 for details of selection process) were completed using CCAM with a uniform grid.
2. These global simulations were dynamically downscaled to fine resolution, using two RCMs, CCAM with variable-resolution or the limited-area RegCM4.2 model, in order to produce current climate or future climate simulations at regional scale.

The process is known as dynamical downscaling, because the equations on which the model is based explicitly simulate atmospheric dynamical and thermodynamical processes, in contrast to other methods, such as statistical ones, that can be used to carry trends into the future for climate projections.

CCAM, a global model, requires only SST and SIC data from the GCMs as inputs to drive the model. RegCM4.2, a limited area model, requires input of more detailed initial and boundary condition data, including atmospheric variables such as MSLP, temperature and wind. In this project, these were supplied by CCAM.

For PRECIS, the third model presented in this study, the downscaling procedure was somewhat different. The initial and boundary conditions for this LAM were obtained from (1) coupled atmosphere-ocean GCM runs from CMIP3 using the older SRES emission scenario and (2) a reanalysis dataset.

The resolutions of the GCM and RCM grids, emission scenarios used, and time periods for the various simulations varied due to technical and computer resource constraints. For details of the set-up of the three types of downscaled simulations, see the following sections and Table 2-5.

2.6.1 CCAM

Step 1: CCAM at 50 km resolution

For these simulations, CCAM is first set up on a C192 grid (with six panels each of 192 x 192 grid points) having a quasi-uniform horizontal resolution of about 50 km over the whole globe (Figure 2-5, top) and 27 vertical levels. It is run for 130 model years (1970–2099) forced by SSTs from each of the six selected CMIP5 GCMs. From 1970 to 2005, historical values of greenhouse gases and aerosols were used. The simulations from 2006 to 2099 are performed for both the RCP 4.5 and RCP 8.5 emission scenarios. As described above in Section 2.4, the biases and variances of the GCM SSTs were corrected before inputting into CCAM. Note that in the rest of report, the end year of the simulations is referred to as 2100.

Step 2: CCAM at 10 km resolution

Each of the CCAM quasi-uniform global simulations is further downscaled using CCAM to 10 km resolution over Indochina, utilizing the C96 grid shown in Figure 2-5 (lower plot). To provide a further degree of consistency with the host CCAM simulation, a scale-selective digital filter (Thatcher and McGregor, 2009) is applied every 6 hours to replace selected broad-scale (with length-scale about the width of Indochina) fields of the high-resolution CCAM simulation with the corresponding fields of the 50 km CCAM simulation. The filter was applied to the MSLP, moisture, temperature, and wind components above pressure-sigma level 0.9 (about 1 km above the surface).

The full model output was saved four times per day at 00, 06, 12 and 18 GMT. These data have been post-processed by interpolating them onto a 0.5° grid for the 50 km simulations, and a 0.1° grid for the 10 km simulations for easier interpretation. Many prognostic and diagnostic fields are available.

2.6.2 RegCM4.2

Step 1: CCAM at 100 km resolution

For the RegCM4.2 simulations, CCAM is first set up on a quasi-uniform C96 grid (with 6 x 96 x 96 grid points) having a resolution of about 100 km over the whole globe and 18 vertical levels. CCAM C96 is run for three 21-year time slices: 1980-2000, 2045-2065 and 2080-2100, forced by the bias-corrected SSTs of two of the global models used in the CCAM downscaling process, ACCESS 1.0 and NorESM1-M. Simulations are performed for both the RCP 4.5 and RCP 8.5 emission scenarios, as above. Because of computing constraints, CCAM was run at a coarser resolution (100 km versus 50 km) and only for three time slices, representing the current, mid-century and the end of the century climates, instead of for a continuous period.

Step 2: RegCM4.2 at 20 km resolution

The CCAM 100 km outputs are then used to create the initial and boundary conditions, updated every 6 hours, for the limited-area RegCM4.2 simulations. The model output was saved four times per day at 00, 06, 12 and 18 GMT. These data cover the domain from 100°E to 120°E and from 6°N to 25.5°N (Vietnam plus part of the East Sea), with horizontal resolution of 20 km for both east-west and north-south directions. The Mercator Conformal projection is used. Many prognostic and diagnostic fields have been saved.

2.6.3 PRECIS

For this project, PRECIS has been configured for a domain extending from about 5°S to 35°N and 92.5°E to 122°E, covering the Indochina Peninsula. Five members of the Hadley Centre perturbed physics ensemble (HadCM3Q) for years corresponding to 1950–2100 and ERA-Interim for years corresponding to 1989–2007 were used to provide the initial and boundary condition data for the PRECIS simulations, which had a resolution of approximately 25 km. The HadCM3Q models used to provide input were from CMIP3, not CMIP5, as for CCAM and RegCM4.2, and the emission scenario used was the older SRES A1B (medium), while the other simulations used the more recent RCP 8.5 (higher) and RCP 4.5 (lower) emission scenarios. There is no bias correction of input data, as there is for the simulations based on CCAM.

A summary of the downscaled simulations used for the project is provided in Table 2-5.

Figure 2-5: CCAM grids used for the 50 km global (C192 grid; top) and 10 km (C96 grid; bottom) downscaled simulations over Vietnam (plotting every 2nd grid point).

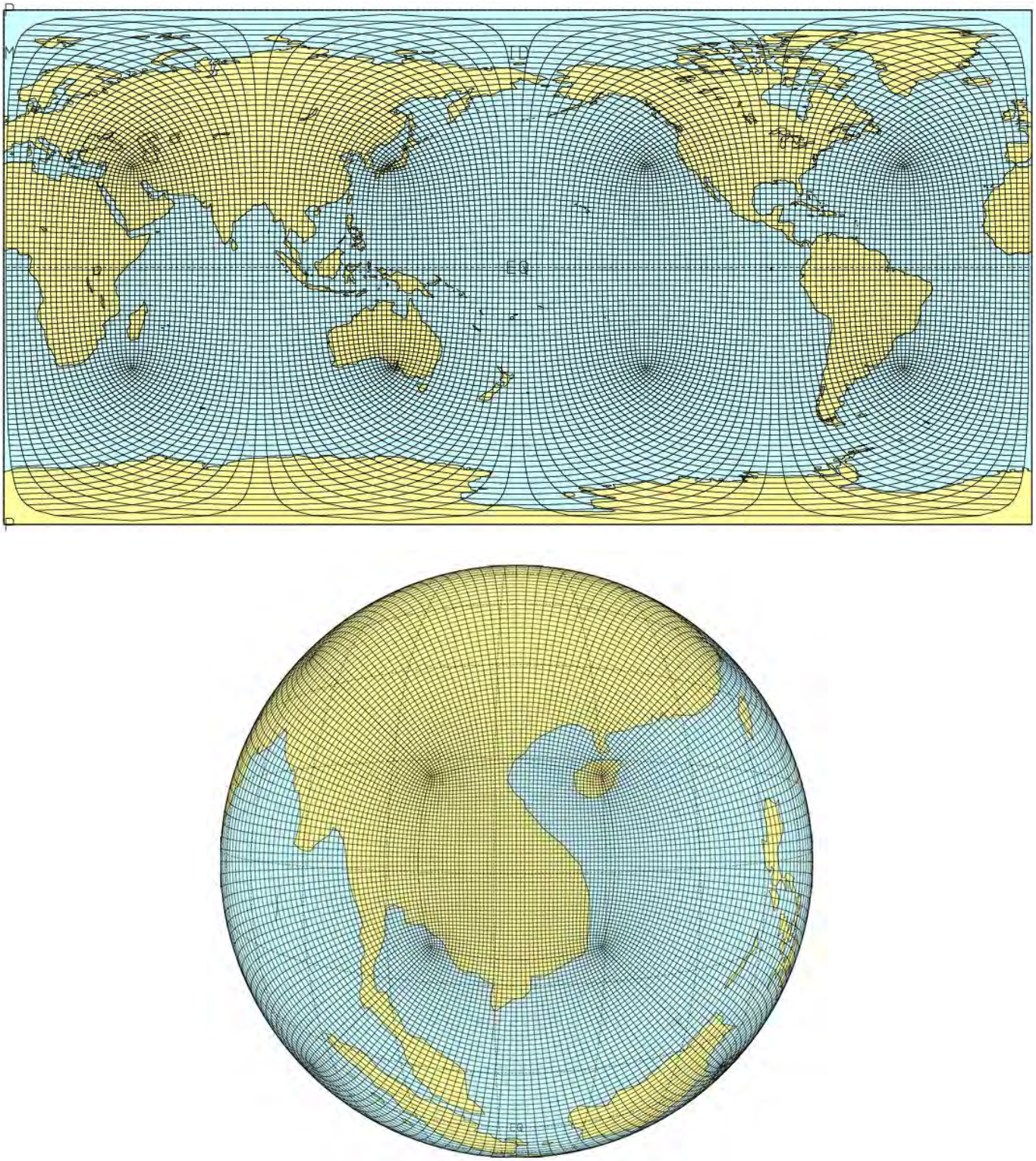

Table 2-5: List of RCMs used in this project, with their resolution, number of levels, and some details of the simulations.

MODEL	RESOLUTION/ VERTICAL LEVELS	GCM DATA USED	INPUT DATA	YEARS SIMULATED	EMISSION SCENARIOS
CCAM	50 km /L27	CNRM-CM5 CCSM4 ACCESS1.0 NorESM1-M MPI-ESM-LR GFDL-CM3 (ERA-Interim for validation)	Sea ice and variance- and bias-corrected SSTs	1970-2100 1979-2009	RCP 8.5 RCP 4.5
CCAM	10 km/L27		CCAM 50 km	1970-2100	RCP 8.5 RCP 4.5
CCAM	100 km/L27	ACCESS1.0 NorESM1-M	Sea ice and variance- and bias-corrected SSTs	1970-2100	RCP 8.5 RCP 4.5
RegCM4.2	20 km/L19	 (ERA-Interim for validation)	CCAM 100 km	1980-2000 2045-2065 2080-2100 1979-2000	RCP 8.5 RCP 4.5
PRECIS	25 km/L19	HadCM3Q (ERA-Interim)	HadCM3Q	1951-2100 1989-2007	SRES A1B

3 OBSERVED CLIMATE VARIABILITY OF VIETNAM

3.1 OVERVIEW

Most of Vietnam has a tropical climate and is controlled by the South West and North East Monsoons, although subtropical northern areas experience cool winters. Figure 3-1 shows a schematic view of large-scale circulation features that influence the climate of Vietnam. The nation is vulnerable to extreme weather and climatic events such as floods and droughts, due to its location within the tropics and in the western part of the Pacific Ocean. The complex topography of the country results in strong spatial variations in temperature and rainfall. Such variations are particularly evident during the monsoon seasons. El Niño-Southern Oscillation (ENSO) is the major phenomenon that dominates the variability of the climate on the inter-annual time scale, and cold wind surges from Siberia and Mongolia during the North East Monsoon Season influence the area on shorter time scales. Tropical cyclones that form over the Western Pacific frequently affect central and northern Vietnam and occasionally also the south. On average five to six tropical cyclones affect Vietnam per year. These tropical cyclones result in floods and salinity intrusion, raise sea levels and also generate storm surges in estuaries, inundating agricultural lands. The Red River basin in the north and the Mekong Delta in the south are flooded almost annually during the peak monsoon seasons. Major droughts and forest fires are associated with failure of monsoon rains, which are associated with ENSO variations on inter-annual time scales.

As mentioned earlier, the weather and climate of Vietnam are primarily controlled by two monsoons, the South West (summer) and North East (winter) Monsoons. These monsoons have their origin outside continental South East Asia and affect a vast area. Therefore, the country's major climatic seasons are defined based on monsoonal influences, with two monsoon seasons (South West and North East) and two inter-monsoon seasons (First and Second). The North East Monsoon Season (NEMS) lasts approximately from December to March and the South West Monsoon Season (SWMS) lasts from June to September. The months of April and May are defined as the First Inter-Monsoon Season (FIMS) and the months of October and November are defined as the Second Inter-Monsoon Season (SIMS).

A monsoon is described as a seasonal reversing wind due to the heating contrast between land and ocean, caused by solar radiation. The monsoon is often accompanied by strong winds and enhanced precipitation. The South West (summer) Monsoon arrives in the East Sea and over Vietnam around mid-May (Qian and Lee, 2000; Ding and Yanju, 2001; Wang *et al.*, 2004b; Nguyen *et al.*, 2009; Pham *et al.*, 2010) starting in early May from southern Vietnam and progressing north to eastern China in July. It is part of the larger scale South East Asian Summer monsoon system, and its arrival signifies the beginning of the summer monsoon over East Asia (Wang *et al.*, 2004b). Accompanying the monsoon are heavy rainfall events.

Figure 3-1: Major climate drivers that influence the climate of Vietnam. ITCZ: Inter-tropical Convergence Zone, ES: East Sea, ENSO: El Niño-Southern Oscillation phenomenon.

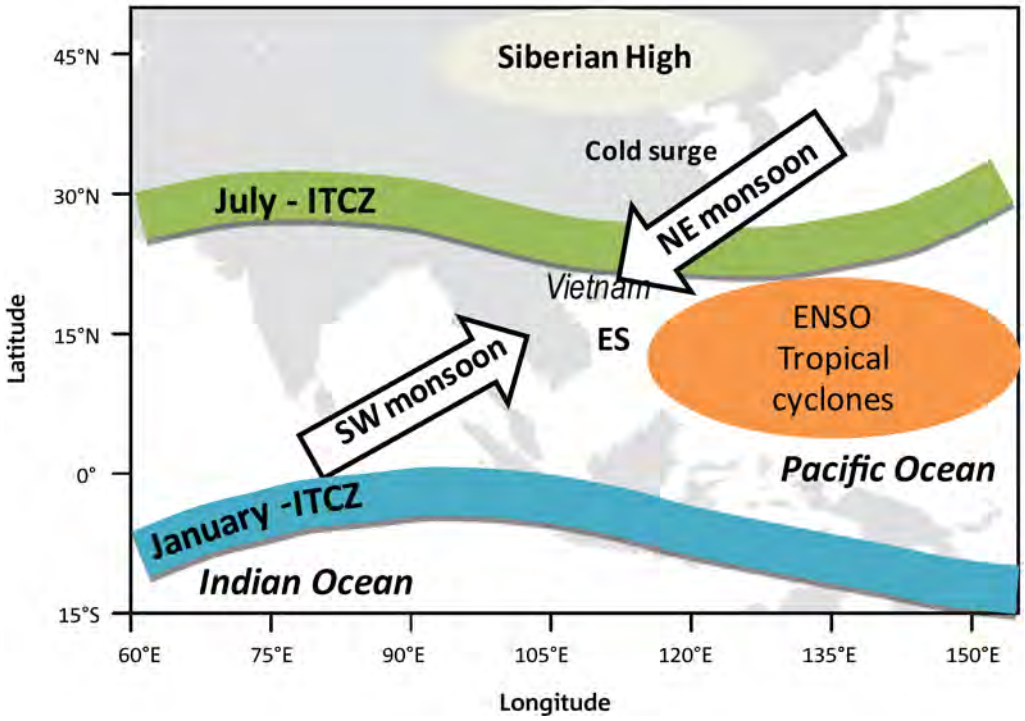

A study by Kajikawa *et al.* (2012) found that the onset of the Asian summer monsoon, including the South East Asian and Western North Pacific Monsoons, has been earlier in the recent decade. Over Vietnam, they show no trend for the regions NW, SC and CH used in this study. Onset dates are later over the NC region by +6 to +8 pentads (five-day periods). The onset dates over the S, NE and ND regions are about -2 to -6 pentads earlier. The authors suggest that the earlier onset and weakening of the South East Asian and Western North Pacific monsoons during early summer (June) can most likely be attributed to the heat contrast between the tropical Indian Ocean and the Asian landmass. Their study also suggests that the upward trend in May rainfall in recent decades reflects the advance of the summer monsoon onsets. Changes in monsoon onset dates and rainfall patterns may have possibly severe consequences for agriculture and water resources in Vietnam (see Section 7.5 for a discussion of changes to monsoon onset date projected by the RCMs used in this study).

In this chapter, we first provide a short description of the monsoonal-based seasonal atmospheric circulation patterns represented by MSLP and winds and their links to rainfall for the present-day climate, based on a number of previous studies (Thompson, 1951; Ramage, 1971; Nieuwolt, 1981; Lau and Chang, 1987; Ding and Sikka, 2006). Spatial patterns of mean seasonal rainfall and rainfall variability are also discussed. Second, trends in regional temperature and rainfall are discussed using station data. Third, characteristics of climate drivers that affect the climate of Vietnam, such as ENSO and tropical cyclones, and their inter-annual variability are described. The last section highlights gaps in the understanding of the present climate variability of Vietnam, providing opportunities for future research.

3.2 ATMOSPHERIC CIRCULATION AND RAINFALL

3.2.1 South West Monsoon Season

Average MSLP for the South West Monsoon Season (Figure 3-2) shows that most of South and South East Asia is occupied by low pressure, with the lowest pressure over the northwest portion of India. The Southern Hemisphere Sub-Tropical High extends northward over the Indian Ocean during this season, as shown by the northward extension of the high pressure belt. Winds at the 850 hPa level are also shown in Figure 3-2. There are two distinct air masses influencing the continental areas in South East Asia during the summer South West Monsoon season: (1) south-westerly winds from the Indian Ocean and (2) south-easterly trade winds from Australia and the southern Pacific.

The South West (summer) Monsoon is the main rainfall season for the region, but is strongest during the initial three months and begins to retreat during September. Orgill (1967) showed an average date of onset of May 17th, with a range of 33 days between May 1 (the earliest) and June 3 (the latest) dates. Analysis of the 850 hPa and 200 hPa winds and rainfall over Vietnam suggests that the mean observed onset date is May 18 for the period from 1979 to 2011, with a range of 53 days between the earliest (April 20) and the latest (June 12) onset date. There is a negligible difference when the onset dates are calculated for the period from 1980 to 2000, with an onset date of May 20 and a range of 50 days between the earliest (April 21) and the latest (June 10) dates (see Section 7.5). Figure 3-3 shows the inter-annual variability of the onset of the South West Monsoon over the South region (S) from 1979 to 2011. It is evident that the monsoon onset tends to be late during El Niño years and earlier during La Niña years. Such a relationship is strong before 1993 and weak thereafter. This figure also shows that onset date tends to be earlier in most years after 1993.

Figure 3-2: Average MSLP (left panel) and winds at the 850 hPa level (right panel) during the South West Monsoon Season (SWMS) for the current climate (1975-2004). Source: ERA-Interim.

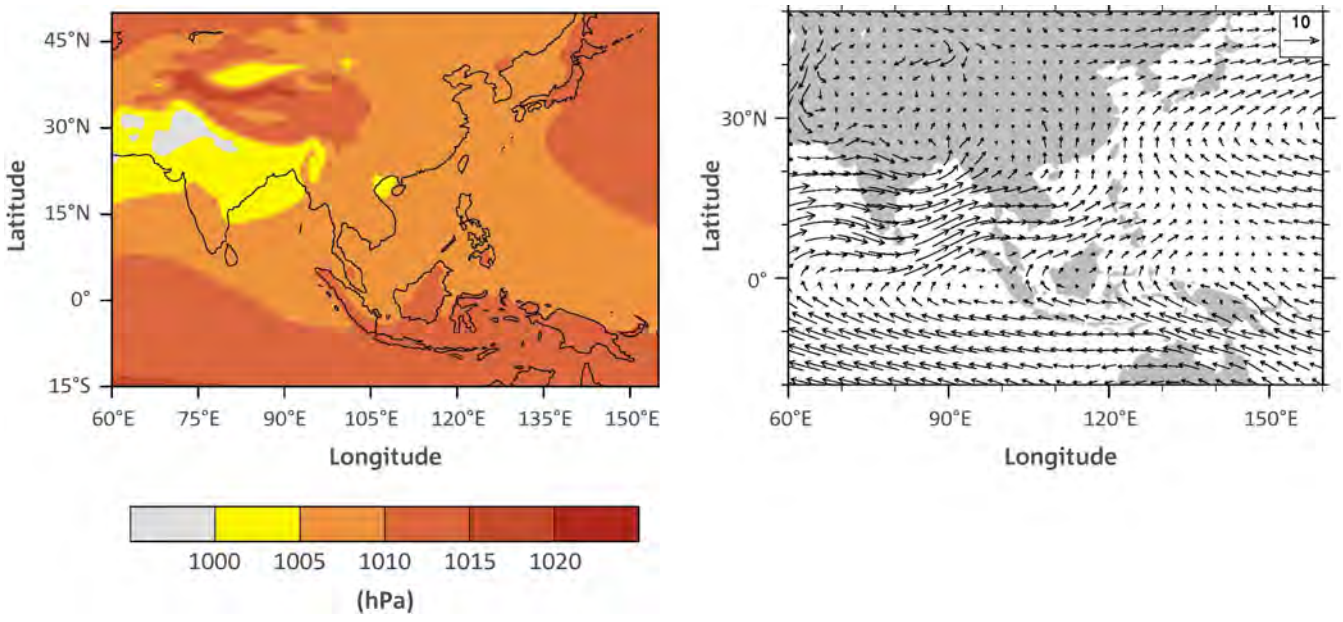

Figure 3-3: Inter-annual variability (days) of the onset (date) of the South West Monsoon over the South region of Vietnam from 1979 to 2011. Grey, red and green bars depict neutral, El Niño and La Niña years, respectively.

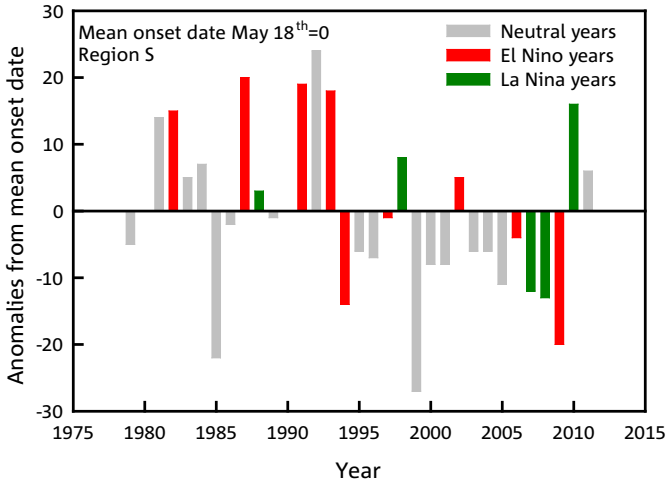

Rainfall during this season is caused by (a) *cyclonic disturbances*, (b) *convection*, (c) *orographic lifting* and (d) *convergence*. Cyclonic disturbances that form outside the region, particularly over the Western Pacific region north of 10°N, can cause rainfall in the coastal areas of Vietnam. These disturbances reach their maximum frequency in September. Convective thunderstorms are frequent over South East Asia, especially south of about 10°N. Strong solar insolation and low wind speeds that prevail during the season are favourable for convective activities in this region. Rainfall due to orographic lifting also occurs over Vietnam during this season. Westerlies or south-westerlies bring ample rainfall to the western part of the mountains and less rainfall to the eastern or coastal regions of Vietnam. The convergence between the equatorial air mass and western northern Pacific air masses also brings rainfall to Vietnam. The amount of rainfall and its spatial and temporal patterns largely depend on the thickness and humidity of the air masses, although other factors such as wind speed and direction and SST anomalies do have some influence.

Average rainfall during the South West Monsoon (Figure 3-4, left panel) shows that areas that are located on the windward side of the mountains receive more than 10 mm day^{-1}, while the areas located on the leeward side of the mountains receive 4-6 mm day^{-1}. For most of South East Asia, this is the main rainy season. However, the rain shadow areas in the eastern parts of Vietnam experience little rain. Rainfall during this season is caused by one or a combination of rain-producing systems.

Inter-annual rainfall variability is generally weak over most of the region where less rainfall is received (right panel of Figure 3-4). However, strong variability of 2-4 mm day^{-1} is observed over the windward side of the mountainous region of Vietnam and the coastal regions facing the Bay of Bengal.

3.2.2 Second Inter-Monsoon Season

October and November are the Second Inter-Monsoon Season months. The Asian continent begins to cool off and the South West Monsoon weakens. Figure 3-5 illustrates MSLP and wind patterns during this season. The pressure pattern is somewhat similar to the First Inter-Monsoon Season (see Section 3.2.4) with the sub-tropical ridge located at 30°N and a low pressure region covering a large area of the Indian and Western Pacific Oceans. Winds are generally weak during this season and weather phenomena that originate within the ITCZ influence the climate of Vietnam.

Figure 3-4: Mean seasonal rainfall (mm day^{-1}) (left panel) and its inter-annual variability (right panel) during the South West Monsoon season (SWMS) for the period 1979-2007. Inter-annual variability is shown by the standard deviation (mm day^{-1}). Source: APHRODITE.

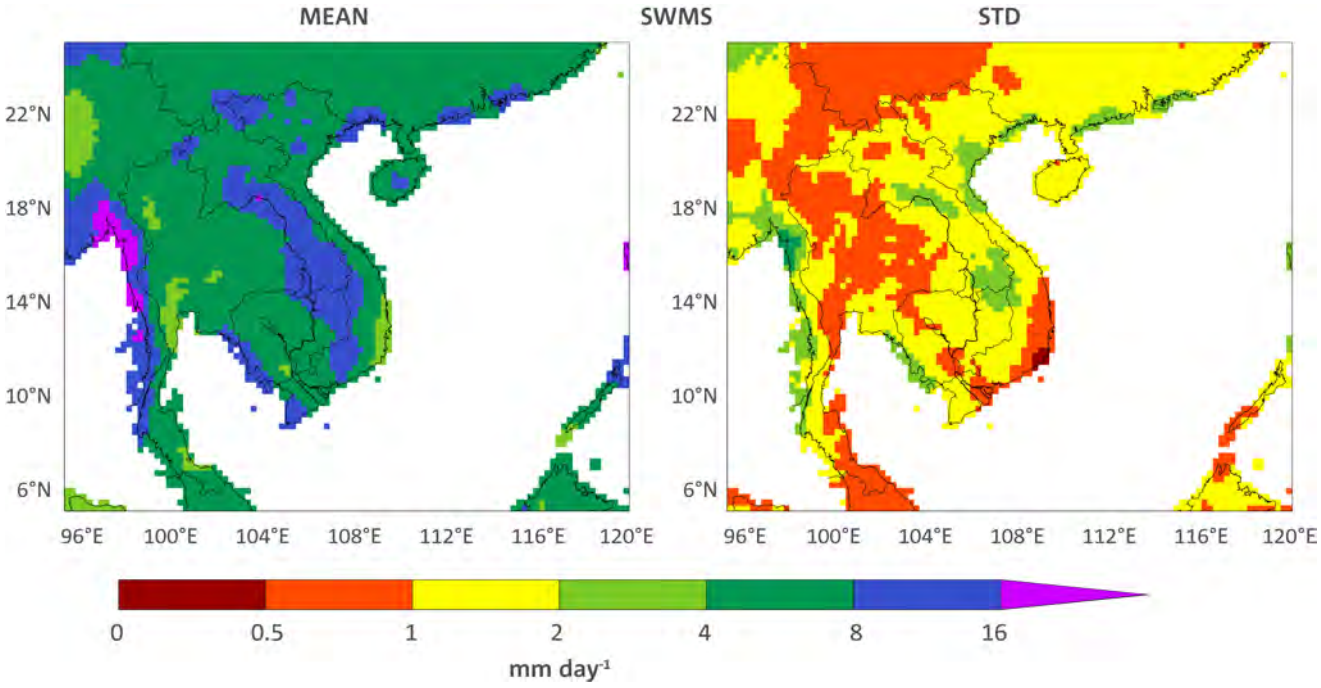

October is the wettest month in some parts of South East Asia. The coastal region of Vietnam receives more than 10 mm day^{-1} of rainfall (Figure 3-6). Rainfall during this season is produced by a number of factors, such as small-scale disturbances, tropical cyclones, orographic lifting and convergence during the latter part of the season. A significant portion of the rainfall is received from tropical cyclones (TCs) that approach Vietnam during the months of October and November and affect much of Vietnam, including the southern and central regions. Sea surface temperature is high over the East Sea, which is one of the factors that keep TCs active over this region. Inter-annual variability of rainfall is strong (4-6 mm day^{-1}) over the east coast of Vietnam (Figure 3-6, right panel), which receives ample rainfall during this season. The other regions of Vietnam experience weak inter-annual variability and less rainfall.

Figure 3-5: Average MSLP (left panel) and winds at the 850 hPa level (right panel) during the Second Inter-Monsoon season (SIMS) for the period 1975-2004. Source: ERA-Interim.

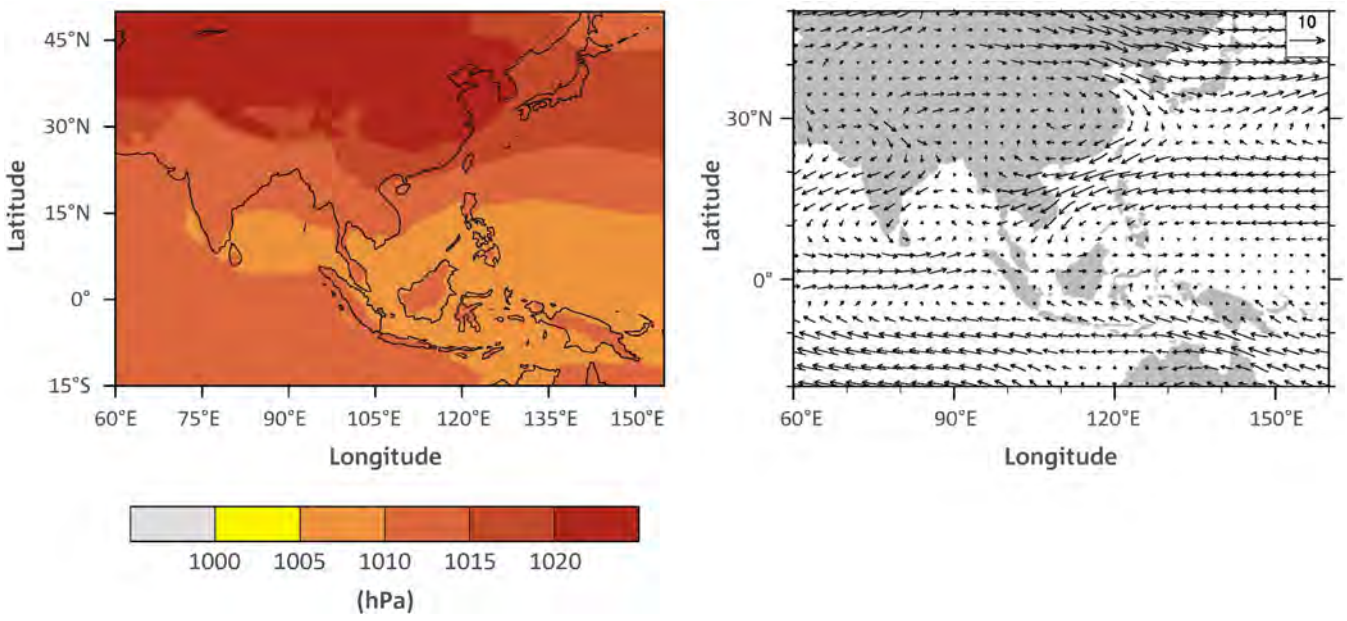

Figure 3-6: Mean seasonal rainfall (mm day^{-1}, left panel) and its inter-annual variability (right panel) during the Second Inter-Monsoon Season (SIMS) for 1979-2007. The inter-annual variability is shown by the standard deviation (mm day^{-1}). Source: APHRODITE.

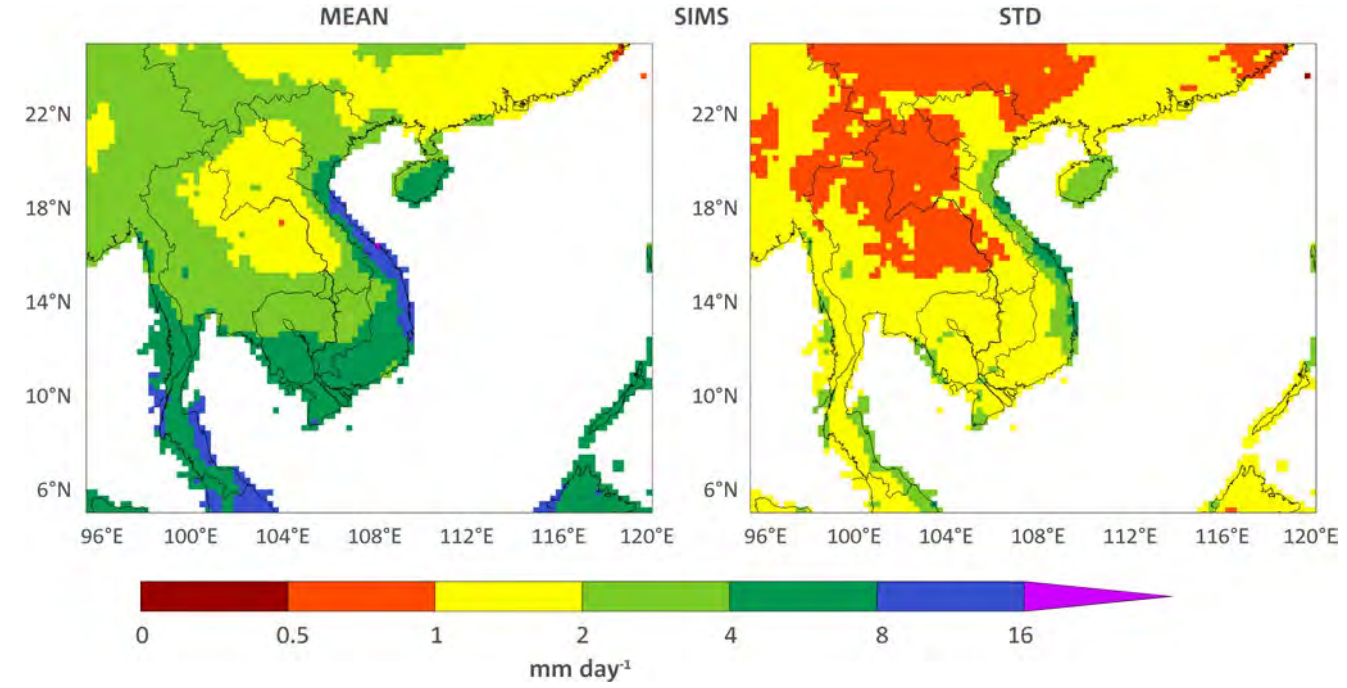

3.2.3 North East Monsoon Season

With the arrival of northerlies from Siberia and Mongolia, the North East Monsoon starts in early December. Figure 3-7 shows MSLP and wind patterns during the North East Monsoon. In general, pressure gradients are small in the tropics compared with higher latitudes. However, a strong pressure gradient is observed during this season over South East Asia. The pressure gradient is stronger over the region centred on Vietnam than in the southern part of South East Asia, resulting in generally high wind velocity. Surface winds from the north are locally deflected by the Annam Mountains that divide Vietnam from Laos.

Two types of air masses influence the climate of Vietnam during the North East Monsoon season:

(1) *Air masses from a large high pressure cell over Siberia and Mongolia*, which are very cold but stable. However, the cold air mass is modified when it reaches the oceanic region of the East Sea. Occasionally, the cold wind surges reach Vietnam, bringing cooler temperatures and rainfall to the north. These cold wind surges are not frequent, but they do explain the strong temperature gradient over Vietnam (Nieuwolt, 1981).

(2) *A warm, tropical air mass carried by north east trade winds*. The air mass has its origin over the Pacific Ocean, north of the Equator. During the cold wind surges of the North East Monsoon, the warm trade winds retreat towards the east over the Pacific Ocean. The boundary between North East Monsoon winds from the northern Asian continent and trade winds from the Pacific Ocean forms part of the polar front. At the surface level, the average position of the polar front in January is around 25°N over the Pacific Ocean, but it can move as far south as 10°N (Ramage, 1971). In an earlier study, Thompson (1951) showed that the polar front position varies in location between 15-20°N.

On the basis of satellite photographs and weather observations, Riehl (1969) documented some important synoptic features responsible for day-to-day variability over South East Asia during the North East (winter) Monsoon Season. These synoptic patterns include (1) the monsoon surge, (2) an eddy and monsoon decay pattern, (3) a reverse flow pattern and (4) a tropical cyclone pattern.

During the North East Monsoon season, the first pattern, a typical cold surge, is characterised by a thick, solid overcast sky covering the Gulf of Tonkin and the northern part of the East Sea. Winds are generally northerlies or north-easterlies and often are diverted parallel to the coast by the Annam Mountains. Skies over the western part of the mountains are clear. The second pattern is the eddy that forms south of the island of Hainan during the North East Monsoon Season, suppressing the north-easterly winds over the Gulf of Tonkin. Subsequently, the shear line moves northward, associated with the weakening of the monsoonal winds. The third circulation pattern is the reverse flow pattern in which south-east winds replace north-east winds, with a low-pressure area located further north of Vietnam (near 25°N). This pattern provides clear weather over the north, with fog patches along the North Vietnam coast and in the Red River Delta during this season (Riehl, 1969). The fourth atmospheric circulation pattern is linked to tropical cyclones that form over the Western Pacific and approach the coast of Vietnam. More details on tropical cyclones and their effects will be discussed later (Section 7). Weather patterns of the North East Monsoon basically remain the same from November to January. However, a gradual decline in northerly wind velocity is noticed, associated with the weakening of the high pressure systems over continental Asia, central Siberia and Mongolia; trade winds over the Pacific Ocean then dominate.

Figure 3-7: Average MSLP (left panel) and winds at the 850 hPa level (right panel) during the North East Monsoon season (NEMS) for the period 1975-2004. Source: ERA-Interim.

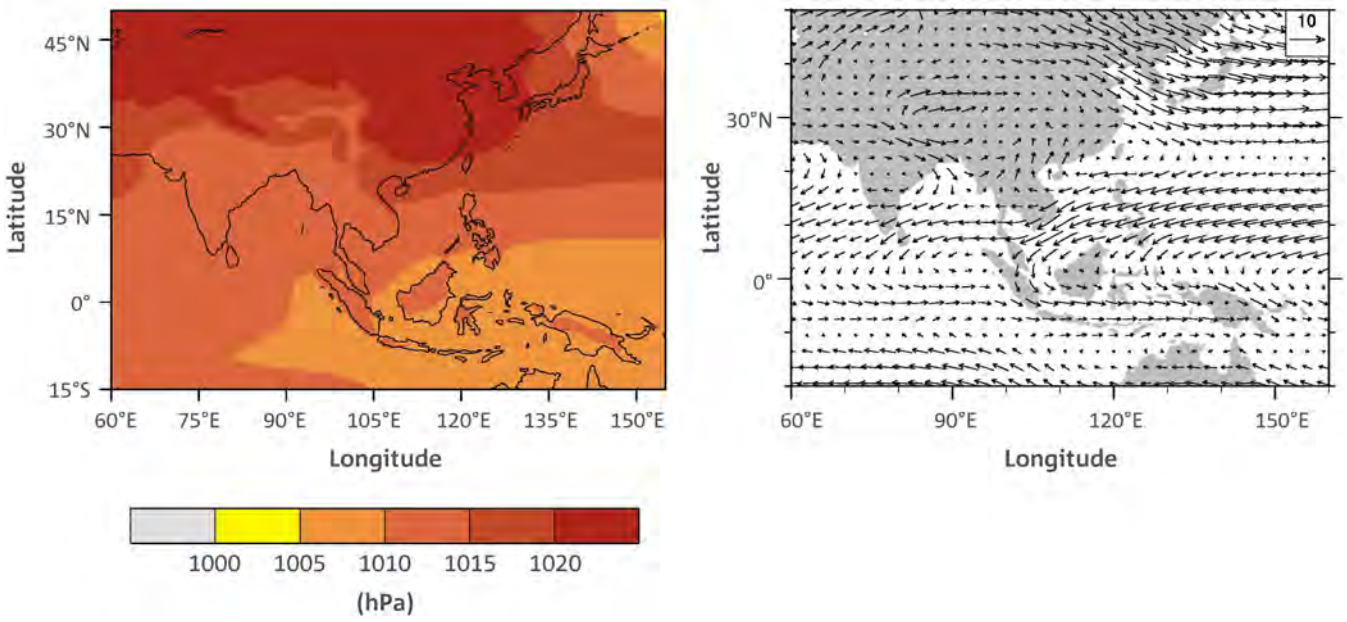

Rainfall during this season over South East Asia is largely caused by disturbances along the tracks of the polar front. On average, most parts of Vietnam receive 1-2 mm day^{-1} of rainfall during this season, but the coastal regions receive 2-4 mm day^{-1} (Figure 3-8, left panel). Rainfall from these disturbances is locally enhanced due to orographic lifting by the mountains in Vietnam and part of Laos. On the western slopes of the mountains, rainfall is reduced due to the rain shadow effect. The condition in northern Vietnam associated with disturbances along the polar front is locally known as '*crachin*' (Nieuwolt, 1981). During *crachin*, the weather is characterised by thick fog and heavily overcast skies and little rain, lasting for three to five days. The main *crachin* season is from the end of January to April and often occurs when a shallow depression forms over the Gulf of Tonkin. Da Nang, on the east coast of central Vietnam, can be used as an example of the influence of the North East Monsoon weather patterns, particularly the polar front. Da Nang shows more rainfall from September to January, with maximum amounts in September and October. The maximum rainfall in these months is linked to the southward migration of the ITCZ following the retreat of the South West summer monsoon. Inter-annual variability of rainfall during the North East Monsoon Season is weak over most parts of Vietnam, except for the coastal regions where 1-2 mm day^{-1} is observed.

3.2.4 First Inter-Monsoon Season

April and May are considered as transitional months between the slowly retreating North East (winter) Monsoon and slowly advancing South West (summer) Monsoon. Generally a broad low pressure region occupies the tropics, with a heat low developing over northwest India. The sub-tropical ridge is located north of 30°N (north of Pakistan). Winds are weak and highly variable during April. During this time of the year, weather phenomena that originate within the Inter-Tropical Convergence Zone (ITCZ) strongly dominate the climate of South and South East Asia. Winds are generally weak during this season (Figure 3-9). Tropical storms are very rare in the East Sea.

The South West (summer) Monsoon does not usually establish itself until the end of May over the northern part of continental South East Asia, particularly over central and northern Vietnam. The onset of the South West Monsoon over this region is related to changes in upper-level circulation. The onset of the monsoon in late May is accompanied by rapid changes in weather conditions over South Asia, but the change is much more gradual over Indochina (Ramage, 1971).

Rainfall during the First Inter-Monsoon Season is strongly influenced by the topography of this region (Figure 3-10, left panel). The western regions of mountains in Vietnam receive between 4-6 mm day^{-1} of rainfall, while the east coastal region receives 2-4 mm day^{-1}. Rainfall variability is generally weak over Vietnam, except for the western slopes of the mountain regions (Figure 3-10, right panel).

Figure 3-8: Mean seasonal rainfall (mm day^{-1}, left panel) and its inter-annual variability (right panel) during the North East Monsoon Season (NEMS). The inter-annual variability is shown by the standard deviation (mm day^{-1}) for the period 1979-2007. Source: APHRODITE.

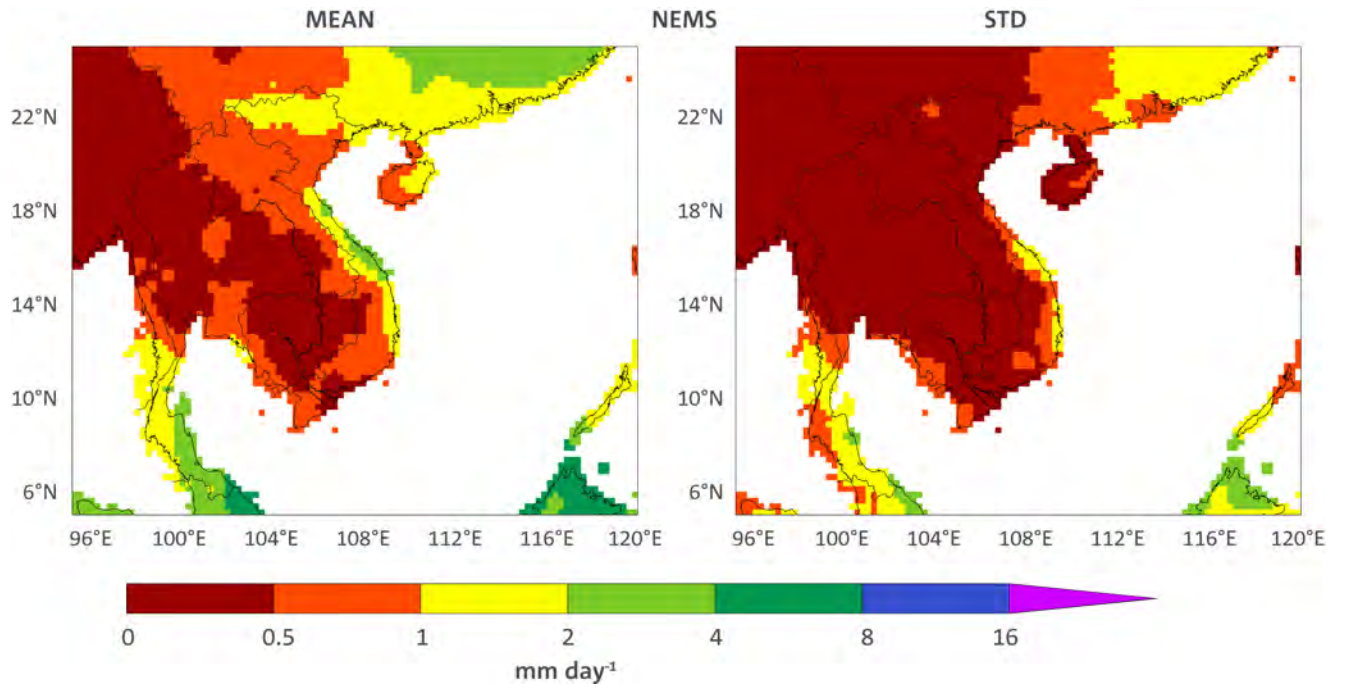

Figure 3-9: Average MSLP (left panel) and winds at the 850 hPa level (right panel) during the First Inter-Monsoon Season (FIMS) for the period 1975-2004 Source: ERA-Interim.

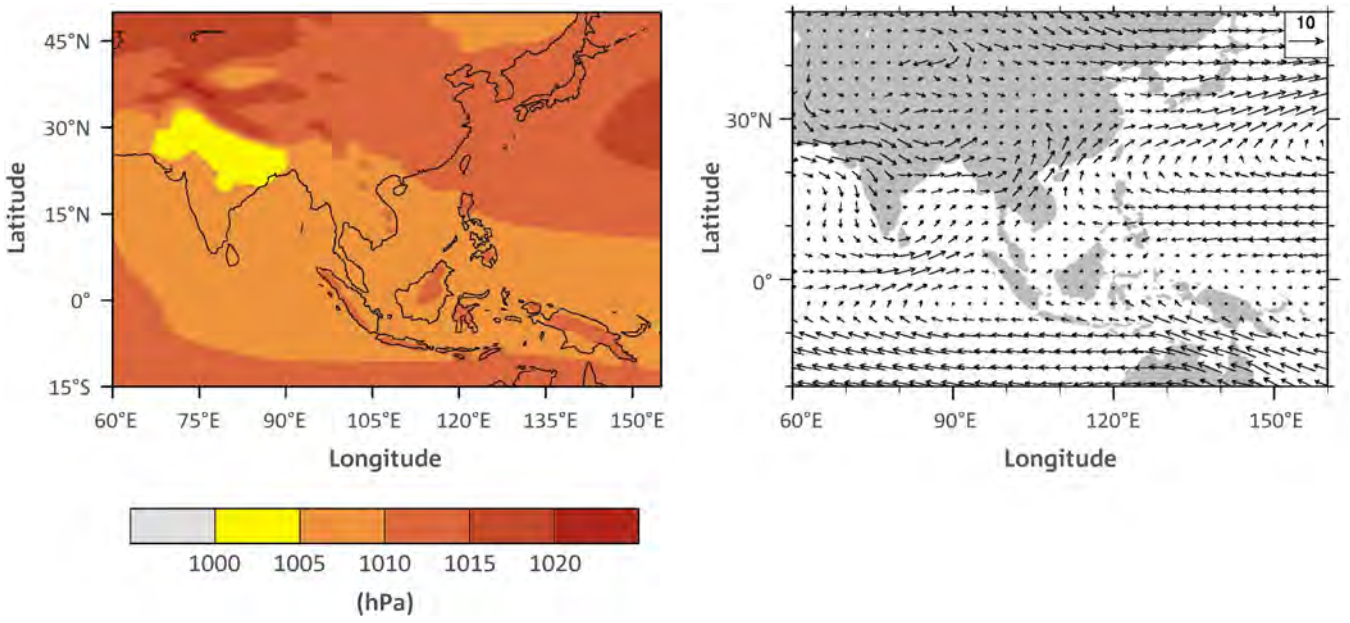

Figure 3-10: Mean seasonal rainfall (mm day^{-1}, left panel) and its inter-annual variability (right panel) during the First Inter-Monsoon Season (FIMS) from 1979-2007. Inter-annual variability is shown by the standard deviation (mm day^{-1}). Source: APHRODITE.

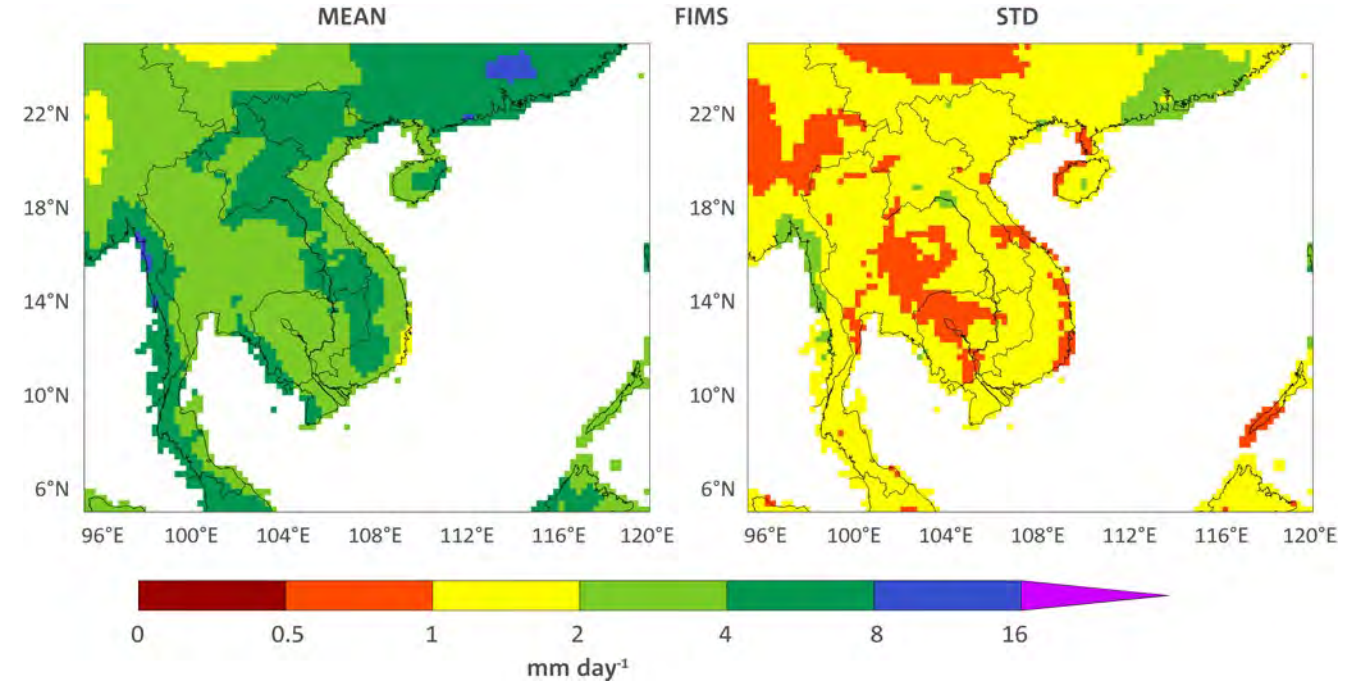

3.3 TRENDS IN TEMPERATURE AND RAINFALL OF VIETNAM

Temperature and rainfall trends during the period 1961-2011 have been investigated using seasonal and annual station observational data. Figure 3-11 shows trends in surface air temperature and rainfall. It is evident that all the stations in Vietnam show warming of between 0.15° and 0.35°C per decade during the past 50 years. The warming is less for coastal stations and more for inland stations. Nguyen *et al*. (2013) reported that Vietnam's average temperature increase of 0.26°C ± 1°C per decade is approximately twice the rate of global warming over the same period. They also showed that greater warming occurs in winter months than in summer and that the southern regions are warming faster than the northern regions.

Trends in rainfall show both increases and decreases. The regions NW, NE, ND and northern stations of NC and stations in the S region show decreases, with region ND showing stronger decreases than the others. Stations in SC, CH and the southernmost stations in NC show large increases during the past 40 years. These results are consistent with the results obtained in recent studies (Endo *et al.,* 2009; Nguyen *et al*., 2013). Endo *et al*. (2009) showed that extreme rainfall events do follow the trends in total rainfall over Vietnam. Since there is a clear pattern in rainfall trends (increase in the middle regions and decrease in northern and southern regions) it is worth looking at any changes in climate drivers that produce rainfall in these regions. Furthermore, changes in meridional circulation and the related rainfall changes provide another topic of research.

3.4 CLIMATE DRIVERS

3.4.1 El Niño-Southern Oscillation (ENSO)

One of the major drivers that affect the climate of Vietnam on the inter-annual time scale is the ENSO phenomenon. The dominant large-scale atmospheric system in the tropics is the Southern Oscillation (SO), a phenomenon defined statistically by Walker and Bliss (1932). The SO is characterized by the variations of pressure difference between the Indonesian low near Darwin and the South Pacific Subtropical High near Tahiti. The inter-annual variability of the SO is measured by the Southern Oscillation Index (SOI) and it is used for seasonal forecasting in the tropics. The SO phenomenon is closely linked with the oceanic event called El Niño, a striking phenomenon involving large-scale inter-annual variations of SSTs, sea level, currents, thermocline, wind and rainfall over the tropical Pacific Ocean, particularly in the east (Bjerknes, 1969; Philander, 1983). El Niño and the SO together comprise a complex system of climate fluctuations termed the ENSO phenomenon. El Niño events are associated with above normal SST anomalies, which are related to weak trade winds, and therefore to a weak pressure gradient between the Indonesian Low and the South Pacific subtropical high. The term La Niña refers to a phase opposite to an El Niño phase and has opposite patterns of SST anomalies, winds and thermocline (Philander, 1985).

Figure 3-11: Mean temperature and rainfall trends from 1961 to 2011. Trends in temperature are shown as °C per decade and rainfall as percentage per decade. Source: Vietnam station observations. Filled circles show that the trend is significant at the 95% level.

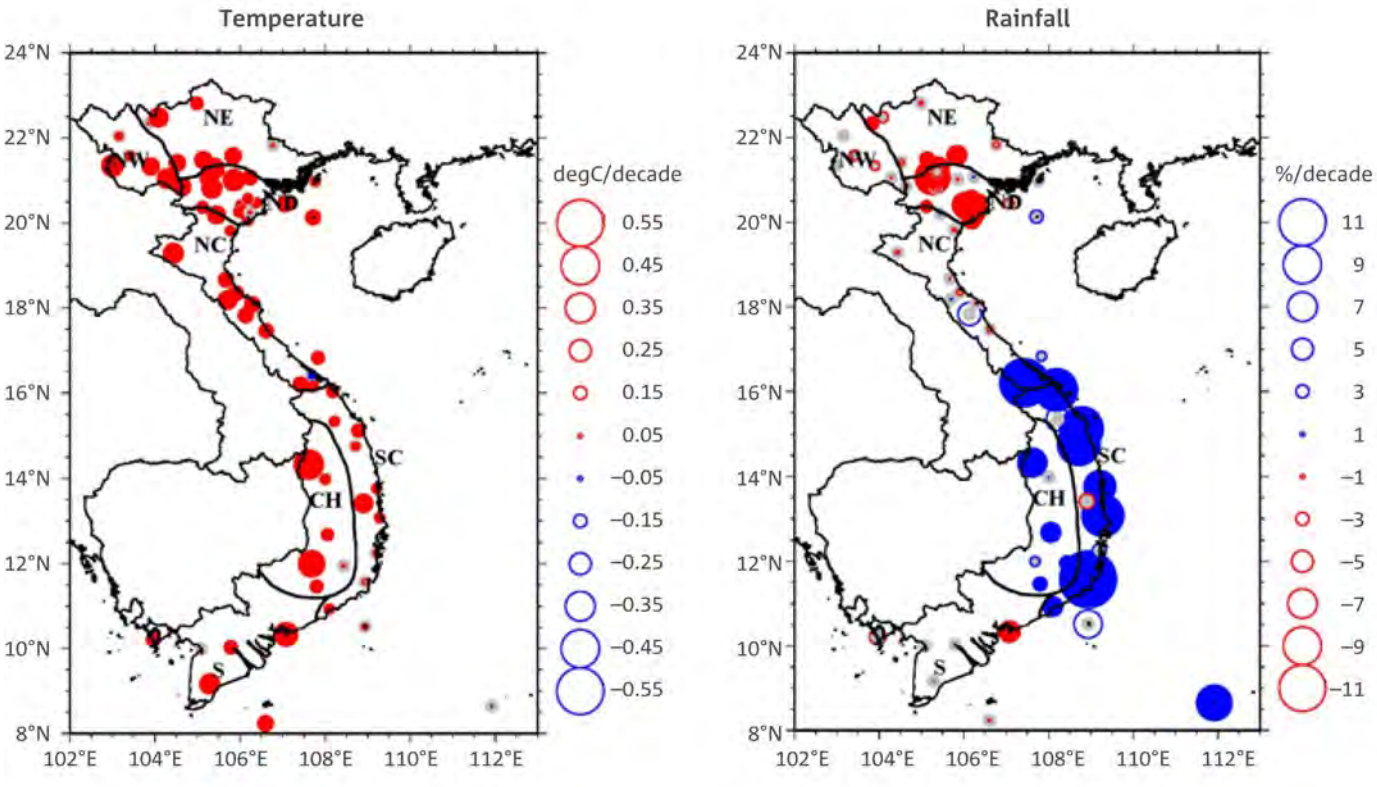

Bjerknes (1969) proposed a thermally-driven east-west circulation pattern along the equator for which the Indonesian region or 'maritime continent' acts as the main source region, releasing a large amount of latent heat to the atmosphere (Ramage, 1968). During El Niño events, (see Figure 3-12a) positive SST anomalies, weaker trade winds, and enhanced rainfall over the central and eastern Pacific are observed. These anomalies are associated with a weaker east-west circulation over the tropics. During these events, negative SST anomalies and suppressed convective activity are observed over the western Pacific region that covers the Indonesian-north Australian region. The thermocline, which is the boundary between the surface mixed layer of the ocean and deep cold water, is deeper over the eastern Pacific. La Niña is essentially the opposite phase of El Niño. During La Niña conditions (see Figure 3-12b) stronger trade winds that cause higher sea levels over the western Pacific and positive SST anomalies are observed over the Indonesian-north Australian region. The thermocline tilt is opposite to El Niño and is shallow over the eastern Pacific. Enhanced rainfall associated with active convection is observed over the western Pacific. Figure 3-12c represents the normal or neutral condition between El Niño and La Niña conditions.

ENSO is the dominant climate driver in the region and it affects the activity of other smaller drivers, such as tropical cyclones, cold surges, and monsoonal variability. A number of studies have demonstrated the influence of ENSO on Vietnam's rainfall and temperature (e.g., Nguyen *et al.*, 2007; Chen *et al.*, 2012; Nguyen *et al.*, 2013). Almost all the studies demonstrated a strong influence of ENSO on rainfall during the First and Second Inter-Monsoon seasons. However, Nguyen *et al.* (2007) also demonstrated the influence of ENSO on monthly rainfall in the central highlands.

For this project, we have investigated the relationship between ENSO and regional and seasonal rainfall of Vietnam. Results based on correlations between NINO3.4[9] (one of several El Niño/ENSO indicators based on sea surface temperature) and seasonal and annual rainfall for the seven sub-regions of Vietnam are shown in Table 3-1. In this table, a negative relationship suggests below normal rainfall during El Niño years and above normal rainfall during La Niña years. It is evident from Table 3-1 that three out of four seasons (all except SWMS) show a negative relationship. However, the relationship is strong only in the four central and southern regions (regions NC, SC, CH and S), but weak in other regions (regions NW, NE and ND). It is also worth mentioning that during SWMS almost all of the regions show a weak positive relationship. The linear relationship between NINO 3.4 and rainfall in the S region is shown in Figure 3-13 as an example of the opposite pattern of correlations between SWMS (upper right) and the other seasons. Changes in the sign of correlation among the seasons and regions suggest changes in circulation patterns which need further investigation.

Figure 3-12: Schematic representations of sea surface temperature anomalies, thermocline, east-west circulations and rainfall along the equator over the Indo-Pacific region for (a) El Niño, (b) La Niña and (c) neutral conditions of the El Niño-Southern Oscillation phenomenon. Source: Australian Bureau of Meteorology.

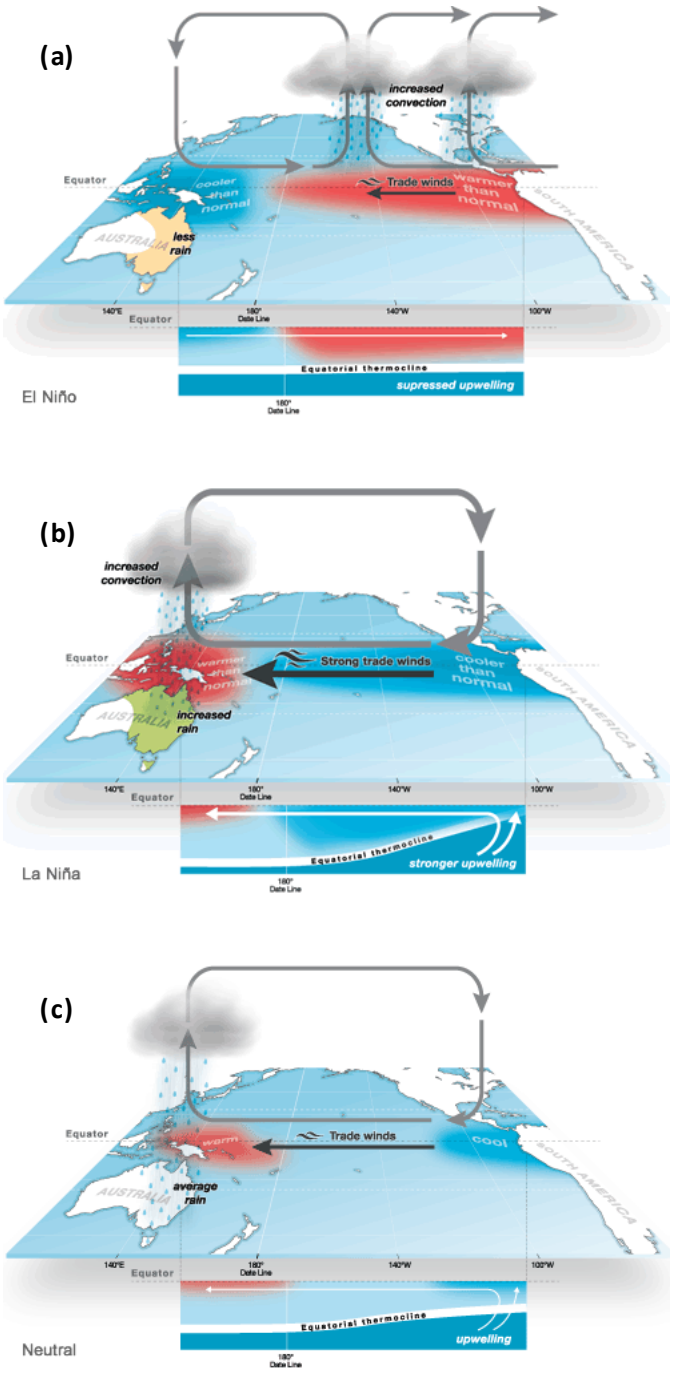

9 NINO3.4 is the average sea surface temperature anomaly in the region bounded by 5°N to 5°S, from 170°W to 120°W. This region has large variability on El Niño time scales, and is close to the region where changes in local sea-surface temperature are important for shifting the large region of rainfall typically located in the far western Pacific.

An El Niño or La Niña event is identified if the 5-month running-average of the NINO3.4 index exceeds +0.4°C for El Niño or -0.4°C for La Niña for at least 6 consecutive months.

Table 3-1: Correlation coefficients between SST anomalies (SSTA), which are represented by the NINO3.4 index, and regional station rainfall anomalies of Vietnam from 1979-2011. Statistically significant values at the 95% confidence level are bold.

NINO3.4 SSTA/ RAINFALL	FIMS	SWMS	SIMS	NEMS
NW	-0.32	0.18	-0.08	-0.03
NE	-0.07	-0.06	0.04	0.06
ND	-0.20	0.17	-0.22	-0.01
NC	**-0.43**	0.16	**-0.57**	-0.28
SC	**-0.52**	0.29	**-0.64**	**-0.48**
CH	**-0.48**	**0.35**	**-0.60**	**-0.36**
S	**-0.76**	0.12	**-0.46**	**-0.52**

3.4.2 Tropical cyclones

Tropical cyclones are one of the deadliest natural disasters affecting Vietnam, particularly in the central and northern regions (the Red River Delta and the coastal zone from Quang Ninh to Khanh Hoa provinces). Strong winds, heavy rains and floods have caused extensive damage to human settlements, infrastructure, ecosystems, etc. In recent years, monthly frequencies of tropical cyclones and their impacts on Vietnam's rainfall have been studied as part of a wider Western Pacific region (Rodgers *et al*., 2000; Wu *et al*., 2004). However, there are also studies that have primarily focused on the effect of tropical cyclones on Vietnam and their link to ENSO variations (Kleinen, 2007; Tan, 2002). The frequency of occurrence of tropical cyclones that affect Vietnam has a clear annual cycle. Monthly frequencies of tropical cyclones for El Niño, La Niña and non-ENSO years or neutral years are shown in Figure 3-14.

Tropical cyclones tend to affect Vietnam during the South West Monsoon and Second Inter-Monsoon seasons, the latter having the highest frequency. It is also clear from Figure 3-14 that more tropical cyclones are recorded during La Niña years and fewer during El Niño years. The frequency for neutral years lies between the frequencies for the two extreme phases of the ENSO phenomenon. In terms of their formation and landfall, most tropical cyclones form between 120°E and 160°E and between 5°N and 15°N. These tropical cyclones give enhanced rainfall to the windward side of the mountains of central Vietnam and cause extensive damage there. It is evident from the past studies (Liu and Chan, 2003; Wu *et al.,* 2004) that there is a strong link between ENSO events and tropical cyclone frequency and distribution over the Western Pacific. SST anomalies, which are strongly associated with ENSO events, have strong persistence over the tropics. Accordingly, it may become possible to foreshadow tropical cyclone activity over the western Pacific a few months in advance by tracking ENSO, thereby potentially reducing casualties over Vietnam. Further details on tropical cyclone characteristics can be found in Section 7 of this report.

Figure 3-13: Relationship between the seasonal NINO3.4 index and normalised seasonal station rainfall amounts for the S region for 1979-2011. Green dots represent individual years. Normalised rainfall is defined as the yearly seasonal rainfall anomalies from the long-term mean divided by the standard deviation of the time series.

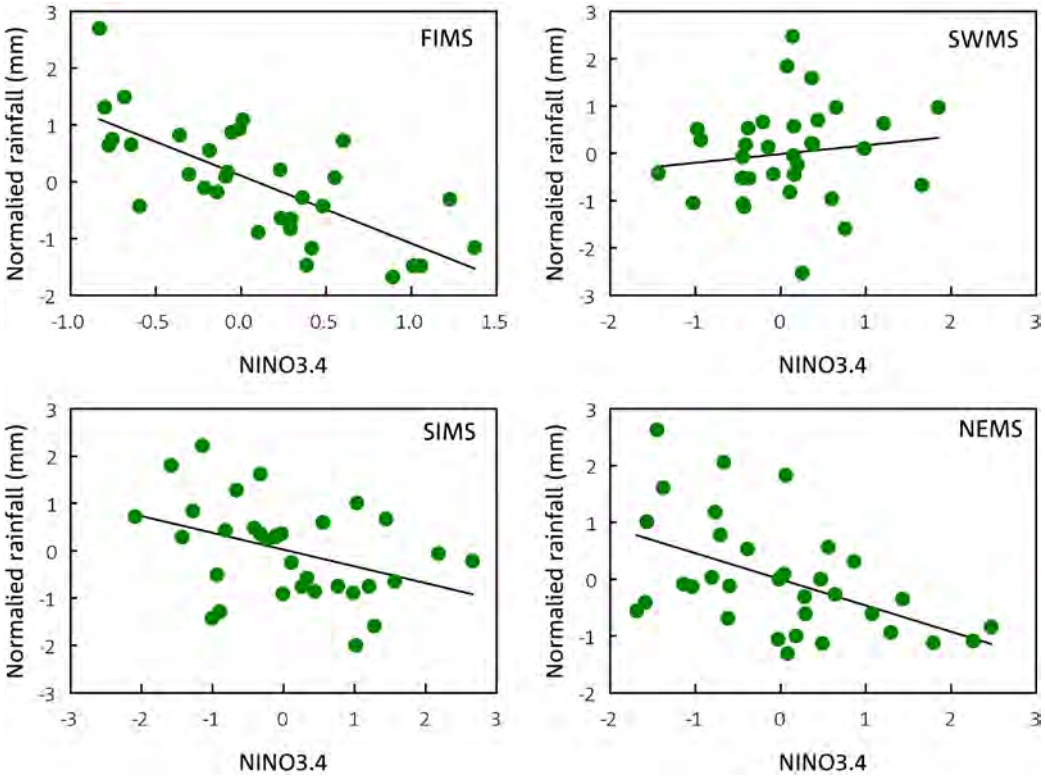

Figure 3-14: Monthly frequency of tropical cyclones affecting Vietnam. Source: Ngu (2000).

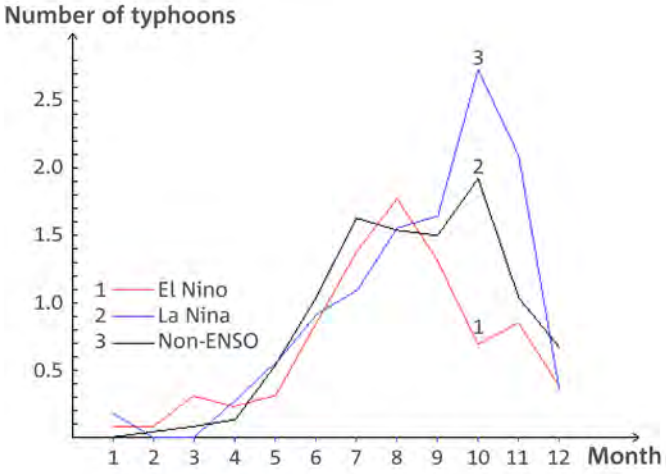

Figure 3-15: Difference in annual rainfall (mm day^{-1}) between CMIP5 GCM ensemble simulations with anthropogenic aerosol-only forcing and those with all anthropogenic forcings for the period 1975-2004.

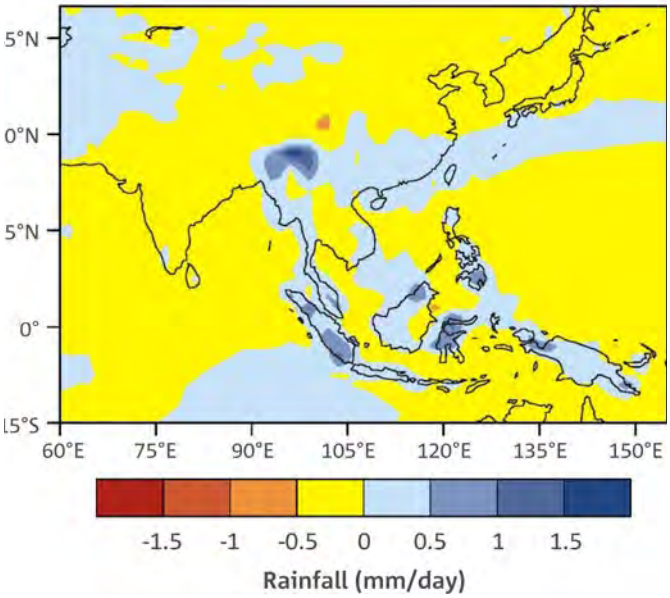

3.4.3 Impact of aerosols on rainfall

The impact of aerosols over South East Asia is investigated using the historical runs from CMIP5 simulations from 1975-2004. Among the available CMIP5 simulations, nine GCMs have simulations particularly focused on anthropogenic aerosol forcings only, which may include indirect effects and black carbon on snow and ice. Some models have multiple simulations, so we have created a multi-model ensemble average using available simulations and calculated seasonal and annual rainfall climatologies for the period 1975-2004 for the runs which have all anthropogenic forcings (greenhouse gases as well as aerosols). The impact of aerosols on rainfall is shown as the difference between rainfall climatologies based on aerosol-only forcing and climatologies based on all forcings. Differences in simulated rainfall under the two conditions are shown for annual and seasonal cases in Figure 3-15 and Figure 3-16, respectively. Overall there is no clear difference in rainfall for a given region. The annual difference in Figure 3-15 shows slight decreases over most of the land areas and also over the western Pacific. However, some areas of South East Asia show a slight increase. Such spatial variations are also seen in the seasonal rainfall patterns.

Spatial patterns of rainfall differences for the four seasons (Figure 3-16) show both decreases and increases. In particular, the northern and southern edges of the ITCZ show relatively stronger decreases compared with other regions. The edges or the boundaries of the ITCZ are found over north India during SWMS, over the equatorial region of the Indian Ocean during SIMS and over the Indonesian-north Australian region during NEMS. The rainfall difference is negative over Vietnam during FIMS and SWMS and positive during SIMS and NEMS.

A number of studies have focused on the impact of aerosols on rainfall (e. g. Frieler *et al*., 2011; Kawase *et al*., 2011; Rotstayn *et al*., 2012). These studies suggest that decrease in rainfall is due to a reduction in evaporation. An increase in black carbon and anthropogenic aerosols tends to enhance the absorption and scattering of short- and long-wave radiation, and hence reduces the radiation reaching the ground, affecting temperature and evaporation at the surface (Kawase *et al.,* 2011).

3.5 SUMMARY AND KNOWLEDGE GAPS

The climate of Vietnam is a complex interplay of large-scale monsoons and smaller scale factors. The various regions of Vietnam have very different climatic regimes related to their location and terrain. In the southern portions, the climate is tropical with strong monsoonal influences. In northern Vietnam, the combination of closeness to China (with associated cold surges in winter), mountainous terrain and monsoonal flow makes the seasonal cycle longer without a clear dry season compared with southern regions. In central Vietnam, the interaction between terrain, mountains on the west and low land along the coast with the different monsoonal flows makes its climate different than the other regions, with a peak in rainfall later in the year than in the north or south. Inter-annual variations of rainfall across Vietnam, particularly in the central and southern regions, show a strong link to ENSO variations. The negative relationship between NINO3.4 SST anomalies and regional rainfall indicates above average rainfall during La Niña years and below average rainfall during El Niño years. Tropical cyclones, which can cause severe damage, can affect all regions of Vietnam, but with greater prevalence in central and northern Vietnam than in the south. More tropical cyclones that affect the Vietnam coast occur during La Niña years compared with El Niño years and this relationship is strong during SIMS. Such relationships suggest that ENSO is a controlling factor of the climate of Vietnam on the inter-annual time scale.

Figure 3-16: Difference in seasonal rainfall (mm day^{-1}) between CMIP5 GCM ensemble simulations with anthropogenic aerosol-only forcing and those with all anthropogenic forcings for the period 1975-2004. (a) First Inter-Monsoon Season (FIMS), (b) South West Monsoon Season (SWMS), (c) Second Inter-Monsoon Season (SIMS) and (d) North East Monsoon Season (NEMS).

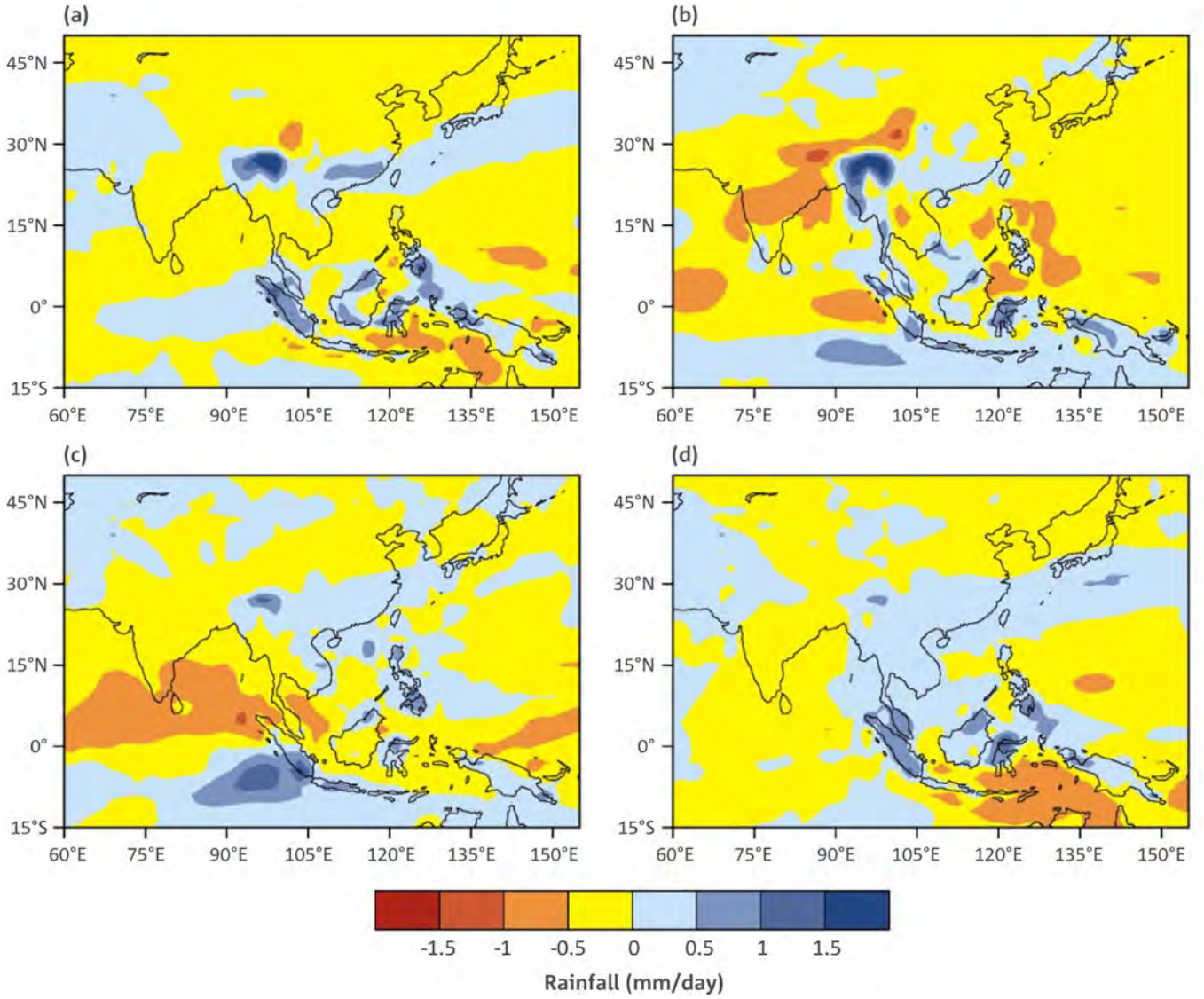

Much more work is needed to understand the impact of ENSO on the climate of Vietnam. It was shown here that especially in the transition seasons (FIMS and SIMS), there appears to be some relationship between ENSO and rainfall (see Table 3-1, which gives correlation coefficients between the NINO3.4 index and regional rainfall of Vietnam). The impact of the Indian Ocean Dipole (IOD) on the rainfall of Vietnam should also be investigated, but this was not attempted in this study. More studies of the seasonal changes in rainfall across Vietnam, especially in SWMS, would greatly increase our understanding of these trends and will also allow more in-depth comparison with the climate projections shown later.

The role and impact of aerosols was only discussed briefly here. Because Vietnam is in close proximity to major sources of aerosols (China and India), further analysis of the effects of aerosols on future climate projections is warranted.

4 UNDERSTANDING AND USE OF CLIMATE PROJECTIONS

The previous chapters have outlined the background of the *High-resolution Climate Projections for Vietnam* project, providing information on climate modelling and details of the models to be used in this study as well as the downscaling methodology to be employed in producing the 10 km resolution projections. The observed climate has also been analysed to determine trends and climate drivers, which is necessary for validation of current climate simulations and for better understanding of the future climate projections that are given in the following chapters.

Before reviewing these projections and applying them to planning and adaptation measures, it is useful to consider some of the factors that may influence them. In addition, one needs to know how best to assess and interpret the results, given the inherent uncertainty in predicting climate change. These uncertainties are influenced by unknowns, such as future technologies and levels of emissions, as well as the physical responses of the earth-atmosphere system and natural variability.

The choice of which climate information may be required for use in any impact or risk assessment is determined by the

1. Climate variable(s) of interest
2. Temporal (time) scales of the assessment
3. Spatial scales of the assessment
4. Management of uncertainty.

The first three factors, properly applied, will determine the relevance of any resulting climate information and the fourth factor will establish confidence in the results. Most projections, such as those detailed in this report, are not forecasts but are conditional upon the assumptions incorporated into the input data and the model that produced those projections. Therefore, although they aim to be physically plausible futures under the assumptions inputted, they would not necessarily be expected to occur.

The following sections give more detailed information on choosing climate information and assessing and managing uncertainty, along with discussion of tools available to help analyse climate projections for impact or risk assessments. Parts of this chapter are based upon the approach of CSIRO and BoM (2007).

4.1 CLIMATE VARIABLES OF INTEREST

A key task in any assessment is to identify the relevant climate variables, either those associated with event risk or those that drive subsequent responses of the environmental systems. For most applications, only a subset of variables is required. A robust physical relationship between the selected variables and the outcome of interest should be ensured. Appropriate variables may be identified by stakeholders, by conceptual models of the system of interest, or through prior research and experience that have determined the key climate drivers of the system. For a list of common climate variables used in risk assessment, see Table 4-1.

Table 4-1: Common climate variables used in impact and risk assessment. Adapted from CSIRO and BoM (2007).

IMPACT AREA	IMPACT	CLIMATE VARIABLES
Agriculture	Rice production	Rainfall Temperature
Water Resources	Stream flows Storage flows	Rainfall Evaporation
Coasts	Aquaculture Saline intrusion Storm surges	Sea level rise Winds Pressure
Infrastructure	Impacts to buildings Road construction and maintenance	Temperature Rainfall Radiation Winds Sea level rise
Terrestrial biodiversity	Primary production Population extinctions	Temperature Rainfall Radiation
Marine biodiversity	Coral bleaching Sea life mortality	Sea surface temperature
Health impacts	Heat related mortality Infectious diseases	Temperature Humidity Rainfall
Fire weather	Fire intensity and frequency Length of fire season Periods for control burns	Precipitation Temperature Relative humidity Wind
Alpine snow conditions	Snow cover Snow depth Snow duration	Precipitation Temperature

The form of a selected variable will differ from system to system, i.e. they may be key atmospheric variables, such as temperature, or they may be derived variables, such as drought indices (intensity and duration of drought). Although many event-based risks will be in response to changes in extreme conditions (IPCC, 2012), it is often difficult to provide reliable estimates of such changes. Instead, changes to mean conditions have most often been relied upon. For example, while past assessments of coastal impacts only applied average sea-level change, the interaction of higher sea levels with extreme tides resulting from natural climatic variability and/or anthropogenic climate changes may need to be assessed to get a more realistic projection of the coastal impacts of climate change.

4.2 TEMPORAL (TIME) SCALES

Each assessment needs to decide the temporal scales over which that assessment will be conducted by considering the following aspects:

The time horizon for the projected climate change or impact

By convention, most of the climate-change projections and estimated impacts developed internationally have employed time horizons of approximately one century (e.g. out to 2100), as illustrated by IPCC global temperature and sea-level projections (IPCC, 2013).

Future time slice or continuous time series?

The Vietnam climate projections presented here focus on two time periods: mid-century (2045-2065) and the end of the century (2080-2100) in order to capture the near-term and the longer term effects of climate change, although some of the high-resolution downscaled simulations in this study also provide data from 1970 to 2100.

Temporal (time) resolution

Climate projections can be presented for annual, seasonal, monthly, weekly, or daily time steps. In this report, we focus on seasonal time periods, calculating means over the 20-year time periods mentioned earlier. However, many complex processes, such as specific hydrological or agricultural systems, may require daily time series data as input, even though the results may be aggregated to seasonal or annual values.

4.3 SPATIAL SCALES

The spatial scales over which the assessment will be conducted must also be considered:

Single point, multiple points, or geographic areas?

Climate projections require data presented in a range of spatial forms. For example, agricultural crop models are often location-specific and hydrological models may require information for specific nodes within the surface water system. In such instances, climate projections at specific geographic locations (grid cells) are necessary to drive impact assessment models for one or more locations. For such applications, climate projections that reflect the spatial variability in future changes are needed, often as gridded data sets of varying geographic and temporal resolutions. The data for some of the downscaled projections in this study are available on a 10 km (0.1° longitude/latitude) grid over Vietnam. Regional averages for the seven climatic sub-regions of Vietnam are presented in this report, and can be accessed with the Climate Futures Tool (Section 4.6). Accessing the more detailed gridded information may require additional processing of the data.

The spatial resolution of the projection

The spatial resolution of climate information is a core challenge for development of climate projections. Global climate model outputs are often produced on a geographic grid of 100-200 km, yet in reality, many climatological gradients (such as temperature variations across terrain) and land surface variations (such as coastlines) have much finer spatial scales. Quantifying the impacts of climate change at the relevant scales is also important for decision-making. The higher resolution projections produced by downscaling in this project help by providing information on a more relevant spatial scale.

4.4 TREATMENT OF UNCERTAINTY

Although science attempts to improve our understanding of how systems work, research does not always reduce uncertainty. For example, when a poorly-known process becomes better quantified and is added to other known uncertainties, the total quantified range may increase, creating the perception that uncertainty has increased. For example, the addition of carbon-cycle uncertainties to the range of global average warming in the IPCC AR4 (2007a) has led to a greater range of global warming than in IPCC AR3 (2001). Examples of uncertainties that were reduced in AR4 include the thermal component of sea-level rise, the 'likely' range of climate sensitivity (IPCC, 2007a) and ranges of warming for selected regions (Figure 2.6 in Carter *et al*., 2007).

Some of the key uncertainties associated with climate projections include:

- Future emissions of greenhouse gases and aerosols
- Climate sensitivity
- Regional expressions of global climate change.

Additional uncertainties arise during the impact assessment process, namely:

- System sensitivity to climatic changes
- System adaptive capacity.

Following the approach of CSIRO and BOM (2007), these key climate uncertainties translate into an 'uncertainty space' bounded by plausible parameters for climate sensitivity, future greenhouse gas emissions, and regional patterns of change. Environmental and socio-economic factors are other uncertainties that may need to be managed during risk assessment since they may contribute to risk as stressors and modifiers of impact and resulting consequences. However, major climate-related uncertainties are the only factors considered in this report, due to space concerns.

A range of statistical methods can be used to explore uncertainty, but there is no completely objective way of applying these statistical methods to manage uncertainties because of the complexity of the problem. Some of the approaches used are multi-model studies that produce probability distributions, various sampling methods applied to quantify ranges of uncertainty, and expert judgement applied to 'what if' scenarios and sensitivity studies. Several of the above approaches can be combined in scenario construction for assessment.

It is important that all approaches used are clearly described and reproducible, with assumptions clearly stated to ensure credibility with stakeholders so results are ultimately accepted. Results can be tested through sensitivity studies where assumptions associated with a specific uncertainty are altered to determine robustness of the uncertain factor (e.g. Jones and Page, 2001; Dessai and Hulme, 2007). If the result is insensitive to changes then that particular source of uncertainty can be overlooked. If the result is sensitive, interpretation of the results will depend on confidence that the uncertainty has been represented well and judgement about how important its contribution is. Sensitivity testing can be applied to methods and assumptions, as well as changing inputs. Sometimes it may be necessary to make a trade-off between uncertainty management and scenario detail (e.g. the degree of spatial and temporal downscaling) in an assessment.

4.4.1 Representing climate uncertainties

Most often, bounded estimates of climate change are used rather than the total uncertainty in adaptation assessments. Figure 4-1 shows an example of sampling effects, where changing the number of models, emission scenarios and climate sensitivities affects the uncertainty space, here represented by a range of temperature changes. In the top line (red), with a single model, one emission scenario, and low, medium, and high climate sensitivities, the three estimates of future change (represented by the dots) are confined to a small region. In the middle line (green), where six emission scenarios are considered instead of just one, a broader range of futures is seen. The bottom (blue) line, with six models and six emission scenarios, has an even wider range of potential changes. As can be seen from the figure, likelihoods and associated statistics such as mean, median or standard deviation will differ considerably depending on the methods and assumptions made (Lopez *et al.*, 2006).

To address uncertainty, current best practice in climate modelling is to include as many models and scenarios as possible to produce a plausible range of futures, as in the lower series in Figure 4-1. The study described in this report used three different models for downscaling for two emission scenarios (lower and higher) with input data from six of the CMIP5 models that best simulate the current climate to capture a plausible range of future climates.

4.4.2 Examples of uncertainty management in impact and risk assessments

Future climate simulations which include a large number of interactions between various components with a broad range of scenarios may not be possible, given the time and resources involved in impact assessments. This can be addressed by:

1. Prior screening of a population of climate scenarios to identify the 'most-likely' future climatic conditions (Jones and Mearns, 2005). This projection is then used in impact assessment, yielding a 'most likely' impact.
2. Prior sensitivity analysis of the impact model of interest with a relatively small number of arbitrary projections. The population of impact outcomes can subsequently be used to generate a simple statistical impact response function that can then be used to comprehensively explore a larger population of global and regional climate model estimates.

When identifying climate variables and selecting the relevant projection information, the information used in the risk assessment should be internally consistent. For example, all projections of rainfall and temperature change applied in an agricultural impact model should have a consistent set of assumptions, including the choice of climate models, time period, and greenhouse gas emission scenario.

Figure 4-1: Projected changes in annual mean temperature in Canberra in 2070 based on simulations with the OzClim scenario generator (**www.csiro.au/ozclim**; Page and Jones, 2001). Results are presented for temperature changes using one model (CSIRO Mark 3.0) with one emission scenario (A1) and three climate sensitivities (red); one model (CSIRO Mark 3.0) with the six IPCC illustrative scenarios (green); and eight models with the six IPCC scenarios (blue). Coloured arrows on the axis identify the minimum and maximum results for each ensemble of results.

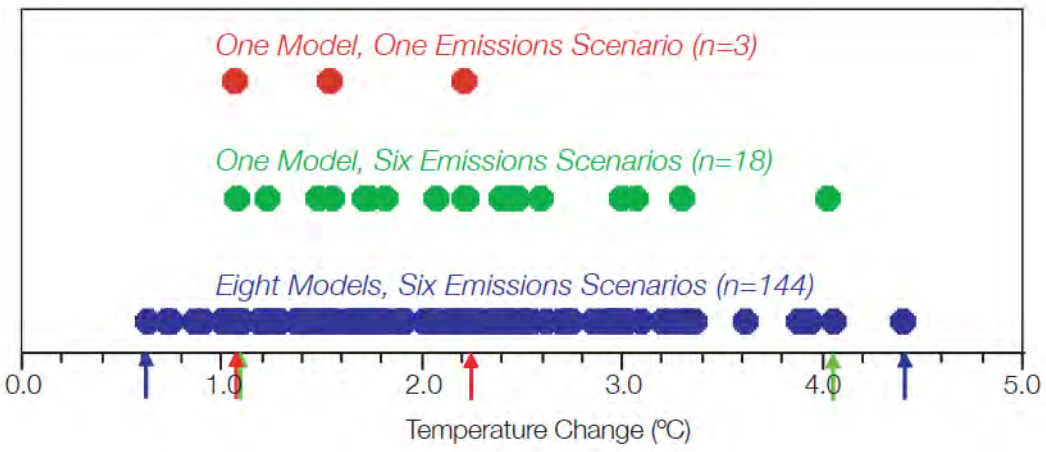

Arbitrary mixing-and-matching of projections degrades the realism of the outcome and limits comparability of different impact and risk assessments. Variables such as temperature, rainfall, evaporation, and humidity are highly interactive, meaning a change in one variable has an effect on other variables. To identify the worst possible outcome from an impact model, it may be tempting to identify the most pessimistic rainfall projection from any climate model and pair that scenario with the most pessimistic temperature projection. However, because the projections for the variables were derived from different climate models, they may be physically inconsistent, providing a spurious estimate of future impacts. The magnitude of projected impacts would therefore be larger than that derived from internally consistent projections (see Figure 4-2). Instead, estimates of impacts should first be calculated independently for each climate model under consideration. This results in a range of impact estimates that are representative of plausible climate futures which can then be ranked according to their relative impact – low, high and/or intermediate outcomes, or combinations of those in probability distributions can be selected for further application.

4.5 UNDERSTANDING CLIMATE PROJECTIONS

The availability of climate data does not ensure that such information will be used effectively for managing climate risk. Recent work on climate change communication has identified challenges in delivering messages to the public regarding climate change and its consequences. Unless overcome, these challenges diminish perceptions of climate risk, reduce incentives for taking risk management actions and limit understanding of what actions may be useful or appropriate.

Considerations for the delivery of climate projection information:

- The need for different data by diverse stakeholders.
- The need for simplicity and transparency in communication of information.
- The limited ability by stakeholders to distinguish between weather forecasts, seasonal climate forecasts and multi-decadal climate projections.
- Confusion by stakeholders in managing information on climate change as new research becomes available, such as successive generations of climate change projections, and the use of different climate models, emission scenarios and model resolutions.
- Conflicting messages from different communicators.
- The need for information on how to respond to projected changes.
- The potential for demands for information to exceed available resources and technical capacity.

Figure 4-2: Example of appropriate and inappropriate use of climate model projections in impact assessment. For both of the above figures, rainfall (R) and temperature (T) projections from three different global climate models (GCMs) are applied in a hypothetical impact model. In (a), each pair of global climate model scenarios is applied independently to the impact assessment model, resulting in a range of different climate impacts. In (b), projections of rainfall and temperature from different models are paired to yield extreme scenarios of climate change, which are then applied to the impact model. Source: CSIRO and BoM (2007).

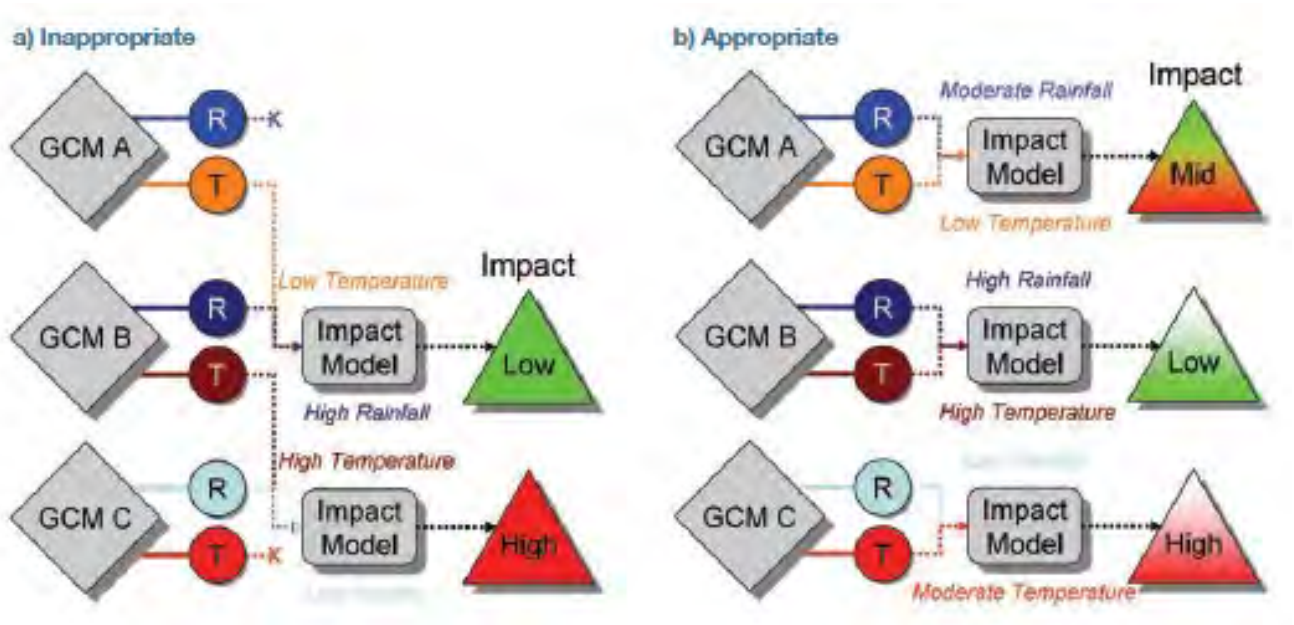

Such sentiments reflect two issues that exist in conflict:

- An intense demand for increasingly detailed information.
- Challenges in meeting demand as well as in interpreting and using the information which is available.

In discussion with stakeholders, several have identified the difficulty in obtaining and applying climate projections. Perhaps the most effective mechanism for overcoming the challenges to using climate information in decision-making is to tailor information about climate change and impacts for a particular decision need, so the projections are relevant and uncertainty is treated in the manner preferred by the stakeholders, who will then have more intimate knowledge of the methods employed. This will increase the chances that the data is appropriately interpreted and effectively used. It is recommended that other stakeholders using the climate projections generated for this project contact IMHEN to explore this option for use of the projections in their applications.

As the demand for climate projections has grown, various tools have been developed which represent different methods for enhancing the delivery of climate information to the public and stakeholders, both for education and for risk assessment and management. The Climate Futures Tool developed for this project is one such tool.

4.6 CLIMATE FUTURES TOOL

Detailed forecasts are often not required in many risk assessment exercises; instead, provision of physically plausible ranges of future climates is more feasible and more useful. A single projection of future climate conditions may be sufficient to illustrate the type of changes that can occur and the potential sensitivity of impacts to that change, or to test a particular method of downscaling. However, for most other purposes, it is better to apply a larger number of projections that represent a larger portion of the uncertainty space.

One commonly used approach is to apply widely divergent estimates of future changes, such as a 'best case' and a 'worst case', for example by constructing two projections combining a higher climate sensitivity (commonly yielding higher temperatures) with drier conditions, and a lower climate sensitivity with wetter conditions (e.g. NAST, 2000; Hayhoe *et al*., 2004; Edmonds and Rosenberg, 2005). The use of disparate emission scenarios can further accentuate the difference in projected futures. However, while both may be plausible, they represent limited uncertainty and it is difficult to determine which, if either, might be more likely. Alternatively, investigators can examine a broad range of climate projections from multiple climate models to identify 'low' and 'high' projections that are more reflective of the full range of uncertainty (AGO, 2006a, 2006b). The Climate Futures Tool allows the end user to explore the range of futures and select the 'most likely', the 'worse case' and the 'best case' for their specific variables.

4.6.1 Delivering climate projections to end-users and stakeholders

Dealing with the complexities of climate projections, such as the expanding number of potentially relevant climate models and the substantial differences in regional projections, is a key challenge in the provision and use of climate-change information for applications. In many cases when conducting impact assessments, localised projection data for multiple climate variables (e.g. both temperature and rainfall) are required. Users of these climate projection data often require a 'best guess' assessment of future climate and prefer to use a single, or small number of climate scenarios in their applications. It is essential that projection data are internally consistent, so when users are applying multiple variables for a possible future climate, the physical relationships between variables are maintained. This ensures that the possible future climates are physically plausible. Values obtained from multi-model distributions, Probability Density Functions (PDFs) or multiple datasets may not have this consistency.

Projection values obtained from a single climate model have this 'internal consistency' and are considered physically plausible. However, with the growing number of available climate models such as CMIP3 (Meehl *et al*., 2007), CMIP5 (Taylor *et al*., 2011), and CORDEX (Giorgi *et al*., 2009), conducting detailed impact assessments using a large number of these climate models is often not feasible. Due to the large number of models there is a temptation to use just one or a few models. Deciding which models to use is not straightforward. While it may be tempting to use a single 'mid-range' model, this overlooks other outlying and potentially important future climates, e.g. a future with potential for large negative impacts. An approach commonly used to deal with this issue is to select a small number of 'best' climate models based on their ability to represent the current climate (e.g. Pitman and Perkins, 2008; Smith and Chandler, 2010; see also discussion in Section 2.3.1). However there is little consensus among climate scientists regarding the assessment of 'best' models, and often a model that performs well in one aspect can show less skill when evaluated for another aspect (e.g. differential skill in simulating different variables or systems). Furthermore, different climate models produce different climate projections, which results in a range of plausible future climates (Watterson, 2008). The approach of model selection does not account for the need to represent the range of uncertainty among the full suite of available model projections. It is important to represent this range of outcomes, as there is currently little justification in ignoring certain models unless they show drastically implausible behaviour from a physical point of view (Whetton *et al*., 2005; Australian Bureau of Meteorology and CSIRO, 2011).

4.6.2 The Climate Futures Framework

The Climate Futures Framework (Whetton *et al*., 2012) addresses these limitations by classifying the projected changes from the full suite of available climate models into categories defined by two climate variables (usually the change in annual mean temperature and rainfall, as in Figure 4-3). Thus, models can be grouped into different categories which have been termed 'climate futures'. For temperature and rainfall, for example the different groups are represented by the simple descriptions 'warmer and little change in rainfall', 'warmer and much wetter', 'hotter and drier' and so on. We can further calculate the relative likelihoods of each category based on the number of climate models that fall within that category. For example, if 7 of 18 models fall into the 'warmer and little change in rainfall' climate future at 2030 under a medium emission scenario, it is given a relative likelihood of 38%, described as 'moderate likelihood'. A subset of models can then be selected to represent any or all of the climate futures identified, overcoming problems associated with working with a large number of climate models, versus user desire for simplicity and internal consistency.

Figure 4-3: Scatter plot representing GCM annual mean temperature vs annual rainfall output classified into climate futures.

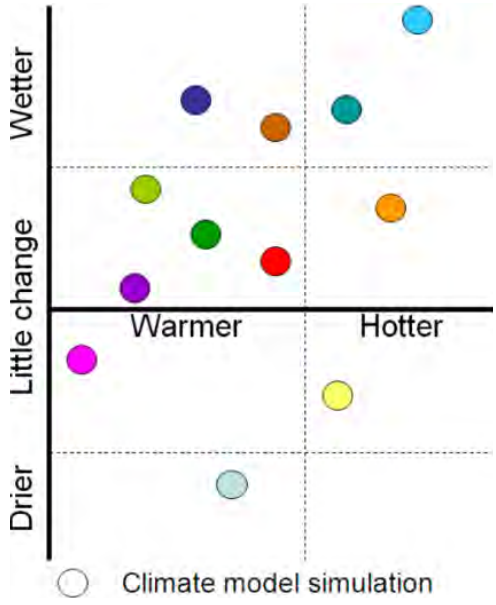

4.6.3 Use of the Climate Futures Tool in impact assessment

The Vietnam Climate Futures web tool (**www.vnclimate.vn**; Figure 4-4) facilitates the use of this framework at a regional level for the seven sub-regions of Vietnam: North West (NW), North East (NE), North Delta (ND), North Central (NC), South Central (SC), Central Highlands (CH) and South (S). By using this tool, the level of complexity is reduced, so users can explore climate projections and generate information tailored to their application, whether it is a general overview of climate change for a region, an investigation of likely threats and opportunities, or a detailed risk assessment using impact models. It also provides an objective means for selecting individual climate models to represent important climate futures for specific impact/risk assessments. For impact assessments, the climate futures approach can provide a pragmatic solution to the issue of dealing with 'too many models'. In sorting the models into defined future climates, the user can easily identify key future climates of interest such as 'best', 'worst' and 'most likely' future climates in terms of their expected impact.

The climate futures web tool provides projections for up to ten climate variables, two time periods (mid- and end-of-century) and two emission scenarios. There are two levels of access to accommodate users with different levels of expertise: Open Access, and Registered Users.

- The **Open Access** interface is accessible for everyone, with no login required. It provides an easy-to-use interface to access summaries of the projected changes in annual mean temperature and rainfall within three key climate futures ('least change', 'most likely', 'potential high impact'), for seven sub-regions throughout Vietnam.
- The **Registered Users** interface is accessible to users who have completed an online registration and requires a higher level of user skill to generate more detailed projections. It is specifically tailored for users involved in detailed impact/risk assessments. Users can generate climate futures based on pairs of climate variables of interest for a selected time period and emission scenario. Additionally, an average period (e.g. annual, seasonal, monthly) can be chosen. Users can also objectively select one or more individual models to represent relevant climate futures and export internally consistent data.

When conducting a study of climate change impacts on a system, some questions are commonly considered:

- Which climate variables are important?
- What is the relevant spatial scale (e.g. grid size)?
- What is the relevant time period?
- What are the uncertainties?

Knowledge of the answers to these questions, as discussed previously, will guide a user of climate-change data to the most appropriate data for their application. In some instances the answers are not straightforward and some additional guidance from data providers or scientific advisors may be required.

Figure 4-4: Home page of Vietnam Climate Futures Tool: **climatetool.vnclimate.vn**.

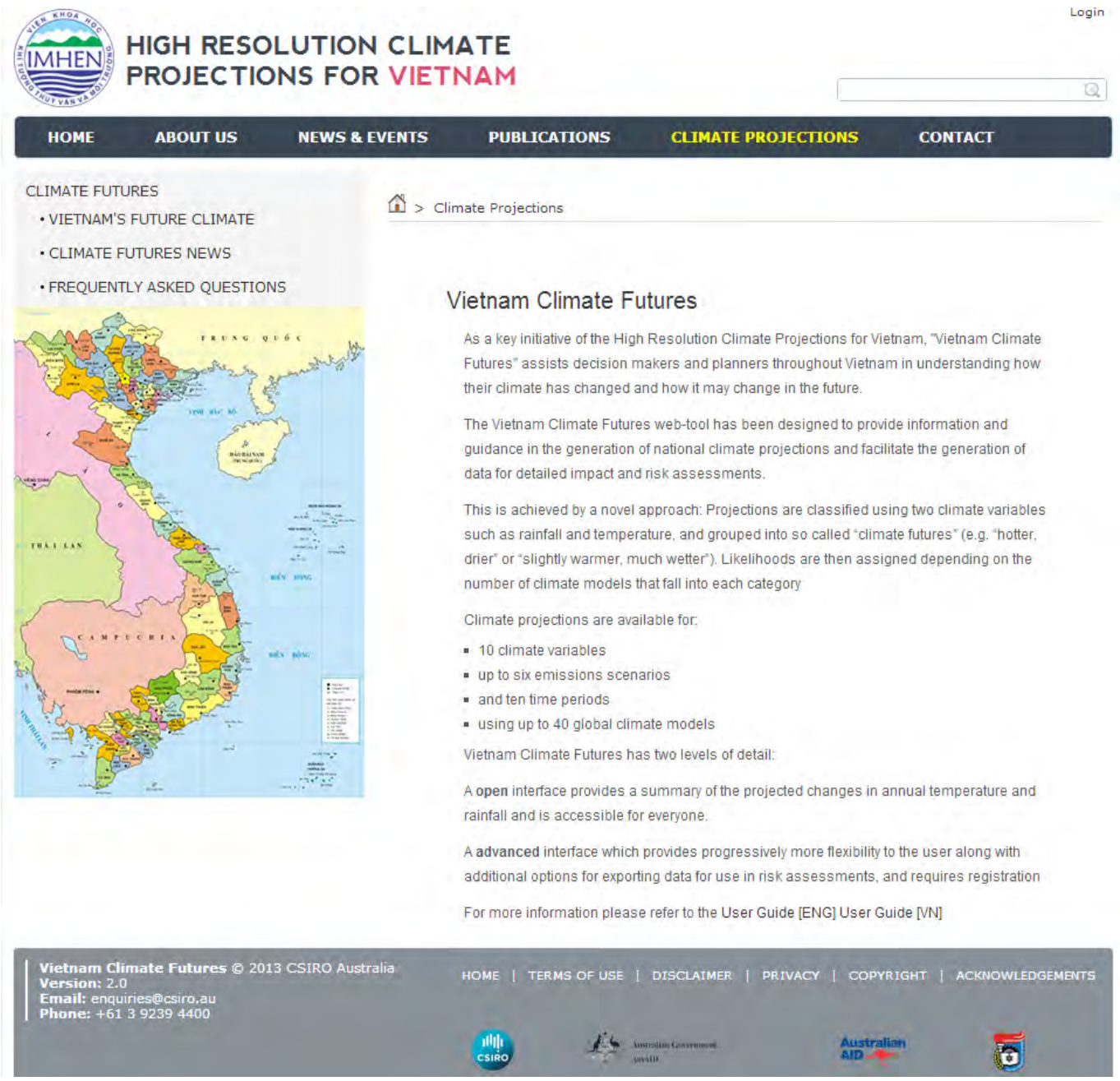

Once the key climate variables have been determined, these are then used to generate the climate futures. Application-relevant cases can then be identified such as (Figure 4-5):

1. The '**most likely'** case, whereby the future is represented by the greatest number of models. This requires that there be at least 10% more models in this category than the next most populous future, and that it is represented by at least one third of the total number of models. Note that it is not always possible to identify a 'most likely' projected future.
2. The '**best case**', which is dependent upon the details of the application or assessment being undertaken. It represents the most desired climate future for the user. For example, in a water availability assessment, a 'best case' future would be one that minimises the need for investment in additional water capture infrastructure; that is, a climate future that has the largest increases in rainfall.
3. The '**worst case**' is also dependent upon the details of the application or assessment being undertaken. It represents the least desired climate future for the user. For example, in a water availability assessment, a worst-case future would be one that results in the largest investment in water-capture infrastructure; that is, a climate future having the largest decreases in rainfall.

These three cases (referred to as 'key climate futures') can have one or more associated consequences identified by the user and a relative likelihood based on model numbers. Once these key climate futures have been identified they can be explored in more detail. One or two models can then be objectively selected to represent each key climate future. The climate futures tool does this by using a statistical multivariate ranking technique (Kokic *et al.*, 2002). Depending on the needs of the application, projected changes can be used directly from the selected models, or users can obtain dynamically downscaled results for higher resolution information. This will result in a small subset of models to represent each key climate future tailored to the impact study (see example in Table 4-2).

Figure 4-5: Example Climate Futures matrix showing a hypothetical 'best' case (green outlined box), 'worst' case (red outlined box) and 'most likely' case (black outlined box) for ND region with RCP 8.5 for end of century. Note likelihood colour coding is based only on the GCMs.

		Annual Surface Temperature (C)			
		Slightly Warmer < 0.50	Warmer 0.50 to 1.50	Hotter 1.50 to 3.00	Much Hotter > 3.00
Annual Rainfall (mm)	Much Drier < -15.00				+ 1 of 4 RCM models
	Drier -15.00 to -5.00			+ 1 of 30 GCM models	+ 2 of 4 RCM models 1 of 30 GCM models
	Little Change -5.00 to 5.00			+ 1 of 30 GCM models	+ 1 of 4 RCM models 9 of 30 GCM models
	Wetter 5.00 to 15.00			+ 1 of 30 GCM models	+ 10 of 30 GCM models
	Much Wetter > 15.00			+ 1 of 30 GCM models	+ 6 of 30 GCM models

Likelihood	Proportion of models
Not projected	No models
Very Low	< 10%
Low	10% - 33%
Moderate	33% - 66%
High	66% - 90%
Very High	> 90%

Table 4-2: Model selection for key climate futures for a hypothetical impact assessment given in Figure 4-5.

KEY CLIMATE FUTURE	CLIMATE FUTURE	LIKELIHOOD	REPRESENTATIVE MODEL
Worst	Much hotter and little change in rainfall	Low	CCAM NorESM1-M
Most Likely	Much hotter and wetter	Moderate	ACCESS1.3
Best	Much hotter and much wetter	Low	GFDL-CM3

4.7 USING AN INTEGRATED ASSESSMENT MODEL TO ASSESS POLICY OPTIONS

From an operational policy perspective, adaptation options need to be identified, assessed and selected before actual investments can be committed. However, for an effective assessment to be conducted, various data inputs are needed to characterise the current state and develop assumptions about the future state (Figure 4-6). Two key data inputs for such an assessment are climate change variables and sea-level rise projections. However, other required data may be important for the complete assessment of impact on a particular sector before consideration of adaptation options, such as hydrological data, spatial information (for example, from a GIS or geographic information system), social information about households and economic data. Combining all this information for an integrated assessment requires a well-defined methodology. The work described here aims to provide insights into the design of an assessment tool, undertaken as part of this project. This tool will ultimately process projections for the purpose of assessing options to adapt to climate change.

4.7.1 Modelling methods

There are various modelling methods that can be used for integrated assessment of possible climate change adaptations.

Statistical models

There are two types of statistical models, both based on analysis of past data:

- *Trend analysis.* This large group of modelling techniques is very powerful if the change we want to assess is captured in past data. For instance, trends or similar previous trend interruptions could be analysed with these methods and interpreted for future purposes. Most of the climate-related changes have not been experienced before and determination of trends is at an early stage. Therefore, these methods might be suitable for developing some parameter assumptions that go into the assessment model, but they cannot provide the actual assessment.
- *Correlations*. These models process past data to identify a relationship between different variables (correlations) or between particular variables and time (trend analysis). This type of modelling can produce parameterised functions (i.e. regression functions) or indicators (i.e. correlation strength) that describe such relationships and quantify their robustness (or uncertainty) (Neale *et al.*, 1999).

Macro-economic models

These modelling techniques operate mostly at the national level. Disaggregating the spatial scope down to provinces or catchments is technically very difficult; the results increasingly lose robustness at smaller scales (Smajgl and Liagre, 2010). Participatory design workshops with stakeholders in Vietnam identified a high relevance of economic information at the household level, while the national level has not been mentioned. Because of this scale mismatch, this group of modelling techniques seems less suitable

- *Input-output modelling.* These models utilise input-output tables. Such tables quantify relationships between different economic sectors in the form of inputs and outputs (valued in dollars) (Lenzen *et al.*, 2004). This methodology is used in nearly all countries to analyse the structure of national economies. It can help quantify options to stimulate an economy, as some sectors have more leverage than other sectors (quantified by value-add multipliers) or employ more people than other sectors (employment multipliers). Newer input-output modelling aims to make such snapshots dynamic or add natural resource considerations (Smajgl and Liagre, 2010).

Figure 4-6: Conceptualisation of link between climate projection data and assessment of adaptation options.

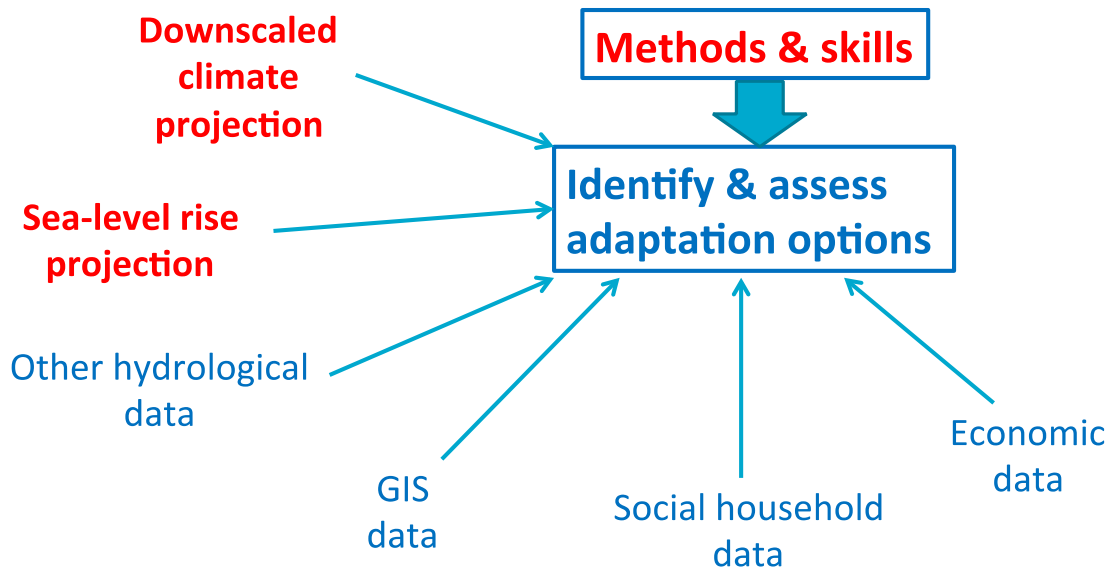

- *Computable General Equilibrium (CGE*). This modelling is a widely implemented type of mathematical modelling that builds on general equilibrium theory (Bergman, 2005; Smajgl, 2003; Smajgl *et al*., 2006). It assumes that all production is consumed, all income is spent and all prices are at the most competitive level (implying zero profit). CGE models are the dominant method used to predict GDP changes, and are used by all major supranational and national economic institutes.

System dynamics models

Some of the required inputs and outputs required in integrated assessment could easily be modelled by system dynamics models. This includes the links between hydrology and agriculture. However, where spatial aspects and human responses (i.e. land use change, livelihood change) gain importance, system dynamics models lose applicability and agent-based models become more effective.

System dynamics models are based on systems thinking (Coyle, 2000), which identifies system components and specifies mathematical relationships between them. System dynamics models can be used to develop only system diagrams for the purpose of conceptualising a problem or visualising certain functions in a particular system. System dynamics models can also be computationally implemented to predict how systems might evolve over time if boundary conditions change.

Bayesian Belief Networks (BBNs)

BBNs are very strong in quantifying uncertainties although the modeller needs to specify the states of all variables. If one is interested in the likelihood of known outcomes, BBNs are a good choice. BBNs would be a good methodology for the assessment of adaptation investments in Vietnam if the context of climate change adaptation could be reduced to a set of pre-known outcomes with quantifiable probabilities. Due to the relevance of emergent dynamics and the complexity of the context, this is unlikely to be the case. Additionally, spatial aspects are not a strength of BBNs and yet they are critical to understand the effectiveness of all relevant adaptation options.

A probabilistic modelling technique described by Cooper (1990) requires the specification of variables that influence the state of a particular indicator, how these variables are linked and the probability of states of variables. Based on Bayesian theory, the overall probability of states of the target indicator can be calculated if the state of explaining variables changes.

Optimal control methods

Optimal control models assume a functional relationship between a target indicator and explaining variables (Sethi, 1977). Utilising algorithms such a function can be solved to maximise or minimise the target indicator. Constraints can be considered by specifying upper and lower bounds for values of explaining variables.

Dynamic optimisation allows for identifying the best solution in a given solution space subject to specified constraints. This group of methods requires specifying a particular behaviour of all involved system components. Thus, optimal control methods do not seem applicable.

Hydro-economic models

These models apply economic values into hydrological modelling and are typically used to determine the economic (monetary) value of water. As the context of assessing adaptation options in Vietnam requires the consideration of a much broader domain of social-ecological interactions, these modelling techniques cannot be recommended.

Agent-based models (ABMs)

These are computational models which contain an explicit and individual representation of the entities of the target system being modelled and of their interactions (Gilbert, 2008; Smajgl *et al*., 2008). Technically ABMs are also based on systems thinking but in comparison to systems dynamics models, ABMs are able to specify qualitative rules, which are critical for simulating human behaviour. Agents in the model can represent individual entities such as humans with various levels of cognitive capacity, and also groups of individuals and non-cognitive environmental entities. As the system representation is developed from the perspective of individual entities (bottom-up approach) agent-based modelling allows for the analysis of 'evolving systems of autonomous interacting agents' (Tesfatsion, 2002).

As Deadman (1999) points out, instead of defining the overall behaviour, in ABMs 'this overall behaviour emerges as a result of the actions and interactions of the individual agents'. This makes agent-based modelling effective in analysing complex adaptive systems (Miller and Page, 2008). In-depth descriptions of agent-based modelling can be found in Holland and Miller (1991), Holland (1992) and Gilbert (2008). ABMs at the local scale are not new to the Mekong Region, as a series of agent-based models has been developed for Thailand, Vietnam and Bhutan using participatory processes (Bousquet *et al*., 2006; Bousquet *et al*., 2007); see also **http://www.ecole-commod.sc.chula.ac.th/pn25/index.php**.

4.7.2 Determining required assessment model inputs and outputs

Choice of which modelling method to use depends upon the inputs and outputs required for the risk assessment to determine adaptation options. The inputs define what the model needs to assess. The outputs specify what information is required from the model. Figure 4-7 shows what interventions a future assessment model would need to be able to assess (in the upper box) and what information it would need to provide (in the lower box) when considering possible future changes in rainfall that may affect flooding and infrastructure needs.

Agent-based modelling is a method that allows for simulating highly complex situations and allowing unexpected phenomena to emerge. Combining an agent-based model with a hydrological floodplain model is a method of addressing the complexities of the assessment needs. The response of households to government interventions is critical and cannot be simply assumed. This was the key argument for choosing agent-based modelling, supported by the need to work with high-resolution data and directly linking hydrological, agricultural and livelihood-related dynamics.

Figure 4-7: List of required features for an integrated assessment model. Inputs are in top box, outputs in bottom box. Colour coding explains the suitability of existing modelling capacity implemented in agent-based methodology: green identifies aspects that can easily implemented in an agent-based model, yellow are dimensions that can be implemented in agent-based modelling depending on the resolution, and red marks aspects that cannot be easily implemented in an agent-based model for Vietnam.

Inputs and Outputs for an Integrated Assessment Model

...the impact of...

- **Changes in sea level, rainfall, temperature, extreme events**
- **Weather monitoring and early warning system**
- **Dykes/sluice gates, water treatment and urban drainage**
- **Resettlements**
- **Crop and land use changes, deforestation**
- **Road upgrades**
- **Building code changes**
- **International water sharing and dam operation agreements**
- **Awareness raising and new crop research**

...on...

- **Vulnerability, sensitivity, adaptive capacity, risk**
- **Agricultural production**
- **Hydrology**
- **Household economics, wellbeing and poverty**
- **Population growth**
- **Food security, nutrition**
- **Biodiversity, environment, endangered species**
- **Gender equality**
- **Migration**

The technical advantage of agent-based modelling when dealing with the requirements listed in Figure 4-7 explains the colour coding. All points in green can be implemented in an agent-based model, some of them more easily than others and some of them requiring more data than others.

The implementation of the yellow points depends on the exact definition of what is needed. Several points were still rather vague and could not be sufficiently specified during early stages of model development, including:

- Building codes (legislation changes)
- Population growth
- Gender equality.

Some yellow points could be implemented in an agent-based model but depend upon further work with other disciplinary models, such as models dealing with

- Dykes/sluice gates
- Water treatment
- Urban drainage
- Hydrology.

Some aspects within hydrology, in particular flooding, depend on the resolution of the model and what data will be available at different levels of resolution. These indicators might be less suitable for the integrated-simulation model and should be addressed by hydrological models. For instance, projecting flood levels for the purpose of infrastructure investments requires a very high resolution, potentially down to the accuracy of a centimetre. Implementing such a function in an agent-based simulation model is technically possible but could be more effectively achieved by the use of existing hydrological models, such as the floodplain model Mike 11 (DHI, 2005), which is in use by Vietnam's government agencies. The effect of flooding on roads requires a high-resolution representation of water levels. Given the availability of floodplain models for parts of Vietnam's coast, in particular the Mekong Delta, it seems more cost effective to integrate indicators such as the risk to roads or other infrastructure of being flooded in those models. However, the data required for this kind of infrastructure-related flood-risk modelling do not seem to be available. Therefore 'road upgrades' is listed in red, because flooding causes erosion, landslides and damage to roads and bridges. In synthesis, this supports the decision to employ existing hydrological floodplain models to assess road upgrades.

4.7.3 Agent-based modelling workshops in Vietnam

In 2011 and early 2012 a series of meetings identified the need for improved capacity at IMHEN to conduct integrated assessments of climate change on the provincial level. This need arose, in part, from the *National Target Plan for Climate Change* and its mandate for provinces to develop climate-change adaptation plans and the need for central government capacity to evaluate and prioritise provincial proposals. The fact that the effectiveness of many strategies, such as investments in dykes and sluice gates, depends on changes occurring in neighbouring countries introduces additional challenges to be considered. The aim is to build capacity at IMHEN and other Vietnamese research institutes on how to use the new regional climate-change projections to help assess various adaptation options and to advise the government on the effectiveness of the adaptation measures.

In order to develop an effective assessment tool, the following steps are needed:

1. Explore assessment needs with government departments and officials who are dealing with planning as well as management agents.
2. Review effective methods and design an integrated assessment tool.
3. Review techniques to prepare datasets for application in the integrated assessment tool.
4. Prepare a plan for the joint development of a model to conduct integrated assessments of climate-change adaptation investments in Vietnam's coastal and inland provinces, to be implemented if funding is available.

Details of a series of workshops held in Vietnam in 2012 to address these issues and develop capacity within Vietnam to continue this process through techniques such as the use of agent-based models are given in Appendix 1. The participatory process provided participants with the fundamentals of agent-based design and the analysis of agent-based models.

The list that synthesises answers to these questions was compiled and discussed with IMHEN.

Key questions about features that the assessment tool would need to cover were:

Inputs:

1. What specific interventions would an integrated assessment tool need to assess to be beneficial to your agency?

Outputs:

1. What information would an assessment tool need to provide (indicators and resolution) in order to be beneficial to your agency?
2. What geographical focus area should such an assessment model have to be beneficial to your agency?

This training connected the data (downscaled climate and sea-level rise projections) to assessment of adaptation options by (1) designing assessment requirements and (2) training staff from IMHEN, SIHYMETE and CTU, so that agent-based modelling can potentially be applied in the future for integrated assessment of climate change risk and adaptation options.

4.8 SUMMARY

Given the inherent variability of Vietnam's climate, combined with other unknowns associated with climate change, projections of future climate are likely to be limited by substantial levels of uncertainty.

To develop meaningful estimates of the risk of future climatic events, simulations using low-resolution climate models to derive average changes in climatic conditions are not sufficient. Instead, high-resolution modelling, such as presented in this report via dynamical downscaling, provides the detail often required to simulate such events. However, there is a trade-off between easy-to-apply methods versus more realistic, detailed assessments and these trade-offs need to be considered against time, money and resources available. Ideally, scenarios should be constructed using the simplest information required to make the decision under consideration.

Detailed risk assessments related to decision-making events with large impacts or large expenses will often require customised climate projections. These customised projections may provide more specific analysis of probability, sensitivity and variability of climate variables, and also require incorporation of other data such as socio-economic data for integrated assessments to directly serve the decision-making requirements. A direct link between those who develop customised climate projections and decision-makers will also allow for more intimate knowledge exchange about methods applied, assumptions and treatment of uncertainties.

It is essential for end-users to identify means for managing uncertainties in a manner appropriate to their specific application and refrain from uncritical use of climate projection information. Sensitivity studies can improve understanding of which climate variables respond to changes in modelling assumptions, and also feed back into modelling studies in terms of where improvements are needed most. Applying these techniques to impact and risk assessment should help constrain uncertainties by providing tighter 'most likely' outcomes.

Use of the Climate Futures Tool can improve user access to and enhance understanding of climate projections by aiding in the selection of internally consistent information that captures the range of future changes, including the 'most likely', 'best case' and 'worst case' for a particular application.

During the workshops held in Vietnam in 2011 and 2012, preliminary work was completed on developing a customised agent-based modelling system to provide integrated assessments of adaptation options through a participatory process. The advantage of using an agent-based modelling system is that it can incorporate socio-economic factors and information from other sources as well as climate projection data. One example of previous use of agent-based modelling in Vietnam is the Mekong region simulation model (Mersim; Smajgl *et al*., 2013). With further funding for development, agent-based modelling can be another approach to use of the high-resolution projections from this study detailed in the following chapters for adaptation planning.

5 MODEL PERFORMANCE FOR CURRENT CLIMATE

5.1 INTRODUCTION

This chapter assesses the performance of both GCMs and RCMs in simulating characteristics of the observed present climate over the area that covers Vietnam. Section 5.2 describes the observational datasets and validation methods. Section 5.3 provides an evaluation of selected CMIP5 GCMs over Vietnam and surrounding regions. Section 5.4 provides an evaluation of the ability of three RCMs forced by ERA-Interim reanalyses to simulate Vietnam's climate, while Section 5.5 provides an evaluation of the same RCMs to simulate the present climate when downscaling the various GCMs.

5.2 OBSERVATIONAL DATASETS AND VALIDATION METHODS

The various observed datasets used for model validation in this chapter are listed in Table 5-1. The datasets are described in Chapter 2. The analysis was performed based on comparison of seasonal averages of observed and simulated precipitation, temperature, and 850 hPa winds. First, an assessment of spatial patterns, annual cycles of circulation, rainfall and temperature was conducted. Then, statistical validation for models was completed. The reference period of 1980 to 2000 was used for validation of all regional climate model simulations, unless otherwise stated. The period 1975-2004 was used in the validation of the GCMs.

5.3 AN ASSESSMENT OF THE NEW GENERATION OF GLOBAL CLIMATE MODELS OVER SOUTH EAST ASIA

5.3.1 Introduction

In this section, we present an assessment of the new generation of GCM simulations performed for the Coupled Model Intercomparison Project Phase 5 (CMIP5) over South East Asia, particularly focused on Vietnam. Statistical measures such as pattern correlation and Root Mean Square Error (RMSE) are calculated using observed and simulated data for four seasons as well as annual values. In this study, 31 simulations were used from 15 organisations, since one or more simulations were submitted by modelling groups of the world. First, observed climatologies of seasonal annual rainfall, temperature and mean sea-level pressure of the historical or the present period from 1975 to 2004 were compared with simulated climatologies of the models. The four seasons considered in this study are the First Inter-Monsoon Season (FIMS, April-May), South West Monsoon Season (SWMS, June-September), Second Inter-Monsoon Season (SIMS, October-November) and North East Monsoon Season (NEMS, December-March).

5.3.2 Data and methods

Monthly data from 31 GCM simulations were obtained from the CSIRO archives. The data were originally extracted from the IPCC Model Output website at **http://www-pcmdi.llnl.gov/**. Some of the models have single simulations for the 20th and 21st centuries, while some models have multiple simulations. For models with multiple simulations, we have computed ensemble-mean changes in climate. The simulations of the 20th century climate were driven by observed changes in greenhouse gases and aerosols. Some simulations included direct and indirect effects of aerosols, some included ozone depletion, and some included volcanic aerosols and solar forcing.

Climatological averages for the MSLP, temperature and rainfall for a 30-year period (1975-2004) for four seasons were constructed. Statistical methods were used to test whether the models adequately reproduce each of these fields over a broader region that covers Asia and South East Asia (60-160°E, 15°S-50°N). A smaller region was also selected to test the reliability of the models, excluding the mountain regions of Asia. The domain for the smaller region covers South East Asia (90-140°E, 0-40°N). A pattern correlation coefficient of 1.0 indicates a perfect match between the observed and simulated spatial pattern, and a Root Mean Square Error (RMSE) of 0.0 indicates a perfect match between the observed and simulated magnitudes.

The RMSE is based on all grid points in the considered domain, and we show results primarily based on annual values. However, we discuss the results based on seasonal values where necessary.

5.3.3 Results

An assessment of the new generation of model simulations over South East Asia using the above-mentioned statistical measures and visual judgements reveal that most of the models simulate the spatial patterns of MSLP fairly well, except some models like HadGEM2-CC and HadCM3 that have relatively weak correlations and large RMSE values (Figure 5-1). Results based on seasonal values indicate that many models fail to capture the observed spatial patterns of MSLP during the South West Monsoon and Second Inter-Monsoon seasons, with large RMSE values presumably due to the complex orography over Central Asia. However, the models capture the observed spatial patterns when the validating domain is reduced in size. These results suggest that the new generation models still find difficulty in simulating the correct atmospheric patterns over orographically complex areas.

Table 5-1: Observational datasets used for validation of RCM simulations for Vietnam.

DATASET	VARIABLES	RESOLUTION	SOURCE	REFERENCES
Stations	Tmax, Tmin, Precipitation	Station locations		
ERA-40	850 hpa winds	2.5°, monthly	Reanalysis	Uppala *et al.,* (2005)
APHRODITE	Precipitation	0.25°, daily	Gridded station data	Yatagai *et al.,* (2009)
CRU 3.0	Temperature	0.5°, monthly	Gridded station data	New *et al.,* (2002)

Figure 5-1: Relationship between pattern correlation and RMSE values for annual MSLP and temperature for the larger domain (60-160°E, 15°S-50°N) for the period 1975-2004. Note the best models tend to sit towards the top left corner and the worst models tend to sit towards the bottom right corner of the figure. Names of the model simulations are shown in the column on the right.

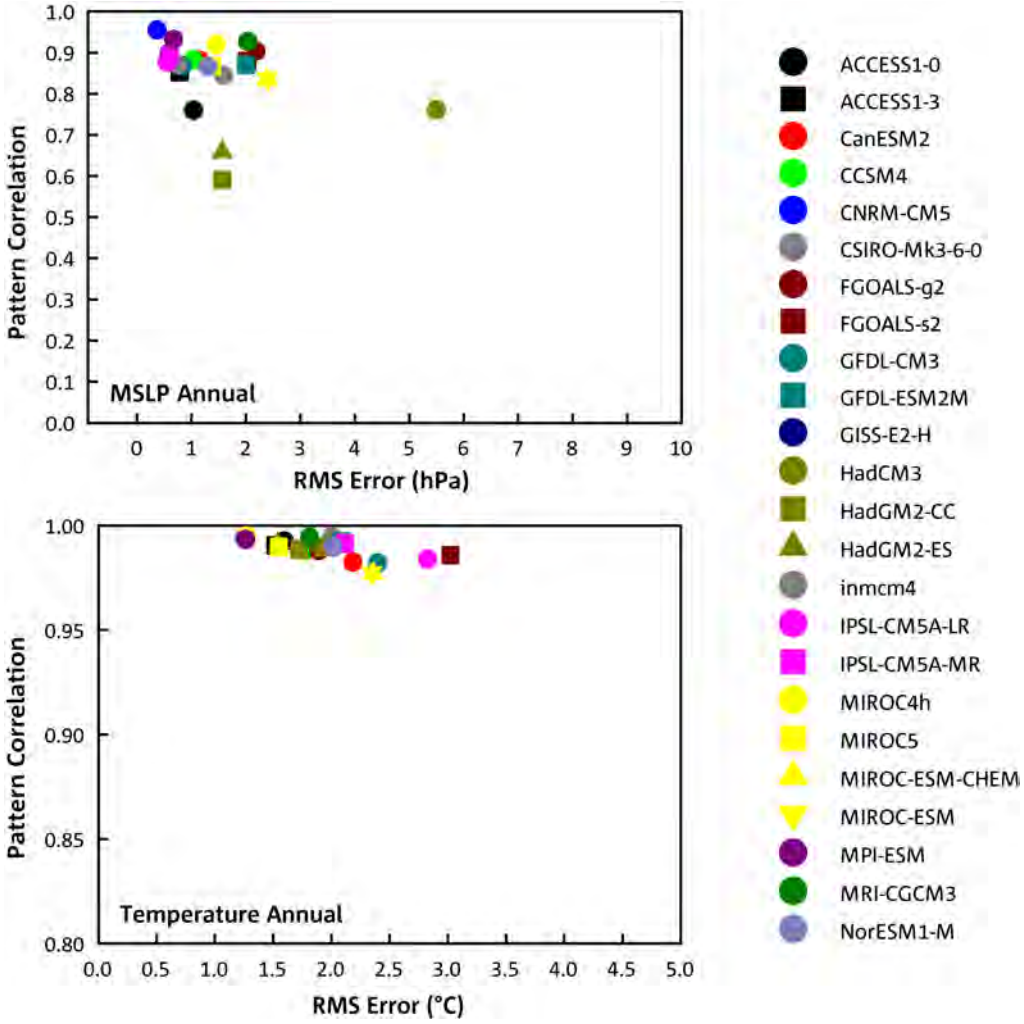

Figure 5-2: Annual average model temperature biases (°C) based on the difference between model simulations and observed values for the period 1975-2004.

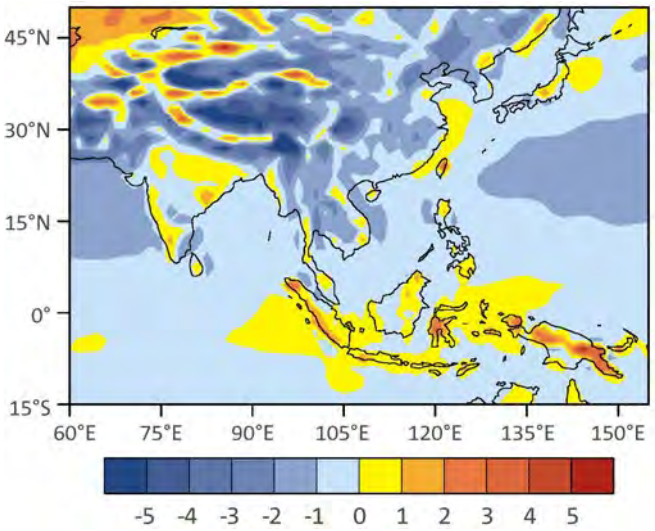

Results for temperature simulations reveal that almost all the models capture the observed annual and seasonal spatial patterns. However, Figure 5-1 shows that there are strong model-to-model variations in RMSE values, which range between 1°C and 3°C. The annual bias between CMIP5 models simulations and observations is shown in Figure 5-2. The models tend to underestimate observed average temperature over the land area and slightly overestimate values over the ocean. The underestimation over land areas is large during three seasons, except for the First Inter-Monsoon season.

Figure 5-3: Relationship between pattern correlation and RMSE values for annual rainfall for ERA-Interim and CRU data for the larger domain (60-160°E, 15°S-50°N) for the period 1975-2004. Note the best models tend to sit towards the top left corner and the worst models tend to sit towards the bottom right corner of the figure. Names of the model simulations are also shown in the column at the right.

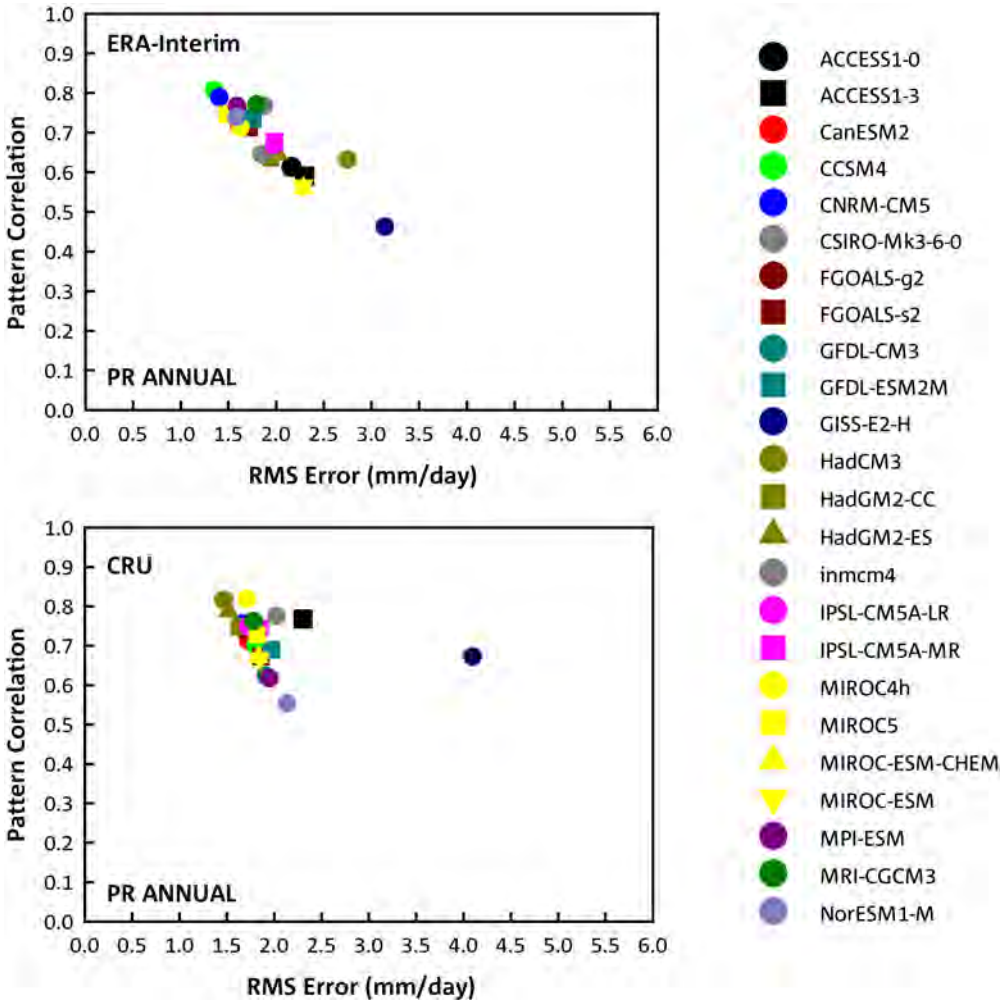

Figure 5-3 depicts the pattern correlation and RMSE for observed and simulated annual rainfall. Here we present results comparing simulated data against two global datasets: the ERA-Interim dataset covers land and ocean areas, while the CRU dataset covers only land areas. Pattern correlations are relatively strong (greater than 0.6), except for a few models. A cluster of models shows strong correlations, with RMSE values between 1.5 and 2.5 mm day^{-1}, indicating that these models are capturing the observed pattern well. Correlations are relatively strong when comparing data from land-only areas, but tend to be weaker when using data from ocean and land areas separately. There are differences in the performance of the models for various seasons. During the North East Monsoon and Second Inter-Monsoon seasons the models perform better than in the South West and First Inter-Monsoon seasons. This may be partly due to deficiencies in the simulations of rainfall during the First Inter-Monsoon and South West Monsoon seasons over orographically complex areas. RMSE values range between 1.5 and 3.0 mm day^{-1} for most of the models, with the exception of a few outliers.

The annual rainfall bias between CMIP5 models and observations based on the NCEP CMAP gridded rainfall dataset for the historical period 1975-2004 is shown in Figure 5-4. Overall the bias ranges between -6 and +4 mm day^{-1}. The models tend to underestimate observed annual average rainfall over South East Asia and the northern Indian and western Pacific Oceans. In particular, the northern part of Indochina shows relatively stronger underestimation. The models also overestimate observed annual rainfall over the Maritime Continent and also slightly over northern Asia. There are significant differences in rainfall bias among the seasons (shown in Figure 5-5). The models tend to underestimate rainfall over land and the Indian and western Pacific Oceans, and overestimate rainfall over the Maritime Continent. The biases are large during the First Inter-Monsoon and the South West Monsoon seasons. The spatial patterns of biases are reflected in the RMSE values.

Deciding on what is acceptable performance of a model is not straightforward. A good performance at simulating current climate does not guarantee that the enhanced greenhouse simulation is accurate. Nor do errors in the current climate performance mean that the enhanced-greenhouse simulated changes in climate are unreliable. This means that focusing on the results of the best-performing models may inadequately represent the underlying uncertainty in projecting regional climate change. Thus our approach to validation has been to view a model as acceptable unless the current climate errors are of a nature which, in our judgement, significantly reduces the likelihood that the enhanced greenhouse simulation is reliable. Absence of key climate features (e.g. pressure patterns and seasonal winds) in the region of interest would be an example of an unacceptable failure. The representation of model processes is important for judging the reliability of enhanced greenhouse changes, and for this reason we have placed emphasis on assessment of multiple variables and of spatial patterns.

Figure 5-4: Annual rainfall bias (mm day^{-1}) between model simulations and observations for the period 1975-2004. Observations are from CMAP data.

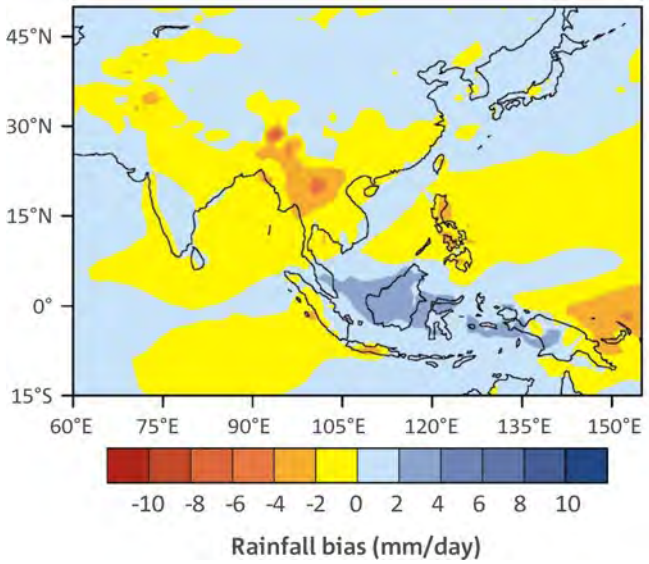

Figure 5-5: Seasonal rainfall bias (mm day^{-1}) between model simulations and observations for four seasons for the period 1975-2004. (a) First Inter-Monsoon Season, (b) South West Monsoon Season, (c) Second Inter-Monsoon Season and (d) North East Monsoon Season.

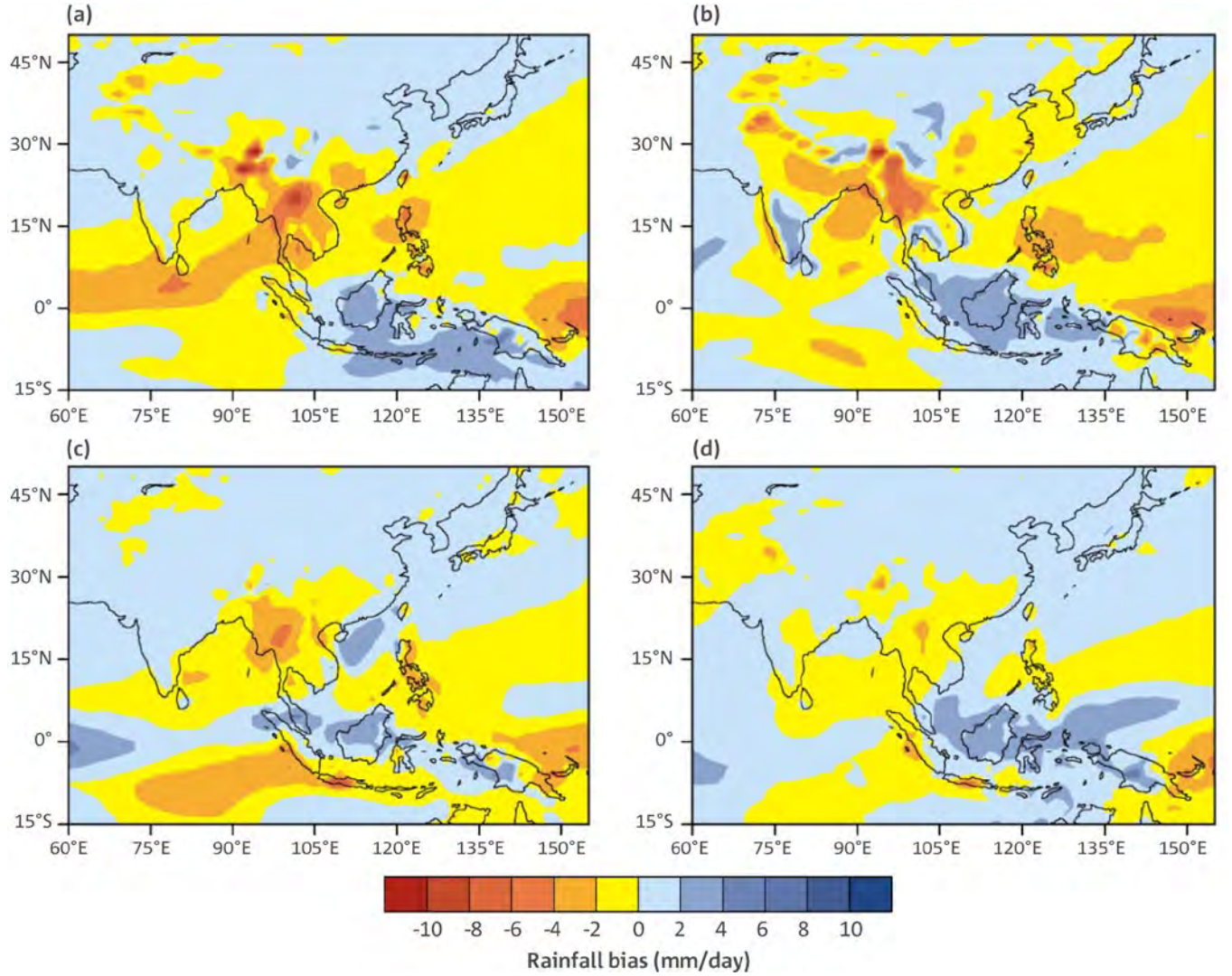

5.4 DOWNSCALED SIMULATIONS WITHIN ERA-Interim

This section assesses the performance of the three models (CCAM, RegCM4.2, and PRECIS) driven by the ERA-Interim reanalyses in simulating characteristics of the observed climate (1990-2007 or 1980-2000) over the area that covers Vietnam. Running models with observed lateral boundary data allows us to assess the skills of the models with accurate boundary forcing. Note that when limited-area models are run with GCM data, the accuracy of the boundary forcing will be reduced due to errors in the GCMs. The analysis compares seasonal averages of observed and simulated precipitation, surface air temperature and 850 hPa wind speed and direction.

The ERA-Interim dataset was used to provide the initial and boundary conditions for PRECIS from 1989-2008. The 1990-2007 validation period for PRECIS simulations was selected as representative of the current observed climate in Vietnam. CCAM used a scale-selective digital filter (see Section 2.6.1 for explanation of this technique) to input data from ERA-Interim for the 50 km global simulation for the period 1979-2009. The 10 km CCAM simulation also used a scale-selective digital filter to input from this 50 km CCAM simulation (so was not directly forced by the ERA-Interim dataset). The validation period was from 1980-2000. RegCM4.2 used ERA-40, instead of ERA- Interim, as initial and boundary condition data for the period 1979-2000, with a validation period from 1980-2000. Table 5-2 provides a summary of the model settings for the dynamically downscaled simulations. We note that a 1–year spin-up period at the beginning of the simulation was removed in all simulations before analysis to ensure that the validation is not influenced by the period necessary for soil moisture and temperature to stabilise.

Validation for the whole of Vietnam is presented first through spatial maps and statistics, followed by validation for the seven sub-regions.

5.4.1 Validation of temperature for Vietnam

Vietnam is characterized by a tropical and monsoonal climate with maximum precipitation and temperature occurring during the South West Monsoon Season (summer; JJAS) and minimum during the North East Monsoon Season (winter; DJFM). These characteristics are related to annual variations in the atmospheric circulation over South East Asia.

The seasonal mean air temperatures using the CRU observational data for NEMS and SWMS are shown in Figure 5-6 (left). A significant seasonal cycle of temperature is evident in northern and central Vietnam, but with little annual variation in southern Vietnam. Cooler temperatures over the higher elevations are also evident

The seasonal mean biases of surface air temperature (Tave) for the PRECIS, CCAM and RegCM4.2 simulations are also presented in Figure 5-6. For NEMS, PRECIS has only small biases, with a slight cold bias in north-western Vietnam and a slight warm bias in the South Central (SC) and Central Highland (CH) regions. A warm bias is evident over Cambodia and Laos. CCAM also shows little bias for this season, with possible cold biases in the higher elevations and in the South (S) region. A slight cold bias is also evident over Cambodia and Laos. RegCM4.2 has the largest bias, being generally cold everywhere, especially inland areas. The South Central (SC) and Central Highland (CH) regions have the smallest biases. For SWMS, all models generally have a cool bias, with RegCM4.2 again the worst. The largest biases (~ -3°C) are over the mountains, with CCAM having larger biases than the other RCMs. It is possible that the CRU dataset is less accurate in these regions, as it is based upon interpolated station data, with stations typically located in valleys, while the model temperatures are at the elevation of the model grid. Both PRECIS and CCAM have little bias along the central Vietnam coastline. While the three models behave similarly to one another in SWMS (summer), in NEMS (winter) there are notable differences, with RegCM4.2 displaying larger regions of cool biases and PRECIS larger regions of warm biases.

Table 5-2: Summary of the RCM set-ups.

MODEL	DRIVING DATA	SIMULATION PERIOD	VALIDATION PERIOD
PRECIS	ERA-Interim	1989-2008	1990-2007
CCAM	ERA-Interim	1979-2009	1980-2000
RegCM4.2	ERA-40	1979-2000	1980-2000

Seasonal and annual validation statistics for surface air temperature (Tave), maximum temperature (Tmax), and minimum temperature (Tmin) for the whole of Vietnam, computed by comparing the station observations with the nearest model grid point, are presented in Table 5-3, Table 5-4 and Table 5-5, respectively. For surface air temperature (Tave), the PRECIS model has a warm bias (ranging from 0.6 to 2.2°C) for all seasons, RegCM4.2 has a cold bias (ranging from -1.3 to -2.2°C) for all seasons, and CCAM has a slight warm bias for FIMS (0.7°C) and NEMS (1.1°C), and a slight cool bias for SWMS (-0.1°C) and SIMS (-0.6°C). Maximum temperatures (Tmax) show negative biases for all seasons and models, with RegCM4.2 exhibiting the largest bias of -6.4°C for NEMS. All models have positive biases in terms of minimum temperature (Tmin), with the largest bias for PRECIS (6.1°C). It is interesting to note that the largest negative biases tend to be for Tmax and the largest positive biases tend to be for Tmin, indicating all models are underestimating the mean diurnal temperature range, and also that the Tave biases tend to be less than those for Tmax and Tmin.

RMSE values show similar magnitudes and sizes to the biases, suggesting that the bias is the main contributor to the error. The pattern correlations are also quite high, indicating that the models are capturing the spatial pattern of temperature well. As temperature is strongly controlled by elevation (with cooler temperatures at higher elevations), there is a general trend to cooler temperatures in northern Vietnam, and as these runs were forced by analyses, this is not too surprising. Note though that Tave, Tmax and Tmin are not actually forced into the models. Only RegCM4.2 has somewhat lower pattern correlation values for Tmax, especially for FIMS and SIMS.

Figure 5-6: Seasonal mean surface air temperature (°C) for NEMS (winter; top) and SWMS (summer; bottom) for CRU (observations, left column) and biases of the three model simulations (PRECIS for the period 1990-2007 and CCAM and RegCM4.2 for 1980-2000).

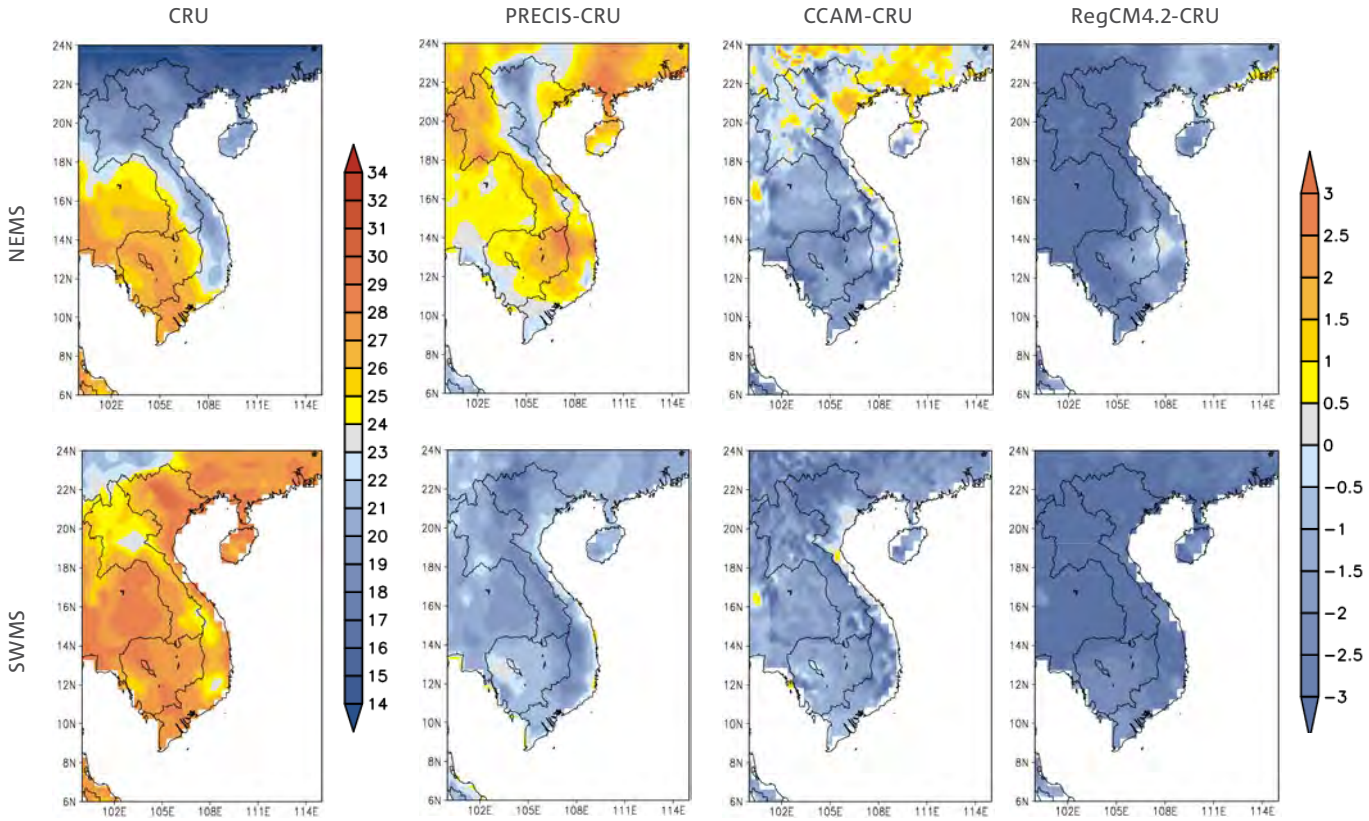

Table 5-3: Tave validation of RCMs relative to station observational data. Bold numbering indicates the best-performing model.

SEASON	BIAS (°C)			RMSE (°C)			PATTERN CORRELATION		
	PRECIS	CCAM	RegCM4.2	PRECIS	CCAM	RegCM4.2	PRECIS	CCAM	RegCM4.2
FIMS	1.6	**0.7**	-1.5	2.0	**1.6**	1.9	**0.88**	0.79	0.85
SWMS	0.6	**-0.1**	-2.1	0.9	**0.6**	2.3	0.96	**0.97**	0.90
SIMS	**0.3**	-0.6	-2.2	**1.0**	**1.0**	2.4	0.92	**0.94**	0.92
NEMS	2.2	**1.1**	-1.3	2.7	2.0	**1.9**	0.88	0.87	**0.92**
ANNUAL	1.3	**0.4**	-1.7	1.5	**1.0**	1.9	**0.93**	0.92	**0.93**

Table 5-4: Tmax validation of RCMs relative to station observational data. Bold numbering indicates the best-performing model.

SEASON	BIAS (°C)			RMSE (°C)			PATTERN CORRELATION		
	PRECIS	CCAM	RegCM4.2	PRECIS	CCAM	RegCM4.2	PRECIS	CCAM	RegCM4.2
FIMS	**-3.4**	-3.7	-5.0	**3.7**	4.2	5.7	**0.82**	0.69	0.58
SWMS	**-3.6**	-3.7	-4.6	**3.8**	3.9	5.0	**0.94**	0.90	0.76
SIMS	**-4.3**	-5.0	-5.3	**4.5**	5.1	5.6	0.86	**0.88**	0.71
NEMS	**-3.5**	-4.1	-6.4	**4.0**	4.5	6.8	**0.82**	0.75	0.78
ANNUAL	**-3.6**	-4.0	-5.4	**3.8**	4.2	5.7	**0.88**	0.84	0.69

Table 5-5: Tmin validation of RCMs relative to station observational data. Bold numbering indicates the best-performing model.

SEASON	BIAS (°C)			RMSE (°C)			PATTERN CORRELATION		
	PRECIS	CCAM	RegCM4.2	PRECIS	CCAM	RegCM4.2	PRECIS	CCAM	RegCM4.2
FIMS	4.9	3.1	**1.5**	5.2	3.6	**2.0**	0.82	0.76	**0.85**
SWMS	3.3	1.7	**0.1**	3.4	2.0	**0.8**	**0.94**	**0.94**	0.92
SIMS	4.4	3.1	**1.4**	4.7	3.5	**2.0**	0.88	0.89	**0.91**
NEMS	6.1	4.5	**2.8**	6.4	4.9	**3.2**	0.89	0.88	**0.92**
ANNUAL	4.7	3.2	**1.5**	4.9	3.5	**1.8**	0.89	0.88	**0.93**

5.4.2 Validation of rainfall for Vietnam

The APHRODITE dataset is used to validate multi-year mean seasonal rainfall for Vietnam. During NEMS (the dry season) the models accurately capture the dry regions over most of Vietnam (Figure 5-7, top). All models also capture the slightly higher rainfall amounts over central Vietnam, with RegCM4.2 showing significantly more rainfall there. The percentage differences (Figure 5-8, top) are generally large, mainly because the mean rainfall is small, so small changes are amplified. All models tend to have too much rainfall (positive bias). CCAM has a slight negative bias in northern Vietnam.

All simulations capture the spatial distribution of precipitation in SWMS (the summer wet season) well, with the wettest regions in the North West, Central Highlands and southern parts of Vietnam (Figure 5-7, bottom). The simulations also capture the higher precipitation over neighbouring Laos and coastal Cambodia. All three simulation correctly place drier conditions over the central coastal regions of Vietnam. The percent biases are generally smaller for this season, with a slight wet bias in PRECIS and a slight dry bias in CCAM (Figure 5-8, bottom).

Validation statistics of the simulated precipitation compared with the observational stations across Vietnam (Table 5-6) show that all models have too little precipitation in SIMS and too much in NEMS. For FIMS and SWMS, PRECIS has slightly too much precipitation, while CCAM and RegCM4.2 have too little precipitation. RegCM4.2 significantly underestimates the rainfall in SIMS and overestimates the rainfall in NEMS.

Of the three models, PRECIS overestimates rainfall in almost all seasons of the year. Conversely, simulations by CCAM and RegCM4.2 underestimate rainfall in almost all seasons except NEMS. The pattern correlation indices show that the simulations of all three models are acceptable. The RMSE statistics show the largest errors in SIMS (values from 4.9 mm day^{-1} for CCAM to 8.2 mm day^{-1} for RegCM4.2). The pattern correlations of rainfall tend to be smaller than for temperature. The highest correlations are for the SIMS, while the worst tend to be for SWMS.

Figure 5-7: Simulations of average precipitation (mm day^{-1}) over Vietnam for two seasons (NEMS, top and SWMS, bottom) for APHRODITE (observations) compared with the three model outputs (CCAM and RegCM4.2 for the 1980-2000 period and PRECIS for 1990-2007).

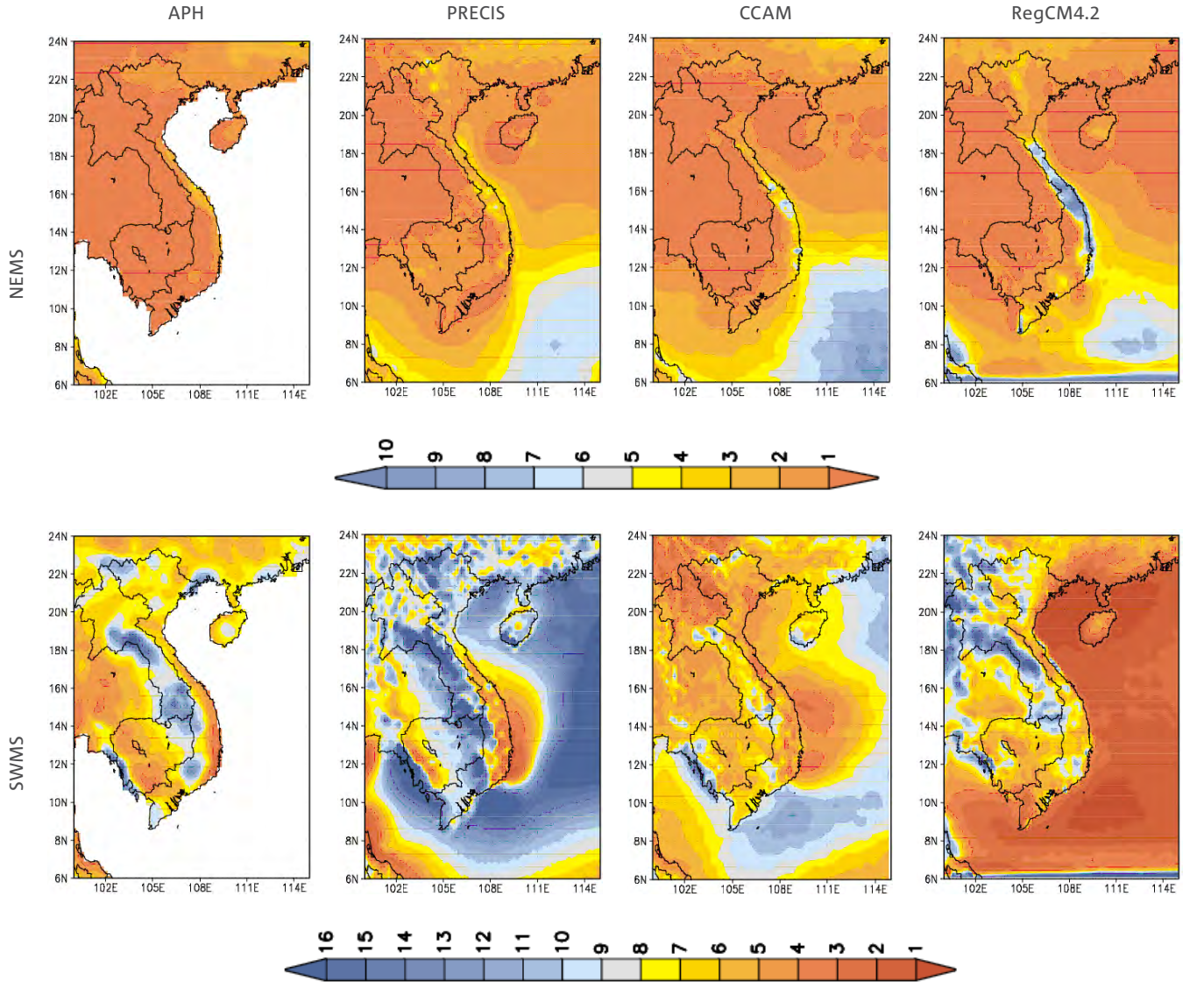

Figure 5-8: Simulations of the percentage difference of rainfall for two seasons (NEMS, top and SWMS, bottom) over Vietnam for APHRODITE (observations) compared with the three model outputs (CCAM and RegCM4.2 for the 1980-2000 period and PRECIS for 1990-2007).

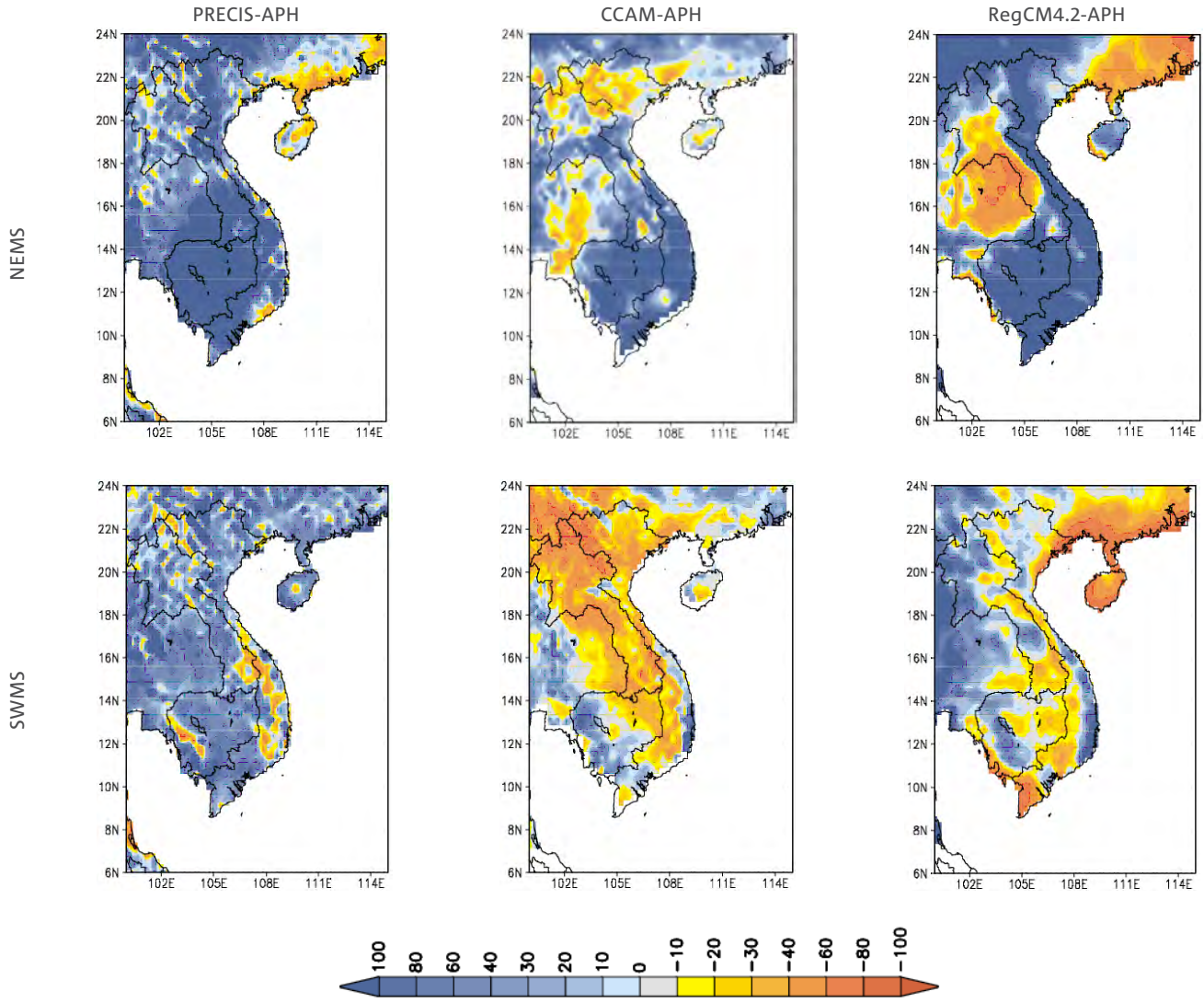

Table 5-6: Rainfall validation of RCMs relative to station data across Vietnam. Bold numbering indicates the best-performing model for each statistic.

SEASON	BIAS (%)			RMSE (MM DAY^{-1})			PATTERN CORRELATION		
	PRECIS	CCAM	RegCM4.2	PRECIS	CCAM	RegCM4.2	PRECIS	CCAM	RegCM4.2
FIMS	**14.2**	-21.3	-25.7	**2.0**	2.6	2.3	**0.61**	0.35	0.55
SWMS	**4.4**	-37.9	-17.2	**4.2**	4.6	4.0	0.50	**0.51**	0.32
SIMS	-24.8	**-22.8**	-59.7	6.3	**4.9**	8.2	0.89	**0.96**	0.77
NEMS	**25.1**	49.0	113.9	**1.4**	1.8	3.2	0.57	**0.87**	0.80
ANNUAL	**-1.7**	-28.8	-19.5	2.5	**2.4**	2.3	0.33	**0.69**	0.57

5.4.3 Validation of the annual cycles of temperature and rainfall for the seven sub-regions

In this section, the annual cycles of temperature and rainfall in the ERA-Interim-driven simulations are compared with observed data from the 61 local stations (STN), as well as from the CRU and APH gridded datasets over the seven sub-regions of Vietnam. In order to reduce the disparity of temperature simulations due to the elevation differences between the models and the station data, the simulations are corrected based on an environmental lapse rate of –0.65°C per 100 m. For the comparison, we selected only those grid cells from the model that correspond with meteorological station locations, and these are averaged to give the climatology for each climatic region. The monthly mean annual cycles of the simulated temperature from three simulations are compared with the observed data over all seven climatic sub-regions, as shown in Figure 5-9. Overall, the models do well in representing the annual cycle of temperature when compared with observations, capturing the high temperature period during June-August, and the low temperature period during December-February. The RegCM4.2 model tends to underestimate temperatures for all regions and all months.

The largest cold biases are found in the NW, NE and ND regions, with a range from -2 to -3°C. Simulations by the PRECIS and CCAM models are more accurate in comparison.

The model-simulated mean annual cycles of precipitation for the seven sub-regions in Vietnam for the 1980-2000 period are compared against APHRODITE and STN data in Figure 5-10. All simulations reproduce the monthly annual cycle fairly well when compared with observations, capturing the wet and dry seasons and the magnitudes of rainfall in these periods. In these simulations, CCAM tends to underestimate rainfall in the North West (NW) and North Central (NC) regions, while PRECIS tends to overestimate rainfall, except in the South Central (SC) and Central Highlands (CH) regions. Both PRECIS and CCAM capture the annual cycle of rainfall well.

Figure 5-9: Annual cycle of temperature (°C) by month, averaged over the seven sub-regions and over the whole of Vietnam for three simulations (RegCM4.2, PRECIS, CCAM), together with station observations (STN) and the CRU gridded dataset, for the period 1980-2000 (PRECIS for 1990-2007).

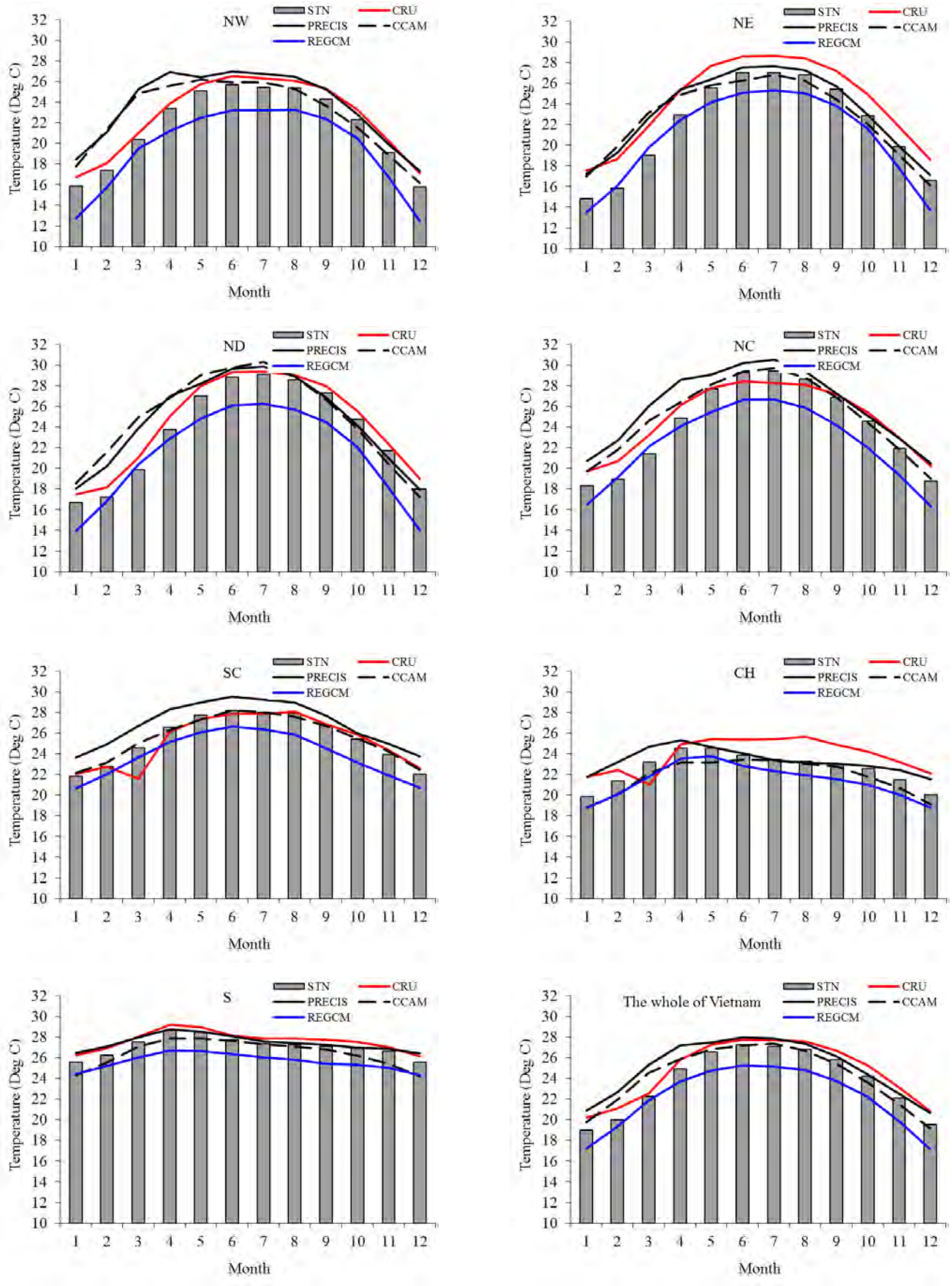

Figure 5-10: Annual cycles of precipitation (mm day^{-1}) averaged over the seven sub-regions and over whole of Vietnam for three simulations (RegCM4.2, PRECIS, CCAM), together with station observations (STN) and APHRODITE gridded dataset (APH) for the period 1980-2000 (PRECIS for 1990-2007).

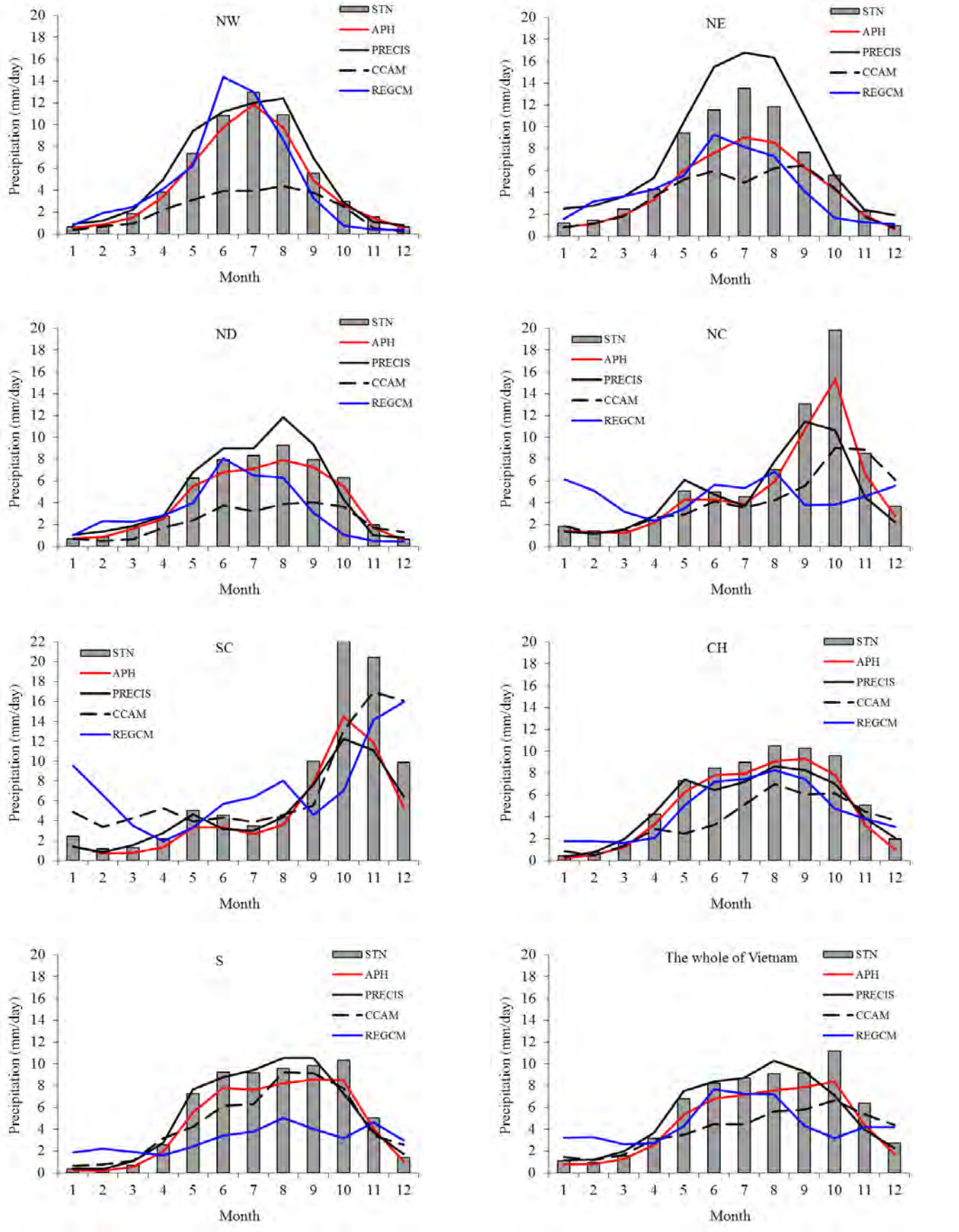

5.4.4 Spatial patterns of circulation

For the evaluation of model performance in simulating wind fields, we consider the patterns of circulation averaged for the period 1980–2000 over South East Asia.

Figure 5-11 shows the horizontal 850 hPa average wind speed and direction in SWMS (summer) and NEMS (winter) from the ERA-40 reanalysis and the three models. The models simulate the spatial patterns of the winter and summer monsoon circulations reasonably well, and the flow is generally accurate in its locations. Among the models, PRECIS has a higher magnitude for the 850 hPa wind speed when compared with the ERA-40 reanalysis.

In NEMS, we also find that the climatology of the horizontal winds at 850 hPa over the region in the model simulations represents the key characteristics of the monsoon circulation well compared with the ERA-40 reanalysis, capturing the location of the north-easterly winds in the southern part and the easterly to south-easterly winds in the northern part of Vietnam. The winter monsoon flow is more accurate in magnitude compared with that in summer for all models.

Figure 5-11: 850 hPa wind speed (m s^{-1}, shown by shading) and direction during NEMS (winter, top) and SWMS (summer, bottom), averaged over the 1980-2000 period for ERA-40 and the RegCM4.2 and CCAM model simulations. The PRECIS period is 1990-2007.

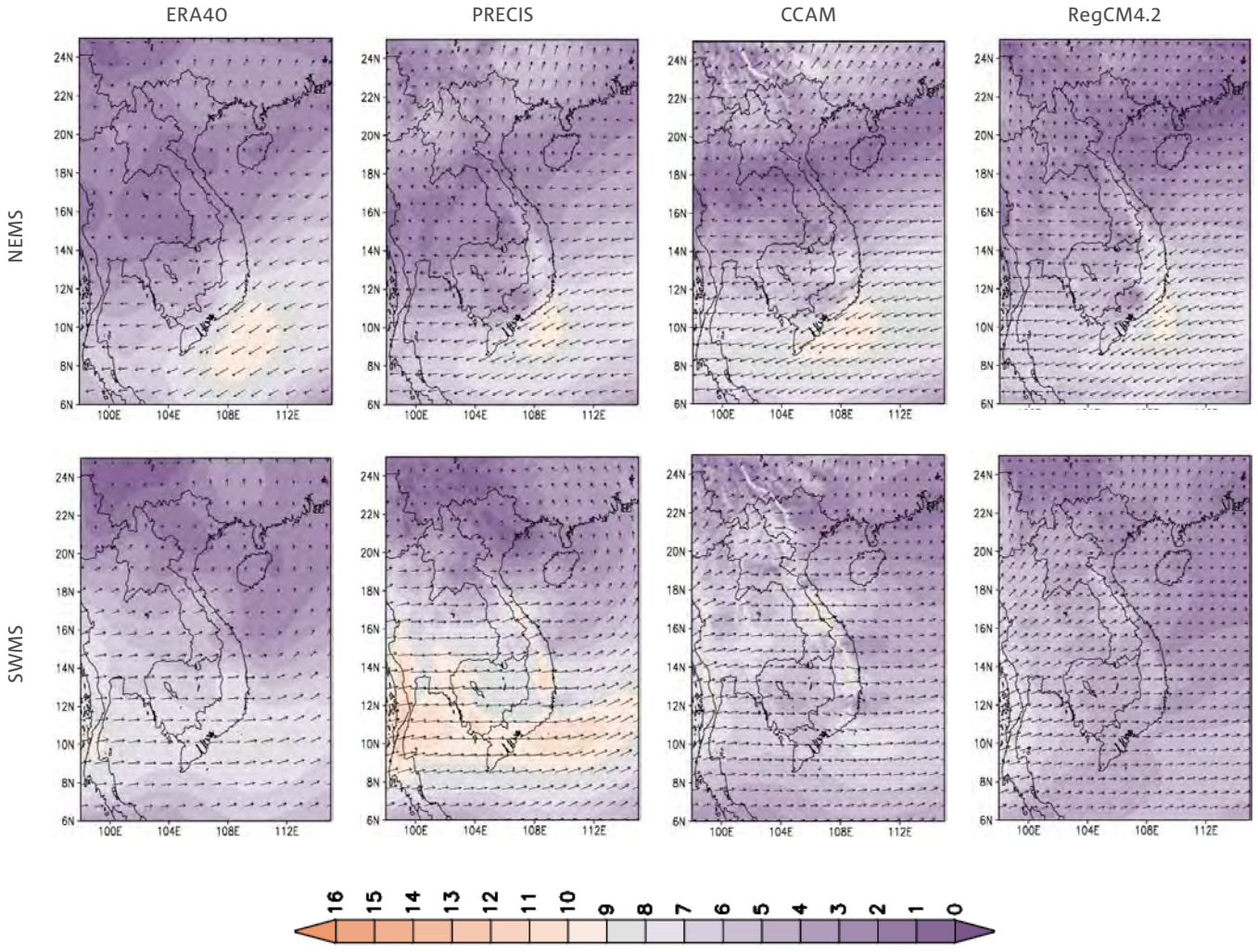

5.5 PERFORMANCE OF RCMs DOWNSCALED FROM GCMs

This section assesses the performance of the two models (CCAM and RegCM4.2) driven by GCM data in simulating characteristics of the observed climate (1980-2000) over the area that covers Vietnam. Validating and comparing model simulations with observed data allows us to assess the skills of the models with no observational data input. Note that when models are run with GCM data, the accuracy of the boundary forcing will be reduced due to errors in the GCMs. Comparison of the results in this section with Section 5.4 gives some measure of this reduced accuracy. The analysis includes comparison of seasonal averages of observed and simulated precipitation and surface air temperature.

For the CCAM simulations, six global 50 km CCAM simulations were completed with bias- and variance-corrected SSTs and with sea ice from the GCMs without atmospheric forcing. Historical values of greenhouse gases and aerosol emissions were used for the period up to 2005 and RCP values used from 2006 onwards (see Section 2.2). The 10 km CCAM simulations were spectrally forced to these 50 km CCAM simulations. For the RegCM4.2 simulations, lateral boundary condition were generated from two global 100 km CCAM simulations which were completed with bias- and variance-corrected SSTs and with sea ice from the GCMs without atmospheric forcing. Table 5-7 provides a summary of the model set-ups for the dynamically downscaled simulations. We note that a 1–year spin-up period was removed before analysis so that the model's land surface scheme (particularly the soil temperature and moisture) can adjust to the model's atmospheric conditions.

5.5.1 Validation of temperature for Vietnam

The spatial distribution of the surface air temperature (Tave) for both NEMS and SWMS from the CRU dataset is shown in Figure 5-12 along with the biases for CCAM and RegCM4.2 simulations. Note that pattern and magnitude of the biases are similar to that for the ERA-Interim-forced runs (Figure 5-6). However, the large cold bias in RegCM4.2 for NEMS noted in the ERA-Interim simulation is mostly gone. In fact, there are some warm biases in certain regions. The cold biases in SWMS are still evident.

Seasonal and annual validation statistics for maximum temperature (Tmax) and minimum temperature (Tmin) for the whole of Vietnam, computed by comparing the station observations with the nearest model grid point, are presented in Table 5-8 and Table 5-9, respectively. Maximum temperatures (Tmax) show negative biases for all seasons and both models, with CCAM exhibiting the largest bias of -4.8°C for NEMS. Both models have positive biases for minimum temperature (Tmin), with the largest bias for RegCM4.2 (6.2°C). These biases are generally slightly larger for CCAM than when downscaling from ERA-Interim, as one might expect, since the model is more constrained when downscaling the ERA-Interim than when only using SSTs and SIC from the GCMs. Interestingly, for RegCM4.2, the Tmax biases are slightly less than when downscaling ERA-Interim. This needs further investigation.

Similar to the ERA-Interim-forced runs, the RMSE shows only slightly larger magnitudes than the biases, suggesting that the bias is the main contributor to the error. And similar to the biases, RegCM4.2 shows smaller values for Tmax and larger values for Tmin than when downscaled from ERA-Interim. The pattern correlations are also quite high, indicating that the models are capturing the spatial pattern of temperature well. These pattern correlation numbers are similar to the ERA-Interim runs.

Table 5-7: Summary of the GCM forced RCM set-ups for current climate validation.

MODEL	DRIVING DATA	INITIAL CONDITIONS	SIMULATION PERIOD	VALIDATION PERIOD
CCAM	Six GCMs	01 Jan 1970 NCEP Reanalysis	1970-2099	1980-2000
RegCM4.2	Two GCMs	01 Jan 1980 ERA-Interim	1980-2000	1980-2000

Figure 5-12: Observed CRU surface air temperature (Tave) (left) and biases for CCAM and RegCM4.2 (°C) for two seasons (NEMS, top and SWMS, bottom) over Vietnam for the 1980-2000 period.

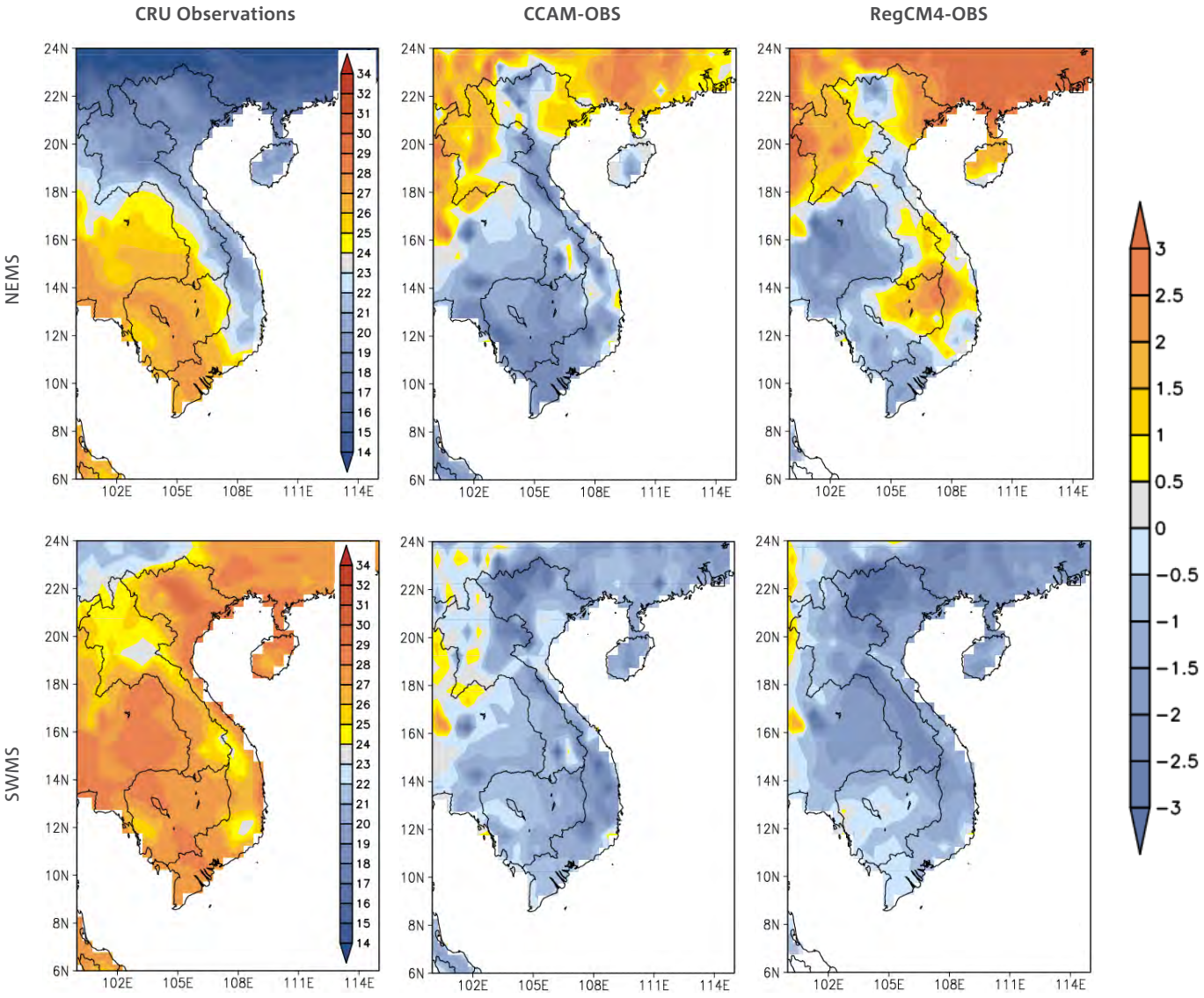

Table 5-8: Tmax validation of multi-model mean of RCMs for current climate (1980-2000) relative to station data. Bold numbering indicates the best-performing model for each statistic.

SEASON	BIAS (°C)		RMSE (°C)		PATTERN CORRELATION	
	CCAM	RegCM4.2	CCAM	RegCM4.2	CCAM	RegCM4.2
FIMS	-4.2	**-2.9**	4.7	**3.5**	0.66	**0.69**
SWMS	-4.1	**-3.3**	4.3	**3.8**	**0.88**	0.77
SIMS	-4.5	**-3.2**	4.7	**3.6**	**0.79**	0.69
NEMS	-4.8	**-3.2**	5.2	**3.8**	0.61	**0.76**
ANNUAL	-4.3	**-3.2**	4.5	**3.6**	**0.70**	**0.70**

Table 5-9: Tmin validation of multi-model mean of RCMs for current climate (1980-2000) relative to station data. Bold numbering indicates the best-performing model for each statistic.

SEASON	BIAS (°C)		RMSE (°C)		PATTERN CORRELATION	
	CCAM	RegCM4.2	CCAM	RegCM4.2	CCAM	RegCM4.2
FIMS	**4.2**	4.5	**4.5**	5.0	**0.76**	0.65
SWMS	2.2	**2.1**	**2.3**	2.4	**0.97**	0.88
SIMS	**3.1**	4.0	**3.5**	4.5	**0.89**	0.82
NEMS	**4.7**	6.2	**5.0**	6.5	**0.92**	0.86
ANNUAL	**3.7**	4.2	**3.9**	4.5	**0.92**	0.82

Comparison of the annual cycle of average surface temperature (Tave) with the station observations and CRU dataset (Figure 5-13) shows close correspondence of the models and the observations. CCAM follows the observations more closely than RegCM4.2, with a warm bias in RegCM4.2 in the first half of the year. Comparing these results with the previous results for Tmax and Tmin suggests that the warm bias in Tmin is larger than the cool bias of Tmax.

Figure 5-13: The annual cycle of the temperature (°C) by month averaged over the whole of Vietnam for two RCM simulations (CCAM and RegCM4.2) compared with CRU gridded observations and local observations (STN) for the period 1980-2000.

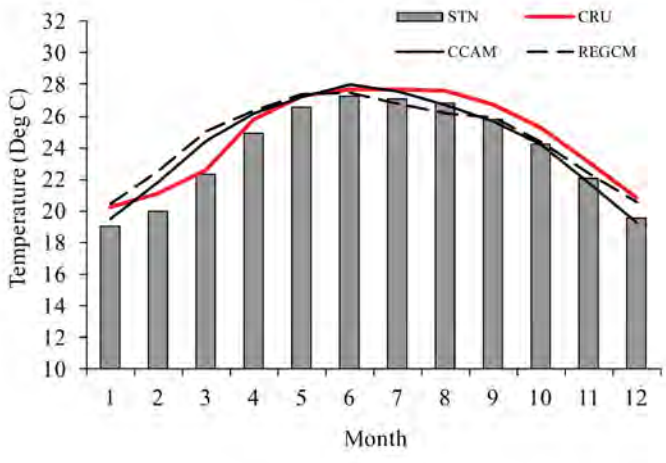

5.5.2 Validation of rainfall for Vietnam

As with the simulations driven by ERA-Interim, the APHRODITE dataset is used to validate multi-year mean seasonal rainfall for Vietnam. The rainfall biases for the GCM-forced simulations (Figure 5-14) are similar in pattern and magnitude to those for the ERA-Interim forced runs (Figure 5-8). The main difference is in SWMS, where both models tend to be slightly wetter than in the ERA-Interim runs. As with the ERA-Interim forced run, RegCM4.2 significantly underestimates the rainfall in SIMS and overestimates the rainfall in NEMS.

Validation statistics for the simulated precipitation compared with the observational stations across Vietnam (Table 5-10) show that both models have too little precipitation in SIMS and too much in NEMS. For FIMS and SWMS, RegCM4.2 has slightly too much precipitation, while CCAM has slightly too little. The RMSE is generally similar to the ERA-Interim runs. The pattern correlations are similar or slightly lower than for the ERA-Interim runs. The main conclusion is that the GCM-forced runs are only slightly less accurate than the ERA-Interim runs.

Finally, the annual cycle of rainfall from the stations, APHRODITE and the two simulations is shown in Figure 5-15. Both models capture the annual cycle reasonably well, except in October and November, where RegCM4.2 is very dry. Both models also tend to overestimate the rain during the dry months.

Figure 5-14: NEMS (winter) and SWMS (summer) precipitation average (mm day^{-1}) during a 1980-2000 baseline period over Vietnam for APHRODITE (observations), and the percentage difference of CCAM and RegCM4.2 relative to the APHRODITE dataset.

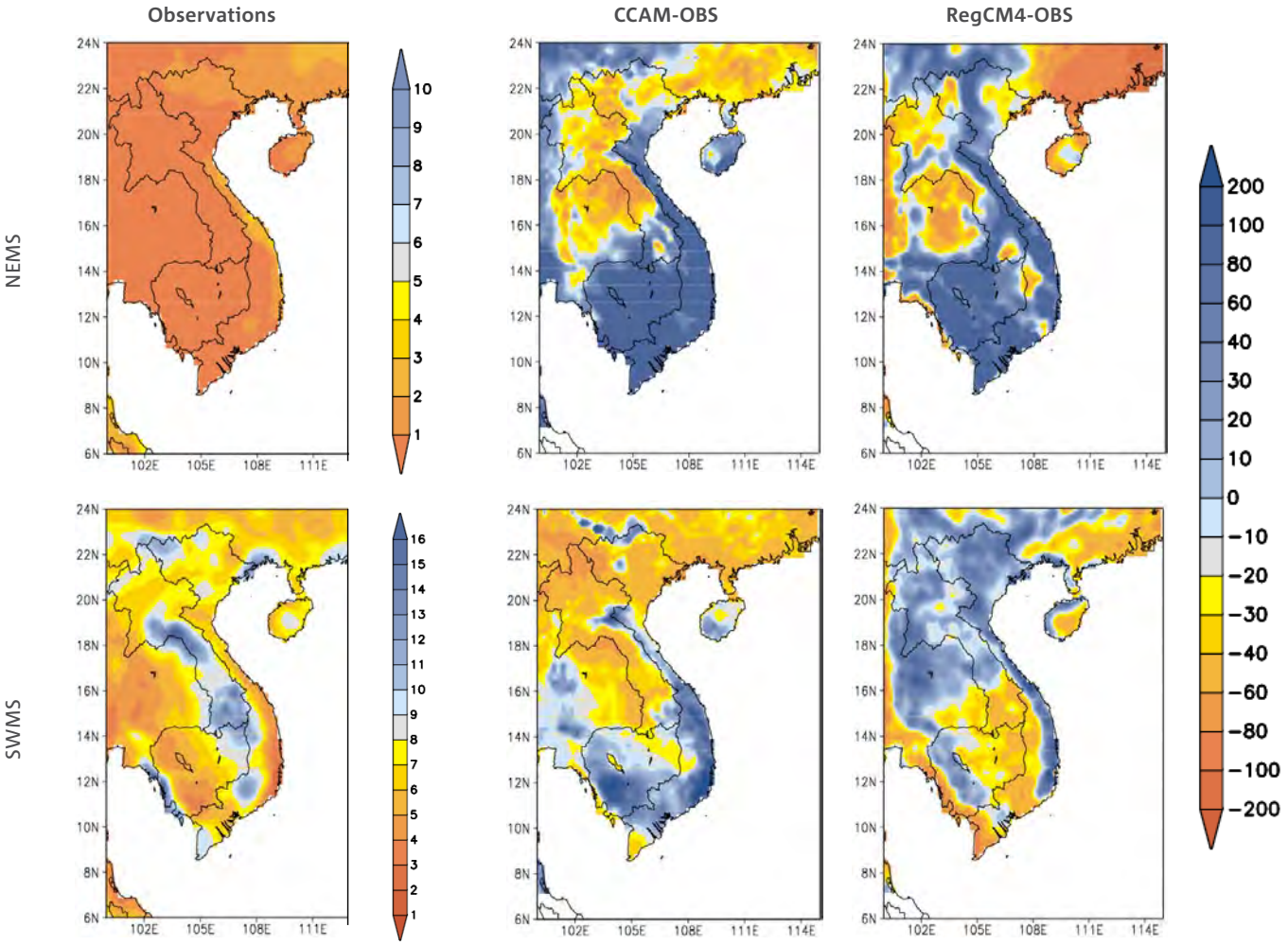

Table 5-10: Rainfall validation of RCMs relative to observational data for the period 1980-2000. Bold numbering indicates the best-performing model for each statistic.

SEASON	BIAS (%)		RMSE (MM DAY^{-1})		PATTERN CORRELATION	
	CCAM	RegCM4.2	CCAM	RegCM4.2	CCAM	RegCM4.2
FIMS	**-12.7**	31.9	**2.3**	2.9	0.49	**0.55**
SWMS	-15.5	**6.0**	**4.3**	4.4	**0.35**	0.32
SIMS	**-16.6**	-66.6	**3.7**	9.7	**0.92**	0.77
NEMS	114.7	**44.8**	3.6	**1.3**	**0.85**	0.80
ANNUAL	**-6.5**	-11.3	2.5	**2.2**	**0.63**	0.57

Figure 5-15: The annual cycle of precipitation (mm day^{-1}) by month averaged over the whole of Vietnam for two RCM simulations (CCAM and RegCM4.2) compared with the APHRODITE dataset and local observations (STN) for the period 1980-2000.

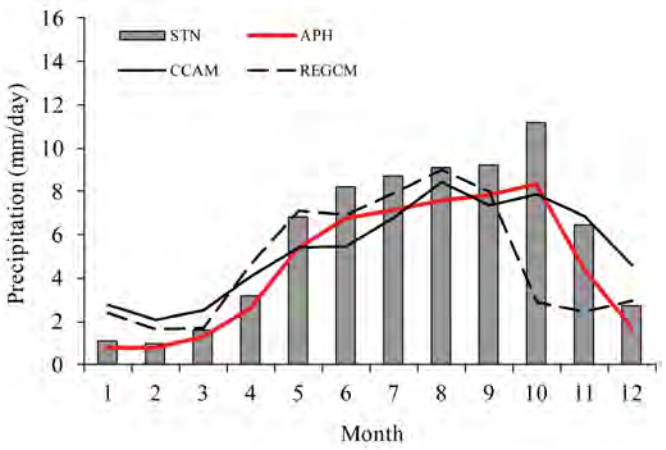

5.6 SUMMARY

This chapter presents an evaluation of the ability of GCMs and RCMs to simulate seasonal climate for the area encompassing Vietnam. Results are presented for GCMs, followed by RCMs driven first by the ERA-Interim reanalyses (using three RCMs) and then driven by GCM data (just two RCMs).

Results based on statistical tests and visual judgements indicate that the current generation of CMIP5 GCMs performed fairly well and captured the observed spatial patterns of temperature and rainfall over a broad region centred on South East Asia. However, most of the models only weakly capture the observed spatial patterns of mean sea level pressure when the topographically complex areas of central Asia are included, particularly during the South West Monsoon. This implies that the current generation of models do not capture the observed circulation patterns over this region. The GCMs also underestimate observed temperature and rainfall over land areas and over some parts of the ocean.

The validation of the regional models driven by fields from the reanalysis and by the SSTs and SIC from GCMs show broadly similar results, with the GCM-driven simulations generally performing slightly worse. This is expected as the GCM-forced runs have no observational data used, so are less constrained.

Our results show that both GCMs and RCMs capture the pattern of present-day climate reasonably well. Although not shown, the RCMs significantly improve upon the accuracy of the climate over Vietnam relative to the GCMs. The simulations accurately reproduced most of the important characteristics of observed spatial patterns, annual cycles and variability of circulation, rainfall and temperature for Vietnam in two main seasons, NEMS (winter) and SWMS (summer).

The models appear to underestimate temperature in most parts of the domain relative to CRU observations in summer. There is also a systematic winter temperature bias, with a tendency for most of the domain to be cooler than observations for RegCM4.2 and CCAM, but for the central parts of the country to be warmer than observations in the PRECIS model.

Investigation of the mean annual cycle of the observed and simulated temperatures over the seven sub-regions shows that the RegCM4.2 model tends to underestimate temperatures for all sub-regions and all months. Simulations by PRECIS and CCAM are more accurate compared with those of the RegCM4.2 model.

When reviewing rainfall, CCAM is too dry for most regions, except in the dry season (NEMS) when it tends to predict slightly too much rainfall. PRECIS and RegCM4.2 tend to have too much rain for most regions. PRECIS captures the rainfall best in the reanalysis-forced runs, with smaller biases than the other simulations in this season.

Analysis of the mean annual cycle of precipitation over the seven sub-regions indicates that all simulations reproduce fairly good monthly variations when compared with observations, capturing the wet and dry seasons as well as the range of rainfall amounts. RegCM4.2 was too dry for the months of October and November.

With respect to spatial patterns of circulation, the models simulate the winter (NEMS) and summer (SWMS) monsoon circulations reasonably, but the summer monsoon flow is too strong in the PRECIS model. The winter monsoon flow is more accurate in direction and speed in comparison with the summer simulations.

The results of this study provide some information about the reliability of the projections and their suitability for use in assessing possible future climate changes in Vietnam and for use of model output as inputs to impact models such as hydrological or crop models. However, it is advised that users make a more detailed assessment before using this data for their application. Potentially, some sort of 'bias correction' of the regional output prior to use in an impact model may be required.

6 VIETNAM'S FUTURE CLIMATE

In this chapter, projected Vietnam-wide changes in temperature and rainfall are presented for the eight downscaled simulations under the high emission scenario, RCP 8.5, for both mid-century (2045-2065) and the end of the century (2080-2100), relative to the period 1980-2000. The multi-model mean changes are presented, along with the percent agreement of the sign-of-change among the downscaled results and the spread among the model projections (using the standard deviation of the model changes as a measure). A further summary of the results for the seven sub-regions across Vietnam, and a comparison with previous projections, is presented in Chapters 9-15. More detailed information is also available on the website.

6.1 CLIMATE CHANGE PROJECTIONS FOR VIETNAM FROM CMIP5 SIMULATIONS

While there were 31 simulations used for validation of the present-day climate over South East Asia (see Chapter 5 for details of GCM and RCM performance), at the time of this report only 24 GCMs had temperature projection data and 22 GCMs had rainfall projection data for the RCP 8.5 emission scenario through to the end of the century. These were used for the multi-model means in this portion of the study.

Figure 6-1 shows the projected increases in temperature and the changes in rainfall projected by the GCM multi-model ensemble for RCP 8.5 by the end of the century. Over Vietnam, the models suggest an increase in annual mean temperature of +2°C to +5°C by 2100, with a mid-value of +4 C by 2100. Annual average rainfall changes range between -8% and +20%, with a mid-value of +7%. However, there are seasonal differences. The largest mean rainfall increase is simulated for SIMS (+20%), while there is a small decrease for FIMS (-4%). Most of the models agree on Vietnam rainfall increases during NEMS, SWMS and SIMS and decreases during FIMS by 2100 (not shown).

The rest of this chapter covers the projections of the various regional climate model simulations when forced with CMIP5 GCM data. We assess ensemble simulations for a number of variables for two models, CCAM and RegCM4.2 (CCAM has six members, and RegCM4.2 has two members).

6.2 CLIMATE CHANGE PROJECTED BY RCMs FOR VIETNAM BY MID-CENTURY (2045-2065)

In this section, the Vietnam-wide changes in temperature and rainfall are presented for the RCP 8.5 (high) emission scenario for mid-century (2045-2065) relative to the period 1980-2000. The multi-model mean changes are presented, along with the percent agreement of the sign-of-change in rainfall among the downscaled results and the spread among the model projections (using the standard deviation of the model changes as a measure). A more detailed summary of the results for the seven climatic sub-regions across Vietnam is presented in Chapters 9-15. Results for other time slices and RCPs are shown in tables.

The multi-model mean rainfall change at mid-century for the four seasons (Figure 6-2) shows rainfall increases over most of Vietnam in FIMS (April-May) except in north-western Vietnam, where the changes are small, or even show minor decreases. SWMS (June-September) is projected to have rainfall decreases in the South Central (SC) region of Vietnam on and in the lee of the mountains, with the southwest flow. SIMS (October-November) shows small rainfall increases in central Vietnam, but little change elsewhere. Finally, NEMS (December-March) shows a similar pattern of small rainfall increases, like SIMS, although the increases extend further south along the coast.

Figure 6-1: Increase in temperature (°C) and changes in rainfall (%) projected by the GCM ensembles by the end of this century over South East Asia. Values are multi-model means.

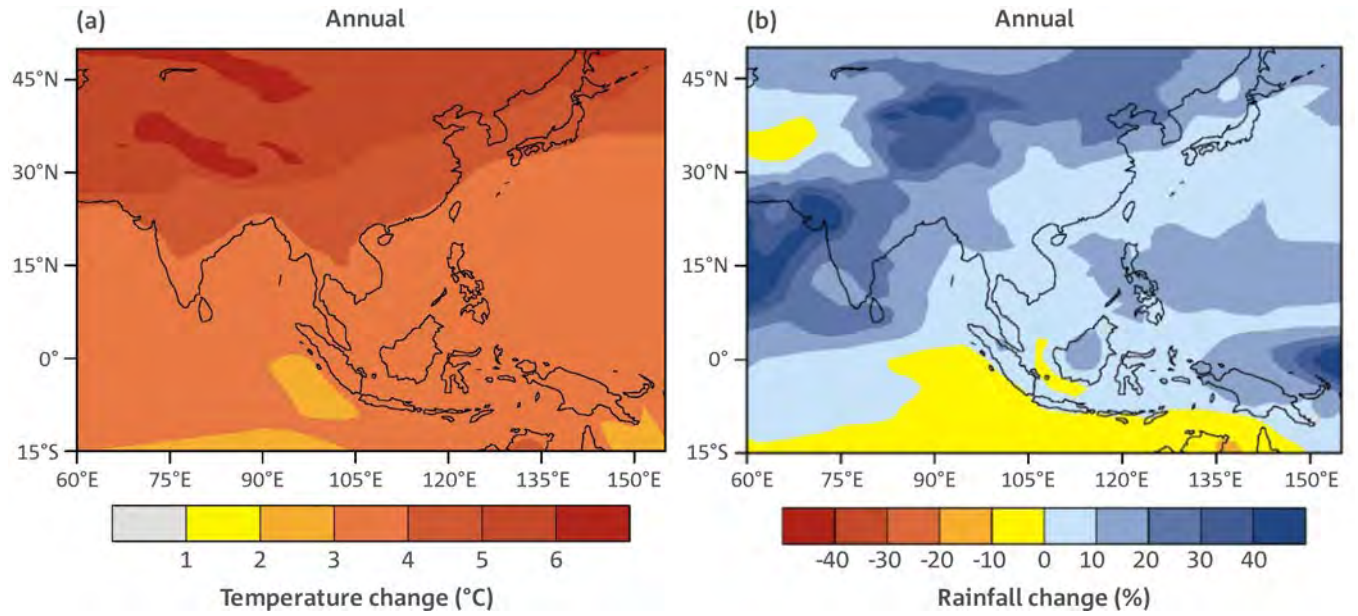

Two measures of the robustness of the climate change signal are (1) the agreement on the sign-of-change among the downscaled model rainfall projections and (2) the spread of the climate-change signal among the models. There are eight downscaled simulations (six for CCAM and two for RegCM4.2) for each time period. For rainfall changes, 100% agreement on sign-of-increase would indicate all models (or eight members) show rainfall increases for the region, suggesting greater confidence that the rainfall will increase for the region. A 0% agreement would indicate that all models project a decrease in rainfall. 50% agreement would indicate that half the simulations show increase and half show decrease, so there is a large uncertainty in the sign-of-change. The spread of the results is computed using the Standard Deviation (SD) of all eight simulations. A small SD indicates that all models have a similar magnitude of the climate change signal, while a large SD indicates a large spread and greater uncertainty in the magnitude of the change signal for the region.

The agreement of the sign-of-increase of the rainfall for the four seasons is shown in Figure 6-3. For FIMS, there is good agreement on rainfall increases for the southern half of Vietnam. Only the northern parts of Vietnam have either small agreement on increase or even some agreement on rainfall decreases. For SWMS, there is relatively good agreement on rainfall decreases in central Vietnam. Elsewhere the agreement is low. Interestingly, in southern Vietnam there is slight agreement on decreases, even though the multi-model mean change shows slight increases, indicating that the models that do show increases have larger magnitude changes than those that indicate decreases. For SIMS, there is some agreement on increases in central Vietnam and in the Mekong Delta region, while there is agreement on decreases in northern Vietnam. Finally, the models tend to agree on the rainfall increases for NEMS across most of Vietnam.

As shown by the spread in the magnitude of the change (Figure 6-4), most locations show little spread, with the only region with large spread in central Vietnam during SIMS. This might be explained due to the small-scale structure of the rainfall in this region, the generally heavy rainfall amounts and that RegCM4.2 had difficulty in capturing this rainfall in the current climate. Although some of these other locations showed disagreement in sign-of-changes in Figure 6-3, those changes were generally small, with only small standard deviation values among the ensemble members.

Figure 6-2: Multi-model mean rainfall changes (mm day^{-1}) projected by the eight-member RCM ensemble for the four seasons at mid-century for RCP 8.5.

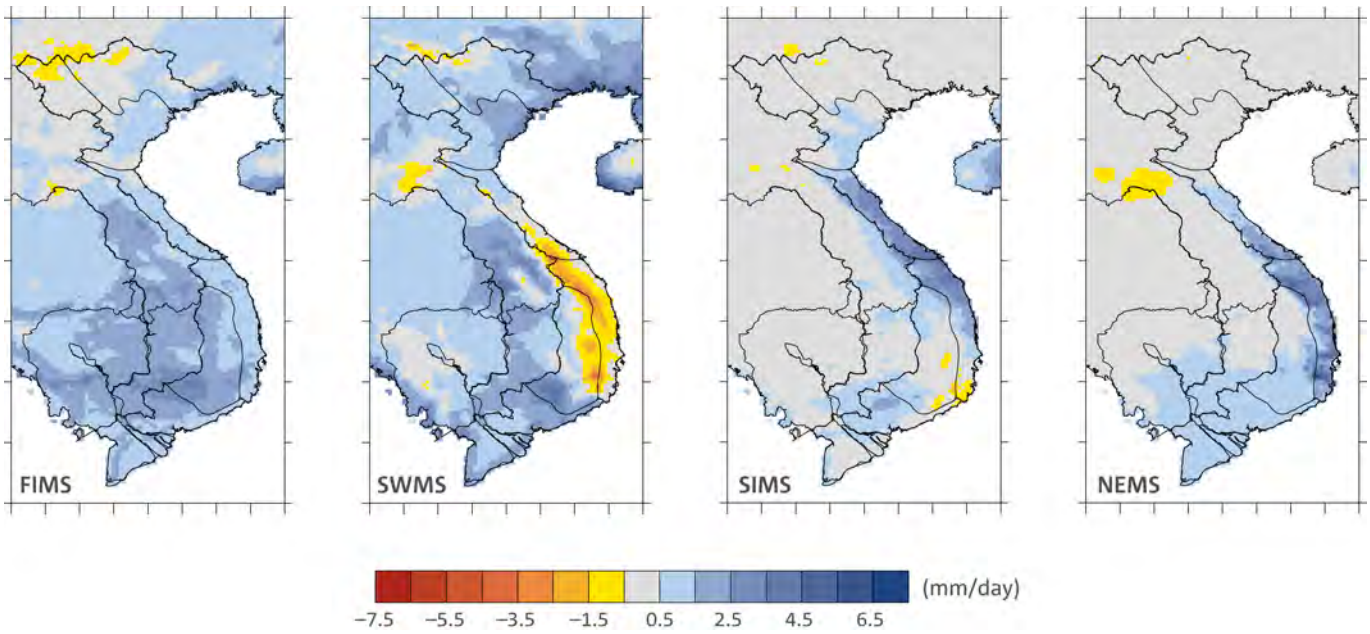

Figure 6-3: Agreement on sign-of-increase of rainfall changes (%) from RCM projections by the eight-member ensemble for the four seasons at mid-century for RCP 8.5.

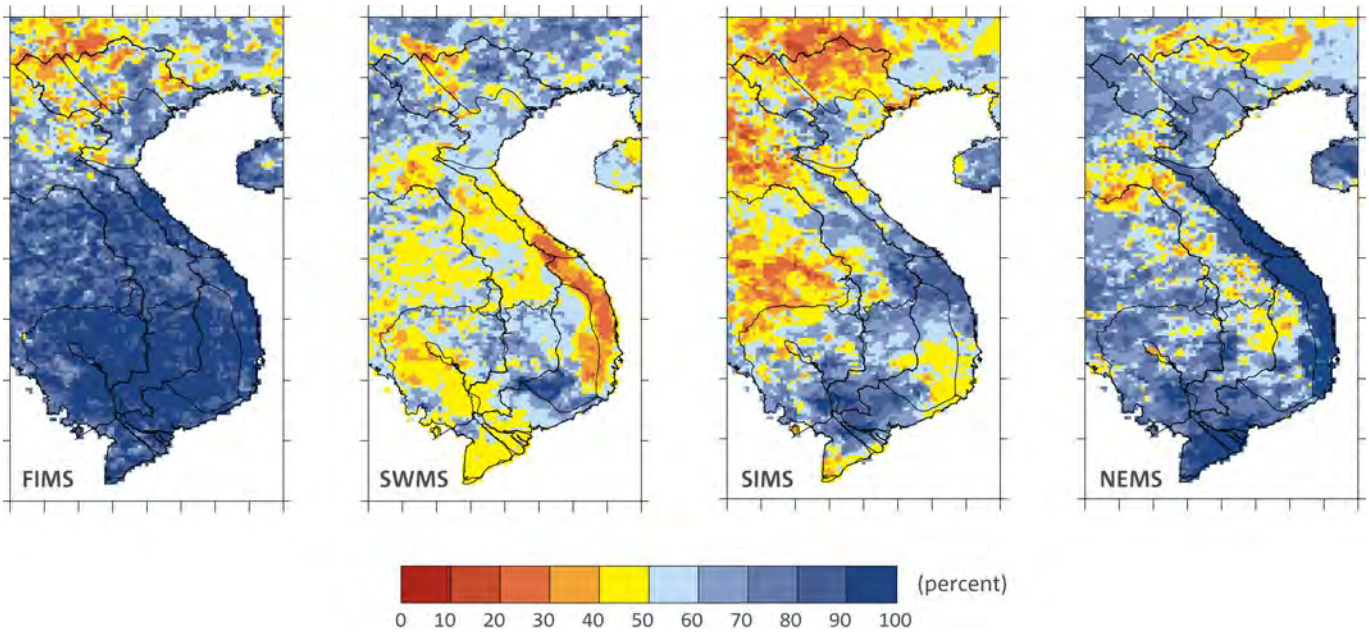

Figure 6-4: Standard deviation of the rainfall changes (mm day^{-1}) from RCM projections by the eight-member ensemble for the four seasons at mid-century for RCP 8.5.

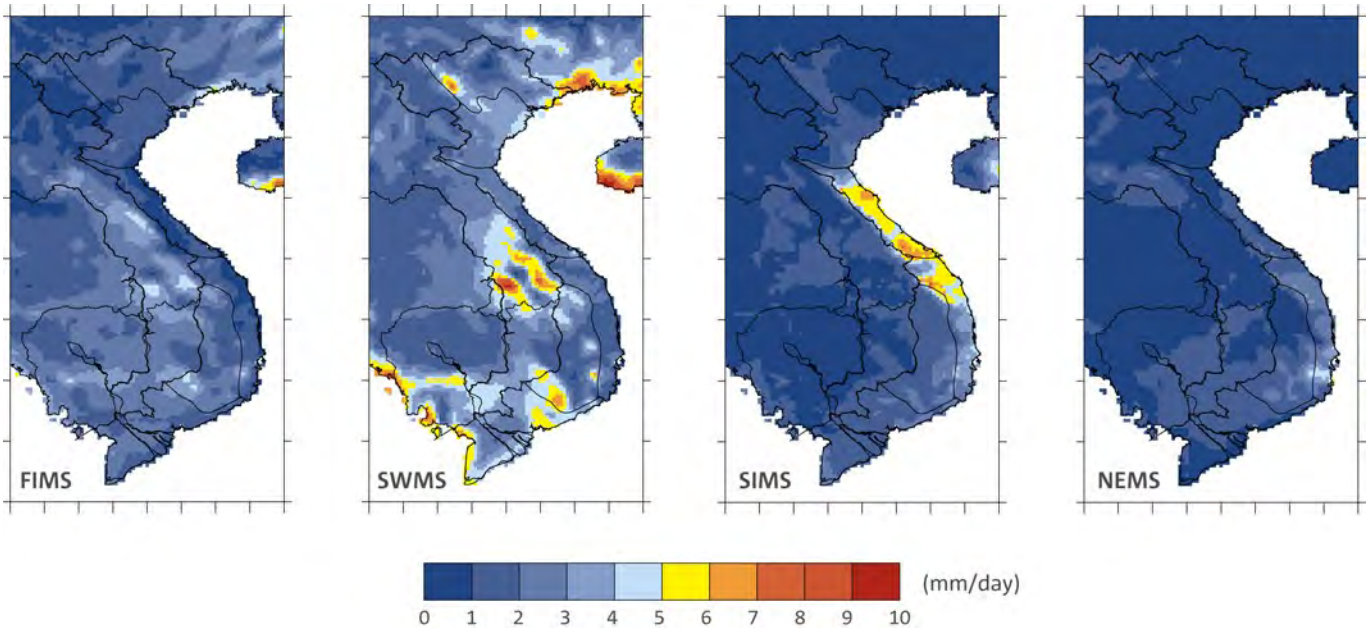

The multi-model mean maximum temperature change (Figure 6-5) shows increases on the order of 1°C for all seasons by mid-century. There is less increase in southern Vietnam for FIMS and SWMS and less increase in central Vietnam for SIMS and NEMS. The largest increases (greater than 2°C) are in northern Vietnam in SWMS and SIMS. All models show increases, so agreement is 100% everywhere and is not shown.

The standard deviation of the signal for maximum temperature change by mid-century for RCP 8.5 (Figure 6-6) shows low spread (good agreement on the amount of change between models) for FIMS and NEMS. Good agreement also is evident in southern Vietnam for all seasons. However, in SWMS the spread is greater than 1°C for northern Vietnam.

Figure 6-5: Multi-model mean maximum temperature changes (°C) projected by the eight-member RCM ensemble for the four seasons at mid-century for RCP 8.5.

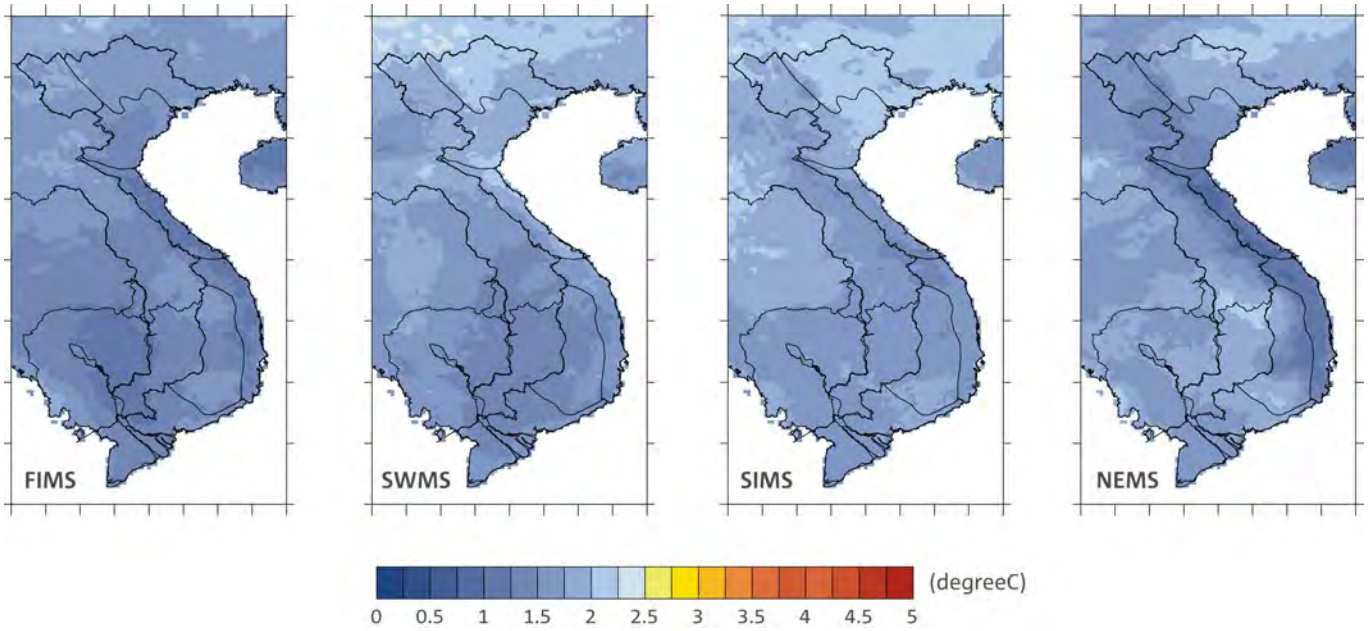

Figure 6-6: Standard deviation of maximum temperature changes (°C) from RCM projections by the eight-member ensemble for the four seasons at mid-century for RCP 8.5.

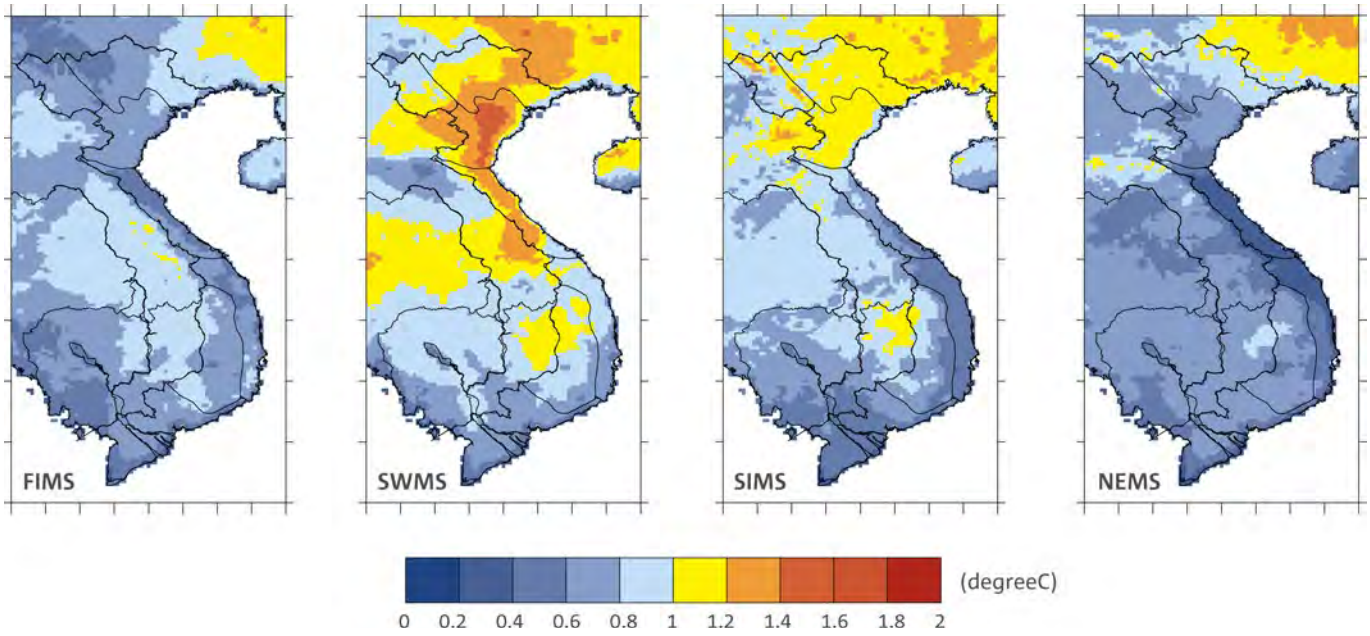

The multi-model mean minimum temperature change (Figure 6-7) shows increases for all seasons by mid-century, of the order of 1.5°C. All models show agreement on increases in maximum temperatures.

The standard deviation of minimum temperature changes by mid-century for RCP 8.5 (Figure 6-8) shows even smaller spread than for maximum temperature changes. This indicates good agreement between the models for all seasons.

As for maximum and minimum temperatures, the multi-model mean of average temperature changes (Figure 6-9) shows warming of about 1.5°C for all seasons. The standard deviation (Figure 6-8) is small, showing good agreement among all the models for all seasons.

Figure 6-7: Multi-model mean of minimum temperature changes (°C) projected by the eight-member RCM ensemble for the four seasons at mid-century for RCP 8.5.

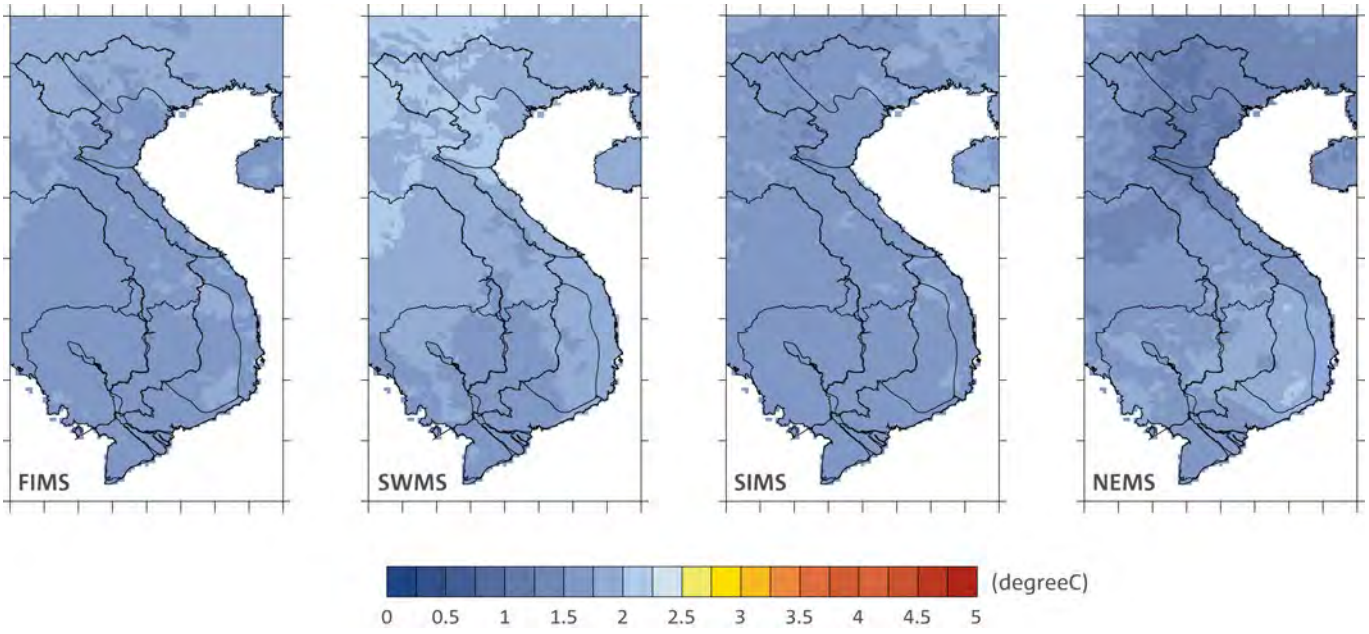

Figure 6-8: Standard deviation of minimum temperature changes (°C) from RCM projections by the eight-member ensemble for the four seasons at mid-century for RCP 8.5.

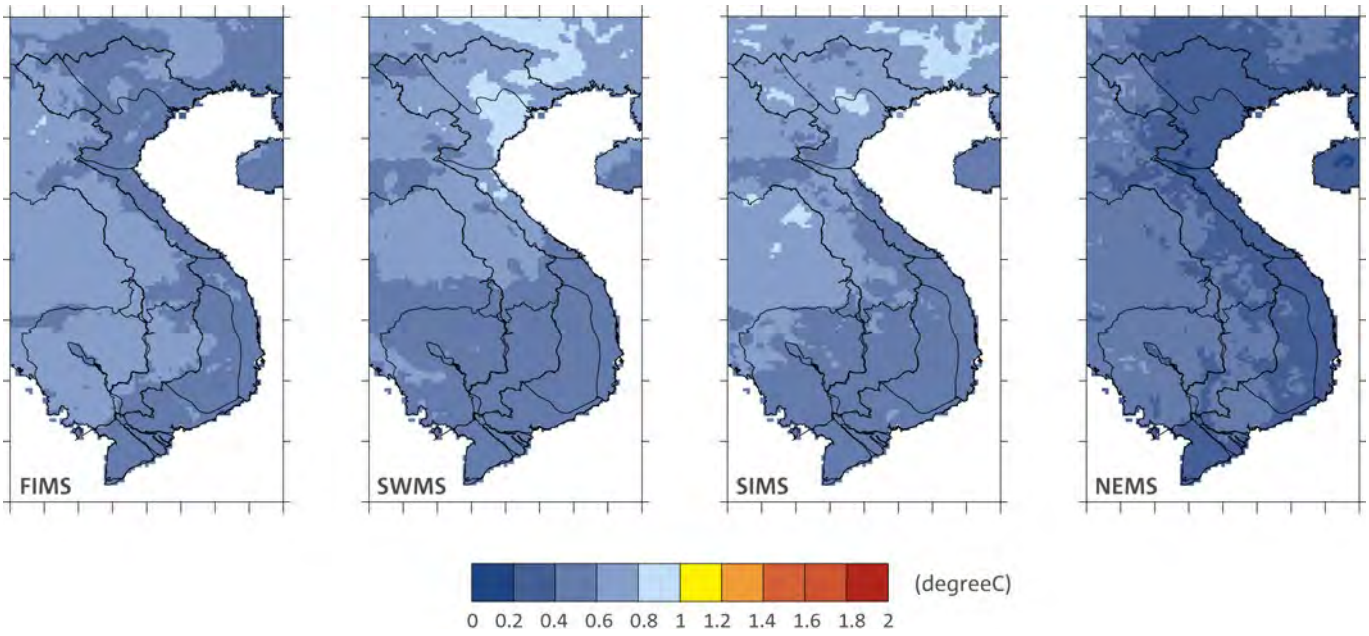

Figure 6-9: Multi-model mean of average temperature changes (°C) projected by the eight-member RCM ensemble for the four seasons at mid-century for RCP 8.5.

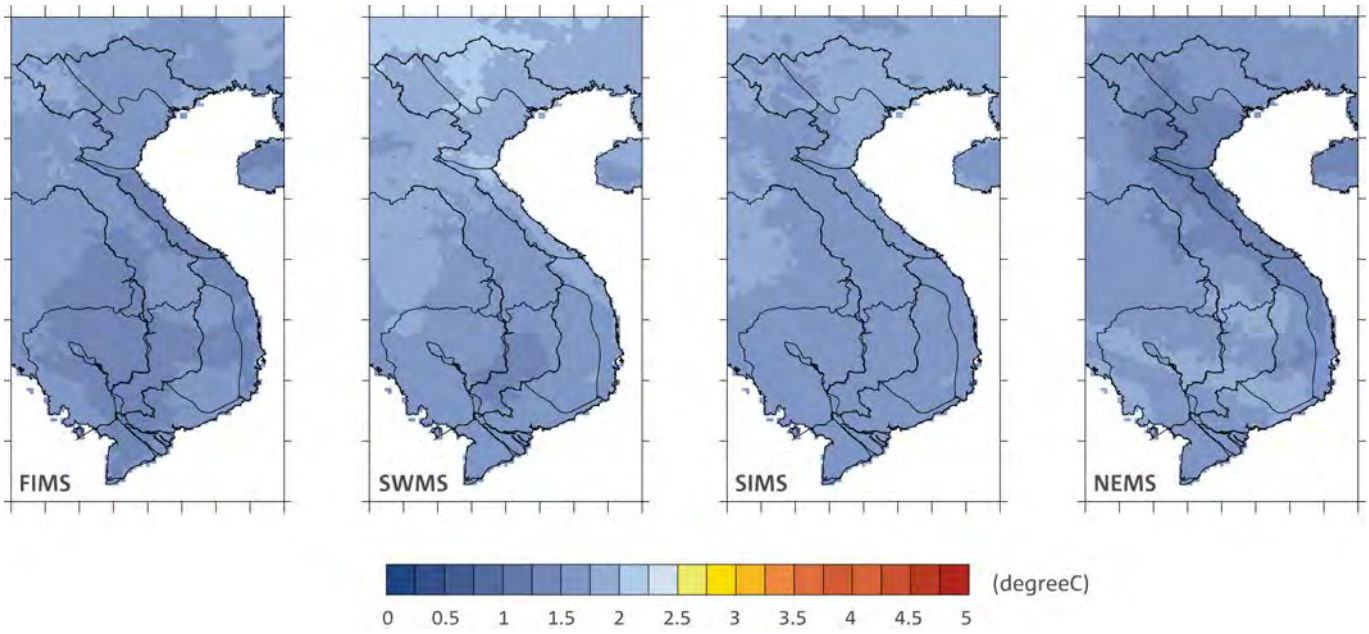

Figure 6-10: Standard deviation of multi-model average temperature changes (°C) from RCM projections by the eight-member ensemble for the four seasons at mid-century for RCP 8.5.

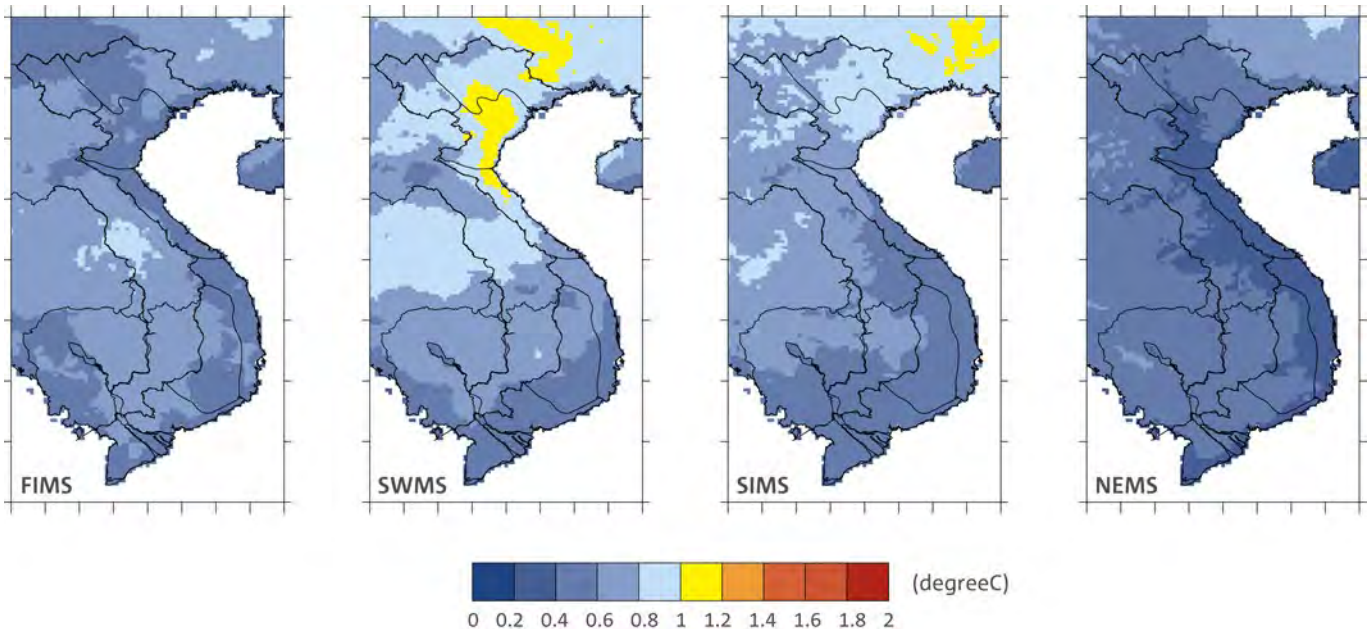

6.3 CLIMATE CHANGE PROJECTED BY RCMs FOR VIETNAM AT THE END OF THE CENTURY (2080-2100)

The multi-model mean annual temperature and rainfall change at the end of the century (Figure 6-11) shows warming over all of Vietnam, with greater warming (greater than 4°C) in northern Vietnam, similar to the GCMs (Figure 6-1). Annual rainfall changes show decreases in inland areas of northern Vietnam and in northern portions of the Central Highlands (CH) region, increases in central Vietnam and along the coast of northern Vietnam, and little change in southern Vietnam. These changes are different than those projected by the GCMs, which showed small increases across Vietnam.

Figure 6-11: Projected changes in annual temperature (Tave, left) and rainfall (right) by 2080-2100 under RCP 8.5. Temperature changes are in °C and rainfall changes are in mm day^{-1}. Values are multi-model means of the eight-member RCM ensemble.

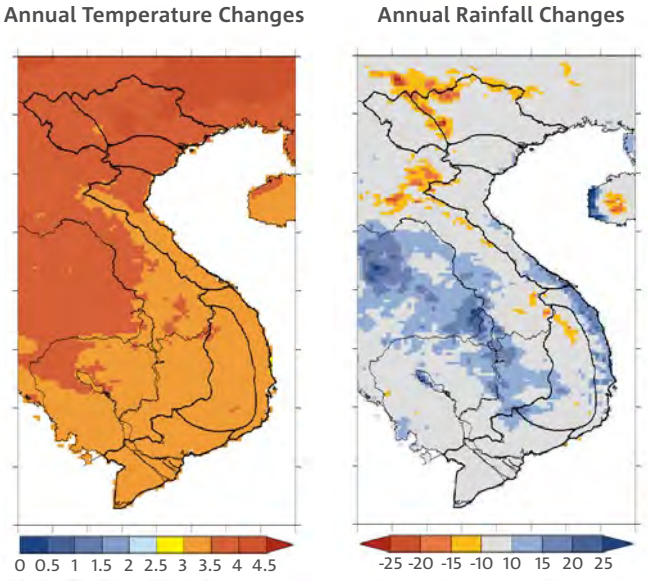

These projected changes in temperature and rainfall can also be compared with the trends of temperature and rainfall already being observed over the last 50 years (Figure 3-11). Both the observations and projections indicate increasing temperatures (observed trends of about 0.25°C per decade, while the trend projected by the RCMs by the end of the century is about 0.4°C per decade, suggesting that the observed trends may be an indication of climate change already happening, with the projected trend slightly larger than the historical observed trend. The pattern of annual rainfall changes in the observations is also similar to the projections, with decreases in northern Vietnam, increases in central Vietnam and little change in southern Vietnam. The magnitudes of the ensemble-mean projected changes are between 1-3% per decade (for main regions of increases and decreases) while the observed trends are on the order of 10% per decade.

The multi-model mean rainfall change at the end of the century for the four seasons (Figure 6-12) shows rainfall increases over most of Vietnam in FIMS, except in north-western Vietnam, where the changes are small or there are even minor decreases. Rainfall decreases are projected in the South Central (SC) region of Vietnam during SWMS, on and in the lee of the mountains, with the south-west flow. SIMS shows rainfall increases in central Vietnam, but smaller changes elsewhere. Finally, NEMS shows a pattern of rainfall increases similar to SIMS, although the increases extend further south along the coast.

The agreement of the sign-of-increase of the rainfall for the four seasons is shown in Figure 6-13. For FIMS, there is good agreement for central and southern Vietnam on rainfall increases. The northern portions of Vietnam have either small agreement on increases or even some agreement on rainfall decreases for this season. For SWMS, there is good agreement on rainfall decreases in central Vietnam, and some agreement on rainfall increases in south-central Vietnam. Interestingly, in southern Vietnam there is some agreement on decreases, even though the multi-model mean change shows slight increases, indicating that the models that do show increases have larger magnitude changes than those that indicate decreases. For SIMS, there is general agreement on increases for most of Vietnam, with some agreement on decreases in the CH region. Finally, the models tend to agree on rainfall increases in NEMS for north and central Vietnam; unlike the mid-century situation, the models show small level of agreement on decreases for southern Vietnam.

Figure 6-12: Multi-model mean rainfall changes (mm day^{-1}) projected by the eight-member RCM ensemble for the four seasons at the end of the century for RCP 8.5.

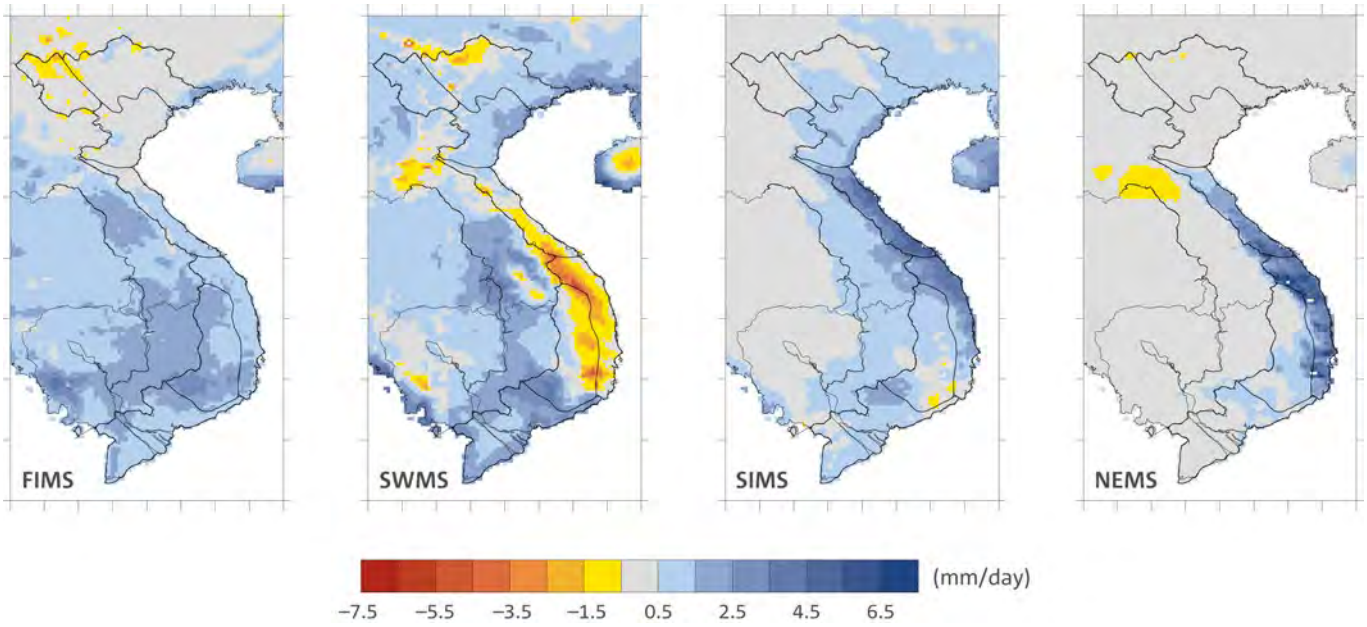

Figure 6-13: Agreement of sign-of-increase of rainfall changes (%) from RCM projections by the eight-member ensemble for the four seasons at the end of the century for RCP 8.5.

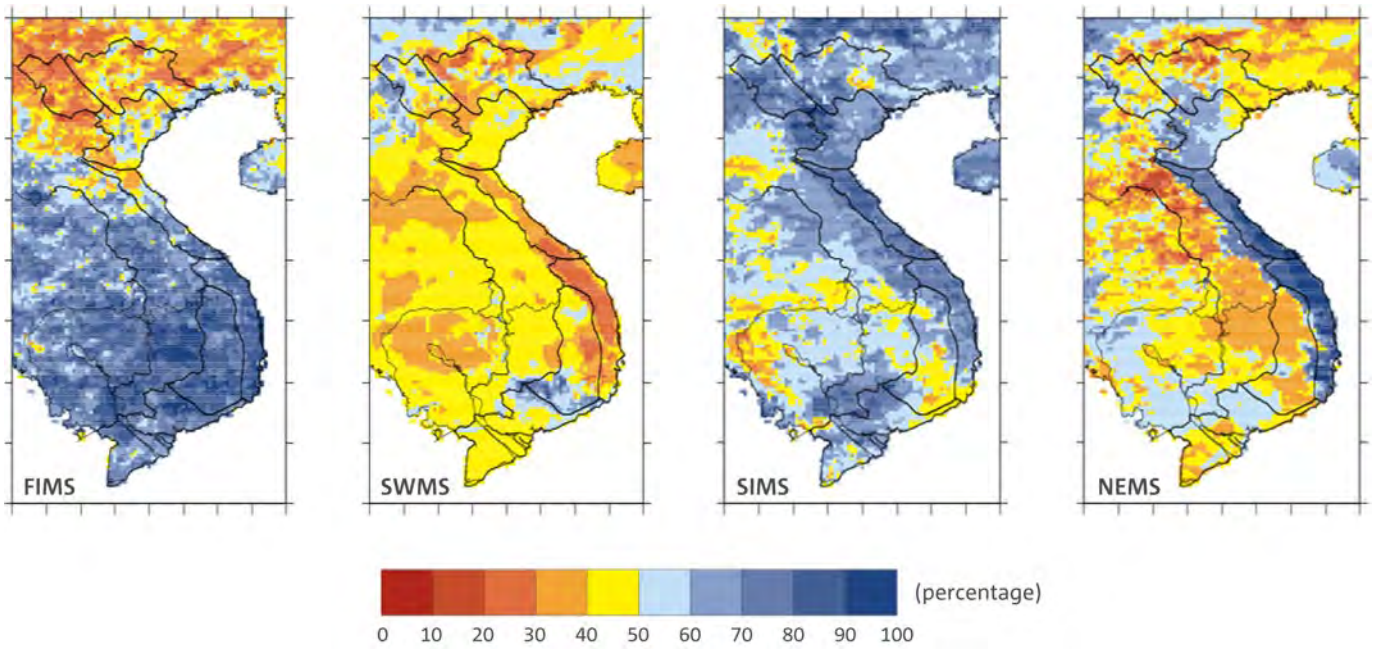

Figure 6-14: Standard deviation of rainfall changes (mm day^{-1}) from RCM projections by the eight-member ensemble for the four seasons at the end of the century for RCP 8.5.

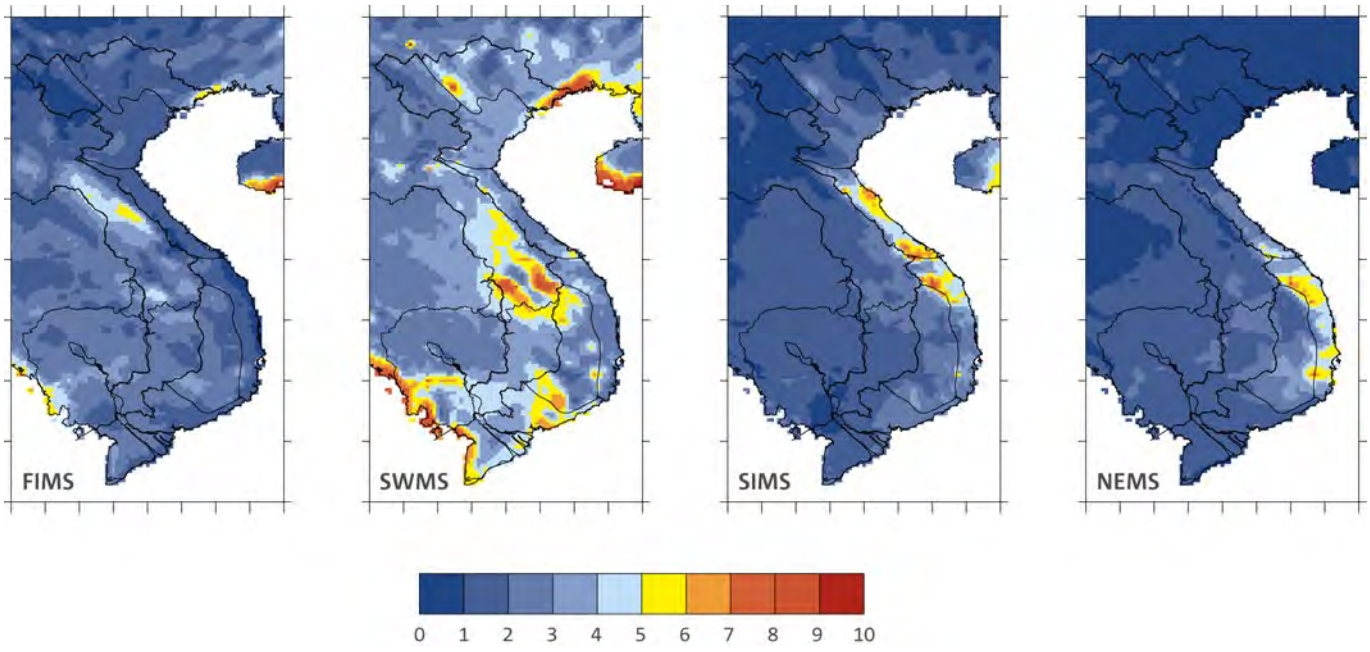

As for the spread in the magnitude of the change (Figure 6-14), the only region with large spread is in central Vietnam during SIMS. Most other locations show little spread in the magnitude of the change signal. Although some of these other locations showed disagreement on sign-of-changes in Figure 6-13, those changes were generally small, with only small standard deviation values among the ensemble members.

The multi-model mean maximum temperature change (Figure 6-15) shows increases on the order of 2.5 to 3°C for all seasons by the end of the century. There is greater increase in north and central Vietnam for SWMS, with the largest increases of greater than 3°C in northern Vietnam in SWMS. The smallest increases are about 2°C for central Vietnam in NEMS. All models show increases, so agreement is 100% everywhere and is not displayed.

The standard deviation of the projected changes (a measure of agreement in magnitude of the change) for the four seasons is presented in Figure 6-16. For all but SWMS, the spread is less than 1°C, indicating strong consistency. The spread between the model projections during SWMS approaches 2°C in northern Vietnam, though this is also the season and region which also has the greatest warming (over 4°C).

The multi-model mean minimum temperature change (Figure 6-17) shows increases for all seasons on the order of 3°C by the end of the century. As for maximum temperatures, all models show agreement on increases.

The standard deviation of minimum temperature changes by the end of the century for RCP 8.5 (Figure 6-18) shows an even smaller spread than for maximum temperature changes. This indicates good agreement between the models for all seasons.

Figure 6-15: Multi-model mean maximum temperature changes (°C) projected by the eight-member RCM ensemble for the four seasons at the end of the century for RCP 8.5.

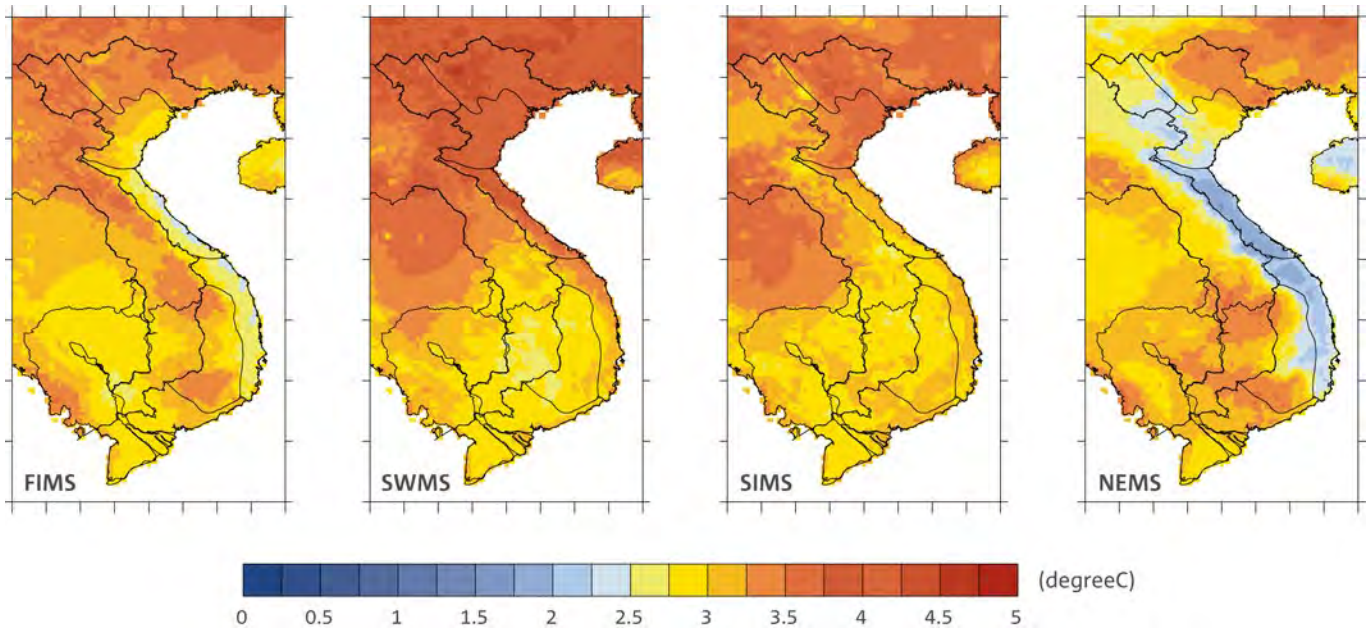

Figure 6-16: Standard deviation of maximum temperature changes (°C) for RCM projections by the eight-member ensemble for the four seasons at the end of the century for RCP 8.5.

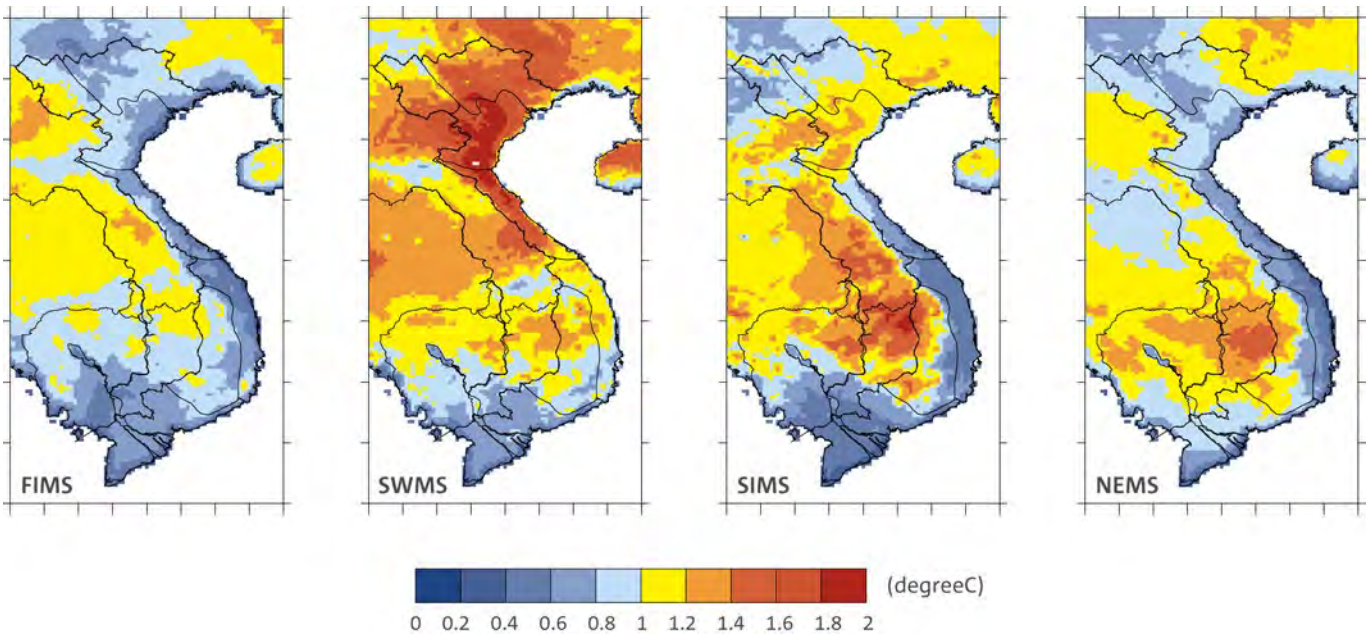

Figure 6-17: Multi-model mean minimum temperature changes (°C) projected by the eight-member RCM ensemble for the four seasons at the end of the century for RCP 8.5.

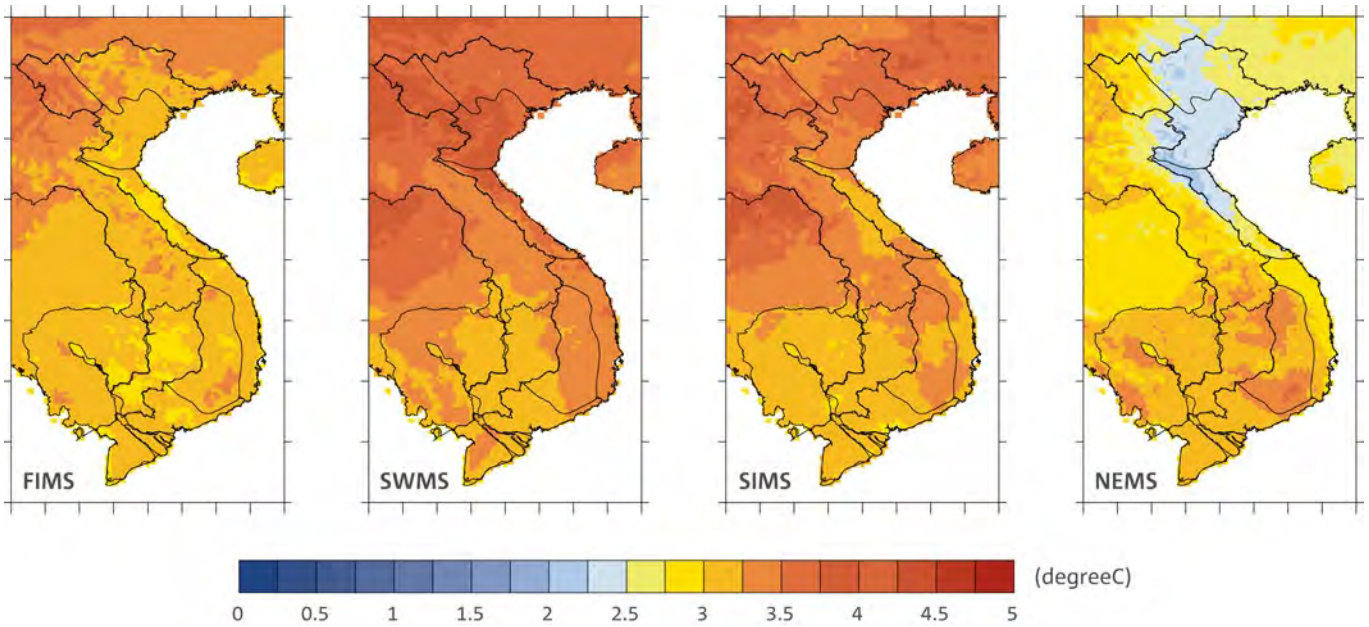

Figure 6-18: Standard deviation of minimum temperature changes (°C) for RCM projections by the eight-member ensemble for the four seasons at the end of the century for RCP 8.5.

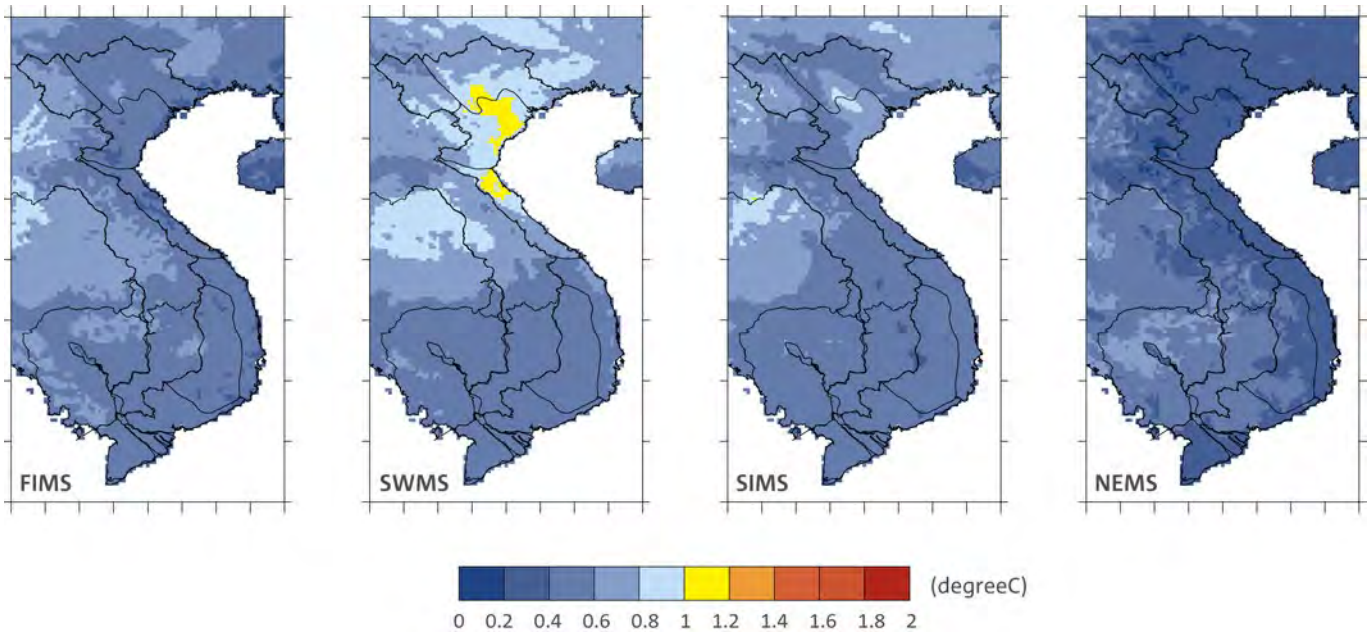

As for maximum and minimum temperatures, the multi-model mean of average temperature changes (Figure 6-19) shows warming of about 2.5 to 3°C for all seasons. The increases for central Vietnam are somewhat smaller, around 2°C in NEMS. The standard deviation (Figure 6-20) is generally small, showing good agreement among all the models for most seasons, except over north Vietnam in SWMS, where it is larger, about 1.2°C.

Projected changes in temperature and rainfall across Vietnam are summarised in the following tables. The changes in temperature across Vietnam by the end of the century show median increases annually of around 1.8°C (with a range of 1.6 to 3.2°C) under RCP 4.5 (Table 6-1) and 3.3°C (with a range of 2.4 to 5.1°C) under RCP 8.5 (Table 6-2). Greater increases are projected for SWMS (2.0°C under RCP 4.5 and 3.9°C under RCP 8.5) and the least increase for NEMS (1.5°C under RCP 4.5 and 2.9°C under RCP 8.5). All models agree on an increase, both annually, seasonally and for the different RCPs. The spread of the change values is about 0.6°C for RCP 4.5 and 0.8°C for RCP 8.5, both seasonally and annually.

Projected rainfall changes across Vietnam by the end of the century show small changes and low levels of agreement (Table 6-3 and Table 6-4). Only for SWMS are the median changes greater than 10 mm day^{-1}, with decreases of -17 mm day^{-1} (with range from -23 to +31 mm day^{-1}) under RCP 4.5 and -22 mm day^{-1} (with a range from -32 to +44 mm day^{-1}) under RCP 8.5. Annual median changes and median changes for other seasons are also small. The generally small projected changes also mean only small levels of agreement on changes across Vietnam, except for SWMS and annually under RCP 4.5 and for SWMS under RCP 8.5, where there is 75% agreement on the sign of rainfall changes (decreases). There is less agreement on the sign-of-change for all other seasons. In addition, the spread of change is larger than the median change, indicating little agreement on the magnitude of the changes.

Figure 6-19: Multi-model mean average temperature changes (°C) projected by the eight-member RCM ensemble for the four seasons at the end of the century for RCP 8.5.

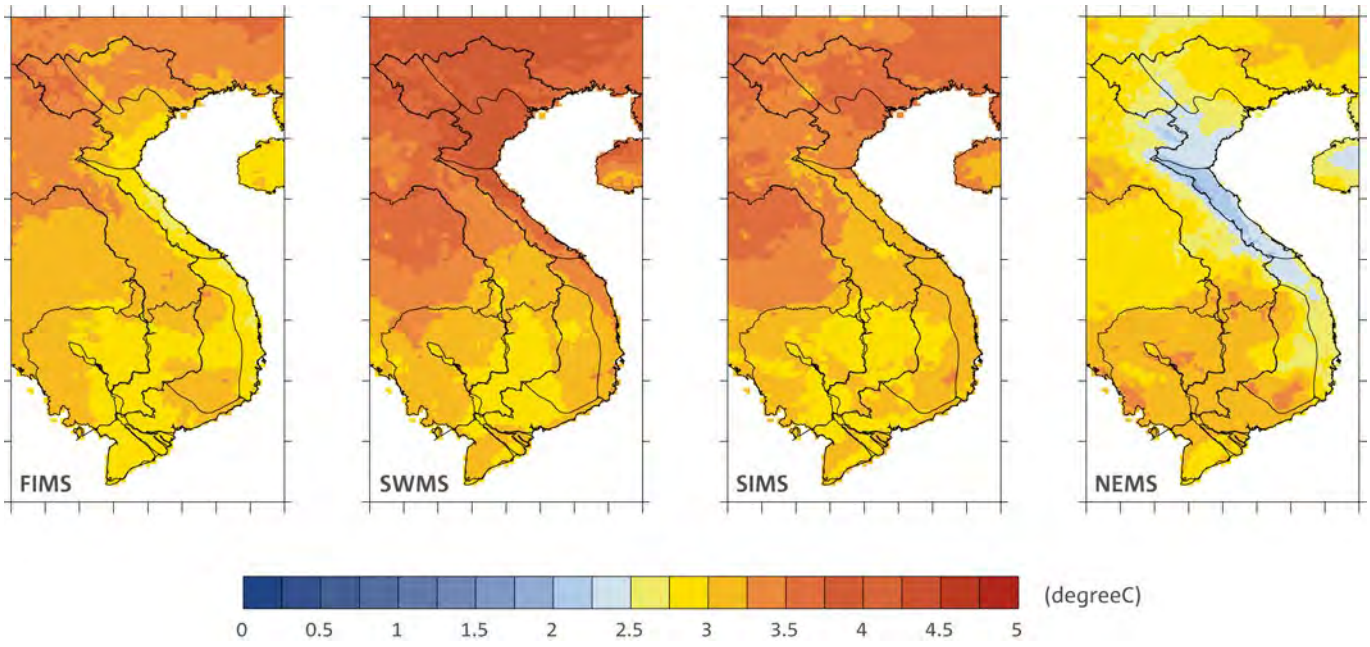

Figure 6-20: Standard deviation of average temperature changes (°C) for RCM projections by the eight-member ensemble for the four seasons at the end of the century for RCP 8.5.

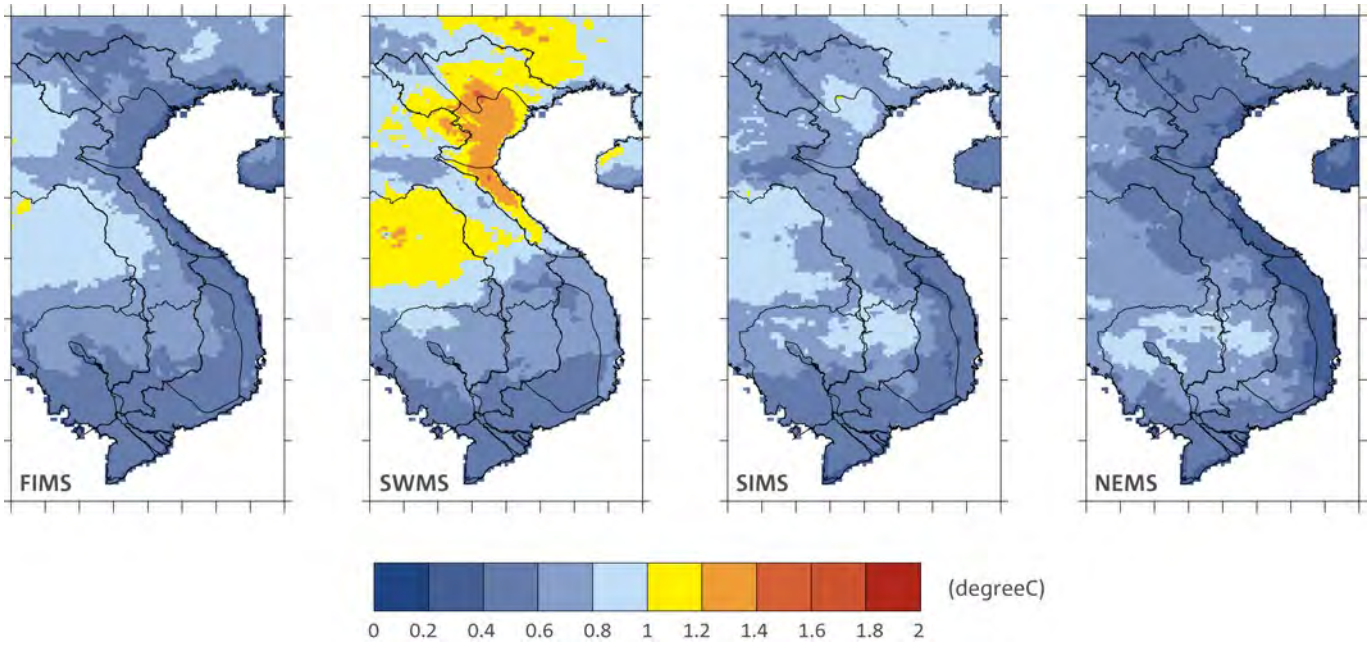

Table 6-1: Temperature changes (°C) for Vietnam annually and by season by the end of the century (2080-2100) under RCP 4.5, including a measure of agreement and spread. Values are RCM ensemble means.

Temperature changes for Vietnam by the end of the century under RCP 4.5

SEASON	MEDIAN CHANGE (AND RANGE) (°C)	MODEL AGREEMENT ON INCREASE (%)	SPREAD (SD) BETWEEN MODELS (°C)
FIMS	1.8 (1.3 to 3.2)	100	0.6
SWMS	2.0 (1.9 to 3.6)	100	0.6
SIMS	1.8 (1.3 to 3.4)	100	0.6
NEMS	1.5 (1.3 to 2.5)	100	0.4
Annual	1.8 (1.6 to 3.2)	100	0.5

Table 6-2: Temperature changes (°C) for Vietnam annually and by season by the end of the century (2080-2100) under RCP 8.5, including a measure of agreement and spread. Values are RCM ensemble means.

Temperature changes for Vietnam by the end of the century under RCP 8.5

SEASON	MEDIAN CHANGE (AND RANGE) (°C)	MODEL AGREEMENT ON INCREASE (%)	SPREAD (SD) BETWEEN MODELS (°C)
FIMS	3.3 (2.4 to 5.0)	100	0.8
SWMS	3.9 (2.4 to 6.0)	100	1.0
SIMS	3.5 (2.6 to 5.4)	100	0.8
NEMS	2.9 (2.2 to 4.2)	100	0.6
Annual	3.3 (2.4 to 5.1)	100	0.8

Table 6-3: Rainfall changes (mm day^{-1}) for Vietnam annually and by season by the end of the century (2080-2100) under RCP 4.5, including a measure of agreement and spread. Values are RCM ensemble means.

Rainfall changes for Vietnam by the end of the century under RCP 4.5

SEASON	MEDIAN CHANGE (AND RANGE) (mm day^{-1})		MODEL AGREEMENT ON INCREASE (%)	SPREAD (SD) BETWEEN MODELS (mm day^{-1})
FIMS	0	(-6 to 8)	50	6
SWMS	-17	(-23 to 31)	25	22
SIMS	3	(-18 to 44)	63	20
NEMS	1	(-9 to 28)	63	11
Annual	-7	(-12 to 20)	25	12

Table 6-4: Rainfall changes (mm day^{-1}) for Vietnam annually and by season by the end of the century (2080-2100) under RCP 8.5, including a measure of agreement and spread. Values are RCM ensemble means.

Rainfall changes for Vietnam by the end of the century under RCP 8.5

SEASON	MEDIAN CHANGE (AND RANGE) (mm day^{-1})		MODEL AGREEMENT ON INCREASE (%)	SPREAD (SD) BETWEEN MODELS (mm day^{-1})
FIMS	1	(-16 to 19)	63	11
SWMS	-22	(-32 to 44)	25	30
SIMS	5	(-13 to 103)	63	42
NEMS	0	(-15 to 45)	50	20
Annual	-9	(-17 to 34)	38	20

6.4 KNOWLEDGE GAPS

The results presented in this section show the multi-model mean annual and seasonal projected changes in temperature and rainfall across Vietnam by both the GCMs and the RCMs. The temperature increases are consistent between the RCM results and CMIP5 GCM results. However, the projected changes in rainfall show less agreement among the models and between the GCMs and the RCMs. In fact, while most GCMs show small increases in SWMS by the end of the century, most of the high-resolution RCMs show decreases. This needs further exploration and more in-depth analysis. It could be related to resolution, the effects of the better resolved terrain on the climate change signal or possibly model configuration. In addition, the causes of the projected rainfall changes need investigating; are they related to circulation changes, temperature or moisture changes, or some other factor? Exploring the changes in circulation (winds and pressure) could lead to insights into the reason for the rainfall changes and provide more confidence in the direction and magnitude of the changes.

Understanding the causes of both the observed and projected changes can lead to better understanding of the dynamics involved and increase confidence in the projected changes. One approach to improving climate change projections is to downscale a greater number of GCMs, using a larger number of downscaling models, in order to see if a more robust signal can be obtained. Comparing the observed changes with the projected changes will (1) show if the observed trends are possibly indicating a climate change signal, and (2) provide increased confidence in the projected changes when the observed and projected changes are similar. When annual temperature and rainfall changes by the end of the century projected by RCMs in this study (Figure 6-11) are compared with observations (Figure 3-11), they show similar trends, increasing confidence that the projections are realistic.

Changes in inter-annual variability were not examined in this document. Since models (both GCMs and RCMs) still have difficulty in simulating inter-annual variations such as ENSO and IOD, the impact of these phenomena on rainfall in Vietnam in a changing climate needs to be explored further.

6.5 SUMMARY

The results presented in this section summarise the projected changes in temperature and rainfall across Vietnam and the surrounding region for mid-century and the end of the century under the high emission scenario (RCP 8.5). Results from multi-model means of more than 20 GCM projections and from eight RCM projections at high resolution were presented. Warming of between 3-4°C is projected across Vietnam, with all models indicating increases and only small variations in the magnitude of the change. The greatest warming is in SWMS (summer) and the least warming in NEMS (winter). There is good agreement between the global models, the regional models and the observed trends.

Projected rainfall changes are less certain. Most projections show only small changes in rainfall, both annually and seasonally. The high-resolution annual projections of decreases in northern Vietnam, increases in central Vietnam and little change in southern Vietnam are in reasonable agreement with the observed rainfall changes. This is in contrast to the GCM ensemble projections, which tend to show slight increases across Vietnam. Examination of the seasonal rainfall changes showed projected decreases for most of Vietnam during SWMS, and increases in the other seasons. There is only small agreement on the sign of change in the regional models, mainly for the decreases for SWMS. But the spread of projected changes is larger than the median change, indicating low confidence in these projected changes.

Changes in the mean temperature and precipitation can be expected to influence the projected changes in key climatic features such as extreme rainfall, droughts, heat waves, tropical cyclones and sea level. Changes in the frequency and intensity of these features can have a greater impact than changes in the annual or seasonal means, since they may have potentially large effects on people and their livelihoods, as well as causing huge economic costs and disruption to society. Projected changes in these climate features and extremes are examined in Chapter 7.

7 CLIMATE FEATURES AND EXTREMES

In this chapter, analyses of the simulations of various climate features and extremes are presented. The various features presented all have particular relevance and importance for the climate of Vietnam: tropical cyclones, extreme rainfall, heat waves and droughts. As is noted below, current extreme events have significant impact for Vietnam; it is likely that changes in extremes could have greater impact on Vietnam than the projected changes in mean temperature and rainfall.

In Section 7.1, a brief summary of the impact of tropical cyclones in Vietnam is first presented. Then, a summary of results using various techniques to analyse GCM data is given in Section 7.1.1, followed by an illustration of application of the direct detection method in regional climate simulations in Section 7.1.2.

7.1 TROPICAL CYCLONES IN VIETNAM

Vietnam is located within the tropical monsoon region and its eastern coast faces the north-west Pacific Ocean, which is one of the major tropical genesis regions of the globe. Due to its location, Vietnam has been heavily affected by storms from the northwest Pacific and therefore it is ranked as one of the top ten countries worldwide suffering from natural disasters, such as storms, floods and landslides. On 2 November 1997, the most destructive Typhoon Linda tore through southern Vietnam and swept away tens of thousands of homes in the Mekong Delta. In the aftermath, Typhoon Linda left behind at least 464 people dead, 857 injured and over 3000 reported missing; 80,000 houses were destroyed and 140,000 were badly damaged. Hundreds of thousands of acres of rice fields were inundated, causing heavy crop losses, and infrastructure such as roads, schools, and hospitals suffered heavily. This was the worst typhoon to strike southern Vietnam during the past 100 years (the International Federation of Red Cross and Red Crescent Societies, IFRC, posted on **http://reliefweb.int/**). The damage caused by Typhoon Linda was enormous in terms of losses to human life and property, with destruction at such a scale that it prompted the Government of Vietnam to officially issue a request for international assistance.

On 8 August 2008, Typhoon Kammuri hit northern Vietnam, causing damage to eight provinces, with 162 dead or missing and 81 injured. On 2 November 2009, Typhoon Mirinae was Category 2 when it hit the Philippines and even though it weakened to a tropical storm during its time in the East Sea before landfall in central Vietnam, the destruction was still enormous. It caused floods and landslides in the central and central highland provinces, leaving 126 people dead or missing and exacting a financial loss of VND 5.6 trillion. On 23-24 August 2010, Typhoon Mindulle originated in the East Sea as a tropical depression and gained strength to become a Category 1 storm when approaching southern North Vietnam; it made landfall at three provinces (Nghe An, Ha Tinh and Quang Binh) killing 10 people, injuring 64 and causing damage to 160 homes (Government of Vietnam). More than 30,287 people were evacuated. By 24-25 August, the associated rainfall caused floods to provinces Thanh Hoa through to Thua Thien Hue.

Figure 7-1 shows the number of storms per month that hit Vietnam during the period 1945 to 1998 (**http://reliefweb.int/**). This figure reveals that the storm season starts in March, when tropical cyclones or typhoons make landfall in the northern part of South Vietnam, then the season moves northward after this month, reaching North Vietnam in May and persisting until September. During these months, the number of storms that make landfall increases; on average there are around 1-5 in May and around 16-20 in September. Central Vietnam is the region with the highest number of hits. In October, the storm season begins to move southward and the peak landfall month is November The region from central to southern Vietnam experiences 16 to 20 storms in November. Due to the widespread damage that they cause, tropical storms play an important role in Vietnam's economy. On average between six and eight major storms hit Vietnam each year, causing human and property losses estimated at 1% of the country's GDP (Government of Vietnam, 26 March 2012).

Since tropical storms or typhoons cause extensive damage to ecosystems, infrastructure, society, economy, etc., we have investigated the characteristics of tropical storms in the present climate and their projected changes by the end of this century.

Figure 7-1: The number of tropical storms and typhoons (per month) that affected Vietnam during the period 1945 to 1998. Source: ReliefWeb.

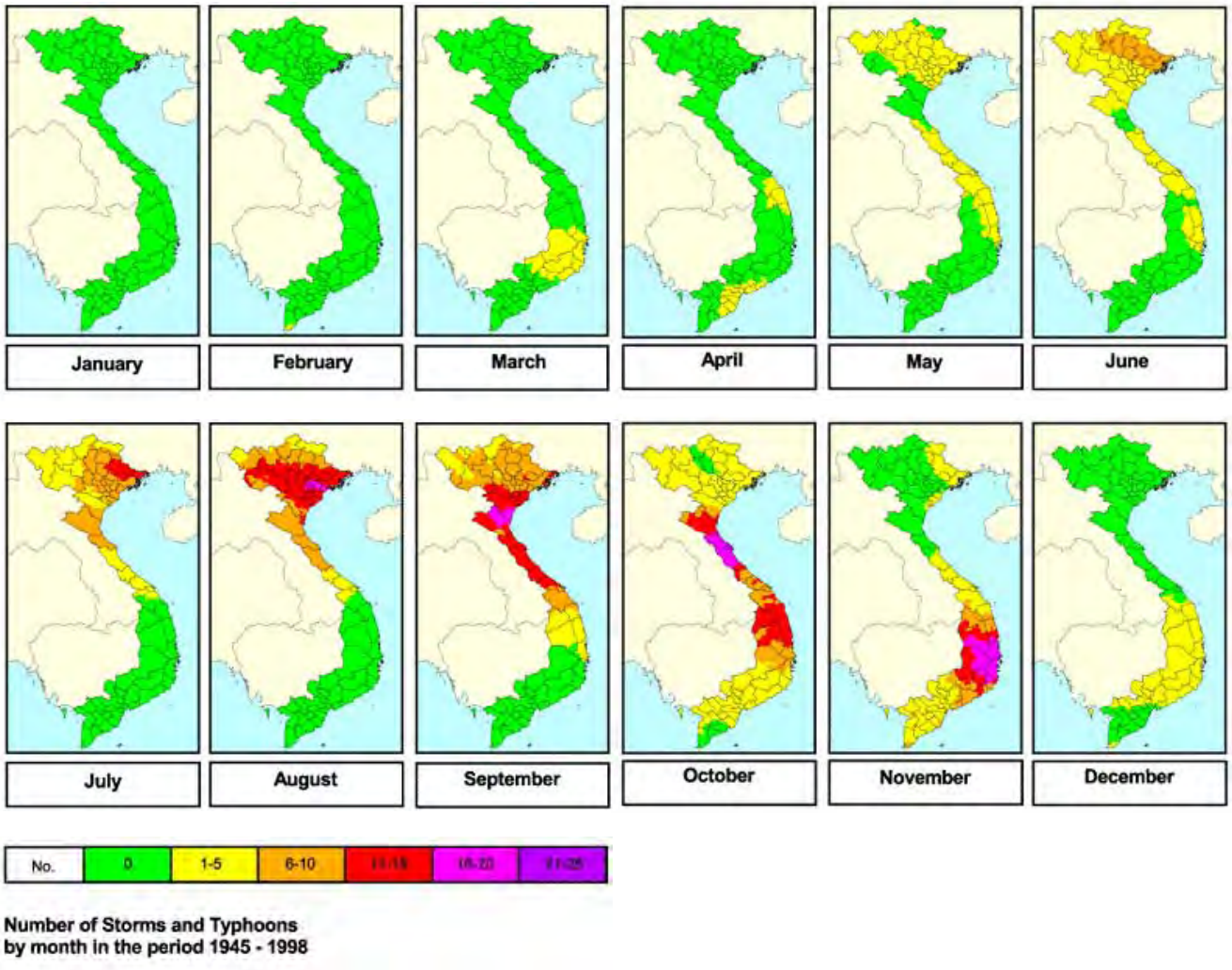

7.1.1 Tropical cyclone detection in GCM simulations

Tropical cyclone methodology using GCMs

The current generation of GCMs is able to simulate the broad-scale atmospheric conditions associated with tropical cyclone activity, but they have insufficient temporal and spatial resolution to capture the high wind speeds and other small-scale features associated with these systems. Despite this limitation, a number of methods exist for making projections of changes in the frequency and location of tropical cyclone activity from GCM data (c.f. Knutson *et al.*, 2010). These methods can be split into two general categories: (1) 'empirical methods' which identify and utilise relationships between tropical cyclones and the large-scale environmental conditions that are known to be associated with their development, and (2) 'direct-detection' schemes to identify synoptic features that have the characteristics of a tropical cyclone directly from climate model output, i.e. a closed low-pressure system accompanied by strong winds and a warm core through the depth of the atmosphere.

The projected changes in tropical cyclone frequency and location were derived using methods falling under both of these general categories:

- Three empirical methods were used to infer tropical cyclone activity from the large-scale environmental conditions and were applied to the outputs of seventeen Coupled Model Intercomparison Project Phase 5 (CMIP5) Global Climate Models. These three schemes are known as the Genesis Potential Index (GPI), the Murakami modification of the GPI (GPI-M) and the Tippett Index.
- Two direct detection schemes, the CSIRO Direct Detection (CDD) and the Okubo-Weiss-Zeta Parameter (OWZP) were applied to a subset of CMIP5 GCM model outputs.

These methods were applied to outputs from CMIP5 GCMs to determine if findings from the Pacific Climate Change Science Program (PCCSP, see Australian Bureau of Meteorology and CSIRO, 2011) are substantiated using this later generation of models, and to provide new projected changes in the frequency of tropical cyclones at the end of the 21st century under a high emissions scenario (RCP 8.5). The TC detection in future simulations under the RCP 8.5 scenario is compared with detection from simulations for the historical period. In addition, the cyclonic wind hazard for both the current climate and for the future climate was assessed using Geoscience Australia's Tropical Cyclone Risk Model (TCRM).

Empirical methods using GCMs

Approaches that use the mean characteristics of the large-scale environment in order to build empirical indices that replicate the key features of tropical cyclone formation are all essentially updates of the Yearly Genesis Parameter (YGP; Gray 1979). For instance, Royer *et al.* (1998) showed that the YGP could not be used to address climate change and therefore refined this index by modifying the thermal component. More recently, Emanuel and Nolan (2004) have proposed the Genesis Potential Index (GPI), which uses the concept of potential intensity (Bister and Emanuel, 1998) to account for thermal conditions. The GPI was developed and tuned using the large-scale environmental conditions of the NCEP/DOE R-2 reanalyses and has since been used in a number of studies to infer tropical cyclone formation in GCMs (e.g. Camargo *et al.*, 2007).

Murakami and Wang (2010) found that when the GPI was applied to the Japanese 25-year reanalysis dataset, it underestimated the frequency of tropical cyclone genesis in the Inter-Tropical Convergence Zone and in the eastern Pacific. Thus they modified the original GPI, herein referred to as GPI-M, by explicitly incorporating a term to represent vertical motion.

Tippett *et al.* (2011) followed the approach of earlier authors with the aim of developing a new index that reduces the limitations of the GPI. The main modification was the use of relative SST (the difference between local SST and mean tropical SST) to replace the potential intensity term in the GPI.

In this study, these three empirical indices were calculated for all CMIP5 GCMs for which relevant data were available.

CSIRO direct detection scheme using GCMs

A number of approaches exist for the direct detection and tracking of tropical cyclone-like vortices in GCMs and downscaled model simulations (e.g., Bengtsson *et al.*, 1982; Broccoli and Manabe, 1990; Walsh and Watterson, 1997; Camargo and Zebiak, 2002). However, due to the low resolution of GCMs and possible model biases and other deficiencies, tropical cyclone detection procedures invariably need to be adjusted to reproduce observed climatologies. Subjective adjustment can lead to model-specific and even basin-specific detection criteria (e.g. Camargo and Zebiak, 2002), which is less than ideal because compensation is made for model deficiencies by the detection procedure, and the same model deficiencies are assumed to be present in the future climate. A method to objectively determine detection criteria that incorporated a resolution-dependent wind-speed threshold was proposed by Walsh *et al.* (2007). While arguably an improvement because of its increased objectivity, it effectively retains model-dependent thresholds for all models of differing grid resolution.

The approach to the direct detection of tropical cyclone-like vortices using a modified version of the Nguyen and Walsh (2001) detection scheme, coupled with the tracking scheme of Hart (2003), is hereafter referred to as the CSIRO Direct Detection (CDD) method. The CDD uses a wind speed threshold set at 70% of the value recommended by Walsh *et al.* (2007) and was applied to outputs from a subset of seventeen CMIP5 GCMs for which suitable sub-daily, multi-level model outputs were available. Of the seventeen CMIP5 models examined, the TC detections in eleven models reproduced the current climate TC climatology with annual TC numbers within ±50% of observed numbers.

Curvature vorticity parameter scheme using GCMs

The Okubo-Weiss-Zeta (OWZP) parameter of Tory *et al.* (2013a, 2013b, 2013c), referred to as the curvature vorticity parameter (CVP) by the Australian Bureau of Meteorology and CSIRO (2011), is an independent and objectively determined detection method developed and tested in reanalysis data and verified against observations. It is based on the observation that the parameter space defining the conditions under which TCs form is large scale in nature, on the order of 1000 km (McBride and Zehr, 1981; Davidson *et al.*, 1990). Thus, rather than detect the structure of TCs directly, it detects the environment that favours their formation – these conditions should be resolvable even in the relatively coarse resolution of GCMs. In particular, recent studies (Dunkerton *et al.*, 2009; Nolan, 2007) have identified the importance of high curvature vorticity and low- to mid-tropospheric relative humidity immediately prior to tropical cyclone formation. Thus, elevated curvature vorticity and relative humidity as well as minimal wind shear have been incorporated into the detection algorithm.

The OWZP has been applied to all tropical cyclone basins in thirteen GCMs. Of the thirteen CMIP5 models examined, the TC detections in all except five models reproduce current-climate TC climatology, with annual TC numbers within ±50% of observed.

The OWZP scheme was tested on 20 years of ERA-Interim reanalysis data, and tuned to best reproduce the International Best Track Archive for Climate Stewardship (IBTrACS; Knapp *et al.*, 2010) observed database. Similarly, the CDD method was tested and tuned to the same reanalysis data to maximise performance and minimise the use of thresholds. The climatology of tropical cyclones based on the application of the CDD and OWZP to ERA-interim reanalyses compares well with the observed climatology derived from IBTrACS, especially for the Western Pacific region (Figure 7-2). No additional tuning or adjustments were made prior to applying these methods to the GCMs, which provides greater confidence that the future changes in tropical cyclone frequency detected actually represent changes in the frequency of tropical cyclone-like circulations that develop in the GCMs.

Figure 7-2: Spatial distribution of annual tropical cyclone genesis in (a) IBTrACS data, (b) detected in ERA-interim using the CDD method and (c) detected in ERA-Interim using the OWZP method. Occurrence is expressed as the number of cyclones per year within a 5° x 5° grid cell.

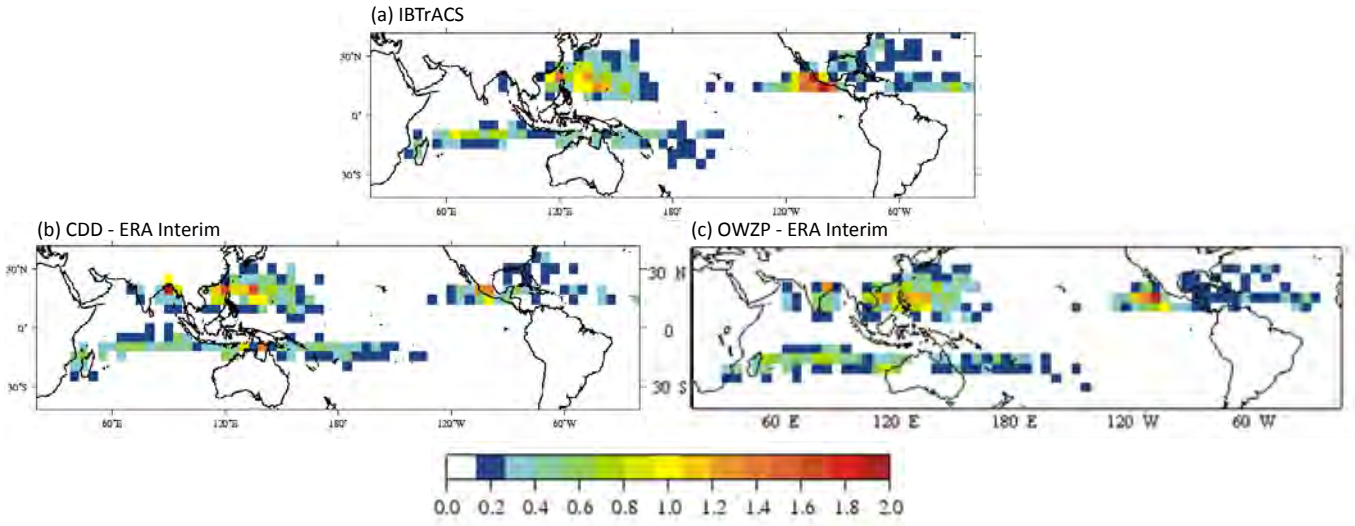

Tropical cyclone wind hazard using GCMs

The current climate wind hazard associated with tropical cyclone activity in the Western Pacific region was estimated by applying Geoscience Australia's Tropical Cyclone Risk Model (TCRM) to the historical track record. TCRM is a statistical-parametric model of tropical cyclone behaviour, enabling users to generate synthetic records of tropical cyclones representing many thousands of years of activity. The model was applied to tracks of tropical cyclone-like vortices detected in the CMIP5 GCM outputs (using the CDD scheme) to determine how the cyclonic wind hazard may change in the future. TCRM uses an auto-regressive model, similar to the model developed by Hall and Jewson (2007), to create synthetic tracks of tropical cyclone events based on the characteristics (speed, intensity, bearing, size and genesis location) of recorded tropical cyclone events. Once a set of synthetic tropical cyclone events has been created, a parametric wind field (Powell *et al.*, 2005) and boundary layer model (Kepert, 2001) is applied to each track, and the maximum wind speed over the life of each event is captured. A generalised extreme value (GEV) distribution is then fitted to the maximum wind speed values for each location (Hosking, 1990).

Projected changes in tropical cyclone frequency by the end of the century for RCP 8.5 based upon GCMs

Changes globally

There is a growing level of agreement among models that on a global basis the frequency of tropical cyclones is likely to decrease by the end of the 21st century. The magnitude of the decrease varies from 6 % to 35 % depending on the modelling study. There is also a general agreement between models that there will be an increase in the mean maximum wind speed of cyclones by between 2% and 11% globally, and an increase in rainfall rates of the order of 20% within 100 km of the cyclone centre (Knutson *et al.*, 2010). Thus, the scientific community has a moderate level of confidence in these global projections.

Changes for the East Sea (0-25°N; 100-180°E)

The GCMs show inconsistent results across a range of methods for projecting changes in TC frequency for the East Sea (Table 7-1, Figure 7-3), using the direct detection methodologies (OWZP or CDD) or the empirical methods described earlier. The direct detection methodologies (CDD and OWZ) and Tippett indicate a decrease in TC numbers, with more than half of the results suggesting decreases of between 5 and 20%. The empirical techniques (GPI-based) assess changes in the main atmospheric ingredients known to be necessary for TC formation. About four-fifths of the results suggest the conditions for TC formation will become more favourable in this region. However, when only the models for which direct detection and empirical methods are available are considered, the assessment is that there will be a decrease in tropical cyclone formation. These projections are consistent with those of the Australian Bureau of Meteorology and CSIRO (2011).

In summary, the global models project a general decrease in TC genesis (formation) frequency for the western North Pacific Basin. However the confidence level for this projection is low.

Table 7-1: Percent change in tropical cyclone formation by the end of the century based upon GCMs using different methods.

MODEL	GPI CHANGE	GPI-M CHANGE	TIPPETT	CDD	OWZP
ACCESS1.0	71	22	-54	15	
ACCESS1.3	55	48	-33	29	
BCCCSM11	13	11	-22		-8
CANESM2	34	22	-47	15	
CCSM4				-81	-14
CNRM-CM5	0	-2	-25	-9	-16
CSIRO-MK3-6-0	7	-1	-30	-11	-4
FGOALS_G2	-5	-15	-10		
FGOALS_S2	-3	-3	-35		
GFDL-ESM2M				8	8
GFDL-CM3	15	5	-17		-31
GFDL-ESM2G				-8	-15
GISS-E2R	14	9	-17		
HADGEM2-ES	13	1	-57		
INMCM4	25	26	-5		
IPSL-CM5-ALR	19	9	-17		
IPSL-CM5-BLR				-31	
MIROC5				-42	-33
MIROC-ESM	17	2	26		
MPI-M	19	17	-45		
MRI-CGCM3	1	-3	-34		
NORESM1-M	-11	-17	-19	-29	
Multi-model mean	17	8	-26	-13	-14
Fraction of models indicating increase	0.8	0.7	0.1	0.4	0.1

Figure 7-3: Percent change in tropical cyclone formation over the East Sea for the end of the century based upon different detection methods for various GCMs.

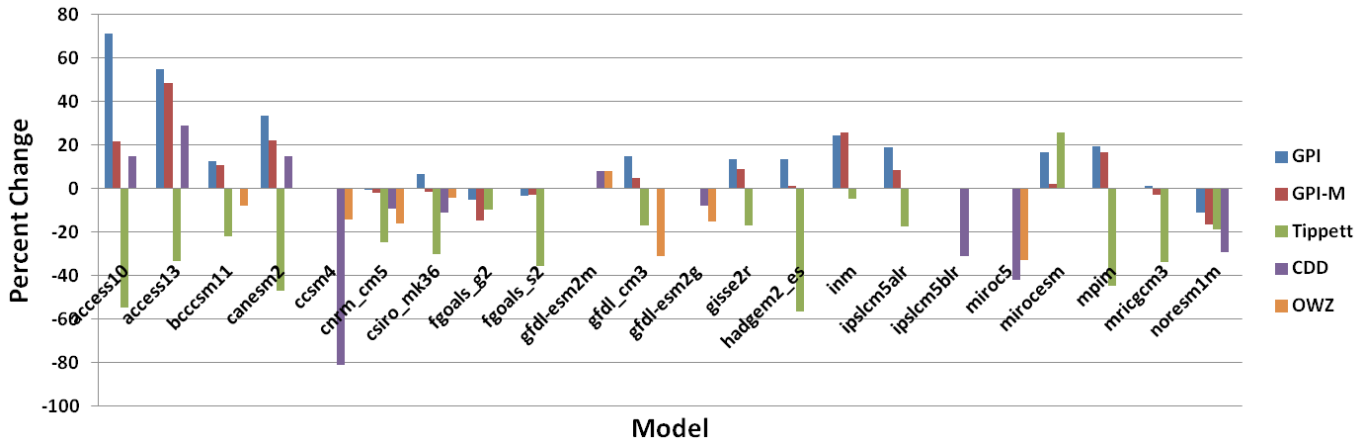

7.1.2 Tropical cyclone detection in CCAM simulations

Data and direct detection scheme for RCM downscaling results using CCAM

The quality of data sources is crucial for computing tropical cyclone (TC) intensity and trends over a region. In this section, first the quality of TC data from various sources is discussed to find the best available dataset to use in this project. There are 15 datasets: Regional Specialized Meteorological Center (RSMC) Miami; RSMC Honolulu; RSMC Tokyo; RSMC New Delhi; RSMC La Reunion; RSMC Nadi; Tropical Cyclone Warning Centre (TCWC) Perth; TCWC Darwin; TCWC Brisbane; TCWC Wellington; Shanghai Typhoon Institute (STI) of the China Meteorological Administration (CMA); Joint Typhoon Warning Center (JTWC); Hong Kong Observatory; NCDC DSI-9636[10]; UCAR ds824.1[11]). Data from all 15 sources were combined into a single dataset called International Best Track Archive for Climate Stewardship (IBTrACS[12]).

This study also focuses on the future trends of TCs over Vietnam using six CCAM simulations at 50 km resolution forced by SSTs from the GCMs selected for this study (see Chapter 2) and one global CCAM simulation at 50 km resolution forced by ERA-Interim for the period 1980-2000. Simulated spatial patterns of TC genesis and TC tracks over the region of interest by CCAM forced by ERA-Interim are compared with JTWC data to check the model performance in simulating TC characteristics.

Observed data for the period from 1884 to 2011 from IBTrACS are used to investigate long-term changes in storm frequency over the northwest Pacific, and the same data are also used to compare storm frequency from 1945 to 2001 with two other sources, JTWC and the World Meteorological Organisation dataset (WMO)[13]. A 20-year (1980-2000) simulation from CCAM representing the current climate is used to compare against observations, and 20-year (2045-2065) simulations representing the future climate at mid-century are used to investigate future changes in TC activity over the domain of interest. Longer period data are more reliable for testing statistical significance. However, we only consider 20-year time slices from the model simulations due to the limitations in computing resources. The region of interest includes the area 5°N-25°N and 110°E-120°E. TCs are counted either if they were generated in the region or have entered into the region. If a TC is re-curved back into the region, then it is counted as one TC.

The extended reconstructed sea surface temperature (SST) data used here is from the NOAA website **http://www.ncdc.noaa.gov/ersst/**. The Southern Oscillation Index (SOI), which is measured as the difference in the monthly pressure anomalies between Darwin (Australia) and Tahiti, is obtained from **http://www.cgd.ucar.edu/cas/catalog/climind/soi.html.** The SST anomalies are calculated as deviations from the long-term mean (1945-2011). Based on the SOI, an El Niño event is defined as SOI ≤ -2 and a La Niña event is defined as SOI ≥ +2. The neutral condition is defined as -2 < SOI < +2. TC characteristics are investigated separately for El Niño, La Niña and neutral events. Trends in the TC frequency are investigated using linear regression and the statistical significance is tested using the Kendall Tau Test.

10 http://gcmd.nasa.gov/records/GCMD_gov.noaa.ncdc.C00076.html

11 http://rda.ucar.edu/datasets/ds824.1/

12 http://www.ncdc.noaa.gov/ibtracs/

13 http://www.ncdc.noaa.gov/ibtracs/index.php?name=wmo-data

We used seven criteria for detecting tropical cyclones from the model simulations, as follows:

1. Vorticity greater than 10^{-6} s^{-1};
2. A closed pressure pattern with minimum pressure anomalies of 0.5 hPa within a radius of 300 km from a point satisfying (1); this minimum pressure is at the centre of the storm;
3. The total tropospheric temperature anomalies, calculated by summing up temperature anomalies at 700, 500 and 300 hPa around the centre of the storm must be greater than 0.5°C;
4. The temperature anomaly at the centre of the storm at 300 hPa must be greater than the temperature anomaly at 850 hPa;
5. The geopotential height anomaly at 500 hPa is less than -10 m;
6. Outer-core wind strength at 850 hPa is 2 m sec^{-1}.

In this chapter, first we discuss the observed characteristics of tropical cyclones over the northwest Pacific region and their impacts on Vietnam. Second, the frequency of tropical cyclones and their intensity simulated by CCAM for the present-day climate are compared with observed frequency and intensity. Third, changes in tropical cyclone activity by the end of the century are given, comparing simulations for the end of the century and the current climate.

Inter-annual variability of tropical cyclone activity

The inter-annual variability of tropical cyclone frequency over the northwest Pacific region from 1945 to 2011 from three sources, IBTrACS, JTWC and WMO, is shown in Figure 7-4. It is evident from this figure that there are considerable differences in annual frequency among the three data sources, in particular before 1975; this is the pre-satellite period. IBTrACS has the largest annual TC frequency compared with the other two sources. JTWC has good agreement with IBTrACS after 1990, but it underestimates IBTrACS numbers before 1990.

The WMO dataset underestimates the IBTrACS annual storm numbers for the entire period of analysis. From 1979 to the current period, on average, JTWC and WMO have around 26 and 31 storms per year, respectively, whereas IBTrACS has an average of 36 storms annually. This difference suggests that JTWC underestimates IBTrACS TC numbers by -12% and WMO by -27%.

The figure suggests that there is considerable uncertainty associated with TC frequency even in observations, particularly before the satellite era. Also, Figure 7-4 shows that TC frequency from IBTrACS decreases around 1980 (solid trend line).

Assessment of CCAM simulations of tropical cyclones for the present-day climate

Inter-annual variability of TC numbers simulated by global CCAM at 50 km resolution forced by ERA-Interim is compared with observed numbers from JTWC, IBTrACS and WMO for 1979-2001 (Figure 7-5). Results based on the 23-year period reveal that the model simulates the TC frequency fairly well over the East Sea, with correlation coefficients for JTWC, IBTrACS, and WMO of 0.67, 0.45 and 0.36, respectively. In 1980 and 1981, CCAM matches well with the observed IBTrACS. After that it matches JTWC most closely until the end of the period, except for 2000, where it underestimates TC numbers compared with JTWC and IBTrACS, but it is still closer to these datasets than to WMO. For this period (1979-2001), on average, CCAM simulates 31 storms annually, which is similar to JTWC for the same period. Further, the correlation among the three observed datasets over this period is 0.65 for IBTrACS and JTWC, 0.57 for IBTrACS and WMO, and 0.25 for WMO and JTWC. These correlations further confirm that CCAM performance is within observed uncertainty.

Figure 7-4: Inter-annual variability of the number of tropical storms over the northwest Pacific from 1945 to 2011 from IBTrACS (blue), JTWC (black) and WMO (green) datasets. Solid black line shows decrease in TC frequency for IBTrACS from 1980.

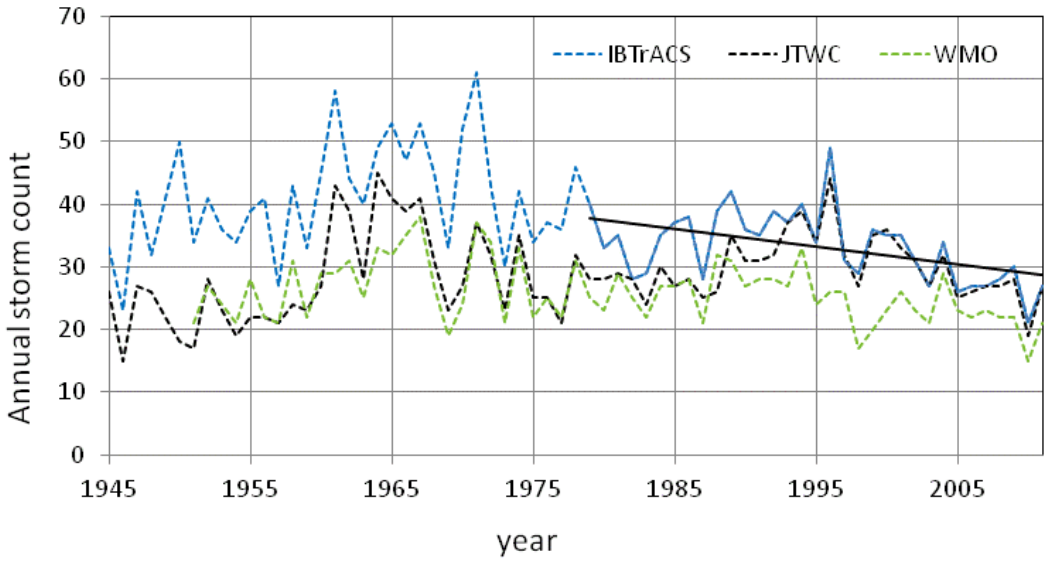

Figure 7-5: Inter-annual variability of observed (JTWC, black; IBTrACS, blue; WMO, green) and CCAM-simulated (red) tropical cyclone numbers over the East Sea from 1979 to 2001. CCAM simulations were at 50 km resolution forced by ERA-Interim.

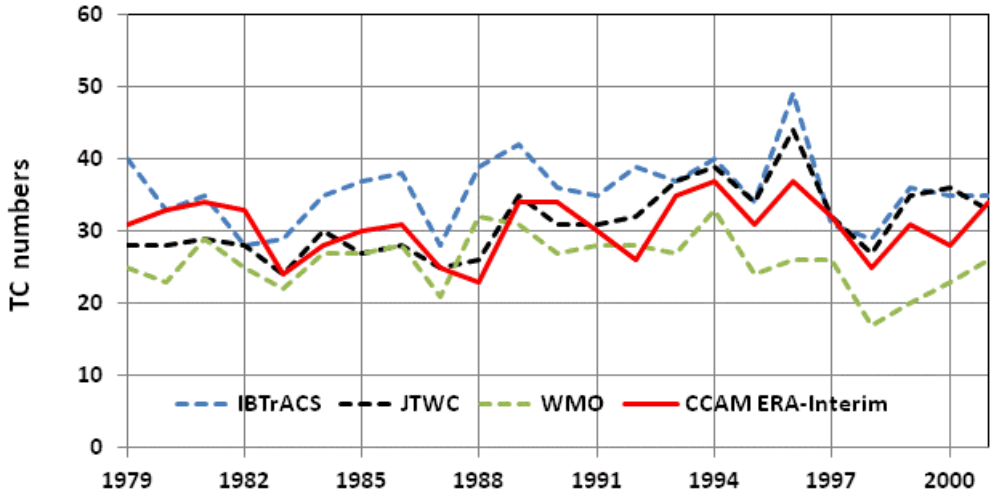

Tropical Cyclones and ENSO in observations and ERA-Interim forced CCAM simulations at 50 km resolution

Since the El Niño-Southern Oscillation (ENSO) phenomenon has a strong influence on the genesis and frequency of tropical cyclones over the western Pacific on the inter-annual time scale, we compared monthly TC frequency simulated by the ERA-Interim-forced CCAM at 50 km resolution with observed JTWC monthly TC frequency over the East Sea for the period 1979-2001. Figure 7-6 shows that the model simulates the annual cycle of TC frequency fairly well, with fewer TCs from March to June and more from July to November. Moreover, more tropical cyclones are simulated during La Niña years compared with El Niño years during the second half of the year, a pattern found in the observed records. However, there are some discrepancies on a monthly basis.

During the analysis period (1979-2001) there were six El Niño years (1982, 1986, 1987, 1991, 1994 and 1997), six La Niña years (1983, 1984, 1988, 1995, 1998 and 2000) and eleven neutral years. Under La Niña conditions, CCAM simulates fewer tropical cyclones in October and more in July than observations. Under El Niño conditions, CCAM simulates fewer tropical cyclones from August to November, resulting in a peak in August instead of a broader peak from August to September, as shown in observed records.

Figure 7-7 shows the relationship between CCAM-simulated tropical cyclones and observed JTWC tropical cyclones for El Niño, La Niña and neutral conditions. For simplicity, we only show the perfect fit (dotted) lines and their equations for the total number of TCs and the numbers in El Niño and La Niña years (not neutral years). Figure 7-7 shows that CCAM simulates the number of tropical cyclones fairly well for El Niño and La Niña conditions, as can be seen from the coefficients of determination, R^2, of the perfect fit for El Niño (dashed red line, 0.78) and La Niña (dashed blue line, 0.82). However, CCAM does not perform well for neutral conditions, with an R^2 of only 0.32 (not shown), which reflects on the R^2 value of the total TCs (dashed black line), which is lower than those in ENSO years. Nevertheless, on average, CCAM only slightly overestimates observed numbers for neutral conditions, simulating 33 storms per year compared with the 31 reported by JTWC for the period 1979-2001.

Knowing how CCAM performs for the current climate is valuable knowledge for further investigation of TCs under projected future climates for the region.

Figure 7-6: Monthly frequencies of tropical cyclones by month from observations (dashed) and from the 50 km ERA-Interim forced CCAM simulation (solid) over the East Sea for El Niño events (red lines) and La Niña events (blue lines) for the period 1979-2001.

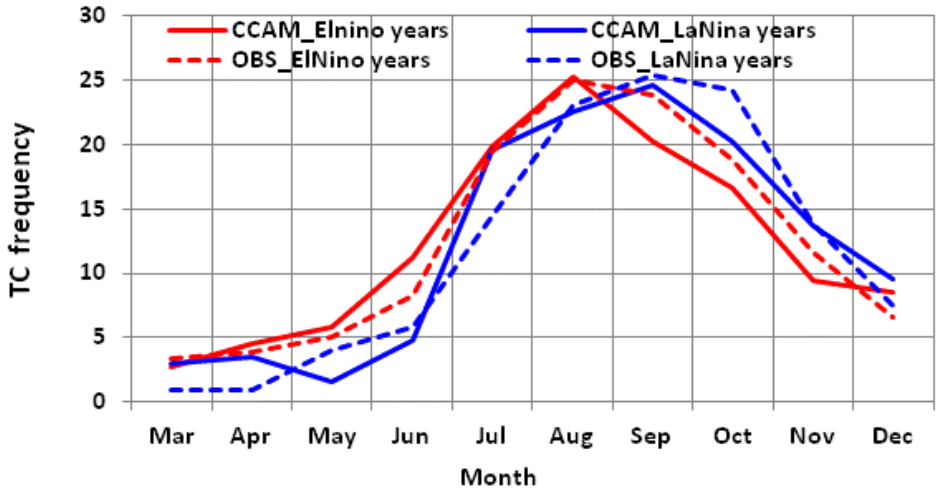

Figure 7-7: Relationship between observed tropical cyclone numbers (JTWC, y-axis) and CCAM-simulated TCs (x-axis) for El Niño, La Niña and neutral conditions over the East Sea for the period 1979-2001. Perfect fit lines and their equations are shown by black, red and blue dashed lines for the total number of TCs and those for El Niño and La Niña years, respectively. The 50 km CCAM simulation was forced by ERA-Interim data.

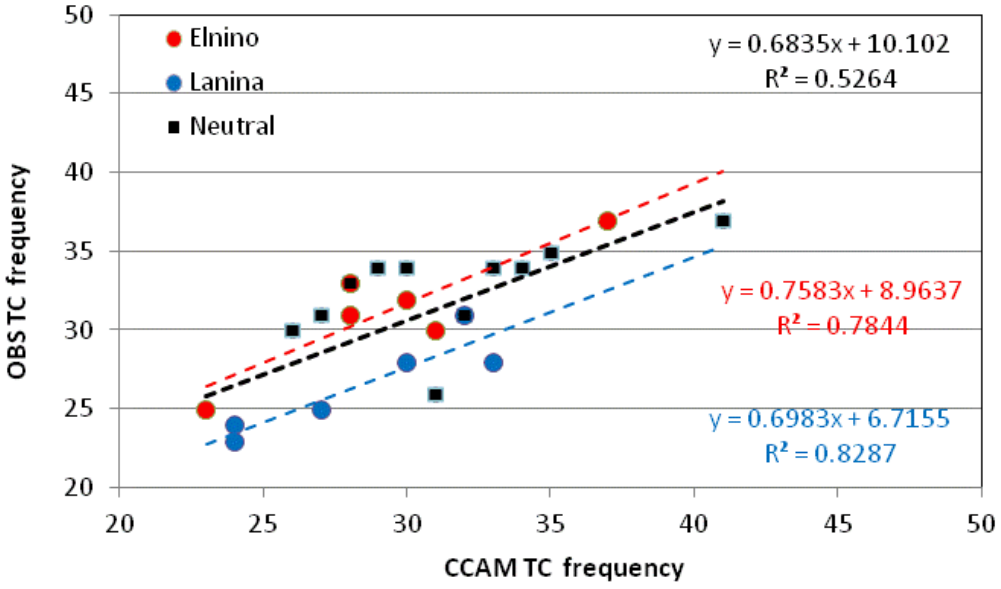

Projected changes in tropical cyclone frequency by the end of the century for RCP 8.5 based upon RCM simulations

At the time of this report, only four of the GCM-forced CCAM 50 km simulations have been analysed for projected changes in tropical cyclones. Due to the need to encompass a larger domain than available for the high-resolution (10 km CCAM or 20 km RegCM4.2) domains, only the 50 km CCAM simulations were used for this analysis. Changes in the number of tropical cyclone days projected by four members of the CCAM 50 km simulations for the end of the century for RCP 8.5 were analysed using direct detection (Figure 7-8). Changes in cyclone days are calculated as the difference between the 21-year period 2079-2100 and the baseline period, 1980-2000. It is evident from this figure that the number of tropical cyclone days shows an overall decrease over the western Pacific by the end of this century, with a maximum decline of 5 to 15 days between latitudes 5°N and 15°N. These results are consistent with the previously mentioned GCM-based direct detection changes.

7.1.3 Summary

In this study, we used three observational datasets of TC numbers: IBTrACS, JTWC and WMO. A comparison among the three datasets reveals a certain degree of uncertainty associated with the data related to TC numbers over this region, with marked differences during the pre-satellite era for the northwest Pacific. In addition, some differences are also found among these observational datasets for the period 1979-2001. WMO always underestimates the IBTrACS annual TC numbers by -27%. Over its long period of record, IBTrACS shows a clear downward trend in the number of tropical cyclones over the northwest Pacific during the satellite era.

Downscaled CCAM simulations forced by ERA-Interim reveal that the model reproduces TC numbers well, with results that are within the observed uncertainties. CCAM also captures year-to-year variations associated with ENSO fairly well from 1979 to 2001, but not so well for the neutral years. When changes in TC days are calculated using an ensemble of four 50 km CCAM simulations forced by GCM SSTs, a decrease in TC days over the western Pacific was found. This result is consistent with results from direct detection in GCMs and other studies conducted overseas (see Knutson *et al.,* 2010). However, most of the studies show that all characteristics of tropical cyclones are not well simulated by models, and therefore we have less confidence in this result. Further investigation is needed to better understand the changes to tropical cyclone characteristics in the future.

Figure 7-8: Projected changes in the number of tropical cyclone days over the western Pacific by the end of the century for RCP 8.5. Changes are calculated as the difference between projections from a four-member 50 km CCAM simulation ensemble for the period 2079-2100 compared with a baseline period, 1980-2000.

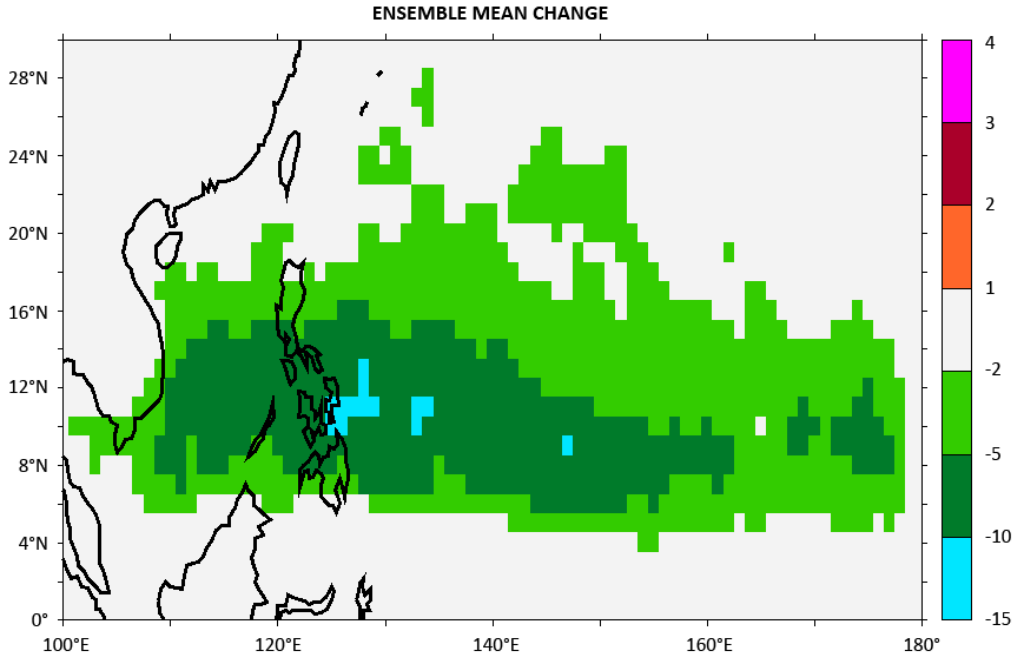

7.2 EXTREME RAINFALL

An understanding of extreme rainfall events for Vietnam is important, as these events can have impact on local infrastructure, economic activities, and environmental systems, as well as human lives. Investigating the changes in intensity (amount) and duration (time span) of these events under a changing climate will improve understanding of risk and planning requirements associated with these events. Central Vietnam is particularly vulnerable to extreme rainfall events such as floods. Heavy rainfall over central Vietnam has therefore received more attention compared with other parts of the country (Yen *et al.,* 2011; Yokoi and Matsumoto, 2008; Chen *et al.*, 2012). The heavy rainfall events typically occur over this region during October to November, with most associated with tropical cyclone activity (Chen *et al.,* 2012). Heavy rainfall over central Vietnam can also occur as a combination of a cold surge and a tropical depression-type disturbance (Yokoi and Matsumoto, 2008). One such event occurred on 2-3 November 1999, when the precipitation over Hue city was more than 1800 mm over these two days, more than eighty-five times the long-term (1979-2011) November mean rainfall (typically 21 mm day^{-1}).

The coastal regions of Vietnam are also influenced by these events, with increased flushing of sediments and water discharge from the Mekong and Red River catchments (Tran *et al.*, 2004). The impact caused by human activity has further diminished the predictability of these events and also led to other environmental impacts, such as erosion, sedimentation and saltwater intrusion, pollution and degradation of ecosystems (Tran *et al.*, 2004).

This section presents the evaluation of extreme rainfall for the current climate, along with projected changes in extreme rainfall by the middle and end of the century for the highest emission scenario (RCP 8.5; refer to Section 2.2 for further details). Extreme rainfall indices generated from observational data and model simulations are used to assess both the duration and intensity of these events. The approach taken, data utilised and results arising from this analysis are summarised below.

7.2.1 Methods and data

This chapter studies extreme rainfall over Vietnam using extreme rainfall indices. The extreme rainfall indices used in this assessment are as follows:

- RX5: annual highest consecutive five-day precipitation amount
- RX1: annual highest one-day precipitation amount
- CWD: annual maximum number of consecutive wet days (days with rainfall greater than or equal to 1 mm)
- CDD: annual maximum number of consecutive dry days (days with rainfall less than 1 mm).

These extreme rainfall indices provide common statistical scales that reveal comparable information on intensities and durations of extreme rainfall events.

Datasets used are daily rainfall from APHRODITE (1979-2007) and station observations (1979-2011) to provide a baseline for the current climate, and the six CCAM simulations at 10 km resolution, (see Section 2.6.1 for more details) to assess likely future climate changes. An advantage of using the APHRODITE dataset as well as station observations in this analysis is that the APHRODITE data are gridded, which means that observed station values are spatially interpolated based on a mathematical extension of trends for all locations across Vietnam, whereas station observation data are limited to the locations of the stations. A possible constraint of the APHRODITE data, however, is that the data might not capture observed climate extremes if the interpolation occurs across a large area with a limited number of station data points.

The extreme indices are computed annually from model simulations of three climate periods: current (1980-2000), mid-century (2045-2065) and end-of-century (2079-2100) under RCP 8.5. Averages are computed for each index for the corresponding periods. The study is conducted over the seven climatic sub-regions of Vietnam, shown in Figure 7-9. The Kendall Tau test is used to examine the statistical significance of projected future changes (for further information on this technique, refer to Kendall, 1975). The statistical significance level provided by this test varies from 0% to 100%, with anything greater than 95% indicating a notable level of significance. The test provides information on whether the projected trends are outside what one would expect from normal variability.

Figure 7-9: The seven climatic sub-regions of Vietnam (outlined in colour) and meteorological stations (squares) used in this project. NW, NE, ND, NC denote regions in northern Vietnam and SC, CH and S denote regions in southern Vietnam.

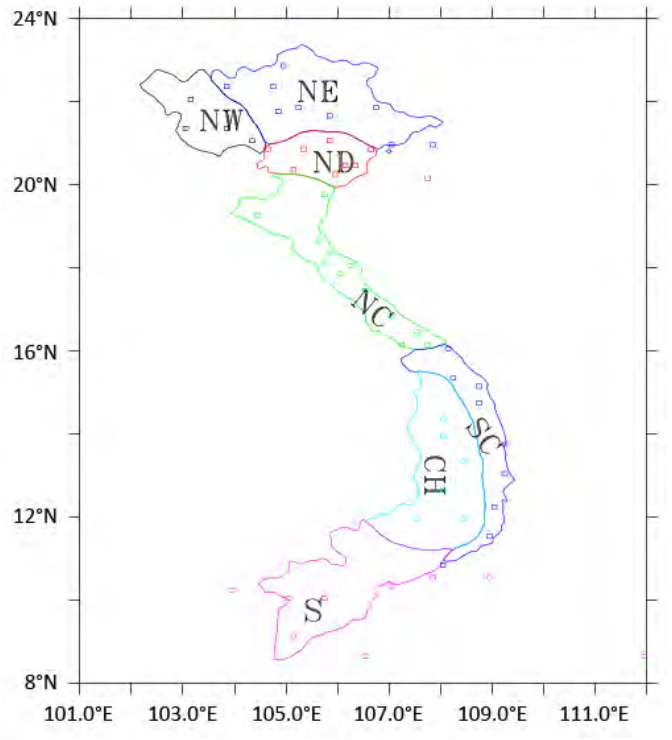

7.2.2 Assessment of downscaled simulations of the current climate (1980-2000)

This section describes how well CCAM simulates the mean condition of the extreme indices of the current climate. Bias (model values minus observation values) is used as a measure of the model performance. The year-to-year variation of these indices is also explained using the standard deviation, where a standard deviation of greater than 1 shows strong year-to-year variability.

Observed indices for the 1979-2007 period

The extreme rainfall indices derived from APHRODITE rainfall data are shown in Figure 7-10. One-day (RX1, a) and five-day (RX5, b) mean rainfall values are largest along the east coast, with amounts between 100 and 200 mm day^{-1} and up to 500 mm day^{-1}, respectively. The longest duration of wet days (CWD, c) is about 10 to 30 days, spread fairly evenly over the entire country, whereas the longest duration of dry days (CDD, d), from 50 to 60 days, is found over the southern part of Vietnam, in particular over the Mekong Delta region. This dry spell also is seen over Cambodia, Laos and Thailand.

Spatial patterns of CCAM-simulated multi-model mean climatologies for RX1, RX5, CWD and CDD are shown in Figure 7-11. A comparison between the observed patterns in Figure 7-10 and simulated patterns in Figure 7-11 suggests that the model captures the magnitude and spatial pattern of the indices of RX5, CWD and CDD over Vietnam fairly well, though the model slightly overestimates RX5, especially over southern Vietnam. In the case of RX1, the model overestimates the magnitude, especially in the south and in the mountainous regions, and also in northern Vietnam. Furthermore, maximum values of simulated CDD are located too far north (centred in northern Laos instead of Cambodia).

The biases of the indices, shown in Figure 7-12, in general indicate that for RX1 and RX5 the percentage bias is still relatively small. However, the CWD index shows a negative bias in the south of around -10 days. The CDD biases are also generally small (less than 5 days).

Figure 7-10: Observed spatial patterns of mean one day (RX1, a) and five day (RX5, b) extreme rainfall indices (mm day^{-1}), consecutive wet days (CWDs, c) and consecutive dry days (CDDs, d) derived from the APHRODITE daily rainfall data for the period from 1979 to 2007.

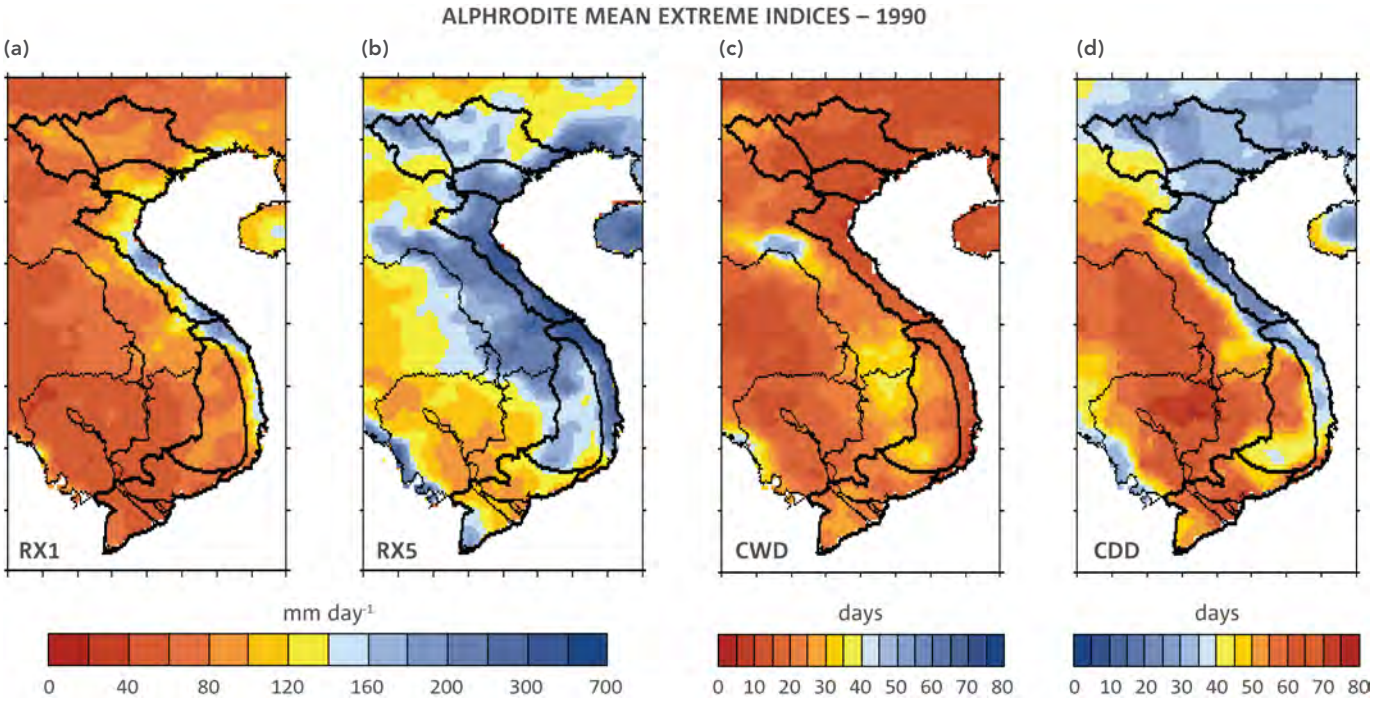

Figure 7-11: Spatial patterns of mean one day (RX1, a) and five day (RX5, b) extreme rainfall indices (mm day^{-1}), consecutive wet days (CWDs, c) and consecutive dry days (CDDs, d) derived from the CCAM multi-model simulations for the period 1980-2000 at 10 km resolution.

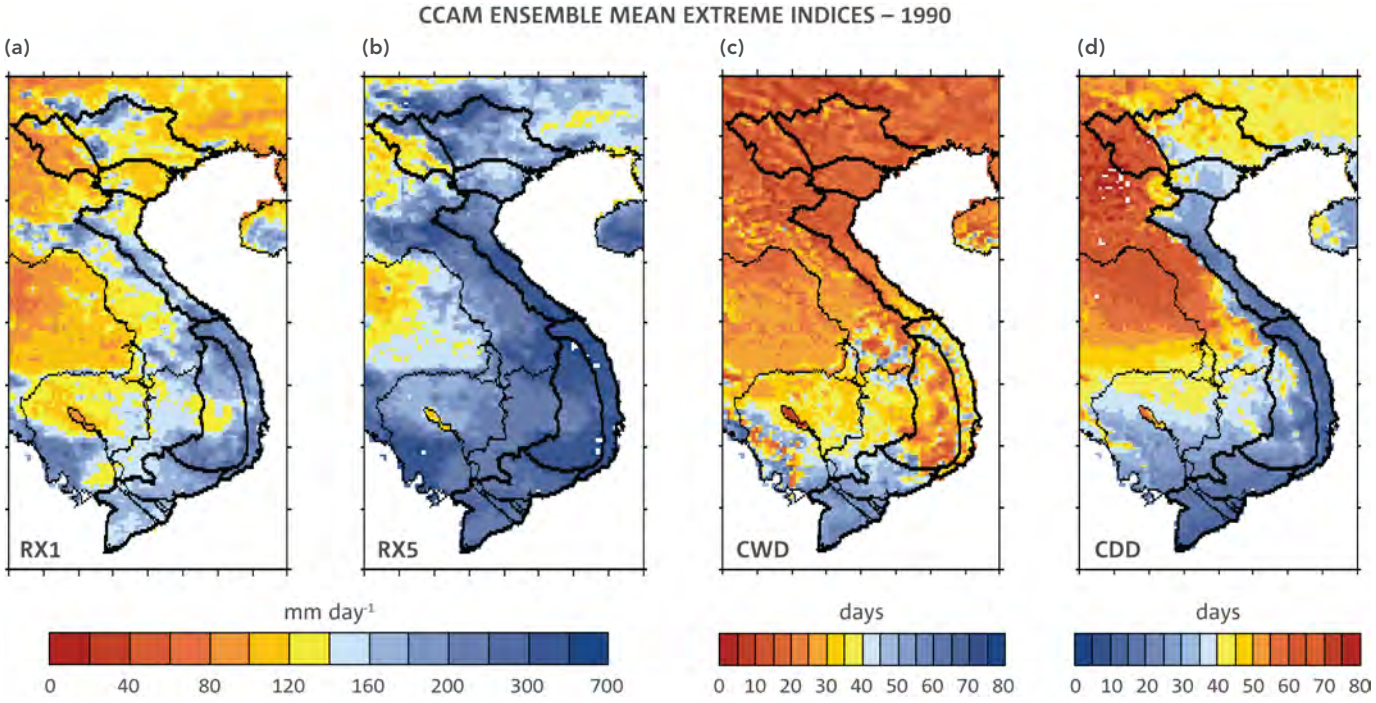

Figure 7-12: Spatial patterns of mean percentage bias of one day (RX1, a) and five day (RX5, b) extreme rainfall indices, consecutive wet days (CWDs, c) and consecutive dry days (CDDs, d) for the period 1980 to 2000. Biases are the multi-model mean of the CCAM simulations for the period 1980-2000 at 10 km resolution relative to the APHRODITE daily rainfall data.

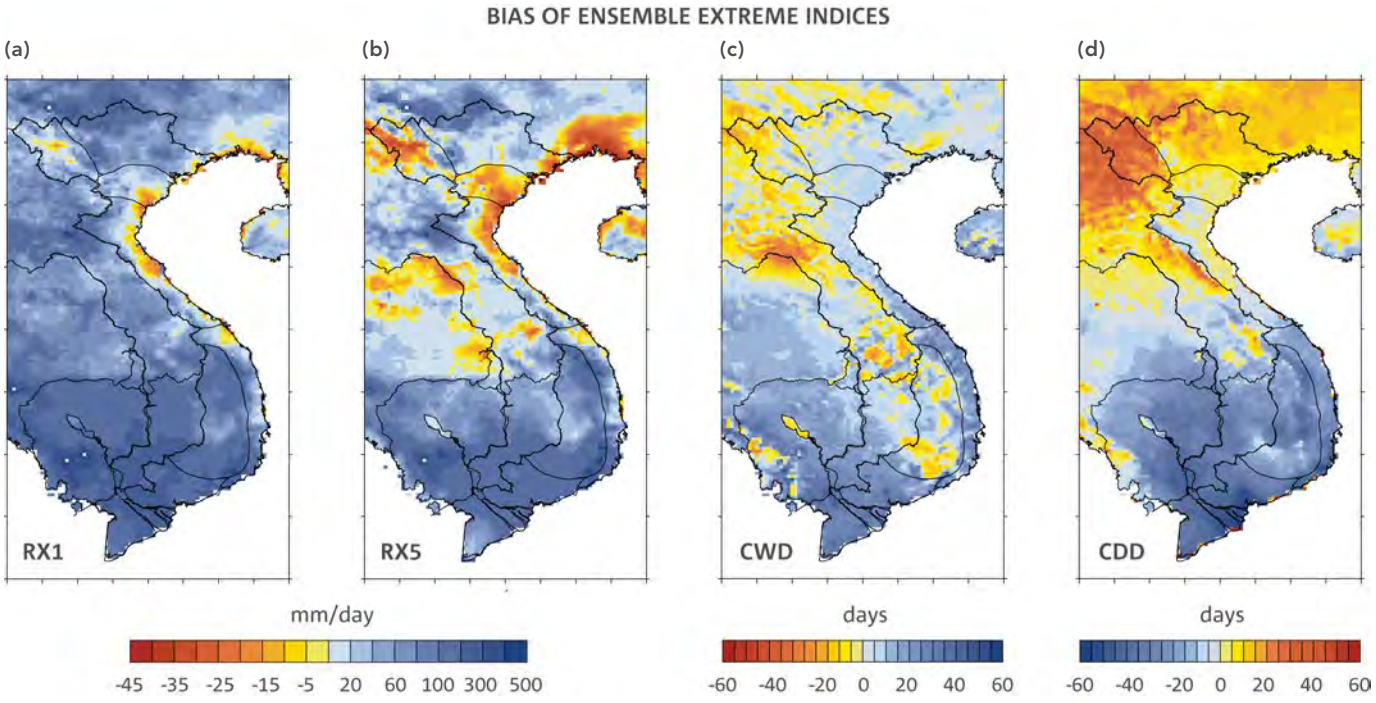

Means, time variability (temporal standard deviations) and biases for the four indices for the seven sub-regions are also given in Table 7-2, where biases are from the regionally averaged APRODITE dataset. Biases for RX1 and RX5 are given as percentages, while biases for CWD and CDD are given in days. The average (median) percent bias across Vietnam is 40% (26%) for RX5 and 97% (66%) for RX1. For RX1 and RX5, CCAM multi-model means tend to overestimate the amount for both, although many regional biases are less than 50% for RX5. Only in the ND and NC regions are the RX5 values underestimated. The largest bias in RX1 (225%) is for the S region, while the largest bias in RX5 (123%) is in the CH region.

The average (median) bias across Vietnam is 0 (-2) days for CWD and 6 (6) days for CDD. The overestimation of rainfall for the S region results in an underestimation (-16 days) of the CDD for this region and overestimation of CWD (16 days). For the northern regions, the model overestimates CDD, with the largest error in the NW region (+29 days), which is followed by the NE region (+24 days). For CWD, the best performance seen in NC (bias of -2 days), whereas the worst CCAM performance is seen in S (bias of -16 days).

In terms of inter-annual variability (SD), CCAM overestimates RX1 for all regions, with the largest SD bias of +506% (+56 mm d-1) seen in the S region. For RX5, the largest SD bias is +329% (76 mm d-1) also in the S region. For regions in northern Vietnam, the SD biases of RX5 and RX1 are around 100%. For CWD and CDD, the SD biases are less than 10 days, except in the S region.

Accurately portraying the extreme rainfall is very difficult for models. Also there may be some issues in relation to the accuracy of the observational datasets. Therefore, except for S (and maybe the CH region for RX1 and RX5), the accuracy of extreme rainfall indices is acceptable.

Table 7-2: Regional values and standard deviation of RX1 and RX5 (with percent bias) and CWD and CDD (day bias) for the observations and the CCAM 10 km ensemble means. The indices are derived from daily station-averaged rainfall (OBS) and area-averaged daily rainfall from CCAM ensemble simulations for the seven sub-regions.

		MEAN				STANDARD DEVIATION			
		RX5 (mm d^{-1})	RX1 (mm d^{-1})	CWD (days)	CDD (days)	RX5 (mm d^{-1})	RX1 (mm d^{-1})	CWD (days)	CDD days)
NW	OBS	134	66	21	36	36	20	8	13
	CCAM	168	104	16	65	66	40	6	19
	BIAS	26	59	-5	29	83	101	-2	6
NE	OBS	180	74	27	20	48	16	8	6
	CCAM	213	144	17	43	96	66	7	15
	BIAS	18	94	-10	24	100	315	-1	9
ND	OBS	192	96	13	31	63	32	4	12
	CCAM	172	120	17	37	91	66	6	12
	BIAS	-11	25	4	6	45	106	2	0
NC	OBS	329	130	22	13	100	31	7	3
	CCAM	298	161	20	26	126	71	7	8
	BIAS	-9	24	-2	13	26	129	0	5
SC	OBS	291	119	24	25	101	34	9	10
	CCAM	394	199	35	15	153	80	13	6
	BIAS	35	66	11	-10	52	134	4	-4
CH	OBS	156	64	45	32	35	18	15	11
	CCAM	348	185	31	26	108	57	14	10
	BIAS	123	189	-14	-6	210	214	-1	-1
S	OBS	133	52	36	34	23	11	13	20
	CCAM	261	169	51	18	99	67	25	7
	BIAS	96	225	16	-16	329	506	12	-13

7.2.3 Projected changes of extreme indices by mid-century (2045-2065) for RCP 8.5

Projected spatial patterns of extreme indices by the middle of the century under the RCP 8.5 (high) emission scenario derived from CCAM simulations at 10 km resolution are displayed in Figure 7-13. This figure shows that projected patterns of these indices are similar to those in the current climate, Figure 7-11, which suggests that no significant changes are expected by mid-century. The actual regional change values for the various indices (Figure 7-14 and Table 7-3) generally confirm this. The RX1 and RX5 values show some increases in the south and far north portions of Vietnam and decreases along the south-east coast. The largest projected increases in both the RX1 and RX5 indices are about 7% and the largest decreases are about -5%.

The year-to-year variability (SD) in RX5 and RX1 is projected to increase (Table 7-3), except for region SC, which shows a reduction of -10%. The largest increases in variability are projected for NW (+21%), NE (+15%) and CH (+11%).

The intensity of RX5 is predicted to increase by less than 10% over the regions NE and NW and to decrease over other regions by mid-century (see Figure 7-13 and Table 7-3). However, the year-to-year variability is projected to increase for all regions, except for SC, which shows a reduction of -9%. The largest change in variability is projected for regions NE (+16%) and NW (+13%).

For CWD and CDD days, the regionally-averaged changes are not statistically significant, with the largest changes only -8 and -4 days for S and CH, respectively. For other regions, the area-averaged change is between 0 and 2 days.

Table 7-3: Extreme indices and standard deviation and the percent change. The two periods used are 1980-2000 (current climate) and 2045-2065 (mid-century) for RCP 8.5.

		MEAN				STANDARD DEVIATION			
		RX5 (mm d^{-1})	RX1 (mm d^{-1})	CWD (days)	CDD (days)	RX5 (mm d^{-1})	RX1 (mm d^{-1})	CWD (days)	CDD days)
NW	1980-2000	168	104	16	65	66	40	6	19
	2045-2065	173	111	15	67	75	49	5	17
	%CHANGE	3	7	-1	2	13	21	0	-1
NE	1980-2000	213	144	17	43	96	66	7	15
	2045-2065	225	153	18	45	111	76	7	15
	%CHANGE	6	6	1	2	16	15	0	1
ND	1980-2000	172	120	17	37	91	66	6	12
	2045-2065	167	118	17	37	98	71	6	12
	%CHANGE	-3	-2	0	0	7	8	0	0
NC	1980-2000	298	161	20	26	126	71	7	8
	2045-2065	288	159	19	26	129	76	7	9
	%CHANGE	-3	-2	-1	0	2	7	0	1
SC	1980-2000	394	199	35	15	153	80	13	6
	2045-2065	376	188	34	15	140	72	12	6
	%CHANGE	-4	-5	-1	-1	-9	-10	0	0
CH	1980-2000	348	185	31	26	108	57	14	10
	2045-2065	344	192	26	26	111	63	11	11
	%CHANGE	-1	3	-4	0	2	11	-3	1
S	1980-2000	261	169	51	18	98	67	24	8
	2045-2065	262	173	43	17	102	71	19	8
	%CHANGE	0	2	-8	-1	4	7	-5	0

Figure 7-13: Projected extreme indices by mid-century (2045-2065) from the 10 km CCAM multi-model mean for RCP 8.5. RX1 (a) and RX5 (b) are shown as mm day^{-1}, while CWD (c) and CDD (d) are shown as number of days.

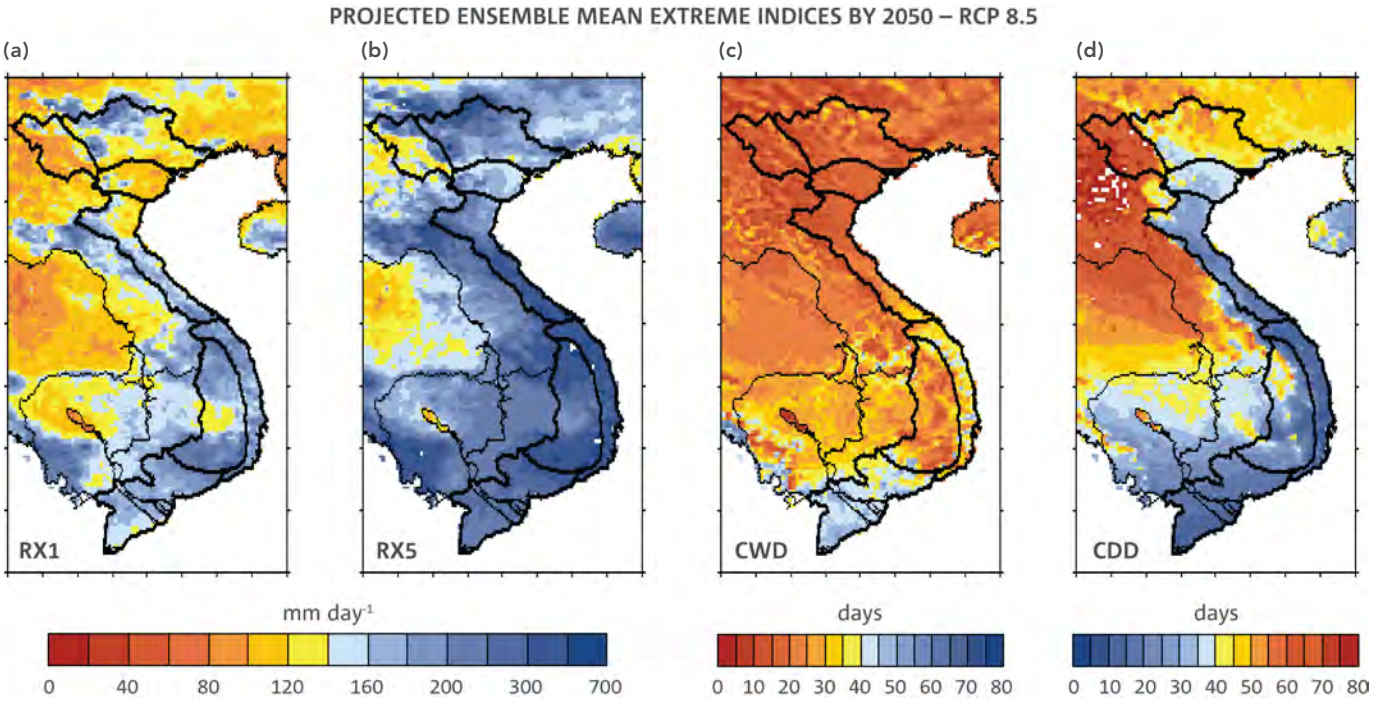

Figure 7-14: Multi-model mean projected changes of extreme indices by mid-century (2045-2065) from 10 km CCAM simulations for RCP 8.5. RX1 (a) and RX5 (b) are shown as changes in mm day^{-1}, while CWD (c) and CDD (d) are shown as number of days. All changes are relative to the baseline period (1980-2000).

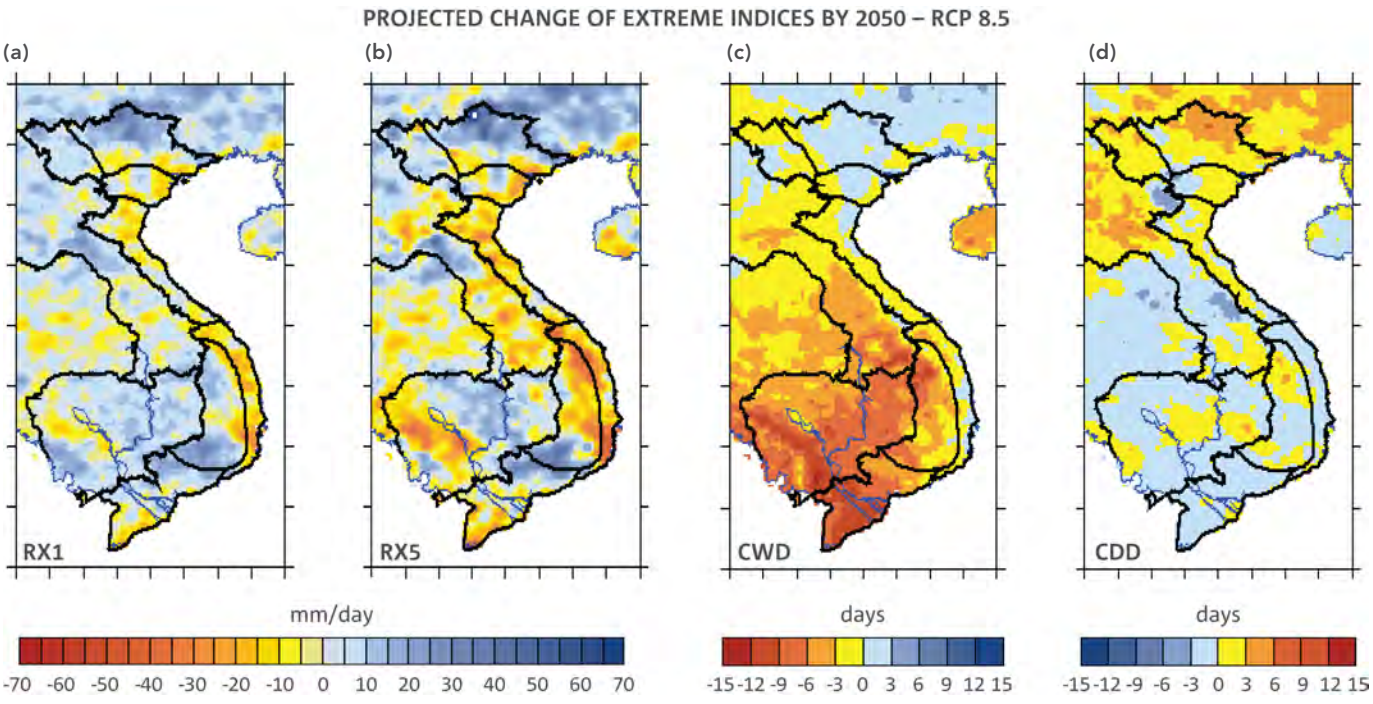

The agreement in the simulated change of the extreme indices among the CCAM multi-model members for mid-century is shown in Figure 7-15. In order to get a more coherent pattern, the changes were interpolated to a 30 km resolution grid. It is evident from this figure that the agreement on decreases in RX5, RX1 and CDD is up to at least 80% in the SC region, and to a lesser extent in the NC region. However, this strong agreement on decreases is fragmented. The CWD shows strong agreement among the multi-model simulations in the south, but fragmented agreement along the east coast. However, the change for each CCAM member (not shown) in RX1 and RX5 is statistically significant at the 95% confidence level for only a few grid points. The change in CWD and CDD is statistically significant for CCAM only for the simulations driven by NorESM1-M and MPI-ESM-LR, whereas CCAM CCSM4 shows no significant change for all the extreme indices.

7.2.4 Projected changes of extreme indices by end of the century (2079-2100) for RCP 8.5

By the end of the century (here defined as 2079-2100), the trends for all extreme indices are projected to continue and become even stronger (Figure 7-16) than for mid-century (Figure 7-14) under RCP 8.5. In particular, the decrease in RX1 and RX5 in central Vietnam is more pronounced. The changes in CWD and CDD, while showing similar patterns over Cambodia and Laos, show some regional changes over Vietnam by the end of the century versus mid-century. In southern Vietnam, the magnitude and patterns are similar. But in SC and NC, both CWD and CDD show changes in sign from mid-century to the end of the century. Changes for ND and NE are similar, but are slightly less for CDD in the NW region.

Model agreement on the sign of change for the extreme indices by the end of the century (Figure 7-17) is generally similar, or shows slightly more agreement than for mid-century, except for CDD, where the pattern of agreement has changed from little agreement to more agreement on increases in CDD, especially over Cambodia and Laos.

Figure 7-15: Percentage of agreement on the direction of change (increase positive)/(decrease negative) of RX1 (a), RX5 (b), CWD (c) and CDD (d) among the 10 km CCAM simulations for the period 2045-2065 compared with the baseline period 1980-2000. The results were interpolated to 30 km resolution.

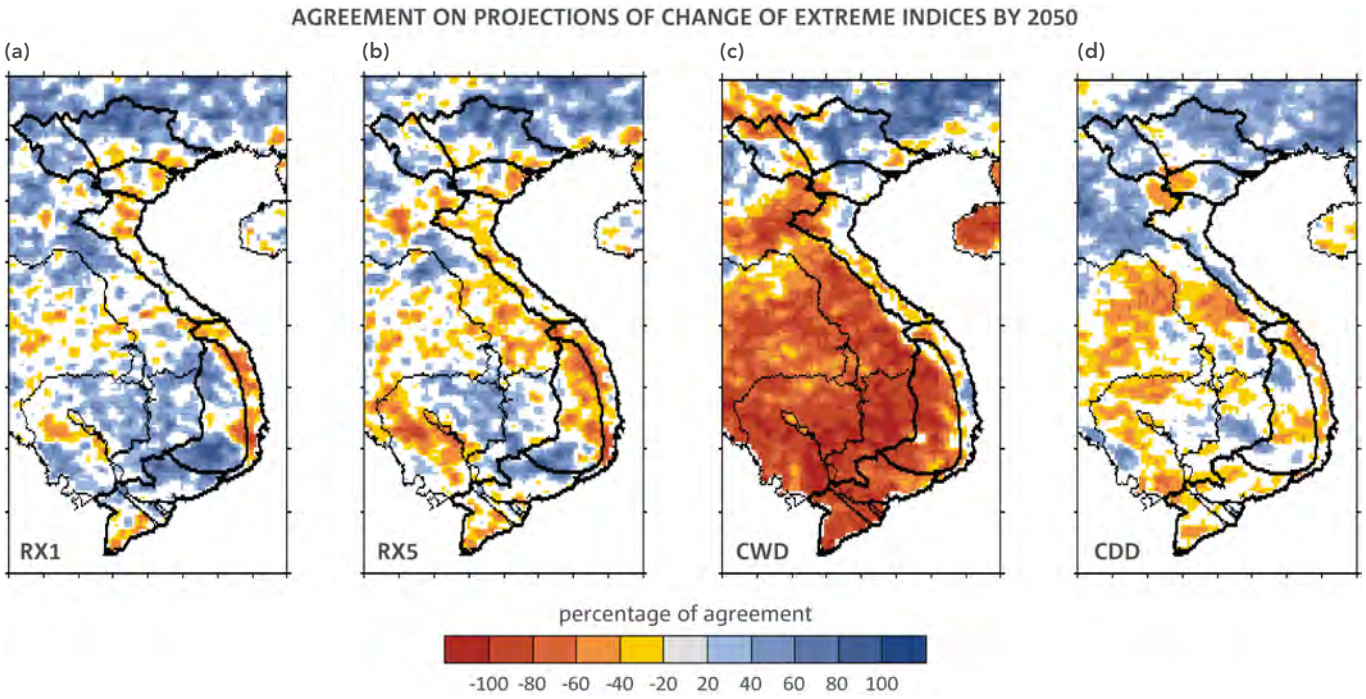

Figure 7-16: Multi-model mean projected changes of extreme indices by end of the century (2079-2100) from 10 km CCAM simulations for RCP 8.5. RX1 (a) and RX5 (b) are shown as changes in mm day^{-1}, while CWD (c) and CDD (d) are shown as number of days. All changes are relative to the baseline period (1980-2000).

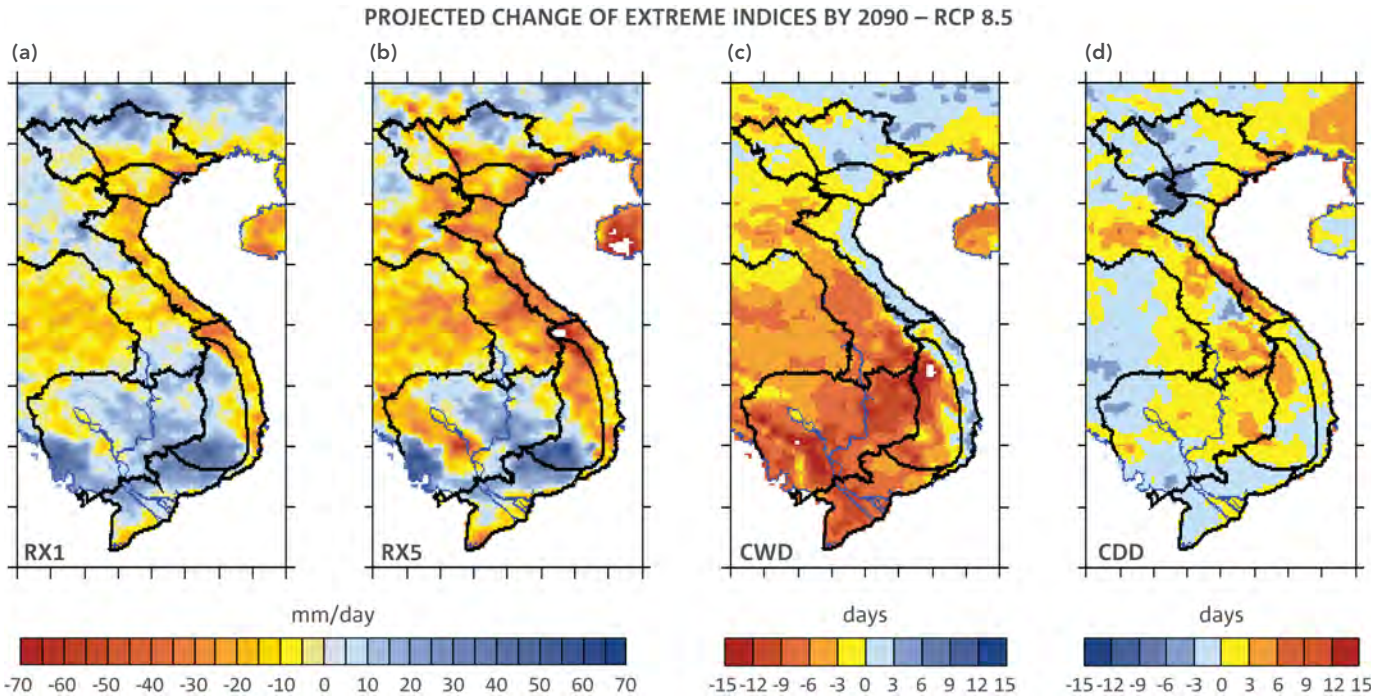

Figure 7-17: Percentage of agreement on the direction of change (increase positive)/(decrease negative) of RX1 (a), RX5 (b), CWD (c) and CDD (d) among the 10 km CCAM simulations for the period 2080-2100 compared with the baseline period 1980-2000. The results were interpolated to 30 km resolution.

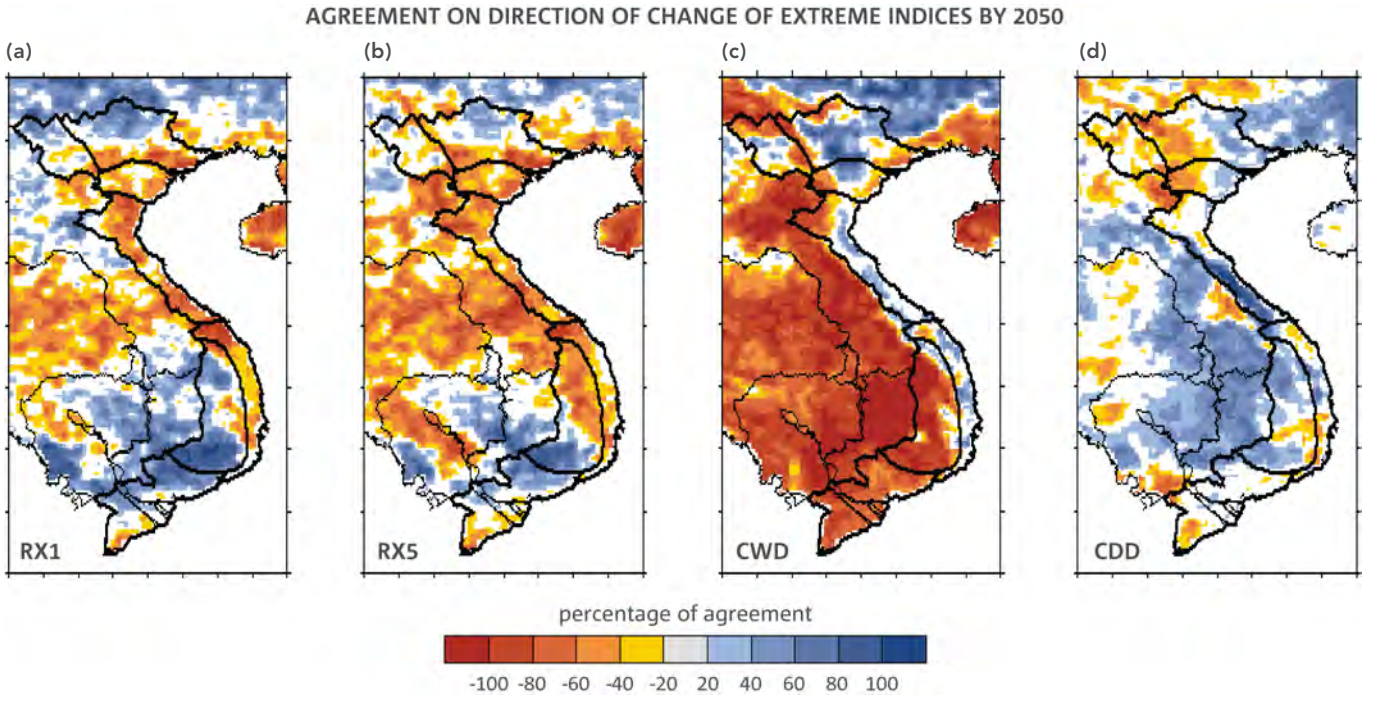

7.2.5 Summary

Spatial and temporal characteristics of extreme rainfall over Vietnam are studied using a set of standard extreme indices: RX1, RX5, CWD and CDD. Present-day 10 km CCAM ensemble-modelled results are compared with observed trends. Finally, the projected changes are presented.

The observed gridded rainfall (from APHRODITE, for the period 1979-2007) shows that the largest one-day (RX1) and five-day (RX5) maximum rainfall events occur along the east coast of Vietnam, with amounts of around 100 to 200 mm day^{-1} for RX1 and up to 500 mm day^{-1} for RX5. The longest duration of wet days (CWD) ranges between 10 and 30 days, spread fairly evenly over the entire country. On the other hand, the longest duration of dry days (CDD) ranges between 50 and 60 days, and is found over South Vietnam, particularly in the Mekong Delta region. A comparison between observed and modelled spatial patterns of RX1, RX5, CWD and CDD indices over Vietnam shows that the model captures the observed characteristics of these indices fairly well, except over southern Vietnam where CCAM significantly overestimates RX1, RX5 and CWD and underestimates CDD. CCAM overestimates the magnitudes of RX5, RX1 and CWD over most parts of Vietnam. In the case of CDD, large values simulated by CCAM over north Vietnam result in positive biases over the north and negative biases over the south portion of the country.

Present-day simulations

Extreme indices simulated by CCAM for the present-day climate for the seven climatic sub-regions are compared with the values derived from the stations.

- CCAM overestimates both the amount and standard deviation of RX1 and RX5, with the largest biases of 225% and 189% for RX1 in the regions of S and CH, respectively. The largest bias (123%) in RX5 is simulated in the region CH. Smaller biases of less than 100% are simulated in regions SC, NC, NE and NW, while ND and NC show biases of less than 30%.
- Compared with observations, CCAM underestimates CDDs for south Vietnam regions, while it overestimates CDDs over north Vietnam regions, with the largest errors in NW (+29 days) and NE (+24 days). CDD shows smaller biases of less than 15 days in other regions, except S.
- CCAM performs well in simulating CWDs over the North Vietnam regions, with the largest bias of 10 days, while the largest biases for regions in the south are around 15 days.
- In terms of variability, CCAM overestimates RX1 for all regions, with the largest bias in the S and NE regions. For RX5, the largest bias is found in the S and CH regions. For CWD and CDD, the largest standard deviation difference (-13 days) is seen in region S, while all other regions exhibit smaller differences.

When comparing model simulations and observations, we can have more confidence in future projected changes if the biases between them are relatively small. However, the direction of change may still provide useful information even if the biases are large. In addition, the spread of projections (as indicated by the ensemble standard deviation of the projected changes) provides additional confidence if it is small.

Mid-century simulations

Projected multi-model mean changes simulated by CCAM for mid-century under RCP 8.5 suggest that:

- RX1 and RX5 are likely to decrease along the east coast and in the southern tip of southern Vietnam (the south side of the Mekong Delta region). RX1 and RX5 are likely to increase in the NE and NW regions located near the border with China. There are also expected to be some increases in the CH region.
- The number of CWDs is projected to decrease between five and 10 days in regions S and CH. However, changes in RX1 and RX5 are insignificant. For other regions, projected changes in CWD are insignificant.
- The number of CDDs is projected to increase by about two days in the NE and NW regions.
- For the NE region, the model suggests that all the four extreme indices, including CDD, will increase in the future.

When the individual CCAM members are investigated, we found that future changes in RX1 and RX5 are not statistically significant. The changes in CWD and CDD are statistically significant at the 95% confidence level in some CCAM members, mainly confined to the southern regions, except for the CDD change in the CCAM MPI-ESM-LR simulation, where a significant decreasing trend covering most parts of Vietnam is evident.

These trends are projected to continue and strengthen by the end of the century.

7.3 HEATWAVES AND HOT DAYS

7.3.1 Introduction

An increase in the frequency of hot days and heatwaves in Vietnam in recent years has affected the population, particularly the older generation, who are more vulnerable to extremes of temperature. Therefore it is considered a serious problem in densely populated regions of Vietnam, where the infrastructure for cooling and health facilities are inadequate to cope with these extreme temperature events. Heat stress has negative impacts on human health and can lead to an increased mortality rate (Muthers *et al.,* 2010). There are several ways to define a heatwave, though most methods use the number of consecutive days above a certain temperature threshold. A widely accepted measure for an index of heatwaves is the Heat-Wave Duration Index (HWDI) defined by Frich *et al.* (2002). HWDI is defined as the maximum number of consecutive days with a maximum temperature (Tmax) at least 5°C above the climatological annual mean Tmax for a reference period (1961-1990) (Frich *et al.,* 2002). It was originally developed for high and mid-latitude regions which have a pronounced annual cycle in temperature. For Vietnam the definition needs to be modified, since it experiences tropical and sub-tropical climates. In particular, no heatwaves can be detected in southern Vietnam using the original definition, because of small seasonal temperature variations in the annual cycle of temperature. Therefore, similar to Perkins *et al.* (2012), we have computed the Tmax threshold using the 95th percentile Tmax for the reference period. The heat stress for hot days is classified as the number of days with Tmax higher than 35°C, the threshold used by the National Centre of Hydro-Meteorological Forecasting, Vietnam.

Future changes in heatwaves are presented through a comparison with present-day model simulations and observations. The climate-change signal is calculated as the difference in mean between the future periods (mid-century, 2045-2065 and end-of-century, 2080-2100 and the current climate period, 1980-2000. The temperature thresholds for the HWDI are calculated for the current climate and applied to the future periods. Future changes in the HWDI index are also shown as differences in their means at mid- and end-of-century and the current climate.

7.3.2 Observed HWDI

The Heat Wave Duration Index (HWDI) and the number of hot days are calculated using station data for the current climatic conditions in Vietnam. Available gridded datasets for Tmax, such as the CRU dataset, were constructed with limited station data for Vietnam and are only available as monthly averages. Results for HWDI based on station data are given in Figure 7-18a, which shows that HWDI ranges from 5 to 30, with the largest values in southern regions. The maximum number of consecutive hot days is shown in Figure 7-18b, with the largest values (> 20 days) in central and southern regions.

Figure 7-18: Observed (a) HWDI, and (b) maximum number of consecutive hot days (Tmax > 35°C) based on station data for the period 1980-2000.

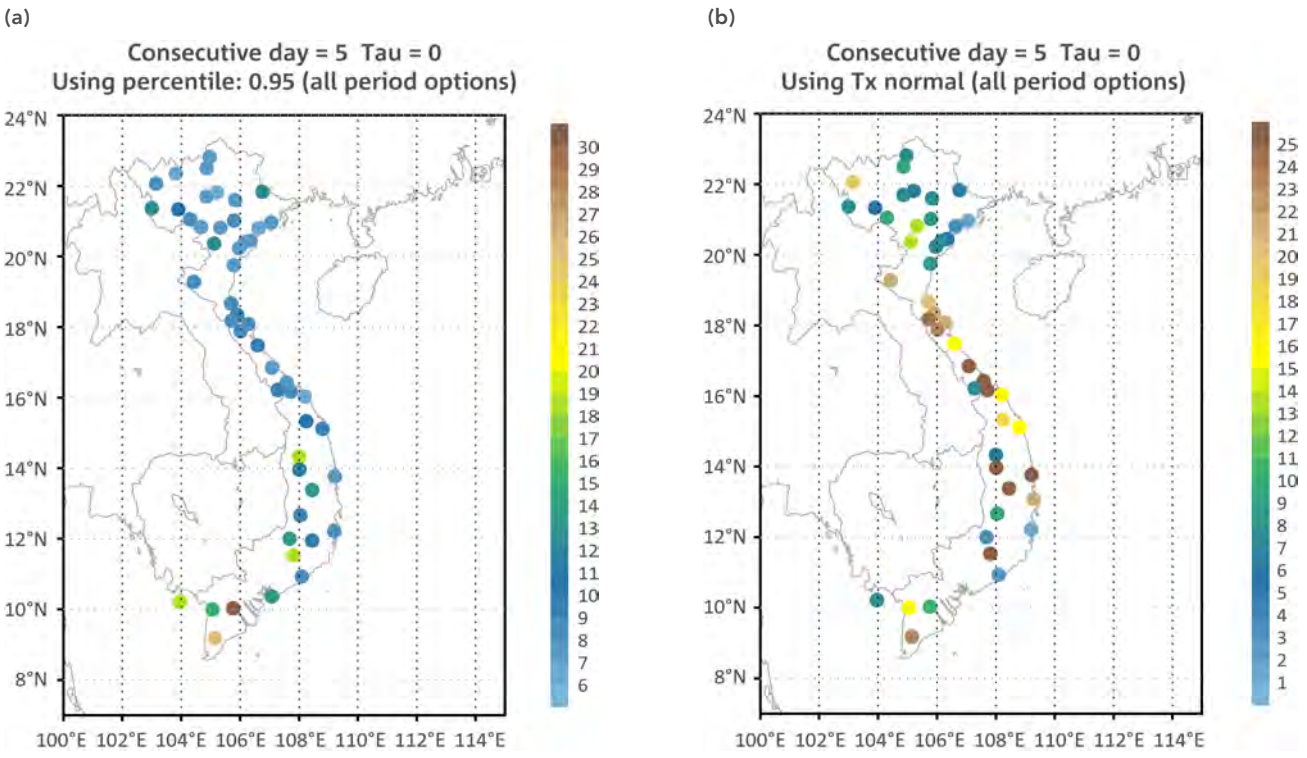

7.3.3 Assessment of model simulations of the current climate

In this section, HWDI from high-resolution CCAM and RegCM4.2 simulations are compared with those from observations to assess how well the models capture these features for the current climate. Only station data are used to validate the model-simulated HWDI and hot days. This is because gridded datasets, such as the CRU dataset, were constructed using data from only a few stations in Vietnam and, more importantly, they are available on a monthly basis but not on a daily basis. Therefore, RCM results are interpolated to the station locations and then compared with observations.

Before analysis of the indices, Tmax needs to be evaluated. Results are based on a comparison against observations of ERA-Interim-forced CCAM and RegCM4.2 simulations, with Tmax given for the whole of Vietnam as in Section 5.4.1. These results suggest that the annual average Tmax is underestimated by -4°C for the 10 km CCAM simulation and by -5.4°C for RegCM4.2 (see Table 5-4). The biases and mean absolute error relative to station observations for the CCAM 10 km simulation forced with ERA-Interim are presented in Figure 7-19.
The biases (Figure 7-19a) show an underestimation of up to -3°C for stations south of 16°N and an overestimation by up to +4°C north of 16°N. The mean absolute error (Figure 7-19b) shows larger errors in northern Vietnam, indicating both positive and negative biases over time, while in southern Vietnam, the mean absolute errors are similar in magnitude to the biases, indicating mainly negative biases over time. It is evident from Figure 7-19 that the underestimation of Tmax by RCMs will have a strong impact on the spatial pattern of the hot days (where the threshold is set to be 35°C), with negative biases over southern Vietnam and positive biases over northern Vietnam (not shown).

7.3.4 Future changes in heatwaves and hot days

Heatwaves

The changes in the number of heatwaves per year and the average duration of heatwaves based on the HWDI for mid-century and the end of the century based upon the high-resolution CCAM and RegCM4.2 simulations are presented in Figure 7-20. The results differ notably in the magnitude of change between mid-century and the end of the century. For mid-century, the models tend to project an increase in the number of heatwaves for most parts of Vietnam, except for the north-west, where no change is projected. The largest increase in heatwaves, with a range of between 3 and 6 events, can be found in South Vietnam and parts of the Central Highlands and South Central Vietnam. Furthermore, the results do not vary significantly among different model simulations. The ensemble standard deviation, a measure of variability, is always less than the projected mean change. This indicates that the changes are robust. However, heatwave duration does show variations between the simulations, with variations in magnitude being larger than the projected mean changes. However, they all agree on an increase in future duration.

Figure 7-19: Tmax biases (a) and mean absolute error (b) for CCAM 10 km simulation forced by ERA-Interim reanalyses compared with observations for the period 1980-2000 (°C).

(a)

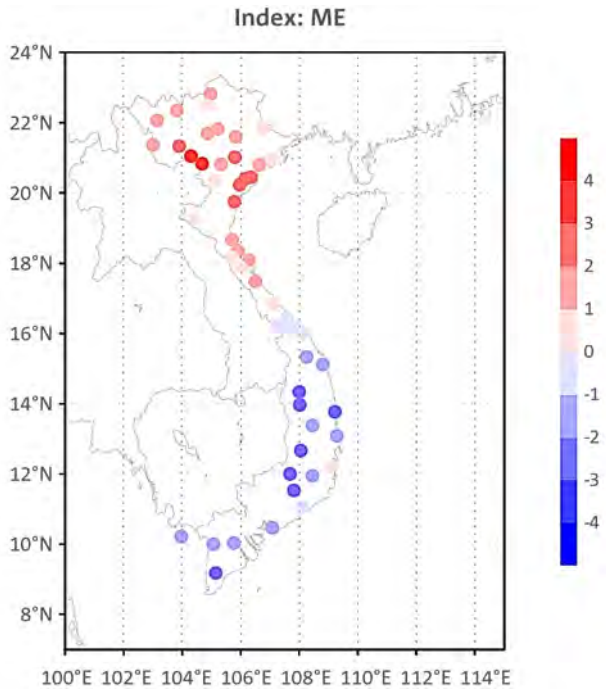

(b)

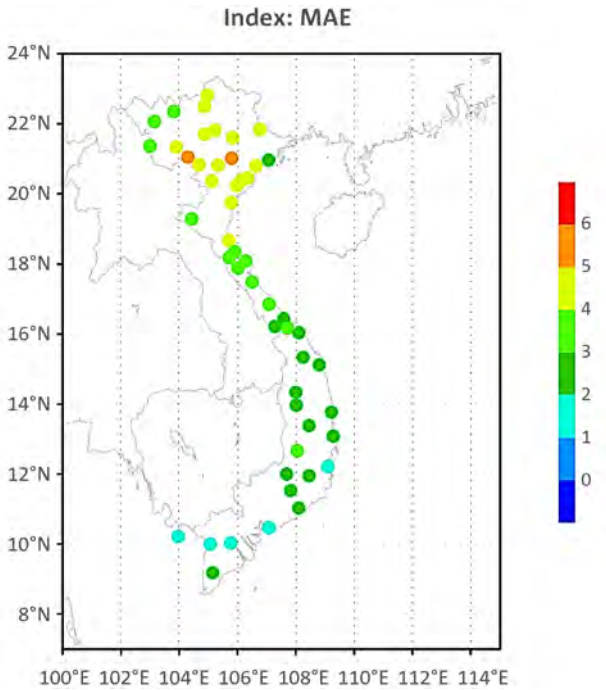

By the end of the century, the number of heatwaves is projected to change significantly in South Vietnam and in the southern Central Highlands. In these regions, the annual average number of heatwaves is projected to increase by between 6 and 10 events. For the rest of Vietnam, increases range between 2 and 5 events. Again, the variations among the simulations are smaller than the mean changes. Therefore an increase in heatwaves is likely, based on the model results. Nevertheless, in the northern parts of South Vietnam and the southern parts of the Central Highlands, the simulations show some differences in the magnitude of changes, which are shown by large ensemble standard deviations in Figure 7-21. The average duration increases between 7 and 15 days in South and south central Vietnam. For the rest of Vietnam, increases are on the order of 2 to 7 days. The regions with the strongest variations among the simulations are coastal areas in South and south central Vietnam, as well as the areas in both regions which showed a large ensemble standard deviation in the number of heatwaves.

Figure 7-20: Changes in the number of heatwaves (a-b, in events) and their average duration (c-d, in days) for 2045-2065 (a,c) and 2080-2100 (b,d) based on the HWDI from the ensemble of CCAM projections at 10 km and RegCM4.2 projections at 20 km for RCP 8.5. Changes are relative to the baseline period 1980-2000.

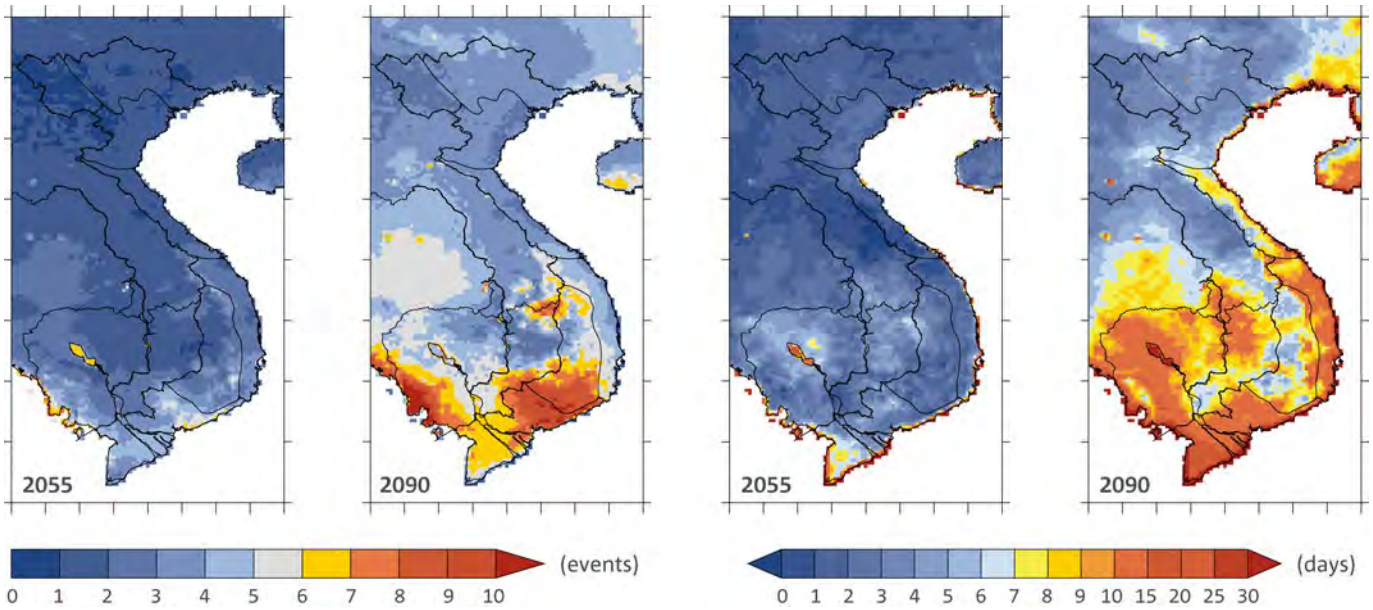

Figure 7-21: Multi-model ensemble standard deviation of the number of heatwaves (events) derived from the HWDI index for 2045-2065 (a) and for 2080-2100 (b) and their average duration (days) for 2045-2065 (c) and for 2080-2100 (d) for RCP 8.5. Based on CCAM simulations at 10 km resolution and RegCM4.2 at 20 km resolution. Changes are relative to the baseline period 1980-2000.

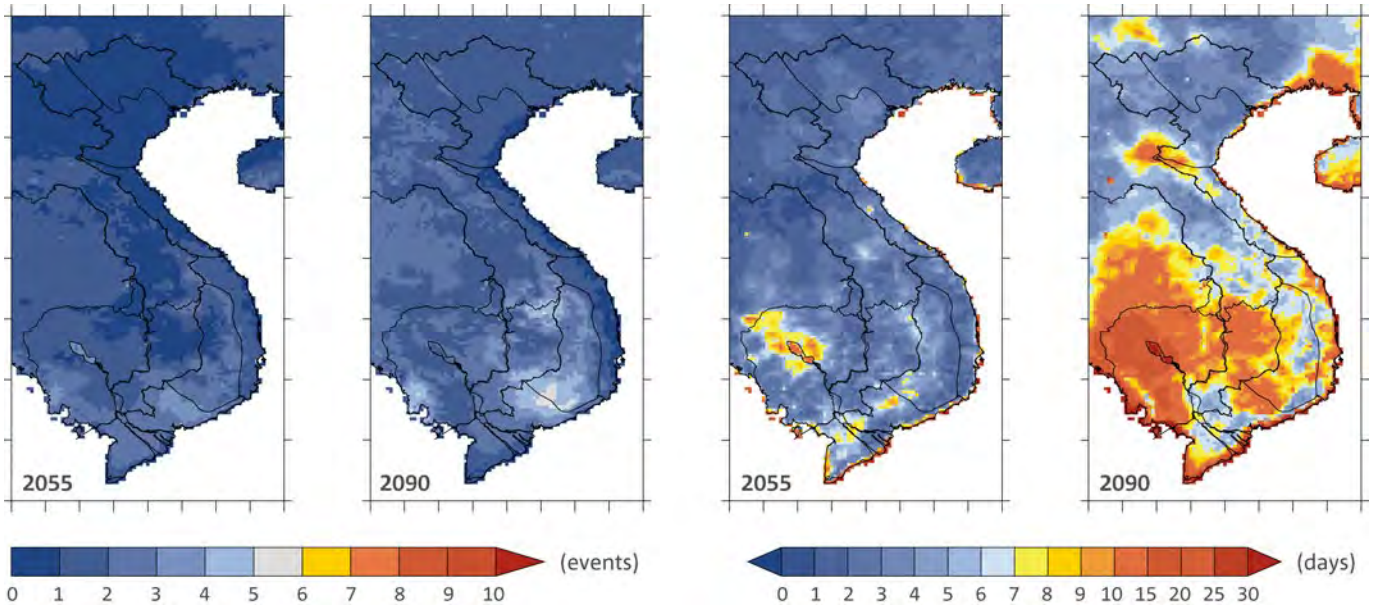

Hot days

Figure 7-22 shows the change in the number of hot days for the multi-model ensemble mean for mid-century (2045-2065) and the end of the century (2080-2100) for RCP 8.5. The ensemble was composed of six CCAM simulations at 10 km resolution and two RegCM4.2 simulations at 20 km resolution. Most parts of northern Vietnam and low-lying areas of central Vietnam show an increase in the number of hot days of between 30 and 45 days per year, whereas a smaller increase of between 15 and 25 days is projected for South Vietnam for mid-century. Model-to-model variability (shown by the standard deviation) is quite large, especially in South Vietnam, because the CCAM projections show only small changes, while RegCM4.2 shows large changes for this region. This might be due to the different model biases in Tmax for this region. In particular, CCAM underestimates Tmax for the current climate by up to 2-3°C. Even with an increase in Tmax, the threshold of 35°C is only exceeded a few times in CCAM simulations during the mid-century period. Nevertheless, all models agree that the number of hot days will increase in the future.

Increases in the number of hot days by the end of the century are quite large, rising by 60 to 95 days per year throughout the low-lying areas of Vietnam. Even in the mountain regions in central and southern Vietnam, increases can be detected. Although these regions did not show days with temperatures in excess of 35°C in the current climate, they show a slight increase in the future. Such an increase in the mountain peaks occurs in RegCM4.2 simulations, probably due to the different representation of the orography in those models. Because of the finer horizontal resolution of CCAM (10 km compared with 20 km for RegCM4.2) the CCAM elevation is higher and the simulated temperature is lower. Model-to-model variations (multi-model standard deviation) show that the models produce similar changes in northern and central Vietnam.

The changes in southern Vietnam vary strongly between the models, but the standard deviation is still smaller than the projected increase.

7.3.5 Summary

Projected changes in the frequency of occurrence and duration of heatwaves, which are defined as consecutive days with extreme temperatures, are investigated using a modified heat wave duration index (HWDI). The threshold of the modified index is the 95th percentile value of the distribution. As a result of the increase in maximum temperatures, general increases in the number and the duration of heatwaves are projected for most parts of Vietnam, except for north-west Vietnam, which shows no changes by mid-century. For the rest of Vietnam, the increase ranges between +1 heatwave per year in the north up to +6 heatwaves per year in South Vietnam for the same time period. This north-south difference in the projected change signal becomes more pronounced by the end of the century. In South Vietnam, the average number of heatwaves per year increases by between 6 and 10 events and at the same time the average duration increases by between +9 and +15 days. However in North Vietnam, the increases in occurrence range between 2 and 4 heatwaves per year, and in duration between 3 and 7 days. Except for some parts of central and South Vietnam the changes in heatwaves are consistent among the different model projections.

In addition to heatwaves, the number of hot days, which are defined for Vietnam as days with a maximum temperature of more than 35°C, is analysed as well. All models show an increase in hot days in the low-lying areas of Vietnam. Due to the high elevation, temperatures above 35°C are never or only rarely reached in the mountains, even at the end of the century. The increase for mid-century ranges between 15 and 25 days per year in South Vietnam, and between 30 and 35 days

Figure 7-22: Changes in the number of hot days for 2045-2065 (a) and 2080-2100 (b) for RCP 8.5. Values are multi-model mean changes from the CCAM and RegCM4.2 ensembles. Also shown are multi-model ensemble standard deviations (days year^{-1}) for 2045-2065 (c) and for 2080-2100 (d). Changes are relative to the baseline period 1980-2000.

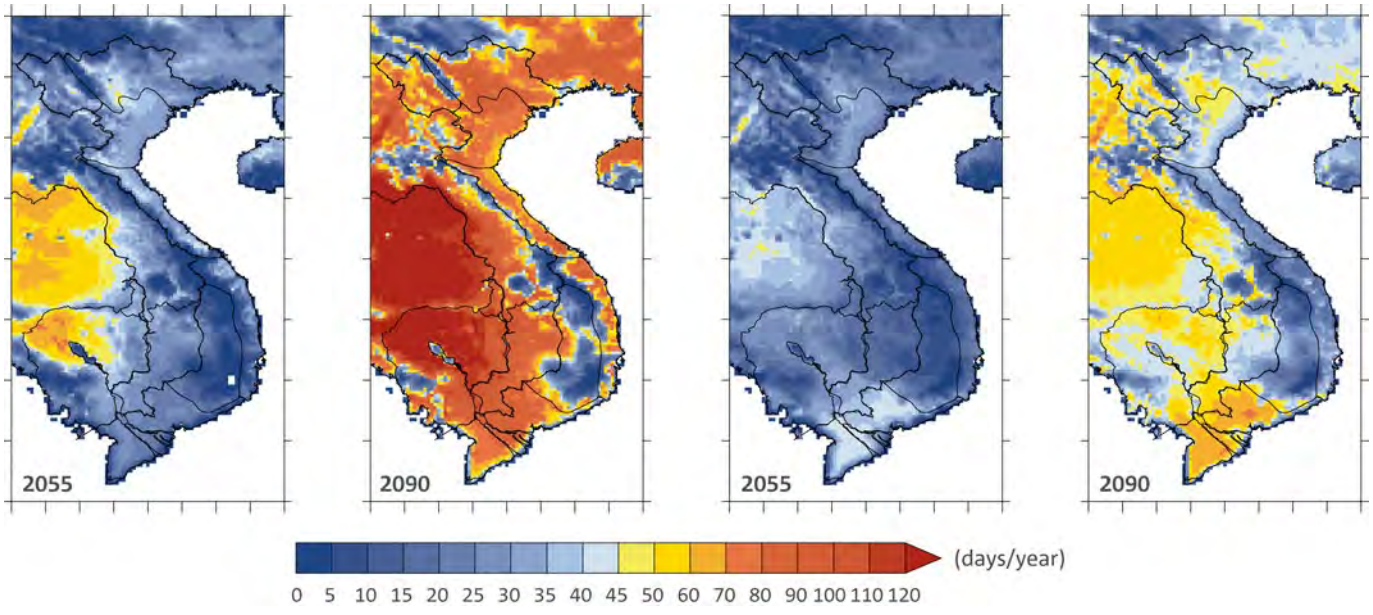

per year in North Vietnam. By the end of the century, the number of hot days is projected to increase between 60 and 95 days per year throughout the low-lying areas of Vietnam. For this period, projected values for South Vietnam depend on which RCM is used for the simulation. Both HWDI and hot day indices do not take into account the other variables such as relative humidity and radiation that contribute to human heat stress. Further investigations are necessary to incorporate other variables, such as relative humidity, solar radiation and wind speed, to fully understand heat stress and human comfort in this region.

7.4 DROUGHTS

7.4.1 Introduction

Another important climatic hazard in Vietnam is drought that affects the agricultural sector, which largely depends on rainfall and plays an important role in Vietnam's economy. An extended period of rainfall deficits can lead to reduced harvests, or even lead to complete failure of crops; it also contributes to lowering of the groundwater table. Similar to heatwaves, there is no universally accepted definition of droughts. The scientific literature classifies the term 'drought' into meteorological, hydrological, agricultural, and socio-economical droughts. Agricultural and hydrological droughts, which affect the agricultural sector and groundwater levels, are probably the most important types in Vietnam. A widely-used drought index called the Standardized Precipitation Index (SPI) developed by McKee *et al.* (1993) covers both agricultural and hydrological droughts. The advantages of the SPI include its simplicity, because it is based on just one variable (rainfall), it is applicable to different locations and seasons, and it has the ability to detect different types of droughts at different temporal scales. Based on the SPI, the changes in the number and duration of severe and extreme agricultural and hydrological droughts are investigated.

Future changes in drought indices are presented through a comparison with present-day model simulations and observations. The climate-change signal is calculated as the difference in the mean for the future periods (mid-century, 2045-2065 and end-of-century, 2080-2100) and the current climate period, 1980-2000. The transformation functions for the SPI are calculated for the current climate and applied to the future periods. Future changes in SPI indices are also shown as differences in their means between mid- and end-of-century and the current climate.

7.4.2 SPI and drought computation

The SPI is based on rainfall data and can be developed by transforming the monthly time series into a normal distribution (Lloyd-Hughes and Saunders, 2002). First, an appropriate probability distribution function (usually the Gamma distribution) is fitted using the rainfall data from a reference period, which should be at least 30 years. The SPI can be calculated for different time scales by averaging the rainfall time series over a different number of months before fitting a distribution function. Depending on this time scale, the SPI can be used for different types of droughts (see Bussay *et al.*, 1998; Szalai and Szinell, 2000). The two types of drought considered in this study are:

- **Agricultural droughts** (time scale of 2-3 months)
- **Hydrological droughts** (time scale of 12-14 months).

The probability distribution function of the SPI is then transformed into a normal distribution with a mean of zero and a standard deviation of 1. The drought classification based on the SPI can be found in Table 7-4. It ranges from extreme drought conditions for an SPI less than -2.0 to extreme wet conditions for an SPI of 2.0 or greater. The values of the SPI are interpreted as the deviation from the climatological mean in units of standard deviation. Consequently, the probability for an SPI of less than -1 is 15.9% and for an SPI of greater than -2 is 2.3%.

Table 7-4: Drought classification based on the standardized precipitation index (SPI). Note only extreme and severe droughts (bold) are considered here.

SPI VALUE	CATEGORY
2 or more	Extremely wet
1.5 to 1.99	Severely wet
1 to 1.49	Moderately wet
0 to 0.99	Mildly wet
0 to -0.99	Mild drought
-1 to -1.49	Moderate drought
-1.5 to -1.99	**Severe drought**
-2 or less	**Extreme drought**

The 3-month and 12-month SPI values are calculated according to Wu *et al.* (2007) using the Gamma distribution and adjusting it by the number of months without rainfall to take into account the dry seasons. Thereafter, the intensity of a drought is defined by the minimum of the SPI between two zero crossings. Consequently, the duration of the drought is defined as the number of months between the zero crossings. Only droughts with duration longer than two months are considered for the computation of the number of events.

The number of droughts and their duration are calculated using APHRODITE data from 1979 to 2007 and the results are shown in Figure 7-23. Agricultural droughts occurred between 5 and 15 times during the 29 year period and had an average duration of 5-15 months in Vietnam. In South Vietnam the number of droughts is less than in North Vietnam, but they lasted longer on average. The frequency of hydrological droughts (ranging from 1 to 10 events) is generally less compared with agricultural droughts, but their duration is longer (average duration ranges from 11 to 38 months). Similar to the agricultural droughts, hydrological droughts are less frequent in the South region than in other regions, but their duration is longer.

Figure 7-23: Number (a, b) and average duration (c, d, in months) of extreme and severe agricultural droughts (a, c) and hydrological droughts (b, d) based on APHRODITE rainfall from 1979 to 2007.

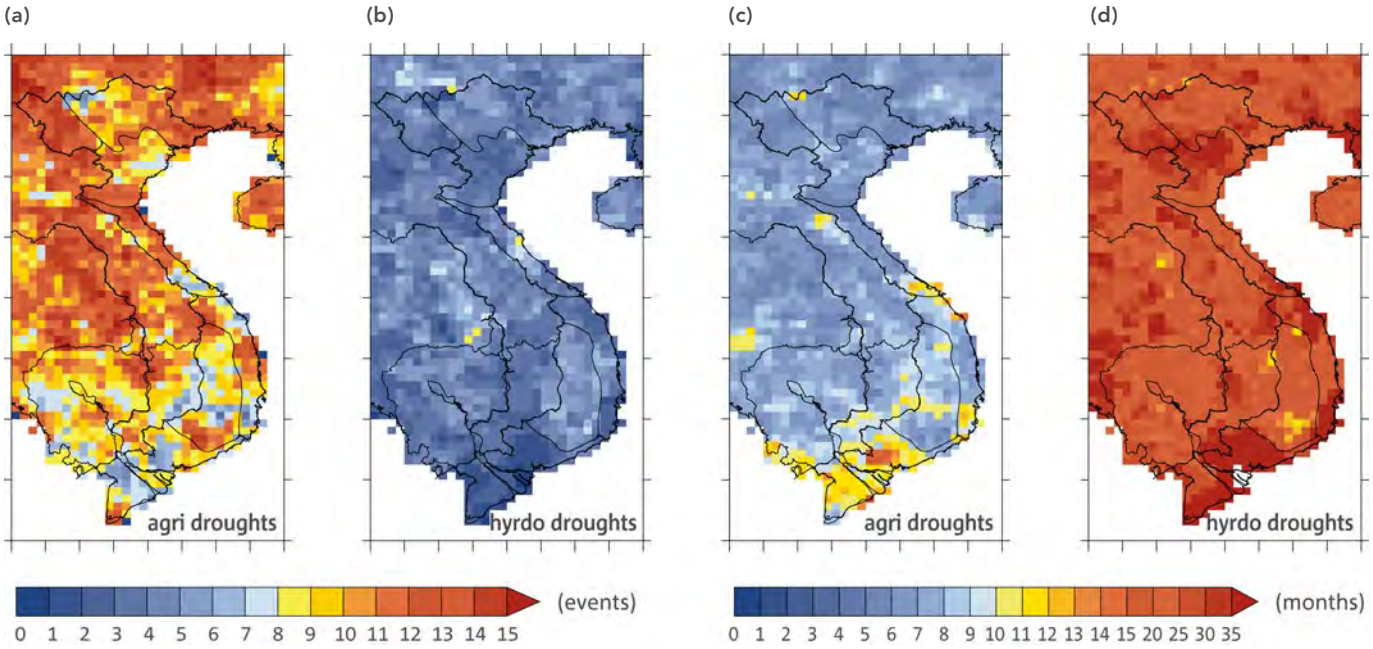

Figure 7-24: Observed trends (year^{-1}) for 3-month SPI (left) and 12-month SPI (right) based on APHRODITE for the period 1979-2007. Note that a positive (negative) trend in SPI is associated with wet (drought) conditions. Note that results have been interpolated to the 25 km APHRODITE grid.

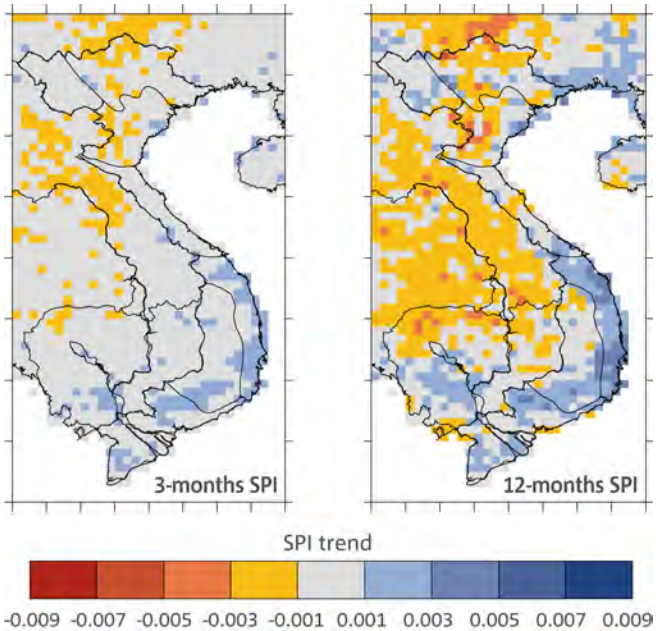

Trends in SPI values are calculated for the period 1979-2007 using APHRODITE data and the results are shown in Figure 7-24. Southern Vietnam has experienced wet conditions since 1979 that led to a decreasing trend in droughts, while some parts of northern Vietnam experienced rainfall deficiencies that resulted in an increasing trend in drought conditions. When comparing trends in both 3-month and 12-month SPIs, there are small differences in the magnitude, but the spatial patterns are very similar.

Figure 7-25 shows the linear trends of modelled 3-month and 12-month SPI based on CCAM simulations forced by ERA-Interim for the period 1979-2007. The general spatial pattern of observed trends in Figure 7-23, with increasing wet conditions in southern Vietnam and increasing drought conditions for parts of northern and central Vietnam, is reproduced. However, the magnitude of the trends is much weaker and also the area of increases in drought conditions in the north is relatively large compared with observations. Although the trends are calculated using a short period of data and weak forcing from the reanalyses dataset, CCAM performs fairly well over Vietnam due to the downscaling procedure (see Section 2.6.1).

Figure 7-25: Observed trends for 3-month SPI (left) and 12-month SPI (right), based on CCAM ERA-Interim results at 10 km resolution for 1979-2007. Note that results have been interpolated to the 25 km APHRODITE grid.

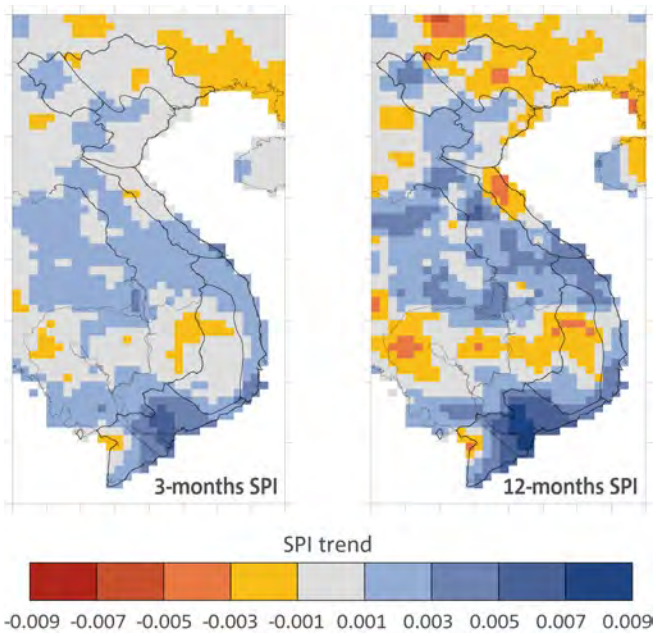

The spatial patterns of SPI calculated using CCAM-simulated rainfall are compared with the APHRODITE dataset. For this purpose, CCAM results are interpolated onto the observed 0.25° longitude by 0.25° latitude (about 25 km) resolution grid before the calculation of the SPI. It is not feasible to compare the absolute SPI values because they are by definition close to zero for the period that is used for the computation of the SPI. Therefore the observed and modelled trends are analysed, as well as the number and duration of severe and extreme drought events.

The CCAM-simulated number and duration of extreme and severe droughts based on the 3-month and 12-month SPI for the period 1979 to 2007 are shown in Figure 7-26 a and b. The range in the frequency of both 3- and 12-month droughts is very close to the observed ranges shown in Figure 7-23. However, there are differences between the observed and simulated spatial patterns of drought frequencies, as shown in Figure 7-26 a and b. In particular, CCAM simulates fewer agricultural droughts in central Vietnam and more in southern Vietnam. However, the observed large number of agricultural droughts in northern Vietnam and in the Central Highlands is reproduced by the model. The simulated duration of both 3-month and 12-month drought types does not show much variation throughout Vietnam, which is opposite to observed (Figure 7-23). However, simulated magnitudes of duration are very similar to observed magnitudes. From these analyses, it is evident that CCAM simulates realistic values of magnitudes of droughts, but a less distinct spatial pattern in drought frequency and duration, which can be partially attributed to using only large-scale forcing from ERA-Interim. Next, the 10 km CCAM simulations are analysed to investigate future changes in the intensity and duration of droughts using the SPI.

Figure 7-26: Number of 3-month (a) and 12-month (b) drought events, and average 3-month (c) and 12-month (d) drought duration based on the CCAM 10 km simulation forced by the ERA-Interim reanalysis from 1979 to 2007. Note that results have been interpolated to the 25 km APHRODITE grid.

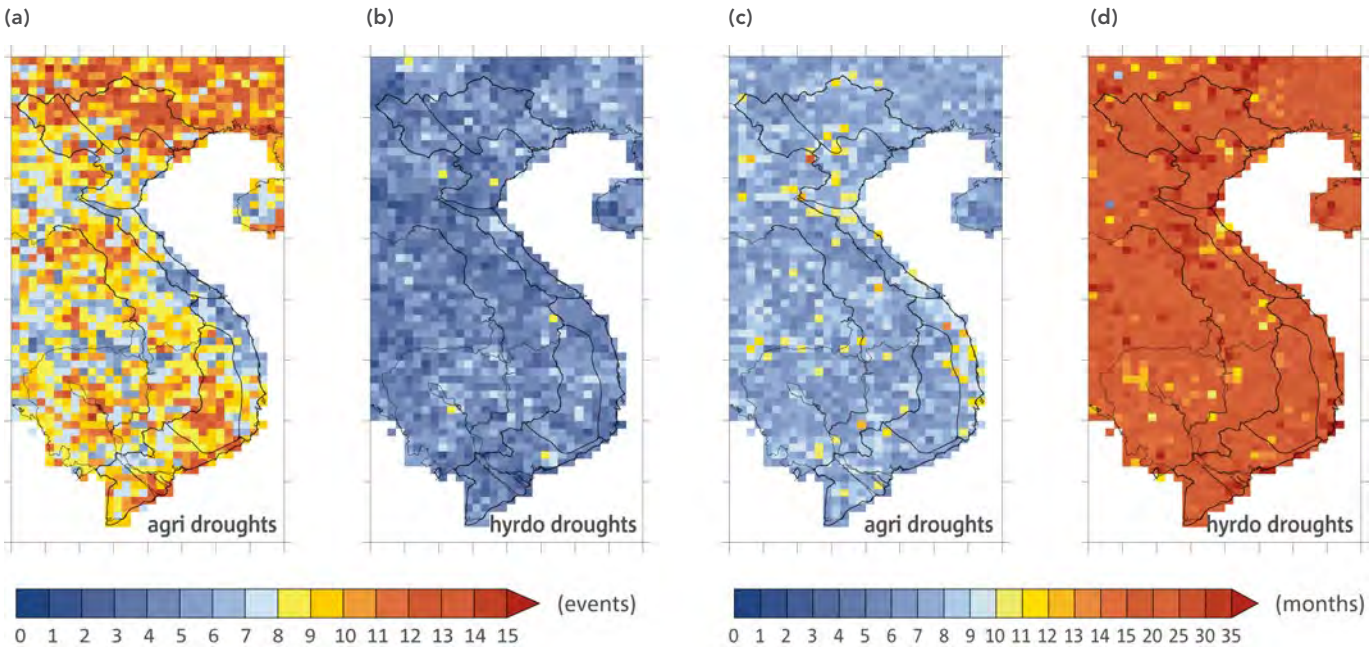

7.4.3 Future changes in droughts

Agricultural droughts

Figure 7-27 shows changes in the number of extreme and severe drought events and their duration, based on the 3-month SPI computed from the 10 km CCAM ensemble projections. Decreases in the number of droughts are projected for most parts of Vietnam for mid-century. Only in the Central Highlands and in north-east Vietnam is a slight increase of about 1 to 3 events projected. Such a projected pattern is similar to the observed trend pattern in the SPI shown in Figure 7-25. Projected changes in drought duration are small except for the northern parts of North Central Vietnam and the southern parts of South Central Vietnam, which exhibit an increase of up to 3 months (i.e. droughts that based upon the 3-month criteria are projected to last 3 months longer). In these areas the standard deviation among the different simulations has a similar magnitude compared with the change signal in Figure 7-28, which indicates that these changes are not robust. In addition, not all CCAM simulations agree on the sign of the change (Figure 7-29).

The projected changes in the number of drought events indicate a decrease by the end of the century for the majority of northern Vietnam (-5 to -8 events), parts of central Vietnam (-3 to -6 events) and southern Vietnam (-2 to -3 events; Figure 7-27). Only the mountain regions of North Central Vietnam and the coastal regions in South Central Vietnam show a considerable increase in the number of drought events (2 to 7 events). These increases, as well as the decreases in northern Vietnam, seem to be a robust change because of the small ensemble standard deviation in these regions, as shown in Figure 7-28. In addition, all models agree on the sign of the change, as depicted in Figure 7-29. The pattern of changes in drought duration by the end of the century is similar to the changes by mid-century, except the magnitude is slightly larger (up to 5 months) and the coastal regions in northern Vietnam show increases as well. Although variations among the different projections are large, they all agree on an increase in the duration of droughts in the future (Figure 7-29). However, there is large uncertainty associated with the magnitude of the change.

Figure 7-27: Projected changes in the number of extreme agricultural droughts for 2045-2065 (a) and severe agricultural droughts for 2080-2100 (b), both in events per period, and their average duration in months for 2045-2065 (c) and for 2080-2100 (d) based on the 3-month SPI values calculated using CCAM ensemble simulations at 10 km resolution for RCP 8.5.

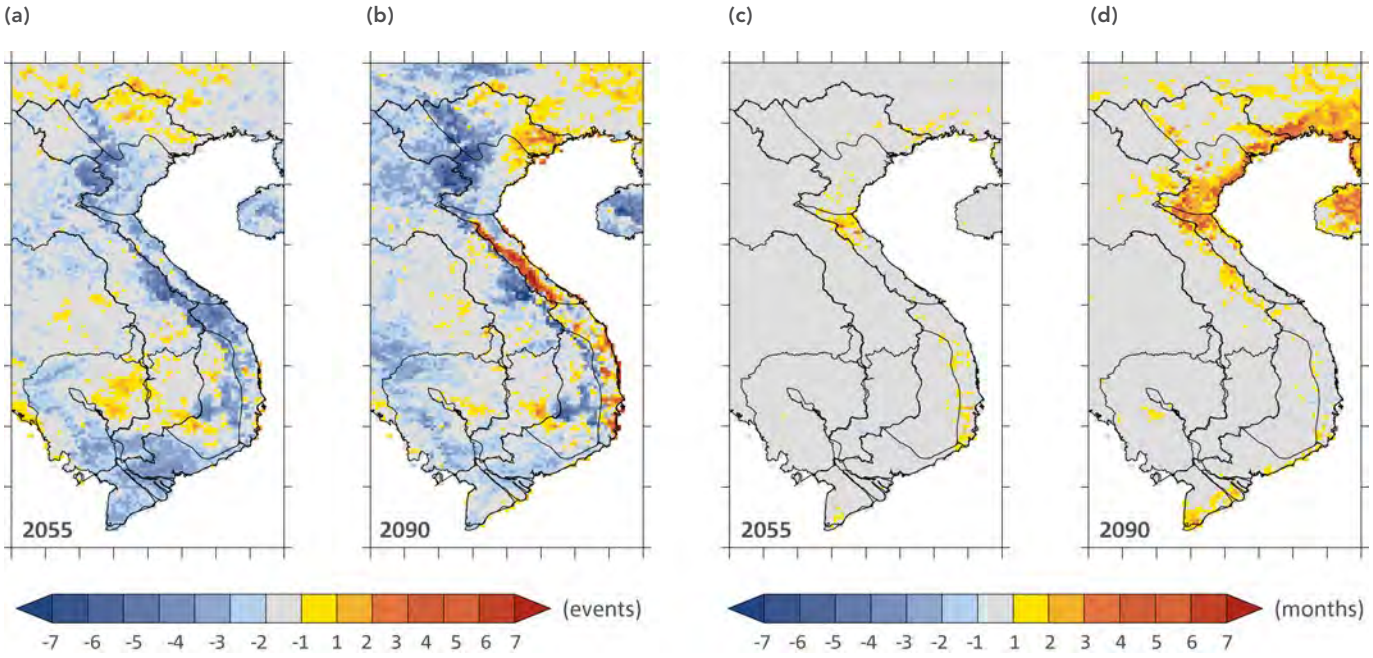

Figure 7-28: Ensemble standard deviations of the number of extreme agricultural droughts for 2045-2065 (a) and severe agricultural droughts for 2080-2100 (b) and their average duration in months for 2045-2065 (c) and for 2080-2100 (d) based on the 3-month SPI values calculated using CCAM ensemble simulations at 10 km resolution for RCP 8.5.

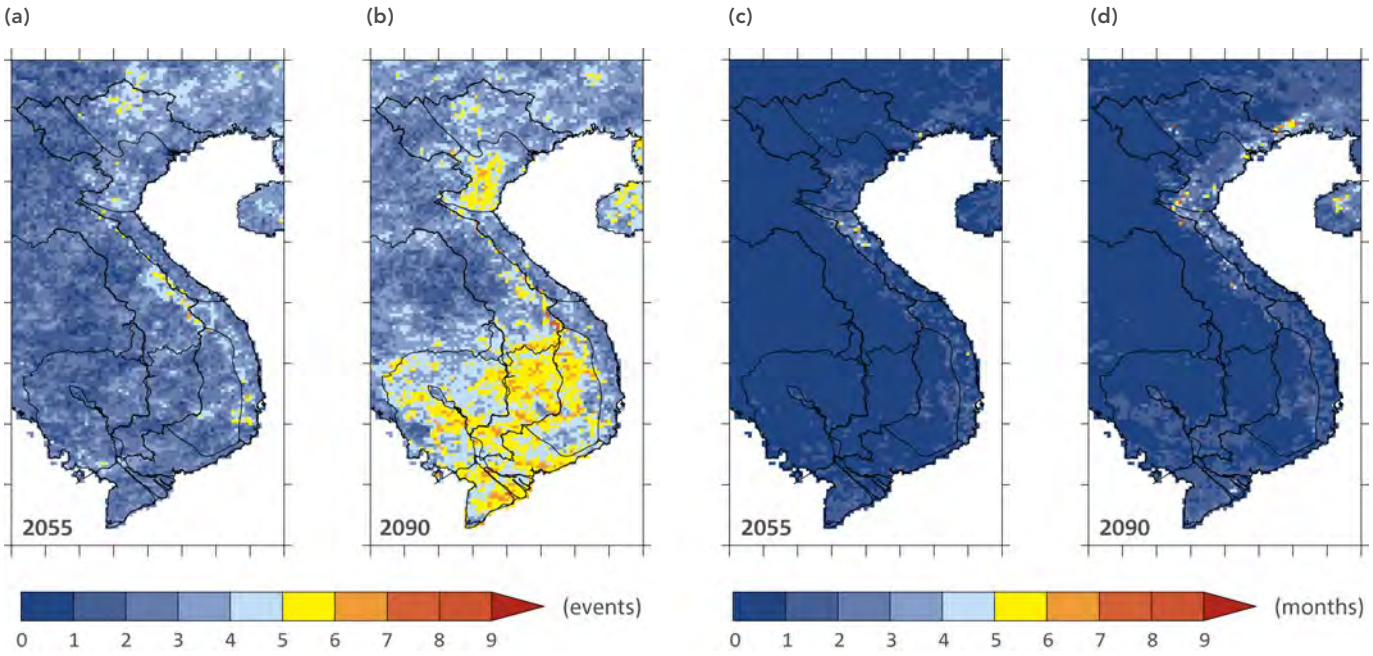

Figure 7-29: Agreement on the increase in the number of extreme agricultural droughts for 2045-2065 (a) and severe agricultural droughts for 2080-2100 (b) and their average duration for 2045-2065 (c) and for 2080-2100 (d) in percent based on the 3-month SPI values calculated using CCAM ensemble simulations at 10 km resolution for RCP 8.5.

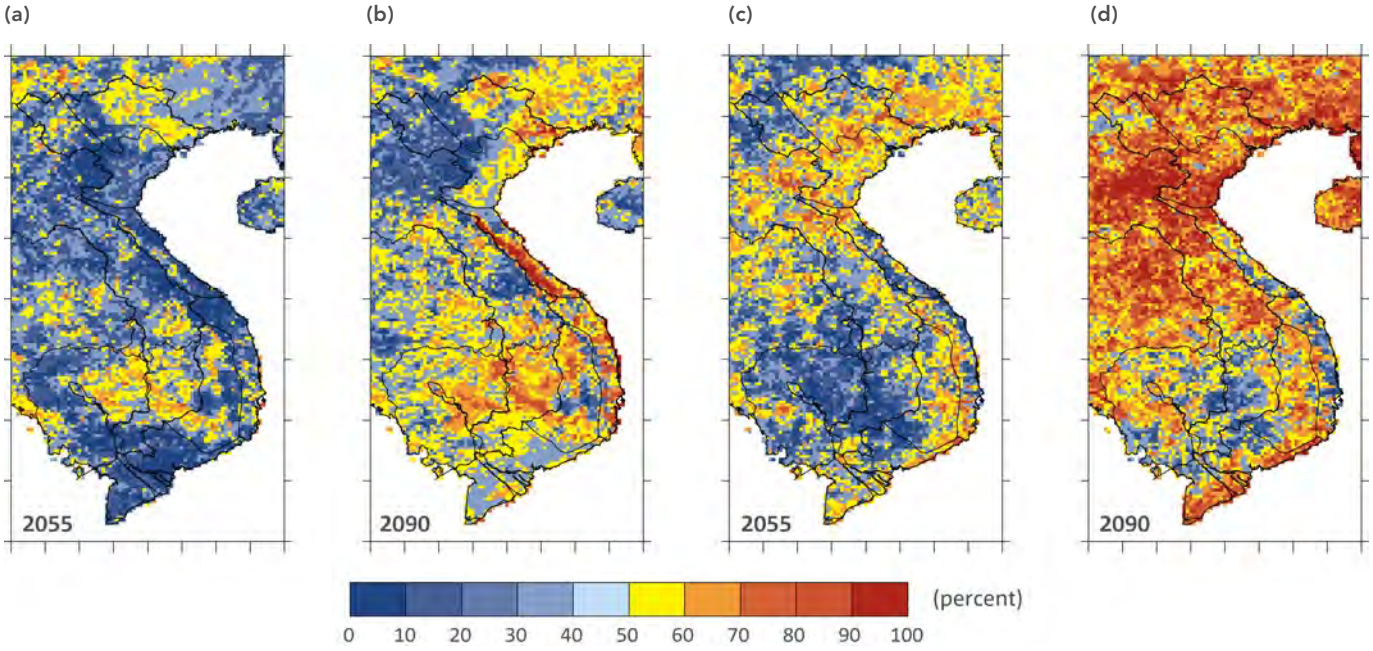

Hydrological droughts

Changes in the number and duration of severe and extreme droughts based on the 12-month SPI values, which can be related to hydrological droughts, are shown in Figure 7-30. By mid-century, many parts of Vietnam show a slight increase in the number and an increased duration of hydrological droughts, especially when compared with the changes based on the 3-month SPI values shown previously. The increase in the number of events is largest (up to +3) in northern Vietnam and in the northern parts of the Central Highlands. The largest increases in duration are projected for South Vietnam (+7-14 months) and the North Delta region (+5-12 months). On the other hand, the number of hydrological drought conditions shows some decrease in most parts of North and South Central Vietnam. From Figure 7-31 (spread, as measured by the standard deviation of the ensemble members) and Figure 7-32 (agreement on sign-of-change), it is evident that the results differ greatly among the different simulations and that only a few grid points agree on the sign of projected change.

The projected end of the century changes in the number of hydrological droughts are more robust (Figure 7-30b) than at mid-century. The number of droughts (frequency) increases by between 1 and 3 events for a 20-year period in the northern regions of Vietnam and in the northern parts of the Central Highlands. In contrast, there is some decrease in the number of droughts in central Vietnam. At the same time, the spread of the projected changes (ensemble standard deviation, Figure 7-31) do not change much compared with the mid-century period, and also most of the simulations agree on an increase in droughts in northern regions and the northern parts of the Central Highlands. However, the simulations do not agree well on the decreases in the number of droughts over North Central Vietnam (Figure 7-32). The duration of severe and extreme hydrological droughts is projected to increase for most of Vietnam. However, only for the North Delta region and for the Mekong Delta do the majority of the simulations agree on this increase.

Figure 7-30: Projected changes in the number of extreme and severe hydrological droughts for 2045-2065 (a) and for 2080-2100 (b) in events per period and their average duration in months for 2045-2065 (c) and for 2080-2100 (d) based on the 12-month SPI values calculated using CCAM ensemble simulations at 10 km resolution for RCP 8.5.

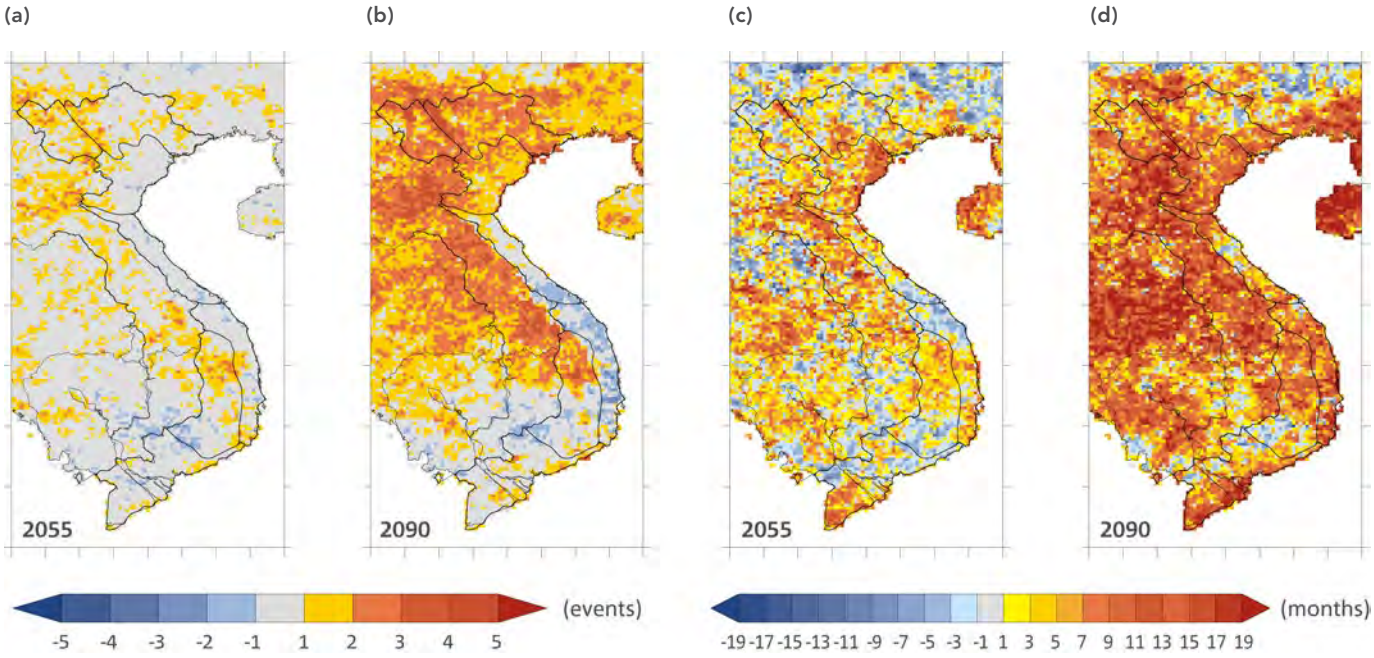

Figure 7-31: Ensemble standard deviations of the number of extreme and severe droughts for 2045-2065 (a) and for 2080-2100 (b) and their average duration in months for 2045-2065 (c) and for 2080-2100 (d) based on the 12-month SPI values calculated using CCAM-ensemble simulations at 10 km resolution for RCP 8.5.

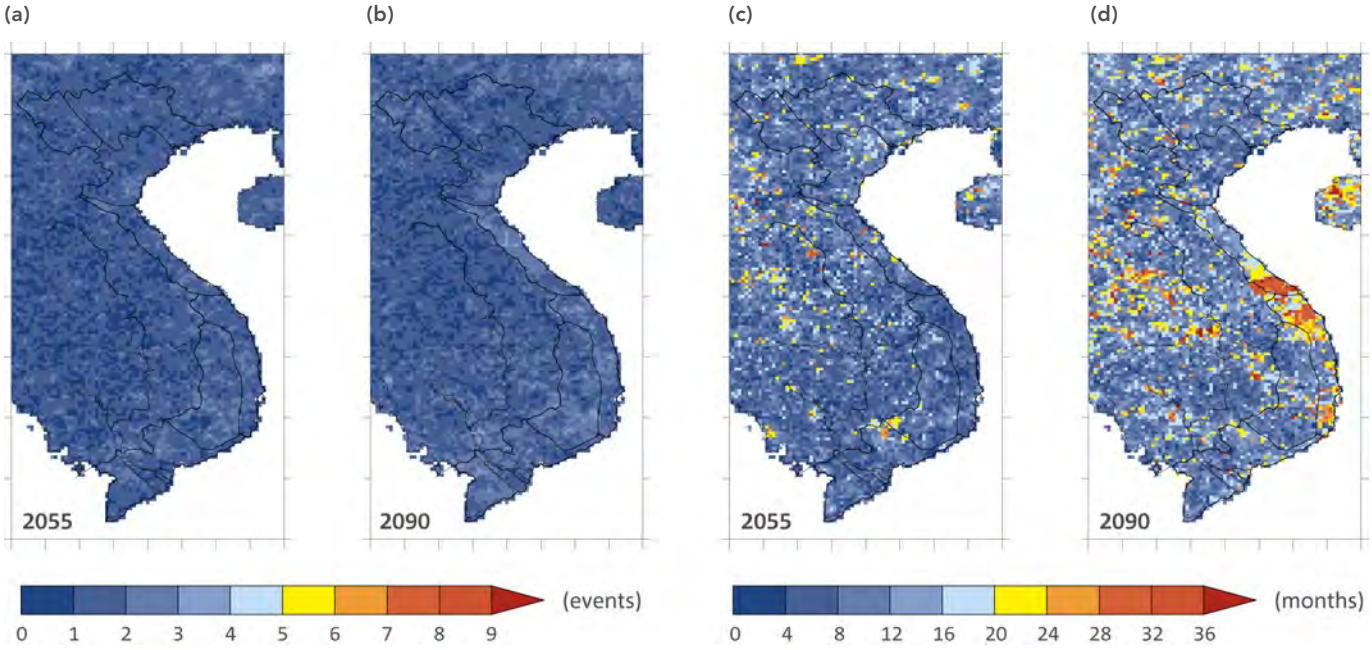

Figure 7-32: Agreement on the increase in the number of extreme and severe droughts for 2045-2065 (a) and for 2080-2100 (b) and their average duration for 2045-2065 (c) and for 2080-2100 (d) in percent based on the 12-month SPI values calculated using CCAM-ensemble simulations at 10 km resolution for RCP 8.5.

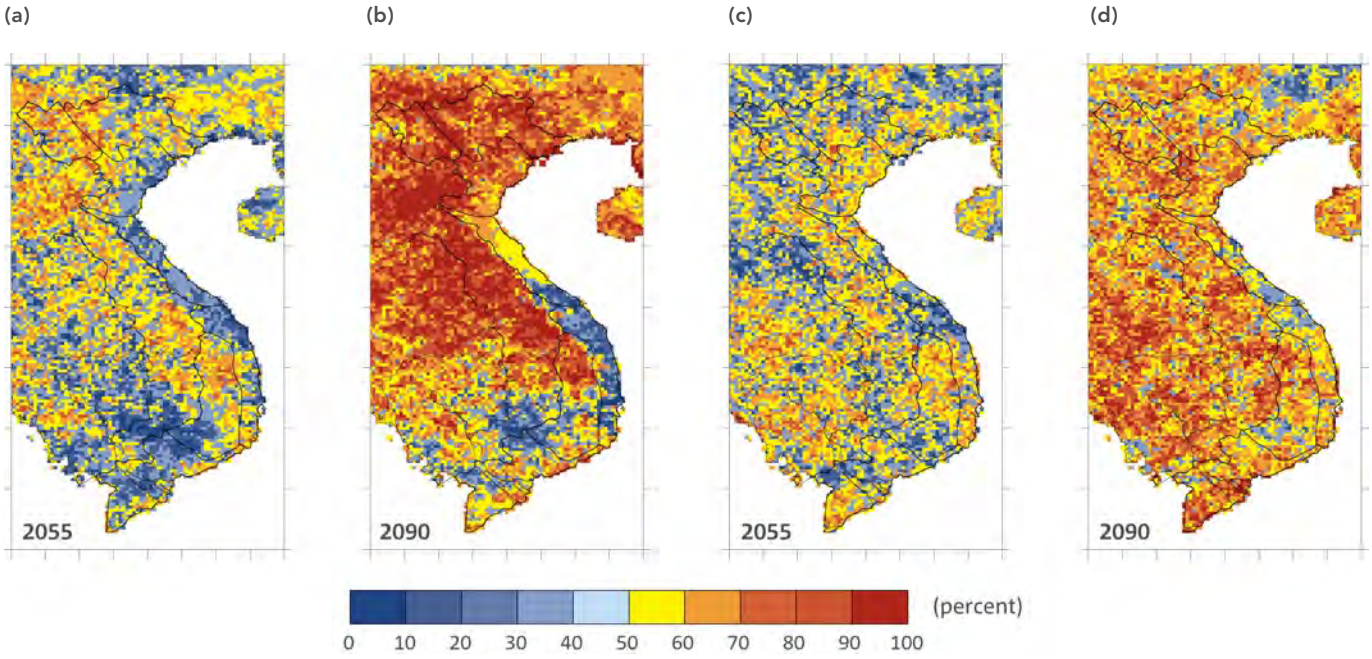

7.4.4 Summary

CCAM-projected changes in severe and extreme short-term (agricultural) droughts and long-term (hydrological) droughts are investigated using the 3-month and 12-month SPI values, respectively. Agricultural droughts are relevant for the large agricultural sector in Vietnam, while hydrological droughts are relevant to changes in groundwater levels, hydro-electricity and dam storages for drinking water. RegCM4.2 results were not used to investigate the changes in drought characteristics due to their short baseline periods (the simulations were for 20-year time slices). CCAM-simulated results show a tendency towards fewer severe and extreme agricultural droughts for most parts of Vietnam by mid-century. However, by the end of the century, the number of droughts increases by 3 to 8 events in the highlands of North Central Vietnam and in the coastal areas of South Central Vietnam. Parts of northern Vietnam and the Central Highlands show a reduction in the number of droughts (up to -8 events). The increase in droughts in central Vietnam can be linked to a large reduction in the South West Monsoon Season rainfall projected by CCAM for this area. A robust increase in the duration of extreme and severe droughts by up to 3 months is also projected for the coastal regions of northern Vietnam and parts of North Central Vietnam.

Results for hydrological droughts show a different pattern of changes when compared with the pattern of changes of agricultural droughts because such long-term droughts are affected by changes in the annual rainfall rather than in the seasonal rainfall. The results also reveal that more, and possibly longer, severe and extreme hydrological droughts (+1 to 3 events) are projected for North Vietnam and the northern parts of the Central Highlands for the end of the century. A possible increase in the duration of droughts of between 6 and 21 months, in combination with a small and less certain increase in the number of droughts, is projected for parts of the Mekong Delta, a region that already faces problems due to a decrease in the amount of groundwater available. For central Vietnam and the southern parts of the Central Highlands, a reduction in the number of droughts of up to -6 events is projected, while the changes of magnitude in the South Central region of Vietnam are less certain. This decrease is probably due to the projected increase in annual rainfall for this part of Vietnam.

7.5 MONSOONS

Vietnam is a developing country that depends heavily on agriculture, so knowing when the rainy season starts is important. Unusual behaviour of the rainy season may lead to droughts or floods, and these greatly affect the livelihood of people living in the region. Monsoon onset is a starting signature of the rainy season. Predicting the onset date is therefore vital for agriculture activities such as crop seeding and fertilizing. The intensity of the rainy season is also important in water resource management and planning.

In this section, an analysis is given of summer monsoon onset dates and the duration of the rainy season over the seven climatic sub-regions of Vietnam (Figure 7-9) using station observations and six numerical simulation results. Future changes of the above variables are also discussed using the downscaled simulations of the Regional Climate Models (RCMs) employed in this study.

7.5.1 Data and method

Data used in this portion of the study came from various sources. Station rainfall data were used to study the onset dates of the monsoon for the current climate. Observed rainfall data was available for a number of stations in Vietnam from 1979 to 2011, as well as gridded data from APHRODITE between 1979 and 2007 (Yatagai *et al.,* 2012). Winds were from the NCEP R-2 reanalysis from 1979 to 2011. CCAM simulations from 1980 to 2000 (representing the current climate) and from 2045 to 2065 (representing the future climate at mid-century) were also used.

Previous studies defined the summer monsoon onset using zonal wind and/or rainfall. These studies showed that the summer monsoon onset occurs over Vietnam between late April and mid-May. In this study, five-day running means of area-averaged daily rainfall and 850 hPa zonal winds are used to define the monsoon onset; this approach is similar to the one used by Qian and Lee (2000), Nguyen *et al.* (2009), and Pham *et al.* (2010).

The method for computing summer monsoon onset dates for the seven climatic regions over Vietnam was:

1. Construction of the daily area-averaged rainfall time series using station data and also CCAM-simulated data for the current and future climates.
2. Area-averaging of the daily 850 hPa wind.
3. Computation of the five-day running means for wind and rainfall.

For monsoon onset to occur:

a. The five-day running mean rainfall rate exceeds the 50th percentile of the current climate amount for the studied region.
b. The five-day running mean winds at 850 hPa become westerly.
c. Both these criteria need to last for at least five consecutive days.

The rainy season retreat date is defined as the first day that the rainfall rate is less than the 50th percentile of the long-term daily mean over the corresponding region, persisting for more than 20 days; this is similar to the approach used by Matsumoto (1997). Monsoon intensity is defined using the rainfall amounts as in Wang and Ho (2002). The duration is defined as the number of days between the onset and retreat dates of the monsoon. The ensemble mean of the various variables is an average of six CCAM simulations.

When comparing the model results against observations for only 20 years, we should keep in mind that the model simulation years used from the climate runs (1980-2000) do not have one-to-one correlation with observed years. Therefore the differences in inter-annual variability between observed and modelled data may have an influence on their means and trends. For example, the results from 20-year sampling dominated by El Niño in modelled data can be very different from those of neutral or La Niña years. As previous studies have reported, rainfall variations in Vietnam are strongly modulated by ENSO variations (Nguyen *et al.,* 2007; Yen *et al.,* 2011; Chen *et al.,* 2012; Sano *et al.,* 2012; Nguyen *et al.*, 2013). The real climate for the period 1980-2000 has seven El Niño and five La Niña years. Furthermore, the rainfall over Vietnam may be influenced by the Pacific Decadal Oscillation (PDO; Dinh, 2009). Therefore, if results obtained are within one standard deviation of the observations, they are considered to be acceptable.

7.5.2 Current climate

In this section, the model simulations are assessed against observed (1) monsoon onset dates, (2) inter-annual variability as measured by the standard deviation, (3) rainfall intensity during the season and (4) duration of the monsoon season. These assessments have been done for the seven climatic sub-regions shown in Figure 7-9.

Mean rainfall and wind conditions

This section discusses the characteristics of the mean rainfall and winds at the surface and upper levels for the months leading up to and after the South West Monsoon Season (SWMS). These two variables are important because they are used to define the summer and winter monsoon onsets for the seven climatic sub-regions in Vietnam. A study of this type was never attempted in the past for such small regions. The monsoon onset dates and the summer rainy season rainfall for the sub-regions are also validated using the downscaled simulations for the current climate (1980 to 2000).

Figure 7-33: NCEP R-2 climatological winds at the 850 hPa level and APHRODITE rainfall (shaded, mm day^{-1}) over Vietnam and surrounding areas for April to December for the period 1979 to 2007.

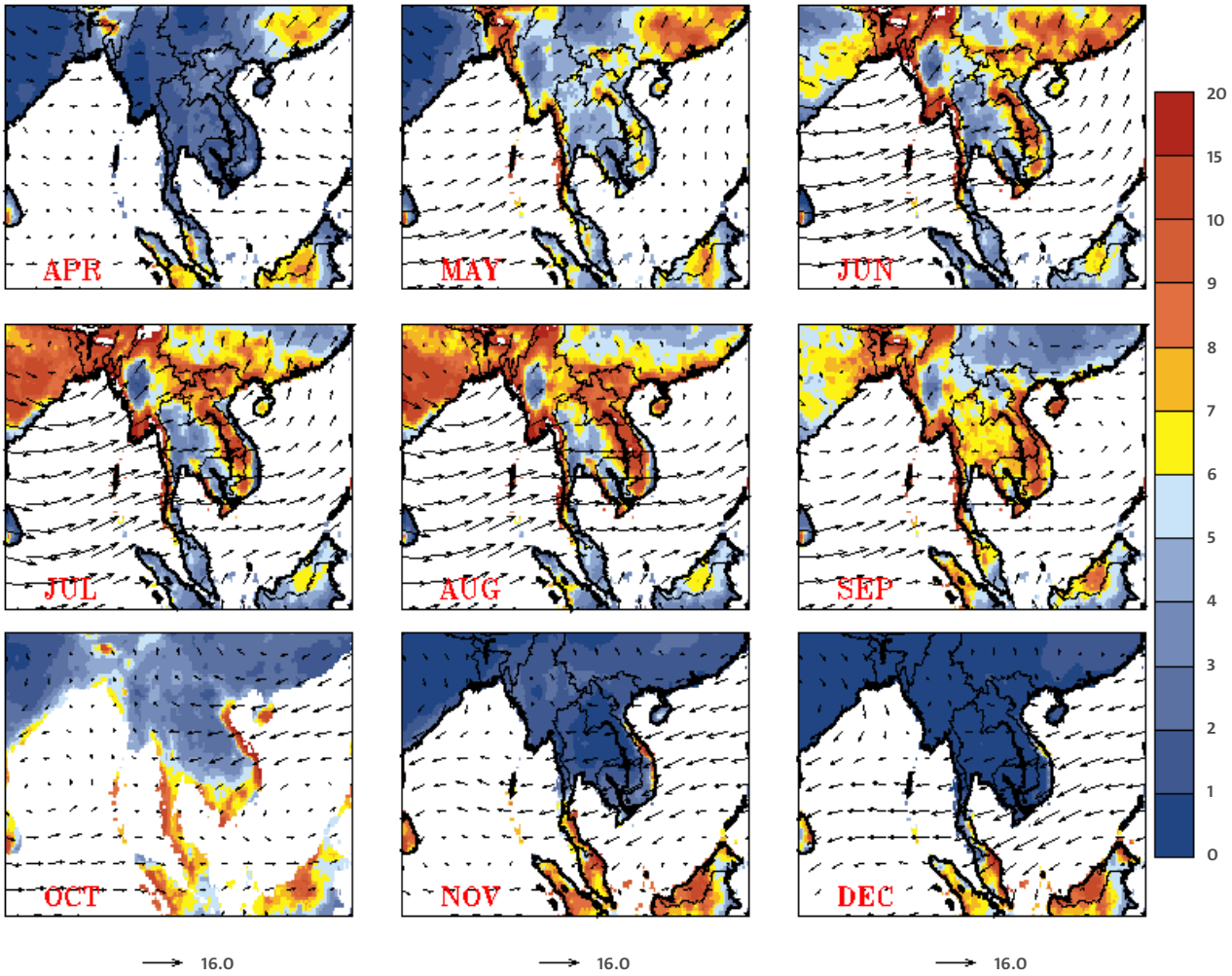

Figure 7-33 shows that the rainy season begins in Vietnam sometime in May and that the rainfall rate is high over the windward side of the mountainous regions. The westerly wind transports moisture from the Bay of Bengal into regions such as Thailand, Laos, Cambodia and Vietnam. In May, more rainfall is received in northern compared with southern Vietnam. South-eastern China also receives high rainfall, which may be attributed to winds from the north western Pacific. The westerly winds strengthen over the Bay of Bengal, leading to widespread rainfall amounts of up to 10-20 mm day^{-1} in September over Vietnam. In October, the westerly winds weaken and a cyclonic circulation is observed over the Bay of Bengal. At the same time, easterly winds are established over the western Pacific, indicating the end of the summer rainy season in Vietnam. In November the cyclonic circulation over the Bay of Bengal shifts southward and the winds over the region are replaced by easterly winds from the northwest Pacific. At this time, rainfall over the region is reduced to 1-2 mm day^{-1}.

Figure 7-34 shows a strong link between the temporal patterns of rainfall and winds. The onset of the summer monsoon is characterised by increased rainfall and westerly winds at lower levels and easterly winds at upper levels. The relationship between winds and rainfall patterns reveals that the rainy season starts in May and ends in September in regions NE and NW in North Vietnam, but extends until November in S and CH in South Vietnam. The rainfall distribution in coastal regions of NC and SC is skewed, with a peak around September to November, which coincides with the tropical cyclone season in Vietnam.

The upper-level winds clearly show the reversal in seasonality from dry to wet for all regions except S, which is located in the extreme southern portion of South Vietnam. However, quite an opposite pattern is seen in low-level winds, where wind reversal in seasonality is apparent in South Vietnam (S, CH and SC) but is not so clear in North Vietnam. This problem may arise due to the coarse resolution (2.5° x 2.5°) of NCEP R2. On the other hand, CCAM upper-level winds display very weak reversal for South Vietnam regions, especially in S, with no reversal in upper-level winds (Figure 7-35). In comparison with station observations (Figure 7-34), CCAM captures the distribution of rainfall well, but not its intensity; for example, CCAM underestimates rainfall for North Vietnam.

Figure 7-34: Observed area-averaged zonal wind at 850 hPa (U850, green) and 200 hPa (U200, red) levels and averaged rainfall (blue) from station data for three regions in South Vietnam (SC, CH and S) and four regions in North Vietnam (NW, NE, ND and NC) for the period 1979-2011. The arrow shows the beginning of the month of May.

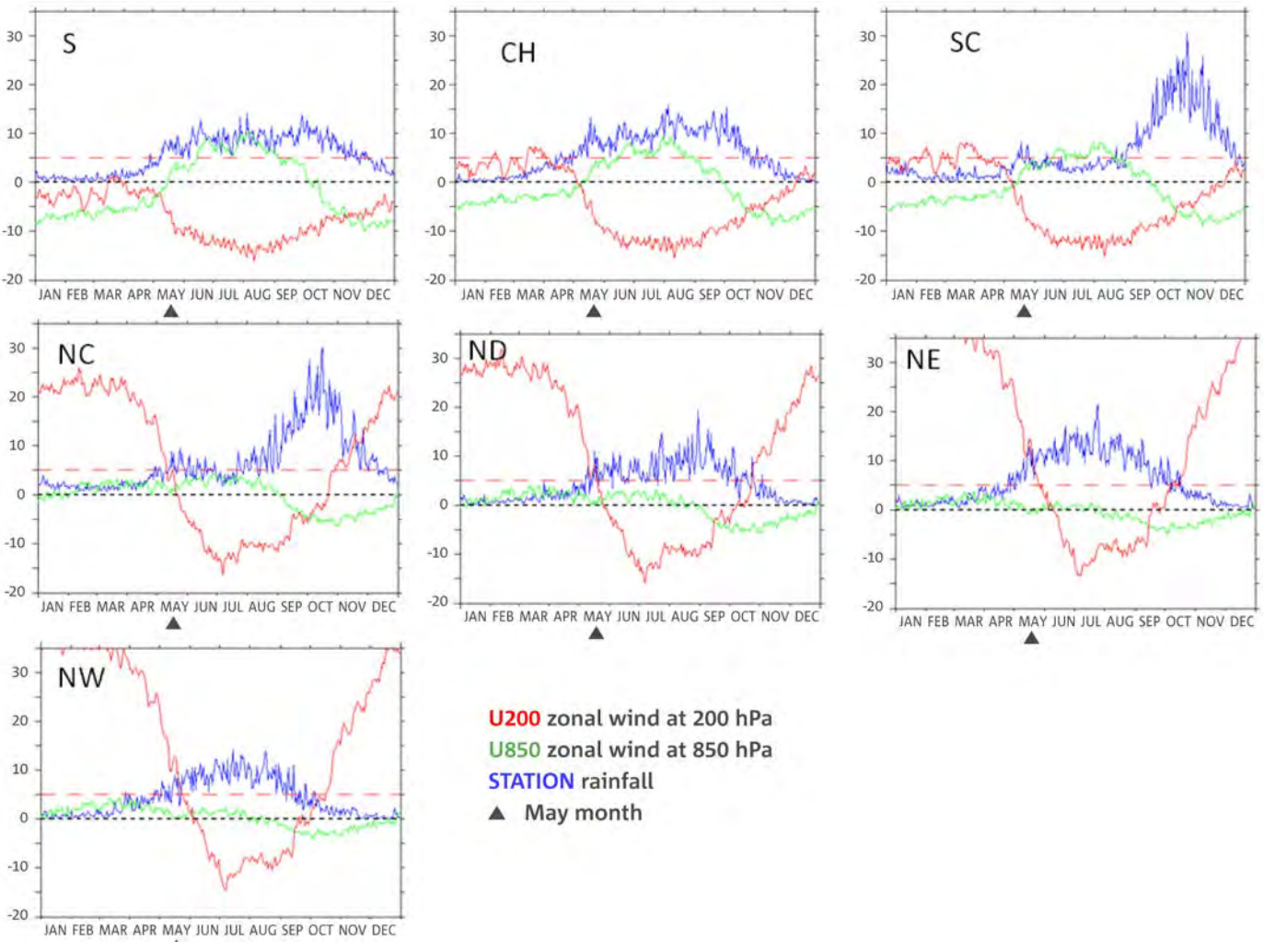

Figure 7-35: As in Figure 7-34 but for the CCAM 10 km simulation.

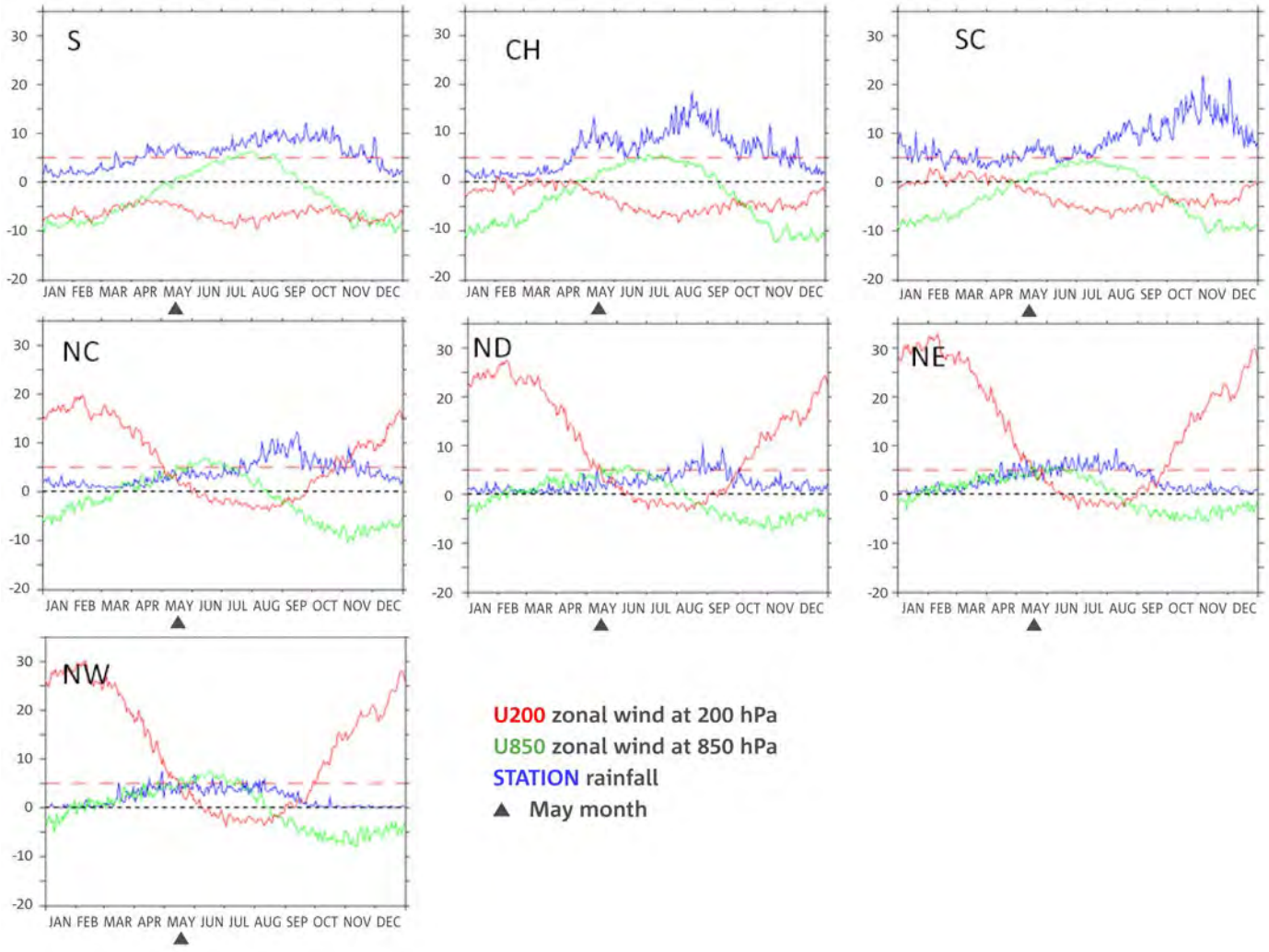

Monsoon onset dates for the current climate

The summer monsoon onset dates for the current climate derived from observations and also from six CCAM simulations are summarized in Table 7-5. Standard deviations of the onset dates are shown and also the ensemble-mean biases.

For region S, the mean observed onset date is 20 May (Julian day 140), varying between 20 April and 12 June, with a standard deviation (SD) of 14 days. The CCAM ensemble-mean onset date for this region is 28 May, which is one week later than the observed onset date, with a spread of between 16 April and 5 August and an SD of 30 days. Thus, the CCAM ensemble-mean onset date is within one observed standard deviation. For this region CCAM CNRM-CM5 and MPI-ESM-LR reproduce the mean onset dates fairly well (24 May and 20 May, respectively). However, as seen in Figure 7-36, all CCAM simulations simulate a much larger range than the observations, with the largest range from -10 to 143 seen in CCAM CCSM4 on the whisker plot (top left), which corresponds to onset dates of 20 April to 20 September and has the largest standard deviation of 42 days (Table 7-5).

For region CH, the mean observed onset date is 20 May, varying from 22 April to 13 June, with an SD of 11 days. The CCAM ensemble mean onset date is 6 May, varying from 15 April to 27 May, with an SD of 12 days. These results show that the CCAM ensemble means underestimate the mean onset date by 14 days but capture the observed standard deviation well. For this region, most CCAM runs are capable of reproducing the mean standard deviation of the onset date, but all the CCAM runs project earlier onset dates than the observations (Table 7-5); CCAM CNRM-CM5 produces the largest variation range (Figure 7-36).

For region SC, all CCAM simulations underestimate the observed mean onset dates and the standard deviation (Table 7-5). The observed mean onset date is 3 June, whereas the CCAM ensemble mean onset date is 17 May, which is 17 days earlier. The observed onset dates have a large spread of -5 to 128 days (Figure 7-36) which corresponds to onset dates of 25 April to 5 September. The best CCAM simulation for this region for the minimum range is CCAM MPI_ESM-LR (23 April), but none of the CCAM simulations are able to simulate the maximum observed range (Figure 7-36).

Table 7-5: Summer monsoon onset dates (as Julian dates) and observed standard deviations for the current climate (1980-2000). Ensemble-mean bias (mean minus observations in days) is shaded.

	S		CH		SC		NC		ND		NE		NW	
	ONSET	SD	ONSET	SD	ONSET	SD	ONSET	SD	ONSET	SD	ONSET	SD	ONSET	SD
OBS	140	14	140	11	154	35	131	21	130	32	119	20	115	15
ENSEMBLE	148	30	126	12	137	16	136	22	137	28	119	19	115	18
BIAS	8	17	-14	0	-17	-19	6	1	7	-3	0	-1	0	3
NorESM1	148	31	132	11	138	13	142	32	151	40	118	23	114	18
MPI_ESM	140	29	125	13	138	14	135	17	134	27	117	20	116	21
CNRM	144	24	126	11	131	13	135	19	137	35	119	16	116	18
CCSM4	151	42	124	11	145	24	137	19	130	20	126	15	117	18
ACCESS1.0	152	28	124	12	135	17	137	24	131	20	114	17	113	16
GFDL-CM3	152	26	123	11	135	13	132	19	138	29	121	20	115	16

Figure 7-36: Onset dates of the summer monsoon for three regions in South Vietnam (S, CH and SC) for the period 1980 to 2000. The mean onset is shown by the dotted line, red and green boxes show spread from the first quartile (Q1) and third quartile (Q3) to the median, respectively, and blue boxes denote Q1. Whiskers show spread from the minimum to Q1 and from the maximum to Q3. The horizontal axis shows station observations (left), six CCAM simulations (middle) and the CCAM ensemble mean (right). The zero value on the vertical axis represents 1 May, with positive numbers indicating later dates and negative numbers earlier dates.

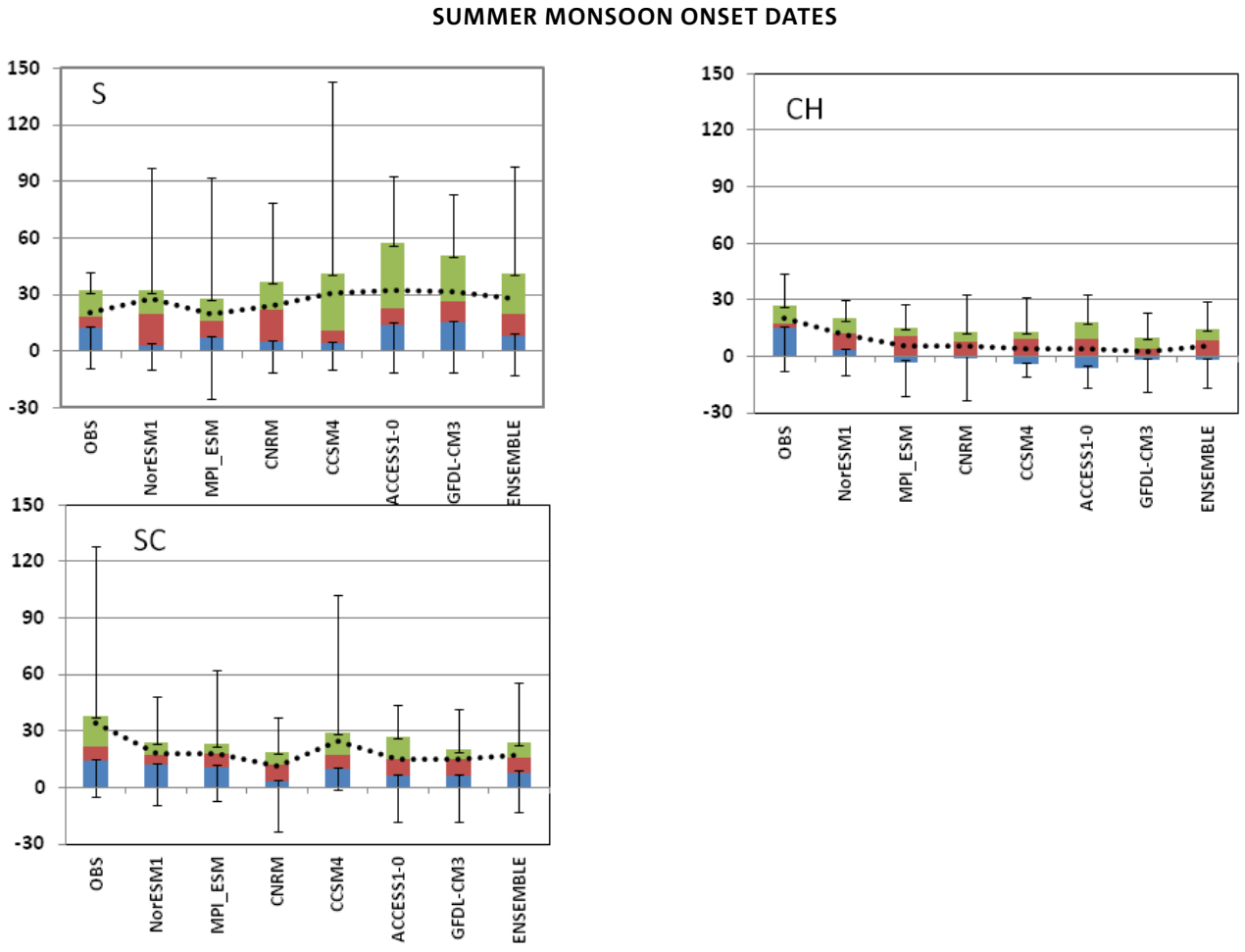

Figure 7-37: As in Figure 7-36 but for North Vietnam.

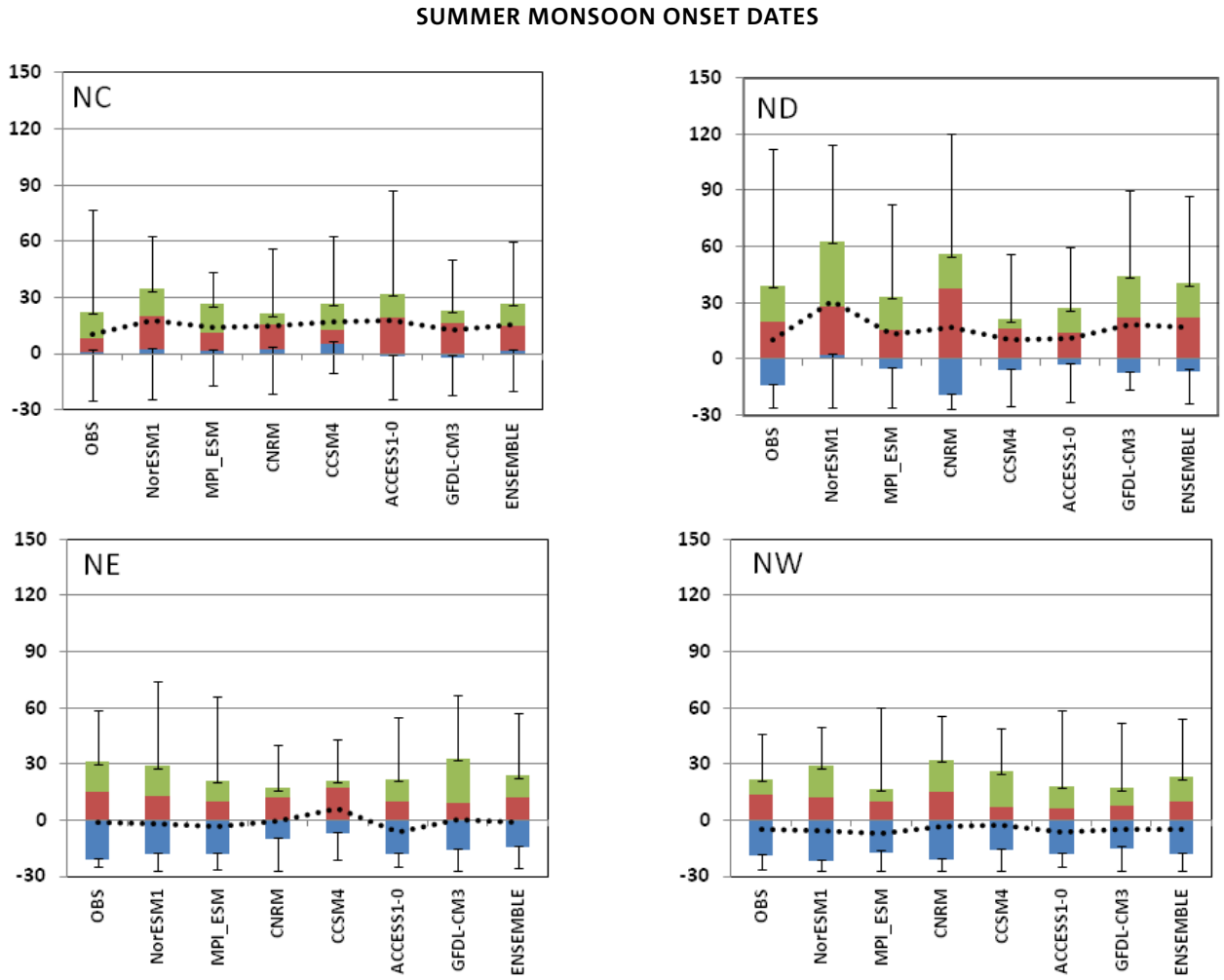

For the NC region, the mean observed onset date is 11 May, but it varies from 5 April to 16 July, with a standard deviation of 21 days. The CCAM ensemble-mean onset date is 16 May, varying from 9 April to 7 July, with a standard deviation of 22 days (Table 7-5). Most CCAM simulations reproduce the observed standard deviation well. CCAM ACCESS1.0 is best at producing mean onset dates compared with the other CCAM runs (Table 7-5). Note that there are some years that do not meet the criteria for defining the onset date for this region.

As in region NC, some CCAM runs are unable to capture the onset dates for some years in the region ND, and CCAM CCSM4 and ACCESS1.0 have some difficulties in reproducing the observed standard deviation for this region (Table 7-5 and Figure 7-37). The observed mean onset date for ND is 10 May and the standard deviation is 32 days, with the onset date ranging from 4 April to 5 August. The CCAM ensemble-mean onset date is 17 May and standard deviation is 28 days, with onset dates ranging from 7 April to 18 July. It is apparent that CCAM is capable of projecting the minimum range but not the maximum range of the onset dates. CCAM CCSM4 is worst in projecting the range of observed onset dates for this region (Figure 7-37).

A plausible reason for the simulations failing to capture the onset dates is the leeward location of these regions. Not only do the westerly monsoon winds bring less moisture, but they are also relatively weak over these regions (Figure 7-35).

CCAM reproduces the mean, standard deviation and the range of the observed onset dates fairly well for region NE. From Table 7-5 and Figure 7-37, the observed mean onset is 29 April and the standard deviation is 20 days, ranging from 5 April to 7 June. The CCAM ensemble-mean onset date is 30 April and the standard deviation is 19 days, ranging from 5 April to 11 June.

For region NW, most CCAM simulations also capture the mean onset date, standard deviation and the range of the observed onset dates (Table 7-5 and Figure 7-37). The observed mean onset is 25 April and the standard deviation is 15 days, ranging from 4 April to 27 May. The CCAM ensemble-mean onset date is 25 April and the standard deviation is 18 days, ranging from 3 April to 7 June.

In summary, CCAM simulates the mean onset date, standard deviation and range well for the North Vietnam regions (NC, ND, NE and NW). On the other hand, CCAM has some difficulties in reproducing the onset dates for the South

Vietnam regions (S, CH and SC); the largest error in the mean onset dates is 17 days in the SC coastal region. This problem may be related to the weak westerly monsoon winds which are unable to lift the moisture-laden air further north to NC, instead depositing most of the moist air on the windward side (CH) and in the south (SC).

Intensity of the rainy season for the current climate (1980-2000)

The rainfall intensity is described as the accumulated rainfall amount (mm) and duration (days) from the monsoon onset date until the rainfall amount is below the 50th percentile of the long-term mean rainfall for at least 20 days. The results are shown in Table 7-6, which also gives the percentage bias of the CCAM ensemble mean.

For region S, all the CCAM simulations underestimate both the observed rainfall amount and the duration by about -55%.

For region CH, CCAM captures the rainfall amount and the duration fairly well. The ensemble-mean errors for the rainfall amount and duration are -5% and -21%, respectively.

For region SC, most CCAM simulations slightly underestimate the rainy season duration, with the CCAM ensemble-mean error being -24%. However, almost all the CCAM runs overestimate the rainfall amount, in particular CCAM ACCESS1.0, resulting in an ensemble-mean error of +24%.

For region NC, all CCAM runs reproduce the rainfall amount and the duration reasonably well. The ensemble-mean biases for rainfall and duration are -3% and -9%, respectively.

For region ND, all CCAM runs underestimate the rainfall amount and most underestimate the duration. The ensemble-mean biases for the rainfall amount and duration are -48% and -16%, respectively.

For NE and NW, CCAM captures the rainfall duration well. The ensemble mean underestimates the observed rainfall amount by about -50%, whereas the error in duration is -7 days.

In summary, the CCAM simulations slightly underestimate the intensity of the rainy season for all regions except SC, where it is too wet. The underestimation of the rainfall amount is within ±50% and the error in duration is less than ±25 days, except for the S region (-51 days).

7.5.3 Future RCM changes in the summer monsoon under RCP 8.5 by mid-century

In this section, the changes projected by the high-resolution CCAM simulations by mid-century (2045-2065) are presented. In general, by mid-century under scenario RCP 8.5, most CCAM simulations suggest that the rainy season will have less rain (Table 7-7) and be shorter (Table 7-8) across all regions. There is little change in onset dates (not shown), with the largest change of +6 in NC, but this change is still within one standard deviation of observed (21 days, Table 7-5). The ensemble mean shows that the strongest reduction in rainfall amount (duration) is in SC at -39% (-15 days) and NC at -37% (-15 days), whereas the reduction in rainfall intensity for other regions is within -20 days.

Table 7-6: Rainfall intensity, or accumulated rainfall amount (mm) and rainfall duration (days) for the seven sub-regions of Vietnam during the summer monsoon season for the current (1980-2000) climate, and the ensemble-mean percentage bias relative to observations (shaded).

	S		CH		SC		NC		ND		NE		NW	
	INTEN-SITY	DURA-TION	INTEN-SITY	DURA-TION	INTEN-SITY	DURA-TION	INTEN-SITY	DURA-TION	INTEN-SITY	DURA-TION	INTEN-SITY	DURA-TION	INTEN-SITY	DURA-TION
OBS	1246	128	1300	127	368	66	369	56	760	98	1353	116	1147	135
ENSEMBLE	566	63	1229	101	455	50	359	51	397	82	705	108	670	123
%BIAS	-55	-51	-5	-21	24	-24	-3	-9	-48	-16	-48	-7	-42	-9
NorESM1	570	65	1142	97	277	32	339	49	303	66	733	111	655	126
MPI_ESM	453	55	1067	88	469	53	303	44	372	82	634	110	607	118
CNRM	592	67	1225	100	428	48	360	53	429	82	756	115	684	125
CCSM4	440	54	1286	108	416	46	443	61	511	100	755	102	721	122
ACCESS1.0	623	62	1380	108	670	68	411	57	432	86	720	109	691	125
GFDL-CM3	716	75	1277	105	466	54	300	43	333	77	630	102	663	124

One way to assess how significant these changes are is to compare the magnitude of the changes relative to the biases in the current climate. If the changes are smaller than the bias, the changes may be considered less reliable. From Table 7-6, the error in the ensemble-mean rainfall amount (duration) for the current climate for SC is 24%, whereas the change is -39% by mid-century, greater than the model error for the rainfall amount. The change for the NC region (Table 7-7) is much larger than the model error in that region (Table 7-6).

In summary, the South West Monsoon Season intensity is projected to decrease by mid-century and also to end earlier than in the current climate. This trend is likely to continue similarly to the end of the century.

Table 7-7: Accumulated rainfall amount (mm) during the summer monsoon season from high-resolution CCAM simulations for the current and future climate at mid-century and the percentage change under RCP 8.5 (shaded).

	S		CH		SC		NC		ND		NE		NW	
	1980-2000	2045-2065	1980-2000	2045-2065	1980-2000	2045-2065	1980-2000	2045-2065	1980-2000	2045-2065	1980-2000	2045-2065	1980-2000	2045-2065
Ensemble Mean	566	449	1229	1028	455	275	359	226	397	375	705	656	670	606
%Chg		-21		-16		-39		-37		-6		-7		-10
NorESM1-M	570	334	1142	724	277	184	339	172	303	417	733	644	655	627
MPI-ESM-LR	453	416	1067	1288	469	399	303	304	372	417	634	588	607	548
CNRM-CM5	592	312	1225	924	428	209	360	262	429	370	756	722	684	635
CCSM4	440	539	1286	1040	416	322	443	257	511	349	755	713	721	577
ACCESS1.0	623	601	1380	1367	670	360	411	148	432	382	720	673	691	611
GFDL-CM3	716	491	1277	827	466	176	300	211	333	314	630	597	663	640

Table 7-8: Duration (in days) of the summer monsoon rainy season from high-resolution CCAM simulations for the current and future climate at mid-century and change under RCP 8.5 (shaded).

	S		CH		SC		NC		ND		NE		NW	
	1980-2000	2045-2065	1980-2000	2045-2065	1980-2000	2045-2065	1980-2000	2045-2065	1980-2000	2045-2065	1980-2000	2045-2065	1980-2000	2045-2065
Ensemble Mean	63	55	101	91	50	35	51	36	82	80	107	104	123	119
%Chg		-8		-10		-15		-15		-2		-3		-5
NorESM1-M	65	42	97	65	32	23	49	28	66	79	111	101	126	129
MPI-ESM-LR	55	57	88	119	53	56	44	53	82	97	102	96	118	110
CNRM-CM5	67	41	100	85	48	29	53	41	82	80	115	108	125	122
CCSM4	54	65	108	89	46	41	61	43	100	76	102	112	122	115
ACCESS1.0	62	68	108	114	68	40	57	21	86	83	109	109	125	120
GFDL-CM3	75	57	105	72	54	22	43	32	77	64	102	96	124	115

7.5.4 Future changes in the summer monsoon under RCP 8.5 by the end of the century

In this section, the changes projected by the high-resolution CCAM simulations by end of the century (2080-2100) are presented. By the end of the century under scenario RCP 8.5, the trends noted at mid-century will continue, with the ensemble mean of the high-resolution CCAM simulations projecting that the rainy season will have even slightly less rain (Table 7-9) and even shorter duration (Table 7-10) across all regions, except for ND, which shows a small increase in duration. The strongest reduction in rainfall amount (duration) is in NC at -59% (-58 days).

One may question how confident it is possible to be in these changes. From Table 7-6, the error in the ensemble-mean rainfall amount (duration) for the current climate for SC is 24% (-16 days), whereas the change is -39% (-15 days) by mid-century and 43% (-33 days) by end of the century. In general, the changes are greater than the current climate bias, which provides some confidence in the changes.

Table 7-9: Accumulated rainfall amount (mm) during the summer monsoon season from high-resolution CCAM simulations for the current and future climate at end of the century and the percentage change under RCP 8.5 (shaded).

	S		CH		SC		NC		ND		NE		NW	
	1980-2000	2080-2100	1980-2000	2080-2100	1980-2000	2080-2100	1980-2000	2080-2100	1980-2000	2080-2100	1980-2000	2080-2100	1980-2000	2080-2100
Ensemble Mean	566	423	1230	840	454	261	359	149	397	354	705	539	670	496
%Chg		-25		-32		-43		-59		-11		-24		-26
NorESM1-M	570	286	1142	661	277	174	339	237	303	364	733	530	655	460
MPI-ESM-LR	453	501	1067	1118	469	446	303	155	372	412	634	635	607	557
CNRM-CM5	592	276	1225	863	428	255	360	146	429	369	756	518	684	493
CCSM4	440	303	1286	615	416	177	443	122	511	381	755	575	721	401
ACCESS1.0	623	614	1380	1031	670	334	411	108	432	394	720	641	691	547
GFDL-CM3	716	561	1277	754	466	178	300	123	333	207	630	333	663	519

Table 7-10: Duration (in days) of the summer monsoon rainy season from high-resolution CCAM simulations for the current and future climate at the end of the century and change under RCP 8.5 (shaded).

	S		CH		SC		NC		ND		NE		NW	
	1980-2000	2080-2100	1980-2000	2080-2100	1980-2000	2080-2100	1980-2000	2080-2100	1980-2000	2080-2100	1980-2000	2080-2100	1980-2000	2080-2100
Ensemble Mean	63	52	101	78	50	34	51	22	82	87	107	97	123	109
%Chg		-17		-22		-33		-58		6		-9		-12
NorESM1-M	65	36	97	63	32	23	49	32	66	92	111	96	126	105
MPI-ESM-LR	55	69	88	106	53	61	44	25	82	102	102	109	118	126
CNRM-CM5	67	38	100	82	48	31	53	22	82	84	115	88	125	101
CCSM4	54	41	108	60	46	24	61	21	100	94	102	104	122	99
ACCESS1.0	62	72	108	89	68	39	57	14	86	93	109	109	125	113
GFDL-CM3	75	58	105	71	54	24	43	16	77	58	102	78	124	109

7.5.5 Summary

The summer monsoon onset for the seven sub-regions of Vietnam was investigated for a 20-year current climate period (1980-2000) and two 20-year future climate periods (2045-2065 and 2080-2100) using ensemble mean values of rainfall and other variables produced by the CSIRO CCAM model simulations. The variables used in this study are onset date and the summer rainy season intensity, based on rainfall amount and the duration of the seasons. The summer monsoon onset date is defined using criteria for rainfall rate and zonal wind at 850 hPa and must last for at least five consecutive days. The model simulations were validated against observations.

The model validation for current climate shows that:

1. The CCAM ensemble mean reproduces the observed monsoon onset date reasonably well, with minimum error (within one observed standard deviation), except for CH, where the error is outside the one standard deviation by three days.
2. In terms of intensity, the ensemble mean underestimates both rainfall amount and duration for all regions, except for rainfall amount in SC. The largest errors in rainfall amount are seen in S, ND and NE (-55%, -48%, and -48%, respectively) and the largest errors in duration are seen in S (-51%).

Future changes by 2050 under scenario RCP 8.5:

1. There is no significant change in onset dates for all regions by 2050. The largest change of +6 days is projected for NC, but this change is within one standard deviation.
2. The rainy season is projected to be shorter in duration by 2050, mainly due to ending earlier, and a less intense rainy season (defined by amount of rain) is projected across almost all regions, with the strongest reduction in coastal regions SC and NC.
3. By end of the century, rainfall amount will decrease by -43% in SC and duration will decrease by -33 days, while in NC, the rainfall amount is projected to decrease by -59% and duration by -58 days.

8 CHANGES IN SEA LEVEL

Globally, sea level changes as a result of changes in the density of the ocean (ocean thermal expansion or contraction) and/or changes in the mass of the ocean through exchanges with the cryosphere (glaciers and ice sheets) and the terrestrial environment (soil moisture, terrestrial reservoirs, lakes, ground water, etc.) In addition to the global-averaged change, sea level changes relative to the land regionally as a result of changes in ocean dynamics (changes in ocean currents related to changes in surface winds, air-sea fluxes of heat and freshwater and internal variability), changes in the Earth's gravitational field with changes in the distribution of water on the Earth and vertical motion of the land (Figure 8-1; see Church *et al.,* 2010 for an overview).

Dasgupta *et al.* (2007) estimated that over 10% of Vietnam's population and GDP could be affected by a sea-level rise of 1 m, with the largest impacts occurring in the Mekong and Red River Deltas. Indeed they argued that most of Vietnam's land area southwest of Ho Chi Minh City would be severely impacted by sea-level rise (Dasgupta *et al.,* 2007).

8.1 SEA-LEVEL RISE: OBSERVATIONS AND METHODS

There are two main sources of instrumental observations of sea-level change. Firstly, coastal tide gauges measure sea level relative to the land (relative sea level, RSL). The first continuous tide-gauge observations, beginning in the 18th century in Europe (Woodworth, 1999), were installed for shipping purposes rather than as climate records. The first Southern Hemisphere observations date from the late 19th century and even today global coverage is not complete. Monthly-average tide-gauge data is available from the Permanent Service for Mean Sea Level (PSMSL; Woodworth and Player, 2003) with high frequency near-real-time data available from the University of Hawaii Sea Level Center (UHSLC) as well as PSMSL. Secondly, high quality ongoing satellite observations of sea level began with the launch of the TOPEX/Poseidon satellite in August 1992, and have been continued with the Jason series of satellites. These two datasets are complementary with the tide-gauge records, which provide a longer but spatially incomplete record, whereas the satellite record gives virtually global coverage of the ocean between 66°S and 66°N, but the record is still short. Various paleo sea-level records (information preserved in rocks, sediments, ice sheets, corals, etc.) can be used to infer local RSL over much longer time scales.

Figure 8-1: Schematic diagram of the major changes that influenced sea level during the 20th century and will continue to drive sea-level change during the 21st century and beyond.

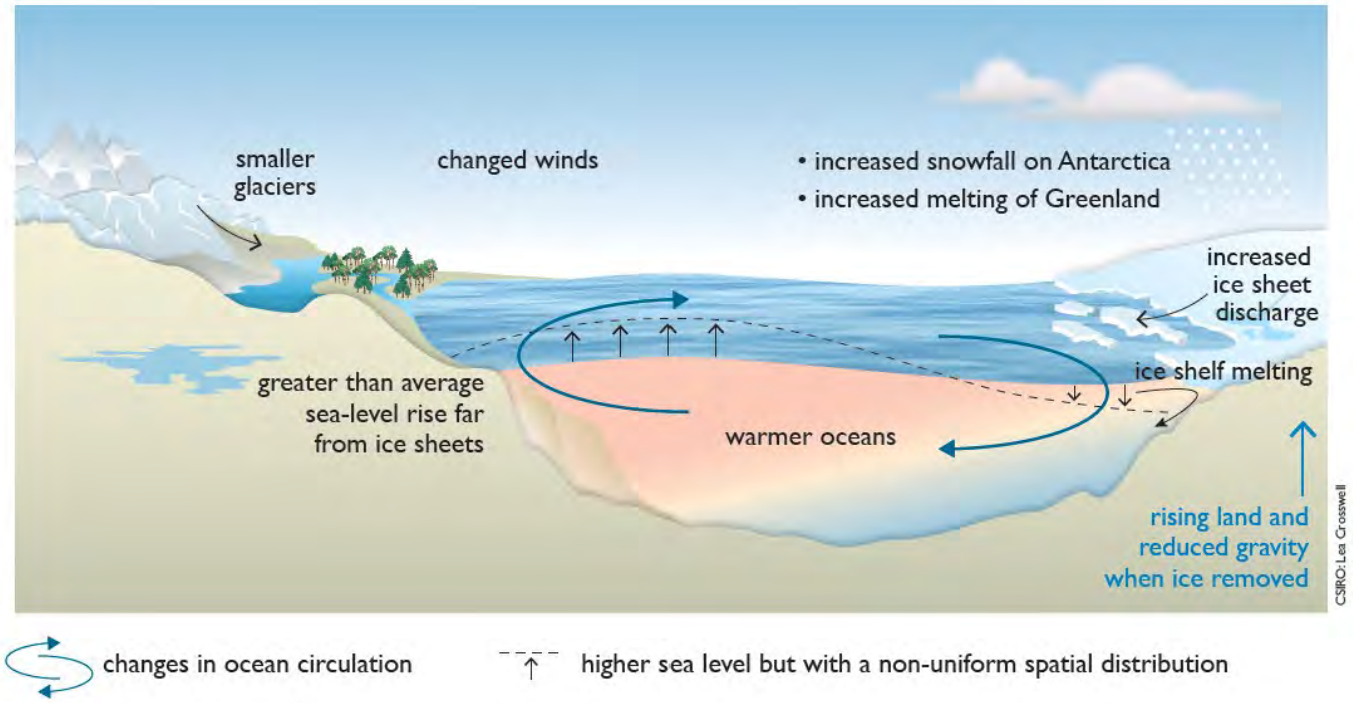

8.1.1 Historical sea-level rise

The multi-century sea-level time series indicate an increase in the rate of sea-level rise (Woodworth, 1999), perhaps starting as early as the 18th century (Jevrejeva *et al.*, 2008), although this latter assessment depends on only three records for the early part of the series. Large-scale spatial correlations estimated from satellite altimeter data have been combined with tide-gauge data in an attempt to improve estimates of 20th (and late 19th) century sea-level rise (Church *et al.*, 2004; Church and White, 2006, 2011; Figure 8-2; Ray and Douglas, 2011). These analyses, and a third dependent on tide-gauge data alone (Jevrejeva *et al.*, 2006), agree on a 20th century rate of sea-level rise of 1.7 ± 0.2 mm year^{-1}. All of these analyses indicate significant changes in the rate of rise during the 20th century, with the largest rates since 1993 and also in the period from 1930-1960. This larger rate of rise since 1993 is also confirmed by the satellite altimeter data (Church *et al.*, 2011; Masters *et al.*, 2012 and the references therein). The Church and White (2011) and the Jevrejeva *et al.* (2006) analyses indicate a small (about 0.01 mm year^{-2}) increase in the rate of sea-level rise from the start of the analysis in the late 19th century. However, Ray and Douglas (2011) found no significant acceleration for the 20th century alone. Paleo data from a number of locations around the world indicate an increase in the rate of rise from several tenths of a mm year^{-1} to modern rates of order 2 mm year^{-1} from the late 19th to the early 20th century (Gerhels and Woodworth, 2013).

The satellite altimeter observations show a very clear pattern of sea-level change since 1993 (Figure 8-3a) with a larger-than-global-average change in the tropical western Pacific Ocean (about three to four times the global-averaged rise), with the eastern Pacific either showing little change or a small fall in sea level. The largest regions of rise are east of the Philippines, with some of these larger rates of rise extending into the East Sea and to the east coast of Vietnam (Figure 8-3b). The altimeter data used here has limited resolution (1°) and as a result, at some locations the mapped altimeter data are some distance from the coast. The trends for the grid points, which are as close as possible to the Vietnam coastal tide gauges (Figure 8-3b; Table 8-1), range from 2.2 to 4.0 mm year^{-1}.

Figure 8-2: Estimates of global mean sea-level rise from 1880 to present from Church and White (2011).

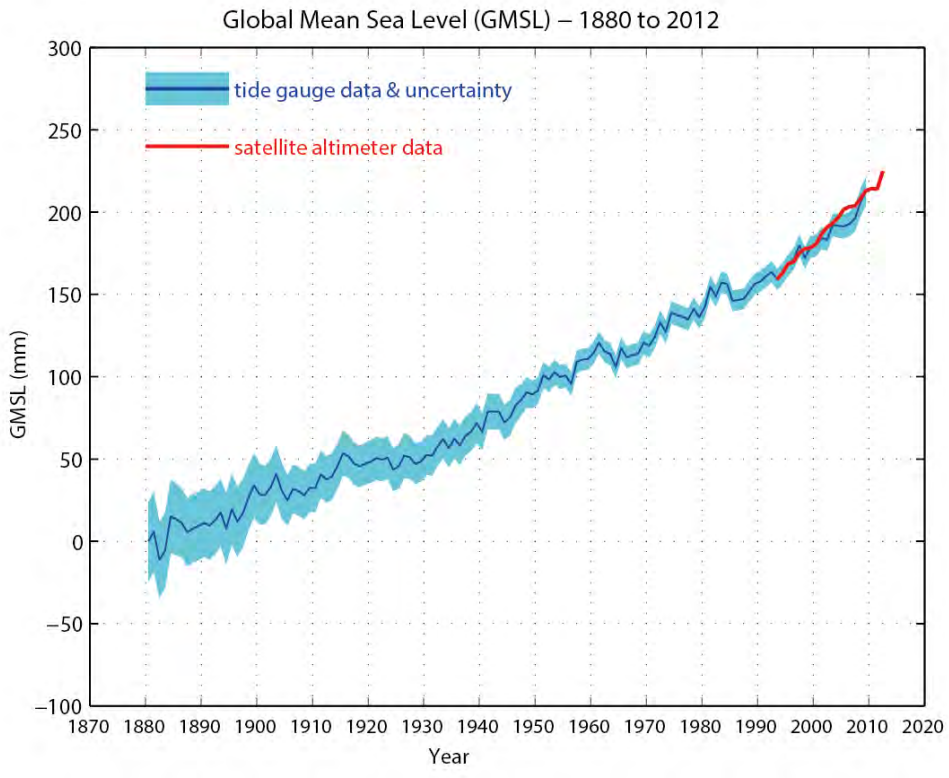

Figure 8-3: The regional trends in sea level over the period 1993 to 2012 based on satellite altimeter data for (a) the globe and (b) the region around Vietnam. The locations of tide gauge data used in Figure 8-4 (following) are indicated in (b).

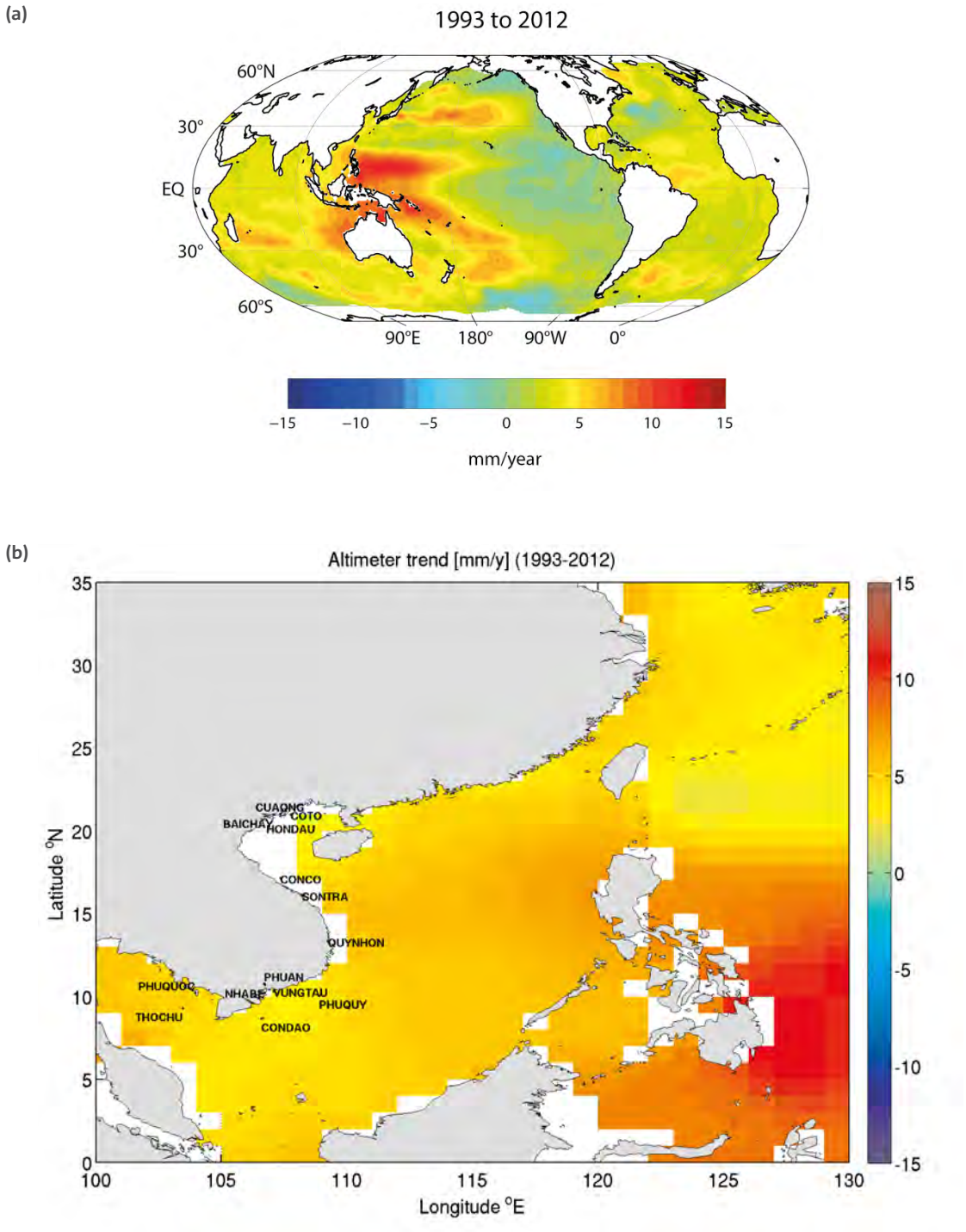

Coastal sea-level data acquired from Hanoi University of Science (HUS) were used in this analysis, as they are more complete than data available through the PSMSL or the UHSLC. However, there appear to be some issues about quality of sections of the data. The better quality data are plotted in Figure 8-4, with the data that appear to be of useful quality bounded by the solid vertical lines, and the locations of the tide gauges shown in Figure 8-3b. Even after focussing on this subset of the data, there is significant variability in the trends between locations and in some case between different periods, suggestive of issues related to the quality of the data and in particular the maintenance of a constant reference level over the length of the records. The average trends of the records shown in Figure 8-4 (each trend was computed for the full length of the useful data and for the period since 1993) are given in Table 8-1. The Cuaong tide-gauge data has very much larger trends than the altimeter data and all other locations, likely a result of compaction of sediments in the region or instability of the tide gauge or its datum. The Coto record indicates falling sea level, in contrast to other nearby gauges over the full length of the record. From 1993 to 2002, both the tide gauge and the altimeter record indicate large positive trends which are likely the result of short-term climate variability over this short period. For Vungtau, there are quite different trends between the first and last half of the record, again suggestive of a reference level problem or strong decadal sea-level variability.

We attempted to estimate a mean sea-level trend for the region. To deal with datum issues, the tide gauge time series were first differenced. The differences were than aggregated for each monthly record where more than five tide gauges were available. The aggregate was then time-integrated to recover the median time series. The median statistics were used here to remove outliers. The median trend of the 14 tide gauge records displayed in Figure 8-4 is 5.8 ± 0.7 mm year^{-1} over the period 1980 to 2008, larger than the global-average 20th century trend of 1.7 ± 0.2 mm year^{-1}, possibly indicative of regional sea-level variability and/or issues with the quality of the data. Since 1993, the trends from the tide gauges are more (spatially) variable than the altimeter trends and the average of these tide gauge trends is -1.7 ± 1.7 mm year^{-1} compared with the equivalent average altimeter data of 3.8 ± 1.6 mm year^{-1}. The large discrepancy between the aggregated tide-gauge trend and the equivalent altimeter trend over the shorter 1993 to 2008 period suggests further tide gauge stability issues, possibly combined with coastal processes and hydrological signals from nearby water courses that remain in the records. A more detailed analysis of these records, together with an analysis of the metadata for the records and the datum control of the records, would be valuable.

Figure 8-4: Monthly sea-level data for the coast of Vietnam from 1960 to 2010. The data that appear to be of useful quality are bounded by the short vertical red lines with the suspect data outside these windows shown in light grey.

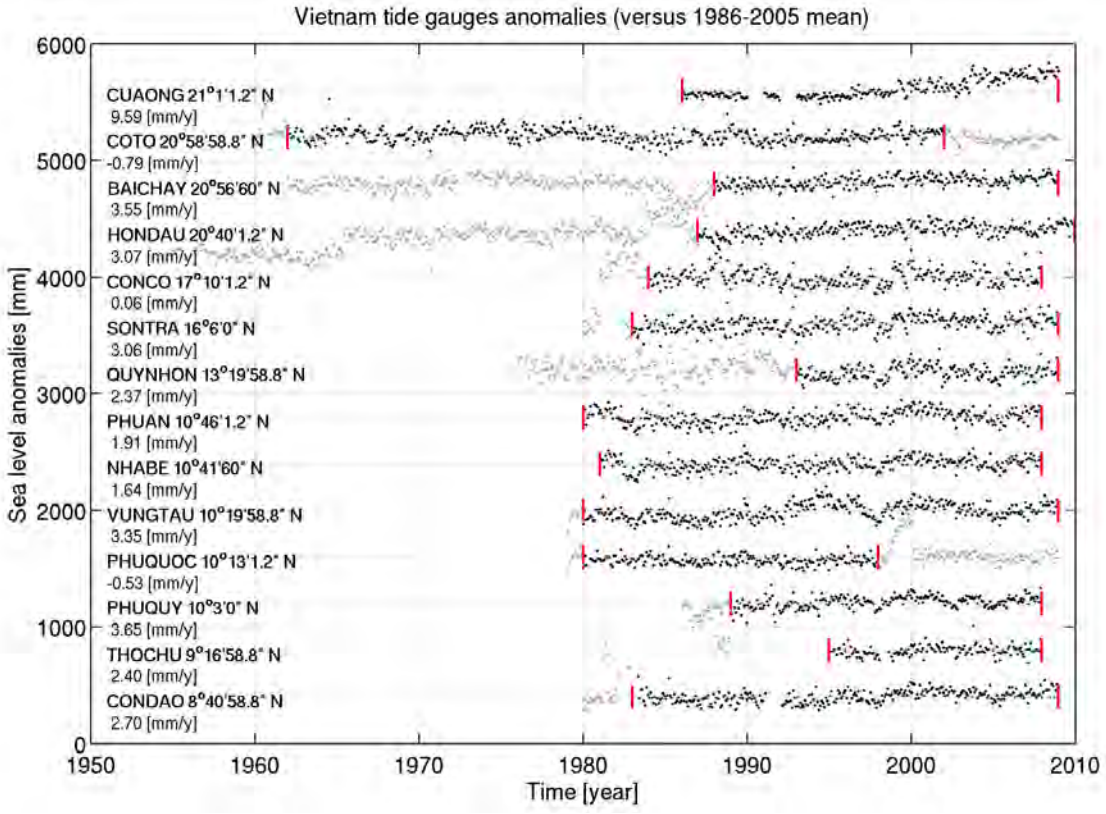

Table 8-1: Sea-level trends. The table gives the locations, start and end dates, record length trend, trend from 1993 to the end of the tide-gauge record, and the altimeter trend for the closest available altimeter grid point from 1993 to the end of the tide-gauge record, each with the standard deviation of the trend in brackets. Note that for Coto and Phuquoc, we have truncated the data to end in 2002 and 1998 because of concerns about the data after this time; these truncations are also applied to the corresponding altimeter data.

STATION	LATITUDE	LONGITUDE	RETAINED PERIOD	RETAINED PERIOD TREND	TREND 1993-END	ALTIMETER TREND 1993-END
CONDAO	840'58.8"	106° 35'60"	1983-2009	2.7 (0.4)	4.6 (0.7)	2.8 (1.0)
THOCHU	9° 16'58.8"	103° 28'1.2"	1995-2008	2.4 (1.0)	2.4 (1.0)	3.3 (0.9)
PHUQUY	10° 3'0"	108° 54'0"	1989-2008	3.7 (0.6)	2.3 (0.7)	2.9 (0.6)
PHUQUOC	10° 13'1.2"	103° 58'1.2"	1980-1998	-0.5 (0.5)	6.4 (3.5)	13.1 (5.9)
VUNGTAU	10° 19'58.8"	107° 4'1.2"	1980-2009	3.4 (0.4)	-3.8 (0.9)	2.7 (1.0)
NHABE	10° 41'60"	106° 43'58.8"	1981-2008	1.6 (0.4)	2.1 (0.8)	2.4 (1.2)
PHUAN	10° 46'1.2"	106° 42'0"	1980-2008	1.9 (0.4)	1.9 (0.9)	2.4 (1.2)
QUYNHON	13° 19'58.8"	109° 15'0"	1993-2009	2.7 (0.9)	2.4 (0.9)	4.3 (0.6)
SONTRA	16° 6'0"	108° 13'1.2"	1983-2009	3.1 (0.4)	3.1 (0.9)	3.8 (0.6)
CONCO	17° 10'1.2"	107° 20'13.2"	1984-2008	0.1 (0.6)	4.3 (1.1)	2.2 (0.7)
HONDAU	20° 40'1.2"	106° 47'60"	1987-2010	3.1 (0.4)	1.1 (0.6)	4.0 (0.9)
BAICHAY	20° 56'60"	107° 4'1.2"	1988-2009	3.6 (0.4)	3.4 (0.6)	3.9 (1.0)
COTO	20° 58'58.8"	107° 46'1.2"	1962-2002	-0.8 (0.2)	6.2 (1.8)	10.7 (2.6)
CUAONG	21° 1'1.2"	107° 20'60"	1986-2009	9.6 (0.5)	15.5 (0.6)	3.9 (1.0)

8.1.2 Reasons for historical sea-level change

Adequately explaining 20th century sea-level change has been a conundrum for many years. However, recently observations and a combination of observations and models have provided a satisfactory explanation for the observed sea-level rise since the early 1970s (Church *et al.*, 2011a; Moore *et al.*, 2011) and for the 20th century as a whole (Gregory *et al.*, 2013a). Ocean thermal expansion, particularly for the upper ocean (Domingues *et al.*, 2008; Levitus *et al.*, 2009; Ishii and Kimoto, 2009), but also for the deeper ocean (Levitus *et al.*, 2012; Purkey and Johnson, 2010), provides one of the major contributions to sea-level rise. Coupled atmosphere-ocean general circulation models (AOGCMs) can also be used for estimating 20th century ocean thermal expansion. These models simulate ocean warming during the 20th century and the observed ocean cooling that follows the injection of aerosols into the stratosphere following major volcanic eruptions (Domingues *et al.*, 2008). However, these models have generally been initialised assuming no volcanic forcing, whereas in reality negative forcing of the climate system associated with volcanic eruptions is a natural part of the climate system. As a result, these models need to be corrected (Gregory, 2010; Gregory *et al.*, 2013b) for this omission. Including this correction, there is good agreement between the models and the observations from 1970 when there are increased ocean data available (Church *et al.*, 2013).

The second major contribution to 20th century sea-level rise is the decay of glaciers. Quantitative estimates of the 20th century contributions of glaciers come from surface mass balance estimates (Cogley, 2009), glacier length (Le Clercq *et al.*, 2011) and models primarily built using surface mass balance estimates (Marzeion *et al.*, 2012). Both the Le Clercq *et al.* and Marzeion *et al.* estimates have maxima in their sea-level contribution in the first half of the 20th century, consistent with the observed faster rate of rise during this period, and near the end of the 20th century.

The Greenland and the Antarctic ice sheets have the potential to make the largest contribution to future sea-level rise. However, the timing of any such contribution and indeed the 20th century contribution is uncertain. The most robust estimates of the ice sheet contributions are dependent on satellite observations commencing in 1992 (Shepherd *et al.*, 2012). These show an accelerating contribution from the Greenland Ice Sheet, both from surface melting and an increased flow of the outlet glaciers (Rignot and Kanaragatnam, 2006). There is also a loss of mass in the West Antarctic Ice Sheet and the Antarctic Peninsula from increased outlet glacier flow. Although the results show increased accumulation over 2009-2010, no significant increase in accumulation has been detected in analyses since 1950 (Monaghan *et al.*, 2006). For both Greenland and Antarctica,

the increased outlet glacier flow has been linked to increased ocean temperatures affecting ice shelves rather than surface warming. Prior to the satellite record, the mass balance estimates for Greenland vary considerably between analyses, with the average of the various analyses quite small (see Gregory *et al.,* 2013a for a full discussion).

The equivalent of about 22 mm of sea-level fall has been impounded in man-made reservoirs, mostly since 1960 with the peak in dam building in the 1970s and 1980s (Chao *et al.,* 2008). There has also been significant anthropogenic withdrawal of water from aquifers (Konikow, 2011; Wada *et al.,* 2012). This withdrawal has increased with time and the rate of withdrawal now exceeds the rate of impoundment resulting in a net positive contribution to sea-level rise.

Since 1993, when estimates of all components are available, the sum of the observed contributions to sea-level rise is in good agreement with the satellite estimates and the tide-gauge reconstruction of global mean sea level.

8.1.3 The ability of models to simulate sea-level rise

The simulations of 20th century and the projections of 21st century sea-level rise reported here are based on coupled AOGCMs that participated in the World Climate Research Programme Coupled Model Intercomparison Project Phase 5 (CMIP5). These models include changes in greenhouse gas concentrations, changes in natural radiative forcing (solar and volcanic), changes in aerosol loading and changes in surface albedo (the amount of sunlight reflected by the surface) for the 20th century and projected changes for the 21st century (Taylor *et al.,* 2011) following the Representative Concentration Pathways (RCPs; Moss *et al.,* 2010; Section 2.2). They provide estimates of changes in ocean temperatures (and hence ocean thermal expansion) in response to changing greenhouse gas concentrations and changes in air-sea fluxes of heat, freshwater and momentum and atmospheric temperatures and precipitation patterns. The air-sea fluxes and internal variability determine ocean circulation and the ocean sea surface height. The changing temperature (and sometimes precipitation) patterns are used to model changes in glacier mass (Radic and Hock, 2011; Slangen *et al.,* 2011; Marzeion *et al.,* 2012). Changes in ocean temperatures and atmospheric temperature and precipitation patterns are used to drive ice sheet models.

When the Marzeion *et al.* (2012) glacier model is forced by observed climate rather than from the climate estimated in climate change simulations, there is an increased Greenland glacier contribution in the 1930s and 1940s (Marzeion *et al.,* 2012). Church *et al.* (2013) argue that this is a result of natural variability and that this contribution needs to be included when evaluating models of 20th century sea-level change. The ice sheets have long time scales and are not necessarily in a state of balance in pre-industrial times and there may also be a small ongoing contribution to past ice sheet conditions. Church *et al.* (2013) use an estimate of 0.1 mm year^{-1} for the 20th century (see Gregory *et al.,* 2013a for a more complete discussion).

Figure 8-5: The sum of the modelled contributions to sea-level change from ocean thermal expansion, increased glacier melting and changes in land-water storage. The light grey lines represent individual models, with the black line showing the adjusted model mean after an allowance for the impact of the lack of volcanic simulations in the model spin-up, natural variability on glacier contributions and a potential long-term ice-sheet contribution are included. The 20th century estimates of global mean sea level are indicated by the blue (Church and White, 2011) and green (Ray and Douglas, 2011) lines with the shading indicating the uncertainty estimates (two standard deviations). The satellite altimeter data since 1993 is shown in red. The results are given (a) for the period 1900 to 2010 and (b) for 1990 to 2010. The dotted black line is after inclusion of the Shepherd *et al.* (2012) ice-sheet observational estimates but excluding the peripheral glacier contribution (to avoid double counting). The red line is the average rate from the altimeter record. Note different vertical scales in the plots. (Adapted from Church *et al.,* 2013).

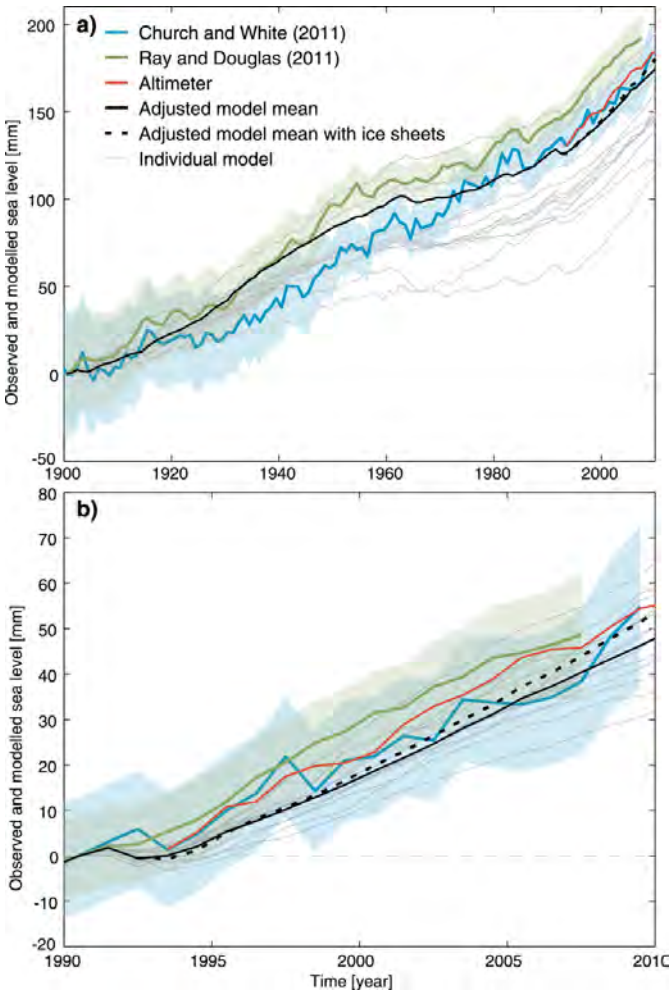

As discussed above, ocean thermal expansion (corrected for the omission of volcanic forcing from the model initialisation; Gregory *et al.,* 2013b) and glacier melting dominate 20th century sea-level change. The ensemble-average estimates of ocean thermal expansion from the CMIP5 20th century simulations, glacier contributions calculated using the model of Marzeion *et al.* (2012) and the adjustment for natural variability, changes in land water storage (Konikow, 2011; Wada *et al.,* 2012) and an assumed small ongoing ice sheet contribution of only 0.1 mm year^{-1} are close to the observed 20th century sea-level rise (Church *et al.,* 2013; Figure 8-5). After adding the observed ice sheet contribution since 1993 (Shepherd *et al.,* 2012), the total sum of terms very nearly explains the observed rise since 1900.

The regional distribution of sea-level rise since 1993 in the Indian and Pacific Oceans is strongly related to natural variability, especially the El Niño Southern Oscillation (ENSO) and the Pacific Decadal Oscillation (PDO) phenomena (Zhang and Church, 2012). Several studies have now demonstrated the importance of changes in winds for the regional distribution of sea level. In particular, Merrifield *et al.* (2011, 2012) have demonstrated that it is the changes in the strength of the trade winds that are responsible for the larger rates of sea-level rise in the western equatorial Pacific. However, the timing and magnitude of natural variation in ENSO and the PDO are not expected to be reproduced in the CMIP5 climate model responses to changes in greenhouse gas forcing. Whether or not there is an additional direct contribution of climate change (from either the greenhouse gas forcing or the regional distribution of anthropogenic tropospheric aerosols) to this regional distribution of sea-level change has not been demonstrated.

8.2 PROJECTIONS OF 21ST CENTURY SEA-LEVEL CHANGE

To project future sea-level rise, we use results from the available CMIP5 coupled AOGCMs simulations. The simulations used here have been forced with the best estimates of historical radiative forcings up to 2005 and then radiative forcing from the RCP 2.6, RCP 4.5, RCP 6.0 and RCP 8.5 scenarios (Moss *et al.,* 2010; Taylor *et al.,* 2011) until 2100 (see Section 2.2 for a more complete description of the RCP scenarios).

8.2.1 Contributions to globally-averaged 21st century sea-level rise

Ocean thermal expansion (Figure 8-6a) is available for up 24 AOGCMs participating in the CMIP5 experiment. They show a rise ranging from 105-198 mm for RCP 2.6 to 236-407 mm for RCP 8.5 for 1995 to 2100, with intermediate values for the other scenarios. For RCP 8.5, the rate of rise increases throughout the 21st century, whereas for RCP 2.6, the rate of rise decreases after 2050.

For the glacier contributions, we use the projections of Marzeion *et al.* (2012) that were used in the evaluation of the 20th century sea-level projections (Figure 8-5). They show (Figure 8-6) a rise ranging from 82-210 mm for RCP 2.6 to 118-292 mm for RCP 8.5 from 1995 to 2100. As for ocean thermal expansion, for RCP 8.5 the rate of rise increases throughout the 21st century, whereas for RCP 2.6, the rate of rise decreases after 2050.

For Greenland, surface melting increases more rapidly than increased snowfall, leading to a positive contribution to 21st century sea-level rise from changes in the surface mass balance (SMB). We use the method developed by Fettweis *et al.* (2013) where changes in SMB are estimated from projected global average temperatures. The values (Figure 8-6) range from 10-56 mm for RCP 2.6 to 59-165 mm for RCP 8.5 by 2100.

In addition to changes in SMB, ocean warming leads to an increased discharge from the Greenland outlet glaciers, as observed over the last two decades (Shepherd *et al.,* 2012). Nick *et al.* (2013) estimate the increased discharge from the four major outlet glaciers in Greenland (Jakobshavn Isbrae, Helheim, Kangerdlugssuaq and Petermann glaciers) for the A1B (AR4) and RCP 8.5 (AR5) scenarios as 8.5–13.1 and 11.3–17.5 mm by 2100. These four glaciers drain 22% of the Greenland Ice Sheet and after multiplying by five to account for drainage from the rest of Greenland, they provide a first order estimate of the total discharge (43–66 mm and 56–88 mm by 2100). The simulated discharge increases rapidly initially, then remains relatively constant and we use a linear trend over the 21st century. Since we have no information on glacial melt for the other RCP scenarios, we use the A1B estimates for RCP 2.6, RCP 4.5 and RCP 6.0 scenarios. Note that Goelzer *et al.* (2013) find an interaction between the dynamics and the SMB such that a combined simulation results in slightly smaller sea-level contribution (central value of 72 mm for the A1B scenario) than the sum of these two contributions (central value of 88 mm) as used here.

Figure 8-6: Contributions (in mm) to 21st century sea-level rise calculated using the results of individual AOGCMs. (a) Global-averaged ocean thermal expansion. (b) Glacier contributions using the Marzeion *et al.* (2012) model. (c) Contributions from the surface mass balance of the Greenland Ice Sheet. For RCP 8.5 and RCP 2.6 the multi-model mean values with 5-95% uncertainty ranges (shaded areas) are shown. For RCP 6.0 and RCP 4.5, only the multi-model mean values are shown.

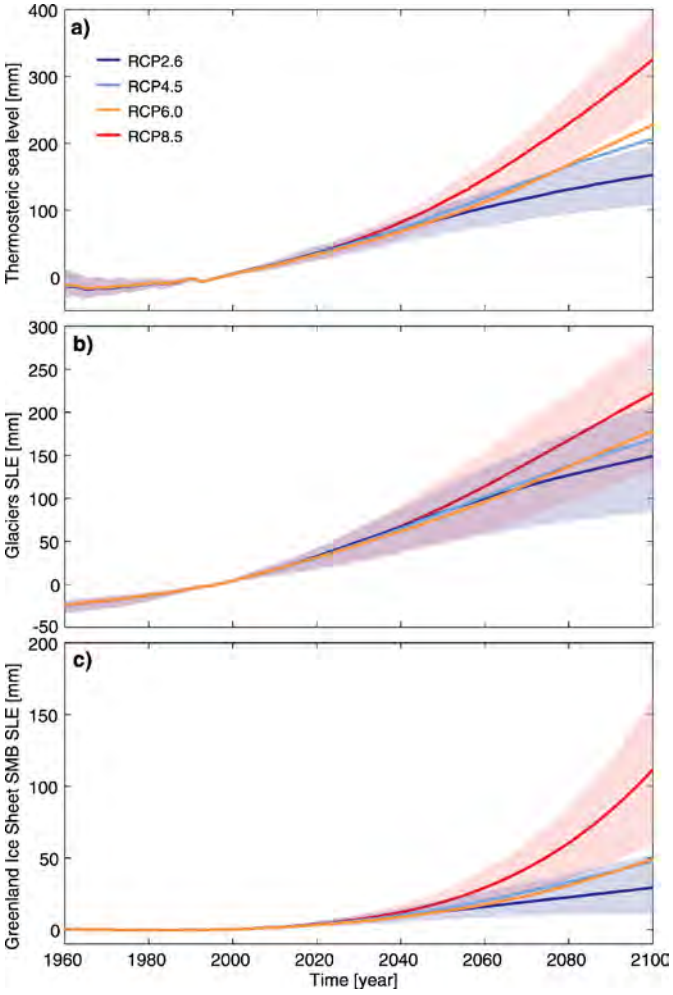

Warming in Antarctica is not projected to be large enough for there to be any significant loss of mass from surface melting. However, atmospheric warming leads to increased moisture transport by the atmosphere and is projected to lead to increased snow accumulation in Antarctica. This was estimated at 5 ± 1.5% °C^{-1} of global surface warming by Gregory and Huybrechts (2006). Other estimates range from 3.7% °C^{-1} by Bengstsson *et al.* (2011), 4.8% °C^{-1} by Ligtenberg *et al.* (2013) and 7% °C^{-1} by Krinner *et al.* (2007). However, as indicated earlier no significant increase in accumulation averaged over Antarctica has yet been detected. Recent observations indicate an increasing sea-level contribution from the West Antarctic Ice Sheet, particularly the Pine Island Glacier (PIG) as well as the Antarctic Peninsula (Shepherd *et al.*, 2012). Recent ice-sheet model simulations are able to reproduce the observed acceleration of the PIG and indicate a maximum sea-level contribution from PIG alone for the 21st century of 27 mm (Joughin *et al.*, 2010). There is at present no published simulation of the dynamic response for the complete Antarctic Ice Sheet for realistic conditions during the 21st century. Little *et al.* (2013) built a statistical relationship between regions and used the available regional PIG simulations to estimate a total Antarctic Ice Sheet contribution (SMB and dynamics) of -80 mm to 130 mm (with a central value of about 25 mm). These estimates have been used in the evaluation presented in this report, starting from the rate over the last decade and extended quadratically to the Little *et al.* (2013) estimates in 2100.

Based on observations of groundwater levels, Konikow (2011) estimated groundwater depletion at the rate of 0.4 ± 0.1 mm year^{-1} sea-level equivalent for 2001-2008 and expected continued depletion. Using a groundwater model and 21st century projections, Wada *et al.* (2012) estimated a somewhat larger groundwater depletion of 70 mm (range of 50 to 90 mm) by 2090. Dam building has significantly reduced from its late 20th century peak, and continuing sedimentation in terrestrial reservoirs is decreasing their storage capacity (Lettenmaier and Milly, 2009). In contrast, Lemperiere (2006) expects dam building to continue. This project takes an average between zero (no additional water impoundment) and a continuation of the average rate for the late 20th century (-0.2 mm year^{-1} SLE). For the regional projections an estimate of 10 mm by 2090, with a range of 0 to 20 mm, was used. The sum of groundwater depletion and reservoir storage gives a total sea-level contribution of 60 mm (30 to 90 mm), assumed to be at a constant rate during the 21st century.

8.2.2 Regional projections for Vietnam

To determine the regional changes in sea level for Vietnam, the approach of Church *et al.* (2011b) and Slangen *et al.* (2012) was used. This involved combining the dynamic ocean sea-level distribution with the regional changes (associated with contemporary changes in mass distribution on the Earth) and an ongoing glacial isostatic adjustment from changes in mass distribution since the last glacial maximum.

For each of the RCPs, the CMIP5 results show that the regional sea-level change due to ocean circulation and density changes in the western equatorial Pacific Ocean is slightly above the global average (Figure 8-7).

Each of the terms associated with a change in mass to the ocean implies changes in the Earth's gravitational field and vertical movement of the crust (sea-level fingerprints). This analysis used the fingerprints calculated by Mitrovica *et al.* (2011). The glacier fingerprints were based on the loss of mass during the latter half of the 20th century, as estimated by Cogley (2009). While the 21st century pattern of glacier mass loss may differ from that assumed by Mitrovica *et al.* (2011), the resultant change in the Vietnam region is likely to be small. The Greenland fingerprint is insensitive to details of the exact location of mass loss on the Greenland Ice Sheet. Lacking more detailed information for Antarctica, we assume that the mass change is uniformly distributed over the continent. We assume that the changes in the terrestrial storage results in a relatively uniform change in sea level around the globe.

In addition to the changes in dynamic ocean signal and changes from the gravitational fingerprints associated with changes in mass of the ocean, we include an estimate of land motions associated with an ongoing Glacial Isostatic Adjustment (GIA) associated with past changes in the ice sheets. For the GIA, we have used sea-level predictions based on the pseudo-spectral algorithm of Kendall *et al.* (2005), taking into account time-varying shorelines, changes in the geometry of grounded marine-based ice, and the feedback into sea level of Earth's rotation changes. The ice-load history is based on the ICE-5G model (Peltier, 2004).

Figure 8-7: Projection of regional sea-level change (in mm) due to ocean density and circulation change for 2081-2100 compared with 1986-2005, derived from CMIP5 models under four different RCPs. The global mean sea level has been removed from each panel; thus positive values indicate higher (and negative values indicate lower) local sea-level change than the global average. The stippling (black shading) indicates regions where climate models tend to agree, with the magnitude of multi-model mean exceeding the inter-model standard deviation.

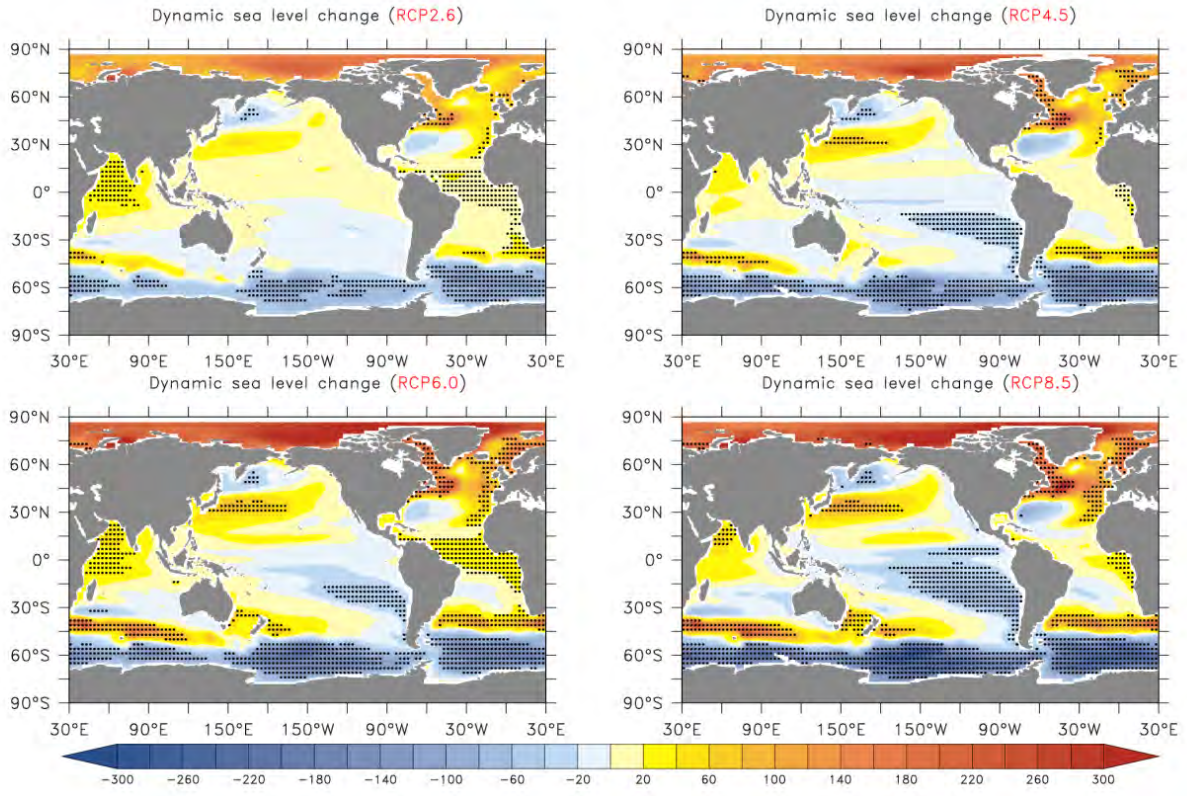

The regional distribution in sea-level change for 2081-2100 compared with 1986-2005 for each of the four scenarios is shown in Figure 8-8. The amount of regional sea-level rise is largest for the RCP 8.5 scenario and smallest for the RCP 2.6 scenario, with RCP 4.5 and 6.0 being similar. The patterns are similar across the scenarios with the largest rise east of southern China, extending westward and then southward into the East Sea. The projections (Figure 8-8) for the coast of Vietnam indicate slightly lower sea-level rise than offshore, as a result of uplift of the coastline by GIA and a small net contribution (maximum around 10-15 mm) from fingerprint patterns associated with redistribution of mass from glaciers and ice sheets. This contribution is positive in south-east Vietnam and the Mekong Delta, and slightly negative in the Gulf of Tonkin and is the sum of a larger-than-global-averaged rise from the Greenland contribution and a smaller-than-global-averaged rise from the smaller glacier fingerprint, because of the proximity of the region of glacier mass loss in the Asian interior. Note that local geodetic effects (such as compaction of sediments) need to be added to the large-scale sea-level changes considered here.

Figure 8-8: Projection of regional sea-level rise for 2081-2100 compared with 1986-2005 for four emission scenarios: RCP 2.6 (top left), RCP 4.5 (top right), RCP 6.0 (bottom left) and RCP 8.5 (bottom right). These regional sea-level projections combine the global-average sea-level projections (thermal expansion, glacier, ice sheets and land storage). Regional 5-95% uncertainties come from uncertainty in the global-mean projections and uncertainty in the regional distribution associated with ocean dynamics, gravitational fingerprints and GIA. These vary little over the displayed domain, with values around 130 mm for RCP 2.6 and 150 mm for RCP 8.5.

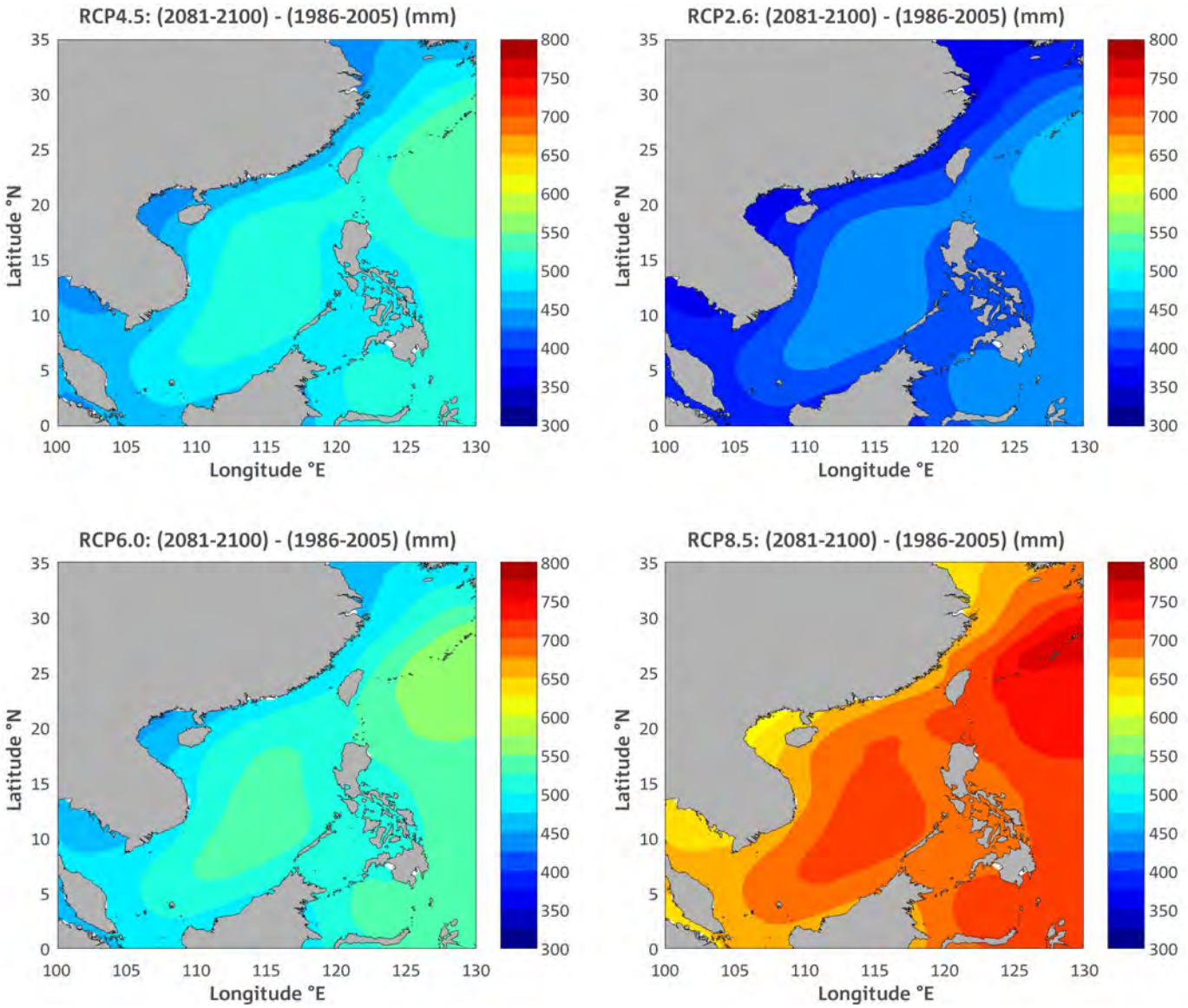

8.3 DISCUSSION

The increase in GMSL in the 1990s was a response to increases in radiative forcing from both anthropogenic and natural sources (Church *et al.,* 2013) and increasing ice sheet contributions (Shepherd *et al.,* 2012). Despite a slowing in the rate of global-average surface temperature in the first decade of the 21st century, the rate of sea-level rise has not decreased significantly because of continued ocean thermal expansion, glacier contributions and increasing contributions from the ice sheets. The projections clearly indicate that both globally and regionally around the Vietnam coast, the rate of sea-level rise during the 21st century will be larger than the average rate during the 20th century as radiative forcing from greenhouse gas emissions continues to grow (Figure 8-9). Even with the lowest emission scenario (RCP 2.6, requiring significant mitigation of greenhouse gas emissions), sea level will continue to rise and some adaptation to rising sea levels will be essential. For the first decades of the 21st century the projections are almost independent of the climate scenario but they begin to separate significantly from about 2050. For the higher greenhouse gas emissions (particularly for RCP 8.5), the rate of rise continues to increase through the 21st century and results in a higher sea-level rise by 2100. Thus the amount of adaptation necessary will depend on the amount of greenhouse gas emissions mitigation.

There remains significant uncertainty about the response of the ice sheets, particularly the West Antarctic Ice Sheet. A sea-level rise a few tens of centimetres higher by 2100 (for example, as in Katsman *et al.,* 2011) is possible if there is a collapse of some component of the ice sheet (Little *et al.,* 2013). There is significant inter-annual variability of the monthly average sea level (Figure 8-9), which has been effectively removed in forming the ensemble-average projections. However, the inter-annual variability will likely continue through the 21st century and beyond. An indication of the magnitude of this inter-annual variability is given by the dotted lines in Figure 8-9, plotted one standard deviation of the historical record above the top and below the bottom of the projections.

The regional distribution of sea-level rise from atmosphere-ocean dynamics remains poorly understood. Changes in the mass of ice stored on land also lead to a regional distribution of sea-level rise (Mitrovica *et al.,* 2001), which is superimposed on the global-mean increase in sea level. Vietnam lies in the far field from the major regions of ice sheet loss but close to regions of glacier mass loss in the Asian interior, and the net effect is small (maximum around 10-20 mm).

It is also important to note that sea level will continue to rise beyond 2100 and that for a sustained global-averaged temperature rise above some threshold, estimated as 3.1 ± 1.5 °C by Gregory and Huybrechts (2006), surface melting will exceed snowfall on Greenland leading to its ongoing decay for centuries and millennia. More recent studies of SMB (e.g. Rae *et al.,* 2012 and Fettweis *et al.,* 2013) indicate a somewhat lower threshold and a dynamic response of the ice sheets may lead to a further significant lowering of this threshold (Robinson *et al.,* 2012).

In addition to sea-level rise from anthropogenic warming, local geological effects could lead to larger local sea-level rise. Particularly important is the compaction of sediments in deltaic regions and also land reclaimed from the sea. This effect is exacerbated by groundwater extraction and there is also a loss of sediment supply to the coastal region as rivers become more managed (Syvitsky *et al.,* 2009; Syvetski and Kettner, 2011). These processes, along with regional developments, may be contributing to the substantially larger rates of relative sea-level rise at locations in Vietnam such as Cua Ong.

The higher sea levels in the 21st century will result in an increase in the frequency of high sea-level extremes. Hunter (2012) demonstrated that even for a 0.5 m sea-level rise, at many locations what is currently a 1-in-100 year flooding event could be occurring annually by 2100. However at the time of publication, the research team was not aware of any such analysis for Vietnam because of the absence of easily accessible high frequency (hourly) sea-level data, although such analysis could be completed in the future. This effect will mean more frequent coastal flooding events for regions that are currently subject to occasional flooding events and adjacent low-lying areas. Most studies to date have argued that changes in mean sea level are the dominant impact on the projected changes in the frequency of extreme sea levels (Sterl *et al.,* 2009; Lowe *et al*., 2010; IPCC SREX, 2012; Colberg and McInnes, 2012) but changes in storminess (frequency or intensity) would also lead to changes in the frequency of extreme sea levels. However, the research team was not aware of any such studies completed for the Vietnamese coastline. These could be completed in the future.

There remains uncertainty in the range of projections. Assuming no changes in storminess, Hunter *et al.* (2013) have combined this uncertainty with the currently observed frequency of extreme sea level to estimate an 'allowance' for sea-level rise. If infrastructure was raised by this allowance, the current risk of coastal flooding would be maintained rather than rising with time. Again, such studies have not been completed for the Vietnamese coast.

Significant uncertainty in sea-level projections comes from the uncertainty surrounding the future of the dynamic response of the ice sheets and the regional distribution of sea-level rise. There is currently significant progress occurring in these fields and a revised assessment of sea-level rise for the Vietnamese coasts should be undertaken after the completion of the Intergovernmental Panel on Climate Change *5th Assessment Report*. Such a study should also examine the interaction between mean sea-level rise and extreme events.

Figure 8-9: Observed and projected relative sea-level change from 1950 to the end of the century near four locations around the coast of Vietnam: (a) Phuquoc, (b) Nhabe, (c) Sontra, and (d) Hondau. The observed tide-gauge relative sea-level records (since the late 1970s) are indicated in light blue, with the satellite record (since 1993) in light green. Multi-model mean projections (black lines) for the RCP 8.5 and RCP 2.6 emission scenarios with 5-95% uncertainty range are shown by the red and blue shaded regions from 1995 to 2100. The dashed lines are an estimate of inter-annual variability in sea level (5–95% uncertainty range about the projections) and indicate that individual monthly averages of sea level can be above or below longer-term averages.

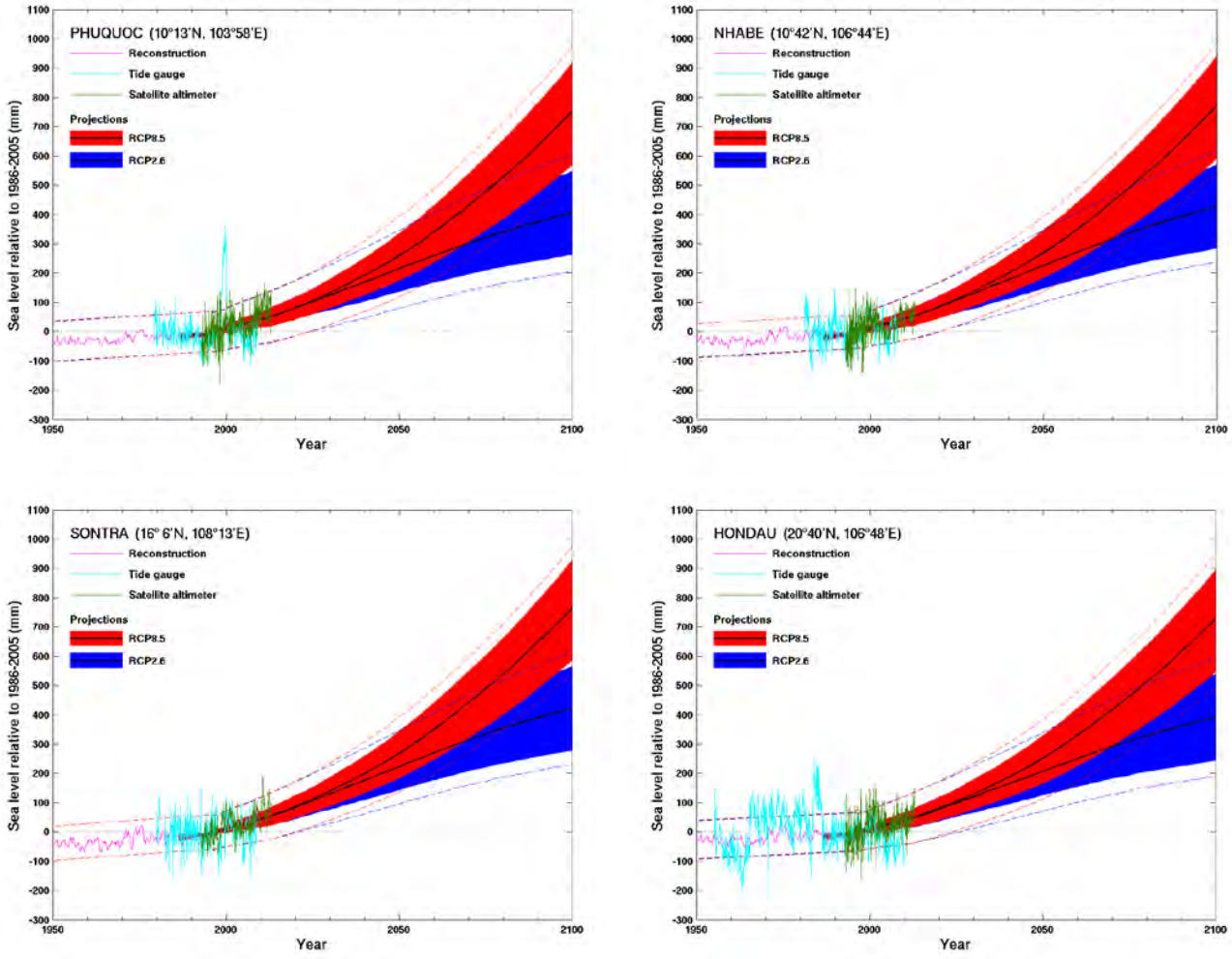


HẢI BỐNG

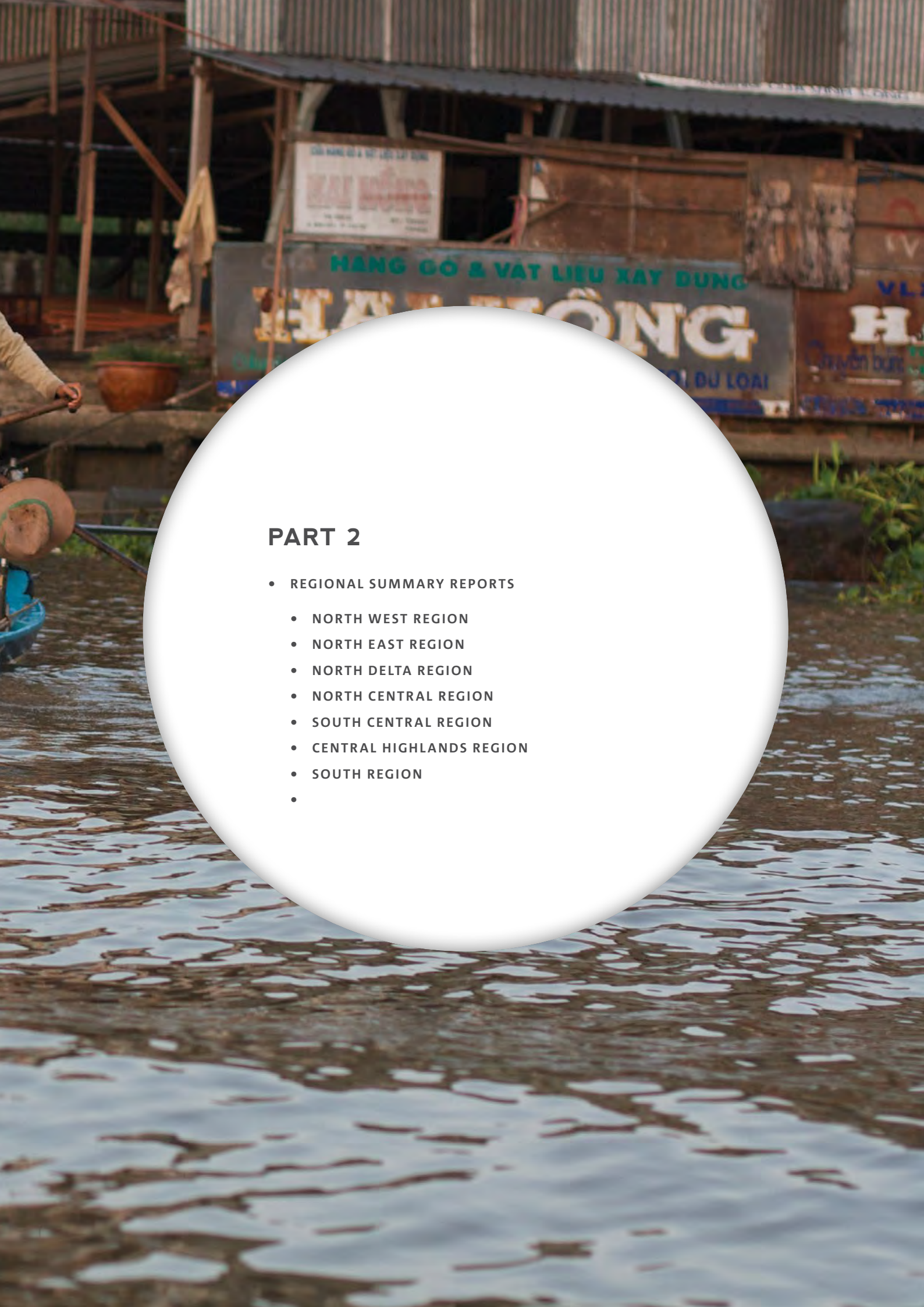

PART 2

- REGIONAL SUMMARY REPORTS
  - NORTH WEST REGION
  - NORTH EAST REGION
  - NORTH DELTA REGION
  - NORTH CENTRAL REGION
  - SOUTH CENTRAL REGION
  - CENTRAL HIGHLANDS REGION
  - SOUTH REGION
  -

EXECUTIVE SUMMARY – PART 2

In Part 2 of this technical report for the *High-resolution Climate Projections for Vietnam* project, detailed information on current climate and projected changes in the future are given for seven sub-regions of Vietnam: North West (NW), North East (NE), North Delta (ND), North Central (NC), South Central (SC), Central Highlands (CH) and South (S).

Each chapter has a general description of the geography and current climatology of the region, followed by analysis of observed trends from station data for the period 1961-2011, including extreme indices (RX1, RX5, R95p, TN10p, TX90p, CDD and CWD; see Section 2 of each chapter for details). Projected changes in temperature and rainfall for the region by mid-century and the end of the century are then presented, first for simulations by CMIP5 GCMs (global climate models), then by RCMs (regional climate models). The RCM projections are from both the new experiments completed for this project using CCAM and RegCM4.2, and the results used for the last official climate change projections completed by IMHEN using the PRECIS model and previous CMIP3 SRES emission scenarios (MONRE, 2012). This provides some indication of the differences among the projections, although it must be kept in mind that they may not be directly comparable, since models have evolved and assumptions about future emission levels have changed.

MAJOR PROJECTED CHANGES BY REGION:

A brief summary of projected changes from the high resolution RCMs over the 21st century under the higher greenhouse gas scenario (RCP 8.5) is given below. These are general trends for the entire region, and there is variation within each region and for different seasons (see individual regional reports for more details).

Temperature is projected to increase in all regions, while rainfall, which is more difficult to project, shows little change annually. Extreme rainfall amounts are lower in the central part of Vietnam (ND, NC, and SC regions), but higher in both the north and south. A decrease in the frequency and an increase in intensity of tropical cyclones (typhoons) are projected, and sea levels will continue to rise.

Rainfall associated with the South West Monsoon decreases slightly for the NW, NE, ND, CH and S regions, with larger decreases for the NC and SC regions. Although little change is projected in annual rainfall, the combination of factors such as the projected decreases in rainfall during the summer monsoon season and the projected increase in the frequency of droughts and more intense extreme rainfall could have significant hydrological implications.

Before application of the results of this study for planning of adaptation measures, it is recommended that a range of possible futures should be considered and that careful analysis is undertaken. Users should collaborate with climate experts and other advisors to identify the best means for applying these new findings in their planning processes and in future project design.

Projected changes by end of century under the higher greenhouse gas scenario (RCP8.5)

REGION	ANNUAL TEMPERATURE	ANNUAL RAINFALL	HOT DAYS	HEATWAVES	DROUGHTS	EXTREME RAINFALL AMOUNTS
NW	Increase by 2.3 to 5.9°C	Little change	More in low-lying areas	Slightly more and longer	Long-term droughts will increase	Small changes
NE	Increase by 2.5 to 6.1°C	Little change	More in low-lying areas	Slightly more and longer	Long-term droughts will increase	More (less) intense in northern (southern) parts
ND	Increase by 2.4 to 5.8°C	Little change	More	Increase	More and longer	Less intense
NC	Increase by 2.2 to 5.0°C	Little change	More	Longer and slightly more	More in mountains	Less intense
SC	Increase by 2.4 to 4.3°C	Little change	More	More and longer	Fewer, but longer	Less intense
CH	Increase by 2.2 to 4.5°C	Little change	More in low-lying areas	More and slightly longer	More and longer in northern parts	Increase in southern parts
S	Increase by 2.6 to 4.4°C	Little change	More	More and longer	Longer in southern part	More (less) intense in northern (southern) parts

9 NORTH WEST REGIONAL REPORT

This chapter summarises the current climate and its trends for the North West region of Vietnam (see Figure 9-1). The projected changes of temperature and rainfall for mid-century and the end of the century are then presented, first from the GCM results, then from the RCM results. The key messages are summarised at the end of the chapter.

9.1 DESCRIPTION

The North West region (NW) of Vietnam (Figure 9-1) contains rugged mountain ranges with alternating narrow valleys and wide plateaus. The terrain exhibits large variations from northwest to southeast. The elevation throughout most of the region does not exceed 1000 m, except for mountain peaks which can be up to 2000 m, such as the Pusilung Mountains in the northwest and the Pudending and Pusamsao mountain ranges which are located along the border between Vietnam and Laos.

Long-term climatological means and ranges of important variables are given in Table 9-1. Within the North West region, Lai Chau and Son La, which are located on the leeward side of the Hoang Lien Son Mountains, have similar altitudes from 100 to 800 m. Due to its location, this region is warmer than the North Delta region to the south. The onset of the rainy season in this region is also earlier than in the others. Moreover, this region is rarely affected by tropical cyclones and experiences a lot of sunshine in summer months (SWMS; June-September). The number of annual sunshine hours in this region (1800-2000 hours) is more than in the North Delta region. Annual temperature amplitude of the North West is 9-11°C, smaller than other regions in the north of Vietnam. The South West Monsoon Season (SWMS) begins a month earlier in this region than the North East (NE) and North Delta (ND) regions. Most rain falls during the months June to August, coinciding with the South West Monsoon Season (SWMS) and less rain and droughts usually occur in December to February, coinciding with the North East Monsoon Season (NEMS).

9.2 OBSERVED CLIMATE

Observed climate trends are analysed using daily data from 70 meteorological stations in Vietnam for the period 1961 to 2011. In addition to trends of mean surface air temperature (or T2m) and precipitation, trends of some extreme indices are also discussed. Definitions of selected extreme indices can be found in ETCCDI (2009), which recommended 27 core Extreme Climate Indices (ECIs) based on daily temperature values or daily precipitation amounts. The indices below are used in this study, mostly following the ETCCDI computational procedures:

- **RX1**: yearly maximum 1-day precipitation (mm).
- **RX5**: annual highest consecutive five-day precipitation amount (mm).
- **R95p**: annual count of days when precipitation exceeds the 95th percentile value for the period 1961-2011.
- **TN10p**: annual count of days when minimum daily temperature is less than the 10th percentile temperature for the period 1961-2011.
- **TX90p**: annual count of days when maximum daily temperature exceeds the 90th percentile temperature for the period 1961-2011.
- **CDD**: consecutive dry days; average annual maximum number of days with daily rainfall less than 1 mm.

Figure 9-1: The North West region with provinces. Insert shows location of region in Vietnam.

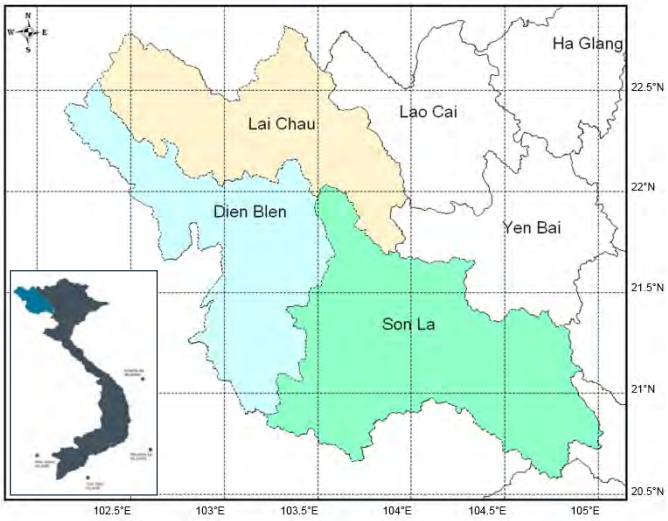

Table 9-1: Observed climate variables and ranges for the NW region. Nguyen and Nguyen (2004).

CLIMATE VARIABLE	VALUE
Altitude	100 to 800 m
Annual average solar radiation	120 to 135 kcal cm^{-2}
Radiation balance	65 to 75 kcal cm^{-2}
Annual sunshine hours	1800 to 2000 h
Annual average temperature	18 to 22°C
Maximum temperature	38 to 40°C
Minimum temperature	-2 to 2°C
Annual temperature amplitude	9 to 11°C
Annual average rainfall	1200 to 1600 mm
Daily maximum rainfall	200 to 500 mm
Rainfall season	Jun to Aug
Humidity	82 to 85%
Annual evaporation	800 to 1000 mm
Annual average wind speed	0.8 to 1.5 m s^{-1}
Maximum wind speed	Less than 35 m s^{-1}

- **CWD**: consecutive wet days; average annual maximum number of days with daily rainfall greater than or equal to 1 mm.
- **Hot days**: days with Tmax greater than 35°C.
- **Cold days**: days with Tmin less than 15°C.

Trends are calculated for each station within the region. Statistical significance of the trends is computed using the non-parametric Mann-Kendall test (Kendall, 1975). In this report, trends with significance levels greater than 90% are considered as statistically significant.

9.2.1 Temperature

There has been a significant increase in annual surface air temperature of approximately 0.2°C per decade for the stations located in the south of this region (Figure 9-2). Two other stations, Lai Chau and Tuan Giao, have a smaller increasing rate of temperature, approximately 0.1°C per decade.

The time series of the regionally-averaged annual temperature (Figure 9-3) shows a warming trend, with strong year-to-year variations. The increasing trend is about 1°C during the past 50 years, or around 0.2°C per decade, as noted above.

9.2.2 Rainfall

Rainfall in this region shows small decreases, less than 2.5% per decade (Figure 9-4). This decrease is not statistically significant.

The time series of the annual rainfall for the region in Figure 9-5 shows strong inter-annual variations, particularly after 1980. Annual rainfall ranges from less than 4 mm day^{-1} to more than 5.5 mm day^{-1}. The trend in annual rainfall for the region is small compared with the year-to-year variability and is not statistically significant.

Figure 9-2: Trend in annual mean surface air temperature (°C per decade) in the North West (NW) region for the period 1961 to 2011. A blue circle indicates a decreasing trend and a red circle shows an increasing trend. A filled circle means that the trend is statistically significant at the 90% confidence level.

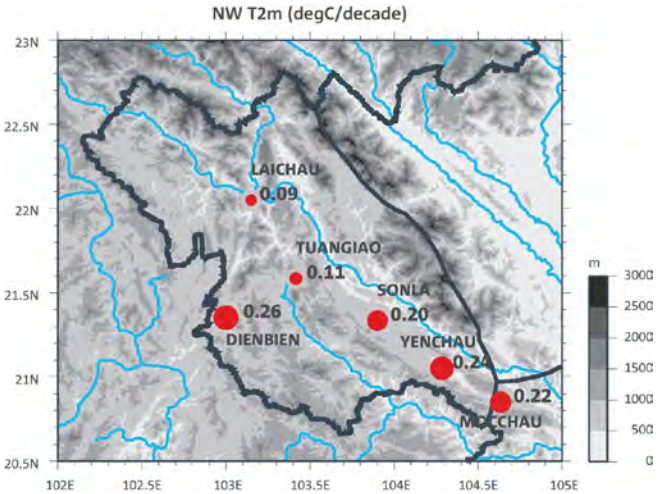

Figure 9-3: Time series of regionally-averaged annual surface air temperature (°C, red) for the NW region with a trend line (dashed). Annual values are shown by black dots.

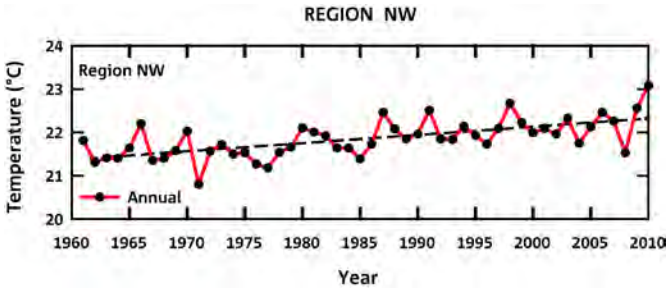

Figure 9-4: Trend in annual rainfall (% per decade) in the NW region for the period 1961 to 2011. A blue circle indicates an increasing trend and a red circle shows a decreasing trend. A filled circle means that the trend is significant at the 90% confidence level.

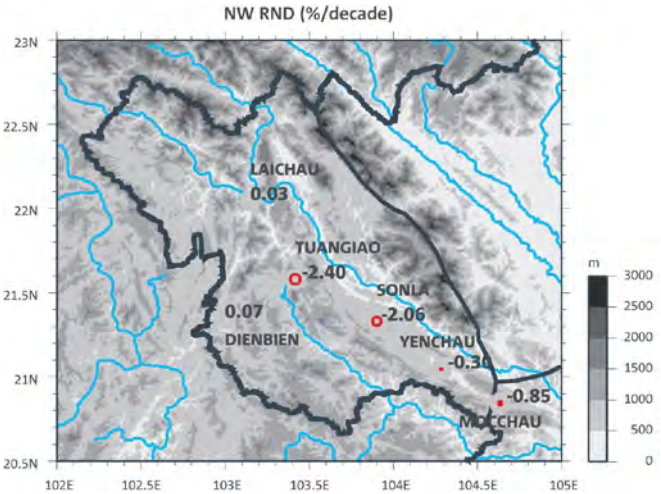

Figure 9-5: Time series of regionally-averaged annual rainfall (mm day^{-1}, blue) for the NW region with a trend line (black dashed line). Annual values are shown by black dots.

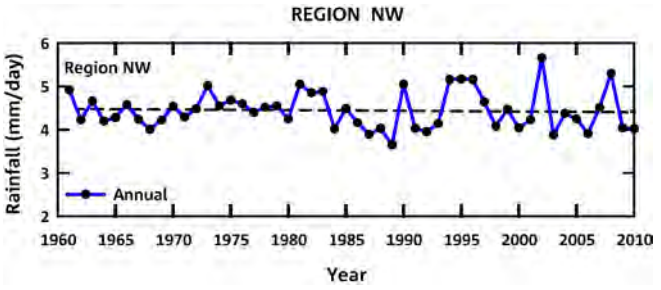

9.2.3 Extremes

Maximum (Tmax) and minimum (Tmin) daily temperatures have increased significantly during the period 1961 to 2011 in this region, as shown in Figure 9-6. Tmax has increased between 0.02 and 0.19°C per decade while Tmin has increased between 0.13 and 0.31°C per decade. It should be noted that greater increase in Tmin and lesser increase in Tmax have resulted in a decrease in the diurnal temperature range in this region during the past 50 years.

The increase in maximum daily temperature has led to a rise in TX90p of up to 7 days per decade (Tuan Giao), whereas the rise in minimum daily temperature has led to a significant decrease in TN10p of more than -15 days per decade (Dien Bien). The number of hot days has increased by up to 3 days per decade at some stations. The number of cold nights has decreased significantly by up to 5 days per decade.

Similar to the annual rainfall, annual maximum daily rainfall (RX1) does not show any significant trends over the region (Figure 9-7). However, it is worth noting that the northwest stations show increasing trends of up to 3.1% per decade, whereas the southeast stations show decreasing trends of up to -5.2% per decade. RX5 shows a similar behaviour to RX1, except for the decreasing trend of about -7% at Son La station, which is significant at the 90% confidence level. R95p and CWD do not show any trends for almost all stations in the NW except Dien Bien and Lai Chau. CDD has a slight but significant increasing trend of up to 3.12% per decade over this region.

Figure 9-6: Trends in Tmax (upper left), Tmin (upper right), TX90p (lower left), and TN10p (lower right) in the NW region for the period 1961 to 2011 (°C per decade for Tmax and Tmin; days per decade for TX90p and TN10p). A blue circle indicates a decreasing and a red circle shows an increasing trend. A filled circle means that the trend is significant at the 90% confidence level.

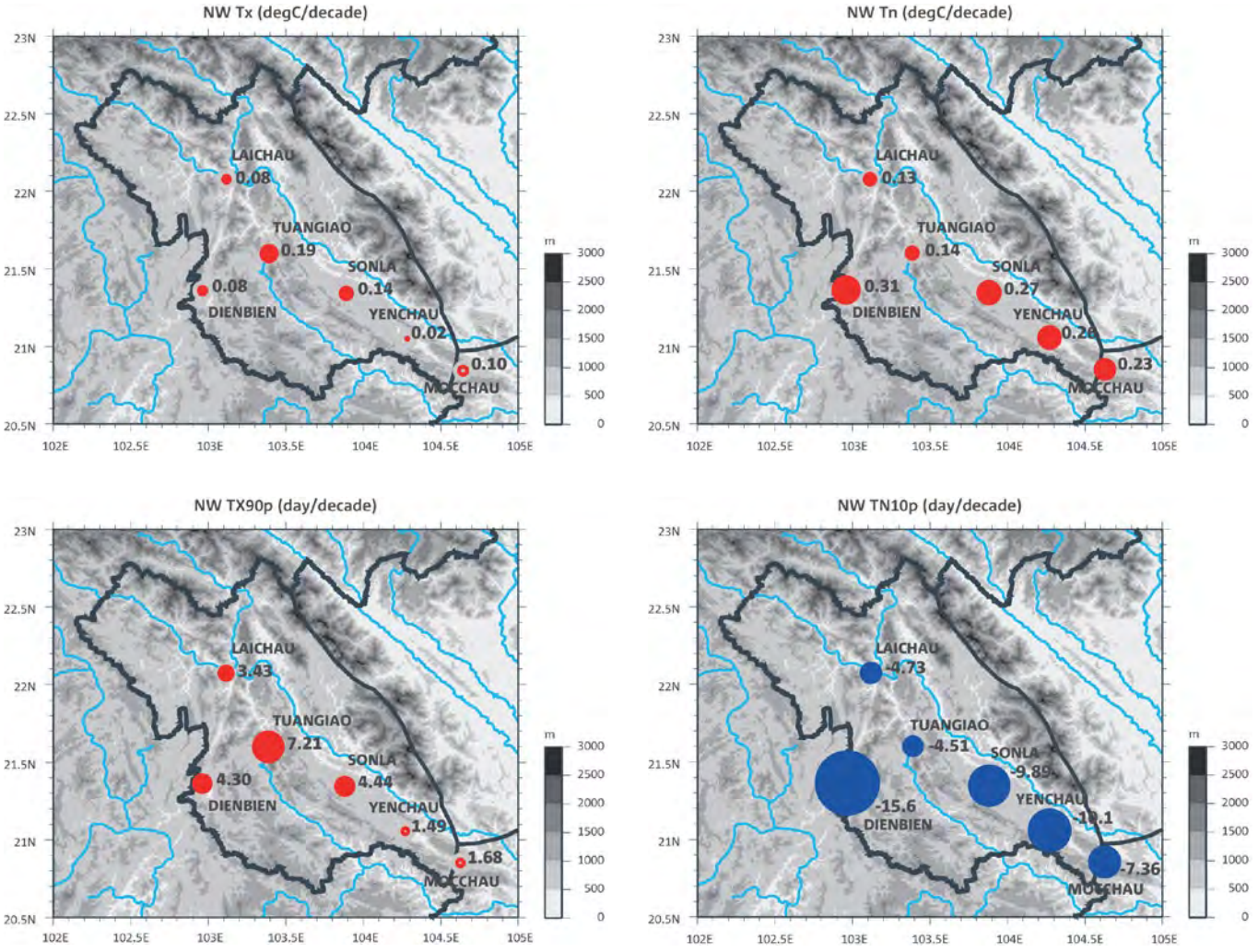

Figure 9-7: Trends in RX1 and RX5 (% per decade), R95p (mm year^{-1}), CWD and CDD (days per decade) in the NW region for the period 1961 to 2011. A blue circle indicates an increasing and a red circle shows a decreasing trend for all but CDD, where red indicates an increasing and blue a decreasing number of days. A filled circle means that the trend is significant at the 90% confidence level.

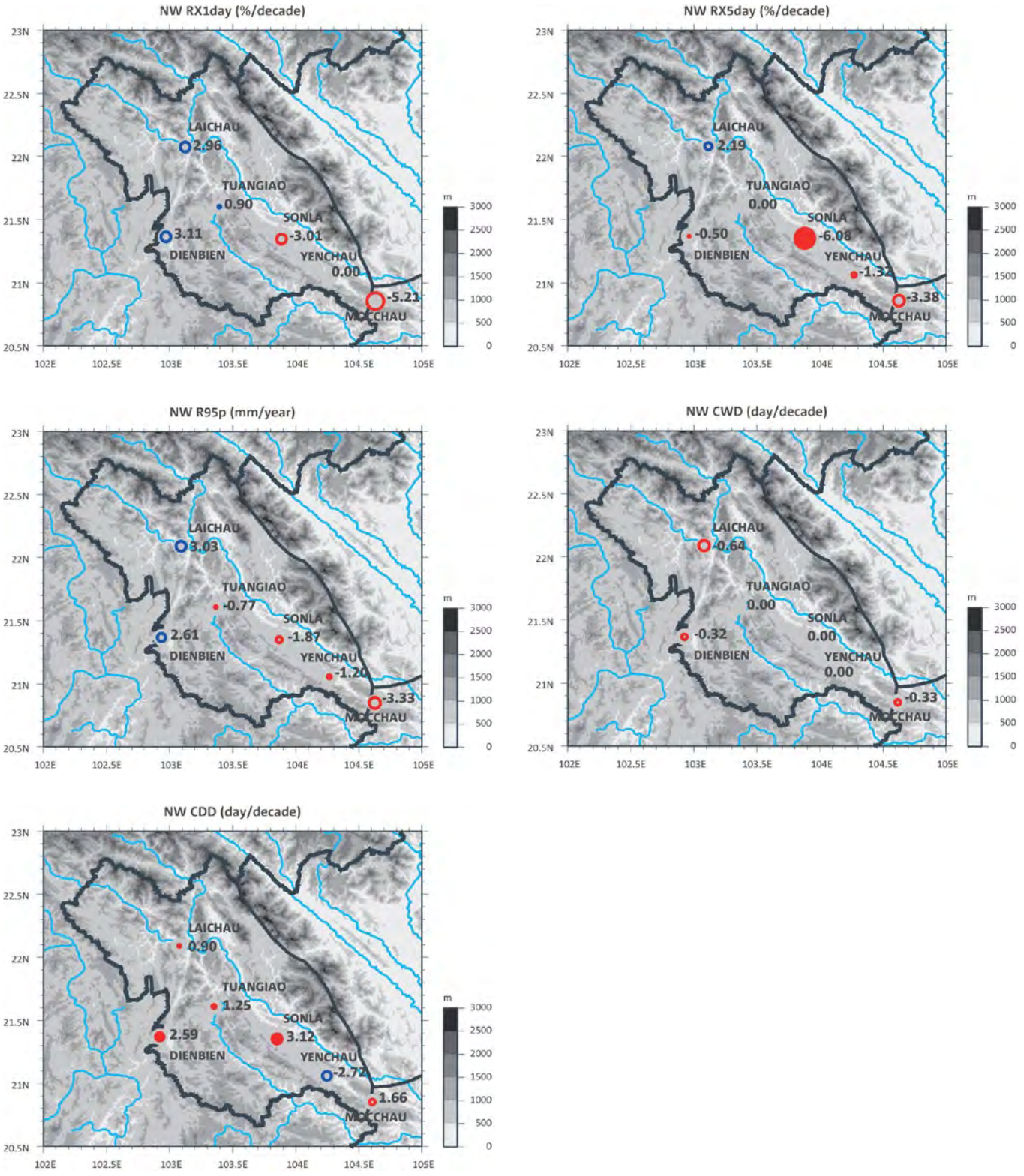

9.3 CLIMATE PROJECTIONS

In this section, projected changes in temperature and rainfall for this region are presented. A summary of the CMIP5 GCM results for different parts of this region is first presented in the form of line graphs. This is followed by the changes projected by regional climate models, both from the new experiments completed for this project and the results used for the last official climate change projections completed by IMHEN (using the previous CMIP3 SRES emission scenarios). This provides some indication of the differences among the projections, though direct comparison is difficult, since different models and different scenarios were used.

9.3.1 GCM results

Surface temperature

Projections for near-surface average temperature for the four seasons for this region from the CMIP5 GCMs are presented in Figure 9-8. The warming signal is very clear, with greatest warming for the high emission scenario (RCP 8.5) and least warming for the low emission scenario (RCP 4.5). There is also slightly greater warming (as measured by the median value – line inside colour bar) during FIMS and SWMS by the end of the century for RCP 8.5, with warming of about 4.2°C, while other seasons show only around 4°C warming by the end of the century.

Figure 9-8: Regionally averaged seasonal surface air temperature changes (°C) for NW. For each season, the time series graph of projections by global climate models (GCM) is shown on the left for the higher (RCP 8.5) greenhouse gas scenario. Black line is from historical GCM runs, red line is the multi-model median projection from GCMs using RCP 8.5. Shadings are between 10% and 90% of 20-year mean values. GCM values have been corrected for 1995-2005 mean bias. Bars on the right for each season show the end-of-century summary of projections by global climate models (GCM, left) and regional climate models (RCM, right) for both lower (RCP 4.5) and higher (RCP 8.5) scenarios.

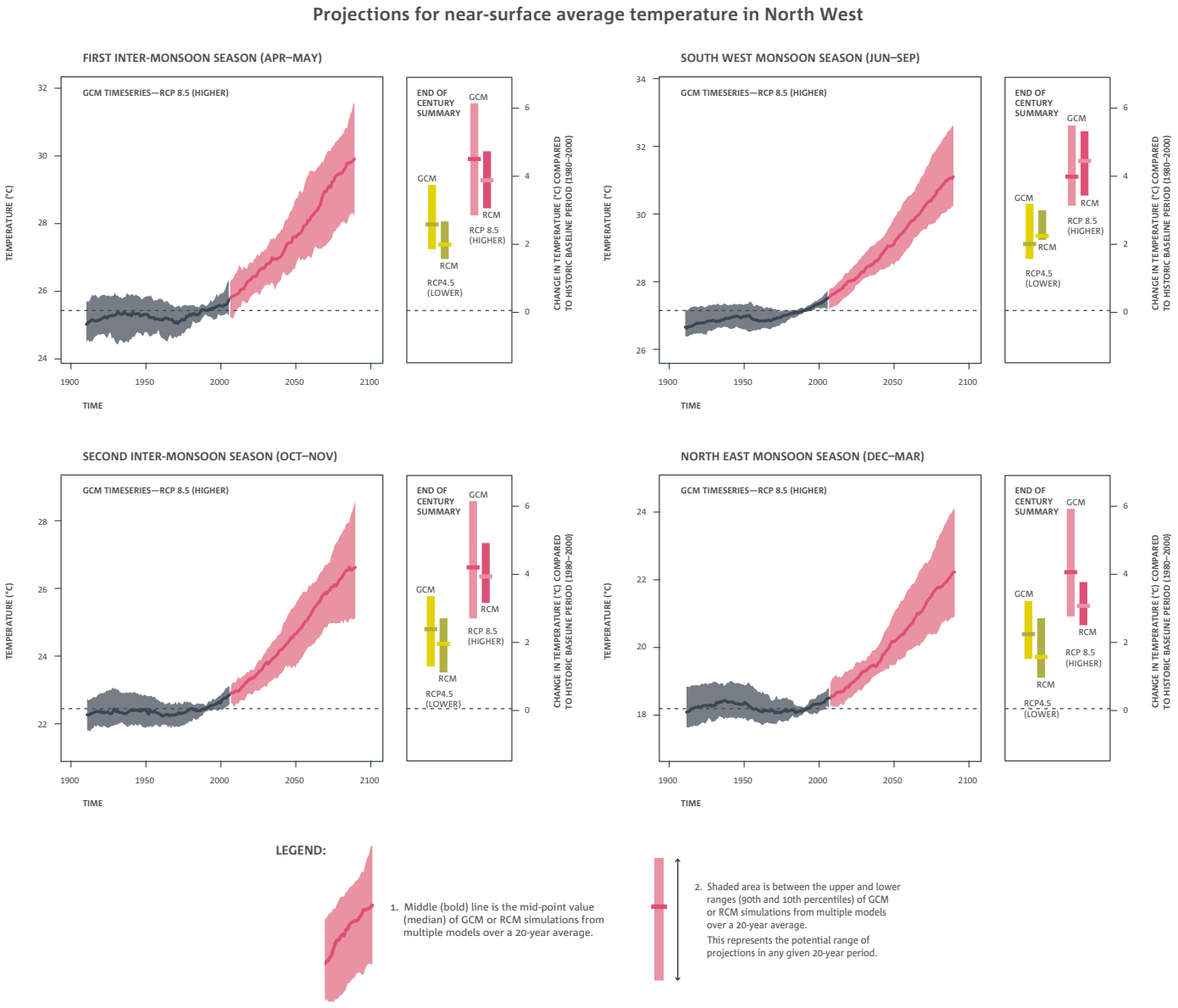

Projections for near-surface maximum temperature for the four seasons for this region from the CMIP5 GCMs are presented in Figure 9-9. Again, the warming signal is very clear and similar to the average temperature. However, there is also slightly greater warming during FIMS and SWMS by the end of the century for RCP 8.5 (more than 4°C), while other seasons show only around 4°C by the end of the century.

Projections for near-surface minimum temperature for four seasons for this region from the CMIP5 GCMs are presented in Figure 9-10. The warming signal is very clear and similar to the average temperature. The warming is similar for all season by the end of the century for RCP 8.5 with values of slightly more than 4°C.

Figure 9-9: Regionally averaged seasonal maximum air temperature changes (°C) for NW. For each season, the time series graph of projections by global climate models (GCM) is shown on the left for the higher (RCP 8.5) greenhouse gas scenario. Black line is from historical GCM runs, red line is the multi-model median projection from GCMs using RCP 8.5. Shadings are between 10% and 90% of 20-year mean values. GCM values have been corrected for 1995-2005 mean bias. Bars on the right for each season show the end-of-century summary of projections by global climate models (GCM, left) and regional climate models (RCM, right) for both lower (RCP 4.5) and higher (RCP 8.5) scenarios.

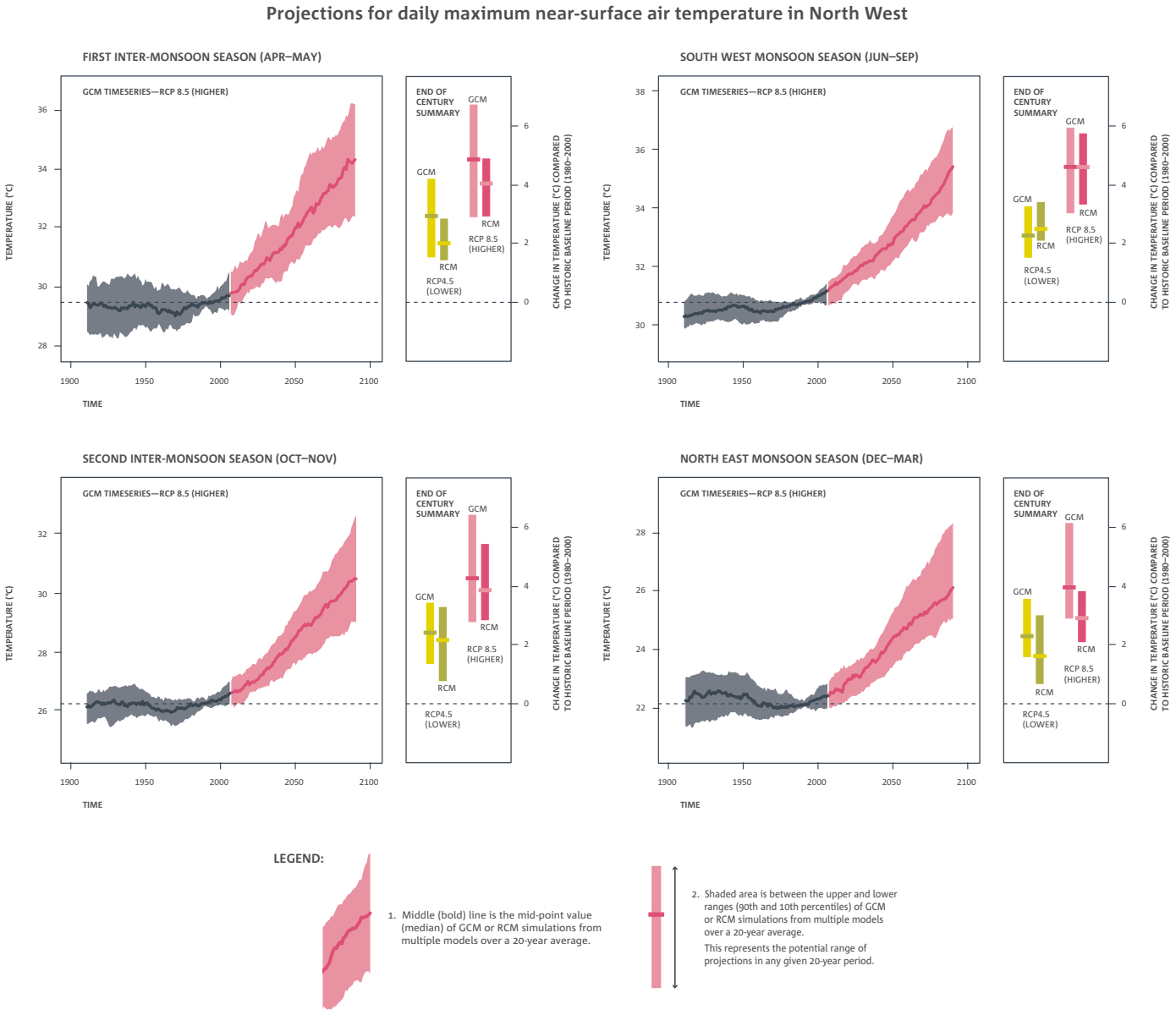

Figure 9-10: Regionally averaged seasonal minimum air temperature changes (°C) for NW. For each season, the time series graph of projections by global climate models (GCM) is shown on the left for the higher (RCP 8.5) greenhouse gas scenario. Black line is from historical GCM runs, red line is the multi-model median projection from GCMs using RCP 8.5. Shadings are between 10% and 90% of 20-year mean values. GCM values have been corrected for 1995-2005 mean bias. Bars on the right for each season show the end-of-century summary of projections by global climate models (GCM, left) and regional climate models (RCM, right) for both lower (RCP 4.5) and higher (RCP 8.5) scenarios.

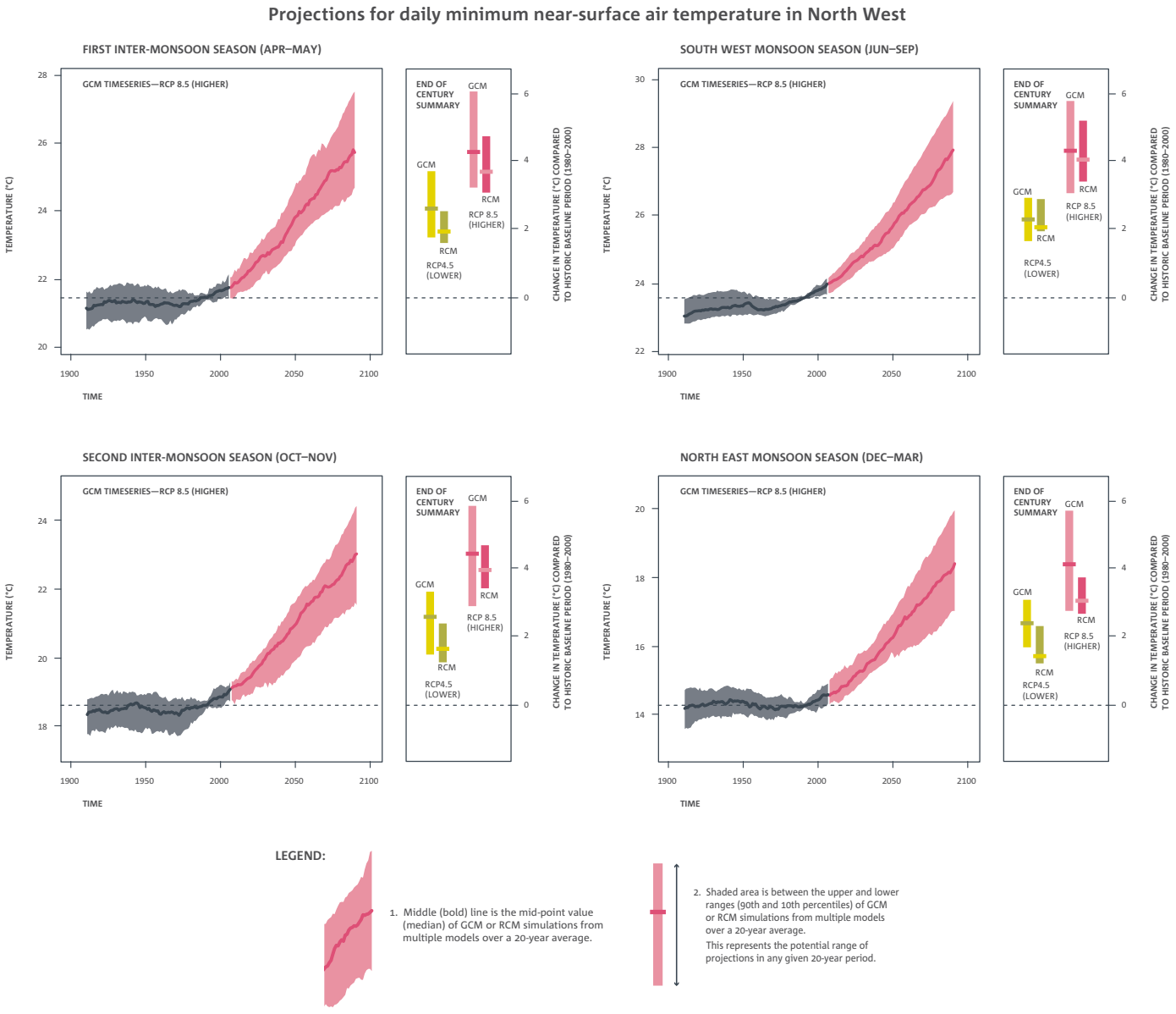

Rainfall

Projections for rainfall for the four seasons for this region from the CMIP5 GCMs are presented in Figure 9-11. There is large range of inter-annual variability simulated by the GCMs for rainfall for this region, as can be seen by the large spread of the colour bar. FIMS and NEMS show little change in projected rainfall by the end of the century. However, both SWMS and SIMS show increases in rainfall by the end of the century for both RCPs.

9.3.2 Regional model results

This section will discuss the projected changes in temperature and rainfall for the future compared with the present climate using ensemble means from eight regional model experiments (shown in Table 9-2 through Table 9-9). In general, these projections do not represent a value specific to any location, but average changes of annual and seasonal values for the North West region.

Figure 9-11: Regionally averaged seasonal precipitation changes (mm month^{-1} on left axis and % on right axis) for NW. For each season, the time series graph of projections by global climate models (GCM) is shown on the left for the higher (RCP 8.5) greenhouse gas scenario. Black line is from historical GCM runs, red line is the multi-model median projection from GCMs using RCP 8.5. Shadings are between 10% and 90% of 20-year mean values. GCM values have been corrected for 1995-2005 mean bias. Bars on the right for each season show the end-of-century summary of projections by global climate models (GCM, left) and regional climate models (RCM, right) for both lower (RCP 4.5) and higher (RCP 8.5) scenarios.

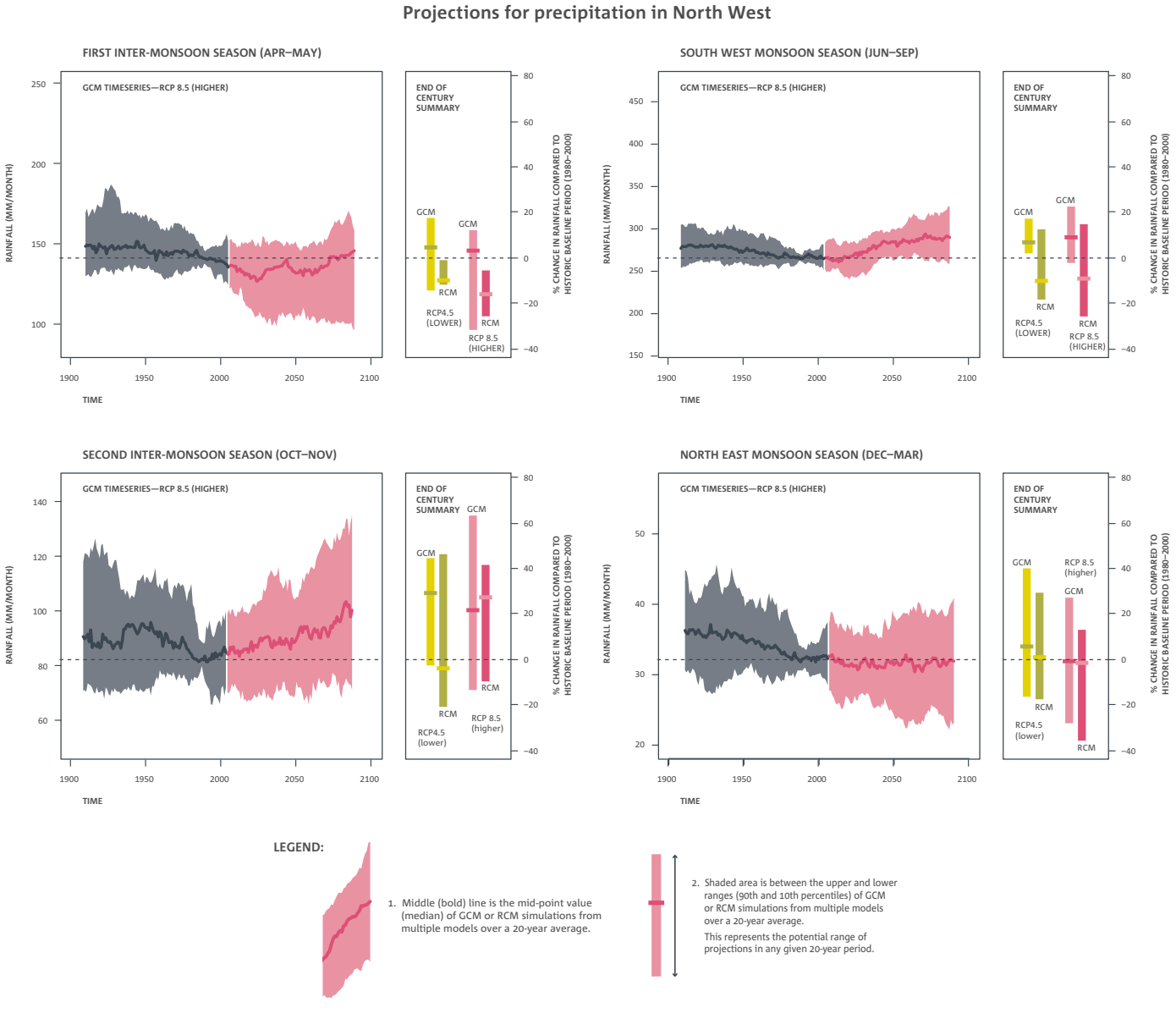

Surface temperature

Table 9-2 to Table 9-6 show projected changes in annual and seasonal surface air temperature (°C) relative to the baseline period 1980-2000 for RCP 8.5 by the middle and the end of the century. As mentioned above, these RCM projections represent an average change over the whole North West geographic region. The increases in annual mean (Tave), maximum (Tmax), and minimum (Tmin) temperatures are quite similar, about 1.9°C by 2045-2065 and 3.8°C by 2080-2100. The projected change in temperature in SWMS is higher than in the other seasons (multi-model mean of 4.4°C for Tave, 4.6°C for Tmax and 4.3°C for Tmin by the end of the century for RCP 8.5), while the temperature during NEMS has the smallest increase (multi-model mean of 3.1°C for Tave, 3.0°C for Tmax and 3.2°C for Tmin by the end of the century for RCP 8.5). The increase in minimum temperature is less than that for maximum temperature in SWMS and annually, resulting in an increase in the diurnal temperature range.

The increase in mean temperature of the multi-model mean is higher than the increase in previous climate projections (MONRE, 2012, see Table 9-3), which showed an annual increase of 2.9°C by the end of the century for the SRES A2 emission scenario. Larger increases are especially noted for SWMS. However, the PRECIS ensemble mean projections show greater warming than the new projections, even with a lower (A1B) emission scenario. Of the eight RCM models, CCAM GFDL-CM3 shows the largest increase and RegCM4.2 NorESM1-M shows the least increase compared with the other models (Table 9-4 to Table 9-6).

Table 9-2: Summary of the multi-model mean and range of projected changes in annual and seasonal average, maximum and minimum temperature (°C) for the NW region relative to the baseline period (1980-2000) for RCP 8.5. Green colouring is for increases less than 2°C, yellow from 2-4°C and orange greater than 4°C.

	MID-CENTURY (2045-2065)					END OF THE CENTURY (2080-2100)				
	ANNUAL	NEMS DEC-MAR	FIMS APR-MAY	SWMS JUNE-SEP	SIMS OCT-NOV	ANNUAL	NEMS DEC-MAR	FIMS APR-MAY	SWMS JUNE-SEP	SIMS OCT-NOV
Tave	1.9	1.6	1.9	2.2	1.9	3.8	3.1	3.9	4.4	4.0
(°C)	1.1 to 3.2	1.0 to 2.7	0.9 to 2.9	1.3 to 3.6	1.2 to 3.6	2.3 to 5.9	2.0 to 4.9	2.3 to 5.8	2.4 to 6.8	2.7 to 6.3
Tmax	1.9	1.5	1.8	2.2	2.1	3.9	3.0	3.9	4.6	4.0
(°C)	0.9 to 3.4	0.5 to 3.0	0.4 to 2.7	1.2 to 3.8	0.9 to 4.0	1.8 to 6.49	1.1 to 5.3	1.7 to 6.3	2.2 to 7.4	2.4 to 7.0
Tmin	1.9	1.7	2.0	2.2	1.8	3.8	3.2	3.9	4.3	4.0
(°C)	1.3 to 3.1	1.2 to 2.5	1.2 to 3.2	1.3 to 3.5	1.3 to 3.2	2.6 to 5.5	2.6 to 4.5	2.6 to 5.5	2.6 to 6.3	2.8 to 5.7

Table 9-3: Projected changes in annual and seasonal mean temperature (°C) for the NW region relative to the baseline period (1980-2000) under different SRES emission scenarios (B1, B2, A2, A1B) from a previous study (MONRE, 2012) and the latest PRECIS projections (ensemble means). Green colouring is for increases less than 2°C, yellow from 2-4°C and orange greater than 4°C. Source: IMHEN.

TAVE (°C)	MID-CENTURY (2045-2065)					END OF THE CENTURY (2080-2100)				
	ANNUAL	NEMS DEC-MAR	FIMS APR-MAY	SWMS JUNE-SEP	SIMS OCT-NOV	ANNUAL	NEMS DEC-MAR	FIMS APR-MAY	SWMS JUNE-SEP	SIMS OCT-NOV
	MONRE 2012					MONRE 2012				
B1	1.4	1.5	1.5	1.1	1.4	1.7	1.9	1.9	1.4	1.7
B2	1.5	1.7	1.6	1.3	1.5	2.4	2.7	2.6	2.0	2.4
A2	1.6	1.8	1.7	1.3	1.6	2.9	3.2	3.1	2.4	2.9
	PRECIS					PRECIS				
A1B	2.6	2.8	2.6	2.3	2.5	4.0	4.3	4.0	3.7	4.0

Table 9-4: Projected changes in annual and seasonal average temperature by model (°C) for the NW region relative to the baseline period (1980-2000) for RCP 8.5 from eight RCM experiments. Green colouring is for increases less than 2°C, yellow from 2-4°C and orange greater than 4°C.

TAVE (°C)	MID-CENTURY (2045-2065)					END OF THE CENTURY (2080-2100)				
	ANNUAL	NEMS DEC-MAR	FIMS APR-MAY	SWMS JUNE-SEP	SIMS OCT-NOV	ANNUAL	NEMS DEC-MAR	FIMS APR-MAY	SWMS JUNE-SEP	SIMS OCT-NOV
Multi-model mean	1.9	1.6	1.9	2.2	1.9	3.8	3.1	3.9	4.4	4.0
	Individual RCM simulations					**Individual RCM simulations**				
CCAM ACCESS1.0	1.7	1.2	2.1	2.2	1.4	3.9	3.1	4.0	4.7	3.7
CCAM NorESM1-M	2.0	1.9	1.7	2.2	1.9	3.8	3.2	3.5	4.5	3.9
CCAM MPI-ESM-LR	1.7	1.3	2.2	2.0	1.2	3.6	2.7	4.3	4.4	3.3
CCAM CCSM4	1.7	1.4	1.6	2.2	1.8	3.6	2.9	3.3	4.4	3.9
CCAM CNRM-CM5	1.8	1.7	1.7	2.0	2.0	3.8	3.0	4.0	4.2	4.3
CCAM GFDL-CM3	3.2	2.7	2.9	3.6	3.6	5.9	4.9	5.8	6.8	6.3
RegCM4.2 ACCESS1.0	2.0	1.5	2.2	2.3	2.3	3.6	3.1	3.7	3.8	4.0
RegCM4.2 NorESM1-M	1.1	1.0	0.9	1.3	1.4	2.3	2.0	2.3	2.4	2.7

	Indicates a range of low results	< 2.0°C
	Indicates a range of medium results	2.0 to 4.0°C
	Indicates a range of high results	> 4.0°C

Table 9-5: Projected changes in annual and seasonal maximum temperature by model (°C) for the NW region relative to the baseline period (1980-2000) for RCP 8.5 from eight RCM experiments. Green colouring is for increases less than 2°C, yellow from 2-4°C and orange greater than 4°C.

TMAX (°C)	MID-CENTURY (2045-2065)					END OF THE CENTURY (2080-2100)				
	ANNUAL	NEMS DEC-MAR	FIMS APR-MAY	SWMS JUNE-SEP	SIMS OCT-NOV	ANNUAL	NEMS DEC-MAR	FIMS APR-MAY	SWMS JUNE-SEP	SIMS OCT-NOV
Multi-model mean	1.9	1.5	1.8	2.2	2.1	3.9	3.0	3.9	4.6	4.0
	Individual RCM simulations					**Individual RCM simulations**				
CCAM ACCESS1.0	1.5	0.9	2.0	1.9	1.2	3.7	2.9	4.1	4.7	3.1
CCAM NorESM1-M	2.0	1.9	1.7	2.3	1.9	3.9	3.1	3.4	5.0	3.8
CCAM MPI-ESM-LR	1.6	1.2	2.2	1.9	0.9	3.5	2.6	4.2	4.3	3.0
CCAM CCSM4	1.9	1.3	1.5	2.4	2.2	3.8	2.8	3.4	5.1	3.9
CCAM CNRM-CM5	1.9	1.7	1.7	2.0	2.2	4.0	3.0	4.3	4.5	4.8
CCAM GFDL-CM3	3.4	3.0	2.7	3.8	4.0	6.4	5.3	6.3	7.4	7.0
RegCM4.2 ACCESS1.0	2.1	1.6	2.4	2.3	2.6	3.7	3.2	4.0	3.8	4.0
RegCM4.2 NorESM1-M	0.9	0.5	0.4	1.2	1.4	1.8	1.1	1.7	2.2	2.4

	Indicates a range of low results	< 2.0°C
	Indicates a range of medium results	2.0 to 4.0°C
	Indicates a range of high results	> 4.0°C

Table 9-6: Projected changes in annual and seasonal minimum temperature by model (°C) for the NW region relative to the baseline period (1980-2000) for RCP 8.5 from eight RCM experiments. Green colouring is for increases less than 2°C, yellow from 2-4°C and orange greater than 4°C.

TMIN (°C)	MID-CENTURY (2045-2065)					END OF THE CENTURY (2080-2100)				
	ANNUAL	NEMS DEC-MAR	FIMS APR-MAY	SWMS JUNE-SEP	SIMS OCT-NOV	ANNUAL	NEMS DEC-MAR	FIMS APR-MAY	SWMS JUNE-SEP	SIMS OCT-NOV
Multi-model mean	1.9	1.7	2.0	2.2	1.8	3.8	3.2	3.9	4.3	4.0
	Individual RCM simulations					**Individual RCM simulations**				
CCAM ACCESS1.0	2.0	1.5	2.2	2.5	1.5	4.1	3.4	4.1	4.7	4.2
CCAM NorESM1-M	2.0	2.0	1.9	2.1	1.9	3.8	3.4	3.7	4.1	4.2
CCAM MPI-ESM-LR	1.8	1.5	2.3	2.1	1.5	3.8	2.9	4.4	4.5	3.7
CCAM CCSM4	1.7	1.5	1.7	2.1	1.4	3.5	3.0	3.3	4.0	4.0
CCAM CNRM-CM5	1.8	1.8	1.8	2.0	1.8	3.6	3.0	3.7	4.0	3.9
CCAM GFDL-CM3	3.1	2.5	3.2	3.5	3.2	5.5	4.5	5.5	6.3	5.7
RegCM4.2 ACCESS1.0	1.9	1.3	2.0	2.2	2.1	3.4	2.7	3.5	3.8	3.9
RegCM4.2 NorESM1-M	1.3	1.2	1.2	1.3	1.3	2.6	2.6	2.6	2.6	2.8

	Indicates a range of low results	< 2.0°C
	Indicates a range of medium results	2.0 to 4.0°C
	Indicates a range of high results	> 4.0°C

Rainfall

The rainfall changes are more complex, with the models simulating both increases and decreases (Table 9-7). Therefore, there is large uncertainty associated with the rainfall change. In general, the majority of RCMs simulate little change (-10% to 10%) in annual rainfall by mid-century (see Table 9-9). However, by the end of the century, all models project decreases during FIMS, although the multi-model mean is only -16%. For SIMS, 6 out of 8 models project increases, with a multi-model mean of +21%. These results suggest greater confidence in these seasonal changes. The CCAM GFDL-CM3 simulation shows the largest decline (-41% for NEMS at the end of the century), while CCAM CCSM4 shows the greatest increase in rainfall (+59% for SIMS at the end of the century).

A comparison between the present and previous climate change projections (MONRE, 2012, Table 9-8) shows no similar changes, but most changes are relatively small and not significant. The largest difference in projected changes is for SIMS, where the previous projections showed little change, but the new projections show significant increases. Interestingly, the PRECIS ensemble mean shows increases for this region for all seasons, with generally greater changes compared with other projections.

Table 9-7: Projected changes in annual and seasonal mean rainfall and its ranges (%) for the NW region relative to the baseline period (1980-2000) for RCP 8.5. Changes are the multi-model means from eight simulations. Orange colouring is for decreases less than -10%, green for changes between -10% to +10% and blue for increases greater than +10%.

RAIN	MID-CENTURY (2045-2065)					END OF THE CENTURY (2080-2100)				
% CHANGE	ANNUAL	NEMS DEC-MAR	FIMS APR-MAY	SWMS JUNE-SEP	SIMS OCT-NOV	ANNUAL	NEMS DEC-MAR	FIMS APR-MAY	SWMS JUNE-SEP	SIMS OCT-NOV
Multi-model mean	-3	8	-4	-4	-7	-9	-5	-16	-8	21
Range	-10 to +3	-26 to +19	-18 to +16	-15 to +10	-28 to +13	-22 to +10	-41 to +23	-31 to -2	-35 to +16	-10 to +59

Table 9-8: Projected changes in annual and seasonal rainfall (%) for the NW region relative to the baseline period (1980-2000) for SRES emission scenarios (B1, B2, A2, A1B) from a previous study (MONRE, 2012) and the latest PRECIS projections (ensemble means). Orange colouring is for decreases less than -10%, green for changes between -10% to +10% and blue for increases greater than +10%. Source: IMHEN.

RAIN	MID-CENTURY (2045-2065)					END OF THE CENTURY (2080-2100)				
% CHANGE	ANNUAL	NEMS DEC-MAR	FIMS APR-MAY	SWMS JUNE-SEP	SIMS OCT-NOV	ANNUAL	NEMS DEC-MAR	FIMS APR-MAY	SWMS JUNE-SEP	SIMS OCT-NOV
	MONRE 2012					MONRE 2012				
B1	3	-4	0	5	0	4	-5	1	6	-1
B2	3	-4	1	5	-1	5	-7	1	8	-1
A2	3	-4	1	5	-1	6	-8	1	10	-1
	PRECIS					PRECIS				
A1B	14	11	9	15	24	19	10	12	22	32

Table 9-9: Projected changes in annual and seasonal mean rainfall by model (%) for the NW region relative to the baseline period (1980-2000) for RCP 8.5 from the eight RCMs. Orange colouring is for decreases less than -10%, green for changes between -10% to +10% and blue for increases greater than +10%.

RAIN (%)	MID-CENTURY (2045-2065)					END OF THE CENTURY (2080-2100)				
	ANNUAL	NEMS DEC-MAR	FIMS APR-MAY	SWMS JUNE-SEP	SIMS OCT-NOV	ANNUAL	NEMS DEC-MAR	FIMS APR-MAY	SWMS JUNE-SEP	SIMS OCT-NOV
Multi-model mean	-3	8	-4	-4	-7	-9	-5	-16	-8	21
	Individual RCM simulations					Individual RCM simulations				
CCAM ACCESS1.0	-3	19	7	-12	3	-6	-1	-7	-7	25
CCAM NorESM1-M	-5	9	-5	-7	-28	-21	-34	-16	-22	-10
CCAM MPI-ESM-LR	-5	1	-16	1	1	-10	7	-24	-5	34
CCAM CCSM4	-10	19	-10	-15	13	-22	23	-15	-35	59
CCAM CNRM-CM5	-6	14	-18	-2	-8	-17	-5	-31	-11	30
CCAM GFDL-CM3	-2	-26	16	-6	-9	-16	-41	-14	-12	-9
RegCM4.2 ACCESS1.0	3	10	-13	10	-23	6	-2	-16	14	35
RegCM4.2 NorESM1-M	2	17	4	0	-2	10	9	-2	16	8

	Indicates a range of low (drier) results	< -10%
	Indicates a range of medium (little change) results	-10 to +10%
	Indicates a range of high (wetter) results	> 10%

9.4 SUMMARY

An analysis of observed records for the NW region shows a significant increasing trend for temperature, while rainfall shows a slight decreasing trend of less than 2.5% per decade, which is not statistically significant. The maximum temperature has increased faster than minimum temperature, but this is not statistically significant. The extreme rainfall indices do not reveal any clear significant trend.

The climate projections based on eight RCM experiments downscaled from the CMIP5 GCMs for RCP 8.5 clearly indicate that the North West region is projected to be warmer in the future. Annual mean surface temperature is projected to increase by 1.9°C by mid-century and by 3.8°C by the end of the century. The end-of-century warming is greatest in SWMS (4.4°C) and least in NEMS (3.1°C). These changes are greater than in the previous projections (MONRE, 2012).

Rainfall projections in the North West region show large uncertainty, with the models simulating both increases and decreases for the future. In general, the majority of RCMs simulate little change (-10% to 10%) in annual rainfall by mid-century and the end of the century for most of the seasons. The most consistent rainfall change simulated by the models by the end of the century is a multi-model mean rainfall decrease of -16% in FIMS (all models project a decrease) and an increase of 21% in SIMS (6 out of 8 models project an increase). Changes in rainfall for other seasons generally show decreases, but are less certain.

10 NORTH EAST REGIONAL REPORT

This chapter summarises the current climate and its trends for the North East region of Vietnam (see Figure 10-1). The projected changes of temperature and rainfall by mid-century and the end of the century are then presented, first from the GCM results, then from the RCM results. The key messages are summarised at the end of the chapter.

10.1 DESCRIPTION

The North East (NE) region of Vietnam includes the northeast and the middle of northern Vietnam areas (Figure 10-1). Hills and valleys alternate in the NE region, with elevations of lower than 500 m, except for the terrain in the north, which has elevations of more than 600-700 m. The Dong Van and Trung Khanh Rocky Mountains and the Ngan Son Range have peaks of over 1000 m in height. The middle portion of North Vietnam has more complex terrain, with mountains alternating with river valleys. The mountain range in the upstream area of the northern Chay River has an elevation between 1000-1500 m. Despite some variations in terrain conditions between the north-eastern and the middle parts of this region, the seasonal cycles of temperature, rainfall, humidity, and sunshine are similar across the region.

Long-term climatological means and ranges of important variables for this region are given in Table 10-1. The climates of Lao Cai, Yen Bai, Ha Giang, Tuyen Quang, Cao Bang, Lang Son, Bac Kan, Thai Nguyen, and Quang Ninh provinces are similar, having elevations between 50-500 m. This region is strongly affected by the North East Monsoon and tropical cyclones, more than the other northern regions. There are many cold, cloudy, and drizzly days, with hoarfrost in winter. The rainy season lasts from May to September, with rainfall maxima in August. This rainy season coincides with the South West (summer) Monsoon season. Rainfall is produced by a combination of storm activities associated with the summer monsoon and convergence within the ITCZ.

10.2 OBSERVED CLIMATE

Observed climate trends are analysed using daily data from 70 meteorological stations in Vietnam for the period 1961 to 2011. In addition to trends of mean surface air temperature (or T2m) and precipitation, trends of some extreme indices are also discussed. Definitions of selected extreme indices can be found in ETCCDI (2009), which recommends 27 core Extreme Climate Indices (ECIs) based on daily temperature values or daily precipitation amounts. The indices below are used in this study, mostly following the ETCCDI computational procedures:

- **RX1**: yearly maximum 1-day precipitation (mm).
- **RX5**: annual highest consecutive five-day precipitation amount (mm).
- **R95p**: annual count of days when precipitation exceeds the 95th percentile value for the period 1961-2011.
- **TN10p**: annual count of days when minimum daily temperature is less than the 10th percentile temperature for the period 1961-2011.
- **TX90p**: annual count of days when maximum daily temperature exceeds the 90th percentile temperature for the period 1961-2011.
- **CDD**: consecutive dry days; average annual maximum number of days with daily rainfall less than 1 mm.
- **CWD**: consecutive wet days; average annual maximum number of days with daily rainfall greater than or equal to 1 mm.
- **Hot days**: days with Tmax greater than 35°C.
- **Cold days**: days with Tmin less than 15°C.

Figure 10-1: The North East region with provinces. Insert shows location of region in Vietnam.

Table 10-1: Observed climate variables and ranges for the NE region. Nguyen and Nguyen (2004).

CLIMATE VARIABLE	VALUE
Terrain height	50 to 500 m
Annual average solar radiation	105 to 130 kcal cm^{-2}
Radiation balance	60 to 70 kcal cm^{-2}
Annual sunshine hours	1400 to 1800 h
Annual average temperature	18 to 23°C
Maximum temperature	38 to 41°C
Minimum temperature	-2 to 2°C
Annual temperature amplitude	12 to 14°C
Annual average rainfall	1400 to 2000 mm
Number of drizzle days	10 to 40 days
Daily maximum rainfall	150 to 500 mm
Rainfall season	May to Sep
Humidity	82 to 88%
Annual evaporation	600 to 1000 mm
Annual average wind speed	0.8 to 1.5 m sec^{-1}
Maximum wind speed	30 to 40 m sec^{-1}

Trends are calculated at stations within the region. The statistical significance of the trends is computed using the non-parametric Mann-Kendall test (Kendall, 1975). In this report, trends with significance levels more than 90% are considered as statistically significant.

10.2.1 Temperature

There has been a significant increase in annual surface air temperature in this region of approximately 0.2°C per decade (Figure 10-2). The highest rate of increase of 0.25°C per decade was observed at Tam Dao station, whereas the lowest rate of increase of 0.02°C per decade was found at Sa Pa station.

The time series of the regionally-averaged annual temperature (Figure 10-3) shows the warming trend, with some year-to-year variations. The warming was about 1°C during the past 50 years, which is about 0.2°C per decade, similar to what was noted above.

10.2.2 Rainfall

Rainfall in this region shows a decreasing trend of up to approximately -6.5% per decade (Figure 10-4) except for the COTO station (off the coast), where a non-significant increasing rainfall trend of approximately 1% per decade was noticed. The trends are more pronounced in the southern part of the region (with some significant decreases) compared with those in the north-west and east portions of this region.

The time series of annual rainfall of the region (Figure 10-5) shows a slight decreasing trend with weak inter-annual variations, with annual values ranging from about 5 mm day^{-1} to 8 mm day^{-1}. The trend in rainfall for this region is small compared with the variability and hence is not statistically significant, as noted above.

Figure 10-2: Trend in annual surface air temperature (°C per decade) in the North East (NE) region for the period 1961 to 2011. A blue circle indicates a decreasing trend and a red circle shows an increasing trend. A filled circle means that the trend is statistically significant at the 90% confidence level.

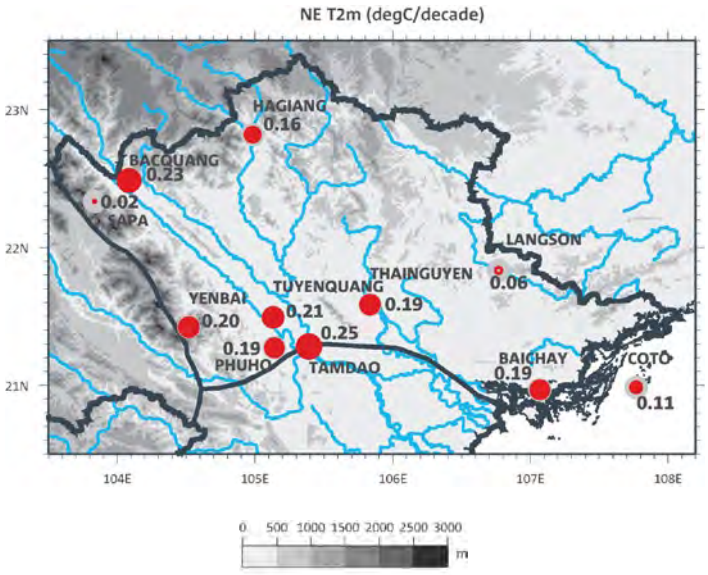

Figure 10-4: Trends in annual rainfall (% per decade) in the NE region for the period 1961 to 2011. A blue circle indicates an increasing trend and a red circle shows a decreasing trend. A filled circle means that the trend is significant at the 90% confidence level.

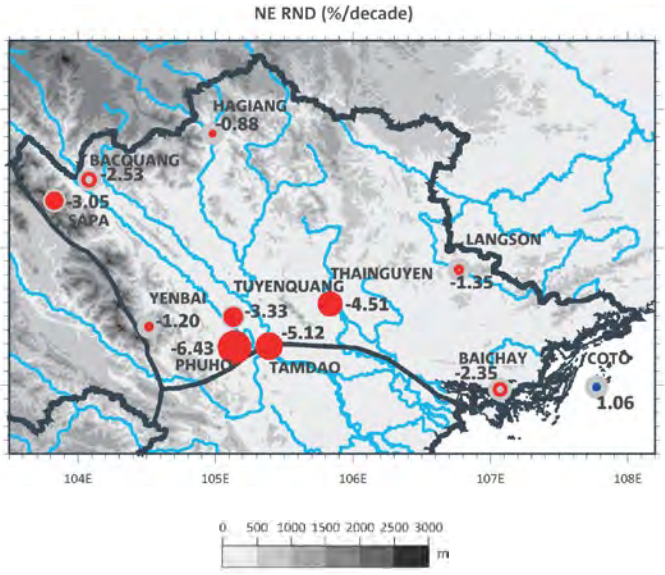

Figure 10-3: Time series of regionally-averaged annual surface air temperature (°C, red) for the NE region with a trend line (dashed). Annual values are shown by black dots.

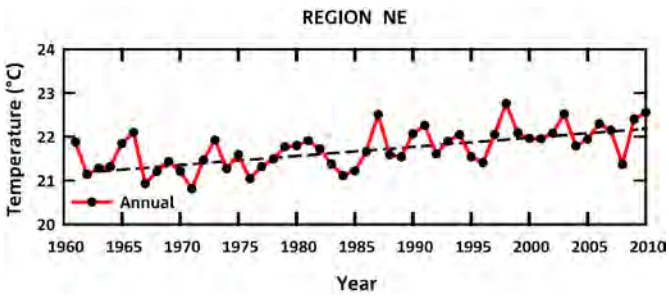

Figure 10-5: Time series of regionally-averaged annual rainfall (mm day^{-1}, blue) for the NE region with a trend line (black dashed line). Annual values are shown by black dots.

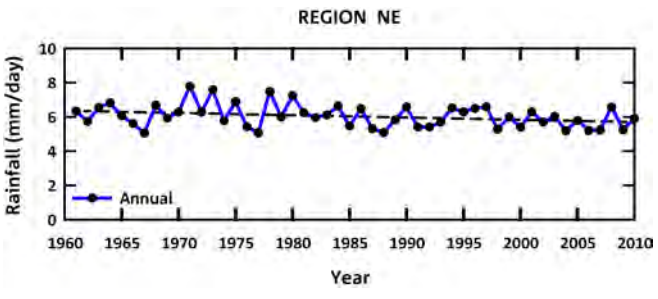

10.2.3 Extremes

Maximum (Tmax) and minimum (Tmin) daily temperatures have increased significantly during the period 1961 to 2011 in the NE region, as shown in Figure 10-6. Tmax has increased by approximately 0.02 to 0.21°C per decade while Tmin has increased by approximately 0.04 to 0.26°C per decade. It should be noted that Tmin shows stronger increase than Tmax, which results in a decline in the diurnal temperature range (DTR) during the past 50 years.

The increase in maximum daily temperature has led to a significant rise in TX90p, whereas the increase in minimum daily temperature has led to a significant decrease in TN10p. The number of extreme hot days has increased significantly by up to approximately 6 days per decade. The number of extreme cold nights has decreased significantly by up to -5 days per decade.

Similar to the annual rainfall trend, annual maximum daily rainfall (RX1) exhibits a weak negative but not statistically significant trend in the region, except for Phu Ho station, where RX1 shows a -6% decline per decade during the past 50 years (Figure 10-7). Trends in RX5 show similar behavior to RX1, except for Sa Pa and Tam Dao stations, which show statistically significant decreases of approximately -4.85% and -5.6% per decade, respectively. R95p and CWD do not show remarkable trends at stations in this region, except for Tam Dao and Phu Ho stations. CDD has a slight but significant increasing trend of up to approximately 2.5% per decade over the NE region.

Figure 10-6: Trends in Tmax (upper left), Tmin (upper right), TX90p (lower left), and TN10p (lower right) in the NE region for the period 1961 to 2011. A blue circle indicates a decreasing and a red circle shows an increasing trend. A filled circle means that the trend is significant at the 90% confidence level.

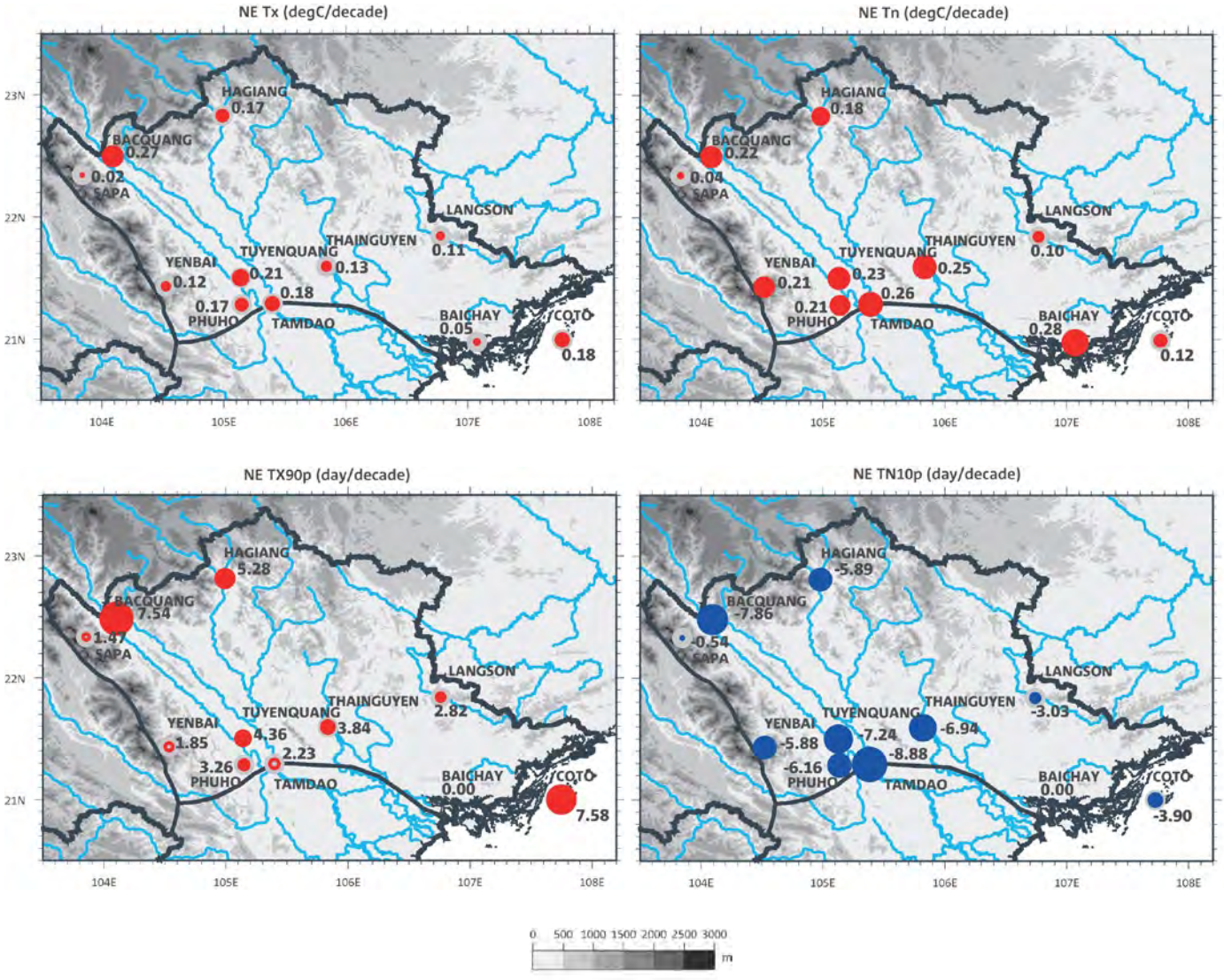

Figure 10-7: Trends in RX1, RX5, R95p, CWD, and CDD in the NE region for the period 1961 to 2011. A blue circle indicates an increasing and a red circle shows a decreasing trend for all but CDD, where red indicates an increasing and blue a decreasing number of days. A filled circle means that the trend is significant at the 90% confidence level.

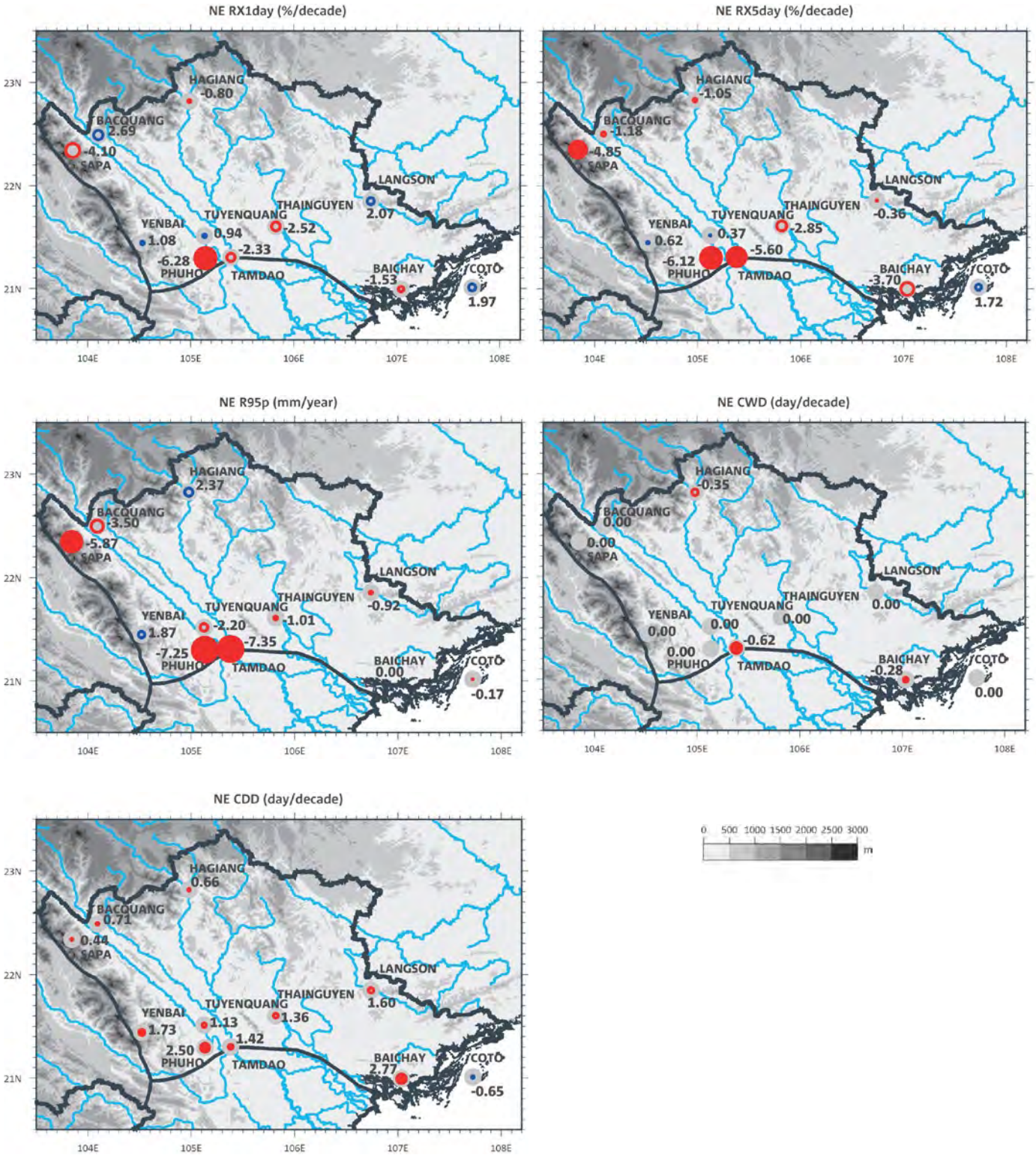

10.3 CLIMATE PROJECTIONS

In this section, projected changes in temperature and rainfall for this region are presented. A summary of the CMIP5 GCM results for different RCPs for this region is first presented in the form of line graphs. This is followed by the changes projected by regional climate models, both from the new experiments completed for this project and from the results used for the last official climate change projections completed by IMHEN (using the previous CMIP3 SRES emission scenarios). This provides some indication of the differences of the projections, though direct comparison is difficult, since different models and different scenarios were used.

10.3.1 GCM results

Surface temperature

Projections for near-surface average temperature for the four seasons for this region from the CMIP5 GCMs are presented in Figure 10-8. The warming signal is very clear, with the greatest warming for RCP 8.5 and the least warming for RCP 4.5. There is also slightly greater warming (as measured by the median value, line inside colour bar) during FIMS by the end of the century for RCP 8.5, with warming of about 4.2°C, while the other seasons show an increase of about 4°C by the end of the century.

Figure 10-8: Regionally averaged seasonal surface air temperature changes (°C) for NE. For each season, the time series graph of projections by global climate models (GCM) is shown on the left for the higher (RCP 8.5) greenhouse gas scenario. Black line is from historical GCM runs, red line is the multi-model median projection from GCMs using RCP 8.5. Shadings are between 10% and 90% of 20-year mean values. GCM values have been corrected for 1995-2005 mean bias. Bars on the right for each season show the end-of-century summary of projections by global climate models (GCM, left) and regional climate models (RCM, right) for both lower (RCP 4.5) and higher (RCP 8.5) scenarios.

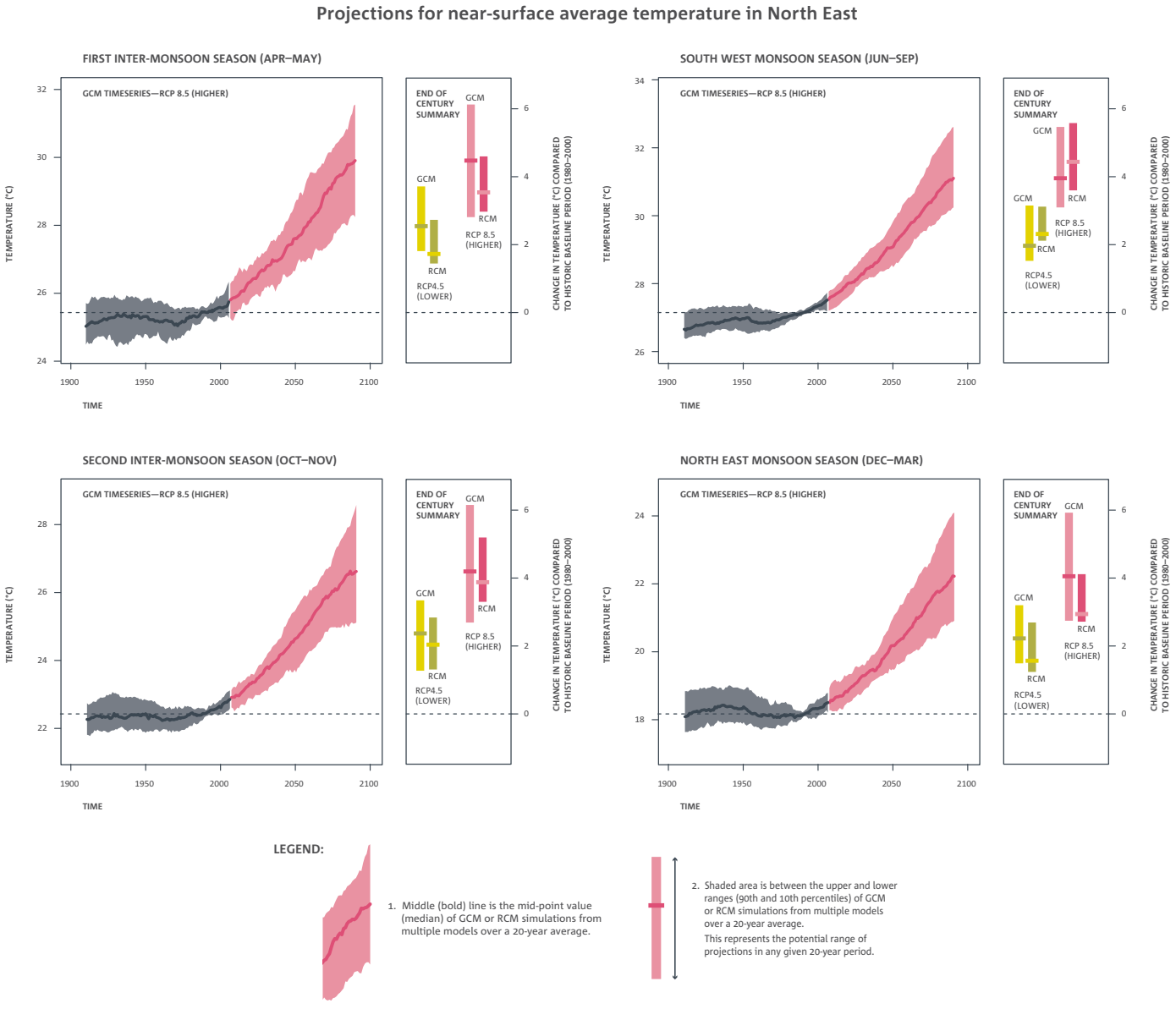

Projections for near-surface maximum temperature for the four seasons for this region from the CMIP5 GCMs are presented in Figure 10-9. Again, the warming signal is very clear and similar to the average temperature. However, there is slightly greater warming during FIMS and SWMS by the end of the century for RCP 8.5 (more than 4°C), while other seasons show increases of around 4°C by the end of the century.

Projections for near-surface minimum temperature for the four seasons for this region from the CMIP5 GCMs are presented in Figure 10-10. The warming signal is very clear and similar to the average temperature. Moreover, the warming of more than 4°C is similar for all seasons by the end of the century for RCP 8.5.

Figure 10-9: Regionally averaged seasonal maximum air temperature changes (°C) for NE. For each season, the time series graph of projections by global climate models (GCM) is shown on the left for the higher (RCP 8.5) greenhouse gas scenario. Black line is from historical GCM runs, red line is the multi-model median projection from GCMs using RCP 8.5. Shadings are between 10% and 90% of 20-year mean values. GCM values have been corrected for 1995-2005 mean bias. Bars on the right for each season show the end-of-century summary of projections by global climate models (GCM, left) and regional climate models (RCM, right) for both lower (RCP 4.5) and higher (RCP 8.5) scenarios.

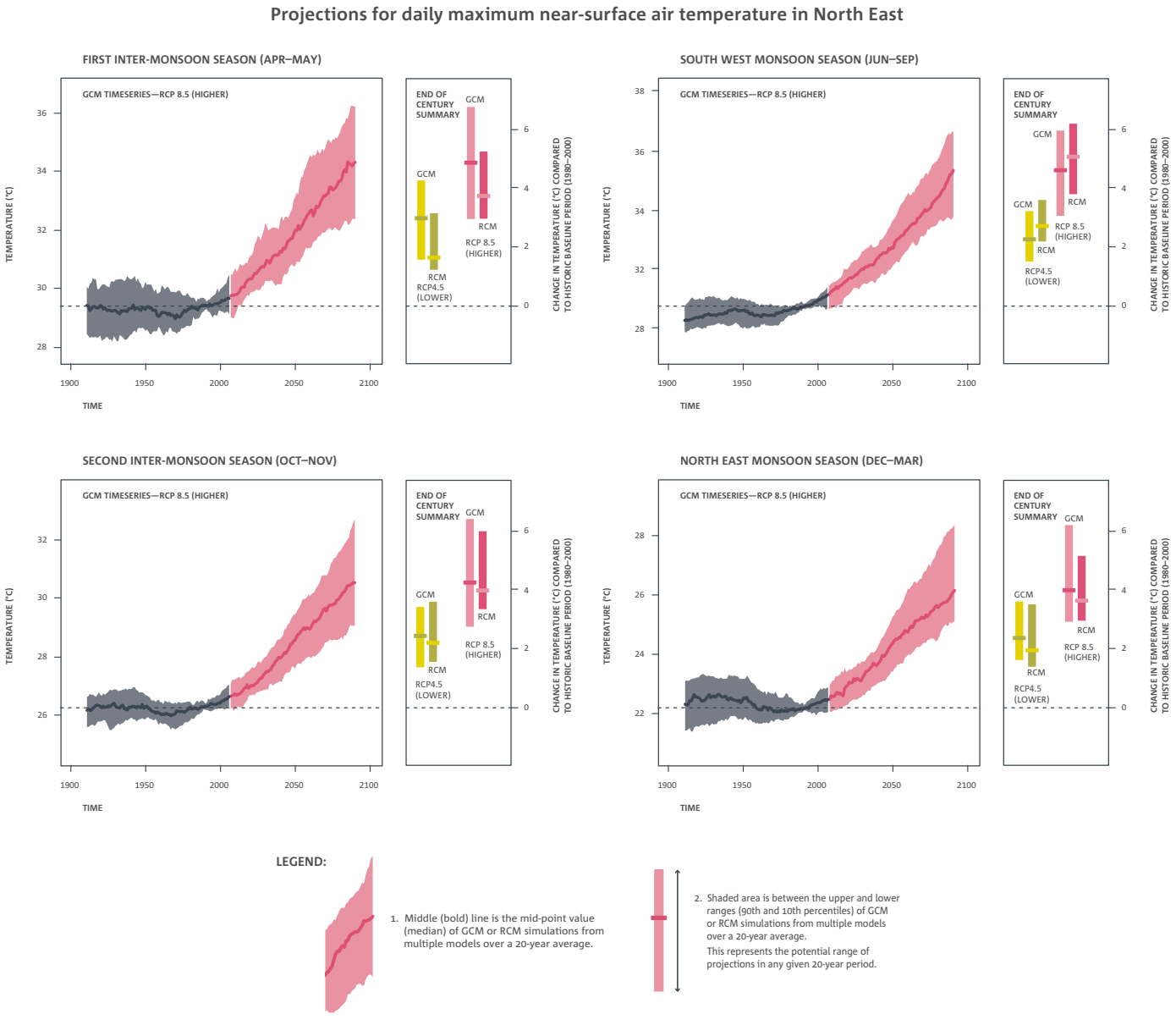

Figure 10-10: Regionally averaged seasonal minimum air temperature changes (°C) for NE. For each season, the time series graph of projections by global climate models (GCM) is shown on the left for the higher (RCP 8.5) greenhouse gas scenario. Black line is from historical GCM runs, red line is the multi-model median projection from GCMs using RCP 8.5. Shadings are between 10% and 90% of 20-year mean values. GCM values have been corrected for 1995-2005 mean bias. Bars on the right for each season show the end-of-century summary of projections by global climate models (GCM, left) and regional climate models (RCM, right) for both lower (RCP 4.5) and higher (RCP 8.5) scenarios.

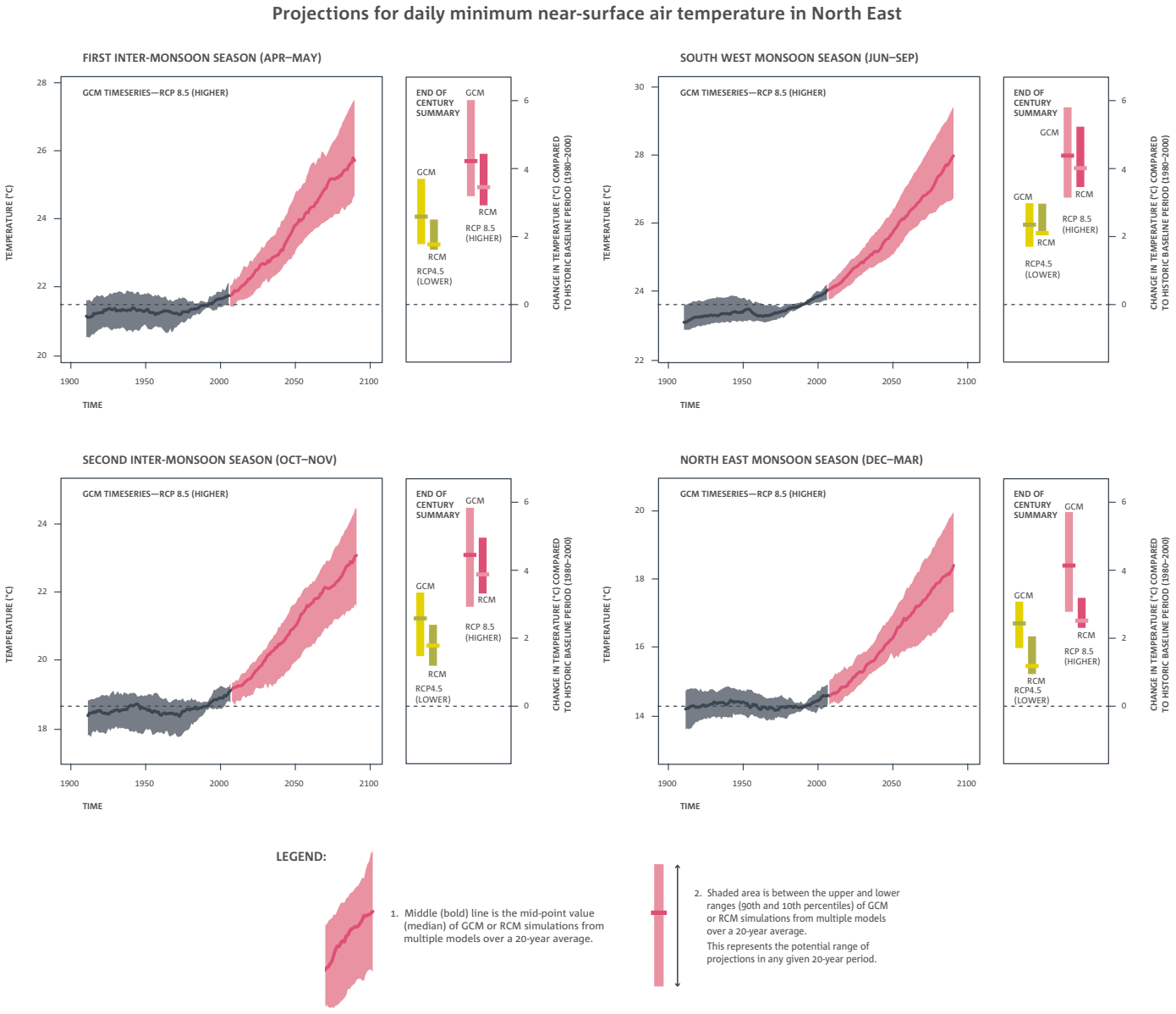

Rainfall

Projections for rainfall for the four seasons for this region from the CMIP5 GCMs are presented in Figure 10-11. There is a large range of inter-annual variability simulated by the GCMs for rainfall for this region, as can be seen by the large spread of the colour bar. FIMS and NEMS show little change in rainfall by the end of the century. However, both SWMS and SIMS show increases in rainfall by the end of the century for all RCPs, with the greatest increases for the higher emission scenario.

10.3.2 Regional model results

This section will discuss the projected changes in climate for the future compared with the present climate using RCM ensemble means from eight experiments, as shown in Table 10-2. In general, these projections do not represent a value specific to any location, since average changes of annual and seasonal values are given for the NE region.

Figure 10-11: Regionally averaged seasonal precipitation changes (mm month^{-1} on left axis and % on right axis) for NE. For each season, the time series graph of projections by global climate models (GCM) is shown on the left for the higher (RCP 8.5) greenhouse gas scenario. Black line is from historical GCM runs, red line is the multi-model median projection from GCMs using RCP 8.5. Shadings are between 10% and 90% of 20-year mean values. GCM values have been corrected for 1995-2005 mean bias. Bars on the right for each season show the end-of-century summary of projections by global climate models (GCM, left) and regional climate models (RCM, right) for both lower (RCP 4.5) and higher (RCP 8.5) scenarios.

Surface temperature

Table 10-2 to Table 10-6 show projected changes in annual and seasonal surface air temperature (°C) relative to the baseline period (1980-2000) for RCP 8.5 by the middle and the end of the century. As mentioned above, these projections represent an average change over the whole NE geographic region.

The increase in annual mean temperature (Tave) is 2.0°C by 2045-2065 and 3.9°C by 2080-2100. The maximum temperature (Tmax) increases faster than the minimum temperature (Tmin), resulting in an increase in the annual mean diurnal temperature range. The projected change in temperature in SWMS is higher compared with other seasons (the multi-model mean is 4.6°C for Tave, 5.1°C for Tmax and 4.2°C for Tmin by the end of the century for RCP 8.5), while the temperature during NEMS has the smallest increase (3.2°C for Tave, 3.9°C for Tmax and 2.7°C for Tmin by end of century for RCP 8.5).

The increase in mean temperature projected by the multi-model mean is higher than in previous climate projections (MONRE, 2012, see Table 10-3), which projected an increase of 2.8°C in annual temperature by the end of the century for the SRES A2 emission scenario and only 2.5°C for SWMS. However, the PRECIS ensemble mean projections show greater warming than the values derived from the CMIP5 simulations, even for lower emission scenarios. Of the eight high-resolution RCM projections produced in this project, CCAM GFDL-CM3 shows the largest increase and RegCM4.2 NorESM1-M shows the least increase compared with the other models (Table 10-4 to Table 10-6).

Table 10-2: Summary of the multi-model mean and range of projected changes in annual and seasonal average, maximum and minimum temperature (°C) for the NE region relative to the baseline period (1980-2000) for RCP 8.5. Green colouring is for increases less than 2°C, yellow from 2-4°C and orange greater than 4°C.

	MID-CENTURY (2045-2065)					END OF THE CENTURY (2080-2100)				
	ANNUAL	NEMS DEC-MAR	FIMS APR-MAY	SWMS JUNE-SEP	SIMS OCT-NOV	ANNUAL	NEMS DEC-MAR	FIMS APR-MAY	SWMS JUNE-SEP	SIMS OCT-NOV
Tave	2.0	1.7	1.8	2.3	2.1	3.9	3.2	3.7	4.6	4.2
(°C)	1.3 to 3.4	1.2 to 2.8	1.2 to 3.1	1.4 to 3.9	1.2 to 3.8	2.5 to 6.1	2.5 to 5.0	2.6 to 5.8	2.4 to 7.1	2.9 to 6.8
Tmax	2.2	2.0	1.8	2.4	2.3	4.4	3.9	4.0	5.1	4.4
(°C)	1.3 to 4.1	1.2 to 3.9	0.8 to 3.4	1.4 to 4.4	1.0 to 4.6	2.3 to 7.5	2.3 to 6.6	2.3 to 7.1	2.2 to 8.3	2.7 to 7.9
Tmin	1.8	1.4	1.9	2.2	1.9	3.5	2.7	3.6	4.2	4.0
(°C)	1.3 to 2.8	1.0 to 1.8	1.4 to 3.0	1.3 to 3.5	1.3 to 3.3	2.6 to 5.1	2.2 to 3.7	2.7 to 5.0	2.5 to 6.3	2.9 to 5.9

Table 10-3: Projected changes in annual and seasonal mean temperature (°C) for the NE region relative to the baseline period (1980-2000) under different SRES emission scenarios (B1, B2, A2, A1B) from a previous study (MONRE, 2012) and the latest PRECIS projections (ensemble means). Green colouring is for increases less than 2°C, yellow from 2-4°C and orange greater than 4°C. Source: IMHEN.

TAVE (°C)	MID-CENTURY (2045-2065)					END OF THE CENTURY (2080-2100)				
	ANNUAL	NEMS DEC-MAR	FIMS APR-MAY	SWMS JUNE-SEP	SIMS OCT-NOV	ANNUAL	NEMS DEC-MAR	FIMS APR-MAY	SWMS JUNE-SEP	SIMS OCT-NOV
	MONRE 2012					MONRE 2012				
B1	1.3	1.4	1.4	1.2	1.3	1.7	1.8	1.7	1.5	1.7
B2	1.5	1.6	1.5	1.3	1.5	2.3	2.5	2.5	2.1	2.3
A2	1.5	1.6	1.6	1.4	1.5	2.8	3.0	2.9	2.5	2.8
	PRECIS					PRECIS				
A1B	2.6	2.9	2.6	2.4	2.6	4.0	4.2	4.0	3.8	4.0

Table 10-4: Projected changes in annual and seasonal average temperature by model (°C) for the NE region relative to the baseline period (1980-2000) for RCP 8.5 from eight RCM experiments. Green colouring is for increases less than 2°C, yellow from 2-4°C and orange greater than 4°C.

TAVE (°C)	MID-CENTURY (2045-2065)					END OF THE CENTURY (2080-2100)				
	ANNUAL	NEMS DEC-MAR	FIMS APR-MAY	SWMS JUNE-SEP	SIMS OCT-NOV	ANNUAL	NEMS DEC-MAR	FIMS APR-MAY	SWMS JUNE-SEP	SIMS OCT-NOV
Multi-model mean	2.0	1.7	1.8	2.3	2.1	3.9	3.2	3.7	4.6	4.2
	Individual RCM simulations					**Individual RCM simulations**				
CCAM ACCESS1.0	2.1	1.8	1.8	2.5	1.9	4.2	3.7	3.7	4.9	4.5
CCAM NorESM1-M	1.8	1.8	1.6	2.1	1.7	3.6	2.9	3.4	4.4	3.6
CCAM MPI-ESM-LR	1.6	1.2	2.2	2.0	1.2	3.8	2.9	4.2	4.7	3.5
CCAM CCSM4	1.7	1.4	1.3	2.2	1.7	3.6	2.9	3.1	4.5	3.5
CCAM CNRM-CM5	1.8	1.5	1.6	2.1	2.0	3.8	2.9	3.8	4.3	4.5
CCAM GFDL-CM3	3.4	2.8	3.1	3.9	3.8	6.1	5.0	5.8	7.1	6.8
RegCM4.2 ACCESS1.0	2.0	1.6	1.7	2.3	2.4	3.6	3.0	3.2	4.1	4.1
RegCM4.2 NorESM1-M	1.3	1.2	1.2	1.4	1.6	2.5	2.5	2.6	2.4	2.9

	Indicates a range of low results	< 2.0°C
	Indicates a range of medium results	2.0 to 4.0°C
	Indicates a range of high results	> 4.0°C

Table 10-5: Projected changes in annual and seasonal maximum temperature by the models (°C) for the NE region relative to the baseline period (1980-2000) for RCP 8.5 from eight RCM experiments. Green colouring is for increases less than 2°C, yellow from 2-4°C and orange greater than 4°C.

TMAX (°C)	MID-CENTURY (2045-2065)					END OF THE CENTURY (2080-2100)				
	ANNUAL	NEMS DEC-MAR	FIMS APR-MAY	SWMS JUNE-SEP	SIMS OCT-NOV	ANNUAL	NEMS DEC-MAR	FIMS APR-MAY	SWMS JUNE-SEP	SIMS OCT-NOV
Multi-model mean	2.2	2.0	1.8	2.4	2.3	4.4	3.9	4.0	5.1	4.4
	Individual RCM simulations					**Individual RCM simulations**				
CCAM ACCESS1.0	2.3	2.3	1.8	2.4	2.3	4.7	4.6	4.0	5.3	4.5
CCAM NorESM1-M	1.9	2.0	1.4	2.2	1.7	4.0	3.3	3.5	5.1	3.6
CCAM MPI-ESM-LR	1.6	1.2	2.2	1.9	1.0	4.2	3.6	4.4	5.0	3.5
CCAM CCSM4	2.0	1.9	1.2	2.4	2.2	4.2	3.8	3.4	5.3	3.7
CCAM CNRM-CM5	1.9	1.6	1.5	2.2	2.3	4.4	3.5	4.4	4.9	5.2
CCAM GFDL-CM3	4.1	3.9	3.4	4.4	4.6	7.5	6.6	7.1	8.3	7.9
RegCM4.2 ACCESS1.0	2.2	2.0	1.7	2.5	2.7	4.0	3.7	3.2	4.5	4.2
RegCM4.2 NorESM1-M	1.3	1.2	0.8	1.4	1.8	2.3	2.3	2.3	2.2	2.7

	Indicates a range of low results	< 2.0°C
	Indicates a range of medium results	2.0 to 4.0°C
	Indicates a range of high results	> 4.0°C

Table 10-6: Projected changes in annual and seasonal minimum temperature by model (°C) for the NE region relative to the baseline period (1980-2000) for RCP 8.5 from eight RCM experiments. Green colouring is for increases less than 2°C, yellow from 2-4°C and orange greater than 4°C.

TMIN (°C)	MID-CENTURY (2045-2065)					END OF THE CENTURY (2080-2100)				
	ANNUAL	NEMS DEC-MAR	FIMS APR-MAY	SWMS JUNE-SEP	SIMS OCT-NOV	ANNUAL	NEMS DEC-MAR	FIMS APR-MAY	SWMS JUNE-SEP	SIMS OCT-NOV
Multi-model mean	1.8	1.4	1.9	2.2	1.9	3.5	2.7	3.6	4.2	4.0
	Individual RCM simulations					**Individual RCM simulations**				
CCAM ACCESS1.0	1.9	1.3	1.9	2.6	1.7	3.9	2.9	3.6	4.7	4.5
CCAM NorESM1-M	1.8	1.6	1.9	2.0	1.7	3.4	2.7	3.5	4.0	3.8
CCAM MPI-ESM-LR	1.7	1.2	2.3	2.1	1.5	3.6	2.3	4.2	4.5	3.6
CCAM CCSM4	1.5	1.0	1.5	2.1	1.3	3.1	2.2	3.1	3.9	3.5
CCAM CNRM-CM5	1.7	1.4	1.8	2.0	1.8	3.3	2.4	3.5	3.9	4.0
CCAM GFDL-CM3	2.8	1.9	3.0	3.5	3.3	5.1	3.7	5.0	6.3	5.9
RegCM4.2 ACCESS1.0	1.8	1.3	1.7	2.2	2.1	3.3	2.6	3.1	3.8	4.0
RegCM4.2 NorESM1-M	1.3	1.2	1.4	1.3	1.4	2.6	2.4	2.7	2.5	2.9

	Indicates a range of low results	< 2.0°C
	Indicates a range of medium results	2.0 to 4.0°C
	Indicates a range of high results	> 4.0°C

Rainfall

The rainfall changes are more complex, since the models simulate both increases and decreases. There is a large amount of uncertainty associated with the rainfall change. In general, the majority of RCMs simulate little change (-10% to 10%) in annual rainfall by mid-century (Table 10-9). However, by the end of the century, more than half of the models (Table 10-9) show decreases in the annual, NEMS, FIMS and SWMS rainfall amounts, while half of the models project increases for SIMS (with a multi-model mean increase of +13%), suggesting greater confidence in these seasonal changes by the end of the century. The CCAM GFDL-CM3 simulation shows the strongest decrease (-33% for NEMS and FIMS), while RegCM4.2 Access1.0 shows the greatest increases in rainfall for SIMS (+94%) by the end of the century (Table 10-9).

A comparison between the present and previous projections (MONRE, 2012, Table 10-8) shows some differences in annual and seasonal changes, though most changes are relatively small and not statistically significant. The largest differences in the changes are for SWMS, where the previous projections showed increases (+11% for the A2 scenario), but the new projections show decreases for this season (-12%). Interestingly, the PRECIS ensemble mean shows increases for this region for all seasons, though most changes are less than 15%. The largest end-of-century PRECIS-projected seasonal increase is in SIMS (+28%), similar to the largest increase projected by the multi-model RCM mean in Table 10-7 (+13%).

Table 10-7: Projected changes in annual and seasonal mean rainfall and its ranges (%) for the NE region relative to the baseline period (1980-2000) for RCP 8.5. Changes are the multi-model means from eight simulations. Orange colouring is for decreases less than -10%, green for changes between -10% to +10% and blue for increases greater than +10%.

RAIN	MID-CENTURY (2045-2065)					END OF THE CENTURY (2080-2100)				
% CHANGE	ANNUAL	NEMS DEC-MAR	FIMS APR-MAY	SWMS JUNE-SEP	SIMS OCT-NOV	ANNUAL	NEMS DEC-MAR	FIMS APR-MAY	SWMS JUNE-SEP	SIMS OCT-NOV
Multi-model mean	-2	-2	-3	-1	-12	-11	-11	-12	-12	13
Range	-11 to +7	-28 to +17	-17 to +8	-12 to +15	-27 to +7	-30 to +5	-33 to +10	-33 to +6	-32 to +13	-21 to +94

Table 10-8: Projected changes in annual and seasonal rainfall (%) for the NE region relative to the baseline period (1980-2000) for SRES emission scenarios (B1, B2, A2, A1B) from a previous study (MONRE, 2012) and the latest PRECIS projections (ensemble means). Orange colouring is for decreases less than -10%, green for changes between -10% to +10% and blue for increases greater than +10%. Source: IMHEN.

RAIN	MID-CENTURY (2045-2065)					END OF THE CENTURY (2080-2100)				
(%)	ANNUAL	NEMS DEC-MAR	FIMS APR-MAY	SWMS JUNE-SEP	SIMS OCT-NOV	ANNUAL	NEMS DEC-MAR	FIMS APR-MAY	SWMS JUNE-SEP	SIMS OCT-NOV
	MONRE 2012					MONRE 2012				
B1	3	-1	-1	5	-1	4	-2	-1	7	-1
B2	3	-2	-1	6	-1	5	-2	-1	9	-1
A2	4	-2	-1	6	-1	6	-3	-1	11	-2
	PRECIS					PRECIS				
A1B	9	4	10	9	17	13	6	15	13	28

Table 10-9: Projected changes in annual and seasonal mean rainfall by model (%) for the NE region relative to the baseline period (1980-2000) for RCP 8.5 from the eight RCMs. Orange colouring is for decreases less than -10%, green for changes between -10% to +10% and blue for increases greater than +10%.

RAIN (%)	MID-CENTURY (2045-2065)					END OF THE CENTURY (2080-2100)				
	ANNUAL	NEMS DEC-MAR	FIMS APR-MAY	SWMS JUNE-SEP	SIMS OCT-NOV	ANNUAL	NEMS DEC-MAR	FIMS APR-MAY	SWMS JUNE-SEP	SIMS OCT-NOV
Multi-model mean	-2	-2	-3	-1	-12	-11	-11	-12	-12	13
	Individual RCM simulations					**Individual RCM simulations**				
CCAM ACCESS1.0	-3	6	8	-8	-16	-7	-2	6	-14	12
CCAM NorESM1-M	-2	11	-2	-2	-25	-13	6	-8	-19	-8
CCAM MPI-ESM-LR	0	-14	-17	11	2	-8	-25	-9	-3	-17
CCAM CCSM4	-5	17	-11	-4	-27	-19	10	-4	-32	12
CCAM CNRM-CM5	-3	6	-8	-2	-12	-18	1	-28	-16	-21
CCAM GFDL-CM3	-11	-28	4	-12	-19	-30	-33	-33	-30	-5
RegCM4.2 ACCESS1.0	7	-14	-6	15	7	1	-29	-13	6	94
RegCM4.2 NorESM1-M	-2	1	6	-5	-3	5	-14	-9	13	40

	Indicates a range of low (drier) results	< -10%
	Indicates a range of medium (little change) results	-10 to +10%
	Indicates a range of high (wetter) results	> 10%

10.4 SUMMARY

An analysis of observed records for the NE region shows a significant increasing trend of temperature in the NE region, while rainfall shows a decreasing trend. Some stations show a decline in rainfall of around -5% per decade. Both maximum and minimum temperatures are increasing, with the minimum temperature increasing slightly more than the maximum. The number of hot days (TX90p) has increased while the number of cold nights has decreased. Most of the extreme rainfall indices do not show any significant trends.

The annual mean surface temperature is projected to increase by 2.0°C by mid-century (projected changes range from 1.3°C to 3.4°C) and by 3.9°C by the end of the century (projected changes range from 2.5°C to 6.1°C). Projected temperature changes show a greater increase in SWMS (4.6°C in Tave) than in other seasons, with the least increase in NEMS (3.2°C in Tave). These temperature changes are greater than the previous projections (MONRE, 2012) but less than for some of the PRECIS ensemble means.

Projected rainfall changes are generally near ±10%, with decreases for all seasons except SIMS, which is projected to increase by +13% by end of the century. These changes are different than the PRECIS projections, which showed increases for all seasons, and from the previous projections (MONRE, 2012), which showed increases in SWMS and little change in SIMS.

11 NORTH DELTA REGIONAL REPORT

This chapter summarises the current climate and trends for the North Delta region of Vietnam (see Figure 11-1). The changes of temperature and rainfall for mid-century and the end of the century are then presented, first from the GCM results, then from the RCM results. The key messages are summarised at the end of the chapter.

11.1 DESCRIPTION

The North Delta (ND) region (Figure 11-1) is a relatively flat delta area. The region is bounded by the Gulf of Tonkin on the east and by the middle of North Vietnam on the west and south-west. The ND region has a dense network of rivers and fertile land, with abundant plant and animal species. Due to favourable natural conditions, the North Delta region has the largest population density of North Vietnam and is a region of growth and socio-economic development.

The ND climate region includes the midland provinces of Vinh Phuc, Hoa Binh, Bac Giang, Bac Ninh, Ha Noi, Hai Phong, Hai Duong, Hung Yen, Nam Dinh, Thai Binh and Ninh Binh provinces, where most areas have an elevation of less than 50 m.

The ND region is strongly influenced by the North East Monsoon and typhoons but to a lesser degree than for the NE. There are cold, cloudy, drizzly days in winter, with hoarfrost occurring in some years in this region. The hottest time of year is early June, when the temperature ranges between 28 and 29°C. The rainy season lasts from April to October, with rainfall maxima in August. North-east winds prevail in winter whereas east and south-east winds dominate the circulation pattern in summer.

11.2 OBSERVED CLIMATE

Observed climate trends are analysed using daily data from 70 meteorological stations in Vietnam for the period 1961 to 2011. In addition to trends of mean surface air temperature (or T2m) and precipitation, trends of some extreme indices are also discussed. Definition of selected extreme indices can be found in ETCCDI (2009), which recommended 27 core Extreme Climate Indices (ECIs) based on daily temperature values or daily precipitation amounts. The indices below are used in this study, mostly following the ETCCDI computational procedures:

- **RX1**: yearly maximum 1-day precipitation (mm).
- **RX5**: annual highest consecutive five-day precipitation amount (mm).
- **R95p**: annual count of days when precipitation exceeds the 95th percentile value for the period 1961-2011.
- **TN10p**: annual count of days when minimum daily temperature is less than the 10th percentile temperature for the period 1961-2011.
- **TX90p**: annual count of days when maximum daily temperature exceeds the 90th percentile temperature for the period 1961-2011.
- **CDD**: consecutive dry days; average annual maximum number of days with daily rainfall less than 1 mm.
- **CWD**: consecutive wet days; average annual maximum number of days with daily rainfall greater than or equal to 1 mm.
- **Hot days**: days with Tmax greater than 35°C.
- **Cold days**: days with Tmin less than 15°C.

Figure 11-1: The North Delta region with provinces. Insert shows location of the region in Vietnam

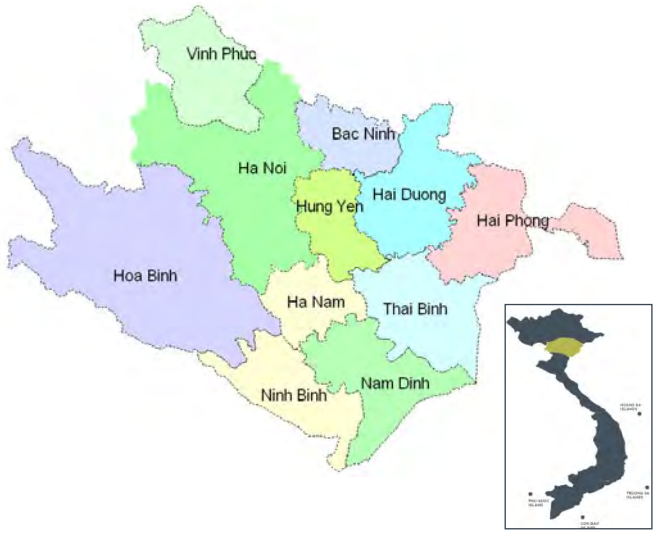

Table 11-1: Observed climate variables and ranges for the ND region. Nguyen and Nguyen (2004).

CLIMATE VARIABLE	VALUE
Terrain height	below 50 m
Annual average solar radiation	105 to 130 kcal cm^{-2}
Radiation balance	65 to 75 kcal cm^{-2}
Annual sunshine hours	1400 to 1700 h
Annual average temperature	23 to 24°C
Maximum temperature	38 to 41°C
Minimum temperature	2 to 5°C
Annual average temperature amplitude	12 to 13°C
Annual average rainfall	1400 to 1800 mm
Daily maximum rainfall	300 to 500 mm
Rainfall season	Apr to Oct
Number of days with drizzle	10 to 30 days
Humidity	84 to 85%
Annual evaporation	700 to 800 mm
Annual average wind speed	1.5 to 2.0 m sec^{-1}
Maximum wind speed	30 to 40 m sec^{-1}

Trends are calculated for each station within this region. Statistical significance of the trends is computed using the non-parametric Mann-Kendall test (Kendall, 1975). In this report, trends with significance levels greater than 90% are considered as statistically significant.

11.2.1 Temperature

Statistically significant increase in temperature has been observed in this region, ranging between 0.15-0.26°C per decade (Figure 11-2). The highest rate of increase (0.26°C per decade) is observed at Ha Noi. Among all the stations in ND, Thai Binh shows the smallest increasing trend of 0.06°C per decade, which is not statistically significant. For the region as a whole, the trend appears to be upward (Figure 10-3), but with larger inter-annual variability than net change.

11.2.2 Rainfall

Observed rainfall records show a significant decreasing trend at most of the stations in the region. In particular, Ba Vi station shows a decline of up to -8% per decade during the past 50 years (Figure 11-4). The regionally averaged trend shows a slight decrease (Figure 11-5), but less than the inter-annual variability.

Figure 11-2: Trend in annual mean surface air temperature in the North Delta (ND) region (°C per decade) for the period 1961 to 2011. A blue circle indicates a decreasing and a red circle shows an increasing trend. A filled circle means that the trend is significant at the 90% confidence level.

Figure 11-4: Trends in annual rainfall in the ND region (% per decade) for the period 1961 to 2011. A blue circle indicates an increasing and a red circle shows a decreasing trend. A filled circle means that the trend is significant at the 90% confidence level.

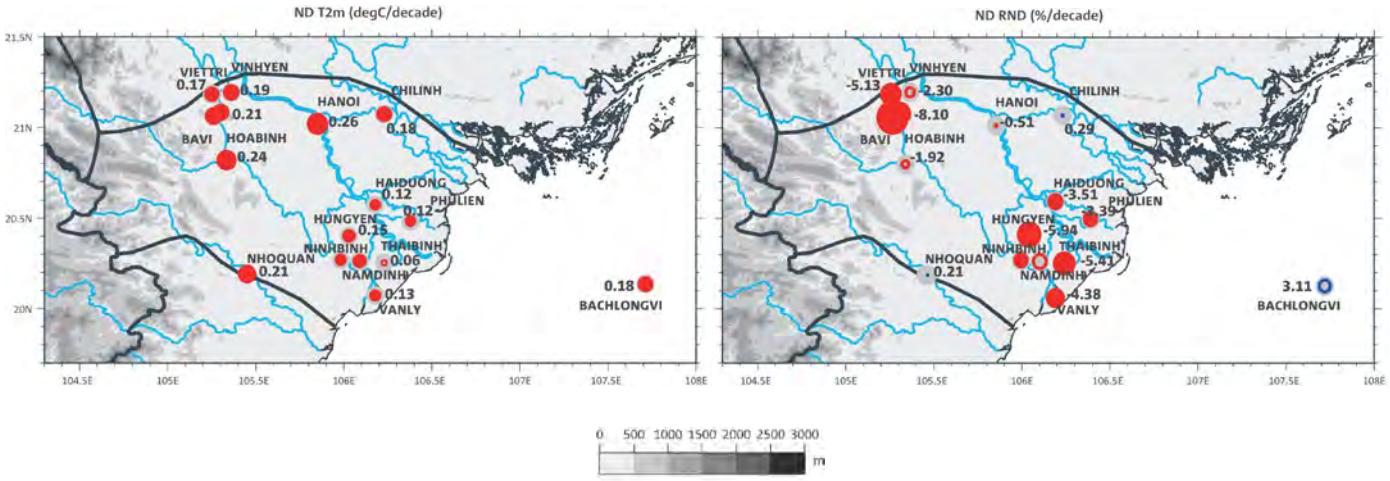

Figure 11-3: Time series of regionally-averaged annual surface air temperature (°C, red) for the ND region with a trend line (dashed black line). Annual values are shown by black dots.

Figure 11-5: Time series of regionally-averaged annual rainfall (mm day^{-1}, blue) for the ND with a trend line (dashed black line). Annual values are shown by black dots.

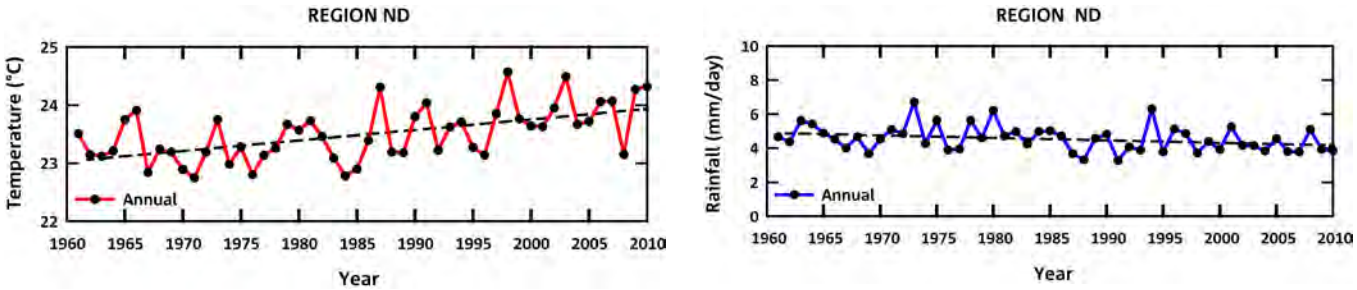

11.2.3 Extremes

Maximum (Tmax) and minimum (Tmin) daily temperatures have increased significantly during the period 1961 to 2011 in this region, as shown in Figure 11-6. Tmax has increased between 0.1 and 0.32°C per decade, while Tmin has increased between 0.04 and 0.29°C per decade. Unlike in the NE and NW regions, the increasing rate of Tmin is similar to Tmax in the ND region.

Extreme maximum temperatures (TX90p) have increased and extreme minimum temperatures (TN10p) have decreased significantly for most stations is this region (Figure 11-6). The significant increase in the number of hot days is associated with the rise in maximum daily temperatures, whereas the decrease in the number of cold nights is associated with the rise in minimum temperatures. The number of extreme hot days has increased by up to 6 days per decade. The number of extreme cold nights has decreased significantly at almost all stations, with the highest rate of -4 days per decade.

The trend in the annual maximum daily rainfall (RX1) shows a decrease in the region (Figure 11-7). The trends are statistically significant at Ba Vi, Hai Duong, Hung Yen and Thai Binh stations with the highest decreasing rate of -13% per decade at Ba Vi station. RX5 rainfall shows a similar decreasing trend as RX1. Similarly, R95p shows a decreasing trend of 5-10% per decade. However, CWD show negligible trends at most stations in ND, while CDD shows a slight increasing trend of up to 2.1% per decade in the region.

Figure 11-6: Trends in Tmax (upper left), Tmin (upper right), TX90p (lower left), and TN10p (lower right) in the ND region for the period 1961 to 2011. A blue circle indicates a decreasing trend and a red circle shows an increasing trend. A filled circle means that the trend is significant at the 90% confidence level.

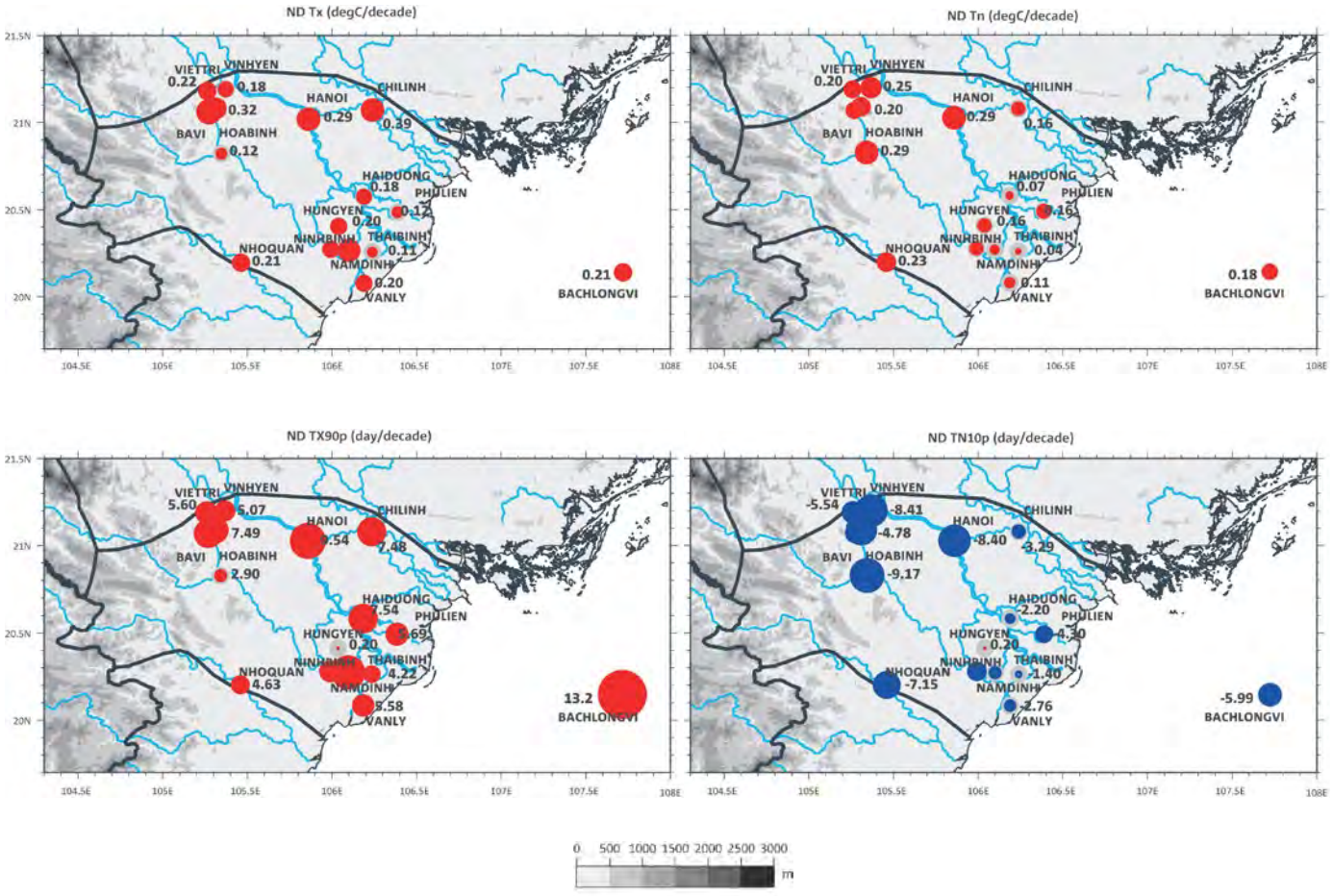

Figure 11-7: Trends in RX1, RX5, R95p, CWD, and CDD in the ND region for the period 1961 to 2011. A blue circle indicates an increasing trend and a red circle shows a decreasing trend for all but CDD, where red indicates an increasing and blue a decreasing number of days. A filled circle means that the trend is significant at the 90% confidence level.

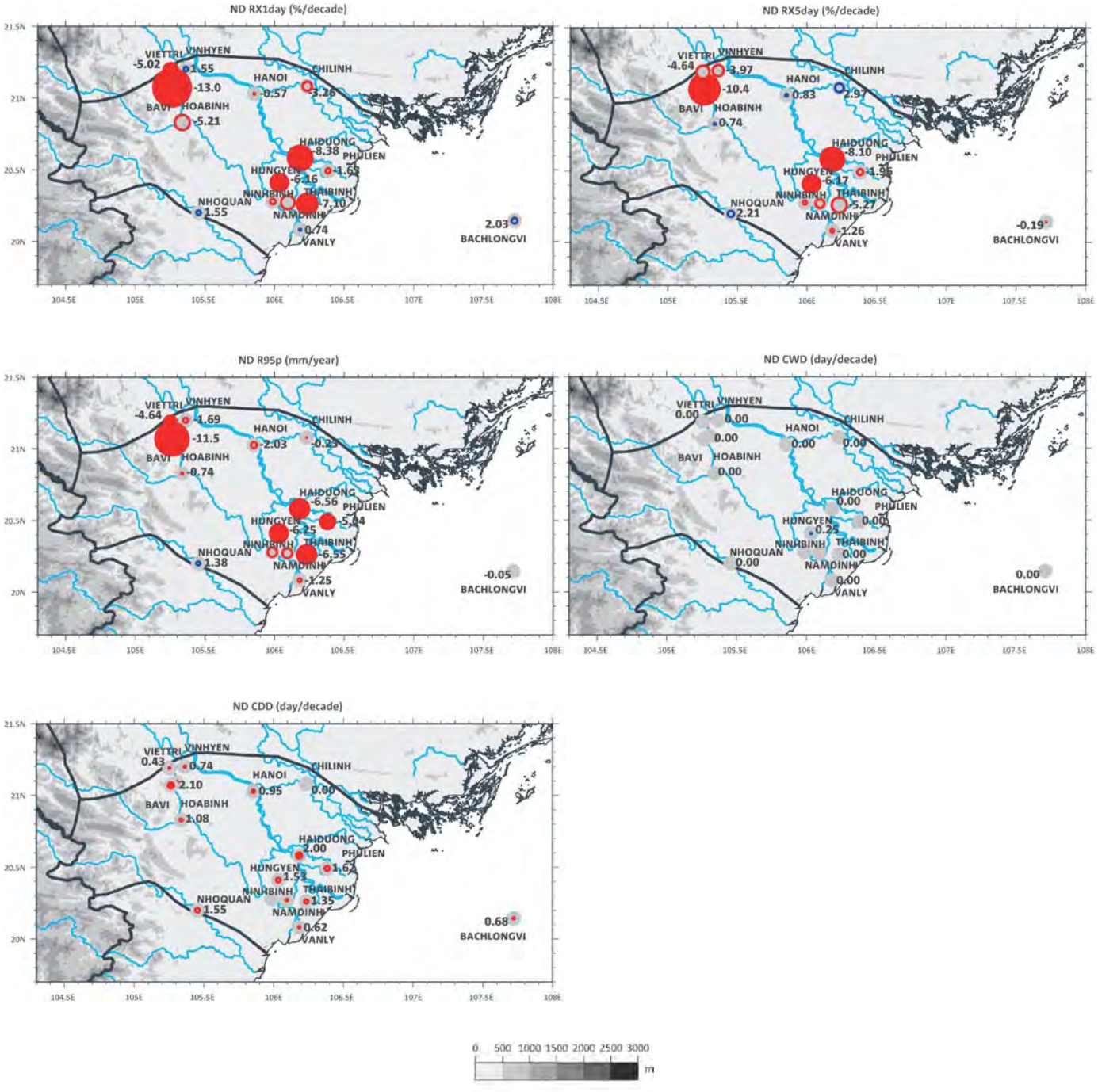

11.3 CLIMATE PROJECTIONS

In this section, projected changes in temperature and rainfall for the ND region are presented. A summary of the CMIP5 GCM results for different RCPs for this region is first presented in the form of line graphs. This is followed by the changes projected by regional climate models, both from the new experiments completed for this project and the results used for the last official projections completed by IMHEN (MONRE, 2012), using the previous CMIP3 SRES emission scenarios. This provides some indication of the differences of the projections, though direct comparison is difficult, since different models and different scenarios were used.

11.3.1 GCM results

Surface temperature

Projections for near-surface average temperature for the four seasons for this region from the CMIP5 GCMs are presented in Figure 11-8. The warming signal is very clear, with greatest warming for the high emission scenario (RCP 8.5) and less warming for the lower emission scenario (RCP 4.5).

There is also slightly greater warming (as measured by the median value, line inside the colour bar) during FIMS by the end of the century for RCP 8.5, with warming of about 4.5°C, while other seasons show slightly less warming by the end of the century.

Projections for near-surface maximum temperature for the four seasons for this region from the CMIP5 GCMs are presented in Figure 11-9. Again, the warming signal is very clear and is similar to the average temperature. However, there is also slightly greater warming during FIMS and SWMS (more than 4°C) by the end of the century for RCP 8.5, while other seasons show slightly less warming.

Figure 11-8: Regionally averaged seasonal surface air temperature changes (°C) for ND. For each season, the time series graph of projections by global climate models (GCM) is shown on the left for the higher (RCP 8.5) greenhouse gas scenario. Black line is from historical GCM runs, red line is the multi-model median projection from GCMs using RCP 8.5. Shadings are between 10% and 90% of 20-year mean values. GCM values have been corrected for 1995-2005 mean bias. Bars on the right for each season show the end-of-century summary of projections by global climate models (GCM, left) and regional climate models (RCM, right) for both lower (RCP 4.5) and higher (RCP 8.5) scenarios.

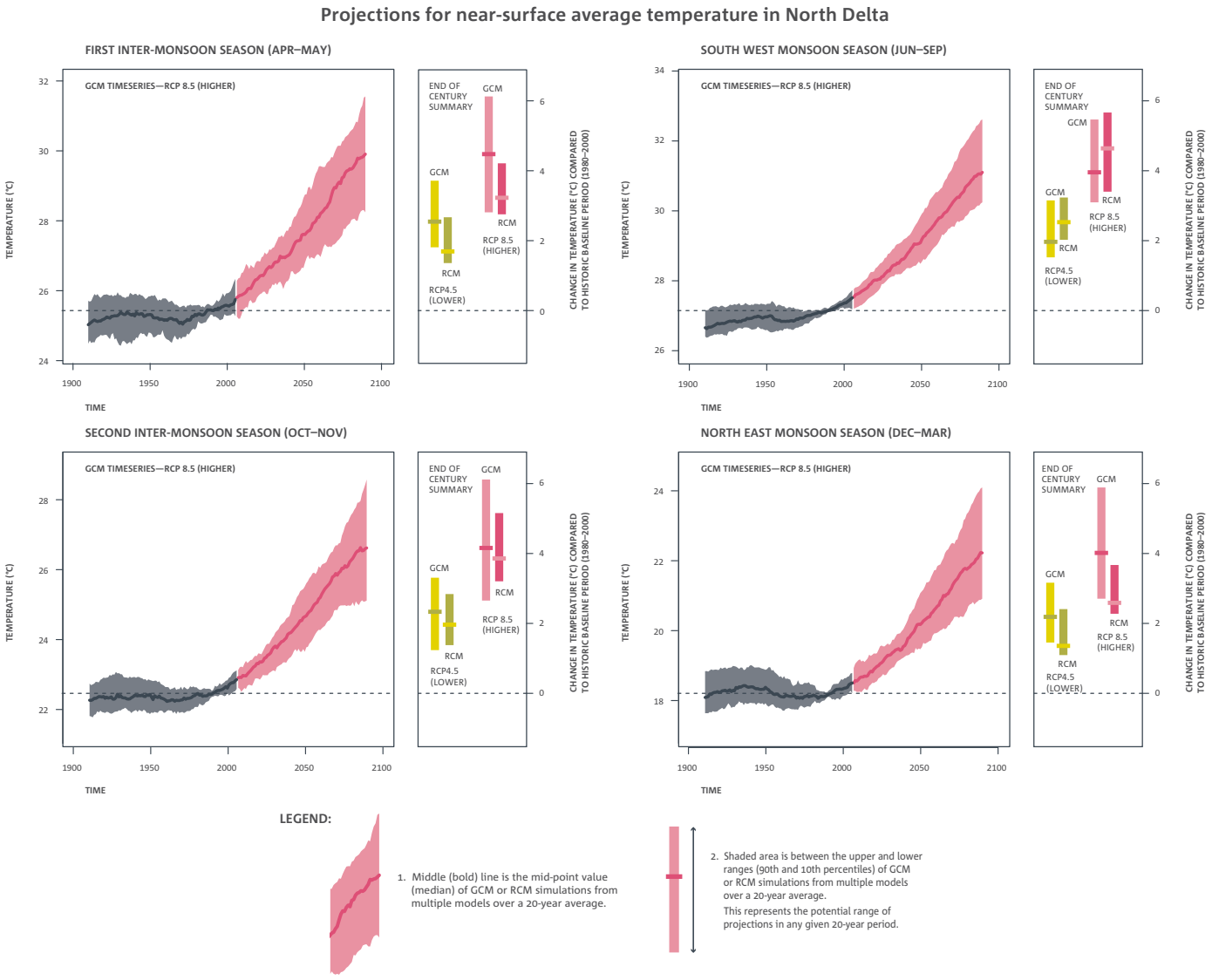

Figure 11-9: Regionally averaged seasonal maximum air temperature changes (°C) for ND. For each season, the time series graph of projections by global climate models (GCM) is shown on the left for the higher (RCP 8.5) greenhouse gas scenario. Black line is from historical GCM runs, red line is the multi-model median projection from GCMs using RCP 8.5. Shadings are between 10% and 90% of 20-year mean values. GCM values have been corrected for 1995-2005 mean bias. Bars on the right for each season show the end-of-century summary of projections by global climate models (GCM, left) and regional climate models (RCM, right) for both lower (RCP 4.5) and higher (RCP 8.5) scenarios.

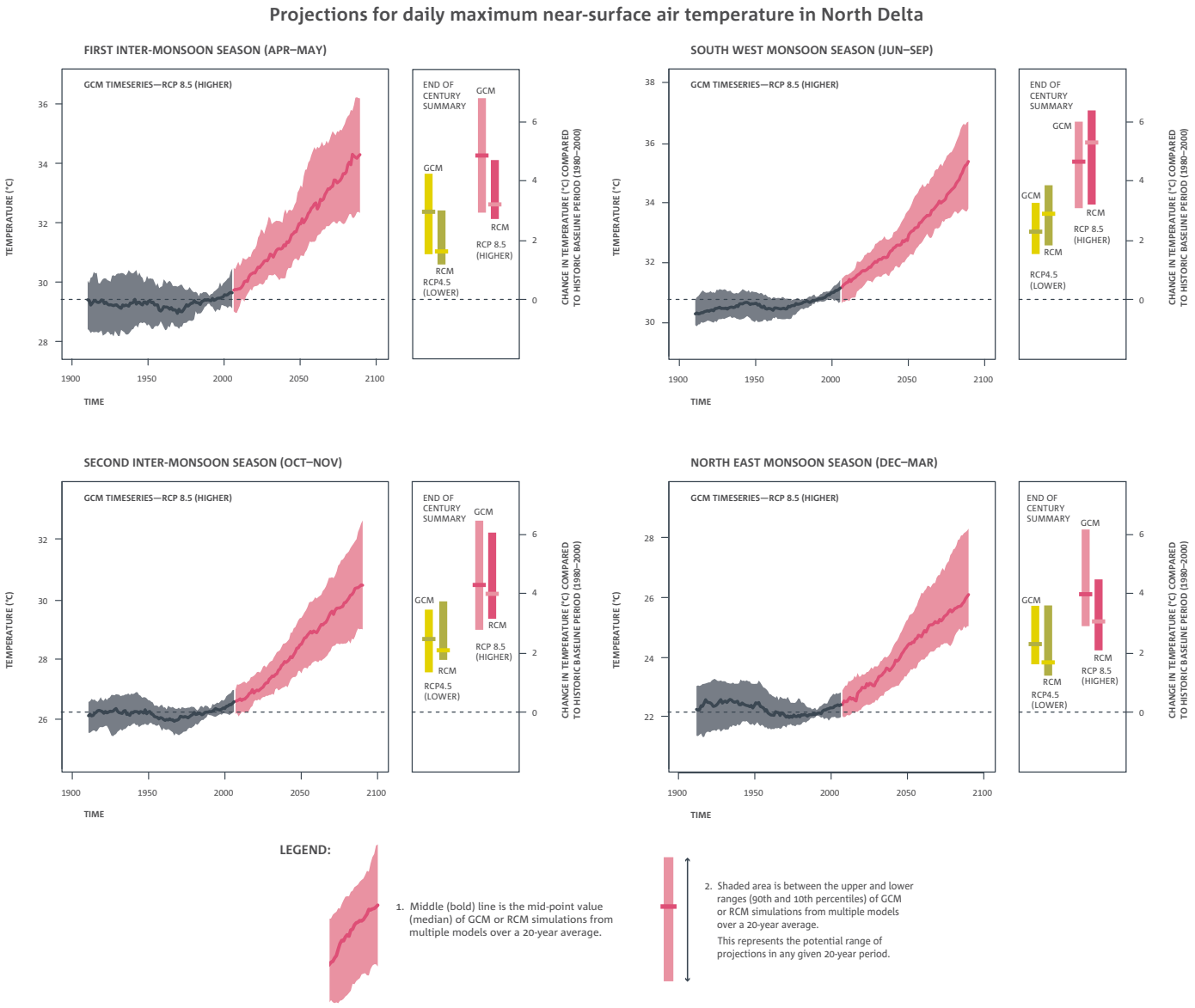

Projections for near-surface minimum temperature for the four seasons for this region from the CMIP5 GCMs are presented in Figure 11-10. The warming signal is very clear and is similar to the average temperature (slightly more than 4°C) for all seasons by the end of the century for RCP 8.5.

Figure 11-10: Regionally averaged seasonal minimum air temperature changes (°C) for ND. For each season, the time series graph of projections by global climate models (GCM) is shown on the left for the higher (RCP 8.5) greenhouse gas scenario. Black line is from historical GCM runs, red line is the multi-model median projection from GCMs using RCP 8.5. Shadings are between 10% and 90% of 20-year mean values. GCM values have been corrected for 1995-2005 mean bias. Bars on the right for each season show the end-of-century summary of projections by global climate models (GCM, left) and regional climate models (RCM, right) for both lower (RCP 4.5) and higher (RCP 8.5) scenarios.

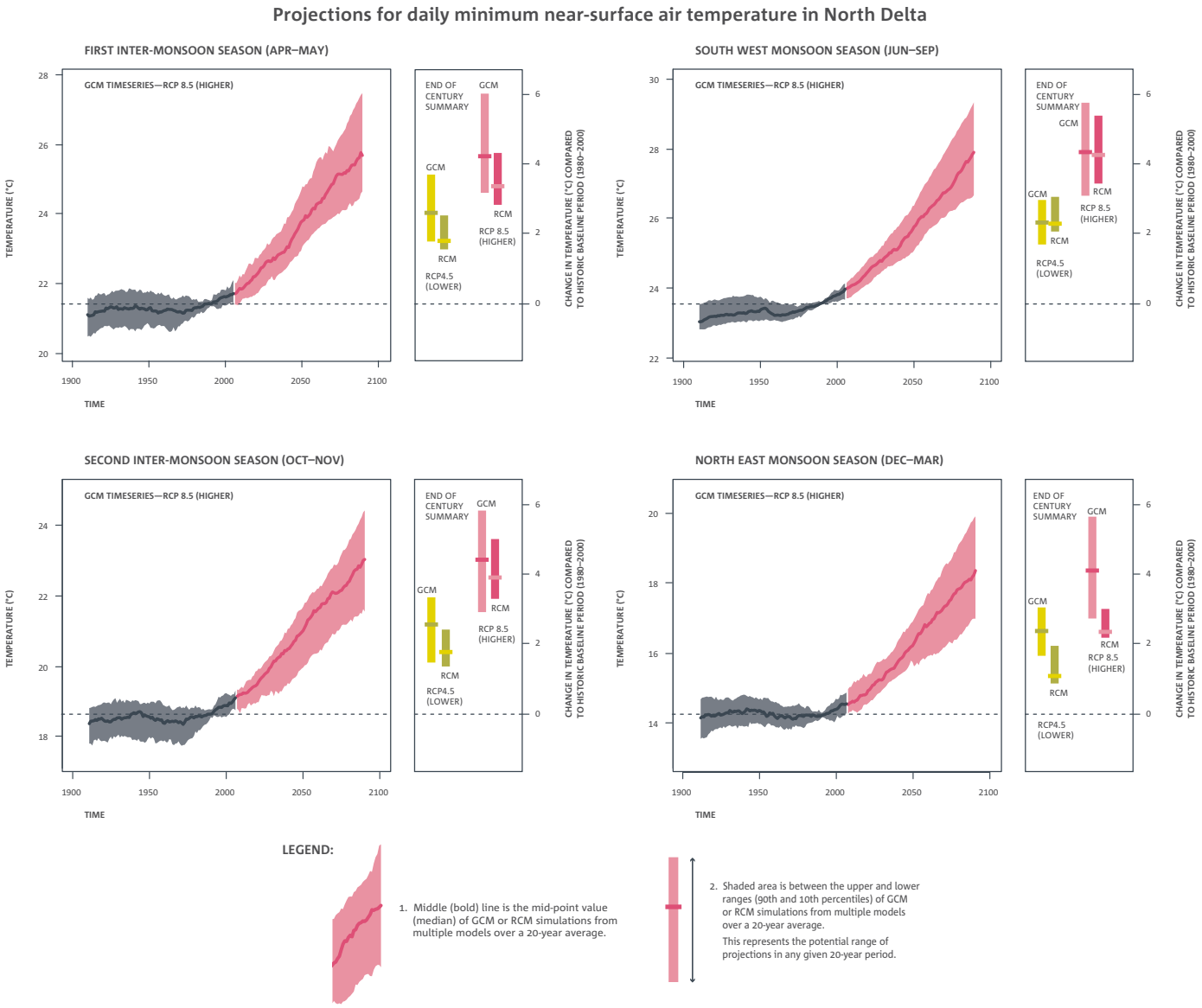

Rainfall

Projected changes in rainfall for the four seasons for this region from the CMIP5 GCMs are presented in Figure 11-11. There is a large range of inter-annual variability simulated by the GCMs for rainfall for this region, as can be seen by the large spread of the colour bar. FIMS and NEMS show little change in rainfall by the end of the century. However, both SWMS and SIMS show increases in rainfall by the end of the century for both RCPs.

Figure 11-11: Regionally averaged seasonal precipitation changes (mm month^{-1} on left axis and % on right axis) for ND. For each season, the time series graph of projections by global climate models (GCM) is shown on the left for the higher (RCP 8.5) greenhouse gas scenario. Black line is from historical GCM runs, red line is the multi-model median projection from GCMs using RCP 8.5. Shadings are between 10% and 90% of 20-year mean values. GCM values have been corrected for 1995-2005 mean bias. Bars on the right for each season show the end-of-century summary of projections by global climate models (GCM, left) and regional climate models (RCM, right) for both lower (RCP 4.5) and higher (RCP 8.5) scenarios.

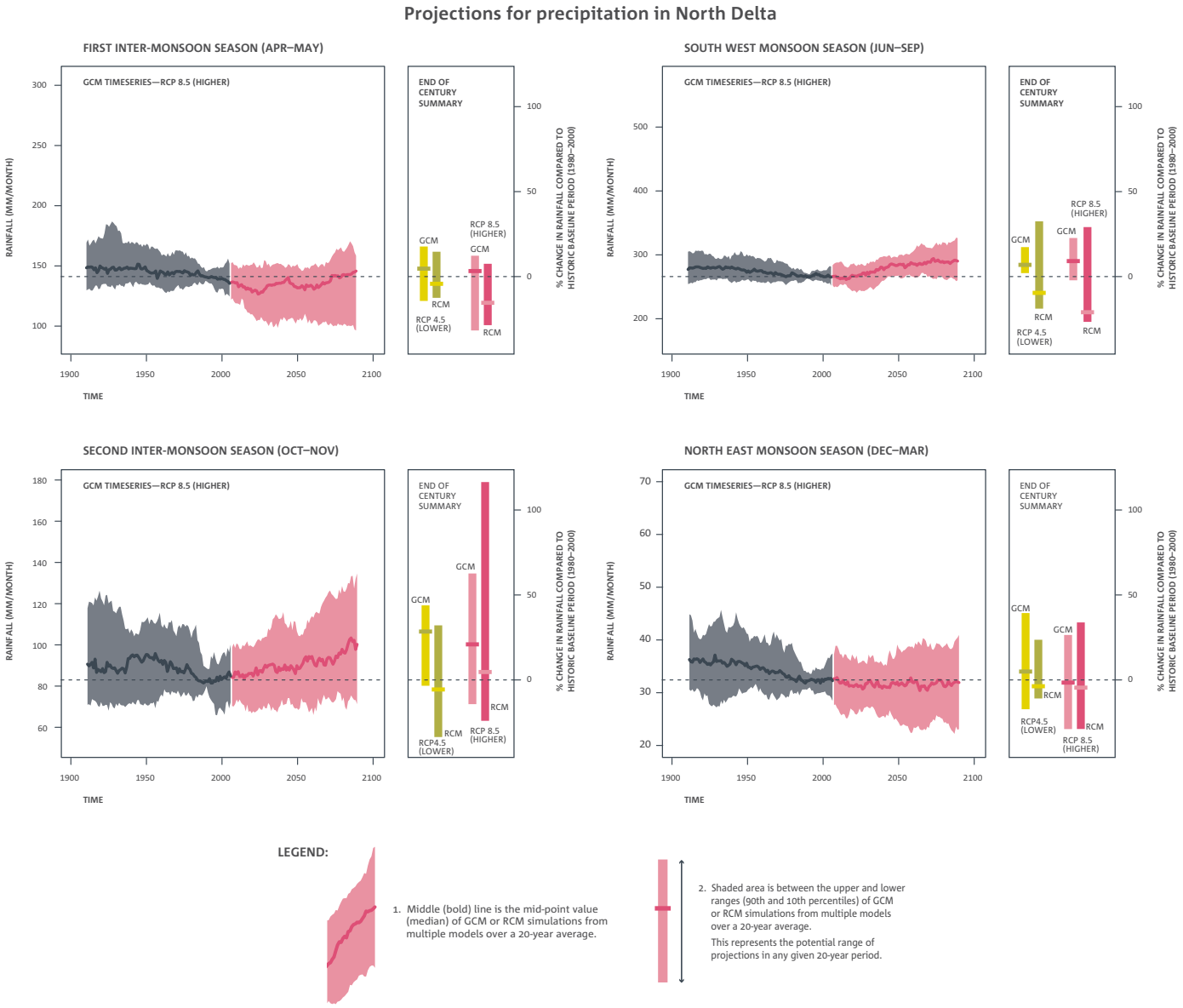

11.3.2 Regional model results

This section will discuss the projected changes in climate for the future compared with the present climate using ensemble means from eight RCM experiments. In general, these projections do not represent a value specific to any location, since average changes of annual and seasonal values are given for the entire ND region.

Surface temperature

Table 11-2 to Table 11-6 show projected changes in annual and seasonal surface air temperature (°C) for RCP 8.5 relative to the baseline period (1980-2000) by the middle and the end of the century. These projections represent an average change over the whole of the ND region. The increases in annual mean temperature (Tave) are 1.9°C by 2045-2065 and 3.8°C by 2080-2100. The maximum temperature (Tmax) increases slightly more than the minimum temperature, which results in an increase in the annual mean diurnal temperature range.

The projected change in temperature in SWMS is higher than the other seasons (the multi-model mean is 4.6°C for Tave, 5.1°C for Tmax and 4.4°C for Tmin by the end of the century for RCP 8.5), while the temperature during NEMS shows the smallest increase (2.9°C for Tave, 3.2°C for Tmax and 2.5°C for Tmin by the end of century for RCP 8.5).

The increase in the mean temperature of the multi-model mean is generally higher than that in previous climate projections (MONRE, 2012; see Table 11-3), which showed an annual increase of 2.8°C by the end of the century for the SRES A2 emission scenario and 2.6°C for SWMS. However, the PRECIS ensemble mean projections show greater warming than the projections derived from CMIP5 simulations, even for the lower emission scenarios. Of the eight RCM experiments, CCAM GFDL-CM3 shows the largest increases and RegCM4.2 NorESM1-M shows the least increase compared with the other models (Table 11-4 to Table 11-6).

Table 11-2: Summary of the multi-model mean and range of projected change in annual and seasonal average, maximum and minimum temperature (°C) for the ND region relative to baseline period (1980-2000) for RCP 8.5. Green colouring is for increases less than 2°C, yellow from 2-4°C and orange greater than 4°C.

	MID-CENTURY (2045-2065)					END OF THE CENTURY (2080-2100)				
	ANNUAL	NEMS DEC-MAR	FIMS APR-MAY	SWMS JUNE-SEP	SIMS OCT-NOV	ANNUAL	NEMS DEC-MAR	FIMS APR-MAY	SWMS JUNE-SEP	SIMS OCT-NOV
Tave	1.9	1.5	1.8	2.3	2.1	3.8	2.9	3.5	4.6	4.1
(°C)	1.3 to 3.3	1.1 to 2.4	1.1 to 3.1	1.3 to 3.9	1.5 to 3.8	2.4 to 5.8	2.3 to 4.3	2.5 to 5.4	2.3 to 7.0	2.7 to 6.5
Tmax	2.0	1.7	1.6	2.4	2.3	4.1	3.2	3.6	5.1	4.4
(°C)	1.1 to 3.8	1.0 to 3.2	0.7 to 3.3	1.2 to 4.4	1.4 to 4.5	2.0 to 6.7	1.9 to 5.3	2.0 to 6.2	1.7 to 8.0	2.4 to 7.4
Tmin	1.8	1.3	1.9	2.3	1.9	3.6	2.5	3.5	4.4	4.1
(°C)	1.3 to 2.9	1.0 to 1.8	1.4 to 3.0	1.4 to 3.7	1.4 to 3.4	2.6 to 5.1	2.0 to 3.5	2.7 to 4.9	2.5 to 6.5	2.9 to 5.9

Table 11-3: Projected changes in annual and seasonal mean temperature (°C) for the ND region relative to baseline period (1980-2000) under different SRES emission scenarios (B1, B2, A2, A1B) from a previous study (MONRE, 2012) and the latest PRECIS projections (ensemble means). Green colouring is for increases less than 2°C, yellow from 2-4°C and orange greater than 4°C. Source: IMHEN.

TAVE (°C)	MID-CENTURY (2045-2065)					END OF THE CENTURY (2080-2100)				
	ANNUAL	NEMS DEC-MAR	FIMS APR-MAY	SWMS JUNE-SEP	SIMS OCT-NOV	ANNUAL	NEMS DEC-MAR	FIMS APR-MAY	SWMS JUNE-SEP	SIMS OCT-NOV
	MONRE 2012					MONRE 2012				
B1	1.3	1.3	1.5	1.2	1.3	1.7	1.7	1.9	1.5	1.6
B2	1.5	1.5	1.7	1.4	1.4	2.4	2.4	2.7	2.2	2.3
A2	1.6	1.6	1.7	1.4	1.5	2.8	2.8	3.2	2.6	2.7
	PRECIS					PRECIS				
A1B	2.6	2.9	2.6	2.3	2.6	4.0	4.2	4.0	3.8	3.9

Table 11-4: Projected changes in annual and seasonal average temperature by model (°C) for the ND region relative to the baseline period (1980-2000) for RCP 8.5 from eight RCM experiments. Green colouring is for increases less than 2°C, yellow from 2-4°C and orange greater than 4°C.

TAVE (°C)	MID-CENTURY (2045-2065)					END OF THE CENTURY (2080-2100)				
	ANNUAL	NEMS DEC-MAR	FIMS APR-MAY	SWMS JUNE-SEP	SIMS OCT-NOV	ANNUAL	NEMS DEC-MAR	FIMS APR-MAY	SWMS JUNE-SEP	SIMS OCT-NOV
Multi-model mean	1.9	1.5	1.8	2.3	2.1	3.8	2.9	3.5	4.6	4.1
	Individual RCM simulations					**Individual RCM simulations**				
CCAM ACCESS1.0	1.9	1.6	1.5	2.4	2.0	4.1	3.4	3.3	5.0	4.6
CCAM NorESM1-M	1.8	1.7	1.5	2.1	1.6	3.4	2.4	3.1	4.5	3.4
CCAM MPI-ESM-LR	1.8	1.3	2.2	2.2	1.5	4.0	2.9	3.9	5.2	3.9
CCAM CCSM4	1.7	1.2	1.4	2.3	1.8	3.4	2.3	2.9	4.7	3.4
CCAM CNRM-CM5	1.8	1.3	1.5	2.2	2.1	3.7	2.6	3.6	4.5	4.6
CCAM GFDL-CM3	3.3	2.4	3.1	3.9	3.8	5.8	4.3	5.4	7.0	6.5
RegCM4.2 ACCESS1.0	1.8	1.4	1.7	2.2	2.2	3.4	2.7	3.1	3.9	3.9
RegCM4.2 NorESM1-M	1.3	1.1	1.1	1.3	1.5	2.4	2.3	2.5	2.3	2.7

	Indicates a range of low results	< 2.0°C
	Indicates a range of medium results	2.0 to 4.0°C
	Indicates a range of high results	> 4.0°C

Table 11-5: Projected changes in annual and seasonal maximum temperature by model (°C) for the ND region relative to the baseline period (1980-2000) for RCP 8.5 from eight RCM experiments. Green colouring is for increases less than 2°C, yellow from 2-4°C and orange greater than 4°C.

TMAX (°C)	MID-CENTURY (2045-2065)					END OF THE CENTURY (2080-2100)				
	ANNUAL	NEMS DEC-MAR	FIMS APR-MAY	SWMS JUNE-SEP	SIMS OCT-NOV	ANNUAL	NEMS DEC-MAR	FIMS APR-MAY	SWMS JUNE-SEP	SIMS OCT-NOV
Multi-model mean	2.0	1.7	1.6	2.4	2.3	4.1	3.2	3.6	5.1	4.4
	Individual RCM simulations					**Individual RCM simulations**				
CCAM ACCESS1.0	2.1	2.0	1.3	2.3	2.5	4.5	4.1	3.2	5.4	4.8
CCAM NorESM1-M	1.8	1.8	1.3	2.2	1.6	3.5	2.2	3.1	5.1	3.4
CCAM MPI-ESM-LR	1.8	1.4	2.2	2.2	1.4	4.4	3.5	4.0	5.6	4.1
CCAM CCSM4	1.9	1.4	1.3	2.6	2.3	3.9	2.7	3.0	5.6	3.6
CCAM CNRM-CM5	1.9	1.4	1.3	2.5	2.5	4.3	3.0	4.0	5.2	5.4
CCAM GFDL-CM3	3.8	3.2	3.3	4.4	4.5	6.7	5.3	6.2	8.0	7.4
RegCM4.2 ACCESS1.0	1.8	1.6	1.6	2.0	2.3	3.4	3.1	3.0	3.8	3.8
RegCM4.2 NorESM1-M	1.1	1.0	0.7	1.2	1.6	2.0	1.9	2.0	1.7	2.4

	Indicates a range of low results	< 2.0°C
	Indicates a range of medium results	2.0 to 4.0°C
	Indicates a range of high results	> 4.0°C

Table 11-6: Projected changes in annual and seasonal minimum temperature by model (°C) for the ND region relative to the baseline period (1980-2000) for RCP 8.5 from eight RCM experiments. Green colouring is for increases less than 2°C, yellow from 2-4°C and orange greater than 4°C.

TMIN (°C)	MID-CENTURY (2045-2065)					END OF THE CENTURY (2080-2100)				
	ANNUAL	NEMS DEC-MAR	FIMS APR-MAY	SWMS JUNE-SEP	SIMS OCT-NOV	ANNUAL	NEMS DEC-MAR	FIMS APR-MAY	SWMS JUNE-SEP	SIMS OCT-NOV
Multi-model mean	1.8	1.3	1.9	2.3	1.9	3.6	2.5	3.5	4.4	4.1
	Individual RCM simulations					**Individual RCM simulations**				
CCAM ACCESS1.0	1.8	1.2	1.8	2.6	1.7	3.9	2.8	3.4	4.9	4.6
CCAM NorESM1-M	1.8	1.6	1.8	2.1	1.8	3.4	2.4	3.3	4.3	3.7
CCAM MPI-ESM-LR	1.8	1.2	2.3	2.2	1.6	3.7	2.3	4.1	4.9	3.8
CCAM CCSM4	1.5	1.0	1.5	2.2	1.4	3.1	2.0	2.9	4.2	3.5
CCAM CNRM-CM5	1.7	1.3	1.7	2.1	1.8	3.4	2.3	3.5	4.2	4.1
CCAM GFDL-CM3	2.9	1.8	3.0	3.7	3.4	5.1	3.5	4.9	6.5	5.9
RegCM4.2 ACCESS1.0	1.8	1.2	1.8	2.3	2.1	3.2	2.4	3.1	3.8	4.0
RegCM4.2 NorESM1-M	1.3	1.1	1.4	1.4	1.4	2.6	2.3	2.7	2.5	2.9

	Indicates a range of low results	< 2.0°C
	Indicates a range of medium results	2.0 to 4.0°C
	Indicates a range of high results	> 4.0°C

Rainfall

Rainfall changes are more complex, since the different simulations show both increases and decreases. Hence, there is large uncertainty associated with rainfall change. Annually and for most seasons, the multi-model mean from the RCM projections shows little change (-10% to 10%) in rainfall by both mid-century and the end of the century (Table 11-7 and Table 11-9). By the end of the century, however, the multi-model mean projection is for an increase during SIMS (multi-model mean of +34%), although only half of the models show increases. For FIMS and SWMS, 6 out of the 8 models project decreases by end of the century. The CCAM MPI-ESM-LR projection shows the greatest decline in rainfall (-39% for SIMS), while RegCM4.2 Access1.0 shows the greatest increase in rainfall in SIMS (+230%). However, this model tended to under-predict rainfall in this season for the current climate, which could lead to large percentage increases in the future (since the percentage is future changes divided by current values).

A comparison between the present and previous projections for rainfall (Table 11-7 and MONRE, 2012 in Table 11-8) shows differences in annual and seasonal changes, although these differences are generally not significant. The largest difference in projected changes in rainfall is found during SWMS, where the previous projections showed increases in rainfall of 11%, while the new projections show decreases of -9% by the end of the century. The PRECIS ensemble mean shows increases for this region for all seasons including FIMS by the end of the century, in contrast to the new projections and MONRE (2012), which project decreases for FIMS.

Table 11-7: Projected changes in annual and seasonal mean rainfall and its ranges (%) for the ND region relative to the baseline period (1980-2000) for RCP 8.5. Changes are the multi-model means from eight simulations. Orange colouring is for decreases less than -10%, green for changes between -10% to +10% and blue for increases greater than +10%.

RAIN	MID-CENTURY (2045-2065)					END OF THE CENTURY (2080-2100)				
% CHANGE	ANNUAL	NEMS DEC-MAR	FIMS APR-MAY	SWMS JUNE-SEP	SIMS OCT-NOV	ANNUAL	NEMS DEC-MAR	FIMS APR-MAY	SWMS JUNE-SEP	SIMS OCT-NOV
Multi-model mean	-1	1	1	-1	2	-6	1	-12	-9	34
Range	-13 to +27	-21 to +29	-13 to +18	-20 to +42	-19 to +85	-24 to +25	-30 to +53	-30 to +21	-29 to +35	-39 to +230

Table 11-8: Projected changes in annual and seasonal rainfall (%) for the ND region relative to the baseline period (1980-2000) for SRES emission scenarios (B1, B2, A2, A1B) from a previous study (MONRE, 2012) and the latest PRECIS projections (ensemble means). Orange colouring is for decreases less than -10%, green for changes between -10% to +10% and blue for increases greater than +10%. Source: IMHEN.

RAIN	MID-CENTURY (2045-2065)					END OF THE CENTURY (2080-2100)				
(%)	ANNUAL	NEMS DEC-MAR	FIMS APR-MAY	SWMS JUNE-SEP	SIMS OCT-NOV	ANNUAL	NEMS DEC-MAR	FIMS APR-MAY	SWMS JUNE-SEP	SIMS OCT-NOV
	MONRE 2012					MONRE 2012				
B1	3	0	-2	5	1	4	0	-2	7	1
B2	4	0	-2	6	1	6	0	-3	9	1
A2	4	0	-2	6	1	7	0	-3	11	2
	PRECIS					PRECIS				
A1B	5	-3	12	5	6	9	1	14	8	12

Table 11-9: Projected changes in annual and seasonal mean rainfall by model (%) for the ND region relative to the baseline period (1980-2000) for RCP 8.5 from the eight RCMs. Orange colouring is for decreases less than -10%, green for changes between -10% to +10% and blue for increases greater than +10%.

RAIN (%)	MID-CENTURY (2045-2065)					END OF THE CENTURY (2080-2100)				
	ANNUAL	NEMS DEC-MAR	FIMS APR-MAY	SWMS JUNE-SEP	SIMS OCT-NOV	ANNUAL	NEMS DEC-MAR	FIMS APR-MAY	SWMS JUNE-SEP	SIMS OCT-NOV
Multi-model mean	-1	1	1	-1	2	-6	1	-12	-9	34
	Individual RCM simulations					**Individual RCM simulations**				
CCAM ACCESS1.0	-5	7	18	-16	-2	-7	2	21	-22	13
CCAM NorESM1-M	7	7	12	12	-19	0	53	-2	-12	-3
CCAM MPI-ESM-LR	-9	-21	-13	-3	-13	-24	-26	-22	-20	-39
CCAM CCSM4	-9	29	-13	-13	-19	-12	26	-9	-29	28
CCAM CNRM-CM5	-11	11	1	-20	-1	-19	17	-28	-24	-17
CCAM GFDL-CM3	-13	-21	0	-17	-5	-24	-28	-25	-26	-8
RegCM4.2 ACCESS1.0	27	-12	-8	42	85	15	-30	-30	27	230
RegCM4.2 NorESM1-M	7	4	10	7	-9	25	-11	2	35	69

	Indicates a range of low (drier) results	< -10%
	Indicates a range of medium (little change) results	-10 to +10%
	Indicates a range of high (wetter) results	> 10%

11.4 SUMMARY

An analysis of observed records for the ND region shows a significant increasing trend of temperature, which ranges between 0.15°C and 0.26°C per decade. Observed rainfall records show a significant decreasing trend at most of the stations in the ND region. The extreme temperature indices show the result of the warming trend, with increases in extreme hot days and decreases in extreme cold days. Extreme rainfall indices show a decreasing trend for RX1, RX5 and R95p. Little trend was noted for CWD and CDD.

The climate projections based on eight RCM experiments downscaled from the CMIP5 GCMs for RCP 8.5 clearly indicate that the ND region is projected to warm in future. Annual mean surface temperature is projected to increase by 1.9°C by mid-century and 3.8°C by the end of the century. The rate of warming is greatest in SWMS and least in NEMS. These changes are greater than in the previous projections (MONRE, 2012).

Rainfall projections in the ND region show large uncertainty, since the models simulate both increases and decreases for the future. In general, the majority of RCMs simulate little change (-10% to 10%) in annual rainfall by mid-century and by the end of the century. The most consistent pattern of seasonal rainfall change projected by the models is the rainfall decrease for FIMS of -12% and for SWMS of -9%, with 6 out of 8 models agreeing on this decrease.

12 NORTH CENTRAL REGIONAL REPORT

This chapter summarises the current climate and its trends for the North Central region of Vietnam (see Figure 12-1). The projected changes of temperature and rainfall by mid-century and the end of the century are then presented, first from the GCM results, then from the RCM results. The key messages are summarised at the end of the chapter.

12.1 DESCRIPTION

The North Central (NC) region is a narrow strip of land stretching from Thanh Hoa to Hai Van Pass, bending north-west to south-east along the coastline. The boundary of the east side of the region is a contiguous beach with narrow plains. The terrain gradually increases in elevation westwards from 100-200 m in the hills, to the complex terrain of the Truong Son Mountains on the border of Vietnam and Laos, with peaks from 1000-1500 m high. There are also mountain ranges that extend from the mountains in the west to the sea (like Hoanh Son Range and Bach Ma Range, with Ngang and Hai Van Passes) which divide the coastal plains into small fields in sequence from north to south. On the coastline strip, from the Hoanh Son mountain range south to the Bach Ma range, there are white sand dunes with narrow fields where rice and vegetables are grown.

In the NC region, winters are cool, with occasional hoarfrost. The summer season is hot, with many hot and dry days associated with westerly winds. Although the region experiences its rainy season during summer, the peak in the annual rainfall cycle is observed during the latter part of the year, due to the influences of tropical cyclones and disturbances within the Inter-Tropical Convergence Zone. Moreover, the warmest temperature period does not coincide with the rainy season.

Long-term climatological means and ranges of important variables of the region are given in Table 12-1. The annual average amplitude of the temperature is 12-14°C, the lowest values in North Vietnam. The main rainy season for NC region is from August to December, with the rainfall maximum in September. A secondary rainy season is from May to June. Significant drought conditions occur during mid-summer in association with prolonged hot and dry westerlies. Northerly winds prevail in winter whereas easterlies or south-easterlies prevail in summer.

12.2 OBSERVED CLIMATE

Observed climate trends are analysed using daily data from 70 meteorological stations in Vietnam for the period 1961 to 2011. In addition to trends of mean surface air temperature (or T2m) and precipitation, trends of some extreme indices are also discussed. Definitions of selected extreme indices can be found in ETCCDI (2009), which recommended 27 core Extreme Climate Indices (ECIs) based on daily temperature values or daily precipitation amounts. The indices below are used in this study, mostly following the ETCCDI computational procedures:

- **RX1**: yearly maximum 1-day precipitation (mm).
- **RX5**: annual highest consecutive five-day precipitation amount (mm).
- **R95p**: annual count of days when precipitation exceeds the 95th percentile value for the period 1961-2011.

Figure 12-1: The North Central region with provinces. Insert shows location of region in Vietnam.

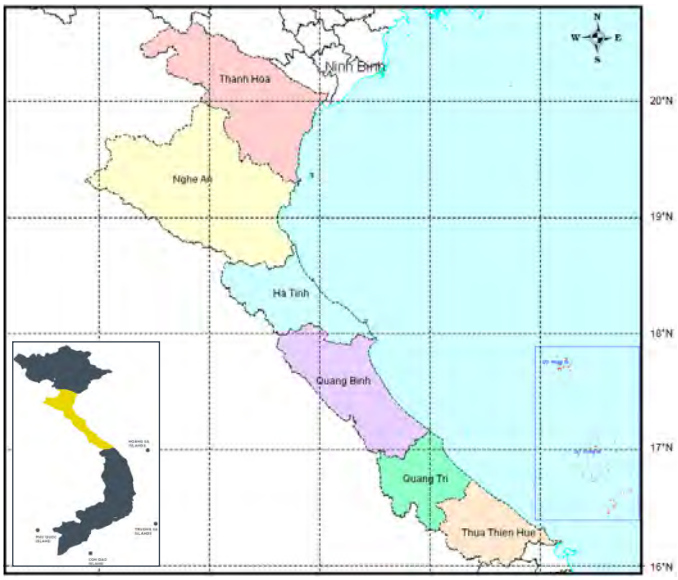

Table 12-1: Observed climate variables and ranges for the NC region. Nguyen and Nguyen (2004).

CLIMATE VARIABLE	VALUE
Terrain height	100 to 1500 m
Annual average solar radiation	110 to 140 kcal cm^{-2}
Radiation balance	65 to 80 kcal cm^{-2}
Annual sunshine hours	1500 to 2000 h
Annual average temperature	23 to 25°C
Maximum temperature	40 to 42.7°C
Minimum temperature	3 to 8°C
Annual temperature amplitude	12 to 14°C
Annual average rainfall	1500 to 2000 mm
Daily maximum rainfall	150 to 500 mm
Rainfall season	Aug to Dec
Number of drizzle days	10 to 30 days
Humidity	84 to 86%
Annual evaporation	700 to 1000 mm
Annual average wind speed	1.5 to 3.0 m sec^{-1}
Maximum wind speed	30 to 40 m sec^{-1}

- **TN10p**: annual count of days when minimum daily temperature is less than the 10th percentile temperature for the period 1961-2011.
- **TX90p**: annual count of days when maximum daily temperature exceeds the 90th percentile temperature for the period 1961-2011.

- **CDD**: consecutive dry days; average annual maximum number of days with daily rainfall less than 1 mm.
- **CWD**: consecutive wet days; average annual maximum number of days with daily rainfall greater than or equal to 1 mm.
- **Hot days**: days with Tmax greater than 35°C.
- **Cold days**: days with Tmin less than 15°C.

Trends are calculated for each station within the region. Statistical significance of the trends is computed using the non-parametric Mann-Kendall test (Kendall, 1975). In this report, trends with significance levels greater than 90% are considered as statistically significant.

12.2.1 Temperature

There has been a significant increase in annual temperature over the last 50 years (Figure 12-2) of between 0.11 and 0.24°C per decade for the stations located in the NC region except for Hue, where the temperature shows a non-statistically significant decreasing trend of -0.08°C per decade. The highest rate of increase, 0.24°C per decade, is at the Tuong Duong station.

The time series of the regionally-averaged annual temperature in Figure 12-3 shows a clear warming trend, with strong year-to year-variations. The warming was less than 1°C during the past 50 years, which gives a regionally-averaged warming of 0.17°C per decade.

12.2.2 Rainfall

From the north of Dong Ha station (except Huong Khe and Tuyen Hoa stations), rainfall shows a small decreasing trend of less than -2.7% per decade, but this trend is not statistically significant (Figure 12-4). In the extreme southern part of the region, rainfall shows a statistically significant increase at three stations, with the largest trend of approximately 11% per decade at the Aluoi station.

The time series of the annual rainfall for the region (Figure 12-5) shows a slight increasing trend with moderate inter-annual variations, with annual values ranging from about 4 mm day^{-1} to almost 9 mm day^{-1}. It is worth mentioning that the increasing trend for the region is dominated by the two southernmost stations.

Figure 12-2: Trend in annual surface air temperature (°C per decade) in the North Central (NC) region for the period 1961 to 2011. A blue circle indicates a decreasing trend and a red circle shows an increasing trend. A filled circle means that the trend is statistically significant at the 90% confidence level.

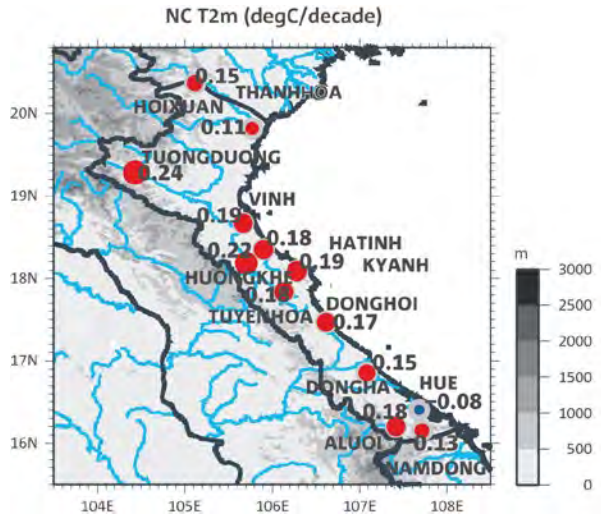

Figure 12-3: Time series of regionally-averaged annual surface air temperature (°C, red) for the NC region with a trend line (dashed). Annual values are shown by black dots.

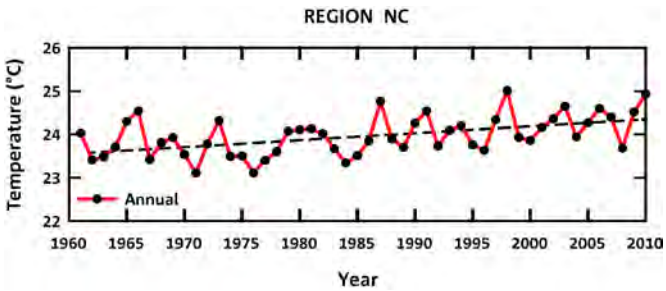

Figure 12-4: Trends in annual rainfall (% per decade) in the NC region for the period 1961 to 2011. A blue circle indicates an increasing trend and a red circle shows a decreasing trend. A filled circle means that the trend is significant at the 90% confidence level.

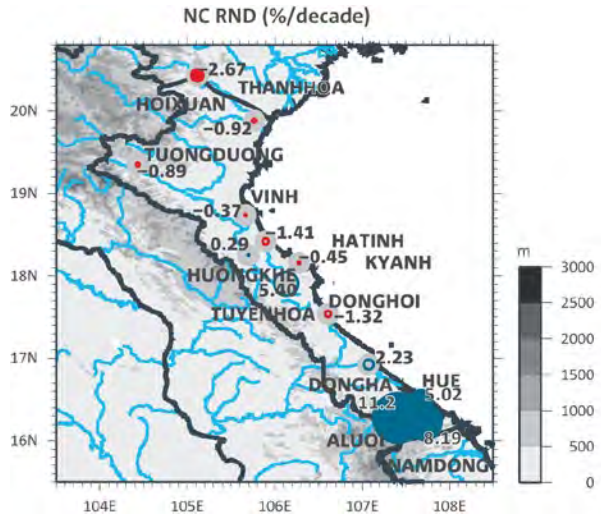

Figure 12-5: Time series of regionally-averaged annual rainfall (mm day^{-1}, blue) for the NC region with a trend line (black dashed line). Annual values are shown by black dots.

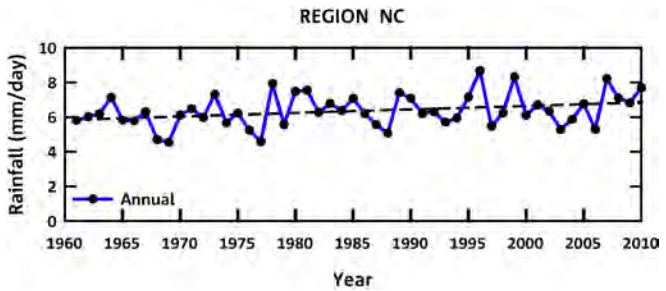

12.2.3 Extremes

Maximum (Tmax) and minimum (Tmin) daily temperatures have increased during the period 1961 to 2011 in the NC region (Figure 12-6). Tmax has increased between 0.13 and 0.26°C per decade in the central part of the region, whereas the rate of increase is smaller in the northern and southern parts. It is noteworthy that the Tmax trends are statically insignificant at the 10% level for the centrally-located stations, while Tmin trends are generally statistically significant everywhere. Tmin has increased faster than Tmax, resulting in a decline in the diurnal temperature range (DTR) over this region during the past 50 years.

The number of hot days has increased significantly by up to 7 days per decade. The number of cold nights has decreased by up to -2 days per decade. The extreme hot days (TX90p) shows a pattern of warming similar to Tmax, with increases in the number of extreme hot days of 3 to 4 days per decade.

The number of extreme cold night (TN10p) is decreasing by five to ten days per decade across the region, like the trend in Tmin.

The annual maximum daily rainfall (RX1) and 5 days extreme rainfall (RX5) do not show a significant trend over the region (Figure 12-7), except for the station Hoi Xuan in the north (for RX1) and for Nam Dong in the south (for both RX1 and RX5). Although the trends are not always significant, it is of interest to note that many stations in the NC region show an increasing trend, which is different than trends in the ND region to the north. The extreme rainfall index R95p also does not show any trends over the region, but three stations show large trends: Tuyen Hoa in central NC with a trend of over +16% and Aluoi and Nam Dong in southern NC with trends of around +20%. CWD shows little trending for most of the stations, except for Aluoi and Nam Dong stations in the south, with increases of more than +1 day per decade. The trend of CDD is small in the region.

Figure 12-6: Trends in Tmax (upper left), Tmin (upper right), TX90p (lower left), and TN10p (lower right) in the NC region for the period 1961 to 2011. A blue circle indicates a decreasing trend and a red circle shows an increasing trend. A filled circle means that the trend is significant at the 90% confidence level.

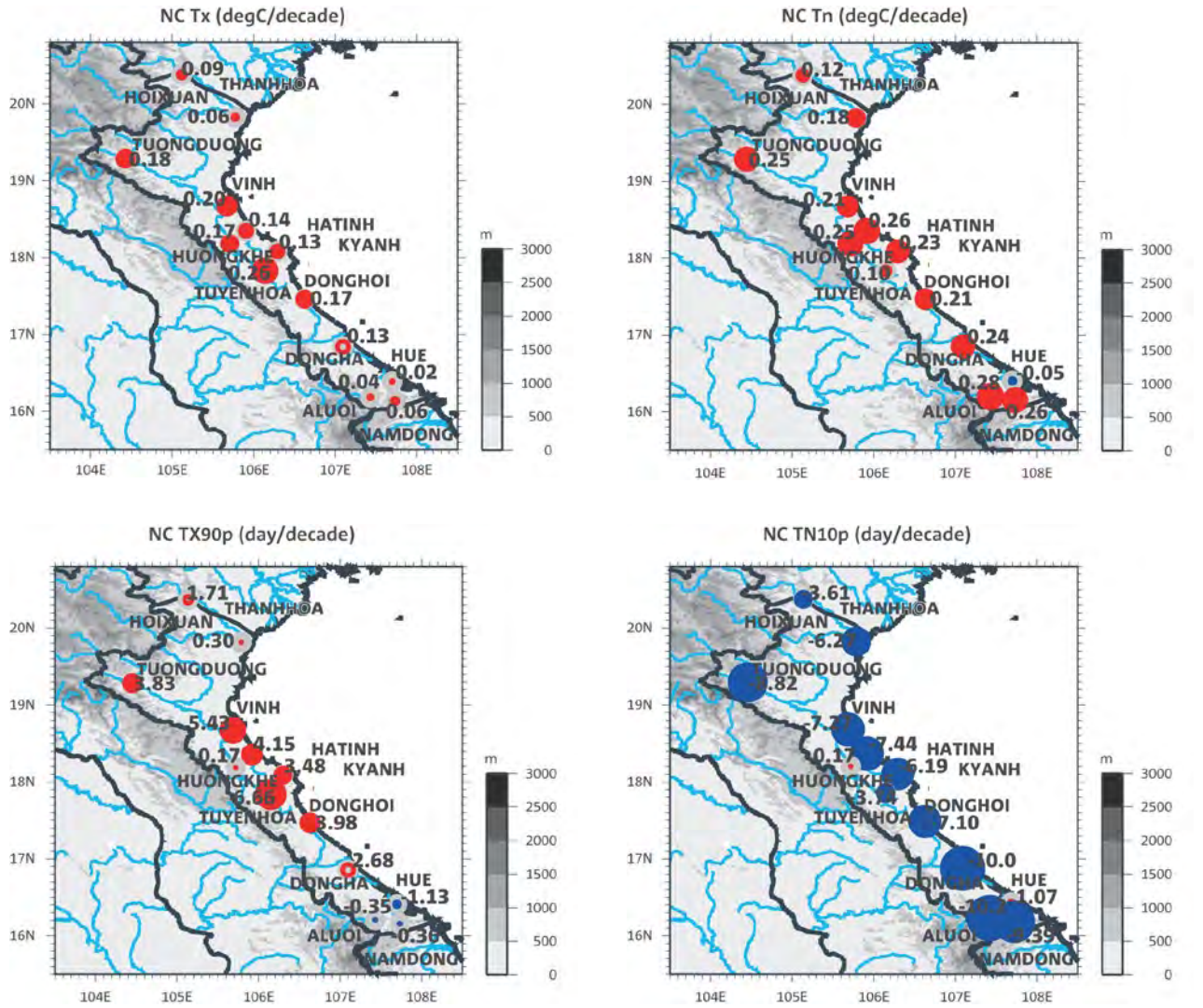

Figure 12-7: Trends in RX1, RX5, R95p, CWD, and CDD in the NC region for the period 1961 to 2011. A blue circle indicates an increasing and a red circle shows a decreasing trend for all but CDD, where red indicates increasing and blue decreasing number of days. A filled circle means that the trend is significant at the 90% confidence level.

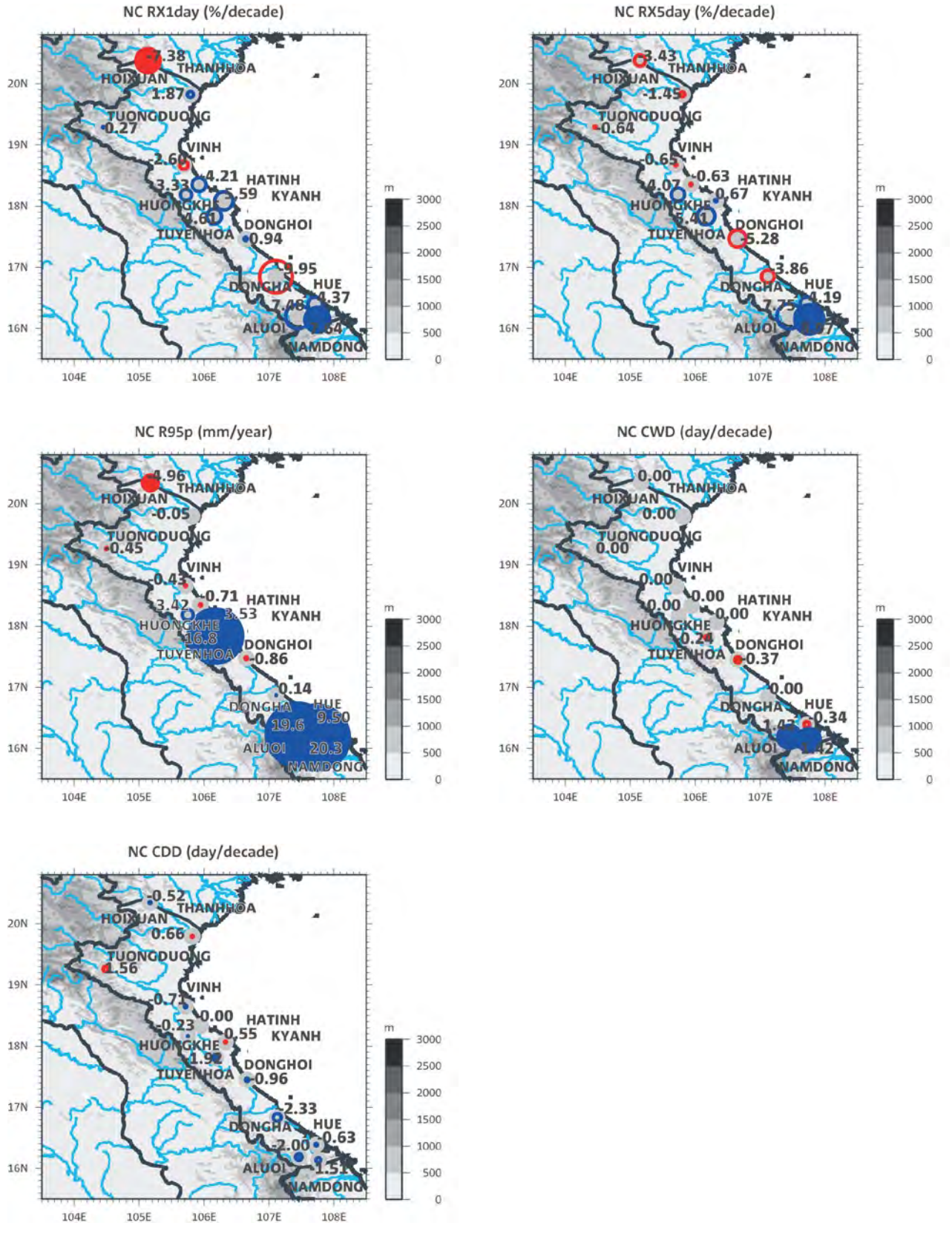

12.3 CLIMATE PROJECTIONS

In this section, projected changes in temperature and rainfall for the NC region are presented. A summary of the CMIP5 GCM results for different RCPs for this region is first presented in the form of line graphs. This is followed by the changes projected by regional climate models, from the new experiments completed for this project, as well as results used for the last official projections completed by IMHEN (MONRE, 2012) using the previous CMIP3 SRES emission scenarios. This provides some indication of the differences in the projections, though direct comparison is difficult, because different models and different scenarios were used.

12.3.1 GCM results

Surface temperature

Projections for near-surface average temperature for the four seasons for the region from the CMIP5 GCMs are presented in Figure 12-8. The warming signal is very clear, with greatest warming for the high emission scenario (RCP 8.5) and less warming for the low emission scenario (RCP 4.5). There is also slightly greater warming of about 4.0°C, (as measured by the median value, line inside colour bar) during FIMS by the end of the century for RCP 8.5, while other seasons show warming of only around 3.5°C by the end of the century.

Figure 12-8: Regionally averaged seasonal surface air temperature changes (°C) for NC. For each season, the time series graph of projections by global climate models (GCM) is shown on the left for the higher (RCP 8.5) greenhouse gas scenario. Black line is from historical GCM runs, red line is the multi-model median projection from GCMs using RCP 8.5. Shadings are between 10% and 90% of 20-year mean values. GCM values have been corrected for 1995-2005 mean bias. Bars on the right for each season show the end-of-century summary of projections by global climate models (GCM, left) and regional climate models (RCM, right) for both lower (RCP 4.5) and higher (RCP 8.5) scenarios.

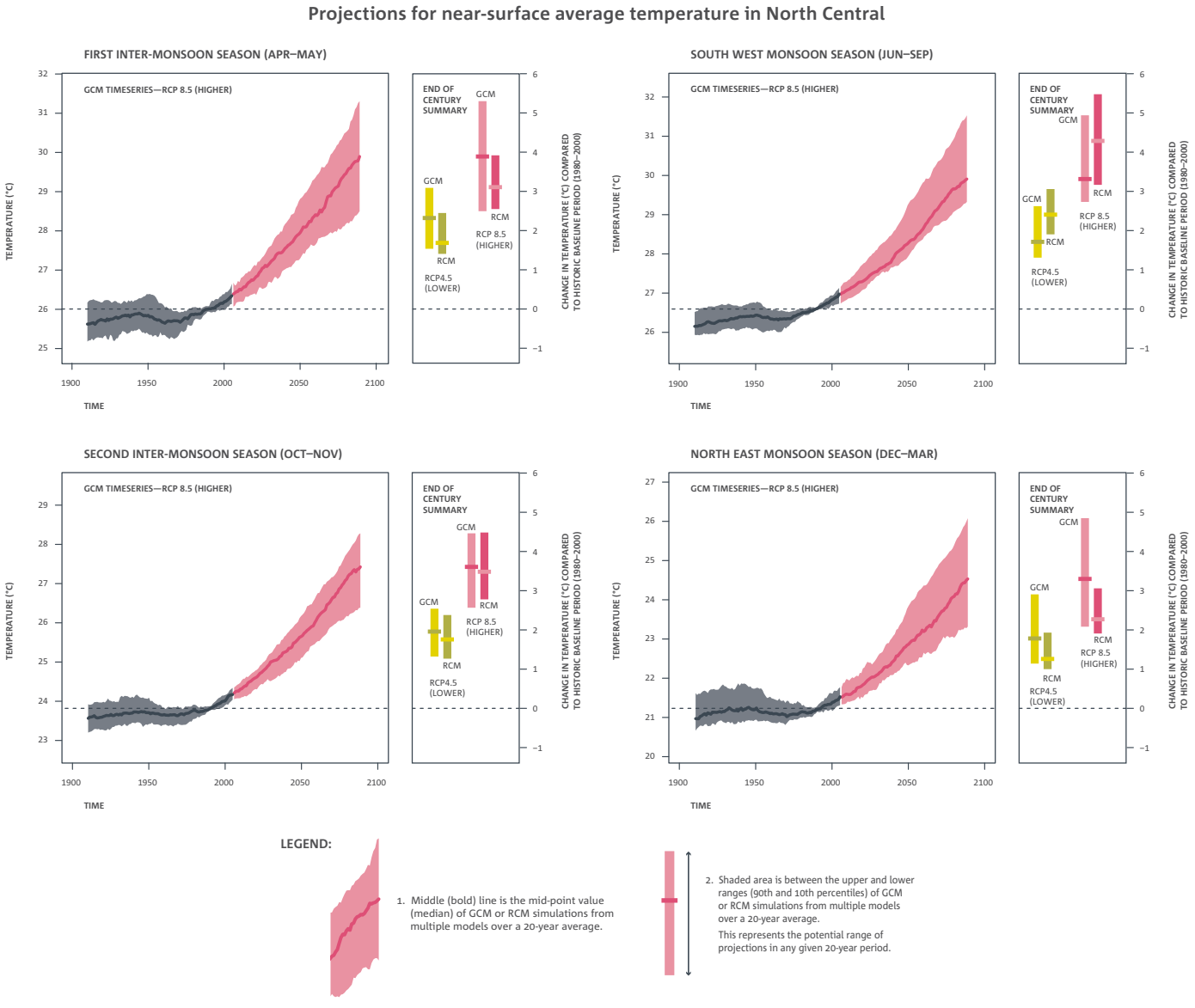

Projections for near-surface maximum temperature for the four seasons for the region from the CMIP5 GCMs are presented in Figure 12-9. Again, the warming signal is very clear and is similar to the average temperature. However, there is also slightly greater warming during FIMS by the end of the century for RCP 8.5 (more than 4°C).

Projections for near-surface minimum temperature for the four seasons for the region from the CMIP5 GCMs are presented in Figure 12-10. The warming signal is again very clear with warming of 3.5 to 4°C for all seasons by the end of the century for RCP 8.5.

Figure 12-9: Regionally averaged seasonal maximum air temperature changes (°C) for NC. For each season, the time series graph of projections by global climate models (GCM) is shown on the left for the higher (RCP 8.5) greenhouse gas scenario. Black line is from historical GCM runs, red line is the multi-model median projection from GCMs using RCP 8.5. Shadings are between 10% and 90% of 20-year mean values. GCM values have been corrected for 1995-2005 mean bias. Bars on the right for each season show the end-of-century summary of projections by global climate models (GCM, left) and regional climate models (RCM, right) for both lower (RCP 4.5) and higher (RCP 8.5) scenarios.

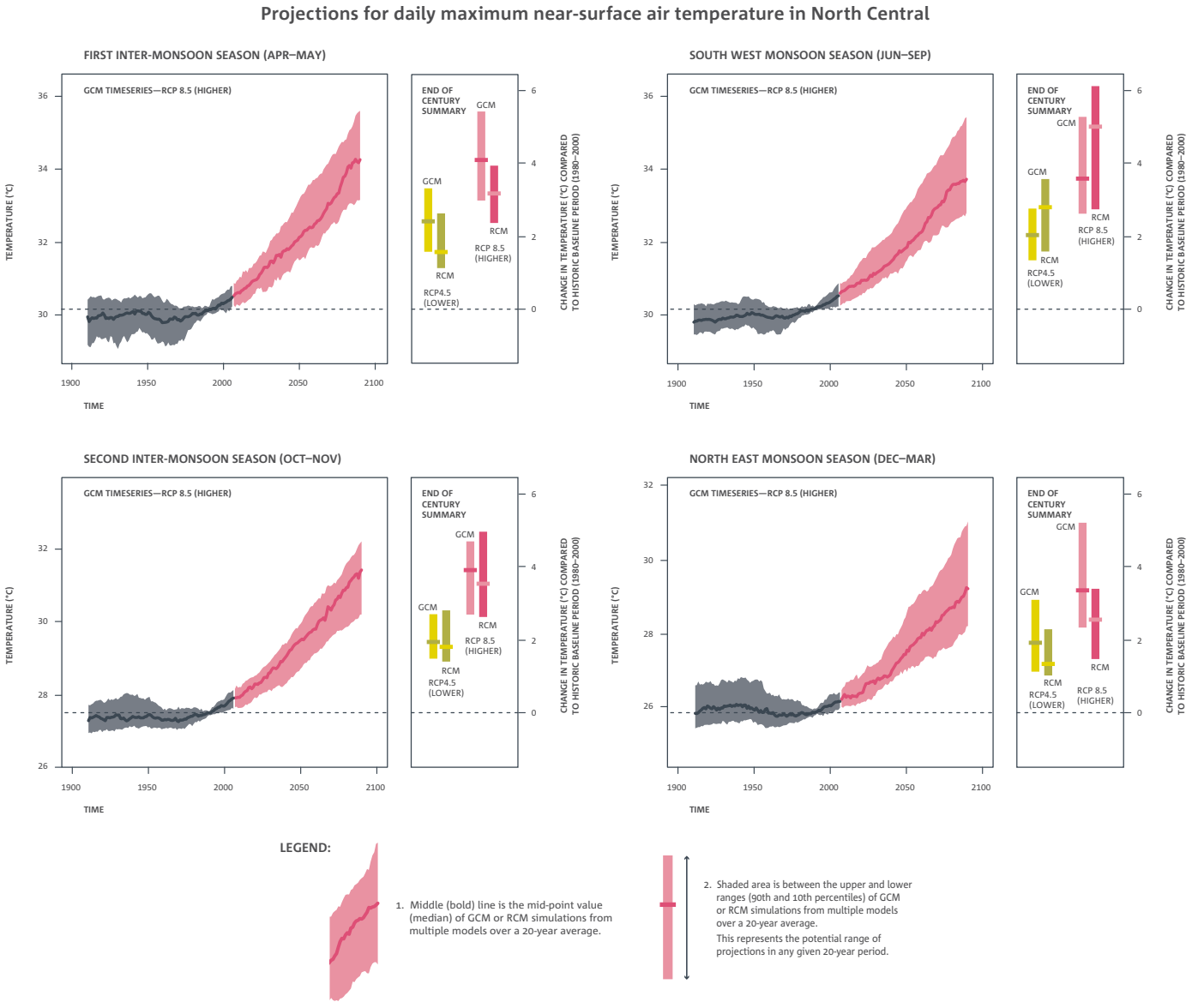

Figure 12-10: Regionally averaged seasonal minimum air temperature changes (°C) for NC. For each season, the time series graph of projections by global climate models (GCM) is shown on the left for the higher (RCP 8.5) greenhouse gas scenario. Black line is from historical GCM runs, red line is the multi-model median projection from GCMs using RCP 8.5. Shadings are between 10% and 90% of 20-year mean values. GCM values have been corrected for 1995-2005 mean bias. Bars on the right for each season show the end-of-century summary of projections by global climate models (GCM, left) and regional climate models (RCM, right) for both lower (RCP 4.5) and higher (RCP 8.5) scenarios.

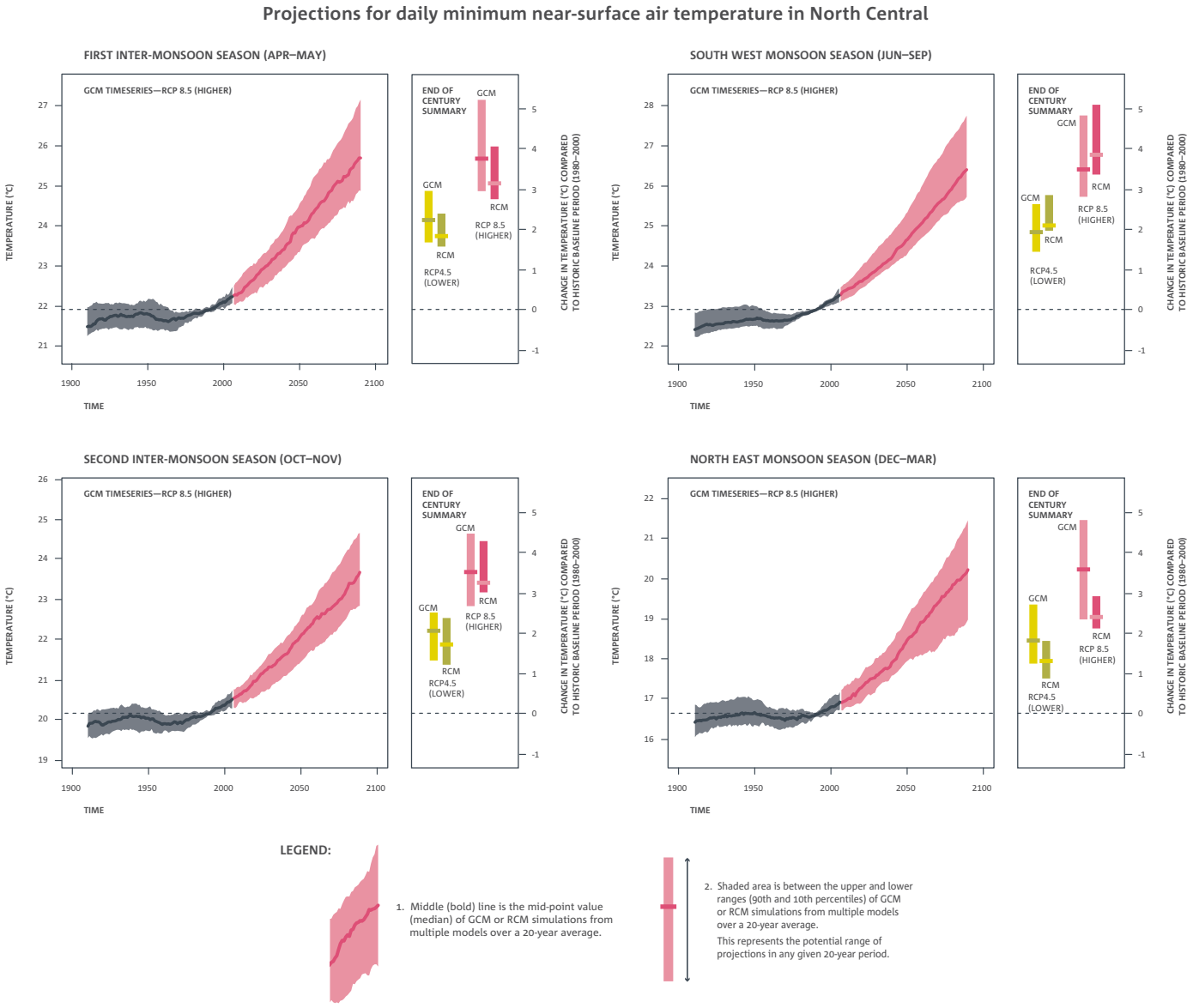

Rainfall

Projections for rainfall for the four seasons for the NC region from the CMIP5 GCMs are presented in Figure 12-11. There is a large range of inter-annual variability simulated by the GCMs for rainfall for this region, as can be seen by the large spread of the colour bar. Most of the seasons show a small increase in rainfall by the end of the century, except FIMS, which shows little change or a very slight decrease.

12.3.2 Regional model results

This section will discuss the projected changes in climate for the future compared with the present climate using ensemble means from eight RCM experiments. In general, these projections do not represent a value specific to any location, since average changes of annual and seasonal values are given for the entire NC region.

Figure 12-11: Regionally averaged seasonal precipitation changes (mm month^{-1} on left axis and % on right axis) for NC. For each season, the time series graph of projections by global climate models (GCM) is shown on the left for the higher (RCP 8.5) greenhouse gas scenario. Black line is from historical GCM runs, red line is the multi-model median projection from GCMs using RCP 8.5. Shadings are between 10% and 90% of 20-year mean values. GCM values have been corrected for 1995-2005 mean bias. Bars on the right for each season show the end-of-century summary of projections by global climate models (GCM, left) and regional climate models (RCM, right) for both lower (RCP 4.5) and higher (RCP 8.5) scenarios.

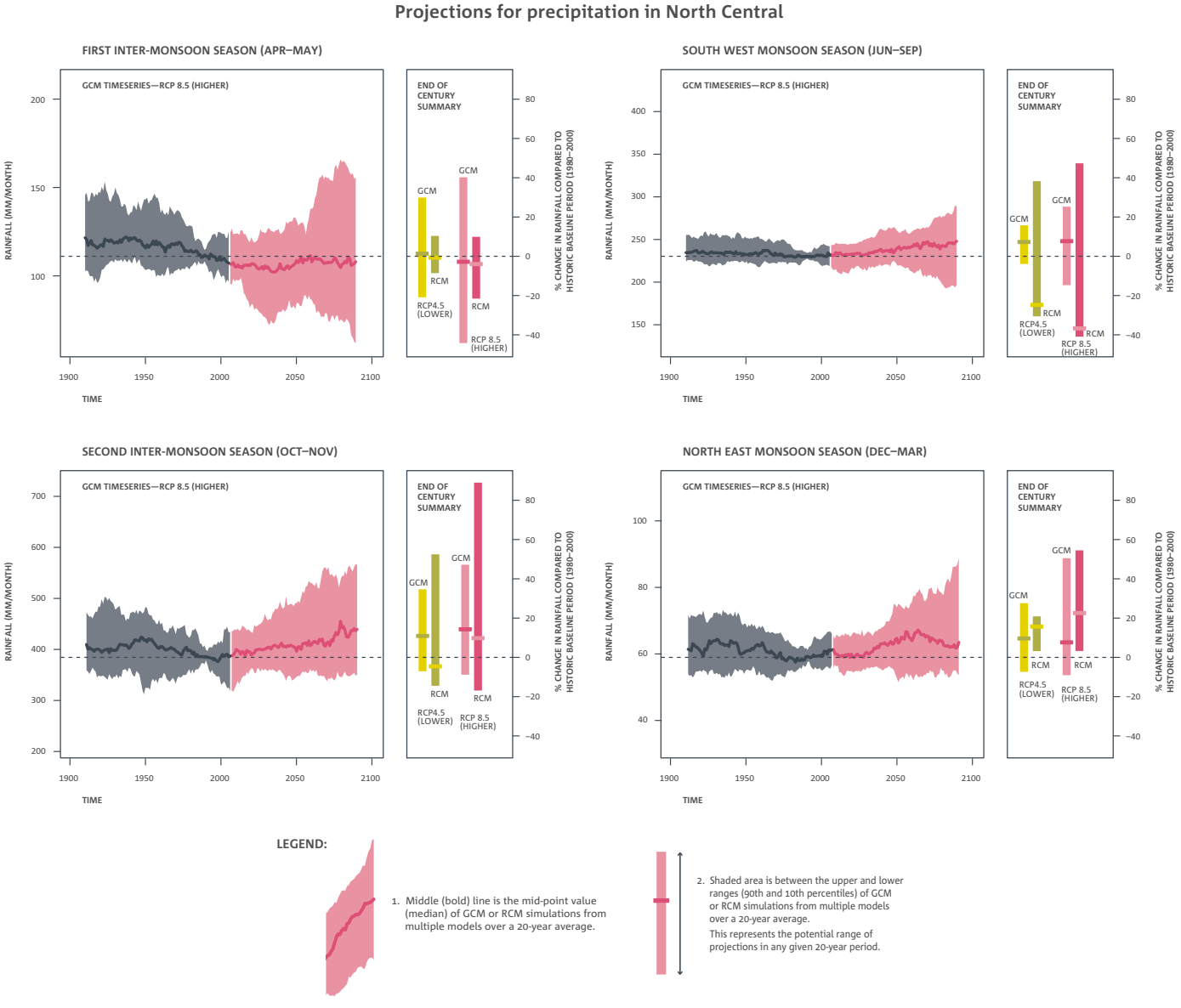

Surface temperature

Table 12-2 to Table 12-6 show projected changes in annual and seasonal surface air temperature (°C) relative to the baseline period (1980-2000) for RCP 8.5 by the middle and the end of the century. As mentioned above, these projections represent an average change over the whole NC geographic region. The increase in annual mean temperature (Tave) is 1.8°C by 2045-2065 and 3.4°C by 2080-2100. The increases in both maximum temperature (Tmax) and minimum temperature (Tmin) are similar to Tave. The projected change in temperature during SWMS is significantly higher than for the other seasons (multi-model mean of 4.4°C for Tave, 4.7°C for Tmax and 4.2°C for Tmin by the end of the century for RCP 8.5), while the temperature during NEMS shows the smallest increase (2.4°C for Tave, 2.4°C for Tmax and 2.5°C for Tmin by the end of century for RCP 8.5).

The increase in annual mean temperature of the multi-model mean is generally greater than the previous climate projections (MONRE, 2012; see Table 12-3), which showed an annual increase of 3.3°C by the end of the century for the SRES A2 emission scenario. However, the new projections show greater warming for SWMS. The PRECIS ensemble mean projections show greater warming than the new projections (except for SWMS), even for the lower emission scenario. Of the eight RCM simulations, CCAM GFDL-CM3 shows the largest increase and RegCM NorESM1-M shows the smallest increase compared with the other models (Table 12-4 to Table 12-6).

Table 12-2: Summary of the multi-model mean and range of projected change in annual and seasonal average, maximum and minimum temperature (°C) for the NC region relative to the baseline period (1980-2000) for RCP 8.5. Green colouring is for increases less than 2°C, yellow from 2-4°C and orange greater than 4°C.

	MID-CENTURY (2045-2065)					END OF THE CENTURY (2080-2100)				
	ANNUAL	NEMS DEC-MAR	FIMS APR-MAY	SWMS JUNE-SEP	SIMS OCT-NOV	ANNUAL	NEMS DEC-MAR	FIMS APR-MAY	SWMS JUNE-SEP	SIMS OCT-NOV
Tave	1.8	1.3	1.7	2.2	1.8	3.4	2.4	3.2	4.4	3.6
(°C)	1.1 to 2.8	1.0 to 1.8	1.0 to 2.7	1.2 to 3.6	1.3 to 3.2	2.2 to 5.0	1.9 to 3.4	2.3 to 4.8	2.2 to 6.6	2.7 to 5.4
Tmax	1.8	1.3	1.5	2.3	2.0	3.5	2.4	3.2	4.7	3.7
(°C)	0.9 to 3.0	0.7 to 1.9	0.7 to 2.7	1.0 to 4.0	1.4 to 3.7	1.6 to 5.6	1.1 to 3.6	1.9 to 5.2	1.6 to 7.5	2.0 to 6.1
Tmin	1.8	1.4	1.9	2.2	1.8	3.4	2.5	3.4	4.2	3.6
(°C)	1.3 to 2.7	1.1 to 1.8	1.3 to 2.8	1.3 to 3.3	1.2 to 2.9	2.6 to 4.7	2.1 to 3.3	2.6 to 4.7	2.6 to 6.0	2.9 to 5.0

Table 12-3: Projected changes in annual and seasonal mean temperature (°C) for the NC region relative to the baseline period (1980-2000) under different SRES emission scenarios (B1, B2, A2, A1B) from a previous study (MONRE, 2012) and the latest PRECIS projections (ensemble means). Green colouring is for increases less than 2°C, yellow from 2-4°C and orange greater than 4°C. Source: IMHEN.

TAVE (°C)	MID-CENTURY (2045-2065)					END OF THE CENTURY (2080-2100)				
	ANNUAL	NEMS DEC-MAR	FIMS APR-MAY	SWMS JUNE-SEP	SIMS OCT-NOV	ANNUAL	NEMS DEC-MAR	FIMS APR-MAY	SWMS JUNE-SEP	SIMS OCT-NOV
	MONRE 2012					MONRE 2012				
B1	1.6	1.5	1.8	1.5	1.5	2.0	1.9	2.3	1.9	1.8
B2	1.7	1.7	2.1	1.7	1.6	2.8	2.6	3.3	2.7	2.6
A2	1.8	1.7	2.1	1.7	1.7	3.3	3.2	3.9	3.2	3.1
	PRECIS					PRECIS				
A1B	2.5	2.6	2.8	2.2	2.3	3.8	3.9	4.2	3.6	3.5

Table 12-4: Projected changes in annual and seasonal average temperature by model (°C) for the NC region relative to the baseline period (1980-2000) for RCP 8.5 from eight RCM experiments. Green colouring is for increases less than 2°C, yellow from 2-4°C and orange greater than 4°C.

TAVE (°C)	MID-CENTURY (2045-2065)					END OF THE CENTURY (2080-2100)				
	ANNUAL	NEMS DEC-MAR	FIMS APR-MAY	SWMS JUNE-SEP	SIMS OCT-NOV	ANNUAL	NEMS DEC-MAR	FIMS APR-MAY	SWMS JUNE-SEP	SIMS OCT-NOV
Multi-model mean	1.8	1.3	1.7	2.2	1.8	3.4	2.4	3.2	4.4	3.6
	Individual RCM simulations					**Individual RCM simulations**				
CCAM ACCESS1.0	1.9	1.5	1.6	2.5	2.0	3.9	3.0	3.3	5.0	4.1
CCAM NorESM1-M	1.7	1.5	1.6	2.1	1.5	3.1	2.1	2.8	4.2	2.9
CCAM MPI-ESM-LR	1.7	1.2	2.0	2.2	1.5	3.6	2.4	3.6	4.9	3.4
CCAM CCSM4	1.5	1.0	1.2	2.1	1.3	3.0	1.9	2.7	4.3	2.9
CCAM CNRM-CM5	1.6	1.2	1.4	2.0	1.7	3.2	2.3	3.1	4.1	3.6
CCAM GFDL-CM3	2.8	1.8	2.7	3.6	3.2	5.0	3.4	4.8	6.6	5.4
RegCM4.2 ACCESS1.0	1.8	1.3	1.7	2.0	2.1	3.2	2.6	3.1	3.6	3.8
RegCM4.2 NorESM1-M	1.1	1.0	1.0	1.2	1.4	2.2	1.9	2.3	2.2	2.7

	Indicates a range of low results	< 2.0°C
	Indicates a range of medium results	2.0 to 4.0°C
	Indicates a range of high results	> 4.0°C

Table 12-5: Projected changes in annual and seasonal maximum temperature by model (°C) for the NC region relative to the baseline period (1980-2000) for RCP 8.5 from eight RCM experiments. Green colouring is for increases less than 2°C, yellow from 2-4°C and orange greater than 4°C.

TMAX (°C)	MID-CENTURY (2045-2065)					END OF THE CENTURY (2080-2100)				
	ANNUAL	NEMS DEC-MAR	FIMS APR-MAY	SWMS JUNE-SEP	SIMS OCT-NOV	ANNUAL	NEMS DEC-MAR	FIMS APR-MAY	SWMS JUNE-SEP	SIMS OCT-NOV
Multi-model mean	1.8	1.3	1.5	2.3	2.0	3.5	2.4	3.2	4.7	3.7
	Individual RCM simulations					**Individual RCM simulations**				
CCAM ACCESS1.0	1.9	1.5	1.4	2.5	2.3	4.2	3.2	3.3	5.5	4.4
CCAM NorESM1-M	1.8	1.6	1.3	2.4	1.4	3.1	1.6	2.6	4.8	2.9
CCAM MPI-ESM-LR	1.7	1.1	1.8	2.3	1.5	3.9	2.6	3.4	5.4	3.7
CCAM CCSM4	1.5	0.9	1.0	2.5	1.5	3.2	1.8	2.6	5.1	2.9
CCAM CNRM-CM5	1.7	1.2	1.2	2.4	2.1	3.7	2.5	3.2	4.7	4.4
CCAM GFDL-CM3	3.0	1.9	2.7	4.0	3.7	5.6	3.6	5.2	7.5	6.1
RegCM4.2 ACCESS1.0	1.6	1.3	1.6	1.7	1.8	3.0	2.6	3.1	3.2	3.3
RegCM4.2 NorESM1-M	0.9	0.7	0.7	1.0	1.4	1.6	1.1	1.9	1.6	2.0

	Indicates a range of low results	< 2.0°C
	Indicates a range of medium results	2.0 to 4.0°C
	Indicates a range of high results	> 4.0°C

Table 12-6: Projected changes in annual and seasonal minimum temperature by model (°C) for the NC region relative to the baseline period (1980-2000) for RCP 8.5 from eight RCM experiments. Green colouring is for increases less than 2°C, yellow from 2-4°C and orange greater than 4°C.

TMIN (°C)	MID-CENTURY (2045-2065)					END OF THE CENTURY (2080-2100)				
	ANNUAL	NEMS DEC-MAR	FIMS APR-MAY	SWMS JUNE-SEP	SIMS OCT-NOV	ANNUAL	NEMS DEC-MAR	FIMS APR-MAY	SWMS JUNE-SEP	SIMS OCT-NOV
Multi-model mean	1.8	1.4	1.9	2.2	1.8	3.4	2.5	3.4	4.2	3.6
	Individual RCM simulations					**Individual RCM simulations**				
CCAM ACCESS1.0	1.9	1.4	1.8	2.5	1.8	3.8	2.8	3.5	4.7	4.1
CCAM NorESM1-M	1.7	1.5	1.8	1.9	1.6	3.2	2.5	3.2	3.9	3.1
CCAM MPI-ESM-LR	1.8	1.3	2.2	2.2	1.6	3.5	2.2	3.8	4.7	3.3
CCAM CCSM4	1.4	1.1	1.4	1.9	1.2	2.9	2.1	2.8	3.9	2.9
CCAM CNRM-CM5	1.5	1.3	1.6	1.8	1.5	3.0	2.2	3.1	3.8	3.2
CCAM GFDL-CM3	2.7	1.8	2.8	3.3	2.9	4.7	3.3	4.7	6.0	5.0
RegCM4.2 ACCESS1.0	1.9	1.3	1.8	2.3	2.3	3.3	2.5	3.1	3.8	4.1
RegCM4.2 NorESM1-M	1.3	1.2	1.3	1.3	1.5	2.6	2.4	2.6	2.6	3.1

	Indicates a range of low results	< 2.0°C
	Indicates a range of medium results	2.0 to 4.0°C
	Indicates a range of high results	> 4.0°C

Rainfall

The rainfall changes are more complex, since the models simulate both increases and decreases. There is also large uncertainty associated with rainfall change. Rainfall projections for the NC region (Table 12-7) show a significant range of changes among the models, both annually and also for the different seasons. Annually, there is a small increase. Larger increases are projected for NEMS and SIMS, while decreases are projected for FIMS and SMWS. The large range suggests large uncertainty in the projected changes of rainfall. In general, the majority of RCMs project increases in NEMS rainfall (7 out of 8 models) and decreases in SWMS (6 out of 8 models) by the end of the century (see Table 12-9), suggesting slightly greater confidence in these seasonal changes. The CCAM CCSM4 simulation shows the greatest seasonal decline (-44% in SWMS), while RegCM4.2 ACCESS1.0 shows the greatest increase in rainfall (+119% for SIMS).

The previous climate change projections (MONRE, 2012; Table 12-8) show small changes, both annually and seasonally, which differs from the new projections. The PRECIS ensemble mean projects decreases for this region for all seasons, though most values are less than 10%. The SWMS decrease is the greatest at -11%, similar to the -17% decrease for the new multi-model mean (Table 12-7).

Table 12-7: Projected changes in annual and seasonal mean rainfall and ranges (%) for the NC region relative to the baseline period (1980-2000) for RCP 8.5. Changes are the multi-model means from eight simulations. Orange colouring is for decreases less than -10%, green for changes between -10% to +10% and blue for increases greater than +10%.

RAIN	MID-CENTURY (2045-2065)					END OF THE CENTURY (2080-2100)				
% CHANGE	ANNUAL	NEMS DEC-MAR	FIMS APR-MAY	SWMS JUNE-SEP	SIMS OCT-NOV	ANNUAL	NEMS DEC-MAR	FIMS APR-MAY	SWMS JUNE-SEP	SIMS OCT-NOV
Multi-model mean	1	13	5	-8	6	3	27	-5	-17	23
Range	-10 to +33	-2 to +27	-9 to +17	-31 to +45	-14 to +81	-18 to +41	-6 to +81	-23 to +17	-44 to +49	-25 to +119

Table 12-8: Projected changes in annual and seasonal rainfall (%) for the NC region relative to the baseline period (1980-2000) for SRES emission scenarios (B1, B2, A2, A1B) from a previous study (MONRE, 2012) and the latest PRECIS projections (ensemble means). Orange colouring is for decreases less than -10%, green for changes between -10% to +10% and blue for increases greater than +10%. Source: IMHEN.

RAIN	MID-CENTURY (2045-2065)					END OF THE CENTURY (2080-2100)				
(%)	ANNUAL	NEMS DEC-MAR	FIMS APR-MAY	SWMS JUNE-SEP	SIMS OCT-NOV	ANNUAL	NEMS DEC-MAR	FIMS APR-MAY	SWMS JUNE-SEP	SIMS OCT-NOV
	MONRE 2012					MONRE 2012				
B1	3	0	-4	4	4	4	1	-6	5	6
B2	3	1	-5	4	5	5	1	-8	7	8
A2	4	1	-5	5	5	6	1	-9	8	9
	PRECIS					PRECIS				
A1B	-5	-1	-1	-6	-6	-7	-6	-7	-11	-1

Table 12-9: Projected changes in annual and seasonal mean rainfall by model (%) for the NC region relative to the baseline period (1980-2000) for RCP 8.5 from the eight RCMs. Orange colouring is for decreases less than -10%, green for changes between -10% to +10% and blue for increases greater than +10%.

RAIN (%)	MID-CENTURY (2045-2065)					END OF THE CENTURY (2080-2100)				
	ANNUAL	NEMS DEC-MAR	FIMS APR-MAY	SWMS JUNE-SEP	SIMS OCT-NOV	ANNUAL	NEMS DEC-MAR	FIMS APR-MAY	SWMS JUNE-SEP	SIMS OCT-NOV
Multi-model mean	1	13	5	-8	6	3	27	-5	-17	23
	Individual RCM simulations					**Individual RCM simulations**				
CCAM ACCESS1.0	-7	12	9	-24	-4	-9	17	0	-36	4
CCAM NorESM1-M	2	13	17	-9	2	12	81	7	-33	17
CCAM MPI-ESM-LR	-5	5	5	-18	-2	-16	7	5	-39	-14
CCAM CCSM4	-4	27	-9	-18	-7	-2	43	-7	-44	16
CCAM CNRM-CM5	-8	26	2	-23	-14	-18	27	-21	-37	-25
CCAM GFDL-CM3	-10	14	0	-31	-5	-17	19	-23	-40	-13
RegCM4.2 ACCESS1.0	33	-2	7	45	81	34	-6	-13	49	119
RegCM4.2 NorESM1-M	11	12	12	12	0	41	26	17	47	77

	Indicates a range of low (drier) results	< -10%
	Indicates a range of medium (little change) results	-10 to +10%
	Indicates a range of high (wetter) results	> 10%

12.4 SUMMARY

An analysis of observational data for the NC region shows a significant increasing trend for temperature of about 0.17°C per decade, while rainfall appears to show little trend (except for three stations in the south, which show statistically significant increases). Both maximum and minimum temperatures have increased, with the minimum temperature showing slightly greater increase in the past 50 years. The number of extreme hot days has increased and the number of cold nights has decreased significantly. Apart from one or two stations in the far south that show increases in extreme rainfall, the rest of the stations in this region do not show any significant trends. In addition to the two southern stations, one central station (Tuyen Hoa) showed large increase in R95p. Most stations had little trend in CWD and CDD.

The annual mean surface temperature of the region is projected to increase by 1.8°C by mid-century (model values range from 1.1°C to 2.8°C) and by 3.4°C by the end of the century (models range from 2.2°C to 5.0°C). The projected seasonal temperature changes show greater increases in SWMS (4.4°C in Tave) and the least increase in NEMS (2.4°C in Tave). These temperature changes are similar to the previous projections (MONRE, 2012), except for SWMS, where the new projections are much larger. The new projections are less than for the PRECIS ensemble mean.

Rainfall projections in the NC region show large uncertainty, since the models simulate both increases and decreases for the future. In general, the majority of RCMs simulate little change (-10% to 10%) in annual rainfall by mid-century and the end of the century. Seasonal changes show increases for NEMS in mid-and end-of-century and for both NEMS and SIMS by the end of the century. The most consistent pattern of rainfall change projected by the models is the rainfall increase for NEMS (multi-model mean of +27%, with 7 out of 8 models projecting an increase) and rainfall decrease for SWMS (multi-model mean of -17%, with 6 out of 8 models agreeing on this decrease by the end of the century).

13 SOUTH CENTRAL REGIONAL REPORT

This chapter summarises the current climate and its trends for the South Central region of Vietnam (see Figure 13-1). The projected changes of temperature and rainfall by mid-century and the end of the century are then presented, first from the GCM results, then from the RCM results. The key messages are summarised at the end of the chapter.

13.1 DESCRIPTION

The South Central region (SC) occupies the southeast area of the Truong Son range, from Hai Van Pass (16°N) to Mui Dinh (11°20'N). The region is situated between the East Sea and the mountainous region to the west and slopes along the east coast. The western boundary is the Truong Son Range, which consists of low hill midlands of weathered basalt. High peaks of the Truong Son Range, such as Ngoc Linh Mountain (2598 m), are located in the northern part of the region, with the eastern slopes covered by dense forest. Eastwards to the Binh Dinh area, the Truong Son Range descends to approximately 1000 m with a few low passes such as the 410 m high Khe Pass connecting eastern and western sides. Except for the Da Rang River, rivers in the SC region are short and steep, but have low discharge levels. They often cause severe flooding during heavy rain periods.

The SC region includes Da Nang city and the provinces of Quang Nam, Quang Ngai, Binh Dinh, Phu Yen, Khanh Hoa, Ninh Thuan and Binh Thuan, all having altitudes of less than 100 m. The southern part of the region is the sunniest area of Vietnam. The main rainy season is from August to December, with a rainfall maximum in October, except to the south of Binh Thuan where the annual cycle is similar to the South region (see Chapter 15). Climatologically, north, north-west, and north-east winds prevail in winter whereas south, south-west, and south-east winds prevail in summer. See Table 13-1 for more details.

13.2 OBSERVED CLIMATE

Observed climate trends are analysed using daily data from 70 meteorological stations in Vietnam for the period 1961 to 2011. In addition to trends of mean surface air temperature (or T2m) and precipitation, trends of some extreme indices are also discussed. Definitions of selected extreme indices can be found in ETCCDI (2009), which recommended 27 core Extreme Climate Indices (ECIs) based on daily temperature values or daily precipitation amounts. The indices below are used in this study, mostly following the ETCCDI computational procedures:

- **RX1**: yearly maximum 1-day precipitation (mm).
- **RX5**: annual highest consecutive five-day precipitation amount (mm).
- **R95p**: annual count of days when precipitation exceeds the 95th percentile value for the period 1961-2011.
- **TN10p**: annual count of days when minimum daily temperature is less than the 10th percentile temperature for the period 1961-2011.
- **TX90p**: annual count of days when maximum daily temperature exceeds the 90th percentile temperature for the period 1961-2011.
- **CDD**: consecutive dry days; average annual maximum number of days with daily rainfall less than 1 mm.

Figure 13-1: The South Central region with provinces. Insert shows location of the region in Vietnam.

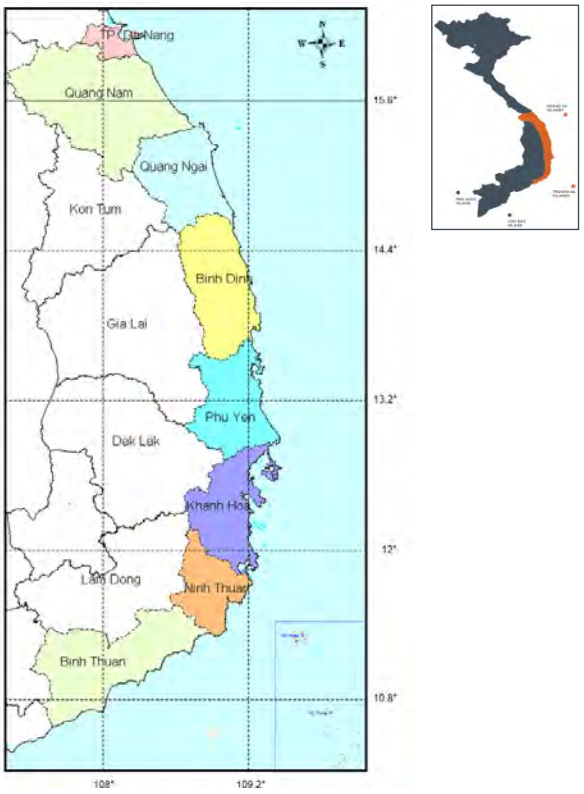

Table 13-1: Observed climate variables and ranges for the SC region. Nguyen and Nguyen (2004).

CLIMATE VARIABLE	VALUE
Terrain height	< 100 m
Annual average solar radiation	140 to 160 kcal cm^{-2}
Radiation balance	75 to 100 kcal cm^{-2}
Annual sunshine hours	2000 to 2500 h
Annual average temperature	25 to 27°C
Maximum temperature	40 to 42°C
Minimum temperature	8 to 13°C
Annual average temperature amplitude	2 to 8°C
Annual average rainfall	1200 to 2000 mm (1600 to 2200 mm in north) (< 800 mm in south)
Daily maximum rainfall	300 to 500 mm
Rainfall season	Aug to Dec
Humidity	80 to 84%
Annual evaporation	1000 to 1600 mm
Annual average wind speed	1.5 to 3.0 m sec^{-1}
Maximum wind speed	30 to 40 m sec^{-1}

- **CWD**: consecutive wet days; average annual maximum number of days with daily rainfall greater than or equal to 1 mm.
- **Hot days**: days with Tmax greater than 35°C.
- **Cold days**: days with Tmin less than 15°C.

Trends are calculated for each station within the region. Statistical significance of the trends is computed using the non-parametric Mann-Kendall test (Kendall, 1975). In this report, trends with significance levels greater than 90% are considered as statistically significant.

13.2.1 Temperature

There has been an increase in annual temperature at stations located in this region, particularly from the mid-1970s to 2010 (approximately 0.08 to 0.16°C). The highest increasing rate of 0.16°C is observed at Quang Ngai (Figure 13-2).

However, the annual area-averaged temperature for the region (Figure 13-3) does not show a clear trend when we consider the whole period from 1961 to 2011, with year-to-year variation of about 0.5°C.

13.2.2 Rainfall

An observed increase of annual rainfall is noted at all stations in the SC region (Figure 13-4). At some stations (Phan Rang), rainfall has increased by up to 13% per decade. However, trends are not statistically significant at the 90% level at Tra My, Nha Trang and Phu Quy stations.

The time series of the regionally-averaged annual rainfall for SC (Figure 13-5) confirms the significant increase in annual rainfall. There is also fairly large inter-annual variability for this region.

Figure 13-2: Trend in annual mean surface air temperature (°C per decade) in the South Central region (SC) for the period 1961 to 2011. A blue circle indicates a decreasing trend and a red circle shows an increasing trend, while a filled circle indicates that the trend is statistically significant at the 90% level.

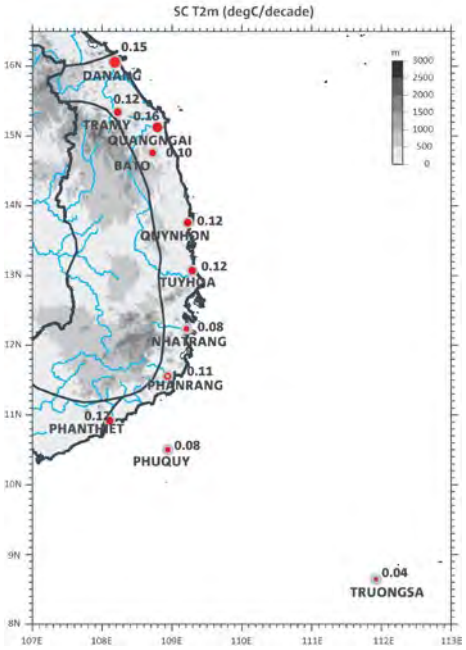

Figure 13-3: Time series of regionally-averaged annual surface air temperature (°C, red) for region SC with a trend line (dashed black line). Annual values are shown by black dots.

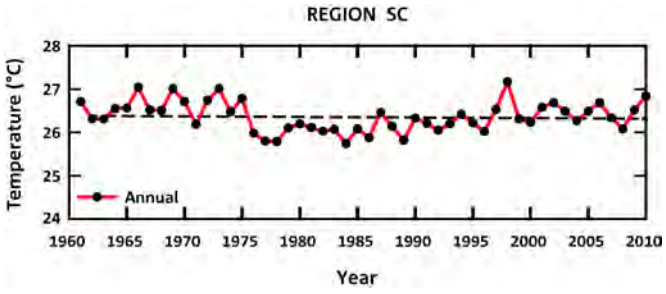

Figure 13-4: Trends in annual rainfall (% per decade) in the SC region for the period 1961 to 2011. A blue circle indicates an increasing trend and red circle shows a decreasing trend, while a filled circle shows that the trend is statistically significant at the 90% level.

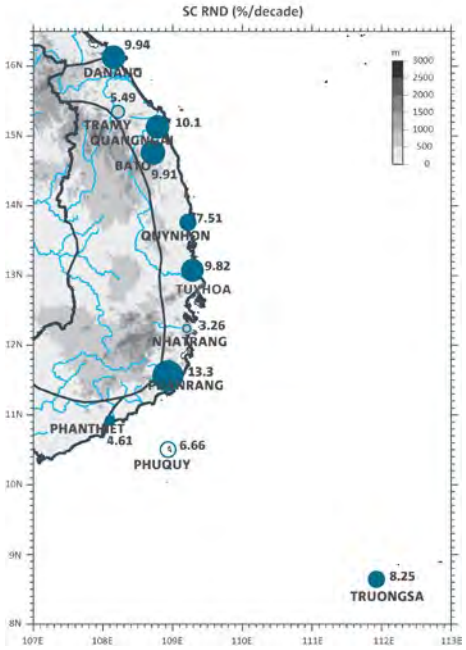

Figure 13-5: Time series of regionally-averaged annual rainfall (mm day^{-1}, blue) for region SC with trend line (dashed black line). Annual values are shown by black dots.

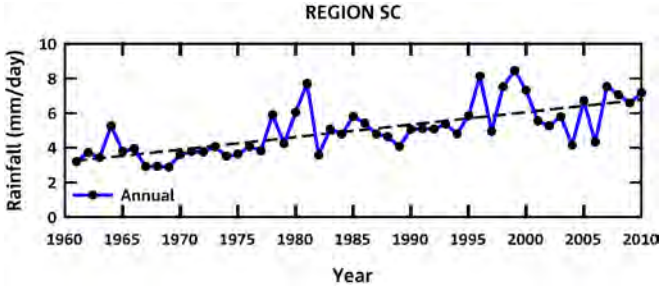

13.2.3 Extremes

Generally, the minimum daily temperature (Tmin) has significantly increased in the region (up to +0.36°C at Quang Ngai), while the increase of the maximum temperature (Tmax) is generally small and insignificant (Figure 13-6). Therefore, the diurnal temperature range (DTR) over the SC region has a decreasing trend during the past 50 years.

The number of hot days has significantly increased by up to 4 days per decade at two stations. The number of cold nights has changed little. The extreme hot days index (TX90p) shows some increases, except at Phu Quy, where it decreases. For many stations, the trend is not significant. A significant decreasing trend (up to -17 days per decade) in extreme cold nights (TN10p) is evident across the region.

An analysis of extreme rainfall indices suggest that RX1, RX5 and R95p rainfall events have increased in the SC region (Figure 13-7). RX1 increased by 14% per decade (at Quang Ngai station), whereas RX5 increased by 13% per decade (at Phu Quy station). R95p has increased significantly at many stations in the region, with an increase of 14.9 mm decade at Tuy Hoa station. Although there are clear increasing trends in these indices, they are not statistically significant at all stations in the region. The number of consecutive wet and dry days (CWD, CDD) does not show a systematic trend in the region. In summary, the systematic increasing trends in the RX1, RX5 and R95p indices are reflected by the increase in flood-related disasters over this region during the past 50 years.

Figure 13-6: Trends in Tmax (upper left), Tmin (upper right), TX90p (lower left), and TN10p (lower right) in the SC region for the period 1961-2011. A blue circle indicates a decreasing trend and red an increasing trend, while a filled circle means that the trend is significant at the 90% level.

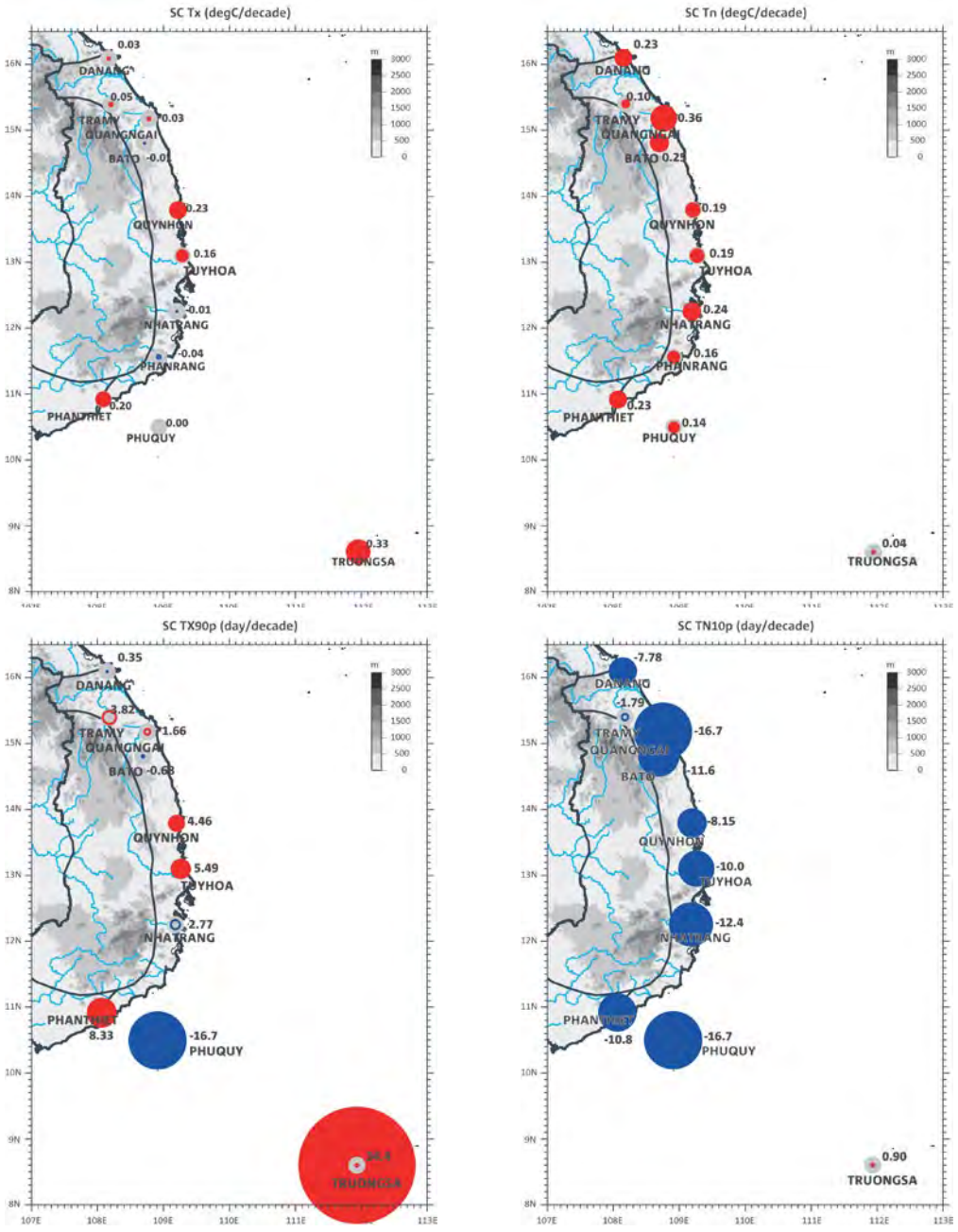

Figure 13-7: Trends in RX1, RX5, R95p, CWD, and CDD in the SC region for the period 1961-2011. A blue circle indicates an increasing and red a decreasing trend for all but CDD, where red indicates an increasing and blue a decreasing number of days. A filled circle means that the trend is significant at the 90% level.

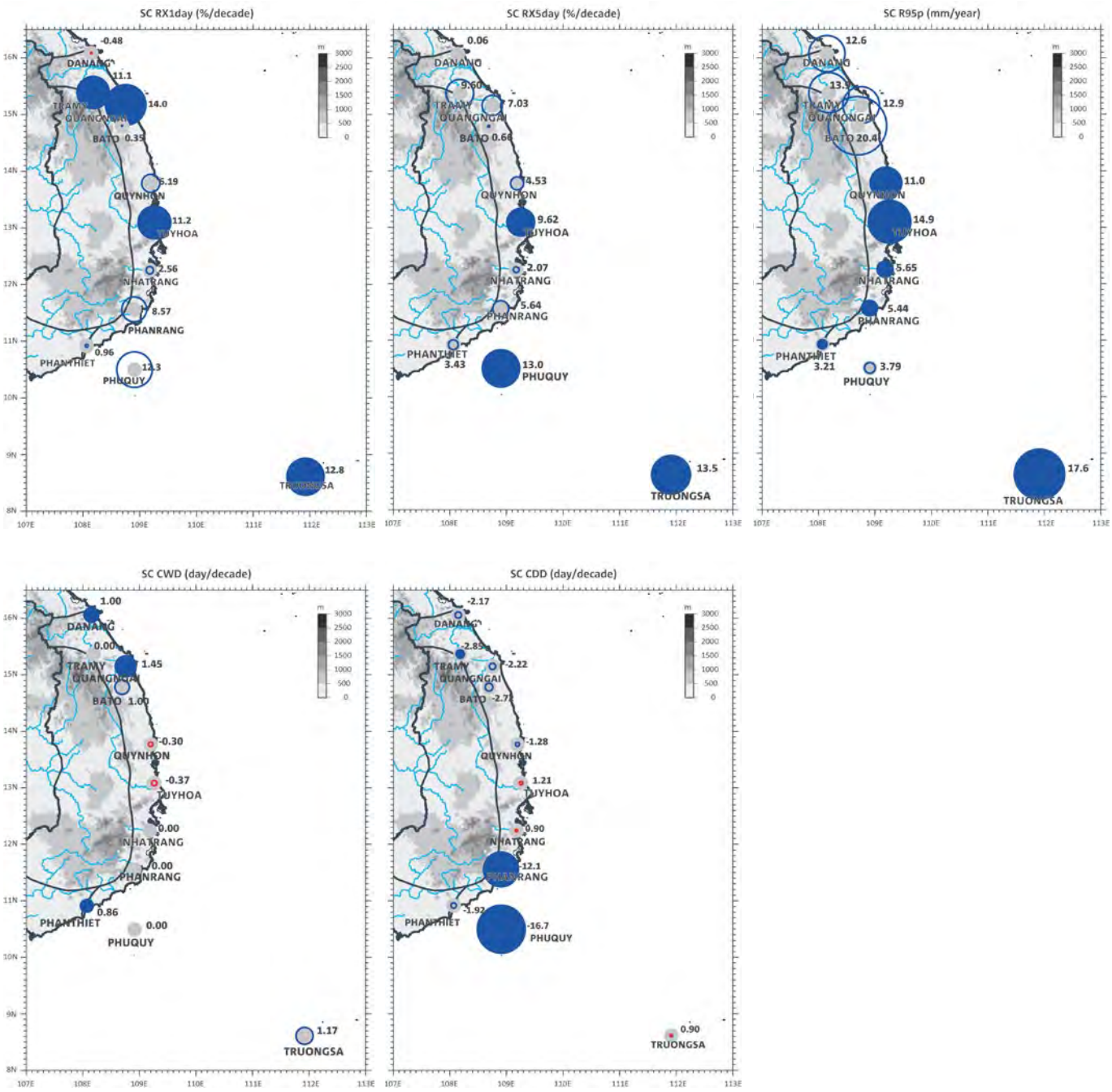

13.3 CLIMATE PROJECTIONS

In this section, projected changes in temperature and rainfall for the SC region are presented. A summary of the CMIP5 GCM results for different RCPs for this region is first presented in the form of line graphs. This is followed by the projected changes by regional climate models, both from the new experiments completed for this project and the results used for the last official projections (MONRE, 2012) completed by IMHEN using the previous CMIP3 SRES emission scenarios. This provides some indication of the differences of the projections, though direct comparison is difficult, since different models and different scenarios were used.

13.3.1 GCM results

Surface temperature

Projections for near-surface average temperature for the four seasons for this region from the CMIP5 GCMs are presented in Figure 13-8. The warming signal is very clear, with greatest warming for the high emission scenario (RCP 8.5) and least warming for the low emission scenario (RCP 4.5). There is also slightly greater warming of about 4.0°C for RCP 8.5 (as measured by the median value – line inside the colour bar) during FIMS by the end of the century, while other seasons have warming of around 3.5°C by the end of the century.

Figure 13-8: Regionally averaged seasonal surface air temperature changes (°C) for SC. For each season, the time series graph of projections by global climate models (GCM) is shown on the left for the higher (RCP 8.5) greenhouse gas scenario. Black line is from historical GCM runs, red line is the multi-model median projection from GCMs using RCP 8.5. Shadings are between 10% and 90% of 20-year mean values. GCM values have been corrected for 1995-2005 mean bias. Bars on the right for each season show the end-of-century summary of projections by global climate models (GCM, left) and regional climate models (RCM, right) for both lower (RCP 4.5) and higher (RCP 8.5) scenarios.

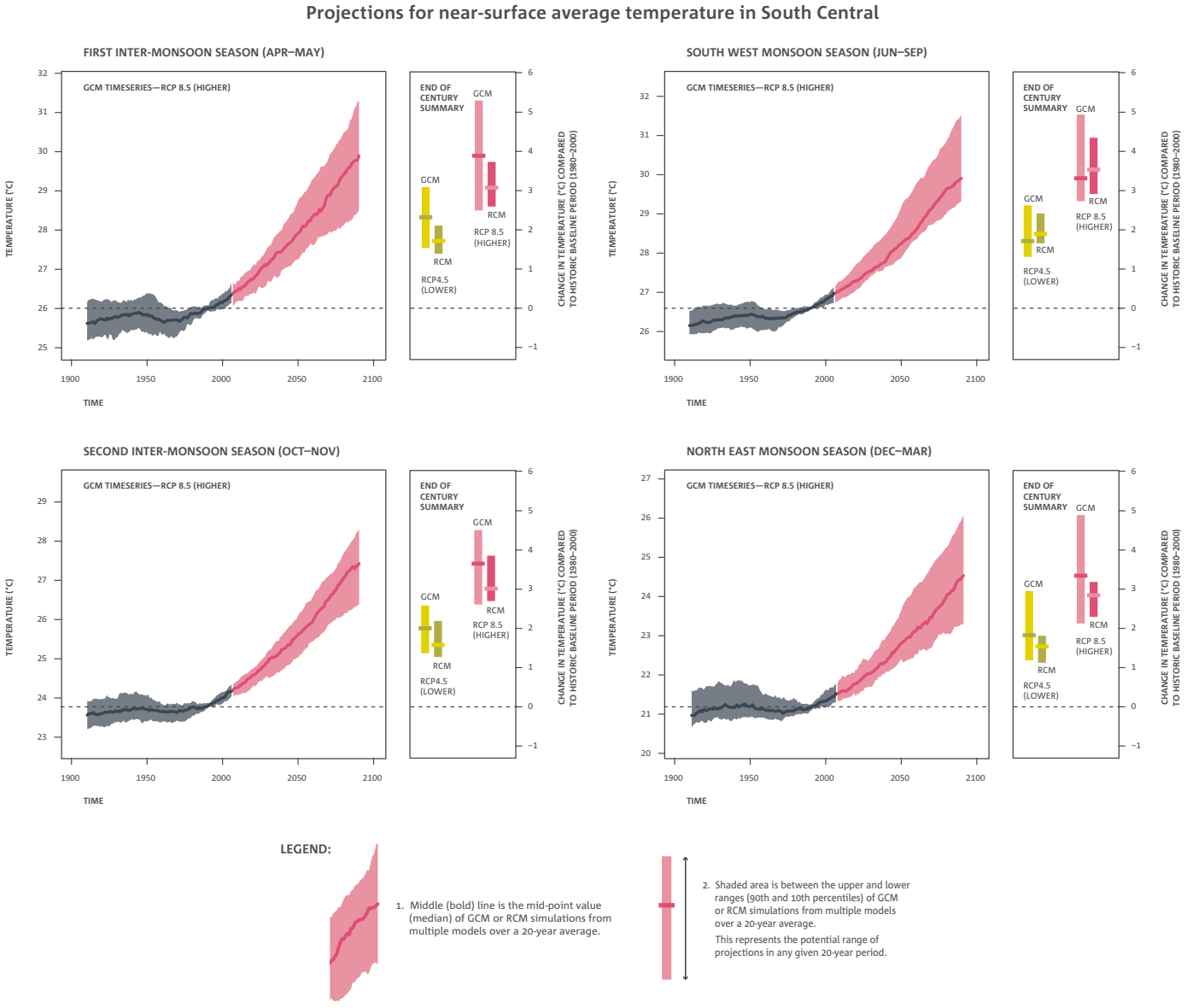

Projections for near-surface maximum temperature for the four seasons from the CMIP5 GCMs are presented in Figure 13-9. Again the warming signal is very clear and is similar to the average temperature.

Projections for near-surface minimum temperature for the four seasons for the region from the CMIP5 GCMs are presented in Figure 13-10. The warming signal is again very clear and is similar to the average temperature. Moreover, the warming in minimum temperature is similar for all seasons by the end of the century for RCP 8.5 (slightly less than 4°C). For FIMS, the maximum temperature is projected to warm slightly faster than the minimum temperature by the end of the century for RCP 8.5.

Figure 13-9: Regionally averaged seasonal maximum air temperature changes (°C) for SC. For each season, the time series graph of projections by global climate models (GCM) is shown on the left for the higher (RCP 8.5) greenhouse gas scenario. Black line is from historical GCM runs, red line is the multi-model median projection from GCMs using RCP 8.5. Shadings are between 10% and 90% of 20-year mean values. GCM values have been corrected for 1995-2005 mean bias. Bars on the right for each season show the end-of-century summary of projections by global climate models (GCM, left) and regional climate models (RCM, right) for both lower (RCP 4.5) and higher (RCP 8.5) scenarios.

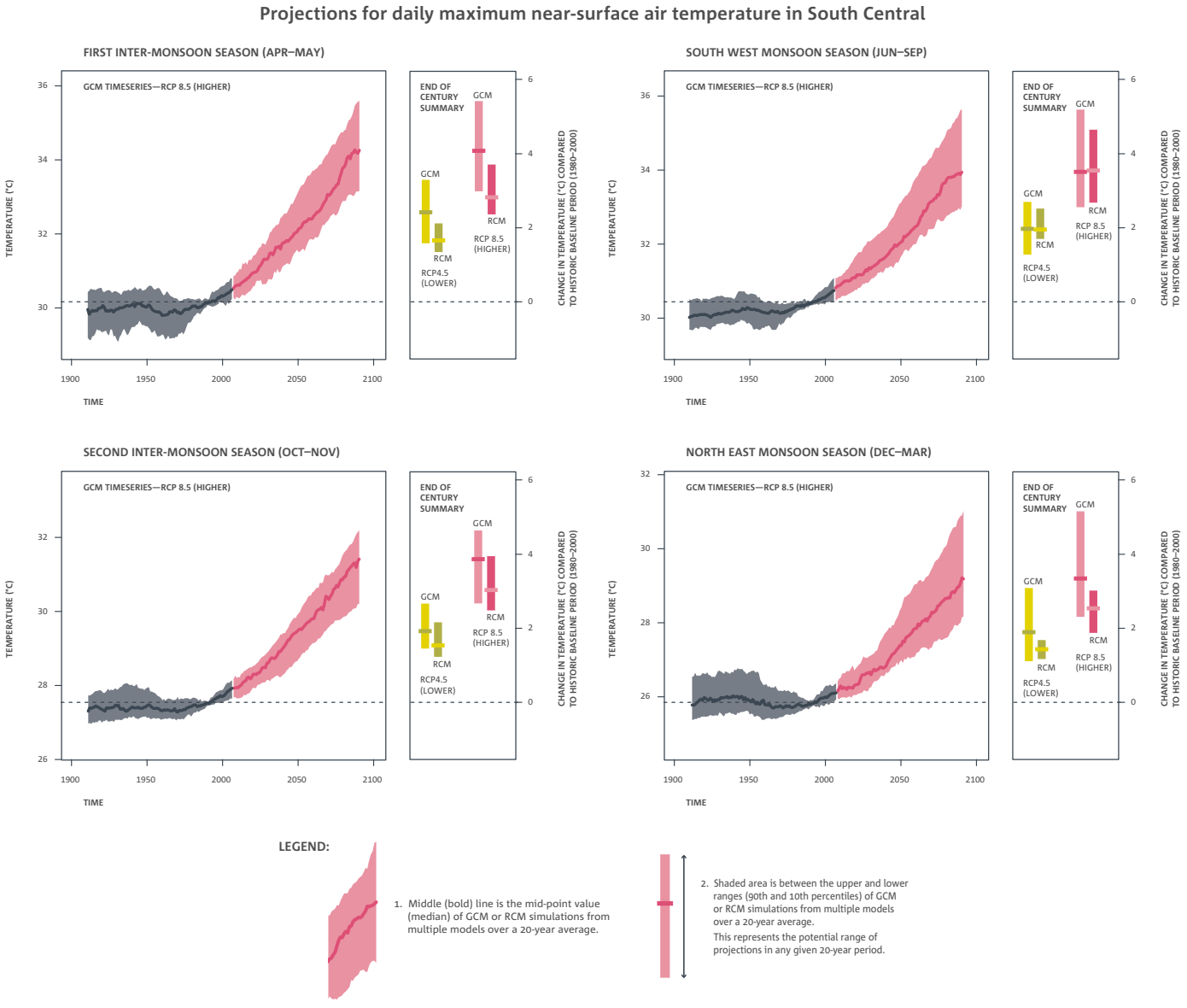

Figure 13-10: Regionally averaged seasonal minimum air temperature changes (°C) for SC. For each season, the time series graph of projections by global climate models (GCM) is shown on the left for the higher (RCP 8.5) greenhouse gas scenario. Black line is from historical GCM runs, red line is the multi-model median projection from GCMs using RCP 8.5. Shadings are between 10% and 90% of 20-year mean values. GCM values have been corrected for 1995-2005 mean bias. Bars on the right for each season show the end-of-century summary of projections by global climate models (GCM, left) and regional climate models (RCM, right) for both lower (RCP 4.5) and higher (RCP 8.5) scenarios.

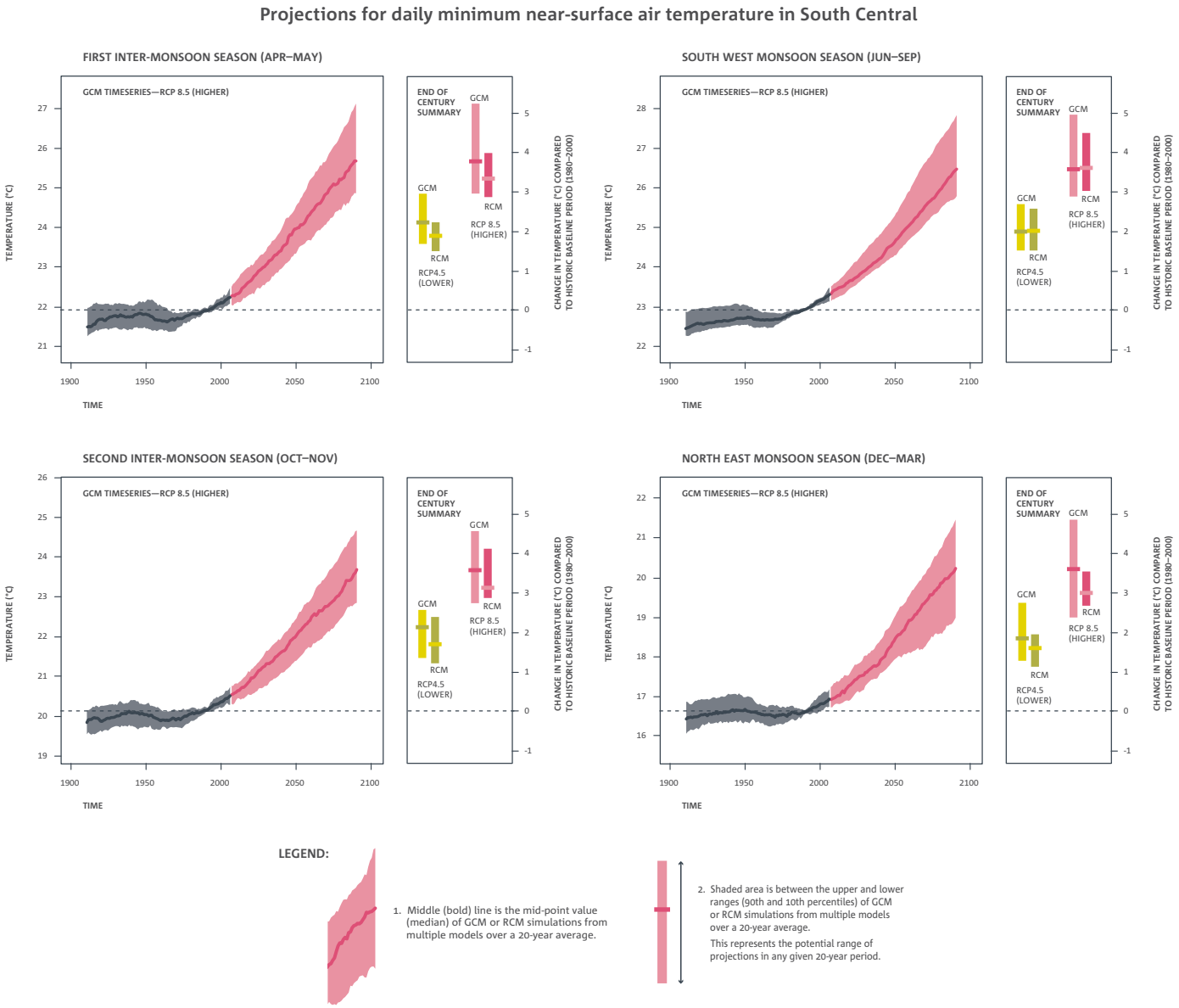

Rainfall

Projected changes in rainfall for the four seasons from the CMIP5 GCMs are presented in Figure 13-11. There is a large range of inter-annual variability simulated by the GCMs for rainfall for this region, as can be seen by the large spread of the colour bar. Most seasons show increases in projected rainfall by the end of the century, except FIMS, which shows little change.

13.3.2 Regional model results

This section will discuss the projected changes by the middle of the century (2045-2065) and by the end of the century (2080-2100) compared with the present climate (1980-2000) using ensemble outputs from the eight RCMs used in this study. In general, these projections do not represent a value for any specific location, since the spatial patterns of climate change across the SC region are not presented. Instead, what is presented here is the average change annually and also for the four seasons for the entire region.

Figure 13-11: Regionally averaged seasonal precipitation changes (mm month^{-1} on left axis and % on right axis) for SC. For each season, the time series graph of projections by global climate models (GCM) is shown on the left for the higher (RCP 8.5) greenhouse gas scenario. Black line is from historical GCM runs, red line is the multi-model median projection from GCMs using RCP 8.5. Shadings are between 10% and 90% of 20-year mean values. GCM values have been corrected for 1995-2005 mean bias. Bars on the right for each season show the end-of-century summary of projections by global climate models (GCM, left) and regional climate models (RCM, right) for both lower (RCP 4.5) and higher (RCP 8.5) scenarios.

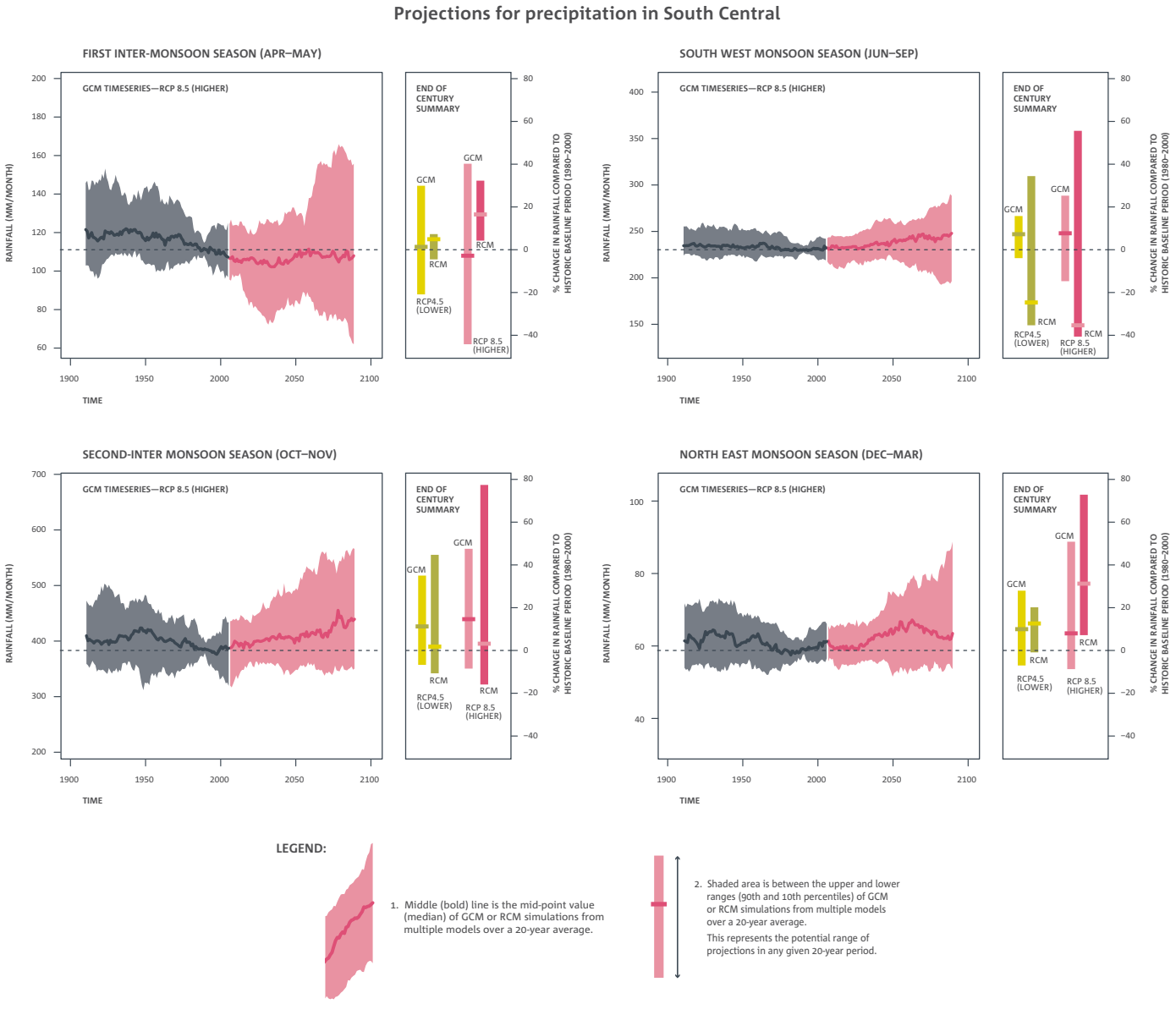

Surface temperature

Table 13-2 to Table 13-6 show projected changes in annual and seasonal surface air temperature (°C) for RCP 8.5 relative to the baseline period 1980-2000. These projections represent an average change over the whole of the SC geographical region. The increase in mean annual temperature (Tave) is 1.7°C by 2045-2065 and 3.2°C by 2080-2100. The maximum temperature (Tmax) increases are similar or slightly less, while the minimum temperature (Tmin) increases slightly more, indicating a projected decrease in the mean annual diurnal temperature range. The projected change in temperature in SWMS is higher than for the other seasons (multi-model mean of 3.6°C for Tave, 3.7°C for Tmax and 3.6 °C for Tmin) by the end of the century for RCP 8.5, while the temperature during NEMS has the smallest increase (2.8°C for Tave, 2.4°C for Tmax and 3.1°C for Tmin by the end of the century for RCP 8.5).

The increase in the multi-model mean temperature (+1.7°C) is similar to the previous projection (1.5°C with A2) at mid-century, but generally greater (+3.2°C vs +2.7°C) at the end of the century (MONRE, 2012; see Table 13-3). However, the new projections show larger increases during SWMS and SIMS than the previous projections. The PRECIS ensemble-mean projections show similar warming to the new projections. Of the eight RCM models, CCAM GFDL-CM3 shows the largest seasonal increase (5.0°C for SWMS at the end of the century) and RegCM4.2 NorESM1-M shows the least increase (2.2°C for NEMS at the end of the century, Table 13-4 to Table 13-6).

Table 13-2: Summary of multi-model mean and range of projected change in annual and seasonal average, maximum and minimum temperatures (°C) for the SC region relative to the baseline period (1980-2000) for RCP 8.5. Green colouring is for increases less than 2°C, yellow from 2-4°C and orange greater than 4°C.

	MID-CENTURY (2045-2065)					END OF THE CENTURY (2080-2100)				
	ANNUAL	NEMS DEC-MAR	FIMS APR-MAY	SWMS JUNE-SEP	SIMS OCT-NOV	ANNUAL	NEMS DEC-MAR	FIMS APR-MAY	SWMS JUNE-SEP	SIMS OCT-NOV
Tave	1.7	1.5	1.7	1.9	1.7	3.2	2.8	3.1	3.6	3.2
(°C)	1.2 to 2.5	1.2 to 2.1	1.2 to 2.6	1.2 to 2.8	1.2 to 2.7	2.4 to 4.3	2.2 to 3.5	2.4 to 4.3	2.4 to 5.0	2.6 to 4.3
Tmax	1.6	1.3	1.5	1.9	1.7	3.1	2.4	3.0	3.7	3.1
(°C)	1.0 to 2.4	0.8 to 1.8	0.9 to 2.4	1.0 to 3.0	1.3 to 2.7	1.7 to 4.3	1.4 to 3.1	1.9 to 4.4	1.8 to 5.5	2.2 to 4.4
Tmin	1.8	1.7	1.9	1.9	1.7	3.3	3.1	3.4	3.6	3.3
(°C)	1.4 to 2.6	1.4 to 2.4	1.4 to 2.7	1.4 to 2.8	1.1 to 2.7	2.8 to 4.4	2.5 to 3.9	2.8 to 4.5	2.9 to 4.9	2.6 to 4.2

Table 13-3: Projected changes in annual and seasonal mean temperature (°C) for the SC region relative to the baseline period (1980-2000) for various SRES emission scenarios (B1, B2, A2, A1B) from a previous study (MONRE, 2012) and the latest PRECIS projections (ensemble mean). Green colouring is for increases less than 2°C, yellow from 2-4°C and orange greater than 4°C. Source: IMHEN.

TAVE (°C)	MID-CENTURY (2045-2065)					END OF THE CENTURY (2080-2100)				
	ANNUAL	NEMS DEC-MAR	FIMS APR-MAY	SWMS JUNE-SEP	SIMS OCT-NOV	ANNUAL	NEMS DEC-MAR	FIMS APR-MAY	SWMS JUNE-SEP	SIMS OCT-NOV
	MONRE 2012					MONRE 2012				
B1	1.2	1.2	1.4	1.1	1.2	1.6	1.5	1.8	1.4	1.5
B2	1.4	1.4	1.7	1.3	1.4	2.3	2.2	2.7	2.0	2.2
A2	1.5	1.5	1.7	1.4	1.4	2.7	2.7	3.2	2.5	2.6
	PRECIS					PRECIS				
A1B	2.1	2.1	2.5	2.1	1.9	3.4	3.3	3.9	3.5	3.0

Table 13-4: Projected changes in annual and seasonal average temperature by model (°C) for the SC region relative to the baseline period (1980-2000) for RCP 8.5 from the eight RCM experiments. Green colouring is for increases less than 2°C, yellow from 2-4°C and orange greater than 4°C.

TAVE (°C)	MID-CENTURY (2045-2065)					END OF THE CENTURY (2080-2100)				
	ANNUAL	NEMS DEC-MAR	FIMS APR-MAY	SWMS JUNE-SEP	SIMS OCT-NOV	ANNUAL	NEMS DEC-MAR	FIMS APR-MAY	SWMS JUNE-SEP	SIMS OCT-NOV
Multi-model mean	1.7	1.5	1.7	1.9	1.7	3.2	2.8	3.1	3.6	3.2
	Individual RCM simulations					**Individual RCM simulations**				
CCAM ACCESS1.0	1.9	1.7	1.8	2.1	2.0	3.5	3.0	3.3	4.0	3.6
CCAM NorESM1-M	1.6	1.7	1.6	1.7	1.5	3.0	2.9	2.9	3.3	2.9
CCAM MPI-ESM-LR	1.7	1.5	1.9	1.9	1.4	3.3	2.8	3.5	3.9	3.0
CCAM CCSM4	1.4	1.3	1.3	1.7	1.3	2.8	2.5	2.7	3.2	2.8
CCAM CNRM-CM5	1.4	1.3	1.4	1.6	1.2	2.7	2.3	2.7	3.1	2.6
CCAM GFDL-CM3	2.5	2.1	2.6	2.8	2.7	4.3	3.5	4.3	5.0	4.3
RegCM4.2 ACCESS1.0	1.9	1.5	1.8	2.2	2.1	3.3	2.8	3.2	3.8	3.6
RegCM4.2 NorESM1-M	1.2	1.2	1.2	1.2	1.3	2.4	2.2	2.4	2.4	2.7

	Indicates a range of low results	< 2.0°C
	Indicates a range of medium results	2.0 to 4.0°C
	Indicates a range of high results	> 4.0°C

Table 13-5: Projected changes in annual and seasonal maximum temperature by model (°C) for the SC region relative to the base line period (1980-2000) for RCP 8.5 from the eight RCM experiments. Green colouring is for increases less than 2°C, yellow from 2-4°C and orange greater than 4°C.

TMAX (°C)	MID-CENTURY (2045-2065)					END OF THE CENTURY (2080-2100)				
	ANNUAL	NEMS DEC-MAR	FIMS APR-MAY	SWMS JUNE-SEP	SIMS OCT-NOV	ANNUAL	NEMS DEC-MAR	FIMS APR-MAY	SWMS JUNE-SEP	SIMS OCT-NOV
Multi-model mean	1.6	1.3	1.5	1.9	1.7	3.1	2.4	3.0	3.7	3.1
	Individual RCM simulations					**Individual RCM simulations**				
CCAM ACCESS1.0	1.9	1.6	1.7	2.1	2.1	3.6	3.0	3.4	4.3	3.8
CCAM NorESM1-M	1.6	1.6	1.4	1.8	1.5	2.9	2.4	2.7	3.5	3.0
CCAM MPI-ESM-LR	1.7	1.3	1.9	2.0	1.5	3.4	2.6	3.4	4.2	3.1
CCAM CCSM4	1.4	1.1	1.1	1.9	1.3	2.8	2.1	2.5	3.6	2.6
CCAM CNRM-CM5	1.5	1.2	1.3	1.9	1.4	2.8	2.2	2.7	3.5	2.8
CCAM GFDL-CM3	2.4	1.8	2.4	3.0	2.7	4.3	3.1	4.4	5.5	4.4
RegCM4.2 ACCESS1.0	1.6	1.3	1.5	1.8	1.7	2.9	2.6	2.9	3.1	3.2
RegCM4.2 NorESM1-M	1.0	0.8	0.9	1.0	1.3	1.7	1.4	1.9	1.8	2.2

	Indicates a range of low results	< 2.0°C
	Indicates a range of medium results	2.0 to 4.0°C
	Indicates a range of high results	> 4.0°C

Table 13-6: Projected changes in annual and seasonal minimum temperature by model (°C) for the SC region relative to the baseline period (1980-2000) for RCP 8.5 from the eight RCM experiments. Green colouring is for increases less than 2°C, yellow from 2-4°C and orange greater than 4°C.

TMIN (°C)	MID-CENTURY (2045-2065)					END OF THE CENTURY (2080-2100)				
	ANNUAL	NEMS DEC-MAR	FIMS APR-MAY	SWMS JUNE-SEP	SIMS OCT-NOV	ANNUAL	NEMS DEC-MAR	FIMS APR-MAY	SWMS JUNE-SEP	SIMS OCT-NOV
Multi-model mean	1.8	1.7	1.9	1.9	1.7	3.3	3.1	3.4	3.6	3.3
	Individual RCM simulations					**Individual RCM simulations**				
CCAM ACCESS1.0	2.0	1.9	2.1	2.2	1.9	3.6	3.2	3.5	4.0	3.6
CCAM NorESM1-M	1.7	1.9	1.8	1.6	1.6	3.2	3.4	3.1	3.2	2.9
CCAM MPI-ESM-LR	1.8	1.8	2.1	1.9	1.5	3.5	3.1	3.8	3.8	3.1
CCAM CCSM4	1.5	1.5	1.6	1.7	1.4	3.0	2.8	3.0	3.1	3.0
CCAM CNRM-CM5	1.4	1.4	1.4	1.4	1.1	2.8	2.5	2.9	3.0	2.6
CCAM GFDL-CM3	2.6	2.4	2.7	2.8	2.7	4.4	3.9	4.5	4.9	4.2
RegCM4.2 ACCESS1.0	2.1	1.6	2.0	2.5	2.4	3.6	2.9	3.5	4.2	4.0
RegCM4.2 NorESM1-M	1.4	1.5	1.5	1.4	1.4	2.8	2.7	2.8	2.9	3.1

	Indicates a range of low results	< 2.0°C
	Indicates a range of medium results	2.0 to 4.0°C
	Indicates a range of high results	> 4.0°C

Rainfall

Rainfall projections in the SC region (Table 13-7) show significant differences in both annual and seasonal changes among the models, although they all project increases in NEMS and FIMS by mid-century (multi-model means of 18% and 13%, respectively) and for the end of the century (multi-model means of 31% and 18%, respectively). The projections are for decreases for SWMS (multi-model mean -10% by mid-century and -13% by the end of the century), although with slightly less agreement (only 6 out of 8 models project decreases). The CCAM CCSM4 simulation projects the largest seasonal decrease (-42% for SWMS at the end of the century), while CCAM NorESM1-M projects the greatest increases in rainfall (+81% for NEMS by the end of the century; Table 13-9).

A comparison between the current projections and previous projections (MONRE, 2012; Table 13-8) shows large differences. The previous projections indicated decreases for NEMS and FIMS and increases for SWMS, while the new projections indicate increases for NEMS and FIMS and decreases for SWMS. The PRECIS ensemble mean shows decreases for this region for all seasons (except NEMS by mid-century). This also contrasts with the new projections, which have increases annually and for all seasons except SWMS (the only season where the new and PRECIS projections agree).

Table 13-7: Projected changes in the annual and seasonal mean rainfall and its range (%) for the SC region relative to the baseline period (1980-2000) for RCP 8.5. Changes are the multi-model means from eight simulations. Orange colouring is for decreases less than -10%, green for changes between -10% to +10% and blue for increases greater than +10%.

RAIN	MID-CENTURY (2045-2065)					END OF THE CENTURY (2080-2100)				
% CHANGE	ANNUAL	NEMS DEC-MAR	FIMS APR-MAY	SWMS JUNE-SEP	SIMS OCT-NOV	ANNUAL	NEMS DEC-MAR	FIMS APR-MAY	SWMS JUNE-SEP	SIMS OCT-NOV
Multi-model mean	5	18	13	-10	5	13	31	18	-13	18
Range	-9 to +35	+6 to +36	0 to +23	-30 to +47	-14 to +55	-13 to +60	+6 to +81	+3 to +43	-42 to +67	-18 to +79

Table 13-8: Projected changes in annual and seasonal rainfall (%) for the SC region relative to the baseline period (1980-2000) for various SRES emission scenarios (B1, B2, A2, A1B) from a previous study (MONRE, 2012) and the latest PRECIS projections (ensemble mean). Orange colouring is for decreases less than -10%, green for changes between -10% to +10% and blue for increases greater than +10%. Source: IMHEN.

RAIN	MID-CENTURY (2045-2065)					END OF THE CENTURY (2080-2100)				
(%)	ANNUAL	NEMS DEC-MAR	FIMS APR-MAY	SWMS JUNE-SEP	SIMS OCT-NOV	ANNUAL	NEMS DEC-MAR	FIMS APR-MAY	SWMS JUNE-SEP	SIMS OCT-NOV
	MONRE 2012					MONRE 2012				
B1	3	-5	-5	3	8	4	-7	-6	4	9
B2	4	-6	-5	3	8	6	-9	-8	5	13
A2	4	-6	-6	3	9	7	-11	-10	6	16
	PRECIS					PRECIS				
A1B	-9	2	-2	-7	-16	-11	-16	-2	-16	-10

Table 13-9: Projected changes in annual and seasonal mean rainfall by model (%) for the SC region relative to the baseline period (1980-2000) for RCP 8.5 from the eight RCM experiments. Orange colouring is for decreases less than -10%, green for changes between -10% to +10% and blue for increases greater than +10%.

RAIN (%)	MID-CENTURY (2045-2065)					END OF THE CENTURY (2080-2100)				
	ANNUAL	NEMS DEC-MAR	FIMS APR-MAY	SWMS JUNE-SEP	SIMS OCT-NOV	ANNUAL	NEMS DEC-MAR	FIMS APR-MAY	SWMS JUNE-SEP	SIMS OCT-NOV
Multi-model mean	5	18	13	-10	5	13	31	18	-13	18
	Individual RCM simulations					Individual RCM simulations				
CCAM ACCESS1.0	-6	11	11	-30	-5	-11	6	6	-37	-5
CCAM NorESM1-M	4	20	23	-25	5	23	81	27	-40	17
CCAM MPI-ESM-LR	-5	11	0	-15	-13	-6	18	16	-28	-15
CCAM CCSM4	-1	12	10	-19	-3	2	24	17	-42	11
CCAM CNRM-CM5	-9	6	13	-27	-14	-13	7	5	-34	-18
CCAM GFDL-CM3	3	35	5	-29	2	-2	37	3	-40	-4
RegCM4.2 ACCESS1.0	35	12	19	47	55	47	8	27	67	77
RegCM4.2 NorESM1-M	22	36	23	15	16	60	69	43	51	79

	Indicates a range of low (drier) results	< -10%
	Indicates a range of medium (little change) results	-10 to +10%
	Indicates a range of high (wetter) results	> 10%

13.4 SUMMARY

An analysis of observed records for the SC region had a small and statistically significant increasing trend in annual temperature (about +0.1°C per decade). Annual rainfall also had a statistically significant increase (about +10% per decade) during the past 50 years. The minimum temperature has increased (about +0.2°C per decade) at a faster rate than the maximum temperature (about +0.05°C per decade, which is not a significant trend). The number of hot days increased by up to 4 days per decade, while the cold nights for the northern part of the region remained unchanged. The number of extreme hot days (TX90p) has increased and the number of extreme cold days (TN10p) has decreased significantly. Extreme rainfall has increased significantly at a number of stations in the region. The CWD has generally not changed significantly except for a couple of stations in northern parts of the region, where there are increases. The CDD has generally not changed significantly except for a couple of stations in southern parts, where there are decreases.

The climate projections based on the eight RCMs downscaled from the CMIP5 GCMS for the high emission scenario (RCP 8.5) clearly indicate that the SC region is projected to warm in future. Annual mean surface temperature is projected to increase by about 1.7°C by mid-century and by 3.2°C by the end of the century. The rate of warming is greatest in SWMS (Tave of +3.6°C) and least in NEMS (Tave of 2.8°C). Tmax is projected to warm less than Tmin. These new projections are generally similar to the previous projections, except for SWMS, where the new projections are much warmer than the old ones by end of the century.

Rainfall projections in the SC region indicate agreement on increases in NEMS (multi-model mean of +31%) and FIMS (multi-model mean of +18%), with all models projecting increases. There is also strong agreement on decreases in SWMS (multi-model mean change of -13%, with 6 out of 8 models projecting decreases).

14 THE CENTRAL HIGHLANDS REGIONAL REPORT

This chapter summarises the current climate and its trends for the Central Highlands region of Vietnam (see Figure 14-1). The projected changes of temperature and rainfall by mid-century and the end of the century are then presented, first from the GCM results, then from the RCM results. The key messages are summarised at the end of the chapter.

14.1 DESCRIPTION

The Central Highlands (CH) region is mountainous, with a vast plateau on the western side of the Truong Son range. The region includes the bulky massif that links the relatively flat plateau, forming many steps as it gradually approaches the Mekong River Valley.

In the northern part of CH, there is the Kon Tum-Pleiku highlands (elevation of 500-700 m), located in the southwestern part of the Kon Tum Thuong Mountains, which have elevations higher than 2000 m. Dak Lak Plateau, which is located in the middle of the region, has elevations of between 300 and 600 m. The highlands south of Lang Bian Plateau 2 are 1500 m high and the Di Linh plateau is between 800 and 1000 m high. The East Highlands (protruding near the coast) have peaks of around 2000 m, and are called Nam Truong Son.

The average temperature of the warmest month ranges between 24 and 28°C, and the temperature of the coldest month is 21°C, with the lowest absolute temperature between 3 and 9°C. The rainy season is from May to October, with maximum rainfall in August. The dry season is from November to March with rainfall of less than 50 mm. Strong winds occur over the plains, with average wind speeds of 1.5-3.5 m sec^{-1}. See Table 14-1 for more details.

14.2 OBSERVED CLIMATE

Observed climate trends are analysed using daily data from 70 meteorological stations in Vietnam for the period 1961 to 2011. In addition to trends of mean surface air temperature (or T2m) and precipitation, trends of some extreme indices are also discussed. Definitions of selected extreme indices can be found in ETCCDI (2009), which recommended 27 core Extreme Climate Indices (ECIs) based on daily temperature values or daily precipitation amounts. The indices below are used in this study, mostly following the ETCCDI computational procedures:

- **RX1**: yearly maximum 1-day precipitation (mm).
- **RX5**: annual highest consecutive five-day precipitation amount (mm).
- **R95p**: annual count of days when precipitation exceeds the 95th percentile value for the period 1961-2011.
- **TN10p**: annual count of days when minimum daily temperature is less than the 10th percentile temperature for the period 1961-2011.
- **TX90p**: annual count of days when maximum daily temperature exceeds the 90th percentile temperature for the period 1961-2011.
- **CDD**: consecutive dry days; average annual maximum number of days with daily rainfall less than 1 mm.
- **CWD**: consecutive wet days; average annual maximum number of days with daily rainfall greater than or equal to 1 mm.
- **Hot days**: days with Tmax greater than 35°C.
- **Cold days**: days with Tmin less than 15°C.

Figure 14-1: The Central Highlands region with provinces. Insert shows location of region in Vietnam.

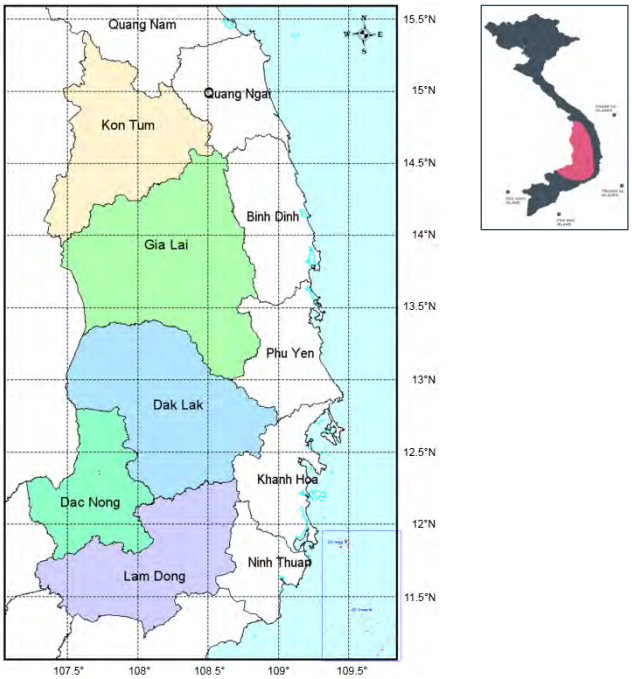

Table 14-1: Observed climate variables and their ranges for the CH region. Nguyen and Nguyen (2004).

CLIMATE VARIABLE	VALUE
Terrain height	300 to 700 m
Annual average solar radiation	150 to 170 kcal cm^{-2}
Radiation balance	70 to 100 kcal cm^{-2}
Annual sunshine hours	200 to 2500 h
Annual average temperature	21 to 24°C
Maximum temperature	37 to 40°C
Minimum temperature	3 to 9°C
Annual temperature amplitude	< 5°C
Annual average rainfall	1400 to 2000 mm
Daily maximum rainfall	Above 200 mm
Rainfall season	May to Oct
Humidity	78-84%
Annual evaporation	900 to 1600 mm
Annual average wind speed	1.5 to 3.5 m sec^{-1}
Maximum wind speed	20 to 25 m sec^{-1}

Trends are calculated for each station within the region. Statistical significance of the trends is computed using the non-parametric Mann-Kendall test (Kendall 1975). In this report, trends with significance levels greater than 90% are considered as statistically significant.

14.2.1 Temperature

The observed surface air temperature has increased over the CH region during the past 50 years (Figure 14-2). The trends range from +0.04°C (Da Lat) to +0.35°C (Kon Tum) per decade. Most trends are statistically significant at the 90% level.

The time series of the regionally-averaged annual temperature in Figure 14-3 clearly shows a warming trend for this region, with some significant year-to-year variations, especially in the early years of the period. The warming is about 1.5°C during the past 50 years, which is about 0.3°C per decade.

14.2.2 Rainfall

Observed rainfall has increased at most of the stations in CH region for the period 1961 to 2011, except for Ayunpa, which shows a non-statistically significant decrease of about -4% per decade (Figure 14-4). The trend is statistically significant at the 90% level for most of the stations. The highest rainfall increase is about +7% per decade at Kon Tum station.

Regionally-averaged annual rainfall from 1961 to 2010 for the region CH (Figure 14-5) has weak inter-annual variations of about 1 mm day^{-1} with a very small positive trend, which is not statistically significant.

Figure 14-2: Trends in annual mean surface air temperature (°C per decade) in the Central Highland (CH) region for the period 1961-2011. A blue circle indicates a decreasing trend and a red circle shows an increasing trend, while a filled circle indicates that the trend is statistically significant at the 90% level.

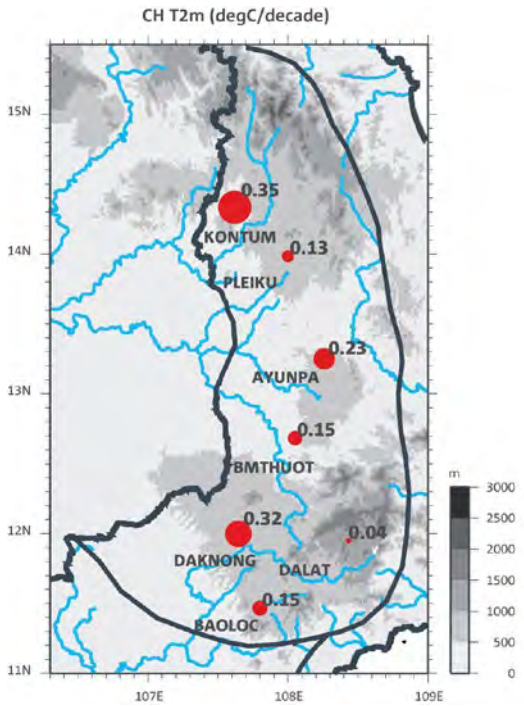

Figure 14-4: Trends in annual rainfall in the CH region (% per decade) for the period 1961-2011. A blue circle indicates an increasing trend and a red circle shows a decreasing trend. A filled circle shows that the trend is statistically significant at the 90% level.

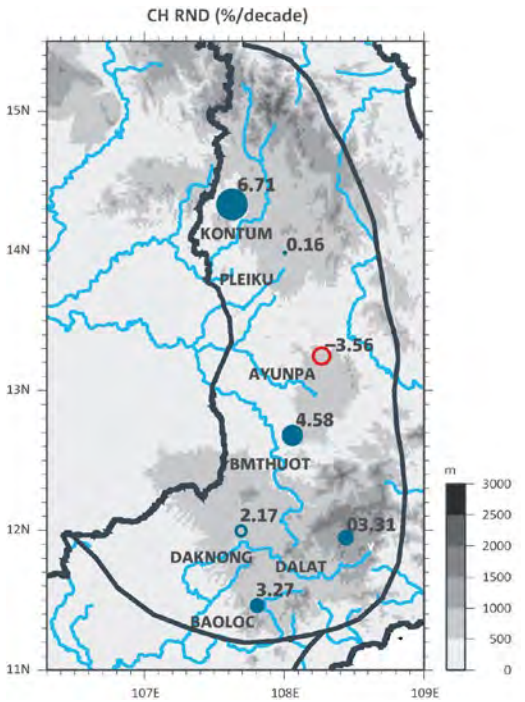

Figure 14-3: Time series of regionally-averaged annual surface air temperature (°C, red) for the CH region, with trend line (dashed black line). Annual values are shown by black dots.

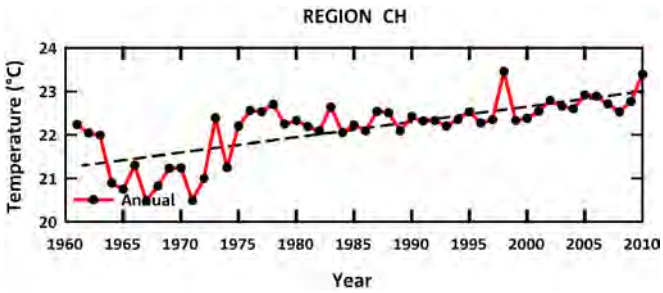

Figure 14-5: Time series of regionally-averaged annual rainfall (mm day^{-1}, blue) for the CH region, with a trend line (dashed black line). Annual values are shown as black dots.

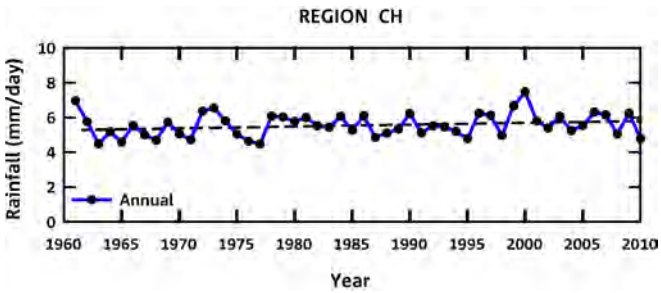

14.2.3 Extremes

While the maximum daily temperature (Tmax) does not have any systematic trend for the CH region, the minimum daily temperature (Tmin) does have significant increases during the period 1961 to 2011 (Figure 14-6). Tmin has increased by approximately 0.18°C (at Da Lat) to 0.65°C (at Kon Tum) per decade. The number of hot days and cold nights have remained largely unchanged at all stations. Trends in extreme hot days (TX90p) are both positive and negative across this region. Extreme minimum temperatures (TN10p) have a significant negative trend (a decreasing number of extreme cold nights on the order of -15 to -20 days per decade).

More extreme rainfall events have been observed in the CH region during the past 50 years (Figure 14-7) except at Ayunpa. Both RX1 and RX5 have generally increased for most stations by about 5-10% per decade. The R95p trend is positive by up to nearly 12 mm day^{-1}. The observed trend in CWD is generally negative and not significant, with only Da Lat having increases. The number of consecutive dry days (CDD) shows little significant trend.

Figure 14-6: Trends in Tmax (top left), Tmin (top right), TX90p (bottom left), and TN10p (bottom right) in the CH region for the period 1961-2011. A blue circle indicates a decreasing trend and a red circle shows an increasing trend. A filled circle means that the trend is statistically significant at the 90% level.

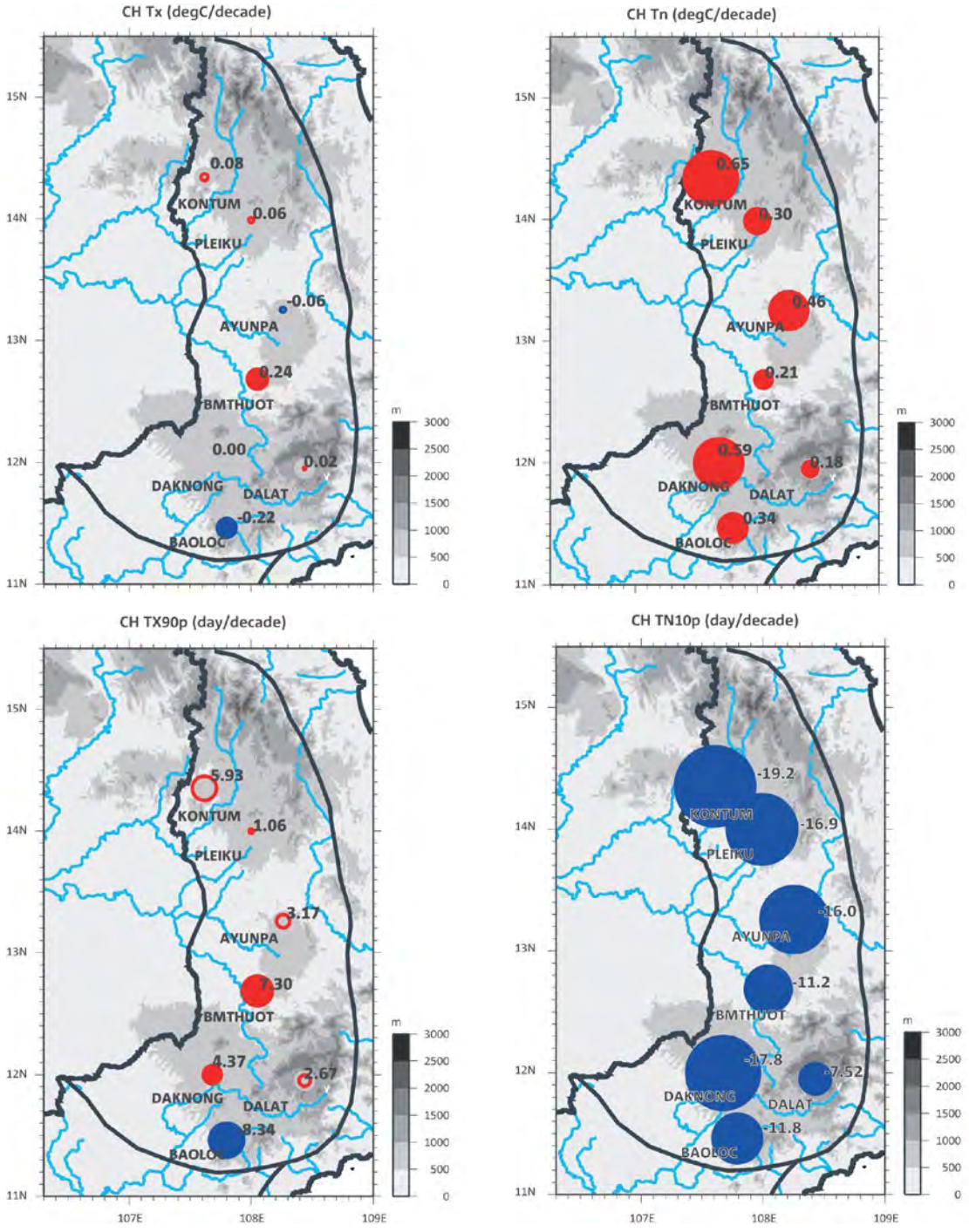

Figure 14-7: Trends in RX1, RX5, R95p, CWD, and CDD in the CH region for the period 1961-2011. A blue circle indicates an increasing trend and red a decreasing trend for all but CDD, where red indicates an increasing and blue a decreasing number of days. A filled circle means that the trend is significant at the 90% level.

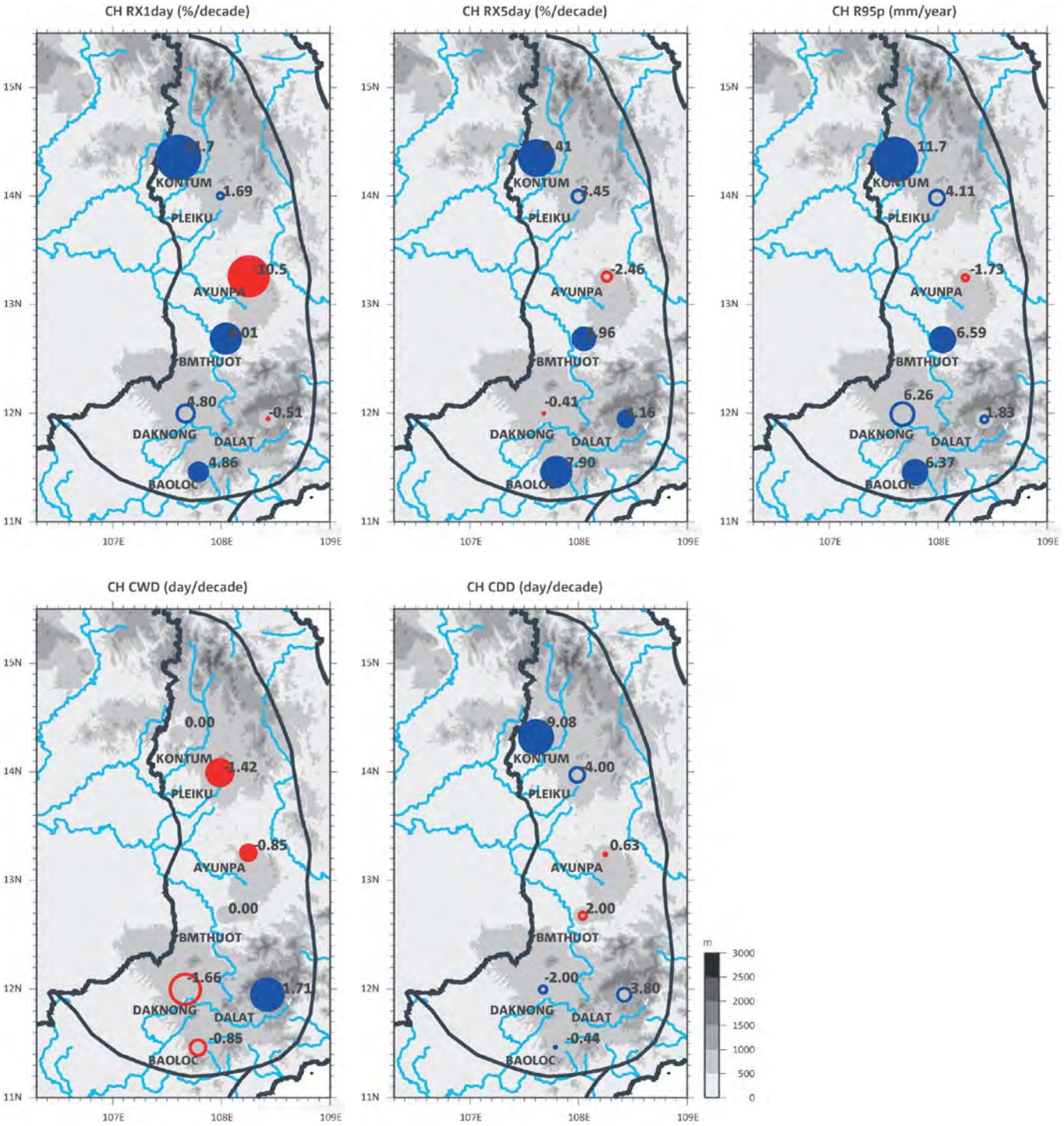

14.3 CLIMATE PROJECTIONS

In this section, projected changes in temperature and rainfall for the region are presented. A summary of the CMIP5 GCM results for different RCPs for this region is first presented in the form of line graphs. This is followed by the projected changes by regional climate models, both from the new experiments completed in this project and results used for the last official projections (MONRE, 2012) completed by IMHEN using the previous CMIP3 SRES emission scenarios. This provides some indication of the differences in the projections, though direct comparison is difficult, since different models and different scenarios were used.

14.3.1 GCM results

Surface temperature

Projections for near-surface average temperature for the four seasons for this region from the CMIP5 GCMs are presented in Figure 14-8. The warming signal is very clear, with greatest warming for the high emission scenario (RCP 8.5) and less warming for the lower emission scenario (RCP 4.5). There is also slightly greater warming of about 3.8°C (as measured by the median value – line inside the colour bar) during FIMS by the end of the century for RCP 8.5, while other seasons project warming of between 3 and 3.5°C by the end of the century.

Figure 14-8: Regionally averaged seasonal surface air temperature changes (°C) for CH. For each season, the time series graph of projections by global climate models (GCM) is shown on the left for the higher (RCP 8.5) greenhouse gas scenario. Black line is from historical GCM runs, red line is the multi-model median projection from GCMs using RCP 8.5. Shadings are between 10% and 90% of 20-year mean values. GCM values have been corrected for 1995-2005 mean bias. Bars on the right for each season show the end-of-century summary of projections by global climate models (GCM, left) and regional climate models (RCM, right) for both lower (RCP 4.5) and higher (RCP 8.5) scenarios.

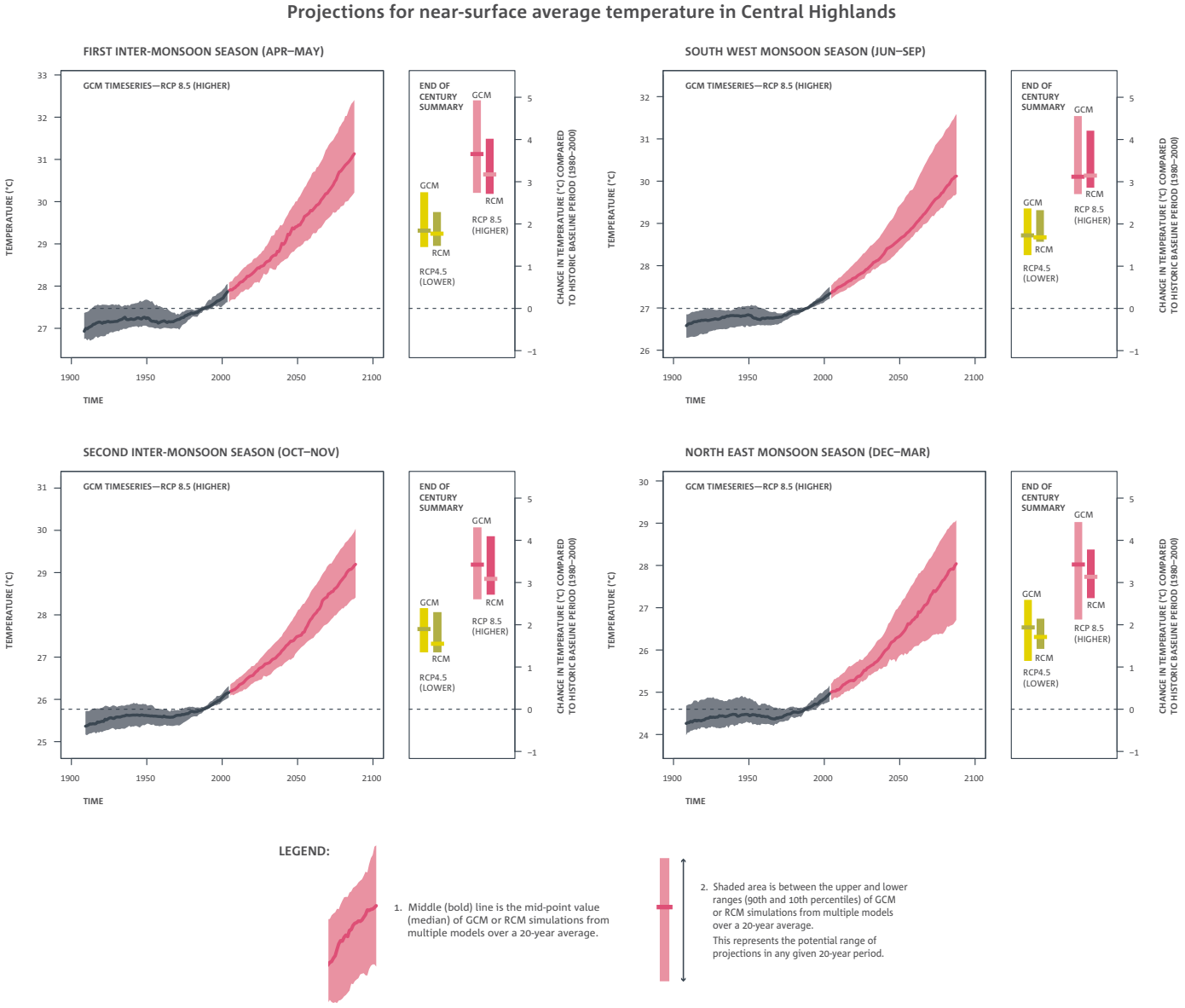

Projections for near-surface maximum temperature for the four seasons from the CMIP5 GCMs are presented in Figure 14-9. Again, the warming signal is very clear and similar to the average temperature. However, there is also slightly greater warming during FIMS (around 4°C) by the end of the century for RCP 8.5, while the other seasons show less warming by the end of the century.

Projections for near-surface minimum temperature for the four seasons for this region from the CMIP5 GCMs are presented in Figure 14-10. The warming signal is again very clear and is similar to the average temperature, with warming of slightly less than 4°C for all seasons by the end of the century for the high emission scenario (RCP 8.5). The maximum temperature is projected to warm more than the minimum temperature by the end of the century under RCP 8.5 during FIMS.

Figure 14-9: Regionally averaged seasonal maximum air temperature changes (°C) for CH. For each season, the time series graph of projections by global climate models (GCM) is shown on the left for the higher (RCP 8.5) greenhouse gas scenario. Black line is from historical GCM runs, red line is the multi-model median projection from GCMs using RCP 8.5. Shadings are between 10% and 90% of 20-year mean values. GCM values have been corrected for 1995-2005 mean bias. Bars on the right for each season show the end-of-century summary of projections by global climate models (GCM, left) and regional climate models (RCM, right) for both lower (RCP 4.5) and higher (RCP 8.5) scenarios.

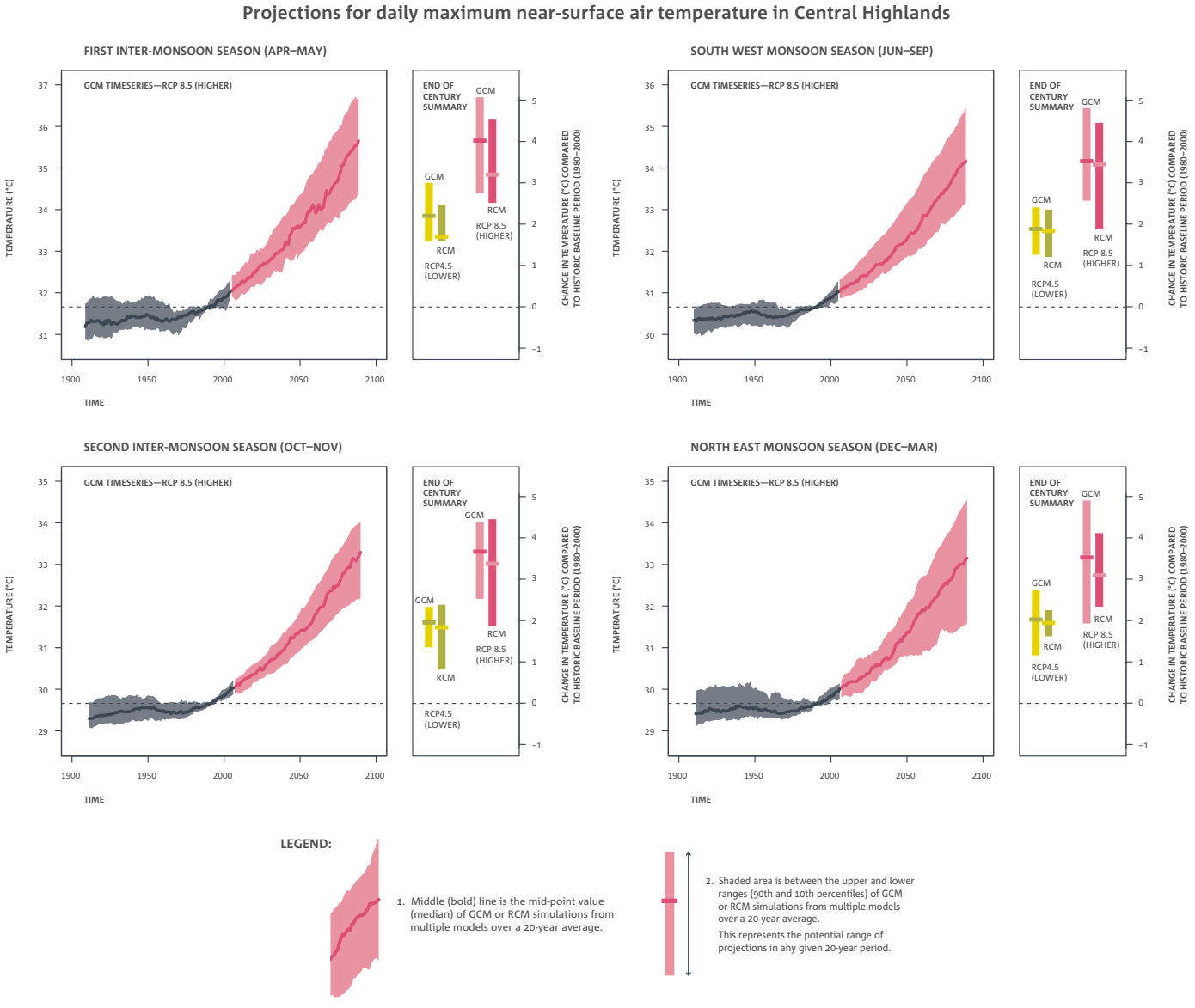

Figure 14-10: Regionally averaged seasonal minimum air temperature changes (°C) for CH. For each season, the time series graph of projections by global climate models (GCM) is shown on the left for the higher (RCP 8.5) greenhouse gas scenario. Black line is from historical GCM runs, red line is the multi-model median projection from GCMs using RCP 8.5. Shadings are between 10% and 90% of 20-year mean values. GCM values have been corrected for 1995-2005 mean bias. Bars on the right for each season show the end-of-century summary of projections by global climate models (GCM, left) and regional climate models (RCM, right) for both lower (RCP 4.5) and higher (RCP 8.5) scenarios.

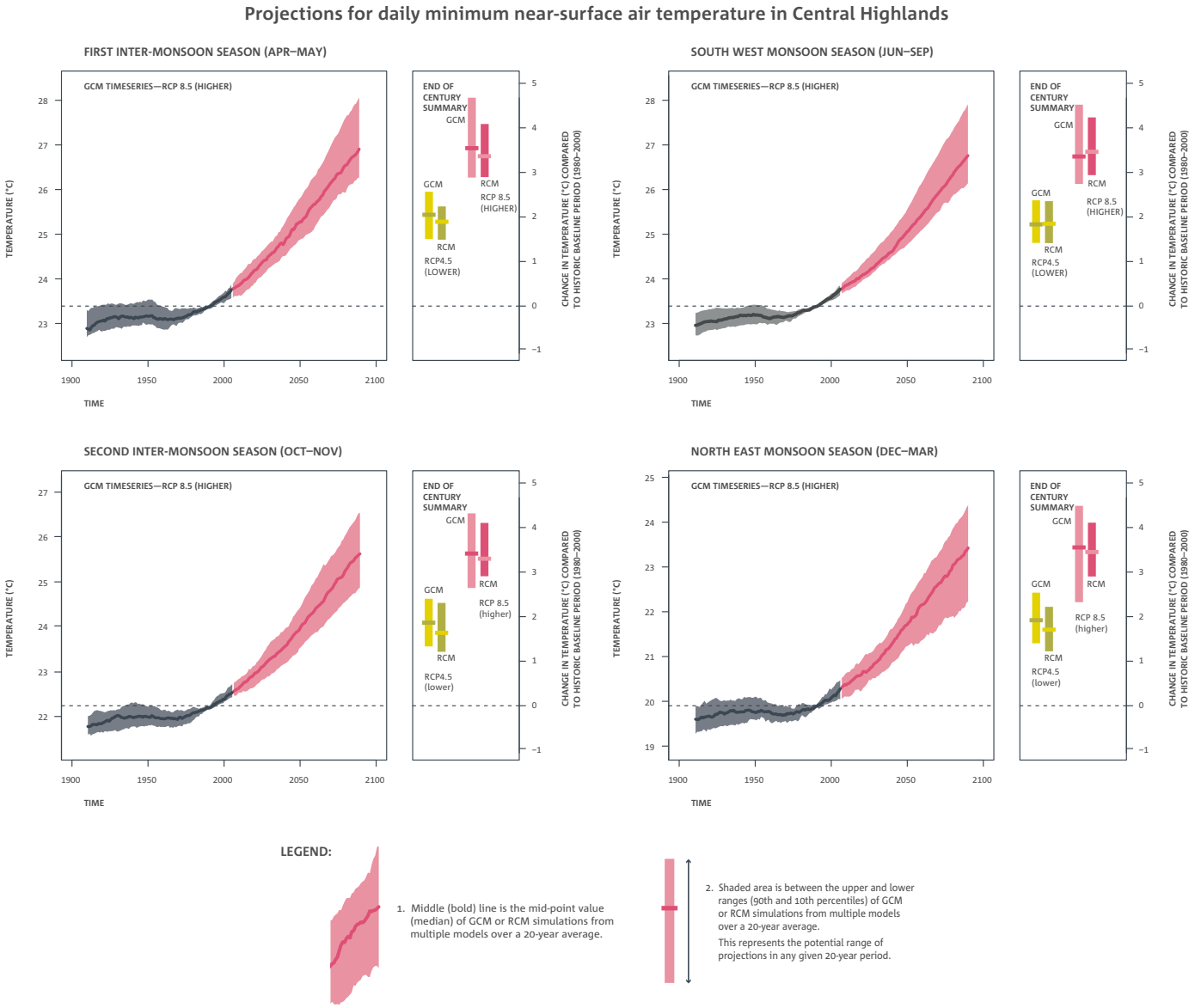

Rainfall

Projections for rainfall for the four seasons from the CMIP5 GCMs are presented in Figure 14-11. There is a large range of inter-annual variability simulated by the GCMs for rainfall for this region, as can be seen by the large spread of the colour bar. Most of the seasons show little change in rainfall by the end of the century. However, SIMS shows some increases in rainfall by this time.

14.3.2 Regional model results

This section will discuss the projected changes in surface temperature and rainfall by the middle of the century (2045-2065) and by the end of the century (2080-2100) compared with the baseline period (1980-2000) using the ensemble means of the eight RCMs employed in this study. These projections do not represent a value specifically for any single station location, but an average for four seasons for the entire region.

Figure 14-11: Regionally averaged seasonal precipitation changes (mm month^{-1} on left axis and % on right axis) for CH. For each season, the time series graph of projections by global climate models (GCM) is shown on the left for the higher (RCP 8.5) greenhouse gas scenario. Black line is from historical GCM runs, red line is the multi-model median projection from GCMs using RCP 8.5. Shadings are between 10% and 90% of 20-year mean values. GCM values have been corrected for 1995-2005 mean bias. Bars on the right for each season show the end-of-century summary of projections by global climate models (GCM, left) and regional climate models (RCM, right) for both lower (RCP 4.5) and higher (RCP 8.5) scenarios.

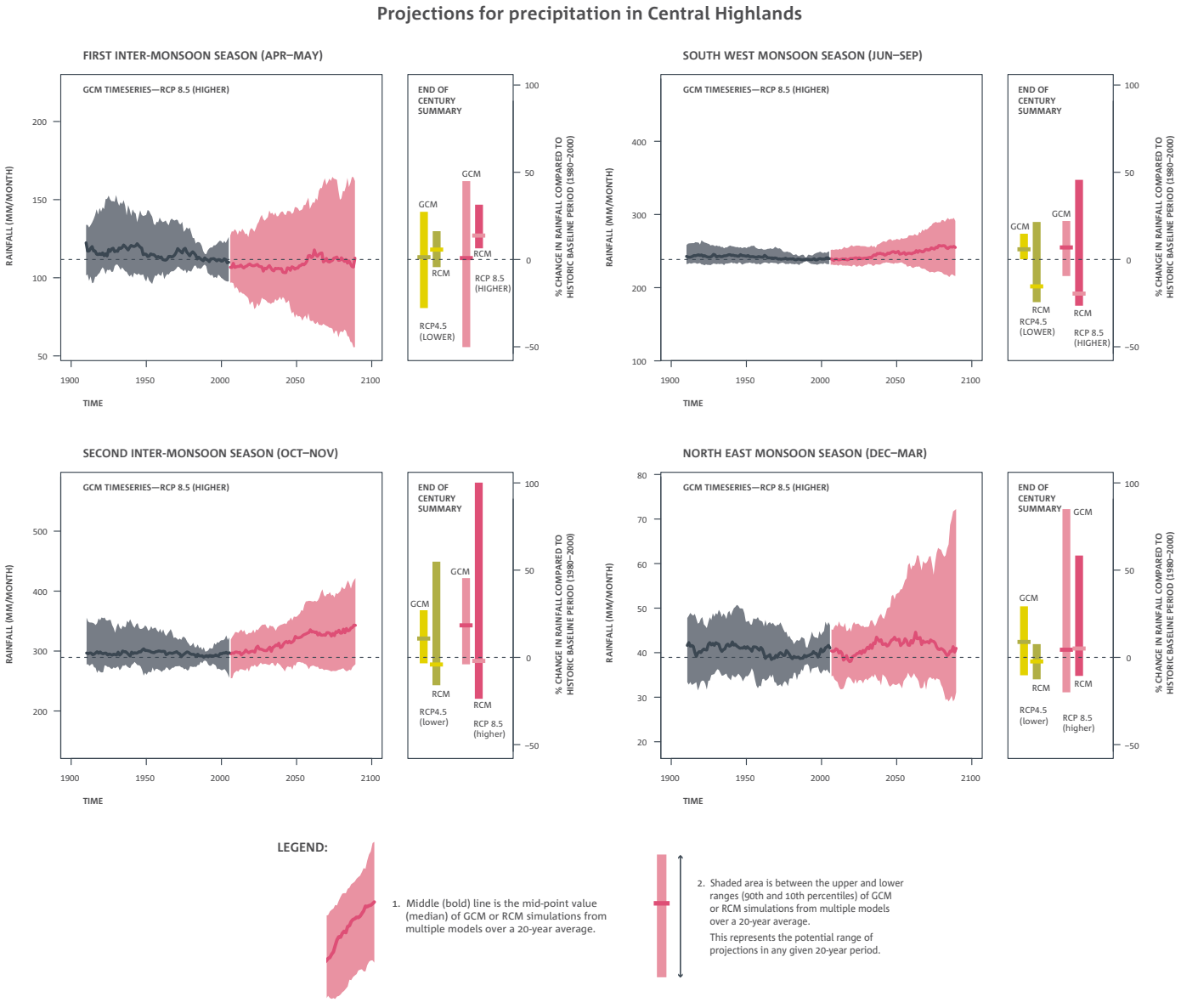

Surface temperature

Projected changes from the eight models suggest a similar warming trend in annual mean average (3.3°C), maximum (3.3°C) and minimum (3.5°C) temperatures for the CH region by the end of the 21st century relative to 1980-2000 for the RCP 8.5 scenario (Table 14-2 to Table 14-6). Moreover, the similar magnitudes of these projected changes by the models suggest that the uncertainty among the model simulations is small. Projected changes for the seasons also are quite similar. However, the projected increase of maximum mean temperature for NEMS is less than for the other seasons. The increase of mean minimum temperature is projected to be slightly more than the projected increase in mean maximum temperature, suggesting a smaller diurnal temperature range in the future. The CCAM GFDL-CM3 run has the largest projected increase in temperature and the RegCM4.2 NorESM1-M has the least projected warming in general.

In comparison with previous projections, the multi-model mean temperature projections produced for the current project are higher than those for the high scenario in the previous projections (SRES A2, MONRE, 2012). The temperatures from the new projection are slightly lower than those for the PRECIS ensemble with the medium emission scenario, SRES A1B (Table 14-3), except for SWMS, where the new projections are slightly higher.

Table 14-2: Summary of multi-model mean and range of projected change in annual and seasonal average, maximum and minimum temperatures (°C) for the CH region relative to the baseline period (1980-2000) for RCP 8.5. Green colouring is for increases less than 2°C, yellow from 2-4°C and orange greater than 4°C.

	MID-CENTURY (2045-2065)					END OF THE CENTURY (2080-2100)				
	ANNUAL	NEMS DEC-MAR	FIMS APR-MAY	SWMS JUNE-SEP	SIMS OCT-NOV	ANNUAL	NEMS DEC-MAR	FIMS APR-MAY	SWMS JUNE-SEP	SIMS OCT-NOV
Tave	1.8	1.8	1.8	1.8	1.8	3.3	3.2	3.3	3.4	3.3
(°C)	1.2 to 2.6	1.2 to 2.4	1.2 to 2.6	1.2 to 2.8	1.3 to 2.8	2.2 to 4.5	2.0 to 4.2	2.3 to 4.6	2.3 to 4.9	2.3 to 4.6
Tmax	1.8	1.8	1.8	1.8	1.8	3.3	3.1	3.4	3.4	3.3
(°C)	1.0 to 2.6	1.0 to 2.3	1.1 to 2.6	1.0 to 2.8	1.0 to 2.9	1.5 to 4.8	1.3 to 4.2	1.9 to 5.0	1.6 to 5.2	1.4 to 4.9
Tmin	1.9	1.9	1.9	1.9	1.8	3.5	3.4	3.4	3.5	3.5
(°C)	1.4 to 2.7	1.5 to 2.6	1.5 to 2.7	1.4 to 2.8	1.1 to 2.8	2.8 to 4.6	2.7 to 4.5	2.8 to 4.6	2.8 to 4.8	2.7 to 4.6

Table 14-3: Projected changes in annual and seasonal mean temperature (°C) for the CH region relative to the baseline period (1980-2000) for various SRES emission scenarios (B1, B2, A2, A1B) from a previous study (MONRE, 2012) and the latest PRECIS projections (ensemble means). Green colouring is for increases less than 2°C, yellow from 2-4°C and orange greater than 4°C. Source: IMHEN.

TAVE (°C)	MID-CENTURY (2045-2065)					END OF THE CENTURY (2080-2100)				
	ANNUAL	NEMS DEC-MAR	FIMS APR-MAY	SWMS JUNE-SEP	SIMS OCT-NOV	ANNUAL	NEMS DEC-MAR	FIMS APR-MAY	SWMS JUNE-SEP	SIMS OCT-NOV
	MONRE 2012					MONRE 2012				
B1	1.2	1.1	1.2	1.2	1.2	1.5	1.5	1.5	1.6	1.5
B2	1.4	1.3	1.4	1.4	1.4	2.2	2.1	2.2	2.3	2.2
A2	1.4	1.4	1.4	1.5	1.4	2.6	2.5	2.6	2.7	2.6
	PRECIS					PRECIS				
A1B	2.2	2.3	2.5	1.9	2.2	3.4	3.5	3.8	3.2	3.3

Table 14-4: Projected change in annual and seasonal average temperature by model (°C) for the CH region relative to the baseline period (1980-2000) for RCP 8.5 from the eight RCM experiments. Green colouring is for increases less than 2°C, yellow from 2-4°C and orange greater than 4°C.

TAVE (°C)	MID-CENTURY (2045-2065)					END OF THE CENTURY (2080-2100)				
	ANNUAL	NEMS DEC-MAR	FIMS APR-MAY	SWMS JUNE-SEP	SIMS OCT-NOV	ANNUAL	NEMS DEC-MAR	FIMS APR-MAY	SWMS JUNE-SEP	SIMS OCT-NOV
Multi-model mean	1.8	1.8	1.8	1.8	1.8	3.3	3.2	3.3	3.4	3.3
	Individual RCM simulations					**Individual RCM simulations**				
CCAM ACCESS1.0	2.1	2.1	2.1	2.2	2.0	3.8	3.6	3.8	4.0	3.8
CCAM NorESM1-M	1.7	1.9	1.5	1.7	1.7	3.1	3.3	2.9	3.1	3.1
CCAM MPI-ESM-LR	1.9	1.9	2.0	1.9	1.7	3.6	3.5	3.7	3.7	3.5
CCAM CCSM4	1.6	1.6	1.5	1.7	1.5	3.0	3.0	2.9	3.2	3.1
CCAM CNRM-CM5	1.5	1.5	1.4	1.6	1.3	3.0	2.9	2.9	3.1	2.9
CCAM GFDL-CM3	2.6	2.4	2.6	2.8	2.8	4.5	4.2	4.6	4.9	4.6
RegCM4.2 ACCESS1.0	1.7	1.6	1.9	1.8	1.7	3.1	3.0	3.4	3.2	3.0
RegCM4.2 NorESM1-M	1.2	1.2	1.2	1.2	1.3	2.2	2.0	2.3	2.3	2.3

	Indicates a range of low results	< 2.0°C
	Indicates a range of medium results	2.0 to 4.0°C
	Indicates a range of high results	> 4.0°C

Table 14-5: Projected change in annual and seasonal maximum temperature by model (°C) for the CH region relative to the baseline period (1980-2000) for RCP 8.5 from the eight RCM experiments. Green colouring is for increases less than 2°C, yellow from 2-4°C and orange greater than 4°C.

TMAX (°C)	MID-CENTURY (2045-2065)					END OF THE CENTURY (2080-2100)				
	ANNUAL	NEMS DEC-MAR	FIMS APR-MAY	SWMS JUNE-SEP	SIMS OCT-NOV	ANNUAL	NEMS DEC-MAR	FIMS APR-MAY	SWMS JUNE-SEP	SIMS OCT-NOV
Multi-model mean	1.8	1.8	1.8	1.8	1.8	3.3	3.1	3.4	3.4	3.3
	Individual RCM simulations					**Individual RCM simulations**				
CCAM ACCESS1.0	2.2	2.2	2.3	2.2	2.2	4.1	4.1	4.3	4.2	4.1
CCAM NorESM1-M	1.8	1.9	1.4	1.9	1.9	3.1	2.8	2.8	3.4	3.3
CCAM MPI-ESM-LR	1.9	1.9	2.0	1.9	2.0	3.8	3.7	3.9	3.9	3.9
CCAM CCSM4	1.8	1.7	1.7	1.9	1.7	3.2	3.0	3.1	3.5	3.1
CCAM CNRM-CM5	1.7	1.7	1.4	1.8	1.8	3.3	3.2	3.3	3.4	3.4
CCAM GFDL-CM3	2.6	2.3	2.6	2.8	2.9	4.8	4.2	5.0	5.2	4.9
RegCM4.2 ACCESS1.0	1.3	1.5	1.6	1.1	1.0	2.4	2.8	3.1	2.0	2.0
RegCM4.2 NorESM1-M	1.0	1.0	1.1	1.0	1.2	1.5	1.3	1.9	1.6	1.4

	Indicates a range of low results	< 2.0°C
	Indicates a range of medium results	2.0 to 4.0°C
	Indicates a range of high results	> 4.0°C

Table 14-6: Projected change in annual and seasonal minimum temperature by model (°C) for the CH region relative to the baseline period (1980-2000) for RCP 8.5 from the eight RCM experiments. Green colouring is for increases less than 2°C, yellow from 2-4°C and orange greater than 4°C.

TMIN (°C)	MID-CENTURY (2045-2065)					END OF THE CENTURY (2080-2100)				
	ANNUAL	NEMS DEC-MAR	FIMS APR-MAY	SWMS JUNE-SEP	SIMS OCT-NOV	ANNUAL	NEMS DEC-MAR	FIMS APR-MAY	SWMS JUNE-SEP	SIMS OCT-NOV
Multi-model mean	1.9	1.9	1.9	1.9	1.8	3.5	3.4	3.4	3.5	3.5
	Individual RCM simulations					**Individual RCM simulations**				
CCAM ACCESS1.0	2.1	2.2	2.1	2.2	2.0	3.8	3.6	3.7	3.9	3.8
CCAM NorESM1-M	1.8	2.0	1.7	1.5	1.7	3.4	3.9	3.1	3.1	3.2
CCAM MPI-ESM-LR	2.0	2.1	2.1	1.9	1.6	3.7	3.6	3.9	3.8	3.4
CCAM CCSM4	1.6	1.7	1.6	1.6	1.5	3.2	3.3	3.0	3.1	3.2
CCAM CNRM-CM5	1.4	1.5	1.5	1.4	1.1	2.9	2.9	2.9	3.0	2.7
CCAM GFDL-CM3	2.7	2.6	2.7	2.8	2.8	4.6	4.5	4.6	4.8	4.6
RegCM4.2 ACCESS1.0	2.0	1.7	2.0	2.3	2.3	3.6	3.0	3.6	3.9	3.9
RegCM4.2 NorESM1-M	1.4	1.5	1.5	1.4	1.4	2.8	2.7	2.8	2.8	3.0

	Indicates a range of low results	< 2.0°C
	Indicates a range of medium results	2.0 to 4.0°C
	Indicates a range of high results	> 4.0°C

Rainfall

The rainfall changes are more complex, since the models simulate both increases and decreases. There is large uncertainty associated with rainfall changes. Projected changes in rainfall (Table 14-7) indicate an increase annually and for most seasons, except SWMS. By the end of the century, rainfall is projected to increase by 5% annually, 16 % for NEMS, 17% for FIMS, -4% for SWMS and +19% for SIMS. All models project an increase in FIMS, while 6 out of 8 models project decreases for SWMS. The CCAM CCSM4 projection (Table 14-9) shows the greatest seasonal decrease (-27% for SWMS) while RegCM4.2 ACCESS1.0 projects the greatest increase (+116% for SIMS).

The previous projections (MONRE, 2012; Table 14-8) projected an increase in rainfall in SIMS (similar to new projections) and a decrease in NEMS and FIMS (opposite to the new projections).

Table 14-7: Projected changes in annual and seasonal mean rainfall and its range (%) for the CH region relative to the baseline period (1980-2000) for RCP 8.5. Changes are the multi-model means from eight simulations. Orange colouring is for decreases less than -10%, green for changes between -10% to +10% and blue for increases greater than +10%.

RAIN % CHANGE	MID-CENTURY (2045-2065)					END OF THE CENTURY (2080-2100)				
	ANNUAL	NEMS DEC-MAR	FIMS APR-MAY	SWMS JUNE-SEP	SIMS OCT-NOV	ANNUAL	NEMS DEC-MAR	FIMS APR-MAY	SWMS JUNE-SEP	SIMS OCT-NOV
Multi-model mean	1	9	11	-3	3	5	16	17	-4	19
Range	-8 to +24	-6 to +27	5 to +19	-14 to +28	-19 to +72	-14 to +47	-19 to +77	+2 to +32	-27 to +55	-25 to +116

Table 14-8: Projected changes in annual and seasonal rainfall (%) for the CH region relative to the baseline period (1980-2000) for SRES emission scenarios (B1, B2, A2, A1B) from a previous study (MONRE, 2012) and the latest PRECIS projections (ensemble means). Orange colouring is for decreases less than -10%, green for changes between -10% to +10% and blue for increases greater than +10%. Source: IMHEN.

RAIN (%)	MID-CENTURY (2045-2065)					END OF THE CENTURY (2080-2100)				
	ANNUAL	NEMS DEC-MAR	FIMS APR-MAY	SWMS JUNE-SEP	SIMS OCT-NOV	ANNUAL	NEMS DEC-MAR	FIMS APR-MAY	SWMS JUNE-SEP	SIMS OCT-NOV
	MONRE 2012					MONRE 2012				
B1	1	-9	-5	1	10	2	-12	-6	1	12
B2	1	-10	-5	1	11	2	-17	-8	2	17
A2	1	-11	-5	1	11	3	-20	-10	2	20
	PRECIS					PRECIS				
A1B	1	-2	-1	7	-10	1	-19	4	0	6

Table 14-9: Projected changes in annual and seasonal mean rainfall by model (%) for the CH region relative to the baseline period (1980-2000) for RCP 8.5 for the eight RCMs. Orange colouring is for decreases less than -10%, green for changes between -10% to +10% and blue for increases greater than +10%.

RAIN (%)	MID-CENTURY (2045-2065)					END OF THE CENTURY (2080-2100)				
	ANNUAL	NEMS DEC-MAR	FIMS APR-MAY	SWMS JUNE-SEP	SIMS OCT-NOV	ANNUAL	NEMS DEC-MAR	FIMS APR-MAY	SWMS JUNE-SEP	SIMS OCT-NOV
Multi-model mean	1	9	11	-3	3	5	16	17	-4	19
	Individual RCM simulations					**Individual RCM simulations**				
CCAM ACCESS1.0	-7	4	9	-13	-11	-14	-8	8	-21	-14
CCAM NorESM1-M	-1	19	19	-13	-1	6	77	23	-26	14
CCAM MPI-ESM-LR	-8	-1	8	-10	-19	-13	-1	32	-25	-24
CCAM CCSM4	-7	5	5	-12	-11	-9	11	14	-27	0
CCAM CNRM-CM5	-8	3	14	-14	-19	-13	-5	2	-15	-25
CCAM GFDL-CM3	0	27	8	-11	1	-6	20	8	-18	-5
RegCM4.2 ACCESS1.0	24	-6	8	28	72	42	-19	13	55	116
RegCM4.2 NorESM1-M	17	18	17	17	11	47	49	31	42	93

	Indicates a range of low (drier) results	< -10%
	Indicates a range of medium (little change) results	-10 to +10%
	Indicates a range of high (wetter) results	> 10%

14.4 SUMMARY

Surface air temperature has increased over the last 50 years for the CH region, from 0.04°C (at Da Lat station) to 0.35°C (at Kon Tum station) per decade. Annual rainfall increased at most stations, though some not significantly. Observed minimum temperatures increased faster than maximum temperatures.

The number of hot days and cold nights did not change significantly over the last 50 years in this region. Extreme hot days also did not change significantly, although extreme cold nights (TN10p) did decrease significantly for this region. Generally, more extreme rainfall events were observed in the CH region during the past 50 years, as indicated by the RX1, RX5 and R95p indices, but CWD and CDD did not have significant trends.

Projected changes in temperature suggest a clear warming trend over the 21st century of the order of 1.8°C by mid-century and 3.3°C by end of the century. Furthermore, simulated small model-to-model differences in the increases in annual and seasonal temperature suggest a small range of uncertainty in the projected changes. These new projections are higher than the previous projections of MONRE (2012).

There is a large model-to-model variation in projected rainfall changes, with some models simulating increases, while others simulate decreases. However, all models project an increase in rainfall for FIMS and 6 out of 8 models project decreases for SWMS. These projected seasonal changes are quite different to the previous projections.

15 SOUTH REGIONAL REPORT

This chapter summarises the current climate and its trends for the South region of Vietnam (see Figure 15-1). The projected changes of temperature and rainfall by mid-century and the end of the century are then presented, first from the GCM results, then from the RCM results. The key messages are summarised at the end of the chapter.

15.1 DESCRIPTION

The South (S) region of Vietnam (Figure 15-1) includes two sub-regions, south-eastern and south-western. The south-eastern sub-region includes one municipality, Ho Chi Minh City, and five provinces: Dong Nai, Binh Duong, Ba Ria-Vung Tau, Binh Phuoc and Tay Ninh. This is the most highly urbanized region in the country, with more than 50% of the people living in urban areas. The south-western sub-region consists of a variety of physical landscapes, but is largely dominated by flat flood plains in the south, with a few hills in the north and west.

Southern Vietnam experiences very little seasonality in temperature. It has a tropical, hot and humid climate with only two seasons: the rainy season and the dry season. In this region, the dry season lasts from December to late April/May (both NEMS and FIMS), and the rainy season from May through November (both SWMS and SIMS). For more details, see Table 15-1.

15.2 OBSERVED CLIMATE

Observed climate trends are analysed using daily data from 70 meteorological stations in Vietnam for the period 1961 to 2011. In addition to trends of mean surface air temperature (or T2m) and precipitation, trends of some extreme indices are also discussed. Definitions of selected extreme indices can be found in ETCCDI (2009), which recommended 27 core Extreme Climate Indices (ECIs) based on daily temperature values or daily precipitation amounts. The indices below are used in this study, mostly following the ETCCDI computational procedures:

- **RX1**: yearly maximum 1-day precipitation (mm).
- **RX5**: annual highest consecutive five-day precipitation amount (mm).
- **R95p**: annual count of days when precipitation exceeds the 95th percentile value for the period 1961-2011.
- **TN10p**: annual count of days when minimum daily temperature is less than the 10th percentile temperature for the period 1961-2011.
- **TX90p**: annual count of days when maximum daily temperature exceeds the 90th percentile temperature for the period 1961-2011.
- **CDD**: consecutive dry days; average annual maximum number of days with daily rainfall less than 1 mm.
- **CWD**: consecutive wet days; average annual maximum number of days with daily rainfall greater than or equal to 1 mm.
- **Hot days**: days with Tmax greater than 35°C.
- **Cold days**: days with Tmin less than 15°C.

Trends are calculated for each station within the region. Statistical significance of the trends is computed using the non-parametric Mann-Kendall test (Kendall, 1975). In this report, trends with significance levels greater than 90% are considered as statistically significant.

Figure 15-1: The South region with provinces. Insert shows location of the region in Vietnam.

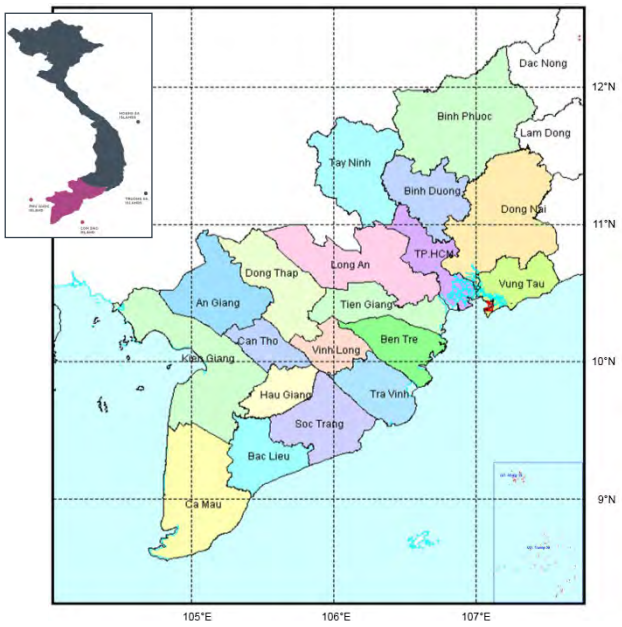

Table 15-1: Observed climate variables and ranges for the South region. Nguyen and Nguyen (2004).

CLIMATE VARIABLE	VALUE
Elevation	< 50 m
Annual average solar radiation	150 to 175 kcal cm^{-2}
Radiation balance	75 to 100 kcal cm^{-2}
Annual sunshine hours	2400 to 3000 h
Annual average temperature	26.5 to 27°C
Maximum temperature	38 to 40°C
Minimum temperature	14 to 18°C
Annual average temperature amplitude	2 to 3°C
Annual average rainfall	1600 to 2000 mm
Daily maximum rainfall	150 to 350 mm
Rainfall season	May to Nov
Humidity	80 to 82%
Annual evaporation	1100 to 1500 mm
Annual average wind speed	1.5 to 3.5 m sec^{-1}
Maximum wind speed	20 to 35 m sec^{-1}

15.2.1 Temperature

There has been an increase in annual temperature in this region for the current climate of between 0.04°C and 0.28°C per decade (Figure 15-2). The regionally-averaged annual temperature has increased by just over 1°C in the last 50 years (Figure 15-3).

Figure 15-2: Trend in annual mean surface air temperature in the South (S) region (°C per decade) for the period 1961-2011. A blue circle indicates a decreasing trend and a red circle shows an increasing trend, while a filled circle indicates that the trend is statistically significant at the 90% level.

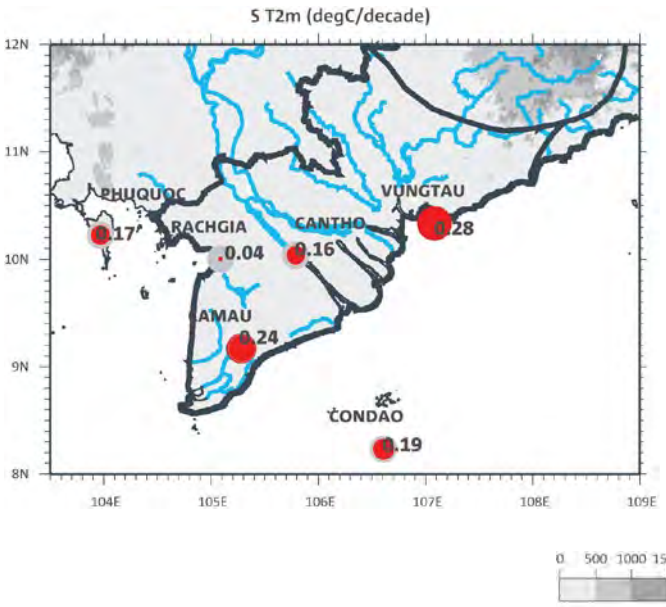

Figure 15-3: Time series of regionally-averaged annual surface air temperature (°C, red) for the S region, with a trend line (dashed). Annual values are shown by black dots.

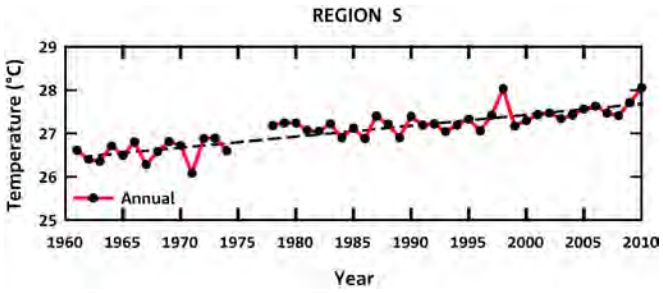

15.2.2 Rainfall

Observed rainfall trends at stations in this region (Figure 15-4) show both increases and decreases. Vung Tau station has the only significant trend, with a decrease of almost -5% per decade. All other stations show either small or insignificant trends. Regionally averaged, the trend in rainfall is very small (Figure 15-5).

Figure 15-4: Trend in annual rainfall (% per decade) in the S region for the period 1961-2011. A blue circle indicates an increasing trend and a red circle shows a decreasing trend. A filled circle indicates that the trend is statistically significant at the 90% level.

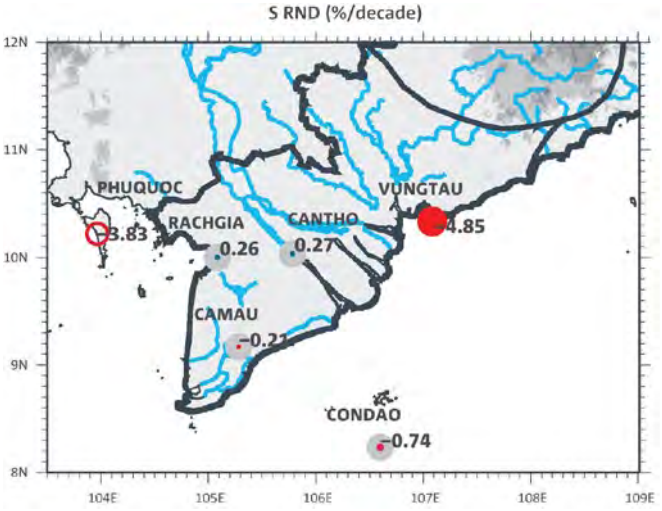

Figure 15-5: Time series of regionally-averaged annual rainfall (mm day^{-1}, blue) for the S region, with a trend line (dashed black line). Annual values are shown by black dots.

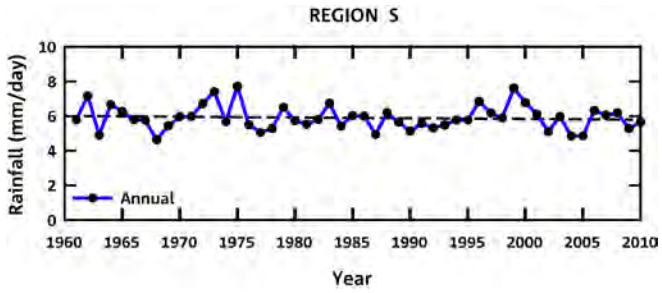

15.2.3 Extremes

Both maximum (Tmax) and minimum (Tmin) daily temperatures have generally increased in the South region (Figure 15-6). Over the whole region, Tmax and Tmin have increased by up to 0.36°C per decade, with greater increases for Tmin. The number of hot days has increased significantly by up to 3 days per decade for Can Tho, while the number of cold nights has decreased significantly. The number of extreme hot days (TX90p) has increased significantly for several stations, with Phu Quoc having an increase of nearly 27 days per decade. Extreme cold nights (TN10p) have also decreased significantly across the region.

Trends in 1-day and 5-day extreme rainfall amounts (RX1 and RX5, Figure 15-7) generally appear to remain unchanged in the Mekong Delta region except for Vung Tau, where both extreme rainfall amounts have decreased significantly (nearly -9%). R95p and CWD has changed little in the region over the last 50 years. CDD does have a statistically significant decrease of up to -20 days per decade.

Figure 15-6: Trends in Tmax (upper left), Tmin (upper right), TX90p (lower left), and TN10p (lower right) in the S region for the period 1961-2011. A blue circle indicates a decreasing trend and a red circle shows an increasing trend, while a filled circle shows that the trend is statistically significant at the 90% level.

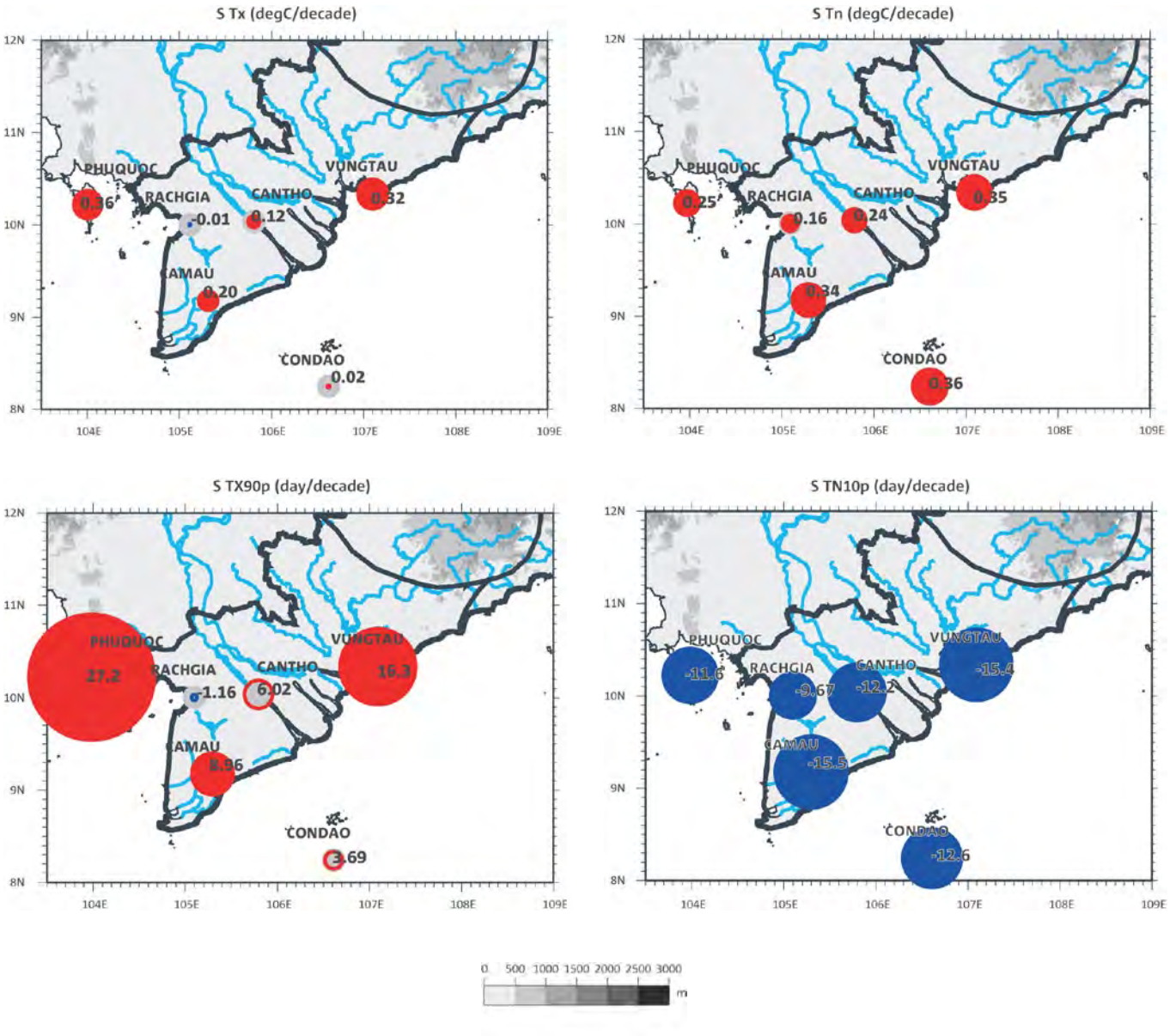

Figure 15-7: Trends in RX1, RX5, R95p, CWD, and CDD in the S region for the period 1961-2011. A blue circle indicates an increasing trend and a red circle shows a decreasing trend for all but CDD, where red indicates increasing and blue decreasing number of days. Filled circles show that the trend is statistically significant at the 90% level.

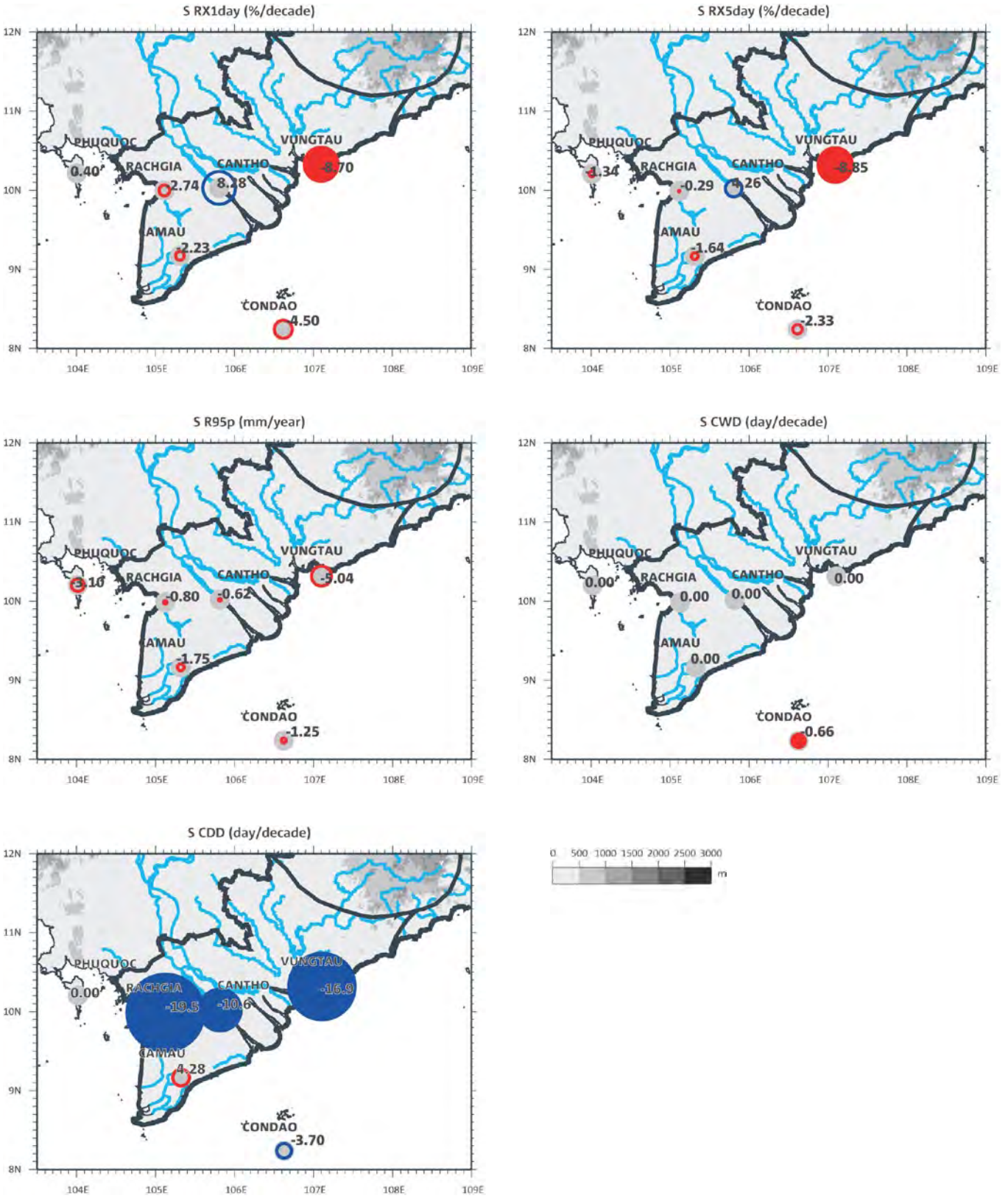

15.3 CLIMATE PROJECTIONS

In this section, projected changes in temperature and rainfall for the S region are presented. A summary of the CMIP5 GCM results for different RCPs for this region is first presented in the form of line graphs. This is followed by the projected changes by regional climate models, both from the new experiments completed for this project and the results used for the last official projections (MONRE, 2012) completed by IMHEN using the previous CMIP3 SRES emission scenarios. This provides some indication of the differences in the projections, though direct comparison is difficult, since different models and different scenarios were used.

15.3.1 GCM results

Surface temperature

Projections for near-surface average temperature for four seasons for this region from the CMIP5 GCMs are presented in Figure 15-8. The warming signal is very clear, with greatest warming for the high emission scenario (RCP 8.5) and a lesser amount of warming for the lower emission scenario (RCP 4.5). There is also slightly greater warming of nearly 4°C (as measured by the median value – line inside the colour bar) for FIMS under RCP 8.5 by the end of the century. Projections for the other seasons are for less than 4°C warming by the end of the century.

Figure 15-8: Regionally averaged seasonal surface air temperature changes (°C) for S. For each season, the time series graph of projections by global climate models (GCM) is shown on the left for higher (RCP 8.5) greenhouse gas scenario. Black line is from historical GCM runs, red line is the multi-model median projection from GCMs using RCP 8.5. Shadings are between 10% and 90% of 20-year mean values. GCM values have been corrected for 1995-2005 mean bias. Bars on the right for each season show the end-of-century summary of projections by global climate models (GCM, left) and regional climate models (RCM, right) for both lower (RCP 4.5) and higher (RCP 8.5) scenarios.

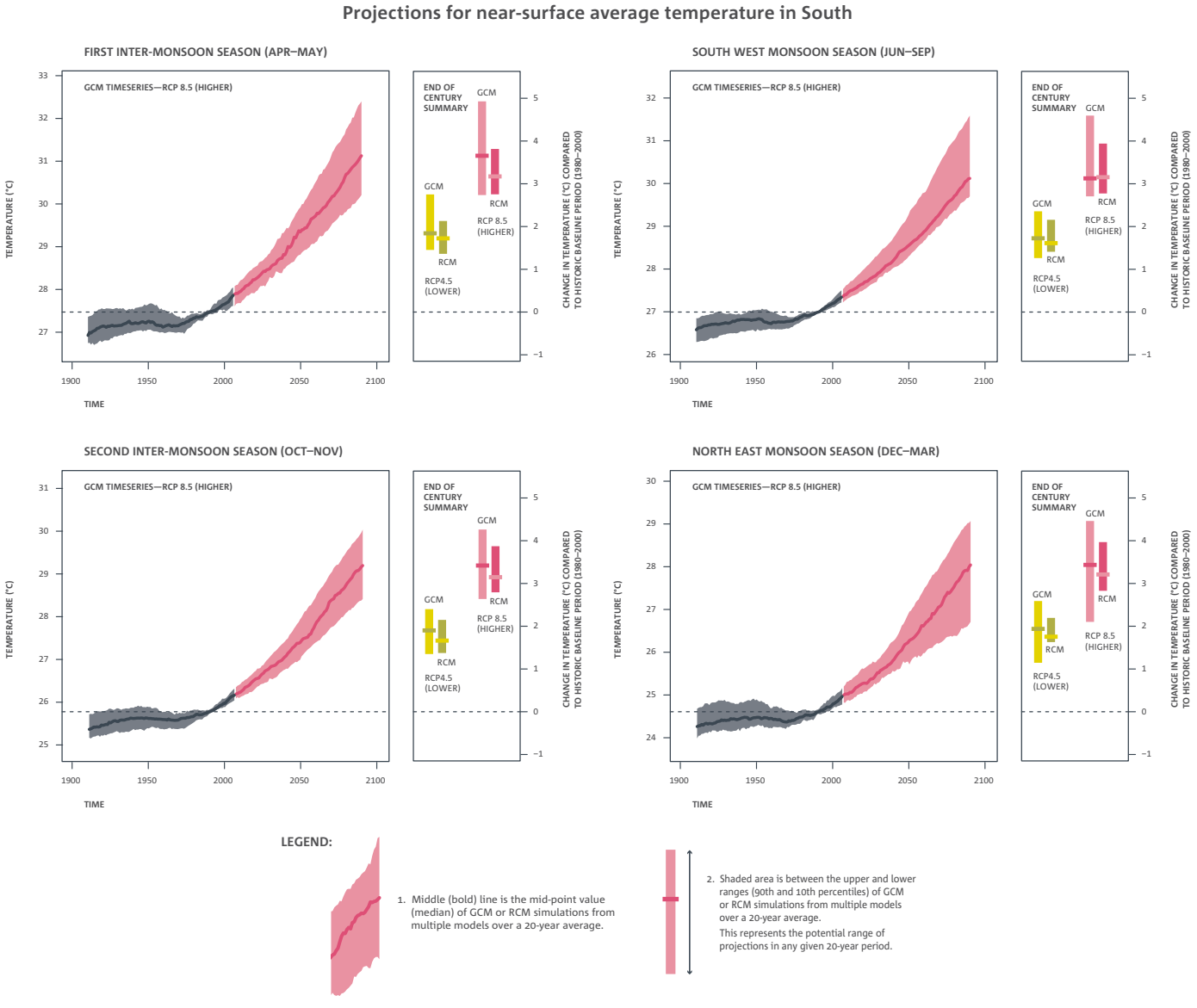

Projections for near-surface maximum temperature for the four seasons from the CMIP5 GCMs are presented in Figure 15-9. Again the warming signal is very clear and is similar to the average temperature.

Projections for near-surface minimum temperature for the four seasons for the region from the CMIP5 GCMs are presented in Figure 15-10. The warming signal is again very clear and is similar to the average temperature. Compared with average temperature warming trends among the seasons, the warming in average minimum temperature is similar or equal for all seasons by the end of the century for RCP 8.5 (less than 4°C).

Figure 15-9: Regionally averaged seasonal maximum air temperature changes (°C) for S. For each season, the time series graph of projections by global climate models (GCM) is shown on the left for the higher (RCP 8.5) greenhouse gas scenario. Black line is from historical GCM runs, red line is the multi-model median projection from GCMs using RCP 8.5. Shadings are between 10% and 90% of 20-year mean values. GCM values have been corrected for 1995-2005 mean bias. Bars on the right for each season show the end-of-century summary of projections by global climate models (GCM, left) and regional climate models (RCM, right) for both lower (RCP 4.5) and higher (RCP 8.5) scenarios.

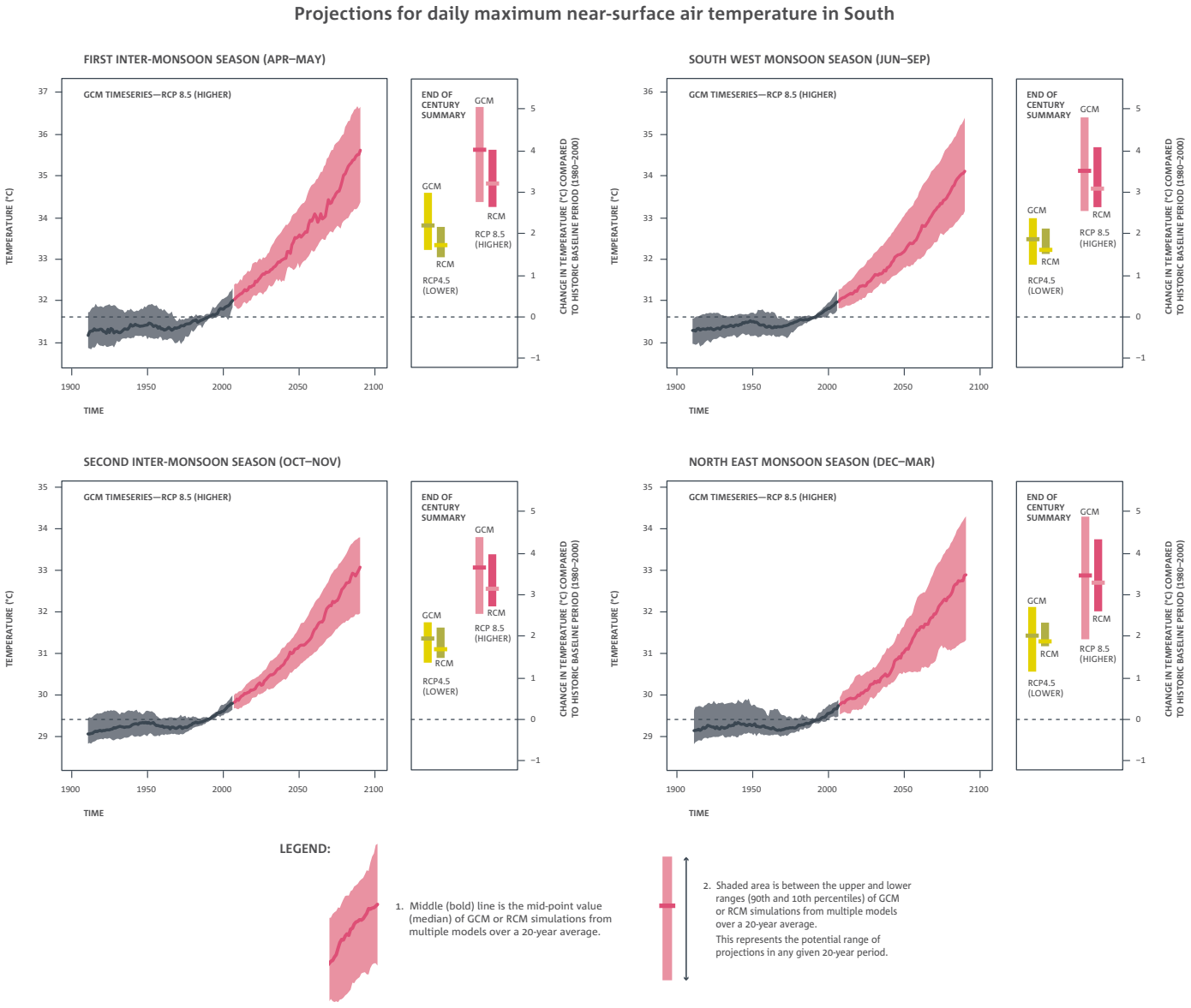

Figure 15-10: Regionally averaged seasonal minimum air temperature changes (°C) for S. For each season, the time series graph of projections by global climate models (GCM) is shown on the left for the higher (RCP 8.5) greenhouse gas scenario. Black line is from historical GCM runs, red line is the multi-model median projection from GCMs using RCP 8.5. Shadings are between 10% and 90% of 20-year mean values. GCM values have been corrected for 1995-2005 mean bias. Bars on the right for each season show the end-of-century summary of projections by global climate models (GCM, left) and regional climate models (RCM, right) for both lower (RCP 4.5) and higher (RCP 8.5) scenarios.

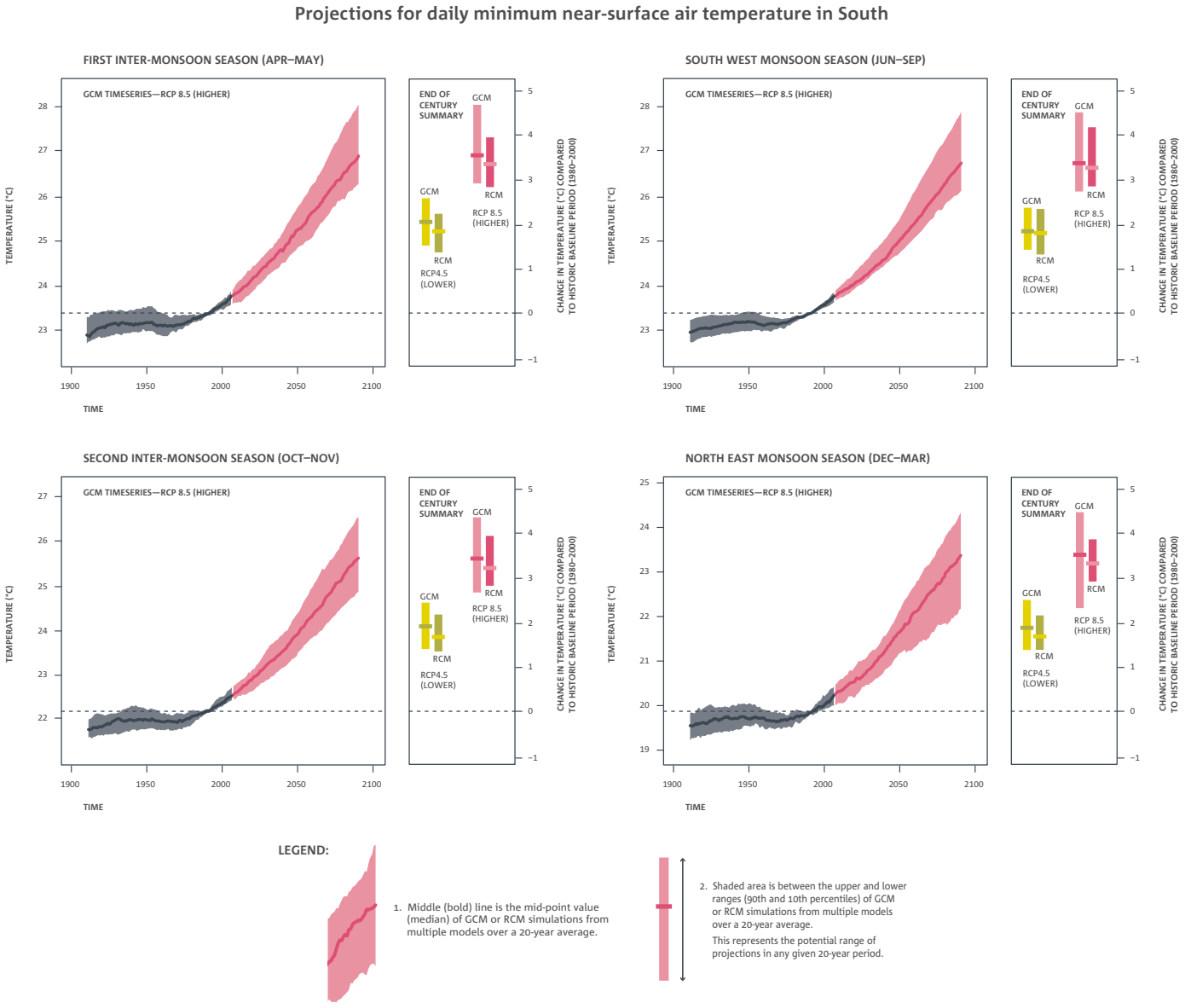

Rainfall

Projections for rainfall for the region from the CMIP5 GCMs are presented in Figure 15-11. There is a large range of inter-annual variability simulated by the GCMs for rainfall for this region, as can be seen by the large spread of the colour bar. Most seasons show little change in rainfall by the end of the century. Only for SIMS are some increases projected by the end of the century.

15.3.2 Regional model results

This section will discuss the projected changes in surface temperature and rainfall by the middle of the century (2045-2065) and by the end of the century (2080-2100) compared with the baseline period (1980-2000) using the ensemble means of the eight RCMs employed in this study. These projections do not represent a value specifically for any single station location, but an average for four seasons for the entire region.

Figure 15-11: Regionally averaged seasonal precipitation changes (mm month^{-1} on left axis and % on right axis) for S. For each season, the time series graph of projections by global climate models (GCM) is shown on the left for the higher (RCP 8.5) greenhouse gas scenario. Black line is from historical GCM runs, red line is the multi-model median projection from GCMs using RCP 8.5. Shadings are between 10% and 90% of 20-year mean values. GCM values have been corrected for 1995-2005 mean bias. Bars on the right for each season show the end-of-century summary of projections by global climate models (GCM, left) and regional climate models (RCM, right) for both lower (RCP 4.5) and higher (RCP 8.5) scenarios.

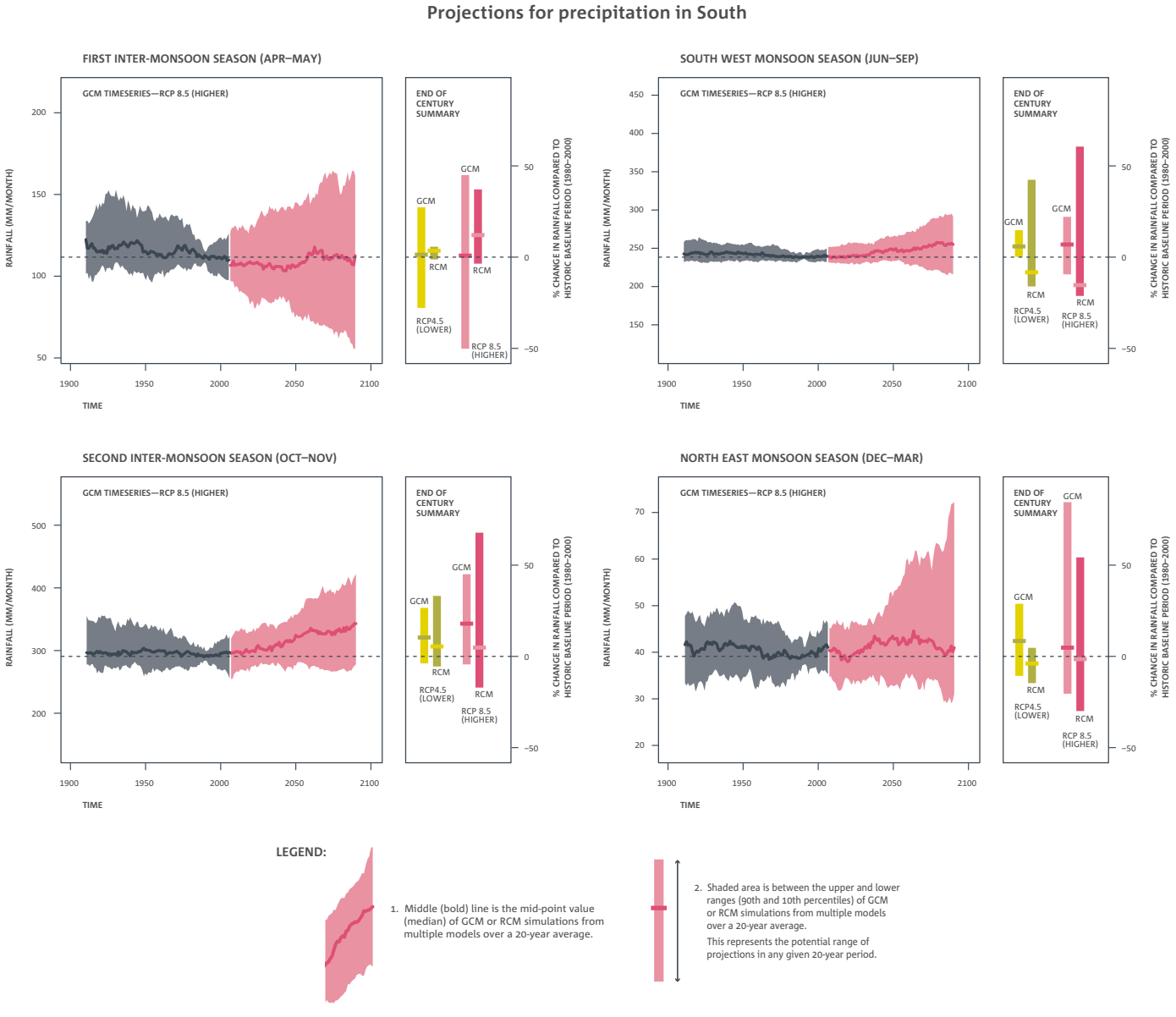

Surface temperature

Table 15-2 to Table 15-6 show projected changes in seasonal and annual surface air temperature (°C) for RCP 8.5 relative to the baseline period 1980-2000 from the high resolution RCMs in this project. Projected changes are the means for two 20-year periods from the 21st century: 2045-2065 and 2080-2100. It is evident from these tables that the increases in mean temperature are quite similar annually (about 1.8°C by mid-century and 3.3°C by the end of the century) and for all seasons. Changes for maximum and minimum temperatures are also similar to the average temperature. The largest projected seasonal increase was by CCAM GFDL-CM3 for SWMS (4.5°C), while the smallest projected increase was by RegCM4.2 NorESM1-M for NEMS (2.5°C).

These projected changes are higher than the previous temperature projections for SRES A2 at the end of the century (MONRE, 2012), both annually and for all seasons. However, the new projections are similar to the PRECIS ensemble-mean projections with SRES A1B at the end of the century (Table 15-3).

Table 15-2: Summary of multi-model mean and range of projected change in annual and seasonal average, maximum and minimum temperatures (°C) for the S region relative to the baseline period (1980-2000) for RCP 8.5. Changes are from eight RCM simulations. Green colouring is for increases less than 2°C, yellow from 2-4°C and orange greater than 4°C.

	MID-CENTURY (2045-2065)					END OF THE CENTURY (2080-2100)				
	ANNUAL	NEMS DEC-MAR	FIMS APR-MAY	SWMS JUNE-SEP	SIMS OCT-NOV	ANNUAL	NEMS DEC-MAR	FIMS APR-MAY	SWMS JUNE-SEP	SIMS OCT-NOV
Tave	1.8	1.9	1.7	1.8	1.8	3.3	3.3	3.3	3.3	3.3
(°C)	1.4 to 2.5	1.4 to 2.5	1.3 to 2.5	1.3 to 2.6	1.4 to 2.6	2.6 to 4.4	2.5 to 4.4	2.8 to 4.3	2.5 to 4.5	2.6 to 4.3
Tmax	1.8	1.9	1.7	1.8	1.9	3.4	3.5	3.3	3.3	3.3
(°C)	1.3 to 2.6	1.4 to 2.6	1.2 to 2.4	1.0 to 2.6	1.5 to 2.6	2.2 to 4.6	2.1 to 4.7	2.4 to 4.3	2.0 to 4.7	2.4 to 4.4
Tmin	1.8	1.9	1.8	1.8	1.8	3.4	3.4	3.4	3.4	3.4
(°C)	1.4 to 2.6	1.5 to 2.5	1.3 to 2.6	1.3 to 2.6	1.2 to 2.7	2.9 to 4.4	2.8 to 4.4	2.8 to 4.4	2.8 to 4.5	2.8 to 4.4

Table 15-3: Projected changes in annual and seasonal mean temperature (°C) for the S region relative to the baseline period (1980-2000) for different SRES emission scenarios (B1, B2, A2, A1B) from a previous study (MONRE, 2012) and the latest PRECIS projections (ensemble means). Green colouring is for increases less than 2°C, yellow from 2-4°C and orange greater than 4°C. Source: IMHEN.

TAVE (°C)	MID-CENTURY (2045-2065)					END OF THE CENTURY (2080-2100)				
	ANNUAL	NEMS DEC-MAR	FIMS APR-MAY	SWMS JUNE-SEP	SIMS OCT-NOV	ANNUAL	NEMS DEC-MAR	FIMS APR-MAY	SWMS JUNE-SEP	SIMS OCT-NOV
	MONRE 2012					MONRE 2012				
B1	1.2	0.9	1.1	1.3	1.3	1.5	1.2	1.4	1.7	1.6
B2	1.3	1.1	1.3	1.5	1.4	2.1	1.7	2.0	2.3	2.2
A2	1.4	1.1	1.3	1.5	1.5	2.5	2.0	2.4	2.8	2.7
	PRECIS					PRECIS				
A1B	2.1	2.1	2.4	1.9	2.2	3.3	3.3	3.6	3.1	3.3

Table 15-4: Projected change in annual and seasonal average temperature by model (°C) for the S region relative to the baseline period (1980-2000) for RCP 8.5 for eight RCMs. Green colouring is for increases less than 2°C, yellow from 2-4°C and orange greater than 4°C.

TAVE (°C)	MID-CENTURY (2045-2065)					END OF THE CENTURY (2080-2100)				
	ANNUAL	NEMS DEC-MAR	FIMS APR-MAY	SWMS JUNE-SEP	SIMS OCT-NOV	ANNUAL	NEMS DEC-MAR	FIMS APR-MAY	SWMS JUNE-SEP	SIMS OCT-NOV
Multi-model mean	1.8	1.9	1.7	1.8	1.8	3.3	3.3	3.3	3.3	3.3
	Individual RCM simulations					**Individual RCM simulations**				
CCAM ACCESS1.0	2.0	2.1	2.0	2.0	2.1	3.7	3.8	3.6	3.7	3.7
CCAM NorESM1-M	1.6	1.8	1.5	1.5	1.6	2.9	3.0	2.8	2.9	2.9
CCAM MPI-ESM-LR	1.8	1.9	1.9	1.7	1.7	3.6	3.7	3.7	3.5	3.4
CCAM CCSM4	1.6	1.7	1.4	1.6	1.5	2.9	3.0	2.8	2.9	2.9
CCAM CNRM-CM5	1.4	1.5	1.3	1.4	1.4	2.9	3.0	2.8	2.9	2.9
CCAM GFDL-CM3	2.5	2.5	2.5	2.6	2.6	4.4	4.4	4.3	4.5	4.3
RegCM4.2 ACCESS1.0	2.0	1.9	2.0	1.9	2.0	3.4	3.4	3.5	3.4	3.4
RegCM4.2 NorESM1-M	1.4	1.4	1.4	1.3	1.4	2.6	2.5	2.8	2.5	2.6

	Indicates a range of low results	< 2.0°C
	Indicates a range of medium results	2.0 to 4.0°C
	Indicates a range of high results	> 4.0°C

Table 15-5: Projected change in annual and seasonal maximum temperature by model (°C) for the S region relative to the baseline period (1980-2000) for RCP 8.5 for eight RCMs. Green colouring is for increases less than 2°C, yellow from 2-4°C and orange greater than 4°C.

TMAX (°C)	MID-CENTURY (2045-2065)					END OF THE CENTURY (2080-2100)				
	ANNUAL	NEMS DEC-MAR	FIMS APR-MAY	SWMS JUNE-SEP	SIMS OCT-NOV	ANNUAL	NEMS DEC-MAR	FIMS APR-MAY	SWMS JUNE-SEP	SIMS OCT-NOV
Multi-model mean	1.8	1.9	1.7	1.8	1.9	3.4	3.5	3.3	3.3	3.3
	Individual RCM simulations					**Individual RCM simulations**				
CCAM ACCESS1.0	2.1	2.2	2.0	1.9	2.2	4.0	4.2	3.9	3.8	3.8
CCAM NorESM1-M	1.6	1.8	1.4	1.7	1.5	2.9	2.8	2.7	3.0	2.8
CCAM MPI-ESM-LR	1.9	2.0	1.9	1.8	1.9	3.9	4.1	3.8	3.8	3.7
CCAM CCSM4	1.7	1.9	1.4	1.7	1.7	3.0	3.1	2.8	3.1	2.9
CCAM CNRM-CM5	1.6	1.7	1.3	1.6	1.6	3.1	3.2	3.1	3.1	3.1
CCAM GFDL-CM3	2.6	2.6	2.4	2.6	2.6	4.6	4.7	4.3	4.7	4.4
RegCM4.2 ACCESS1.0	1.8	1.9	1.8	1.7	1.9	3.2	3.4	3.3	2.9	3.2
RegCM4.2 NorESM1-M	1.3	1.4	1.2	1.0	1.5	2.2	2.1	2.4	2.0	2.4

	Indicates a range of low results	< 2.0°C
	Indicates a range of medium results	2.0 to 4.0°C
	Indicates a range of high results	> 4.0°C

Table 15-6: Projected change in annual and seasonal minimum temperature by model (°C) for the S region relative to the baseline period (1980-2000) for RCP 8.5 for eight RCMs. Green colouring is for increases less than 2°C, yellow from 2-4°C and orange greater than 4°C.

TMIN (°C)	MID-CENTURY (2045-2065)					END OF THE CENTURY (2080-2100)				
	ANNUAL	NEMS DEC-MAR	FIMS APR-MAY	SWMS JUNE-SEP	SIMS OCT-NOV	ANNUAL	NEMS DEC-MAR	FIMS APR-MAY	SWMS JUNE-SEP	SIMS OCT-NOV
Multi-model mean	1.8	1.9	1.8	1.8	1.8	3.4	3.4	3.4	3.4	3.4
	Individual RCM simulations					**Individual RCM simulations**				
CCAM ACCESS1.0	2.1	2.1	2.1	2.1	1.9	3.7	3.7	3.6	3.7	3.7
CCAM NorESM1-M	1.6	1.9	1.5	1.5	1.6	3.1	3.5	2.9	2.9	3.0
CCAM MPI-ESM-LR	1.8	2.0	1.9	1.8	1.7	3.6	3.6	3.8	3.5	3.4
CCAM CCSM4	1.6	1.6	1.5	1.6	1.5	3.0	3.1	2.8	2.9	3.0
CCAM CNRM-CM5	1.4	1.5	1.3	1.3	1.2	2.9	3.0	2.8	2.8	2.8
CCAM GFDL-CM3	2.6	2.5	2.6	2.6	2.7	4.4	4.4	4.4	4.5	4.4
RegCM4.2 ACCESS1.0	2.1	1.8	2.1	2.3	2.1	3.6	3.2	3.6	4.0	3.7
RegCM4.2 NorESM1-M	1.5	1.5	1.7	1.5	1.4	2.9	2.8	3.1	3.0	2.8

	Indicates a range of low results	< 2.0°C
	Indicates a range of medium results	2.0 to 4.0°C
	Indicates a range of high results	> 4.0°C

Rainfall

Rainfall is projected to increase in the future annually and for all seasons (Table 15-7) for this region. Annual rainfall is projected to increase by about 5% during 2045-2065 (with only 3 out of 8 models agreeing on an increase), and by 7% during 2080-2100 (with 3 out of 8 models agreeing on an increase) relative to the baseline period 1980-2000 for RCP 8.5. The largest projected rainfall increase is for FIMS (multi-model mean of +15%, with 7 out of 8 models projecting increases), with a similar increase for SIMS (+14%, with 5 out of 8 models projecting increases) by the end of the century (Table 15-9).

The largest projected seasonal rainfall increase is by RegCM4.2 ACCESS1.0 for SWMS (+93%) while the largest decrease projected was by CCAM ACCESS1.0 for NEMS (-31%), both for the end of the century.

These results for rainfall projections are significantly different from the previous climate projections (MONRE, 2012; Table 15-8). The previous projections had decreases in NEMS (while the new projections show little change) and increases in SIMS (similar to the new projections). The PRECIS ensemble-mean projections are similar to the previous MONRE projections.

Table 15-7: Projected changes in annual and seasonal mean rainfall and its range (%) for the S region relative to the baseline period (1980-2000) for RCP 8.5. Changes are the multi-model means from eight simulations. Orange colouring is for decreases less than -10%, green for changes between -10% to +10% and blue for increases greater than +10%.

RAIN % CHANGE	MID-CENTURY (2045-2065)					END OF THE CENTURY (2080-2100)				
	ANNUAL	NEMS DEC-MAR	FIMS APR-MAY	SWMS JUNE-SEP	SIMS OCT-NOV	ANNUAL	NEMS DEC-MAR	FIMS APR-MAY	SWMS JUNE-SEP	SIMS OCT-NOV
Multi-model mean	5	8	12	3	3	7	1	15	5	14
Range	-10 to +36	-5 to +22	0 to +27	-16 to +61	-14 to +28	-18 to +52	-31 to +57	-11 to +51	-21 to +93	-18 to +72

Table 15-8: Projected changes in annual and seasonal rainfall (%) for the S region relative to the baseline period (1980-2000) for SRES emission scenarios (B1, B2, A2, A1B) from a previous study (MONRE, 2012) and the latest PRECIS projections (ensemble means). Orange colouring is for decreases less than -10%, green for changes between -10% to +10% and blue for increases greater than +10%. Source: IMHEN.

RAIN (%)	MID-CENTURY (2045-2065)					END OF THE CENTURY (2080-2100)				
	ANNUAL	NEMS DEC-MAR	FIMS APR-MAY	SWMS JUNE-SEP	SIMS OCT-NOV	ANNUAL	NEMS DEC-MAR	FIMS APR-MAY	SWMS JUNE-SEP	SIMS OCT-NOV
	MONRE 2012					MONRE 2012				
B1	3	-9	-3	2	10	3	-11	-4	2	12
B2	3	-10	-3	2	11	5	-16	-5	3	17
A2	3	-10	-3	2	11	6	-19	-6	4	20
	PRECIS					PRECIS				
A1B	2	-17	-9	5	6	3	-35	-4	4	15

Table 15-9: Projected changes in annual and seasonal mean rainfall by model (%) for the S region relative to the baseline period (1980-2000) for RCP 8.5 for the eight RCMs. Orange colouring is for decreases less than -10%, green for changes between -10% to +10% and blue for increases greater than +10%.

RAIN (%)	MID-CENTURY (2045-2065)					END OF THE CENTURY (2080-2100)				
	ANNUAL	NEMS DEC-MAR	FIMS APR-MAY	SWMS JUNE-SEP	SIMS OCT-NOV	ANNUAL	NEMS DEC-MAR	FIMS APR-MAY	SWMS JUNE-SEP	SIMS OCT-NOV
Multi-model mean	5	8	12	3	3	7	1	15	5	14
	Individual RCM simulations					Individual RCM simulations				
CCAM ACCESS1.0	-2	-1	17	-6	-7	-9	-31	32	-15	-9
CCAM NorESM1-M	3	20	13	-12	15	3	53	0	-18	13
CCAM MPI-ESM-LR	-9	-5	0	-11	-14	-14	-23	16	-21	-18
CCAM CCSM4	-3	8	13	-10	-7	-5	5	5	-16	1
CCAM CNRM-CM5	-10	1	0	-16	-14	-18	-19	-11	-21	-18
CCAM GFDL-CM3	0	19	8	-11	6	-1	-1	8	-9	8
RegCM4.2 ACCESS1.0	36	0	20	61	28	52	-30	19	93	72
RegCM4.2 NorESM1-M	25	22	27	28	16	52	57	51	46	66

	Indicates a range of low (drier) results	< -10%
	Indicates a range of medium (little change) results	-10 to +10%
	Indicates a range of high (wetter) results	> 10%

15.4 SUMMARY

For current climate in the S region, there is a trend of temperature increase of 0.04°C to 0.28°C per decade from 1961 to 2010. The annual rainfall shows increases and decreases at various stations in this region, with no regional consistency.

The temperature extremes tend to increase in this region. Over the whole region, maximum and minimum temperatures have increased by up to 0.36°C per decade at Con Dao, with somewhat greater increases for minimum temperatures. The number of hot days increased by 3 days per decade over the last 50 years, while the extreme hot days (TX90p) increased. Extreme cold nights (TN10p) decreased significantly throughout the region by up to 15 days per decade. Extreme rainfall indices RX1, RX5, R95p and CWD showed little trend over the last 50 years. However, the number of CDDs did decrease significantly.

Mean annual temperature (Tave) is projected to increase about 1.8°C by mid-century and by about 3.3°C by the end of the century, with little seasonal variation. Both Tmax and Tmin show similar changes to Tave. Rainfall is projected to increase in all seasons in the future. Annual rainfall is projected to increase by about 5% by 2045-2065 and by 7% by 2080-2100, respectively. Increases are projected to be larger in FIMS (+15%) and SIMS (+14%), with the other seasons showing only small increases. The previous projections and the PRECIS ensemble both projected decreases in NEMS (different to the new projections) and increases in SIMS (similar to the current projections).

REFERENCES

Adler RF, Huffman GJ, Chang A, Ferraro R, Xie P-P, Janowiak J, Rudolf B, Schneider U, Curtis S, Bolvin D, Gruber A, Susskind J, Arkin P and Nelkin E (2003) The Version-2 Global Precipitation Climatology Project (GPCP) Monthly Precipitation Analysis (1979–Present). J Hydromet 4:1147-1167

Afiesimama EA, Pal JS, Abiodun BJ, Gutowski WJ and Adedoyin A (2006) Simulation of West African Monsoon using the RegCM3. Part I: Model validation and interannual variability. Theor Appl Climatol 86:23–37

AGO (Australian Greenhouse Office) (2006a) Climate Change Impacts & Risk Management: A Guide for Business and Government. Department of Environment and Heritage, Commonwealth of Australia, 72 pp

AGO (Australian Greenhouse Office) (2006b) Climate Change Scenarios for Initial Assessment of Risk in Accordance with Risk Management Guidance. Department of Environment and Heritage, Commonwealth of Australia, 35 pp

Arakawa A and Schubert WH (1974) Interaction of a cumulus cloud ensemble with the large-scale environment: Part 1. J Atmos Sci 31:674-701

Asian Development Bank (1994) Climate Change in Asia: Vietnam Country Report. Asian Development Bank, PO Box. 789, Manila, Philippines, 102pp

Asian Disaster Preparedness Center (2003) Climate change and development in Vietnam: Agriculture and adaptation for the Mekong Delta region. Bangkok Deutsche Gesellschaft für Technische Zusammenarbeit (GTZ) GmbH, Postfach 51 80, D - 65726 Eschborn, Division 44 - Environment and Infrastructure, 27pp

Australian Bureau of Meteorology and CSIRO, 2011. Climate Change in the Pacific: Scientific Assessment and New Research. Volume 1: Regional Overview. http://www.pacificclimatechangescience.org/wp-content/uploads/2013/08/Climate-Change-in-the-Pacific.-Scientific-Assessment-and-New-Research-Volume-1.-Regional-Overview.pdf

Bengtsson L, Bottger H and Kanamitsu M (1982) Simulation of hurricane-type vortices in a general circulation model. Tellus 34:440–457

Bengtsson L, Koumoutsaris S and Hodges K (2011) Large-scale surface mass balance of land ices from a comprehensive atmosphere model. Surveys Geophys 32:459-474

Bergman L (2005) Chapter 24 CGE modeling of environmental policy and resource management. In: Karl-Göran M, Jeffrey RV (eds) Handbook of Environmental Economics. Elsevier 1273-1306

Bhend J and Whetton P (2013) Consistency of simulated and observed regional changes in temperature, sea level pressure and precipitation. Clim Change doi:10.1007/s10584-012-0691-2 1-12

Bister M and Emanuel KA (1998) Dissipative heating and hurricane intensity. Meteor Atm Phys 52:233–240

Bjerknes J (1969) Atmospheric teleconnections from the equatorial Pacific. Mon Wea Rev 97:163-172

Bousquet F, Barnaud C, Barreteau O, Cernesson F, Dumrongrojwatthana P, Dung LC, Ekasingh B, Gajaseni N, Hoanh CT, LePage C, Naivinit W, Promburom P, Raj Gurung T, Ruankaew N and Trebuil G (2006) Companion modelling for resilient water management: Stakeholders' perceptions of water dynamics and collective learning at the catchment scale, France and the CGIAR: Delivering scientific results for agricultural development 98-101

Bousquet F, Castella JC, Trébuil G, Barnaud C, Boissau S and Kam SP (2007) Using multi-agent systems in a companion modelling approach for agro-ecosystem management in South-east Asia. Outlook on Agriculture 36:57-62

Broccoli AJ and Manabe S (1990) Can existing climate models be used to study anthropogenic changes in tropical cyclone climate? Geophys Res Lett 17:1917–1920

Bussay AM, Szinell C, Hayes M and Svoboda M (1998) Monitoring drought in Hungary using the standardized precipitation index. Annales Geophysicae 11 (Supplement)

Camargo SJ and Zebiak SE (2002) Improving the detection and tracking of tropical cyclones in atmospheric general circulation models. Wea Forecasting 17:1152–1162

Camargo SJ, Sobel AH, Barnston AG and Emanuel KA (2007) Tropical cyclone genesis potential index in climate models. Tellus 59A:428-443

Carter TR, Jones RN, Lu X, Bhadwal S, Conde C, Mearns LO, O'Neill BC, Rounsevell MDA, and Zurek MB (2007) New Assessment Methods and the Characterisation of Future Conditions. In: Parry, ML, Canziani OF, Palutikof JP, van der Linden PJ and Hanson CE (eds). Climate Change 2007: Impacts, Adaptation and Vulnerability. Contribution of Working Group II to the Fourth Assessment Report of the Intergovernmental Panel on Climate Change. Cambridge University Press, Cambridge, UK

Chao BF, Wu YH and Li YS (2008) Impact of artificial reservoir water impoundment on global sea level. Science 320:212-214

Chen TC, Tsay JD, Yen MC and Matsumoto J (2012) Interannual variation of the late fall rainfall in Central Vietnam. J Climate 25:392-413

Church JA, Gregory JM, White NJ, Platten SM and Mitrovica JX (2011b) Understanding and projecting sea level change. Oceanography 24:130-143

Church JA, Monselesan D, Gregory JM and Marzeion B (2013) Evaluating the ability of process based models to project sea-level change. Envir Res Lett 8(1) 014051

Church J and White N (2011) Sea-Level Rise from the Late 19th to the Early 21st Century. Surveys in Geophys 32:585-602

Church JA and White NJ (2006) A 20th century acceleration in global sea-level rise. Geophys Res Lett 33 L10602, doi:10610.11029/12005GL024826

Church JA, White NJ, Coleman R,Lambeck K and Mitrovica JX (2004) Estimates of the regional distribution of sea level rise over the 1950-2000 period, J Climate, 17:2609-2625

Church JA, White NJ, Konikow IF, Domingues CM, Cogley JG, Rignot E, Gregory JM, van den Broeke MR, Monaghan AJ and Velicogna I (2011a) Revisiting the Earth's sea-level and energy budgets from 1961 to 2008. Geophys Res Lett 38 L18601 doi:10.1029/2011GL048794

Church, JA, Woodworth PL, Aarup T and Wilson WS (Eds) (2010) Understanding Sea-level Rise and Variability, Wiley-Blackwell Publishing, Chichester, UK, 427pp

Cogley JG (2009) Geodetic and direct mass-balance measurements: comparison and joint analysis. Annals Glaciology 50:96-100

Colberg F and McInnes KL (2012) The impact of future changes in weather patterns on extreme sea levels over southern Australia. J Geophys Res 117(C8) C08001

Cooper GF (1990) The computational complexity of probabilistic inference using Bayesian belief networks. Artificial Intelligence 42:393-405

Coyle G (2000) Qualitative and quantitative modelling in system dynamics: some research questions. System Dynamics Rev 16:225-244

CSIRO and the Australian Bureau of Meteorology (2007) Climate change in Australia: technical report 2007. CSIRO Marine and Atmospheric Research, Aspendale, VIC, 148 pp, **http://www.climatechangeinaustralia.gov.au/technicalreport.php**

Dasgupta S, Laplante B, Meisner C, Wheeler D and Yan JP (2007) The impact of sea level rise on developing countries: A comparative analysis. World Bank Policy Research Working Paper 4136

Davidson NE, Holland GJ, McBride JL and Keenan TD (1990) On the formation of AMEX Tropical Cyclones Irma and Jason. Mon Wea Rev 118:1981-2000

Deadman P (1999) Modelling individual behaviour and group performance in an intelligent agent-based simulation of the tragedy of the commons. J Environ Management 56:159-172

Dessai S and Hulme M (2007) Assessing the robustness of adaptation decisions to climate change uncertainties: A case study on water resources management in the East of England. Global Environmental Change 17:59-72

DHI (2005) MIKE 11-A modeling system for rivers and channels. DHI – water and environment. Hørsholm, Denmark

Dickinson RE, Henderson-Sellers A and Kennedy PJ (1993) Biosphere-Atmosphere Transfer Scheme (BATS) version 1E as coupled to the NCAR Community Climate Model. NCAR Tech Note, Nat Cent Atmos Res, Boulder, Colo, 72pp

Ding Y and Sikka DR (2006) Synoptic systems and weather. In: The Asian Monsoons, Wang B (Ed), Praxis, Springer, Berlin, Heidelberg 131-201

Ding Y and Yanju L (2001) Onset and the evolution of the summer monsoon over the South China Sea during SCSMEX field experiment in 1998. Meteor Soc Japan 79:255-276

Dinh VU (2009) Long-term variation and trend estimation for tropical cyclone and typhoon in the north-western Pacific, East Sea and Vietnamese coastal areas. J Nat Science Technology 25:542- 550

Domingues CM, Church JA, White NJ, Gleckler PJ, Wijffels SE, Barker PM and Dunn JR(2008) Improved estimates of upper-ocean warming and multi-decadal sea-level rise. Nature 453:1090-1093

Dunkerton TJ, Montgomery MT and Z Wang (2008) Tropical cyclogenesis in a tropical wave critical layer: Easterly waves. Atmos Chem Phys Disc 8:11149-11292

Eckert R and Waibel M (2009) Climate change and challenges for the urban development of Ho Chi Minh City / Vietnam Pacific News 31:18-20

Edmonds JA and Rosenberg NJ (2005) Climate change impacts for the coterminous USA: An integrated assessment summary. Climatic Change 69:151-162

Emanuel KA and Nolan DS (2004) Tropical Cyclone activity and global climate. 26th Conf hurricanes and tropical meteorology, Amer Met Soc, Miami, Florida

Endo N, Matsumoto J and Lwin T (2009) Trends in precipitation extremes over Southeast Asia. SOLA 5:168-171

ETCCDI (2009) **http://etccdi.pacificclimate.org/list_27_indices.shtml**

Evans JP, McGregor JL and McGuffie K (2012) Future regional climates. In "Future of the World's Climate" Henderson-Sellers A and McGuffie K (Eds). Elsevier, Amsterdam, 223-250

Fettweis X, Franco B, Tedesco M, van Angelen JH, Lenaerts JTM, van den Broeke MR and Gallée H (2013) Estimating the Greenland ice sheet surface mass balance contribution to future sea level rise using the regional atmospheric climate model MAR. The Cryosphere 7:469-489

Francisco RV, Argete J, Giorgi F, Pal J, Bi X and Gutowski WJ (2006) Regional model simulation of summer rainfall over the Philippines: Effect of choice of driving fields and ocean flux schemes. Theor Appl Climatol 86:215–227

Freidenreich SM and Ramaswamy V (1999) A new multiple-band solar radiative parameterization for general circulation models. J Geophys Res 104:31,389–31,409

Frich P, Alexander LV, Della-Marta P, Gleason B, Haylock M, Tank AK and Peterson T (2002) Observed coherent changes in climatic extremes during the second half of the twentieth century. Clim Res 19:193-212

Frieler K, Meinshausen M, Schneider von Deimling T, Andrews T and Forster P (2011) Changes in global-mean precipitation in response to warming, greenhouse gas forcing and black carbon. Geophys Res Lett 38 L04702, doi:10.1029/2010GL045953

Gehrels WR and Woodworth PL (2013) When did modern rates of sea-level rise start? Global and Planetary Change 100:263-277

Gilbert N (2008) Agent-based models. SAGE Publications, Los Angeles

Giorgi F, Jones C and Asrar GR (2009) Addressing climate information needs at the regional level: the CORDEX framework. World Meteorological Organization (WMO) Bulletin 58(3):175.

Goelzer H, Huybrechts P, Fürst JJ, Nick FM, Andersen ML, Edwards TL, Fettweis X, Payne AJ and Shannon S (2013) Sensitivity of Greenland ice sheet projections to model formulations. J Glaciology, in press.

Gordon C, Cooper C, Senior CA, Banks H, Gregory JM, Johns TC, Mitchell JFB, and Wood RA (2000) The simulation of SST, sea ice extents and ocean heat transports in a version of the Hadley Centre coupled model without flux adjustments. Clim Dyn 16:147–168

Gray WM (1979) Hurricanes: Their formation structure and likely role in tropical circulation. Meteorology over the tropical oceans, Shaw DB (Ed) Roy Meteor Soc pp 155-218

Gregory JM (2010) Long-term effect of volcanic forcing on ocean heat content, Geophys Res Lett 37 L22701

Gregory JM, Bi D, Collier MA, Dix MR, Hirst AC, Hu A, Huber M, Knutti R, Marsland SJ, Meinshausen M, Rashid HA, Rotstayn LD, Schurer A and Church JA (2013b) Climate models without pre-industrial volcanic forcing underestimate historical ocean thermal expansion. Geophys Res Lett 40:1600-1604 doi: 10.1002/grl.50339

Gregory JM, White NJ, Church JA, Bierkens MFP, Box JE, van den Broeke M, Cogley JG, Fettweis X, Hanna E, Huybrechts P, Konikow LF, Leclercq PW, Marzeion B, Oerlemans J, Tamisiea ME, Wada Y, Wake LM and van de Wal RSW (2013a) Twentieth-century global-mean sea-level rise: Is the whole greater than the sum of the parts? J Climate 26:4476-4449

Gregory M and Huybrechts P (2006) Ice-sheet contributions to future sea-level change. Phil Trans Roy Soc A-Math Phys Eng Sci 364:1709-1731

Grell GA (1993) Prognostic evaluation of assumptions used by cumulus parameterization. Mon Wea Rev 121:764-787

Grose MR, Brown JN, Narsey S, Brown JR, Murphy BJ, Langlais C, Sen Gupta A, Moise AF and Irving DB (2013) Assessment of the CMIP5 global climate model simulations of the western tropical Pacific climate system and comparison to CMIP3. Submitted to Int J Climatology

Hall TM and S Jewson S (2007) Statistical modelling of North Atlantic tropical cyclone tracks. Tellus A 59:486-498

Hart RE (2003) A cyclone phase space derived from thermal wind and thermal asymmetry. Mon Wea Rev 131:585-616

Hayhoe K, Cayan D, Field CB, Frumhoff PC, Maurer EP, Miller NL, Moser SC, Schneider SH, Cahill NC, Cleland CC, Dale L, Drapek R, Hanemann RN, Kalkstein LS, Lenihan J, Lunch CK, Neilson RP, Sheridan SC and Verville JH (2004) Emissions pathways, climate change, and impacts on California. Proceedings of the National Academy of Science USA 101:12422-12427

Holland JH (1992) Adaptation in natural and artificial systems: An introductory analysis with applications to biology, control and artificial intelligence. MIT Press, Cambridge

Holland JH and Miller JH (1991) Artificial adaptive agent in economic theory. Amer Econ Rev 81:365-370

Hong S-Y, Dudhia J and Chen S-H (2004) A revised approach to ice microphysical processes for the bulk parameterization of clouds and precipitation. Mon Wea Rev 132:103–120

Hosking JRM (1990) L-moments: Analysis and estimation of distributions using linear combinations of order statistics. J Roy Stat Soc 52:105-124

Hulme M and Viner D (1998) A climate change scenario for the tropics. Clim Change 39:145–176

Hunter J (2012) A simple technique for estimating an allowance for uncertain sea-level rise. Clim Change 113:239-252

Hunter JR, Church JA, White NJ and Zhang X (2013) Towards a global regionally varying allowance for sea-level rise, Ocean Engineering(0)

IPCC (Intergovernmental Panel on Climate Change) SRES (2000) Special Report on Emissions Scenarios: A special report of Working Group III of the Intergovernmental Panel on Climate Change. Nakićenović N and Swart R (eds). Cambridge University Press, UK, 570 pp

IPCC (Intergovernmental Panel on Climate Change) AR3 (2001) Climate Change 2001: The Scientific Basis. Contribution of Working Group I to the Third Assessment Report of the Intergovernmental Panel on Climate Change. Houghton JT, Ding Y, Griggs DJ, Noguer M, van der Linden PJ, and Xiaosu D (eds). Cambridge University Press, UK 944 pp

IPCC (Intergovernmental Panel on Climate Change) AR4 (2007a) Climate Change 2007: The Physical Science Basis. Contribution of Working Group I to the Fourth Assessment Report of the Intergovernmental Panel on Climate Change. S. Solomon S, D. Qin D, M. Manning M, Z. Chen Z, M. Marquis M, K.B. Averyt KB, M. Tignor M and H.L. Miller HL (eds). Cambridge University Press, Cambridge, United Kingdom and New York, NY, USA 996 pp

IPCC (Intergovernmental Panel on Climate Change) AR4 (2007b) Climate Change 2007: Impacts, Adaptation and Vulnerability. Contribution of Working Group II to the Fourth Assessment Report of the Intergovernmental Panel on Climate Change. Parry ML, Canziani OF, Palutikof JP, van der Linden PJ and Hanson CE (eds). Cambridge University Press, Cambridge, UK 1000 pp

IPCC (Intergovernmental Panel on Climate Change) SREX (2012) Managing the Risks of Extreme Events and Disasters to Advance Climate Change Adaptation. A Special Report of Working Groups I and II of the Intergovernmental Panel on Climate Change [Field, C.B., V. Barros, T.F. Stocker, D. Qin, D.J. Dokken, K.L. Ebi, M.D. Mastrandrea, K.J. Mach, G.-K. Plattner, S.K. Allen, M. Tignor, and P.M. Midgley (eds.)]. Cambridge University Press, Cambridge, UK, and New York, NY, USA, 582 pp

IPCC (Intergovernmental Panel on Climate Change) AR5 (2013) Climate Change 2013: The Physical Science Basis. Contribution of Working Group I to the Fifth Assessment Report of the Intergovernmental Panel on Climate Change [Stocker, T.F., D. Qin, G.-K. Plattner, M. Tignor, S.K. Allen, J. Boschung, A. Nauels, Y. Xia, V. Bex and P.M. Midgley (eds.)]. Cambridge University Press, Cambridge, United Kingdom and New York, NY, USA, 1535 pp.

Ishii M and Kimoto M (2009) Reevaluation of historical ocean heat content variations with time-varying XBT and MBT depth bias corrections. J Oceanography 65:287-299

Jevrejeva S, Grinsted A, Moore JC and Holgate S (2006) Nonlinear trends and multiyear cycles in sea level records. J Geophys Res 111(C9) C09012

Jevrejeva S, Moore JC, Grinsted A and Woodworth PL (2008) Recent global sea level acceleration started over 200 years ago. Geophys Res Lett 35 L08715 doi:08710.01029/02008GL033611

Jones RN, and Mearns LO (2005) Assessing future climate risks. In Lim, B. et al. (eds), Adaptation Policy Frameworks for Climate Change: Developing Strategies, Policies and Measures. United Nations Development Programme, Cambridge University Press, Cambridge, UK, 119-143

Jones RG, Noguer M, Hassell DC, Hudson D, Wilson SS, Jenkins GJ and Mitchell JFB (2004) Generating high resolution climate change scenarios using PRECIS. Met Office Hadley Centre: Exeter, UK 40 pp

Jones RN and Page CM (2001). Assessing the risk of climate change on the water resources of the Macquarie River Catchment. In Integrating models for natural resources management across disciplines, issues and scales, 673-678

Joughin I, Smith BE and Holland DM (2010) Sensitivity of 21st century sea level to ocean-induced thinning of Pine Island Glacier, Antarctica. Geophys Res Lett 37 L20502

Kajikawa Y, Yasunari T, Yoshida S and Fujinami H (2012) Advanced Asian summer monsoon onset in recent decades. Geophys Res Lett 39 L03803 doi:10.1029/2011GL050540

Kalnay E, Kanamitsu M, Kistler R, Collins W, Deaven D, Gandin L, Iredell M, Saha S,White G, Woollen J, Zhu Y, Chelliah M, Ebisuzaki W, Higgins W, Janowiak J, Mo K C, Ropelewski C, Wang J, Leetmaa A, Reynolds R, Jenne R and Joseph D (1996) The NCEP/NCAR40-year reanalysis project. Bull Amer Meteor Soc 77:437–471

Katsman CA, Sterl A, Beersma JJ, van den Brink HW, Church JA, Hazeleger W, Kopp RE, Kroon D, Kwadijk J, Lammersen R, Lowe J, Oppenheimer M, Plag H.P, Ridley J, von Storch H, Vaughan DG, Vellinga P, Vermeersen LLA, van de Wal RSW and Weisse R (2011) Exploring high-end scenarios for local sea level rise to develop flood protection strategies for a low-lying delta - the Netherlands as an example. Clim Change 109:617-645 DOI: 10.1007/s10584-011-0037-5

Katzfey JJ, McGregor JL, Nguyen KC and Thatcher M (2009) Dynamical downscaling techniques: Impacts on regional climate change signals. In MODSIM09 Int. Congress on Modelling and Simulation, www.mssanz.org.au/modsim09 13:2377-2383

Katzfey JJ (2013) Chapter 15: Regional Climate Modelling for the Energy Sector. In A. Troccoli et al. (eds.), Weather Matters for Energy, DOI: 10.1007/978-1-4614-9221-4_15

Kawase H, Takemura T and Nozawa T (2011) Impact of carbonaceous aerosols on precipitation in tropical Africa during the austral summer in the twentieth century. J Geophys Res 116 D18116 doi:10.1029/2011JD015933

Kendall MG (1975) Rank correlation methods. Charles Griffin, London 272pp

Kendall RA, Mitrovica JX and Milne GA (2005) On post-glacial sea level – II Numerical formulation and comparative results on spherically symmetric models. Geophys J Int 161:679-706

Kepert JD (2001) The dynamics of boundary layer jets within the tropical cyclone core. Part I: Linear theory. J Atmos Sci 58:2469-2484

Kim ST and Yu JY (2012) The two types of ENSO in CMIP5 models. Geophys Res Lett 39

Kleinen J (2007) Historical perspectives on typhoons and tropical storms in the natural and socio-economic system of Nam Dinh (Vietnam). J Asian Earth Sci 29:523-531

Knapp KR, Kruk MC, Levinson DH, Diamond HJ and Neumann CJ (2010) The International Best Track Archive for Climate Stewardship (IBTrACS). Bull Amer Meteor Soc 91:363-376

Knutson TR, McBride JL, Chan J, Emanuel K, Holland G, Landsea C, Held I, Kossin JP, Srivastava AK and Sugi M (2010) Tropical cyclones and climate change. Nature Geoscience 3:157-163

Kokic, P, Beckling, J and Lübke, O (2002) A New Definition of Multivariate M-quantiles. In Statistical Data Analysis Based on the L1-Norm and Related Methods. Statistics for Industry and Technology pp 15-24

Konikow LF (2011) Contribution of global groundwater depletion since 1900 to sea-level rise. Geophys Res Lett 38 L17401

Kowalczyk EA, Wang YP, Law RM, Davies HL, McGregor JL and Abramowitz G (2006) The CSIRO Atmosphere Biosphere Land Exchange (CABLE) model for use in climate models and as an offline model. CSIRO Marine and Atmospheric Research Paper 13 37pp.

Krinner G, Magand O, Simmonds I, Genthon C and Dufresne J (2007) Simulated Antarctic precipitation and surface mass balance at the end of the twentieth and twenty-first centuries. Clim Dyn 28:215-230

Kug JS, Ham YG, Lee JY and Jin FF (2012) Improved simulation of two types of El Niño in CMIP5 models. Env Res Lett 7 Doi: 10.1088/1748-9326/7/3/039502

Lau K-M and Chang C-P (1987) Planetary scale aspects of the winter monsoon and atmospheric teleconnections. In: Monsoon Meteorology, Chang C-P and Krishnamurti T (Eds), Oxford University Press, New York 161-202

Le Clercq PW, Oerlemans J and Cogley JG (2011) Estimating the glacier contribution to sea-level rise for the period 1800-2005. Surveys Geophys 32:519-535

Lemperiere F (2006) The role of dams in the XXI century. Int J Hydropower Dams 3

Lenzen M, Pade LL and Munksgaard J (2004) CO2 multipliers in multi-region input-output models. Econ Systems Res 16:391-412

Lettenmaier DP and Milly PCD (2009) Land waters and sea level. Nature Geoscience 2:452-454

Levitus S, Antonov JI, Boyer TP, Locarnini RA, Garcia HE and Mishonov AV (2009) Global ocean heat content 1955-2007 in light of recently revealed instrumentation problems. Geophys Res Lett 36 L07608 doi:07610.01029/02008GL037155

Levitus S, Antonov JI, Boyer TP, Baranova OK, Garcia HE, Locarnini RA, Mishonov AV,Reagan JR, Seidov D, Yarosh ES and Zweng MM (2012) World ocean heat content and thermosteric sea level change (0-2000 m), 1955-2010. Geophys Res Lett 39 L10603

Ligtenberg SRM, van de Berg WJ, van den Broeke MR, Rae JGL and van Meijgaard E (2013) Four scenarios for the future surface mass balance of the Antarctic ice sheet: a contribution to ice2sea. Clim Dyn, submitted

Little CM, Oppenheimer M and Urban NM (2013) Upper bounds on twenty-first-century Antarctic ice loss assessed using a probabilistic framework. Nature Clim Change, advance online publication

Liu KS and Chan JCL (2003) Climatological characteristics and seasonal forecasting of tropical cyclones making landfall along the South China Coast. Mon Wea Rev 131:1650-1662

Lloyd-Hughes B and Saunders MA (2002) A drought climatology for Europe. Int J Climatol 22:1571–1592 doi:10.1002/joc.846

Lopez A., Tebaldi C, New M, Stainforth D, Allen M and Kettleborough J (2006) Two approaches to quantifying uncertainty in global temperature changes. Journal of Climate 19: 4785-4796

Lowe JA, Woodworth PL, Knutson T, McDonald RE, McInnes KL, Woth K, von Storch H, Wolf J, Swail V, Bernier NB, Gulev S, Horsburgh KJ, Unnikrishnan AS, Hunter JR and Weisse R (2010) Past and Future Changes in Extreme Sea Levels and Waves, in Understanding Sea-Level Rise and Variability. Church JA, Woodworth PL, Aarup T and Wilson WS (eds). Wiley-Blackwell, Oxford, UK, pp 326-375.

Marzeion B, Jarosch AH and Hofer M (2012) Past and future sea-level change from the surface mass balance of glaciers. The Cryosphere 6:1295-1322

Masters D, Nerem RS, Choe C, Leuliette E, Beckley B, White N and Ablain M (2012) Comparison of global mean sea level time series from TOPEX/Poseidon, Jason-1 and Jason-2. Marine Geodesy 35(supp1):20-41

Matsumoto J (1997) Seasonal transition of summer rainy season over Indochina and adjacent monsoon region. Adv Atmos Sci 14:231-245

McBride JL and Zehr R (1981) Observational analysis of tropical cyclone formation. Part II: Comparison of non-developing versus developing systems. J Atmos Sci 38:1132-1151

McGregor JL (1993) Economical determination of departure points for semi- Lagrangian models. Mon Wea Rev 121:221-230

McGregor JL (1996) Semi-Lagrangian advection on conformal-cubic grids. Mon Wea Rev 124:1311-1322

McGregor JL (1997) Regional climate modelling. Meteor Atmos Phys 63:105-117

McGregor JL (2003) A new convection scheme using a simple closure. In "Current issues in the parameterization of convection", BMRC Research Report 93:33–36

McGregor JL (2005a) Geostrophic adjustment for reversibly staggered grids. Mon Wea Rev 133:1119-1128

McGregor JL (2005b) C-CAM: Geometric aspects and dynamical formulation [electronic publication]. CSIRO Atmospheric Research Tech Paper 70 43pp

McGregor JL and Dix MR (2001) The CSIRO conformal-cubic atmospheric GCM. In IUTAM Symposium on Advances in Mathematical Modelling of Atmosphere and Ocean Dynamics, Hodnett PF (Ed), Kluwer, Dordrecht, 197-202

McGregor JL and Dix MR (2008) An updated description of the Conformal-Cubic Atmospheric Model. In: "High Resolution Simulation of the Atmosphere and Ocean", Hamilton K and Ohfuchi W (Eds), Springer, 51–76

McGregor JL, Gordon HB, Watterson IG, Dix MR and Rotstayn LD (1993) The CSIRO 9-level atmospheric general circulation model. CSIRO Div. Atmospheric Research Tech Paper 26 89pp

McKee TB, Doesken NJ and Kleist J (1993) The relationship of drought frequency and duration to time scales. In Proc 8th Conf Applied Climatology, Amer Meteor Soc, 17:179-183

Meehl, G.A., Stocker TF, Collins WD, Friedlingstein P, Gaye AT, Gregory JM, Kitoh A, Knutti R, Murphy JM, Noda A, Raper SCB, Watterson IG, Weaver AJ and Zhao Z-C (2007) Global climate projections. In: IPCC 2007a

Meinshausen M, Smith SJ, Calvin K, Daniel JS, Kainuma M, Lamarque JF, Matsumoto K, Montzka S, Raper S, Riahi K, Thomson A, Velders GJM and van Vuuren D (2011) The RCP greenhouse gas concentrations and their extensions from 1765 to 2300. Clim Change 109:213–241

Merrifield MA and Maltrud ME (2011) Regional sea level trends due to a Pacific trade wind intensification. Geophys Res Lett 38 L21605

Merrifield MA, Thompson PR and Lander M (2012) Multidecadal sea level anomalies and trends in the western tropical Pacific. Geophys Res Lett 39 L13602

Miller JH and Page SE (2008) Complex adaptive systems: An introduction to computational models of social life. Princeton University Press, Princeton and Oxford

Mitchell TD and Jones PD (2005) An improved method of constructing a database of monthly climate observations and associated high-resolution grids. Int. J Climatol 25:693-712 doi:10.1002/joc.1181

Mitrovica JX, Gomez N, Morrow E, Hay C, Latychev K and Tamisiea ME (2011) On the robustness of predictions of sea level fingerprints. Geophys J Int 187:729-742 doi:10.1111/J1365-246X2011.05090

Mitrovica JX, Tamisiea M, Davis JL and Milne GA (2001) Recent mass balance of polar ice sheets inferred from patterns of global sea-level change. Nature 409:1026-1029

Monaghan AJ, Bromwich DH, Fogt RL, Wang S-H, Mayewski PA, Dixon DA, Ekaykin A, Frezzotti M, Goodwin I, Isaksson E, Kaspari SD, Morgan VI, Oerter H, Van Ommen TD, Van der Veen CJ and Wen J (2006) Insignificant change in Antarctic snowfall since the International Geophysical Year. Science 313:827-831

MONRE (2009) Climate change and sea level rise scenarios for Viet Nam. Hanoi Agriculture Press, Hanoi

MONRE (2012) Climate change, sea level rise scenarios for Viet Nam. Ministry of Natural Resources and Environment, Hanoi

Moore JC,.Jevrejeva S and Grinsted A (2011) The historical global sea level budget. Annals Glaciology 52(59): 8-14

Moss RH, Edmonds JA, Hibbard KA, Manning MR, Rose SK, van Vuuren DP, Carter TR, Emori S, Kainuma M, Kram T, Meehl GA, Mitchell JFB, Nakicenovic N, Riahi K, Smith SJ, Stouffer RJ, Thomson AM, Weyant JP, Wilbanks TJ (2010) The next generation of scenarios for climate change research and assessment. Nature 463:747-756

Murakami H and Wang B (2010) Future change of North Atlantic tropical cyclone tracks: Projection by a 20-km-mesh global atmospheric model. J Clim 23:2699–2721

Muthers S, Matzarakis A and Koch E (2010) Climate change and mortality in Vienna—A human biometeorological analysis based on regional climate modeling. Int J Envir Res and Public Health 7:2965-2977

NAST (National Assessment Synthesis Team) (2000) Climate Change Impacts on the United States: The Potential Consequences of Climate Variability and Change, National Assessment Synthesis Team, U.S. Global Change Research Program. Cambridge University Press, New York, NY, USA

Neale MC, Boker SM, Xie G, Maes HM (1999) Statistical modeling. Richmond, Virginia: Dept Psychiatry

New M, Hulme M and Jones PD (1999) Representing twentieth century space-time climate variability. Part 1: development of a 1961-90 mean monthly terrestrial climatology. J Climate 12:829-856

New M, Lister D, Hulme M and Makin I (2002) A high-resolution data set of surface climate over global land areas. Clim Res 21:1-25 doi: 10.3354/cr021001

Ngu DN (2000) Knowledge of El Niño and La Niña. Science and Technology Publishing House, Hanoi

Nguyen D-Q, Renwick J and McGregor J (2013) Variations of surface temperature and rainfall in Vietnam from 1971 to 2010. Int J Climatol DOI:10.1002/joc.3684

Nguyen DT, Uvo C and Rosbjerg D (2007) Short communication: Relationship between the tropical Pacific and Indian Ocean sea-surface temperature and monthly precipitation over the Central Highlands, Vietnam. Int J Climatol DOI:10.1002/joc.1486 27:1439–1454

Nguyen KC and McGregor JL (2009) Modelling the Asian summer monsoon using CCAM. Clim Dyn 32:219-236

Nguyen KC, Katzfey JJ, and McGregor JL (2012) Global 60 km simulations with CCAM: evaluation over the tropics. Clim Dyn 39:637-654 10.1007/s00382-011-1197-8

Nguyen KC, Katzfey JJ, and McGregor JL (2013) Downscaling over Vietnam using the stretched-grid CCAM: verification of the mean and interannual variability of rainfall. Clim Dyn 10.1007/s00382-013-1976-5

Nguyen DN and Nguyen TH (2004). Climate and climate resources of Vietnam. Agriculture Publisher, Hanoi.

Nguyen KC and Walsh KJE (2001) Interannual, decadal and transient greenhouse simulation of tropical cyclone-like vortices in a regional climate model of the South Pacific. J Climate 14:3043–3054

Nick FM, Vieli A, Andersen ML, Joughin I, Payne A, Edwards TL, Pattyn F and Van De Wal RSW (2013) Future sea level rise from Greenland's major outlet glaciers in 935 a warming climate. Nature, accepted.

Nieuwolt S (1981) The climates of continental southeast Asia. In: World Survey of Climatology, Takahashi K and Arakawa H (Eds), Elsevier, Amsterdam 9:1-59

Nolan DS (2007) What is the trigger for tropical cyclogenesis? Aust Meteor Mag 56:241-266

Orgill MM (1967a) Some aspects of the onset of the summer monsoon over southeast Asia. Final Report, Second Technical Report, Southeast Asia Monsoon Study, Dept Atmos Science, Colorado State University, Fort Collins, Colorado 75pp

Orgill MM (1967b) Rainfall patterns associated with monsoon disturbances over southeast Asia. Report No. 3. Third Technical Report, Southeast Asia Monsoon Study, Dept Atmos Science, Colorado State University, Fort Collins, Colorado 51pp

Page CM and Jones RN (2001). OzClim: the development of a climate scenario generator for Australia. In MODSIM 2001: International Congress on Modelling and Simulation: proceedings, 667-671

Peltier WR (2004) Global glacial isostasy and the surface of the Ice-Age Earth: The ICE-5G(VM2) model and GRACE Annual Rev Earth Planetary Sci 32:111–149

Perkins SE, Alexander LV and Nairn JR (2012) Increasing frequency, intensity and duration of observed global heatwaves and warm spells. Geophys Res Lett 39 *L20714*

Pham XT, Fontaine B and Philippon N (2010) Onset of the summer monsoon over the southern Vietnam and its predictability. Theor Appl Climatol 99:105-113

Philander SGH (1983) El-Nino Southern Oscillation Phenomena. Nature 302: 295-301 doi: 10.1038/302295a0

Philander SGH (1985) El Niño and La Niña. J Atmos Sci 42:2652-2662

Powell M, Soukup G, Cocke S, Gulati S, Morisseau-Leroy N, Hamid S, Dorst N and Axe L (2005) State of Florida hurricane loss projection model: Atmospheric science component. J Wind Engineering and Industrial Aerodynamics 93:651-674

Purkey SG and Johnson GC (2010) Warming of Global Abyssal and Deep Southern Ocean Waters between the 1990s and 2000s: Contributions to global heat and sea level rise budgets. J Climate 23:6336-6351

Qian W and Lee DK (2000) Seasonal march of Asian summer monsoon. Int J Clim 20:1371-1386

Radic V and Hock R (2011) Regionally differentiated contribution of mountain glaciers and ice caps to future sea-level rise. Nature Geoscience 4:91-94

Rae JGL, Aðalgeirsdóttir G, Edwards TL, Fettweis X, Gregory JM, Hewitt HT, Lowe JA, Lucas-Picher P, Mottram RH, Payne AJ, Ridley JK, Shannon SR, van de Berg WJ, van de Wal RSW and van den Broeke MR (2012) Greenland ice sheet surface mass balance: evaluating simulations and making projections with regional climate models. The Cryosphere Discuss 6:1275-1294

Ramage CS (1968) Role of a tropical “maritime continent” in the atmospheric circulation. Mon Wea Rev 96:365–370

Ramage CS (1971) Monsoon meteorology. Academic Press, New York and London 296pp

Ray RD and Douglas BC (2011) Experiments in reconstructing twentieth-century sea levels. Progress In Oceanography 91:496-515

Riehl H (1967) Southeast monsoon study. Final report. Southeast Asia monsoon study. Dept Atmos Sci, Colorado State University, Fort Collins, Colorado 1-33

Riehl H (1969) Weather patterns over southeast Asia during the northeast monsoon season. Navy Weather Research Facility, Norfolk, Virginia, NAVWEARSCHFAC Technical Paper No. 18-69

Reynolds RW, Smith TM, Liu C, Chelton DB, Casey KS and Schlax MG (2007) Daily high-resolution blended analyses for sea surface temperature. J Climate 20:5473-5496

Rignot E and Kanagaratnam P (2006) Changes in the velocity structure of the Greenland Ice Sheet. Science 311:986-990

Robinson A, Calov R and Ganopolski A (2012) Multistability and critical thresholds of the Greenland ice sheet. Nature Clim Change 2:429-432

Rodgers EB, Adler RF and Pierce HF (2000) Contribution of tropical cyclones to the North Pacific climatological rainfall as observed from satellites. J Appl Meteor 39:1658–1678

Rotstayn LD (1997) A physically based scheme for the treatment of stratiform clouds and precipitation in large-scale models. I: Description and evaluation of the microphysical processes. Quart J R Meteor Soc 123:1227–1282

Rotstayn LD, Jeffrey SJ, Collier MA, Dravitzki SM, Hirst AC, Syktus JI and Wong KK (2012) Aerosol and greenhouse gas-induced changes in summer rainfall and circulation in the Australasian region: a study using single-forcing climate simulations. Atmos Chem Phys 12:6377-6404 doi:10.5194/acp-12-6377-2012

Rotstayn LD and Lohmann U (2002) Simulation of the tropospheric sulfur cycle in a global model with a physically based cloud scheme. J Geophys Res 107 doi:10.1029/2002JD002128

Royer J-F, Chauvin F, Timbal B, Araspin P and Grimal D (1998) A GCM study of the impact of greenhouse gas increase on the frequency of occurrence of tropical cyclones. Clim Change 38:307-343

Sano M, Xu C and Nakatsuka T (2012) A 300-year Vietnam hydroclimate and ENSO variability record resconstructied from tree ring $\delta^{18}O$. J Geophy Res (Atmos) DOI:10.1029/2012JD017749

Schmidt F (1977) Variable fine mesh in spectral global model. Beitr Phys Atmos 50:211–217

Schwarzkopf MD and Ramaswamy V (1999) Radiative effects of CH4, N2O, halocarbons and the foreign-broadened H2O continuum: A GCM experiment. J Geophys Res 104:9467–9488

Sen PK (1968) Estimates of the regression coefficient based on Kendall’s Tau. J Amer Stat Assoc 63:1379-1389

Sethi SP (1977) Dynamic optimal control models in advertising: A survey. SIAM Rev 19:685-725

Shepherd A et al. (2012) A reconciled estimate of ice-sheet mass balance. Science 338:1183-1189

Slangen ABA, Katsman CA, van de Wal RSW, Vermeersen LLA and Riva REM (2012) Towards regional projections of twenty-first century sea-level change based on IPCC SRES scenarios. Clim Dyn 38:1191-1209

Slangen ABA and van de Wal RSW (2011) An assessment of uncertainties in using volume-area modelling for computing the twenty-first century glacier contribution to sea-level change. The Cryosphere 5:673-686

Smajgl A (2003) Conceptual and institutional aspects in implementing an emissions trading scheme. In: Brebbia CA and Patania F (Eds) Air Pollution XI - Eleventh International Conference on Modelling, Monitoring and Management of Air Pollution. WIT Press: Southampton.

Smajgl A, Egan S, Ward J and Kroon F (2013) The Mekong region simulation (Mersim) model - Design Document CSIRO Climate Adaptation Flagship, Townsville

Smajgl A, Greiner R and Mayocchi C (2006) Estimating the implications of water reform for irrigators in a sugar growing region. Environ Mod and Software 21:1360-1367

Smajgl A, Izquierdo L and Huigen M (2008) Modelling endogenous rule changes in an institutional context: The ADICO sequence. Adv Complex Systems 2:199-215

Smajgl A and Liagre L (2010) Multiplier analysis for Great Barrier Reef catchments: Policy implications of water availability. Econ Systems Res 22:263-277

Smith I, Chandler E (2009) Refining rainfall projections for the Murray Darling Basin of south-east Australia - the effect of sampling model results based on performance. Climatic Change 102:377–393. doi:10.1007/s10584-10009-19757-10581

Sterl A, van den Brink VH, Haarsma R and van Meijgaard E (2009) An ensemble study of extreme North Sea storm surges in a changing climate. Ocean Sciences Discussions 6:1031-1059

Syvitski J and Kettner A (2011) Sediment flux and the Anthropocene, Phil Trans Roy Soc A-Math Phys Eng Sci 369:957-975

Syvitski J, Kettner AJ, Overeem I, Hutton EWH, Hannon MT, Brakenridge R, Day J, Vorosmarty C, Saito Y, Giosan L and Nicholls RJ (2009) Sinking deltas due to human activities. Nature Geoscience 2:681-686

Szalai S and Szinell CS (2000) Comparison of two drought indices for drought monitoring in Hungary — a case study. In: Drought and drought mitigation in Europe, Springer, Netherlands, 161-166

Tan PV (2002) On the tropical cyclone activity in the Northwest Pacific basin and Bien Dong Sea in relationship with ENSO J Science, Vietnam National University, Hanoi 18:51-58

Taylor KE, Stouffer RJ and Meehl GA (2011) An Overview of CMIP5 and the experiment design. Bull Amer Meteor Soc 93:485-498

Tesfatsion L (2002) Agent-based computational economics: Modelling economies as complex adaptive systems. Department of Economics, Iowa State University, **http://www.econ.iastate.edu/tesfatsi/aceISpdf**

Thatcher M and McGregor JL (2009) Using a scale-selective filter for dynamical downscaling with the conformal cubic atmospheric model. Mon Wea Rev 137:1742-1752

Thompson BW (1951) An essay on the general circulation of the atmosphere over South-East Asia and the West Pacific. Quart J Roy Meteor Soc 77:569-597

Tippett MK, Camargo SJ, Sobel AH (2011) A Poisson regression index for tropical cyclone genesis and the role of large-scale vorticity in genesis. J Clim 24:2335–2357

Tory KJ, Chand SS, Dare RA and McBride JL (2013a) The development and assessment of a model-, grid- and basin independent tropical cyclone detection scheme. J Clim, in press

Tory KJ, Chand SS, Dare RA and McBride JL (2013b) An assessment of a model-independent tropical cyclone detection procedure in selected CMIP3 global climate models. J Climate, in press

Tory KJ, Dare RA, Davidson NE, McBride JL and Chand SS (2013c) The importance of low-deformation vorticity in tropical cyclone formation. Atmos Chem Phys 13:2115–2132

Tran DT, Saito Y, Dinh VH, Nguyen VL, Ta TKO and Tateishi M (2004) Regimes of human and climate impacts on coastal changes in Vietnam. Reg Environ Change 4:49-62

Uppala SM, Kallberg PW, Simmons AJ, Andrae U, Da Costa Bechtold V, Fiorino M, Gibson JK, Haseler J, Hernandez A, Kelly GA, Li X, Onogi K, Saarinen S, Sokka N, Allan RP, Andersson E, Arpe K, Balmaseda MA, Beljaars ACM, Van De Berg L, Bidlot J, Bormann N, Caires S, Chevallier F, Dethof A, Dragosavac M, Fisher M, Fuentes M, Hagemann S, Holm E, Hoskins BJ, Isaksen L, Janssen PAEM, Jenne R, Mcnally AP, Mahfouf J-F, Morcrette J-J, Rayner NA, Saunders RW, Simon P, Sterl A, Trenberth KE, Untch A, Vasiljevic D, Viterbo P and Woollen J (2005) The ERA-40 re-analysis. Quart J R Meteor Soc 131:2961–3012 doi:10.1256/qJ04.176

Wada Y, van Beek LPH, Sperna Weiland FC, Chao BF, Wu Y-H and Bierkens MFP (2012) Past and future contribution of global groundwater depletion to sea-level rise. Geophys Res Lett 39 L09402

Waibel M (2008) Implications and challenges of climate change for Vietnam. Pacific News 29:26-27

Walker GT and Bliss BW (1932) World weather. V Mem R Meteor Soc 36:53-84

Walsh KJE, Fiorino M, Landsea CW and McInnes KL (2007) Objectively determined resolution-dependent threshold criteria for the detection of tropical cyclones in climate models and reanalyses. J Clim 20:2307-2314

Walsh KJE and Watterson IG (1997) Tropical cyclone–like vortices in a limited area model: Comparison with observed climatology. J Clim 10:2240–2259

Wang B and Ho L (2002) Rainy season of the Asian-Pacific summer monsoon. J Climate 15:386-398

Wang B, Ho L, Zanh Y and Lu MM (2004b) Definition of South China Sea monsoon onset and commencement of the East Asia summer monsoon. J Climate 17:699-710

Wang Y, Leung LR, McGregor JL, Lee D-K, Wang WC, Ding Y and Kimura F (2004a) Regional climate modeling: progress, challenges and prospects. J Meteor Soc Japan 82:1599-1628

Watterson IG, Bathols J and Heady C (2013a) What influences the skill of climate models over the continents? Submitted to Bull Amer Meteor Soc

Watterson IG, Hirst AC and Rotstayn LD (2013b) A skill-score based evaluation of simulated Australian climate. In press, Aust Meteor Ocean J

Whetton PH, McInnes KL, Jones RN, Hennessy KJ, Suppiah R, Page CM, Bathols J and Durack PJ (2005) Australian Climate Change Projections for Impact Assessment and Policy Application: A Review. Climate Impact Group, CSIRO Marine and Atmospheric Research, Aspendale, Victoria, Australia

Whetton PH, Hennessy K, Clarke J, McInnes K and Kent D (2012) Use of Representative Climate Futures in impact and adaptation assessment. Climatic Change 115: 433-442

Woodworth PL (1999) High waters at Liverpool since 1768: the UK's longest sea level record. Geophys Res Lett 26:1589-1592

Woodworth PL and Player R (2003) The Permanent Service for Mean Sea Level: An update to the 21st century. J Coastal Res 19:287-295

Wu H, Svoboda MD, Hayes MJ, Wilhite DA and Wen F (2007) Appropriate application of the standardized precipitation index in arid locations and dry seasons. Int J Climatol 27:65–79 doi:10.1002/joc.1371

Wu MC, Chang WL, Leung WM (2004) Impacts of El Niño–Southern Oscillation events on tropical cyclone landfalling activity in the Western North Pacific. J Climate 17:1419–1428

Xu Z and Yang ZL (2012) An improved dynamical downscaling method with GCM bias corrections and its validation with 30 years of climate simulations. J Climate 25:6271-6286

Yatagai A, Arakawa O, Kamiguchi K, Kawamoto H, Nodzu MI and Hamada A (2009) A 44-year daily gridded precipitation dataset for Asia based on a dense network of rain gauges. SOLA 5:137-140 DOI:10.2151/sola.2009-035

Yatagai A, Kamiguchi K, Arakawa O, Hamada H, Yasutomi N and Kitoh A (2012) APHRODITE: Constructing a Long-term daily gridded precipitation dataset for Asia based on a dense network of rain gauges. Bull Amer Meteor Soc 1401-1415

Yen MC, Chen TC, Hu HL, Tzeng RY, Dinh DT, Nguyen TTT and Wong CJ (2011) Interannual variation of the fall rainfall in Central Vietnam. J Meteor Soc Japan 89A:259-270

Yokoi S and Matsumoto J (2008) Collaborative effects of cold surge and tropical-type disturbance on heavy rainfall in Central Vietnam. Mon Wea Rev 136:3275-3287

Zhang X and Church JA (2012) Sea level trends, interannual and decadal variability in the Pacific Ocean. Geophys Res Lett 39 L21701

APPENDIX 1: DEVELOPMENT OF AN INTEGRATED ASSESSMENT TOOL

This appendix gives details of a series of workshops held in Vietnam with various stakeholders in 2012 to develop an integrated assessment tool to apply to climate change projections, such as those developed in this project, using agent-based modelling in a participatory process.

DESCRIPTION OF TRAINING AND PARTICIPATORY PROCESS

Step 1: Seminars and workshops in Hanoi and HCMC on participatory assessment design

Key decision-makers from IMHEN and other agencies were invited to an initial workshop in Hanoi and Ho Chi Minh City (HCMC) during the week of 14 May 2012, with a total of 50 participants attending from IMHEN. Seminars were given which covered the following topics:

- What is integrated assessment?
- Traditional assessment methods.
- The complexity of the system at hand.
- Emergent phenomena or issues.
- Methods for implementing integrated assessments.

Based on these seminars, a workshop was held to identify a robust list of features that the assessment tool would need to cover. The key questions were:

Inputs:

- What specific interventions would an integrated assessment tool need to assess to be beneficial to your agency?

Outputs:

- What information would an assessment tool need to provide (indicators and resolution) in order to be beneficial to your agency?
- What geographical focus area should such an assessment model have to be beneficial to your agency?

The inputs define what the model needs to assess. The outputs specify what information is required from the model. The list that synthesises answers to these questions was compiled and discussed with IMHEN. For a summary of issues discussed at the workshops see Figure 4-7, which shows what interventions a future assessment model would need to be able to assess in the upper box and what information it would need to provide in the lower box.

Step 2: Selection of assessment methodology

In the next step, the project participants identified which methodology, or which combination of methods, would suit the requirements specified in Figure 4-7. The following questions were asked:

1. Is the assessment going to cover only changes that are captured in past data?
2. Will the assessment model need to capture variables from different disciplines (i.e. hydrology, agriculture, social science, economics, etc.)?
3. Does the assessment aim for identifying an optimal solution?
4. Can human behaviour be prescribed (outside of the model) or do household-level adaptation processes need to be modelled?

The first question tests the principal suitability of statistical and econometric methods, because if changes need to be modelled that are not captured in the past data, statistical methods are generally less effective. The second question asks if there is a need for, and relevance of, cross-disciplinary dynamics. If these needs are low, then a whole-of-system approach can be replaced by disciplinary methods. The third question queries the relevance of optimality while the fourth question targets the relevance of disaggregated (household level) simulations of human behaviour.

MODELLING METHODS

During this process, a list of methods was considered and discussed based on the four questions listed at the beginning of this section:

Statistical models

- *Trend analysis.*
- *Correlations*.

Macro-economic models

- *Input-output modelling.*
- *Computable General Equilibrium (CGE*).

System dynamics models

Bayesian Belief Networks (BBNs)

Optimal control methods

Hydro-economic models

Agent-based models (ABMs)

Statistical models

These questions were discussed with IMHEN and it was decided, as an example, to combine agent-based modelling with a hydrological floodplain model. (For a more complete description of the capabilities of the different modelling methods, see Section 4.7.1; for further discussion of the reasons for the choice of an agent-based model, see Section 4.7.2.)

Step 3: First training of staff of IMHEN, SIHYMETE, and CTU on integrated assessment, complexity and agent-based modelling

This training was conducted 16-17 July 2012 in Hanoi and covered the following sessions:

Integrated assessment
Participants were presented with the contrast between disciplinary and integrated research and how disciplinary integration holds the key to analysing sustainability-related issues. Examples were presented for integrated research and for triple-bottom-line assessments.

Complexity and emergence
Participants were shown that with disciplinary integration more variables needed to be linked, which increases complexity. The discussion of this topic was concerned with conveying the relevance of choosing adequate methods to avoid inappropriate simplifications. Such inappropriate simplifications often come with assumptions that some methods implicitly make. Inadequate simplifications can lead to maladaptive investments. This is particular true in the case of situations that have not yet been experienced. The context of sea-level rise in the Mekong Delta is an example of such a situation. Analysing the effectiveness of adaptation options to sea-level rise in the Mekong Delta depends on various factors and how these factors interact. Such factors include salinity intrusion and the underpinning hydrological processes, upstream change to hydrological dynamics, including tributary and mainstream dams, water diversions, large-scale irrigation and large-scale land use change. Additionally, household-level adaptations to situational changes are a key determinant for the effectiveness of adaptation options. Any assessment of adaptation options would need to take such complex interactions into account. This debate on complexity introduced the concept of *emergence*. Participants explored what emergence means, and how emergence could be captured in integrated assessment modelling.

Agent-based modelling
Agent-based modelling was introduced as a method that allows for simulating highly complex situations and allowing unexpected phenomena to emerge. This session explained what agent-based modelling is and provided the participants with examples. One example shown was the Mekong region simulation model (Mersim; Smajgl *et al*., 2013). Participants discussed the utility of the existing Mersim model shell for the context task of assessing the effectiveness of adaptation options in Vietnam. A clear message from the floor was that the model could be useful if it was extended for a wider area, and that all other coastal provinces need to implement it.

Model design
This session was the core of the training and explained the four steps of successful agent-based model design: (1) determine system boundaries, (2) specify the system and its variables unambiguously, (3) specify possible states (or attributes) for each variable (or agent entities), and (4) develop a robust response function. Students were taken through techniques to successfully implement each of these four steps.

Model-based analysis
This session started laying out the kind of analysis agent-based models allow. The discussion emphasised the importance of knowing upfront what indicators decision-makers require from the model. Examples were shown for analysis conducted with Mersim.

Step 4: Second training of staff of IMHEN, SIHYMETE and CTU in design and analysis of agent-based models

This training was conducted 23-24 August 2012. During these two days, participants were guided to design their own model. These hands-on sessions aimed to create the necessary space for participants to experience model design actively. Participants developed system diagrams and agent rules. In this context much time was spent on the underpinning structure of agent-based model architecture. This included specifying agents, the attributes that define them, and the state of the attributes. Contexts were discussed that exemplify these three tiers (agents/attributes/states). At the end of this training, participants developed a solid understanding of the language used in agent-based modelling and what model design entails.

Step 5: Third training of staff of IMHEN, SIHYMETE and CTU in agent-based model analysis and modelling processes

This training was conducted 15 November 2012 and focused on agent-based analysis. The first type of analysis this training addressed was the (statistical) analysis of results from Monte Carlo runs. For Monte Carlo runs, the model is run many hundreds of times. As some parameters are stochastic (they can range between two values), each run leads to a different result. Plotting these results delivers the solution space with a probability distribution. Participants were shown Excel spreadsheets with results from the Mersim model and were given the task of interpreting some results. A pattern-based analysis of the results was then presented, which explains the temporal or spatial patterns. Also in this session, participants were asked to provide their own interpretation. Results based on single model runs were then discussed. This included the task of identifying typical runs, and how to take, interpret and present screenshots of such typical runs. The final session focused on the overarching modelling process. This included discussions on how modellers can effectively inform the decision-making processes and why the design of the engagement process is critical. The final hour was spent on repeating material on model design and model analysis, which provided insights in the skills participants had obtained.

Summary

The training provided participants with the fundamentals of agent-based design and the analysis of agent-based models. The interactions with participants have shown that a core group of participants were successfully trained and could be ready to work on an integrated assessment model for climate adaptation in Vietnam. The skills some of the participants obtained would be sufficient to become effective project team members during an implementation phase of such model development. This was not successfully achieved for participants from CTU because not every training session was attended by the same people. But most of the IMHEN and SIHYMETE staff that attended were able to engage successfully in the final discussion, showing the basic understanding this training aimed to convey. These participants would require a real model development project to practice their basic skills in on-the-job training.

This training connects the data (downscaled climate and sea-level rise projections) to assessment of adaptation options by (1) designing assessment requirements and (2) training staff from IMHEN, SIHYMETE and CTU, with potential positive outcomes if the model development actually occurs.

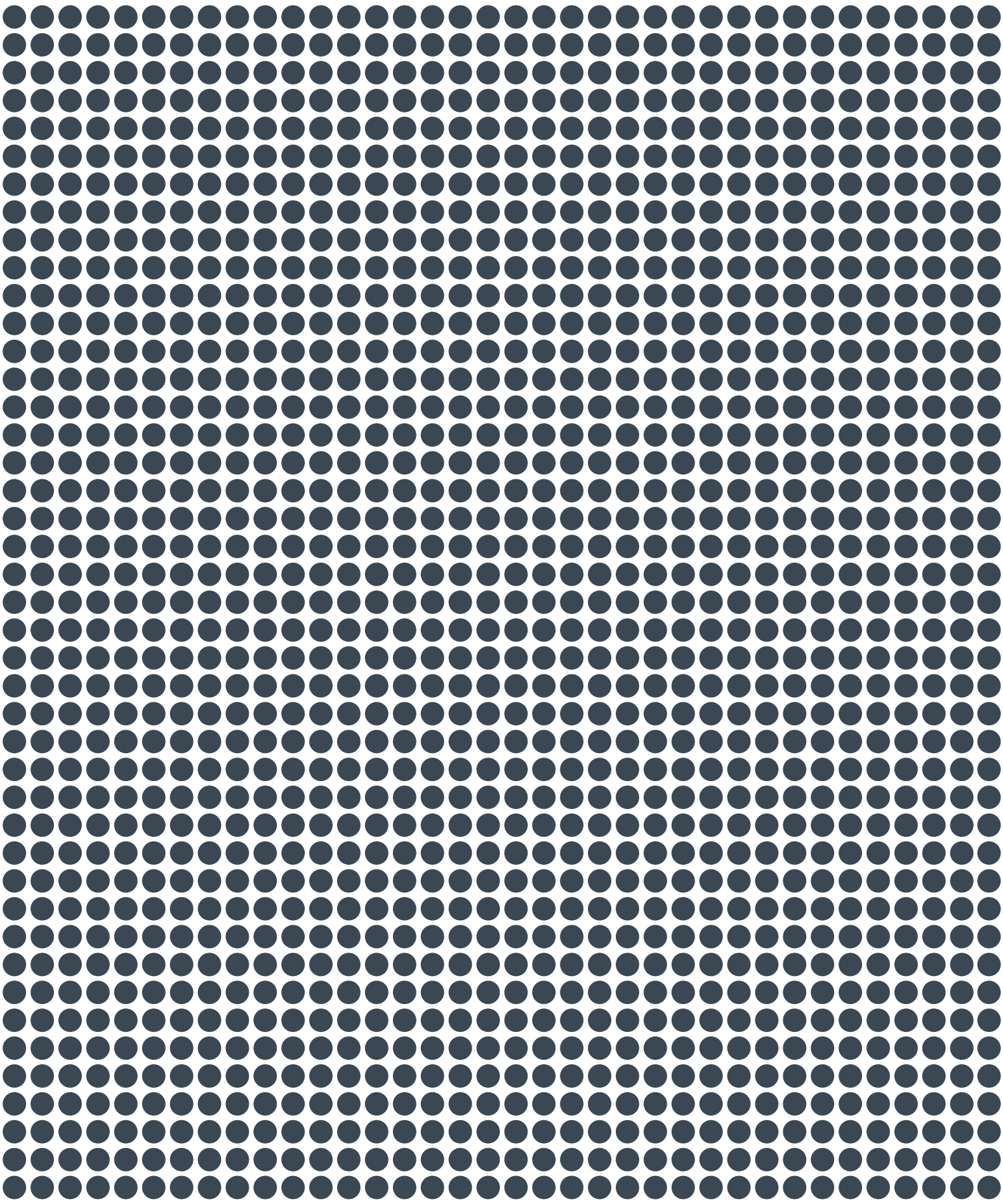

CONTACT

VIETNAM INSTITUTE OF METEOROLOGY, HYDROLOGY AND ENVIRONMENT

WEB http://www.imh.ac.vn/

Assoc. Prof. Dr. Nguyen Van Thang

EMAIL nvthang@imh.ac.vn

PHONE +84 - 4 - 38359415

For more information, please visit the project website:

WWW.VNCLIMATE.VN

B&M 13-00212